Methods in Molecular Biology 849

Springer Protocols

Einar M. Sigurdsson
Miguel Calero
María Gasset *Editors*

Amyloid Proteins

Methods and Protocols

Second Edition

Humana Press

METHODS IN MOLECULAR BIOLOGY™

Series Editor
John M. Walker
School of Life Sciences
University of Hertfordshire
Hatfield, Hertfordshire, AL10 9AB, UK

For further volumes:
http://www.springer.com/series/7651

Amyloid Proteins

Methods and Protocols

Second Edition

Edited by

Einar M. Sigurdsson

Departments of Physiology and Neuroscience, and Psychiatry,
School of Medicine, New York University,
New York, NY, USA

Miguel Calero

Centro Nacional de Microbiología, Instituto de Salud Carlos III,
Majadahonda, Madrid, Spain

María Gasset

Instituto de Química-Física Rocasolano, CSIC, Madrid, Spain

Humana Press

Editors
Einar M. Sigurdsson
Departments of Physiology and
Neuroscience, and Psychiatry
School of Medicine
New York University
New York, NY, USA

María Gasset
Instituto de Química-Física Rocasolano
CSIC, Madrid, Spain

Miguel Calero
Centro Nacional de Microbiología
Instituto de Salud Carlos III
Majadahonda, Madrid, Spain

ISSN 1064-3745 e-ISSN 1940-6029
ISBN 978-1-61779-550-3 e-ISBN 978-1-61779-551-0
DOI 10.1007/978-1-61779-551-0
Springer New York Dordrecht Heidelberg London

Library of Congress Control Number: 2012930138

Cover illustration: The cover art depicts fibers assembled from full-length Tau and observed by Atomic Force Microscopy. Courtesy of Susanne Wegmann (D. Müller laboratory, ETHZ Basel, Switzerland).

Printed on acid-free paper

Humana Press is part of Springer Science+Business Media (www.springer.com)

Preface

Amyloid diseases are characterized by the deposition of insoluble fibrous amyloid proteins. The word "amyloid" indicates a starch-like compound, and though a misnomer, continues to be the accepted term for this group of protein conformational disorders. Approximately 30 different proteins can form amyloid and although there is usually no homology in their amino acid sequence, all share a β-pleated sheet as the polymer scaffold. Historically, these β-pleated deposits were detected by histological dyes, and the characteristic fibril structure confirmed with electron microscopy. As these amyloids were purified and sequenced, various in vitro techniques were developed, often using synthetic peptides and/or highly purified amyloids derived from diseased tissue. Development of animal models occurred concurrently and some of these diseases can now be passed on to animals by injecting them with amyloid-rich tissue fractions, or shown to spread between cells in vivo or in culture, suggesting a transmissible nature of these protein polymers. However, for most amyloidoses, transgenic technology has been necessary for recapitulating the disease. Together, these in vitro and in vivo models have been used to understand the etiology and pathogenesis of amyloid diseases as well as to screen for drugs to prevent the formation of and/or clear these aggregates.

Several of these methods and protocols are detailed in this second edition of *Amyloid Proteins: Methods and Protocols*, using examples from various amyloids. Substantial changes have been made from the first edition of this volume. Several classic methods/protocols that did not warrant updates are not included in the second edition. Importantly, numerous new chapters have been added that cover new techniques and/or topics not addressed in the first edition. Such expansion was made possible with the help of two new editors, Drs. María Gasset and Miguel Calero, who graciously agreed to participate in this project. The volume is divided into three parts. Part I contains in vitro assays, starting with a few chapters that focus on the preparation of amyloid and its precursors. These are followed by chapters detailing specific analytical methods for studying these proteins. Part II describes cell culture models and assays for production of amyloid proteins, and Part III consists of protocols for amyloid extraction from tissue, its detection in vitro and in vivo, as well as nontransgenic methods for developing amyloid mouse models. Most of the chapters follow a similar format and are detailed protocols for performing a particular procedure. However, certain chapters focus more on the general principles and theoretical issues of a particular method.

It is our hope that these chapters will be useful for both students and scientists new to the amyloid field, as well as for seasoned investigators learning new techniques to further their research.

We would like to thank the authors for their contribution and the series editor, Dr. John M. Walker, for the opportunity to edit this book.

New York, NY, USA — *Einar M. Sigurdsson*
Madrid, Spain — *Miguel Calero*
Madrid, Spain — *María Gasset*

Contents

Contributors

Umberto Agrimi • *Department of Veterinary Public Health and Food Safety, Istituto Superiore di Sanità, Rome, Italy*

Marcelo A. Barria • *Mitchell Center for Alzheimer's Disease and Related Brain Disorders, Department of Neurology, University of Texas Houston Medical School, Houston, TX, USA*

Ilia V. Baskakov • *Center for Biomedical Engineering and Technology, Department of Anatomy and Neurobiology, University of Maryland, Baltimore, MD, USA*

Gal Bitan • *Department of Neurology, David Geffen School of Medicine at UCLA, Los Angeles, CA, USA*

Luz P. Blanco • *Department of Molecular, Cellular, and Developmental Biology, University of Michigan, Ann Arbor, MI, USA*

Hugo M. Botelho • *Instituto de Tecnologia Química e Biológica, Universidade Nova de Lisboa, Oeiras, Portugal*

Allal Boutajangout • *Departments of Physiology and Neuroscience, and Psychiatry, New York University School of Medicine, New York, NY, USA*

Alexander K. Buell • *Nanoscience Centre, University of Cambridge, Cambridge, UK*

Ashley I. Bush • *Mental Health Research Institute, University of Melbourne, Parkville, VIC, Australia*

Erica Caballero • *Instituto de Biología y Genética Molecular (IBGM), Universidad de Valladolid and Consejo Superior de Investigaciones Científicas (CSIC), Valladolid, Spain*

Miguel Calero • *Centro Nacional de Microbiología, Instituto de Salud Carlos III, Majadahonda, Madrid, Spain*

Matthew R. Chapman • *Department of Molecular, Cellular, and Developmental Biology, University of Michigan, Ann Arbor, MI, USA*

Subashchandrabose Chinnathambi • *Max Planck Unit for Structural Molecular Biology c/o DESY, Hamburg, Germany*

Paula Desplats • *Department of Neurosciences, UCSD School of Medicine, La Jolla, CA, USA*

Christopher M. Dobson • *Department of Chemistry, University of Cambridge, Cambridge, UK*

Michele A. Di Bari • *Department of Veterinary Public Health and Food Safety, Istituto Superiore di Sanità, Rome, Italy*

Herman K. Edskes • *Laboratory of Biochemistry and Genetics, National Institute of Diabetes Digestive and Kidney Diseases, National Institutes of Health, Bethesda, MD, USA*

Günter Fritz • *Department of Neuropathology, University of Freiburg, Freiburg, Germany*

María Gasset • *Instituto de Química-Física Rocasolano, CSIC, Madrid, Spain*
Sebastien A. Gauthier • *Departments of Psychiatry and Pharmacology, New York University School of Medicine, New York, NY, USA; Center for Dementia Research, Nathan S. Kline Institute for Psychiatric Research, Orangeburg, NY, USA*
Anna L. Gharibyan • *Department of Medical Biochemistry and Biophysics, Umeå University, Umeå, Sweden*
Jorge Ghiso • *Departments of Pathology and Psychiatry, New York University School of Medicine, New York, NY, USA*
Cláudio M. Gomes • *Instituto de Tecnologia Química e Biológica, Universidade Nova de Lisboa, Oeiras, Portugal*
Dennisse Gonzalez-Romero • *Mitchell Center for Alzheimer's Disease and Related Brain Disorders, Department of Neurology, University of Texas Houston Medical School, Houston, TX, USA*
Adam P. Gunn • *Mental Health Research Institute, University of Melbourne, Parkville,VIC, Australia*
Per Hammarström • *Department of Chemistry, IFM, Linköping University, Linköping, Sweden*
Dung Minh Hoang • *Department of Radiology, Center for Biomedical Imaging New York University School of Medicine, New York, NY, USA*
Indiana E. Ingolfsdottir • *Faculty of Medicine, University of Iceland, Reykjavik, Iceland*
Asad Jan • *Laboratory of Molecular and Chemical Biology of Neurodegeneration, Brain Mind Institute, École Polytechnique Fédérale de Lausanne (EPFL), Lausanne, Switzerland*
Sadasivam Jeganathan • *Max-Planck-Unit for Structural Molecular Biology c/o DESY, Hamburg, Germany; Department of Experimental Oncology, IFOM-IEO Campus, Milan, Italy*
Carl Julien • *Axe Neurosciences, Centre Hospitalier de l'Université Laval, Québec, QC, Canada*
Sonia S. Jung • *Departments of Psychiatry and Pharmacology, New York University School of Medicine, New York, NY, USA; Center for Dementia Research, Nathan S. Kline Institute for Psychiatric Research, Orangeburg, NY, USA*
Dmitry Kryndushkin • *Laboratory of Biochemistry and Genetics, National Institute of Diabetes Digestive and Kidney Diseases, National Institutes of Health, Bethesda, MD, USA; Department of Pharmacology, Uniformed Services University of the Health Sciences, Bethesda, MD, USA*
Annette Eva Langkilde • *Faculty of Pharmaceutical Sciences, University of Copenhagen, Copenhagen, Denmark*
Hilal A. Lashuel • *Laboratory of Molecular Neurobiology and Neuroproteomics, Brain Mind Institute, Ecole Polytechnique Fédérale de Lausanne (EPFL), Lausanne, Switzerland*
He-Jin Lee • *Department of Anatomy, School of Medicine, Institute of Biomedical Science and Technology, Konkuk University, Seoul, Korea*
Seung-Jae Lee • *Department of Biomedical Science and Technology, Institute of Biomedical Science and Technology, Konkuk University, Seoul, Korea*

Efrat Levy • *Departments of Psychiatry and Pharmacology, New York University School of Medicine, New York, NY, USA; Center for Dementia Research, Nathan S. Kline Institute for Psychiatric Research, Orangeburg, NY, USA*
Yong Sheng Li • *Department of Neurology, New York University School of Medicine, New York, NY, USA*
Mikael Lindgren • *Department of Chemistry, IFM, Linköping University, Linköping, Sweden*
Aleksey Lomakin • *Materials Processing Center, Massachusetts Institute of Technology, Cambridge, MA, USA*
Dahabada H.J. Lopes • *Department of Neurology, David Geffen School of Medicine at UCLA, Los Angeles, CA, USA*
Devin K. Lowenstein • *Department of Neurology, David Geffen School of Medicine at UCLA, Los Angeles, CA, USA*
Natallia Makarava • *Center for Biomedical Engineering and Technology, Department of Anatomy and Neurobiology, University of Maryland, Baltimore, MD, USA*
Eckhard Mandelkow • *Max-Planck-Unit for Structural Molecular Biology c/o DESY, Hamburg, Germany; DZNE, German Center for Neurodegenerative Diseases c/o CAESAR, Hamburg, Germany*
Eva-Maria Mandelkow • *Max-Planck-Unit for Structural Molecular Biology c/o DESY, Hamburg, Germany; DZNE, German Center for Neurodegenerative Diseases c/o CAESAR, Hamburg, Germany*
Eliezer Masliah • *Departments of Neurosciences, and Pathology, University of California, San Diego, La Jolla, CA, USA*
Paul M. Mathews • *Center for Dementia Research, Nathan S. Kline Institute for Psychiatric Research, Orangeburg, NY, USA; Department of Psychiatry, New York University School of Medicine, New York, NY, USA*
Matthew J. Mazzella • *Center for Dementia Research, Nathan S. Kline Institute for Psychiatric Research, Orangeburg, NY, USA*
Ryan McGlinchey • *Laboratory of Biochemistry and Genetics, National Institute of Diabetes Digestive and Kidney Diseases, National Institutes of Health, Bethesda, MD, USA*
Ludmilla A. Morozova-Roche • *Department of Medical Biochemistry and Biophysics, Umeå University, Umeå, Sweden*
Kyle L Morris • *School of Life Sciences, University of Sussex, Brighton, UK*
Daniel J. Muller • *Department of Biosystems Science and Engineering, ETH Zürich, Basel, Switzerland*
Kazuma Murakami • *Molecular Gerontology, Tokyo Metropolitan Institute of Gerontology, Tokyo, Japan; Division of Food Science and Biotechnology, Graduate School of Agriculture, Kyoto University, Kyoto, Japan*
K. Peter R. Nilsson • *Department of Chemistry, IFM, Linköping University, Linköping, Sweden*
Ralph A. Nixon • *Center for Dementia Research, Nathan S. Kline Institute for Psychiatric Research, Orangeburg, NY, USA; Departments of Psychiatry and Cell Biology, New York University School of Medicine, New York, NY, USA*

Romolo Nonno • *Department of Veterinary Public Health and Food Safety, Istituto Superiore di Sanità, Rome, Italy*
Lucía Núñez • *Instituto de Biología y Genética Molecular (IBGM), Universidad de Valladolid and Consejo Superior de Investigaciones Científicas (CSIC), Valladolid, Spain*
Ingvar H. Olafsson • *Faculty of Medicine/Department of Neurosurgery, University of Iceland/Landspitali University Hospital, Reykjavik, Iceland*
Kenjiro Ono • *Department of Neurology & Neurobiology of Aging, Kanazawa University Graduate School of Medical Science, Kanazawa, Japan*
Valeriy Ostapchenko • *Center for Biomedical Engineering and Technology, Department of Anatomy and Neurobiology, University of Maryland, Baltimore, MD, USA*
Emmanuel Planel • *Axe Neurosciences, Centre Hospitalier de l'Université Laval, Québec, QC, Canada*
David Quartermain • *Department of Neurology, New York University School of Medicine, New York, NY, USA*
Hameetha B. Rajamohamedsait • *Department of Physiology and Neuroscience, New York University School of Medicine, New York, NY, USA*
Dina Raveh • *Department of Life Sciences, Ben Gurion University of the Negev, Beersheba, Israel*
Roland Riek • *Physical Chemistry, ETH Zurich, ETH Honggerberg, Zurich, Switzerland*
Blaine R. Roberts • *Mental Health Research Institute, University of Melbourne, Parkville, VIC, Australia*
Clark Rosensweig • *Department of Neurology, David Geffen School of Medicine at UCLA, Los Angeles, CA, USA*
Agueda Rostagno • *Department of Pathology, New York University School of Medicine, New York, NY, USA*
Susmita Sahoo • *Departments of Psychiatry and Pharmacology, New York University School of Medicine, New York, NY, USA; Center for Dementia Research, Nathan S. Kline Institute for Psychiatric Research, Orangeburg, NY, USA*
Sara Sanz-Blasco • *Instituto de Biología y Genética Molecular (IBGM), Universidad de Valladolid and Consejo Superior de Investigaciones Científicas (CSIC), Valladolid, Spain*
Stephen D. Schmidt • *Center for Dementia Research, Nathan S. Kline Institute for Psychiatric Research, Orangeburg, NY, USA; Vaccine Research Center, National Institute of Allergy and Infectious Diseases, National Institutes of Health, Bethesda, MD, USA*
Louise C Serpell • *School of Life Sciences, University of Sussex, Brighton, UK*
Frank Shewmaker • *Department of Pharmacology, Uniformed Services University of the Health Sciences, Bethesda, MD, USA*
Einar M. Sigurdsson • *Departments of Physiology and Neuroscience, and Psychiatry, New York University School of Medicine, New York, NY, USA*
Sharmistha Sinha • *Department of Neurology, David Geffen School of Medicine at UCLA, Los Angeles, CA, USA; Department of Biochemistry, Biophysics and Molecular Biology, Iowa State University, Ames, IA, USA*

Daniel R. Smith • *Department of Molecular, Cellular, and Developmental Biology, University of Michigan, Ann Arbor, MI, USA*
Claudio Soto • *Mitchell Center for Alzheimer's Disease and Related Brain Disorders, Department of Neurology, University of Texas Houston Medical School, Houston, TX, USA*
Brian Spencer • *Department of Neurosciences, UCSD School of Medicine, La Jolla, CA, USA*
David B. Teplow • *Department of Neurology, David Geffen School of Medicine at UCLA, Los Angeles, CA, USA*
Finnbogi R. Thormodsson • *ValaMed ehf, KIM Medical Park, Reykjavik, Iceland*
Belen Tizon • *Departments of Psychiatry and Pharmacology, New York University School of Medicine, New York, NY, USA; Center for Dementia Research, Nathan S. Kline Institute for Psychiatric Research, Orangeburg, NY, USA*
Bente Vestergaard • *Faculty of Pharmaceutical Sciences, University of Copenhagen, Copenhagen, Denmark*
Marçal Vilar • *Neurodegeneration Unit, Centro Nacional de Microbiología, Instituto de Salud Carlos III, Madrid, Spain*
Dadi Th. Vilhjalmsson • *Department of Surgery (Colorectal section), Malmö University Hospital (SUS Malmö), Malmö, Sweden*
Carlos Villalobos • *Instituto de Biología y Genética Molecular (IBGM), Universidad de Valladolid and Consejo Superior de Investigaciones Científicas (CSIC), Valladolid, Spain*
Youssef Zaim Wadghiri • *Department of Radiology, Center for Biomedical Imaging New York University School of Medicine, New York, NY, USA*
Lei Wang • *Physical Chemistry, ETH Zurich, ETH Honggerberg, Zurich, Switzerland*
Susanne Wegmann • *Department of Biosystems Science and Engineering, ETH Zurich, Basel, Switzerland*
Mark E. Welland • *Nanoscience Centre, University of Cambridge, Cambridge, UK*
Per Westermark • *Department of Immunology, Genetics and Pathology, Uppsala University, Uppsala, Sweden*
Reed B. Wickner • *Laboratory of Biochemistry and Genetics, National Institute of Diabetes Digestive and Kidney Diseases, National Institutes of Health, Bethesda, MD, USA*
Thomas Wisniewski • *Departments of Neurology, Pathology and Psychiatry, New York University School of Medicine, New York, NY, USA*
Yizhou Zhou • *Department of Molecular, Cellular, and Developmental Biology, University of Michigan, Ann Arbor, MI, USA*
Alexis Bretteville • *Axe Neurosciences, Centre Hospitalier de l'Université Laval, Québec, QC, Canada*

Part I

In Vitro Models and Assays

Chapter 1

Rapid Generation of Dityrosine Cross-linked Aβ Oligomers via Cu-Redox Cycling

Adam P. Gunn, Blaine R. Roberts, and Ashley I. Bush

Abstract

There is a great interest in the role of free radicals and oxidative stress in Alzheimer's disease and for the role of transition metals in the generation of oligomers of Aβ peptides. In the literature, there are a multitude of varying methods that can be used to create soluble oligomers of Aβ, however, the processes that create these oligomers are often stochastic by nature and thus reproducibility is an issue. Here we report a simple and reproducible method for the production of radically derived dityrosine cross-linked oligomers of Aβ, through reaction with copper and ascorbic acid.

Key words: Amyloid beta, Aβ, Alzheimer's disease, Dityrosine, Hydroxyl radical, Copper

1. Introduction

The amyloid beta (Aβ) peptide is a central contributor to the neuronal degeneration typical of Alzheimer's disease (AD). An amphipathic peptide, Aβ is cleaved from the amyloid precursor protein (APP) by the action of beta and gamma secretase. Aβ is highly metastable, and is capable of rapid aggregation via hydrophobic self-association as well as through interaction with cellular ions such as Ca, Cu, Fe, and Zn. The characteristic senile plaques of AD brains are primarily composed of fibrillar Aβ and are especially enriched for the transition metals Fe, Cu, and Zn, of which Cu and Zn are complexed with the aggregated Aβ (1). However, it has been consistently reported that the level of soluble Aβ in AD cerebral tissue, rather than fibrillar plaque-bound Aβ, correlates with neuronal and synaptic damage (2–4).

Soluble Aβ, including oligomeric forms, represent roughly 1–3% of total brain Aβ (4), although overall, post-translationally

Einar M. Sigurdsson et al. (eds.), *Amyloid Proteins: Methods and Protocols*, Methods in Molecular Biology, vol. 849,
DOI 10.1007/978-1-61779-551-0_1,

altered species comprise a considerably greater proportion of the Aβ found in the brains of AD patients (5, 6). Post-translational modifications to Aβ identified in AD brain include isomerised amino acid side chains such as D-aspartate, D- or L-isoaspartate (7), D-serine (8), and amino-terminal pyroglutamate (9, 10), as well as products of oxidation including methionine sulfoxide (11). These modifications are thought to enhance resistance to protease degradation and have been detected both in soluble Aβ and in amyloid deposits, suggesting that they may form during the early stages of AD pathogenesis.

Oxidatively modified proteins accumulate during ageing and result from the imbalance between production and detoxification of reactive oxygen species (ROS). This 'oxidative stress' is a prevalent feature of AD brain (12, 13), and oxidative damage precedes the appearance of anatomical or cognitive changes in humans (14) and animal models (15). In AD brain, there is also extensive evidence of dysregulated metal homeostasis (16), and we propose that abnormal interactions between Aβ and physiological transition metals, particularly copper and iron, contribute significantly to this stress. Conditions which prevail in the aged commonly include physiological acidosis, mitochondrial insufficiency, hypercholesterolaemia, and transient or chronic ischemia (for a discussion of their relationship to AD pathogenesis, see refs. 17–19). In this pro-oxidant environment, the usual tight restraints on copper trafficking are subtly perturbed, permitting Aβ to participate in aggressive redox chemistry. Aβ possesses a high-affinity copper binding site (20) and can react with biological reductants (e.g., dopamine, cholesterol, and ascorbic acid) to form an Aβ–Cu(I) complex. In vitro, re-oxidation of the Aβ–Cu(I) complex by molecular oxygen generates H_2O_2, which can further degrade to produce highly reactive hydroxyl radicals via Fenton and Haber–Weiss reactions. As a consequence, Aβ can form soluble dityrosine cross-linked dimers via radicalisation of the single tyrosine residue (Y10) (21). Furthermore, mutation of this tyrosine to alanine (Y10A) abolished neurotoxicity and significantly diminished H_2O_2 production, highlighting the critical role of the tyrosine residue in Aβ-mediated neurotoxicity (21).

Herein we describe a method for the rapid generation of dityrosine cross-linked Aβ oligomers, mediated by the reaction of Aβ with Cu and ascorbic acid. This method reproducibly generates a disperse mixture of Aβ oligomers, with a proportion containing dityrosine cross-links that can be detected by fluorescence spectrometry and immunoblotting techniques.

2. Materials

2.1. Aβ Preparation

1. $A\beta_{1-42}$ peptide, lyophilised (synthesised using standard Fmoc chemistry, commercially sourced).
2. Anti-static gun (or other anti-static apparatus).
3. 1,1,1,3,3,3-Hexafluoro-2-propanol (HFIP). Store at 4°C.
4. Phosphate-buffered saline (PBS; pH 7.4): 137 mM NaCl, 2.7 mM KCl, 10 mM Na_2HPO_4, and 2 mM KH_2PO_4.
5. NaOH (20 mM) dissolved in water.

2.2. Dityrosine Cross-linking and Detection

1. $CuCl_2$ (1 mM) present as a glycine counter-ion (6 mM): Dissolve 8.5 mg $CuCl_2{\cdot}2H_2O$ and 22.5 mg of glycine in 50 mL of water, filter through a 0.2-μm filter.
2. Ascorbic acid (5 mM): Prepare a 50 mM stock in water, then dilute (must be prepared fresh for each experiment).
3. Ethylenediaminetetraacetic acid (EDTA; 25 mM): prepared in water and filtered through a 0.2-μm filter.
4. Black microplate (quartz or plastic), or fluorescence microcuvette (see Note 1).

2.3. Immunoblotting Components

1. Nitrocellulose membranes: 0.2 μm Trans-Blot® (Bio-Rad, California, USA).
2. Filter Paper: 3 mm Chromatography grade (Whatman, New Jersey, USA).
3. Tris-buffered saline (TBS; 10×): 0.1 M Tris, 1.5 M NaCl, adjust to pH 8.0 with concentrated HCl.
4. TBS containing 0.1% v/v Tween 20 (TBS-T).
5. Blocking solution: 2% w/v Bovine serum albumin (BSA) in TBS buffer.
6. 1C3 antibody (Cat# NWA-DIY020, Northwest Life Science Technologies, Washington, USA).
7. Polyclonal rabbit anti-mouse IgG, HRP conjugated (Dako, California, USA).
8. ECL detection reagents: Immobilon® (Millipore, Massachusetts, USA).

3. Methods

3.1. Pretreatment and Preparation of Aβ Stock

1. Weigh out an appropriate amount (e.g. 0.1–0.3 mg) of lyophilised Aβ1–42 peptide using a clean spatula and a 1.5-mL centrifuge tube on a microbalance, under minimal static conditions

(see Note 2). The microbalance should be pre-zeroed using the empty tube.

2. The Aβ peptide is dissolved in HFIP to 1 mg/mL and the tube (cap closed) left to incubate at room temperature for 1 h. Initially this solution will be cloudy, but should become clear after the incubation.
3. The HFIP can be removed by either leaving the tube uncapped in the fumehood overnight (see Note 3) or by vacuum centrifugation. If air-drying over night, any residual HFIP should be removed by a brief (10 min) vacuum centrifugation step or by running a stream of nitrogen/argon gas over the residue. Dried preparations of Aβ should be visible only as a 'glassy' film towards the bottom of the tube (see Note 4). HFIP-treated Aβ can be stored at –80 C for later use (see Note 5).
4. An aliquot of HFIP-pretreated Aβ is redissolved in NaOH (20 mM) and PBS (pH 7.4) to 1 mg/mL. Firstly, NaOH is added to the pretreated Aβ to 20% vol/wt (i.e. 20 μL NaOH for a 100 μg aliquot). The Aβ should be left to dissolve for 3 min at room temperature without agitation. Deionised water (dH_2O) is added (3.5 volumes) to the NaOH dissolved Aβ (i.e. 70 μL dH_2O to the 20 μL NaOH-treated Aβ). 10× PBS is added to neutralise the mixture and bring the final concentration of Aβ to 1 mg/mL (i.e. 10 μL of 10× PBS to the 90 μL mixture).
5. The Aβ is then sonicated in a water bath for 5 min.
6. Following sonication, the Aβ is centrifuged for 10 min at 16,000 × *g* at 4°C to remove any large aggregated material remaining in the tube.
7. The supernatant (top 80% of preparation only) is removed to a pre-chilled 1.5-mL tube and kept on ice.
8. For UV quantification of the Aβ stock, make a 50-fold dilution of the Aβ in PBS (pH 7.4, room temperature). The volume of diluted Aβ required for quantitation is dependent on the UV/Vis spectrophotometer being used.
9. Measure the absorbance of Aβ at 214 nm, using a wavelength scanning protocol from 350 to 200 nm (see Note 6). Calculate the concentration of Aβ from the OD_{214} value (ε_{214} $A\beta_{1-42}$ = 94,500 M^{-1}/cm), correcting for the dilution factor and background absorbance (see Note 7).

3.2. Formation and Fluorescent Detection of Aβ-Dityrosine

1. In a 2-mL centrifuge tube (rounded bottom), combine the 10× PBS, dH_2O, Aβ, $CuCl_2$, and ascorbic acid as per Table 1, in that order.
2. Vortex the mixture briefly (2 s) and incubate at 37°C on a vertically rotating wheel (to ensure good aeration) at approximately 30 rpm.

Table 1
Components of the Aβ-dityrosine reaction mixture. The reaction is directly scalable, providing that an adequate size reaction vessel is used to ensure proper aeration

Reagent	[Stock]	[Final]	Dilution	Volume
PBS	10×	1×	10	$(1{,}000 - y)/10$
dH_2O	–	–	–	to 1 mL
Aβ	xμM	10 μM	$x/10$	yμL
$CuCl_2$ $Glycine_6$	1 mM	10 μM	100	10 μL
Ascorbate	5 mM	100 μM	50	20 μL
				1,000 μL

Note: the volume of 10× PBS added is calculated on the total volume minus the volume of Aβ added, as the Aβ stock is already in PBS

3. At selected time points (0–120 min), an aliquot is removed and EDTA (25 mM) is added to 1% v/v (see Note 8). Samples should be analysed immediately following the addition of EDTA, but can be kept on ice for short periods of time if taking multiple aliquots across a time-course (see Note 9).
4. In a quartz microcuvette or microplate, measure the amount of dityrosine fluorescence. The excitation light is set to 320 nm, and the emission wavelengths scanned from 380 to 500 nm. The dityrosine fluorescence appears as a broad peak at 420 nm.
5. Retain the samples in tubes on ice for subsequent immunoblotting (see Note 10).

3.3. Immunodetection of Aβ-Dityrosine

1. Prepare a nitrocellulose membrane for dot-blotting (see Note 11) by allowing the membrane to soak in PBS (pH 7.4) for 1 min. Also soak a piece of filter paper, in PBS.
2. Assemble a dot-blotting assembly as follows: On a clean working surface, place two sheets of paper towel. On top of the paper towels, place a piece of dry filter paper. On top of the dry filter paper, place the pre-soaked filter paper, and then on top of this place the pre-soaked membrane (see Note 12).
3. Apply 3–5 μL of each sample per membrane spot.
4. Allow the membrane to dry at room temperature for 5 min by laying the membrane on top of a separate dry piece of filter paper.
5. Once dry, block the membrane in BSA blocking solution (2% w/v in TBS) for 1 h at room temperature.

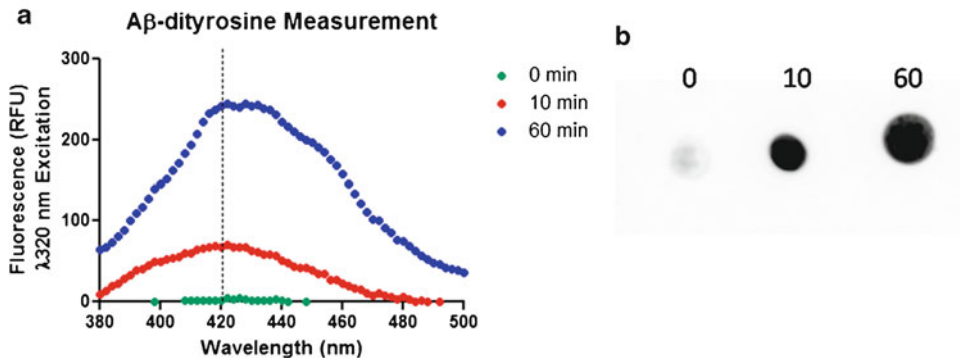

Fig. 1. Detection of Aβ-dityrosine crosslinking. (**a**) Fluorescence emission spectra of Aβ-dityrosine at selected time-points. The spectra were baseline corrected using PBS as a blank. (**b**) Identical samples as in (**a**) immunoblotted and probed for dityrosine using the 1C3 antibody.

6. Drain the blocking solution and apply the 1C3 antibody (1:1,000 diluted in 2% BSA solution in TBS-T) for 1 h at room temperature or overnight at 4°C.
7. Wash the blot 4 × 5 min in TBS-T
8. Apply secondary detection antibody (anti-mouse IgG) to the blot for 1 h at room temperature (see Note 13).
9. Wash the blot 4 × 5 min in TBS-T
10. Drain excess TBS-T from the blot, and apply ECL detection reagent to the blot. Incubate for 1–2 min at room temperature. Drain excess ECL reagent from the membrane and image the chemiluminescence signal.

4. Notes

1. Quartz glass is the best material for transmittance of light in the UV region. Some black plastic microplates (e.g. Fluotrac 200, Greiner) can also be used for the measurement of dityrosine fluorescence, however the absorbance of light at 320 nm should be minimal (if reading through the bottom of the plate), as well as exhibiting low autofluorescence. Suitability of the microplate for dityrosine measurement should first be determined by fluorescence and absorbance scans of PBS alone.
2. Static electricity can create difficulty for accurate weighing of lyophilised peptides, as static makes the peptide stick to spatulas, tubes, etc. We have found the use of an anti-static gun invaluable for reducing peptide wastage and increasing ease of handling.
3. Be sure to protect open tubes from falling debri and dust in the fume hood by placing a cover above the tubes. Any dust entering

the tubes could act as a potential nucleation seed for peptide fibrillation.

4. Do not use preparations that appear as opaque or white pellets, these preparations will not be fully disaggregated and will not give consistent reaction kinetics.
5. Wrap parafilm M® around the cap to further prevent any moisture accumulation in the tubes.
6. The use of spectrum scanning can help to identify light scatter arising from poorly prepared Aβ. Preparations that show significant change in absorbance spectra may have some pelleted material carried over from step 7. A small amount of absorbance drift (±3%) is normal, providing it is random (not consistently moving up or down). It is also for this reason that the solution of Aβ being measured is equilibrated to room temperature.
7. The UV spectrophotometer must either be 'zeroed' on PBS or the OD_{214} value of the PBS subtracted.
8. EDTA addition is essential for observing dityrosine fluorescence. Any Cu that is coordinated with the Aβ will cause quenching of the fluorescence.
9. Equilibrate the samples to room temperature before reading.
10. Alternatively, take a separate aliquot of each time-point for dot-blotting to reduce sample loss or cross-contamination during the fluorescence reads.
11. Aβ-dityrosine oligomers can also be detected by western blot of PAGE separated mixtures of Cu-reacted Aβ; however, the use of dot-blots allows for simplified and rapid detection of total Aβ-dityrosine.
12. It is important to ensure the dot-blotting assembly is flat with good contact between the nitrocellulose membrane and the filter paper. This allows the sample to be drawn through the membrane due to capillary action, reducing lateral diffusion and making spots more compact.
13. Whilst our laboratory routinely uses rabbit anti-mouse IgG at a 1:15,000 dilution, certain ECL reagents are capable of working with much higher dilutions of secondary detection antibody.

Acknowledgments

This work was supported by the Mental Health Research Institute (Parkville, VIC, Australia) and the Centre for Neuroscience, University of Melbourne (Parkville, VIC, Australia).

References

1. Dong J, Atwood CS, Anderson VE, Siedlak SL, Smith MA, Perry G and P.R. Carey (2003) Metal binding and oxidation of amyloid-beta within isolated senile plaque cores: Raman microscopic evidence, *Biochemistry* **42**, 2768–2773.
2. Lue L-F, Kuo Y-M, Roher AE, et al. (1999) Soluble amyloid β peptide concentration as a predictor of synaptic change in Alzheimer's disease. *Am J Pathol* **155**, 853–862.
3. Wang J, Dickson DW, Trojanowski JQ, Lee VM (1999) The levels of soluble versus insoluble brain Aβ distinguish Alzheimer's disease from normal and pathologic aging. *Experimental Neurology* **158**, 328–337.
4. McLean CA, Cherny RA, Fraser FW, Fuller SJ, Smith MJ, et al. (1999) Soluble pool of Aβ amyloid as a determinant of severity of neurodegeneration in Alzheimer's disease. *Ann Neurol* **46**, 860–866.
5. Portelius E, Bogdanovic N, Gustavsson MK, Volkmann I, Brinkmalm G, et al. (2010) Mass spectrometric characterization of brain amyloid beta isoform signatures in familial and sporadic Alzheimer's disease. *Acta Neuropathol.*
6. Guntert A, Dobeli H, Bohrmann B (2006) High sensitivity analysis of amyloid-beta peptide composition in amyloid deposits from human and PS2APP mouse brain. *Neuroscience* **143**, 461–475.
7. Roher AE, Lowenson JD, Clarke S, Wolkow C, Wang R, et al. (1993) Structural alterations in the peptide backbone of β-amyloid core protein may account for its deposition and stability in Alzheimer's disease. *J Biol Chem* **268,** 3072–3083.
8. Kaneko I, Morimoto K, Kubo T (2001) Drastic neuronal loss in vivo by β-amyloid racemized at Ser(26) residue: conversion of non-toxic (D-Ser(26))β-amyloid 1–40 to toxic and proteinase-resistant fragments. *Neuroscience* **104**, 1003–1011.
9. Saido TC, Iwatsubo T, Mann DM, Shimada H, Ihara Y, et al. (1995) Dominant and differential deposition of distinct β-amyloid peptide species, $A\beta_{N3(pE)}$, in senile plaques. *Neuron* **14,** 457–466.
10. Piccini A, Russo C, Gliozzi A, Relini A, Vitali A, et al. (2005) Beta amyloid is different in normal aging and in Alzheimer disease. *J Biol Chem* **280,** 34186–34192.
11. Head E, Garzon-Rodriguez W, Johnson JK, Lott IT, Cotman CW, et al. (2001) Oxidation of Aβ and plaque biogenesis in Alzheimer's disease and Down syndrome. *Neurobiol Dis* **8**, 792–806.
12. Butterfield DA, Perluigi M, Sultana R (2006) Oxidative stress in Alzheimer's disease brain: new insights from redox proteomics. *Eur J Pharmacol* **545,** 39–50.
13. Bush AI, Tanzi RE (2008) Therapeutics for Alzheimer's disease based on the metal hypothesis. *Neurotherapeutics* **5**, 421–432.
14. Nunomura A, Perry G, Aliev G, Hirai K, Takeda A, et al. (2001) Oxidative damage is the earliest event in Alzheimer disease. *J. Neuropath. Exp. Neurology* **60**, 759–767.
15. Pratico D, Uryu K, Leight S, Trojanoswki JQ, Lee VM (2001) Increased lipid peroxidation precedes amyloid plaque formation in an animal model of Alzheimer amyloidosis. *J Neurosci* **21**, 4183–4187.
16. Duce JA, Bush AI (2010) Biological metals and Alzheimer's disease: implications for therapeutics and diagnostics. *Prog Neurobiol* **92,** 1–18.
17. Atwood CS, Moir RD, Huang X, Scarpa RC, Bacarra NM, et al. (1998) Dramatic aggregation of Alzheimer Aβ by Cu(II) is induced by conditions representing physiological acidosis. *J Biol Chem* **273**, 12817–12826.
18. Schapira AH (1996) Oxidative stress and mitochondrial dysfunction in neurodegeneration. *Curr Opin Neurol* **9**, 260–264.
19. Sparks DL (1997) Coronary artery disease, hypertension, ApoE, and cholesterol: a link to Alzheimer's disease? *Ann N Y Acad Sci* **826**, 128–146.
20. Atwood CS, Scarpa RC, Huang X, Moir RD, Jones WD, et al. (2000) Characterization of copper interactions with Alzheimer amyloid β peptides: identification of an attomolar-affinity copper binding site on amyloid beta1-42. *J Neurochem* **75,** 1219–1233.
21. Barnham KJ, Haeffner F, Ciccotosto GD, Curtain CC, Tew D, et al. (2004) Tyrosine gated electron transfer is key to the toxic mechanism of Alzheimer's disease β-amyloid. *FASEB J* **18**, 1427–1429.

Chapter 2

Application of Photochemical Cross-linking to the Study of Oligomerization of Amyloidogenic Proteins

Dahabada H.J. Lopes, Sharmistha Sinha, Clark Rosensweig, and Gal Bitan

Abstract

Assembly of amyloidogenic proteins into toxic oligomers and fibrils is an important pathogenic feature of over 30 amyloid-related diseases. Understanding the structures and mechanisms involved in the assembly process is necessary for rational approaches geared at inhibiting formation of these toxic species. Here, we review the application of photo-induced cross-linking of unmodified proteins (PICUP) to two disease-related amyloidogenic proteins (1) islet amyloid polypeptide (IAPP), whose toxic oligomers are thought to cause the demise of pancreatic β-cells in type-2 diabetes mellitus and (2) α-synuclein, which aggregates into toxic oligomers and precipitates in Lewy bodies in Parkinson's disease. PICUP is an effective method allowing chemical "freezing" of dynamically changing oligomers and subsequent study of the oligomer size distribution that existed before cross-linking. The method has provided insights into the factors controlling early oligomerization, which could not be obtained by other means. We discuss sample preparation, experimental details, optimization of parameters, and troubleshooting.

Key words: PICUP, Cross-linking, IAPP, α-Synuclein, Oligomers, Protein assembly

1. Introduction

Parkinson's disease (PD) and type-2 diabetes mellitus (T2DM) belong to a group of diseases characterized by amyloid formation and hence termed amyloidoses (1). In all of these diseases, one or more proteins that are part of normal physiology respond to genetic, environmental, or yet unknown stimuli by self-assembly leading to the formation of toxic oligomers and amyloid fibrils.

Islet amyloid polypeptide (*IAPP*). IAPP is the major component of the pancreatic islet amyloid associated with the development of T2DM. IAPP, also known as amylin, is a 37-amino acid residue polypeptide hormone (2, 3) that belongs to the calcitonin gene-related family (4). It is one of the most amyloidogenic polypeptides

Einar M. Sigurdsson et al. (eds.), *Amyloid Proteins: Methods and Protocols*, Methods in Molecular Biology, vol. 849,
DOI 10.1007/978-1-61779-551-0_2,

known (5–8). A number of studies have shown that IAPP-mediated degeneration of β-cells does not require amyloid formation (9–12). Rather, prefibrillar oligomers of IAPP have been shown to be more cytotoxic than IAPP fibrils and to cause membrane disruption (13–15). Similar findings have been reported for most other amyloidogenic proteins (16).

Although intensively studied, little is known about the size distribution or structure of early IAPP oligomers. The characterization of early oligomeric species of IAPP is difficult because the oligomers exist as metastable, heterogeneous mixtures comprising a wide range of molecular sizes. Multiple analytical methods have been used to study IAPP oligomer mixtures, each one with its unique advantages and limitations (17).

A useful method for the characterization of oligomer size distribution in vitro is photo-induced cross-linking of unmodified proteins (PICUP). PICUP is a well-established method, first developed to analyze stable proteins complexes (18) and later applied to quantitative study of metastable amyloid protein assemblies, including amyloid β-protein (Aβ) (19), prion (20), and α-synuclein (α-syn) (21).

A major problem found in studies involving amyloidogenic proteins is the significant differences in assembly kinetics and toxicity observed using proteins or peptides from different sources or even using different lots from the same source (22, 23). This irreproducibility likely results from the presence of preexisting aggregates in the peptide stocks. Such aggregates serve as seeds for fibril formation and therefore must be removed or dissociated to improve experimental reproducibility. Here we use 1,1,1,3,3,3-hexafluoroisopropanol (HFIP) treatment (24, 25) as a method for dissociating IAPP aggregates. Importantly, in the case of IAPP, HFIP treatment does not remove preformed aggregates entirely (26). However, we found that for efficient cross-linking, IAPP must be treated with HFIP. This finding suggests that the C-terminal tyrosine, which is the most active side-chain in IAPP in the PICUP chemistry, likely, is buried in IAPP aggregates and becomes exposed upon HFIP treatment.

In our hands, attempts to cross-link IAPP without treatment with HFIP yielded mainly monomer and dimer bands, which were observed also in uncross-linked samples (Fig. 1a). A trimer band also was apparent but its low abundance suggested that low efficiency cross-linking took place. We interpreted these observations as indicating that the presence of preformed aggregates in the lyophilized IAPP powder and rapid aggregation upon dissolution of IAPP attenuated the cross-linking reaction. Attempts to remove preformed aggregates using size exclusion chromatography (SEC) or filtration through 10,000 Da molecular-weight cutoff filters yielded solutions with IAPP concentrations below the detection limit of the UV detector of the SEC system or of silver staining. In contrast, treatment with HFIP was found to yield IAPP in a state that was amenable to photo-cross-linking. When following HFIP treatment,

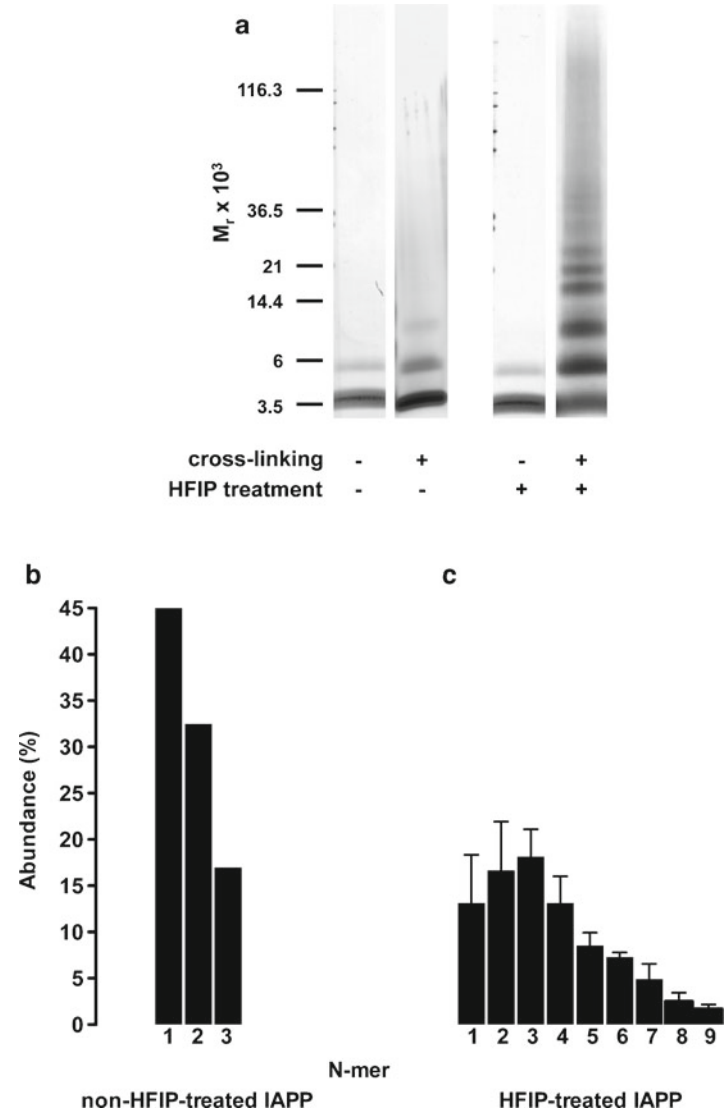

Fig. 1. SDS-PAGE analysis of IAPP following PICUP. HFIP-treated or untreated samples were subjected to PICUP. (**a**) The resulting mixtures were analyzed by SDS-PAGE using a 10–20% gradient Tris-tricine gel and silver stained. The mobilities of molecular mass markers are shown to the left. (**b** and **c**) Densitometric analysis of gels bands for HFIP-untreated IAPP (**b**) and HFIP-treated IAPP (**c**). The abundance of each band is normalized to the entire lane.

the dry peptide film was solubilized in phosphate buffer (see below) and cross-linked immediately, it produced an oligomer distribution comprising monomer through nonamer (Fig. 1), which was consistent with a theoretical distribution under high-efficiency conditions, as described previously (27).

The oligomer size distribution of HFIP-treated IAPP suggested the existence of metastable oligomers. The abundance of IAPP

monomer through tetramer diverged significantly from an exponential curve (Fig. 1c), similar to oligomer size distributions observed previously for Aβ(1–40) and calcitonin (27). This suggests that IAPP monomer, dimer, trimer, and tetramer are in quasi-equilibrium in the initial steps of the self-assembly process.

α-*Syn*. A protein with poorly defined cellular roles, α-syn is known mostly for its association with neurodegenerative diseases. α-Syn self-assembly into neurotoxic oligomers and fibrillar aggregates is thought to be causative in a group of diseases called "synucleinopathies," such as Parkinson's disease, dementia with Lewy bodies, and multiple system atrophy (28). Aggregated α-syn is the major component of the hallmark pathological lesions in PD, Lewy bodies and Lewy neurites (29). In the past, research has focused on the fibrillar form of α-syn. Current research indicates that oligomeric α-syn is the form of the protein most likely to cause neuronal death (30, 31). The role of α-syn in cell death still is unclear as is the relationship between assembly state and toxicity. Prefibrillar α-syn can take a variety of forms, including spherical oligomers, annuli, and protofibrils (32). The characterization of these species and their relative toxicity is of considerable importance for understanding the mechanisms of α-syn-induced neuronal loss in Parkinson's disease and other synucleinopathies.

A PICUP study of α-syn was reported by Li et al. who showed that solutions of recombinant α-syn contained a mixture of monomers, dimers, and trimers (21). The authors suggested that the amphipathic N-terminal region was required for dimerization and trimerization of α-syn and that the later aggregation of α-syn originated from dimeric and trimeric seeds.

We applied PICUP to α-syn at concentrations ranging from 2 to 100 μM (data not shown). Protein concentration of 2 μM produced the best resolution of individual bands without compromising sensitivity. At higher concentrations (20–100 μM), when fractionated by SDS-PAGE, the cross-linked mixture produced a smear in which individual oligomers could not be identified. Control, uncross-linked α-syn samples showed a band with an apparent mobility corresponding to dimer in addition to the monomer band (Fig. 2). This band likely represents an SDS-induced artifact similar to that seen in uncross-linked Aβ42 (33–35). In our hands, application of PICUP to freshly prepared solutions of α-syn yielded oligomer size distributions in which oligomers higher than trimer clearly were observed (Fig. 2). However, the experimental reproducibility of the relative abundance of each oligomer was low as a result of large batch-to-batch variability (Fig. 2). This variability could not be attributed to other causes because the oligomer size distribution was unaffected when the same sample was incubated for several days and cross-linked at different time points.

Two representative α-syn oligomer size distributions are shown in Fig. 2. In some experiments, we observed bands corresponding

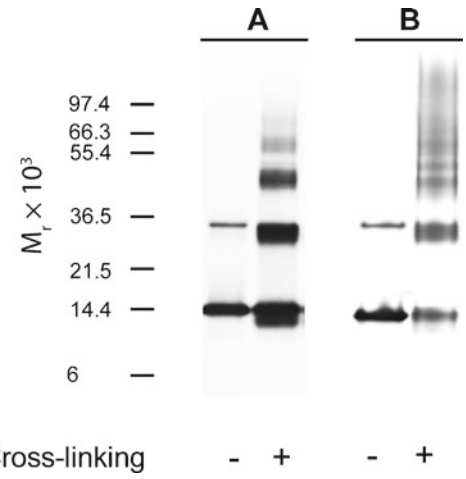

Fig. 2. PICUP analysis of α-syn. α-Syn (2 μM) was cross-linked, fractionated by SDS-PAGE and silver stained. Two representative cross-linking patterns (A and B) are shown.

to monomer through pentamer (Fig. 2, pattern A). In others, a complex pattern was found, wherein bands corresponding to individual oligomers up to a heptamer were observed in addition to larger species that could not be resolved by SDS-PAGE (Fig. 2, pattern B). These results demonstrate the importance of the source of α-syn used in PICUP experiments. One way of improving reproducibility in experiments using α-syn is by measuring the concentration of the protein immediately after dissolution[1] using a molar extinction coefficient $\varepsilon_{274\ nm} = 5{,}600\ M^{-1}/cm^{-1}$ (36) and using exactly the same concentration for all experiments. Using this approach, batch-to-batch variation can be reduced, though not eliminated, in PICUP experiments. Thus, we caution researchers using PICUP to study α-syn oligomerization and suggest that they must characterize the protein structure by complementary means and preferably use the same batch in all experiments.

2. Materials

1. Orbital shaker (INFORS AG, Labotron, Bottmingen, Switzerland).
2. Water-bath sonicator (Branson 1510, Branson Ultrasonic, Danbury, CT).
3. Light source: Dolan-Jenner 200 W incandescent lamp.

[1] Measuring the concentration immediately after dissolution is essential because as proteins aggregate, the absorbance values vary compared with the freshly dissolved proteins. Hence, for aggregating proteins, it is recommended to measure the concentration immediately after dissolution in appropriate buffer.

4. Reaction apparatus allowing controlled exposure and positioning of samples a fixed distance from the light source (see Note 1). An inexpensive, yet highly reliable and flexible apparatus may be constructed using any 35-mm, single lens release (SLR) camera body and an attached bellows.
5. 0.2-mL, clear, thin-walled plastic PCR tubes (Eppendorf).
6. 1.8-mL glass vial (Kimble Chromatography).
7. 1.7-mL, clear, silicon-coated tubes (Denville Scientific, INC).
8. 1,1,1,3,3,3-Hexafluoro-2-propanol (HFIP) (TCI America, Portland, OR).
9. Tris(2,2′-bipyridyl)dichlororuthenium(II) hexahydrate (Ru(Bpy)), $M_r = 748.63$ g/mol (Sigma).
10. Ammonium persulfate (APS, $M_r = 228.2$ g/mol) (Sigma).
11. Quenching reagent: 5% (v/v) β-mercaptoethanol (Sigma) in 2× SDS-tricine sample buffer (Invitrogen) or 1 M dithiothreitol (DTT, $M_r = 154.5$ g/mol) (Fisher) in water (see Note 1).

3. Methods

The most important factors that must be considered when designing a PICUP experiment are the reagent stoichiometry, irradiation time, and sample preparation procedure. The former two issues require empirical optimization, whereas the latter largely affects interpretation of the experimental data. For amyloidogenic proteins in particular, determination of size distributions of metastable oligomers requires using aggregate-free starting preparations. PICUP can be used to generate stable, soluble protein oligomers which, following fractionation and purification, may be used for structural studies, cytotoxicity assays (37), oligomerization-inhibition studies (38, 39), and/or as targets for the development of molecular-recognition tools (40).

The background, mechanism, instrumentation, protocol, optimization, scope, modifications, applications, and limitations of PICUP were discussed in previous publications (19, 25, 41, 42). This chapter focuses on sample preparation and experimental troubleshooting for IAPP and α-syn.

3.1. Preparing HFIP-Treated IAPP for Photo-cross-linking

The following is a method for preparation of aggregate-free IAPP by treating the lyophilized peptide with HFIP, drying the solution, and resolubilizing the resulting peptide film initially in dilute NaOH to increase solubility and decrease de novo peptide aggregation, which can account for poor reproducibility among experiments (43). The method illustrated below also can be applicable to other amyloidogenic proteins.

(a) Weigh out ~300–360 μg of lyophilized peptide using a microbalance and transfer into labeled, silicon-coated, low-adsorbent tubes.

(b) Before dissolving the peptide in HFIP, chill the HFIP container on ice inside a fume hood wearing adequate protection (HFIP is volatile and toxic). Cooling of a 250-mL bottle typically requires 10–15 min. Also, it is advised to chill all the tubes used.

(c) Add HFIP to prechilled tubes containing peptide lyophilizates to obtain a nominal peptide concentration of 0.1 mM.

(d) Sonicate the peptide solutions in a water-bath sonicator for 5 min at room temperature.

(e) Incubate the tubes for 30 min at room temperature with agitation using an orbital shaker at 200 rpm.

(f) Chill the tubes on ice (for 1 min), and divide the solutions into 100–120-μL aliquots in labeled silicon-coated low-adsorbent tubes (see Note 2).

(g) Remove HFIP by leaving the tubes open in the fume hood overnight. Place the open tubes in a rack and cover them with a large sheet of Kimwipe to prevent dust contamination.

(h) Exsiccate the remaining HFIP in vacuo in a lyophilizer or a centrifugal concentrator for 2 h, or in an exsiccator attached to a vacuum inlet for 4 h. The final product will be a peptide film at the bottom of the tubes. If properly exsiccated, the tubes can be stored airtight for extended periods (months) at −20 or −80°C.

3.2. Solubilizing the HFIP-Treated IAPP Films

Before solubilizing the HFIP-treated peptides for cross-linking reactions, one needs to prepare the cross-linking and quenching reagents.

(a) Prepare the Ru(Bpy) solution in 10 mM sodium phosphate, pH 7.4, using a vortex to mix the solution until particulate material is no longer observed. The Ru(Bpy) solution is sensitive to light and should be protected from ambient light. A simple method is to use aluminum foil to wrap the tube (see Notes 3 and 5).

(b) Prepare the APS solution in 10 mM sodium phosphate, pH 7.4. Mix the solution using a vortex until particulate material is no longer observed (see Notes 4 and 5).

(c) For SDS-PAGE analysis following cross-linking, a convenient quenching reagent is 5% β-mercaptoethanol in 2× SDS-PAGE sample buffer. Alternatively, 1 M DTT in deionized water or a suitable buffer can be used.

(d) HFIP-treated peptide films now can be dissolved in dilute NaOH first and then sodium phosphate buffer is added to get ~10 μM peptide concentration as follows.

(e) Add 60 mM NaOH followed by deionized water into the tube containing the peptide film such that NaOH and water constitute 10 and 45% of the final volume, respectively (see Note 6).

(f) Gently mix the peptide film by pipetting up and down and sonicate for 1 min in a water-bath sonicator (see Note 7).

(g) Add 45% 20 mM sodium phosphate, pH 7.4, and mix gently by pipetting. The peptide solution is ready. It should be kept on ice and used immediately after preparation.

3.3. α-Syn Sample Preparation

The aggregation kinetics of α-syn is considerably slower than that of IAPP and does not require HFIP treatment. Rather, freshly dissolved protein is used for cross-linking.

(a) Dissolve lyophilized α-syn at 20 μM in 10 mM phosphate buffer and incubate at 37 °C with mechanical agitation.

(b) Measure the solution's absorbance using a UV spectrometer at $\lambda = 274$ nm, subtract the buffer's absorbance, and calculate the protein concentration using $\varepsilon_{274} = 5{,}600\ M^{-1}/cm^{-1}$ (36).

(c) Remove ~2 μL aliquots of the aggregating solution and dilute tenfold in 10 mM phosphate buffer for cross-linking.

3.4. PICUP Reaction

(a) Adjust the camera shutter delay to 1 s. At longer irradiation times, extensive radical reactions may cause protein degradation. Irradiation time may need to be optimized when using the method with a new protein. Wind the camera shutter.

(b) A typical PICUP reaction is performed in a 20-μL reaction volume. Transfer 18 μL of the protein solution into a thin-walled, clear, 0.2-mL PCR tube.

(c) Add the PICUP reagents in this order: 1 μL Ru(Bpy) followed by 1 μL APS, and mix the reagents by pipetting.

(d) Quickly place the reaction tube inside a 1.8-mL glass vial. Place the vial inside the bellows attached in front of the camera body. Attach the lens protector, turn on the light, and press the shutter so that the sample is irradiated for 1 s inside the bellows. Turn off the light to avoid heating.

(e) After sample irradiation, quickly take the vial out of the bellows and the PCR tube out of the vial. Quickly quench the reaction by adding 1 μL DTT or 10 μL reducing PAGE sample buffer. Repeat the reaction for each peptide aliquot.

(f) The reaction mixtures can now be frozen at −20°C for storage for no longer than 7 days or kept on ice before analysis by SDS-PAGE and silver staining.

3.5. SDS-PAGE and Silver Staining of Cross-linked Peptide Products

(a) Routine SDS-PAGE and silver staining are performed to visualize cross-linked peptides.

(b) Load 100–150 pmol of protein per lane.

(c) Include similar amounts of uncross-linked proteins for comparison. Also include a standard protein ladder for visual approximation of molecular weight of peptide bands.

(d) Run the gel using a standard gel electrophoresis apparatus. We use the XCell SureLock Mini-Cell system from Invitrogen and perform silver staining according to Invitrogen publication IM-1002, Novex Pre-Cast Gel Electrophoresis Guide.

4. Notes

1. The technical details of PICUP were addressed in a previous edition of Amyloid and Proteins Methods and Protocol Part I, In Vitro Assays, Chapter 2. Determination of Peptide Oligomerization State Using Rapid Photochemical Cross-linking (41).
2. HFIP is volatile. Therefore, this step should be done on ice to avoid evaporation.
3. It is important to consider the protein:Ru(Bpy) ratio for optimization of the experimental system. Based on our experience, we recommend for IAPP: A reaction volume of 18 μL, 10 μM IAPP with 1 μL of 2 mM Ru(Bpy). For α-syn: The same reaction volume, 2 μM α-syn and 1 μL of 1 mM Ru(Bpy).
4. The Ru(Bpy):APS concentration ratio should be kept 1:20.
5. The APS and Ru(Bpy) solutions should be prepared fresh and, in case of a series of experiments, can be stored at room temperature and used for up to 48 h following preparation.
6. When working with IAPP, it is advised to prechill all the solutions on ice prior to use and always keep the tubes on ice to avoid aggregation during the sample preparation.
7. Brief sonication is an efficient way to break apart loosely attached aggregates but times longer than 1 min can induce aggregation and should be avoided.

Acknowledgments

This work was supported by grants from American Health Assistance Foundation (A2008-350), the Jim Easton Consortium for Alzheimer's Drug Discovery and Biomarker Development at UCLA, UCLA Center for Gene-Environment Studies in Parkinson's Disease, and the Michael J. Fox Foundation.

References

1. Selkoe, D. J. (2004) Cell biology of protein misfolding: the examples of Alzheimer's and Parkinson's diseases. *Nat. Cell Biol.* **6**, 1054–1061.
2. Cooper, G. J., Willis, A. C., Clark, A., Turner, R. C., Sim, R. B., and Reid, K. B. (1987) Purification and characterization of a peptide from amyloid-rich pancreases of type 2 diabetic patients. *Proc. Natl. Acad. Sci. USA* **84**, 8628–8632.
3. Westermark, P., Wernstedt, C., Wilander, E., Hayden, D. W., O'Brien, T. D., and Johnson, K. H. (1987) Amyloid fibrils in human insulinoma and islets of Langerhans of the diabetic cat are derived from a neuropeptide-like protein also present in normal islet cells. *Proc. Natl. Acad. Sci. USA* **84**, 3881–3885.
4. Martinez-Alvarez, R. M., Volkoff, H., Cueto, J. A., and Delgado, M. J. (2008) Molecular characterization of calcitonin gene-related peptide (CGRP) related peptides (CGRP, amylin, adrenomedullin and adrenomedullin-2/intermedin) in goldfish (Carassius auratus): cloning and distribution. *Peptides* **29**, 1534–1543.
5. Kahn, S. E., Andrikopoulos, S., and Verchere, C. B. (1999) Islet amyloid: a long-recognized but underappreciated pathological feature of type 2 diabetes. *Diabetes* **48**, 241–253.
6. Hull, R. L., Westermark, G. T., Westermark, P., and Kahn, S. E. (2004) Islet amyloid: a critical entity in the pathogenesis of type 2 diabetes. *J. Clin. Endocrinol. Metab.* **89**, 3629–3643.
7. Clark, A., Cooper, G. J., Lewis, C. E., Morris, J. F., Willis, A. C., Reid, K. B., and Turner, R. C. (1987) Islet amyloid formed from diabetes-associated peptide may be pathogenic in type-2 diabetes. *Lancet* **2**, 231–234.
8. Kapurniotu, A. (2001) Amyloidogenicity and cytotoxicity of islet amyloid polypeptide. *Biopolymers* **60**, 438–459.
9. Lorenzo, A., Razzaboni, B., Weir, G. C., and Yankner, B. A. (1994) Pancreatic islet cell toxicity of amylin associated with type-2 diabetes mellitus. *Nature* **368**, 756–760.
10. Kapurniotu, A., Bernhagen, J., Greenfield, N., Al-Abed, Y., Teichberg, S., Frank, R. W., Voelter, W., and Bucala, R. (1998) Contribution of advanced glycosylation to the amyloidogenicity of islet amyloid polypeptide. *Eur. J. Biochem.* **251**, 208–216.
11. Saafi, E. L., Konarkowska, B., Zhang, S., Kistler, J., and Cooper, G. J. (2001) Ultrastructural evidence that apoptosis is the mechanism by which human amylin evokes death in RINm5F pancreatic islet β-cells. *Cell Biol. Int.* **25**, 339–350.
12. Muthusamy, K., Arvidsson, P. I., Govender, P., Kruger, H. G., Maguire, G. E., and Govender, T. (2010) Design and study of peptide-based inhibitors of amylin cytotoxicity. *Bioorg. Med. Chem. Lett.* **20**, 1360–1362.
13. Engel, M. F., Khemtemourian, L., Kleijer, C. C., Meeldijk, H. J., Jacobs, J., Verkleij, A. J., de Kruijff, B., Killian, J. A., and Hoppener, J. W. (2008) Membrane damage by human islet amyloid polypeptide through fibril growth at the membrane. *Proc. Natl. Acad. Sci. USA* **105**, 6033–6038.
14. Khemtemourian, L., Killian, J. A., Hoppener, J. W., and Engel, M. F. (2008) Recent insights in islet amyloid polypeptide-induced membrane disruption and its role in β-cell death in type 2 diabetes mellitus. *Exp. Diabetes Res.* **2008**, 421287.
15. Sparr, E., Engel, M. F., Sakharov, D. V., Sprong, M., Jacobs, J., de Kruijff, B., Hoppener, J. W., and Killian, J. A. (2004) Islet amyloid polypeptide-induced membrane leakage involves uptake of lipids by forming amyloid fibers. *FEBS Lett.* **577**, 117–120.
16. Kirkitadze, M. D., Bitan, G., and Teplow, D. B. (2002) Paradigm shifts in Alzheimer's disease and other neurodegenerative disorders: The emerging role of oligomeric assemblies. *J. Neurosci. Res.* **69**, 567–577.
17. Li, H., Murakami, K., Rahimi, A. F., Maiti, P., Sinha, S., and Bitan, G. (2009) Amyloids and Protein Aggregation–Analytical Methods, in Encyclopedia of Analytical Chemistry (Sagi, I., Ed.), John Wiley: Chichester. DOI: 10.1002/9780470027318.a9038.
18. Fancy, D. A., and Kodadek, T. (1999) Chemistry for the analysis of protein-protein interactions: Rapid and efficient cross-linking triggered by long wavelength light. *Proc. Natl. Acad. Sci. USA* **96**, 6020–6024.
19. Bitan, G., and Teplow, D. B. (2004) Rapid photochemical cross-linking–a new tool for studies of metastable, amyloidogenic protein assemblies. *Acc. Chem. Res.* **37**, 357–364.
20. Piening, N., Weber, P., Hogen, T., Beekes, M., Kretzschmar, H., and Giese, A. (2006) Photo-induced crosslinking of prion protein oligomers and prions, *Amyloid* **13**, 67–77.
21. Li, H. T., Lin, X. J., Xie, Y. Y., and Hu, H. Y. (2006) The early events of α-synuclein oligomerization revealed by photo-induced cross-linking, *Protein Peptide Lett.* **13**, 385–390.
22. Padrick, S. B., and Miranker, A. D. (2002) Islet amyloid: Phase partitioning and secondary nucleation are central to the mechanism of fibrillogenesis. *Biochemistry* **41**, 4694–4703.

23. Rahimi, A. F., Shanmugam, A., and Bitan, G. (2008) Structure–Function Relationships of Pre-Fibrillar Protein Assemblies in Alzheimer's Disease and Related Disorders. *Curr. Alzheimer Res.* **5**, 319–341.
24. Stine, W. B., Jr., Dahlgren, K. N., Krafft, G. A., and LaDu, M. J. (2003) In vitro characterization of conditions for amyloid-β peptide oligomerization and fibrillogenesis. *J. Biol. Chem.* **278**, 11612–11622.
25. Rahimi, F., Maiti, P., and Bitan, G. (2009) Photo-induced cross-linking of unmodified proteins (PICUP) applied to amyloidogenic peptides. *J. Vis. Exp.*, **23**, http://www.jove.com/index/details.stp?id=1071.
26. Rahimi, F., Murakami, K., Summers, J. L., Chen, C. H., and Bitan, G. (2009) RNA aptamers generated against oligomeric Aβ40 recognize common amyloid aptatopes with low specificity but high sensitivity. *PLoS One* **4,** e7694.
27. Bitan, G., Lomakin, A., and Teplow, D. B. (2001) Amyloid β-protein oligomerization: prenucleation interactions revealed by photo-induced cross-linking of unmodified proteins. *J. Biol. Chem.* **276**, 35176–35184.
28. Spillantini, M. G., and Goedert, M. (2000) The α-synucleinopathies: Parkinson's disease, dementia with Lewy bodies, and multiple system atrophy. *Ann. N. Y. Acad. Sci.* **920**, 16–27.
29. Spillantini, M. G., Crowther, R. A., Jakes, R., Cairns, N. J., Lantos, P. L., and Goedert, M. (1998) Filamentous α-synuclein inclusions link multiple system atrophy with Parkinson's disease and dementia with Lewy bodies. *Neurosci. Lett.* **251**, 205–208.
30. Kazantsev, A. G., and Kolchinsky, A. M. (2008) Central role of α-synuclein oligomers in neurodegeneration in Parkinson disease. *Arch. Neurol.* **65**, 1577–1581.
31. van Rooijen, B. D., Claessens, M. M., and Subramaniam, V. (2010) Membrane interactions of oligomeric α-synuclein: potential role in Parkinson's disease. *Curr. Protein Pept. Sci.* **11**, 334–342.
32. Caughey, B., and Lansbury, P. T. (2003) Protofibrils, pores, fibrils, and neurodegeneration: separating the responsible protein aggregates from the innocent bystanders. *Annu. Rev. Neurosci.* **26**, 267–298.
33. Bitan, G., Kirkitadze, M. D., Lomakin, A., Vollers, S. S., Benedek, G. B., and Teplow, D. B. (2003) Amyloid β-protein (Aβ) assembly: Aβ40 and Aβ42 oligomerize through distinct pathways. *Proc. Natl. Acad. Sci. USA* **100**, 330–335.
34. Bitan, G., Fradinger, E. A., Spring, S. M., and Teplow, D. B. (2005) Neurotoxic protein oligomers–what you see is not always what you get. *Amyloid* **12**, 88–95.
35. Hepler, R. W., Grimm, K. M., Nahas, D. D., Breese, R., Dodson, E. C., Acton, P., Keller, P. M., Yeager, M., Wang, H., Shughrue, P., Kinney, G., and Joyce, J. G. (2006) Solution state characterization of amyloid β-derived diffusible ligands. *Biochemistry* **45**, 15157–15167.
36. Weinreb, P. H., Zhen, W., Poon, A. W., Conway, K. A., and Lansbury, P. T., Jr. (1996) NACP, a protein implicated in Alzheimer's disease and learning, is natively unfolded. *Biochemistry* **35**, 13709–13715.
37. Ono, K., Condron, M. M., and Teplow, D. B. (2009) Structure-neurotoxicity relationships of amyloid β-protein oligomers. *Proc. Natl. Acad. Sci. USA* **106**, 14745–14750.
38. Fradinger, E. A., Monien, B. H., Urbanc, B., Lomakin, A., Tan, M., Li, H., Spring, S. M., Condron, M. M., Cruz, L., Xie, C. W., Benedek, G. B., and Bitan, G. (2008) C-terminal peptides coassemble into Aβ42 oligomers and protect neurons against Aβ42-induced neurotoxicity. *Proc. Natl. Acad. Sci. USA* **105**, 14175–14180.
39. Li, H., Monien, B. H., Lomakin, A., Zemel, R., Fradinger, E. A., Tan, M., Spring, S. M., Urbanc, B., Xie, C. W., Benedek, G. B., and Bitan, G. (2010) Mechanistic investigation of the inhibition of Aβ42 assembly and neurotoxicity by Aβ42 C-terminal fragments. *Biochemistry* **49**, 6358–6364.
40. Rahimi, F., and Bitan, G. (2010) Selection of aptamers for amyloid β-protein, the causative agent of Alzheimer's disease, *J. Vis. Exp.* **39**, http://www.jove.com/index/details.stp?id=1955.
41. Vollers, S. S., Teplow, D. B., and Bitan, G. (2005) Determination of Peptide oligomerization state using rapid photochemical crosslinking. *Methods Mol. Biol.* **299**, 11–18.
42. Bitan, G. (2006) Structural study of metastable amyloidogenic protein oligomers by photo-induced cross-linking of unmodified proteins. *Methods Enzymol.* **413**, 217–236.
43. Fezoui, Y., Hartley, D. M., Harper, J. D., Khurana, R., Walsh, D. M., Condron, M. M., Selkoe, D. J., Lansbury, P. T., Fink, A. L., and Teplow, D. B. (2000) An improved method of preparing the amyloid β-protein for fibrillogenesis and neurotoxicity experiments. *Amyloid* **7**, 166–178.

Chapter 3

Preparation of Stable Amyloid β-Protein Oligomers of Defined Assembly Order

Clark Rosensweig, Kenjiro Ono, Kazuma Murakami, Devin K. Lowenstein, Gal Bitan, and David B. Teplow

Abstract

Oligomeric assemblies of the amyloid β-protein, Aβ, are thought to be the proximate neurotoxic agents in Alzheimer's disease (AD). Oligomer formation is a complex process that produces a polydisperse population of metastable structures. For this reason, formal structure–activity correlations, both in vitro and in vivo, have been difficult to accomplish. An analytical solution to this problem was provided by the application of a photochemical cross-linking method to the Aβ assembly system. This method, photo-induced cross-linking of unmodified proteins (PICUP), enabled the quantitative determination of the oligomer size distribution. We report here the integration of PICUP with SDS-PAGE and alkaline extraction procedures to create a method for the isolation of pure populations of oligomers of defined order. This method has been used successfully to provide material for formal structure–activity studies of Aβ oligomers.

Key words: Amyloid β-protein, Oligomers, PICUP, Purification

1. Introduction

Alzheimer's disease (AD) is a neurodegenerative disorder characterized by the formation of extracellular amyloid deposits in the brain parenchyma and vasculature and within neuronal cells (1). These deposits are composed of the amyloid β-protein, Aβ, and the microtubule-associated protein, tau, respectively (1, 2). An important current working hypothesis of AD causation posits that Aβ oligomers are the proximate pathologic agents (3–5). In vivo and in vitro studies have revealed a diversity of such assemblies (6), including dimers (7), Aβ*56 (8), Aβ-derived diffusible ligands (ADDLs) (9), paranuclei (10), protofibrils (11, 12), globulomers (13), and amylospheroids (14). To establish how each of these assemblies is involved in disease causation, structure–activity

Einar M. Sigurdsson et al. (eds.), *Amyloid Proteins: Methods and Protocols*, Methods in Molecular Biology, vol. 849,
DOI 10.1007/978-1-61779-551-0_3,

correlations must be established. However, achievement of this goal has been difficult due to the complexity of Aβ assembly, the metastability of Aβ oligomers, and the polydispersity of the oligomer population (6, 15).

Bitan et al. (16) applied the method of photo-induced cross-linking of unmodified proteins (PICUP) (17, 18) to "freeze" the oligomer equilibria and allow analytical studies of Aβ oligomerization. PICUP is a highly efficient, zero-length cross-linking method that can be applied to native (no *pre facto* protein modification is required) Aβ populations. Following cross-linking, monomer interchange among cross-linked oligomer species does not occur because the monomers are covalently bound to each other. This eliminates the metastability problem discussed above and allows quantitative determination of the polydispersity of the population. Bitan et al. observed that the shorter isoform of Aβ, Aβ40, and the longer isoform, Aβ42, each produced a distinct oligomer distribution when studied by SDS-PAGE (10). This distinction is correlated with the strong disease linkage of Aβ42.

The successful application of PICUP to the problem of quantitatively determining the Aβ oligomer size distribution suggested that PICUP might be incorporated into a protocol for the production of Aβ oligomers of defined order. Initial work in this area focused on coupling PICUP with size exclusion chromatography (SEC). SEC is a useful method for the separation of soluble proteins on the basis of Stokes radius. SEC has the advantage of being carried out in the solution phase, which results in sample fractions that can be used immediately in other experiments. Unfortunately, preliminary experiments showed that the molecular weight resolution of SEC was insufficient to produce pure populations of oligomers larger than dimers (unpublished results). For this reason, we attempted to combine PICUP with SDS-PAGE, which has very high molecular weight resolution. To do so, an efficient method of extraction of the oligomer populations from the gel matrix had to be developed. This goal was achieved through modification of an alkaline extraction protocol originally reported by Jin and Manabe (19). The ability to produce pure populations of oligomers of specific order enabled formal structure–activity studies of Aβ40 oligomers (20). We communicate here details of the method used in this study.

2. Materials

All solutions were prepared using water provided by a Milli-Q system (18 MΩ/cm, Millipore Corp., Bedford, MA). All reagents were of the highest purity available and were purchased from Sigma-Aldrich, unless otherwise noted.

2.1. PICUP

1. Ammonium persulfate (APS): 60 mM solution in water (13.7 mg/ml). Vortex until the APS has dissolved, place on ice, and then use immediately thereafter.
2. Tris (2,2′-bipyridyl)dichlororuthenium (II) hexahydrate (Ru (Bpy)): 3 mM solution in water (2.24 mg/ml). Vortex the solution until the solid is dissolved and then place on ice, wrapped in aluminum foil, to protect from light. Use immediately.
3. Sodium hydroxide (NaOH): 60 mM (2.4 g/l) in water, pH 11.
4. Sodium phosphate, dibasic buffer (Na_2HPO_4): 20 mM (2.84 g/l) in water, pH 7.4. Prepare and store at room temperature.
5. β-Mercaptoethanol: 5% (v/v) solution in 2× sample buffer (Cat. Num. LC1676, Invitrogen, Carlsbad, CA).
6. 200-W incandescent lamp: model 170-D (Dolan-Jenner, Lawrence, MA) (see Note 1, Fig. 1).
7. 35-mm Pentax camera body with bellows (see Note 1, Fig. 1).
8. Sonicator (model 1510R-DTH; Branson Ultrasonics).

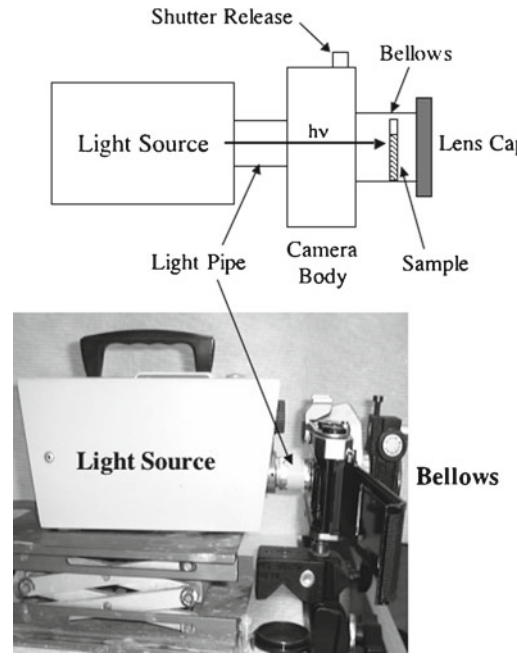

Fig. 1. The irradiation system. A light source is linked to the shutter side (*back*) of a 35-mm SLR camera body through a cylindrical tube (*light pipe*). The sample is placed within a bellows attached to the lens opening, after which a lens cap closes the open end of the bellows. Irradiation then occurs by actuation of the shutter release, with the time adjusted using the shutter speed control of the camera.

2.2. SDS-PAGE and Gel Staining

1. 10–20% Tricine gels, 1-mm thick, 10 wells (Cat. Num. EC6625BOX, Invitrogen, Carlsbad, CA) (Note 2). Store at 4°C.
2. Tricine SDS Running Buffer (10×) (Cat. Num. LC1675, Invitrogen, Carlsbad, CA). Dilute 50 ml of 10× buffer in 450 ml water. Mix thoroughly. Store at room temperature.
3. Mark12 unstained standard: protein standard (Cat. Num. LC5677, Invitrogen, Carlsbad, CA). 2.5–200 kDa standard. Store at 4°C.
4. Coomassie Blue: SimplyBlue™ (Cat. Num. LC6060, Invitrogen, Carlsbad, CA).
5. Orbital shaker, model ZD-9556 (Madell Technology Corporation, Ontario, CA).

2.3. Alkaline Extraction

1. 1.5-ml Disposable pellet pestle (Cat. Num. K749521-1590, Fisher Scientific, Rockford, IL).
2. Ammonium hydroxide (NH_4OH): 0.1 M (0.35% w/v) in water.
3. Rotator (Mini LabRoller, Labnet International, Inc., Woodbridge, NJ) (8.4″×4″×5″, 20–24 rpm).

2.4. Purification

1. SDS Removal: SDSOut (Pierce, Rockford, IL).
2. Dialysis membrane: Spectra/Por Biotech CE Dialysis Membranes; 2,000 MWCO (molecular weight cutoff); 7.5-mm diameter (Spectrum Laboratories, Rancho Dominguez, CA).
3. Urea: 10 M (60% w/v) in water.
4. Silver staining kit: SilverXpress (Cat. Num. LC6100, Invitrogen, Carlsbad, CA).

3. Methods

The method described involves the production of multiple samples of cross-linked peptide, followed by the pooling of the samples, their fractionation by SDS-PAGE, and their extraction from the resultant gel (Fig. 2).

3.1. PICUP

1. Dissolve Aβ40 (see Note 3) to a concentration of 90 μM in a solution of 6 mM NaOH/9 mM Na_2HPO_4. First, dissolve 195 μg of the peptide in 50 μl of 60 mM NaOH gently agitating the tube to aid in dissolution. Add 225 μl water, continuing to gently agitate, until the solution is clear. Finally, add 225 μl of 20 mM Na_2HPO_4, pH 7.4 (see Notes 4 and 5).
2. Sonicate the Aβ40 solution for 1 min.

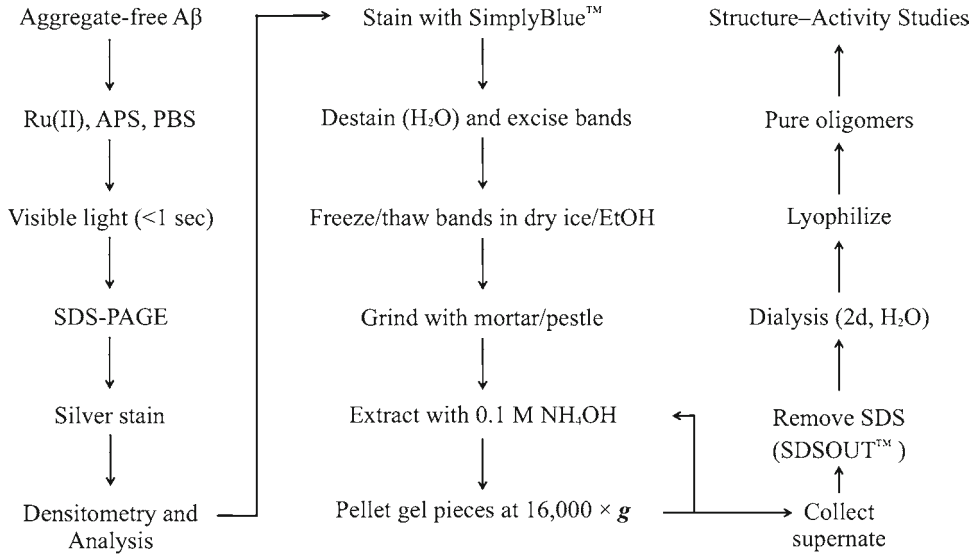

Fig. 2. Outline of the method.

3. Centrifuge the solution at 16,000 × *g* for 10 min, then aliquot the supernate into 0.2-ml clear, thin-walled PCR tubes (18 µl/tube).
4. Add 1 µl of APS and 1 µl Ru(Bpy) into one reaction tube. Place the tube into the camera bellows in the irradiation system (Fig. 2), cap the end, and then irradiate the tube for 1 s. Immediately quench the reaction with 20 µl of β-mercaptoethanol/sample buffer.
5. Multiple reactions may be done to produce larger amounts of cross-linked peptide (see Note 6). These reactions may be pooled and stored at –20°C if subsequent experiments are not to be done immediately (see Note 7).

3.2. SDS-PAGE

1. Prepare the gel for electrophoresis by creating a two-lane gel, one lane being an outermost lane and the other being the remaining lanes in the gel from which you have removed the intervening polyacrylamide teeth between the sample wells. This can be done using a small scalpel. Wash the two sample wells with running buffer and assemble the gel system.
2. Heat the cross-linked oligomers at 100°C for 10 min. This can be done in a boiling-water bath or a heating block. Centrifuge the pooled oligomers briefly in a microcentrifuge (16,000 × *g*).
3. Load molecular weight markers (10 µl) in the small well and the supernate of the cross-linked oligomers in the large well (up to 400 µl).
4. Electrophorese at 100 V, constant voltage, until the sample has stacked at the interface between the stacking and separating gels.

Electrophorese the samples at 120 V, constant voltage, until the dye front has reached the bottom of the gel.

5. After electrophoresis, open the gel cartridge by prying it open with a spatula, knife, or other thin, flat implement. Carefully detach the gel from the bottom plate of the cartridge into a staining tray filled with water.
6. Add enough water to cover the gel by a few centimeters and gently agitate on an orbital shaker for 5 min. Discard the water and replace it with fresh water. Repeat wash three times.
7. Pour out the last water wash and add sufficient SimplyBlue™ stain solution to cover the gel. Place the gel on the orbital shaker for 1 h. After staining, pour out the staining solution and replace it with water. Place the gel on the orbital shaker for 1 h to destain the gel and to reveal the protein bands.

3.3. Alkaline Extraction

1. Place the stained gel on a glass plate (scrupulously cleaned with soap and water, then water, and finally with methanol or ethanol) and excise the oligomer bands with a scalpel or razor blade (see Note 8).
2. Dice each band into small (1 mm) cubes and place the cubes into a 1.5-ml microcentrifuge tube (see Note 9). Wash the gel cubes with 1 ml of water three times. Briefly centrifuge ($16{,}000 \times g$) and remove the supernatant water each time.
3. Pre-heat a water bath to 70°C and prepare a small vessel (of geometry appropriate for immersing 1.5-ml microcentrifuge tubes) containing dry ice and ethanol. Subject the gel cubes to three cycles of rapid freezing and thawing by alternately placing the tubes in the water and dry ice/ethanol baths. The cubes will become brittle during this process, after which they are crushed into a homogeneous state using a 1.5-ml pellet pestle.
4. Extract the crushed gel pieces in 1 ml of 0.1 M NH_4OH for 10 min at room temperature while rotating at 24 rpm. Centrifuge at $16{,}000 \times g$ for 5 min and collect the supernate. Repeat the extraction, rotation, and centrifugation twice more.

3.4. Purification

1. Pool the final supernates of the extracted gel pieces and treat with SDS-Out™ to remove SDS. Transfer the protein sample to one of the microcentrifuge tubes provided with the kit. Add the SDS-Out Precipitation Reagent to the protein sample (1:20, v/v) and vortex to mix. Incubate on ice for 20 min, then centrifuge at $16{,}000 \times g$ for 10 min. Transfer up to 500 µl of the supernate to one of the spin cup columns provided with the kit and centrifuge at $16{,}000 \times g$ for 1 min.
2. Prepare dialysis membrane by cutting into short lengths (suitable for up to 1 ml of sample) and soaking in enough water to fully immerse the membrane for 30 min at room temperature

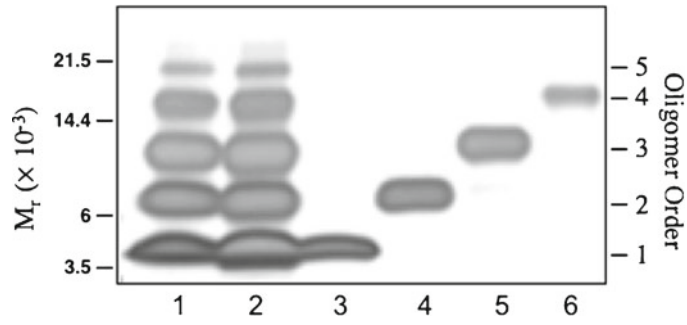

Fig. 3. Evaluation of the method by SDS-PAGE and silver staining. *Lanes*: 1, cross-linked Aβ40 prior to purification; 2, cross-linked Aβ40, for which the entire lane from the first Coomassie-stained gel was subjected to the purification procedure; 3, final product from the monomer band of the first gel; 4, final product from the dimer band; 5, final product from the trimer band; and 6, final product from the tetramer band.

(this removes sodium azide and other chemical contaminants). Without letting the membrane dry out, fold one end of the tubing back onto itself and clamp the tubing closed across the double-thickness region using a dialysis tube clamp. Introduce up to 1 ml of the SDS-Out™-treated mixture into each piece of dialysis tubing and then clamp this end as specified above. When this end of the membrane is folded, ensure that as little air as possible is left inside the bag.

3. Dialyze the 1 ml samples in dialysis membranes against 5 L of 10 M urea at 4°C for 12 h. Remove the urea by dialysis twice with 5 L of water for 12 h at 4°C each time.
4. After dialysis, open one end of the bag, collect the solution, and lyophilize. Store the lyophilizate at –20°C (see Note 10).
5. Lyophilizates can be reconstituted in a variety of solvents. We routinely evaluate protein amount and purity by reconstitution of the lyophilizate in 200 µl of 50 mM sodium bicarbonate, after which 5 µl of this solution is mixed with 5 µl of 2× sample buffer/5% 2-mercaptoethanol, boiled for 10 min, and then analyzed by SDS-PAGE and silver staining (Fig. 3).

4. Notes

1. The camera body/bellows system is a convenient means of precisely irradiating samples for chosen amounts of time. Any system that can accomplish the same thing can be used. The incandescent lamp provides visible light to photooxidize the Ru^{II} in the Ru(Bpy) complex. The critical considerations here are the wavelength distribution of the light source and the photon flux. Adjustments to these parameters generally are not

possible, but the modification of irradiation time is a simple and effective method for optimizing cross-linking efficiency and minimizing radical damage to the protein to be cross-linked (see (16) for a complete discussion of these points).

2. 10–20% Gradient gels also can be prepared manually. We have chosen to purchase pre-cast gels for convenience.
3. The Aβ used in our experiments is synthesized "in house," as described (20). The method of synthesis and the source of Aβ is not critical, *as long as the peptide is chemically pure*. Our peptides are characterized by HPLC, amino acid analysis, and mass spectrometry. Peptide purity is >90%, as determined by HPLC. The protein content of our peptide lyophilizates generally is >85%.
4. The calculation used here should provide enough material to run two gels of cross-linked material, but it can be scaled up or down to fit the needs of the user. The volume of NaOH used should be 10% of the final solution volume. Add water to 55% of the final volume. Add the final 45% solution volume as 20 mM Na_2HPO_4, pH 7.4.
5. Any remaining unsolubilized peptide should be solubilized following addition of the water. After addition of the phosphate buffer, the pH should change to 7.6. Any unsolubilized peptide should be removed at this point by centrifugation for 15 min at 16,000 × *g* at room temperature.
6. It is important to do one reaction at a time. Do not add the APS and Ru(Bpy) reagents to all the tubes and then irradiate them one at a time. Only add reagents to a tube once the irradiation and quenching of the prior tube has been completed.
7. The –20°C freezer should not have an auto-defrost function because this function produces freeze–thaw cycles that can affect peptide structure.
8. Place a plain white sheet of paper under the glass plate to enhance contrast and make the oligomer bands easier to distinguish.
9. Diced gel pieces can be stored at –20°C for several weeks prior to use.
10. Oligomers should be stable indefinitely in an anhydrous state at –20°C under N_2 or Ar gas.

Acknowledgments

We gratefully acknowledge the support of NIH grants AG027818, NS038328, the Jim Easton Consortium for Alzheimer's Drug Discovery and Biomarkers at UCLA, and the California Department of Public Health, Alzheimer's Disease Program, grant #07-65806.

References

1. Selkoe DJ (1991) The molecular pathology of Alzheimer's disease. *Neuron* **6**, 487–498.
2. Selkoe DJ (1994) Cell biology of the amyloid β-protein precursor and the mechanism of Alzheimer's disease. *Annu Rev Cell Biol* **10**, 373–403.
3. Haass C, and Selkoe DJ (2007) Soluble protein oligomers in neurodegeneration: lessons from the Alzheimer's amyloid β-peptide. *Nat Rev Mol Cell Biol* **8**, 101–112.
4. Kirkitadze MD, Bitan G, and Teplow DB (2002) Paradigm shifts in Alzheimer's disease and other neurodegenerative disorders: the emerging role of oligomeric assemblies. *J Neurosci Res* **69**, 567–577.
5. Walsh DM, and Selkoe DJ (2007) Aβ oligomers - a decade of discovery. *J Neurochem* **101**, 1172–1184.
6. Roychaudhuri R, Yang M, Hoshi MM, and Teplow DB (2009) Amyloid β-protein assembly and Alzheimer disease. *J Biol Chem* **284**, 4749–4753.
7. Shankar GM, Li S, Mehta TH, Garcia-Munoz A, Shepardson NE, Smith I, Brett FM, Farrell MA, Rowan MJ, Lemere CA, Regan CM, Walsh DM, Sabatini BL, and Selkoe DJ (2008) Amyloid-β protein dimers isolated directly from Alzheimer's brains impair synaptic plasticity and memory. *Nat Med* **14**, 837–842.
8. Lesne S, Koh MT, Kotilinek L, Kayed R, Glabe CG, Yang A, Gallagher M, and Ashe KH (2006) A specific amyloid-β protein assembly in the brain impairs memory. *Nature* **440**, 352–357.
9. Lambert MP, Barlow AK, Chromy BA, Edwards C, Freed R, Liosatos M, Morgan TE, Rozovsky I, Trommer B, Viola KL, Wals P, Zhang C, Finch CE, Krafft GA, and Klein WL (1998) Diffusible, nonfibrillar ligands derived from Aβ1-42 are potent central nervous system neurotoxins. *Proc Natl Acad Sci USA* **95**, 6448–6453.
10. Bitan G, Kirkitadze MD, Lomakin A, Vollers SS, Benedek GB, and Teplow DB (2003) Amyloid β-protein (Aβ) assembly: Aβ40 and Aβ42 oligomerize through distinct pathways. *Proc Natl Acad Sci USA* **100**, 330–335.
11. Harper JD, Wong SS, Lieber CM, and Lansbury PT (1997) Observation of metastable Aβ amyloid protofibrils by atomic force microscopy. *Chem Biol* **4**, 119–125.
12. Walsh DM, Lomakin A, Benedek GB, Condron MM, and Teplow DB (1997) Amyloid β-protein fibrillogenesis. Detection of a protofibrillar intermediate. *J Biol Chem* **272**, 22364–22372.
13. Barghorn S, Nimmrich V, Striebinger A, Krantz C, Keller P, Janson B, Bahr M, Schmidt M, Bitner RS, Harlan J, Barlow E, Ebert U, and Hillen H (2005) Globular amyloid β-peptide1-42 oligomer - a homogenous and stable neuropathological protein in Alzheimer's disease. *J Neurochem* **95**, 834–847.
14. Hoshi M, Sato M, Matsumoto S, Noguchi A, Yasutake K, Yoshida N, and Sato K (2003) Spherical aggregates of β-amyloid (amylospheroid) show high neurotoxicity and activate tau protein kinase I/glycogen synthase kinase-3β. *Proc Natl Acad Sci USA* **100**, 6370–6375.
15. Teplow DB (2006) Preparation of amyloid β-protein for structural and functional studies. *Methods Enzymol* **413**, 20–33.
16. Bitan G, Lomakin A, and Teplow DB (2001) Amyloid β-protein oligomerization: prenucleation interactions revealed by photo-induced cross-linking of unmodified proteins. *J Biol Chem* **276**, 35176–35184.
17. Fancy DA (2000) Elucidation of protein-protein interactions using chemical cross-linking or label transfer techniques. *Curr Opin Chem Biol* **4**, 28–33.
18. Fancy DA, and Kodadek T (1999) Chemistry for the analysis of protein-protein interactions: Rapid and efficient cross-linking triggered by long wavelength light. *Proc Natl Acad Sci USA* **96**, 6020–6024.
19. Jin Y, and Manabe T (2005) High-efficiency protein extraction from polyacrylamide gels for molecular mass measurement by matrix-assisted laser desorption/ionization-time of flight-mass spectrometry. *Electrophoresis* **26**, 1019–1028.
20. Ono K, Condron MM, and Teplow DB (2009) Structure-neurotoxicity relationships of amyloid β-protein oligomers. *Proc Natl Acad Sci USA* **106**, 14745–14750.

Chapter 4

Purification and Fibrillation of Full-Length Recombinant PrP

Natallia Makarava and Ilia V. Baskakov

Abstract

Misfolding and aggregation of prion protein (PrP) is related to several neurodegenerative diseases in humans such as Creutzfeldt–Jacob disease, fatal familial insomnia, and Gerstmann–Straussler–Sheinker disease. Certain applications in prion area require recombinant PrP of high purity and quality. Here, we report an experimental procedure for expression and purification of full-length mammalian PrP. This protocol has been proved to yield PrP of extremely high purity that lacks PrP adducts, which are normally generated as a result of spontaneous oxidation or degradation. We also describe methods for the preparation of amyloid fibrils from recombinant PrP in vitro. Recombinant PrP fibrils can be used as a noninfectious synthetic surrogate of PrP^{Sc} for development of prion diagnostics including the generation of PrP^{Sc}-specific antibody.

Key words: Recombinant prion protein, Inclusion body, Protein purification, Amyloid fibrils, Conformational transition, Prion diseases

1. Introduction

Recombinant prion protein (PrP) expressed in *Escherichia coli* has been used extensively in prion research for various applications. These applications include modeling of prion conversion in vitro; utilization of PrP as immunogen for generating anti-PrP antibody; developing anti-prion therapeutic strategies that involve active immunization using PrP refolded in β-sheet-rich conformations; screening of anti-prion drugs using in vitro conversion assays; and others. These applications require PrP of very high purity with minimal amounts of chemical modifications or degradation. While several methods for purification and refolding of recombinant PrP have been previously described by different groups (1–6), some of the previously developed protocols required a fusion of PrP to a histidine tags or produced PrP of insufficient purity or partially degraded. Inconsistent results in converting of PrP into β-sheet-rich conformations described in the past are attributed, at least in part,

Einar M. Sigurdsson et al. (eds.), *Amyloid Proteins: Methods and Protocols*, Methods in Molecular Biology, vol. 849,
DOI 10.1007/978-1-61779-551-0_4,

to differences in experimental protocols for expression and purification of PrP employed by different laboratories. Here, we describe a reliable experimental protocol for the expression of tag-free full-length recombinant PrP of high purity and with minimal amount of chemical modifications or degradation. This protocol yields approximately 10 mg of mouse PrP or 6–8 mg of hamster PrP per liter of bacterial culture.

The current chapter also describes experimental protocols for converting full-length recombinant PrP into amyloid fibrils developed by our group in the past (7–10). While recombinant PrP fibrils were able to induce transmissible prion diseases in wild-type animals, their infectivity was found to be very low (11). Nevertheless, the immunoconformational assay that utilized conformational, PrP^{Sc}-specific antibodies and a broad panel of non-conformational antibodies revealed that the PrP fibrils produced in vitro acquired a surface structure similar to that of PrP^{Sc} (12). In this regard, PrP fibrils appear to be a suitable synthetic surrogate of PrP^{Sc} and can be utilized for the development of prion diagnostics, high-throughput screening of anti-prion drugs, development of anti-prion decontamination procedures, and other important applications in the field.

2. Materials

Unless otherwise noticed, all reagents are from Sigma (St. Louis, MO). All solutions are prepared with deionized water purified using Synergy 185 UV Ultrapure Water System (Millipore, Bedford, MA). Water and solutions for desalting and high-performance liquid chromatography (HPLC) are degassed under vacuum. HPLC buffers are purged with helium. Shaking procedures at 37°C were performed in an Innova 4300 incubator (New Brunswick Scientific) set at 200 rpm.

2.1. Protein Expression

1. Plasmid DNA encoding mouse PrP 23-230 or Syrian hamster PrP 23-231 (see Note 1) in pET101/D-TOPO (Invitrogen).
2. Competent BL21Star (DE3) One Shot *E. coli* cells and their SOC medium (Invitrogen).
3. Luria-Bertani (LB) Broth (Biosource).
4. 100 mg/mL Carbenicillin disodium salt (American Bioanalytical) in water and stored in aliquots at –20°C.
5. Two 2,800-ml baffled PYREX flasks (Fisher Scientific).
6. TB medium composition for 1,200 ml (see Note 2): 14.4 g Bacto trypton (BD Biosciences, Sparks, MD), 28.8 g Bacto yeast extract (BD Biosciences), 4.8 ml glycerol (American Bioanalytical), water to adjust 1,080 ml. TB medium needs to be autoclaved and then supplemented with 120-ml

filter-sterilized solution of 0.17 M KH_2PO_4 and 0.72 M K_2HPO_4 and 100 μg/ml carbenicillin.

7. 1 M Isopropyl-beta-D-thiogalactopyranoside (IPTG, American Bioanalytical) in water and stored in aliquots at –20°C.

2.2. Isolation of Inclusion Bodies

1. Cell lysis buffer: 50 mM Tris–HCl, 1 mM ethylenediamine tetraacetic acid (EDTA), 100 mM NaCl, pH 8.0.
2. 9 mg/ml Phenylmethylsulphonylfluoride (PMSF) in acetonitrile and stored at –20°C.
3. Lysozyme (American Bioanalytical) solution: prepare at 10 mg/ml in lysis buffer. Store in aliquots at –20°C.
4. Deoxycholic acid (Alfa Aesar).
5. 2 mg/ml Deoxyribonuclease I (DNaseI, type II) in water and stored in aliquots at –20°C.

2.3. Immobilized Metal Ion Affinity Chromatography and Oxidative Refolding

1. 9 M Urea. After urea is dissolved in MiliQ water, add 10 g/l mixed bed amberlite (MB-150), and stir further the solution for at least 1 h. Before use, the solution is filtered using disposable filter units with polyethersulfone (PES) membrane (Nalgene Nunc). 9 M Urea can be stored at –20°C.
2. Chelating Sepharose Fast Flow (GE Healthcare).
3. 0.2 M Nickel sulfate ($NiSO_4$).
4. Acidic buffer for elution of loosely bound ions from Sepharose: 0.02 M Na-acetate, 0.5 M NaCl, pH 3.0.
5. Immobilized metal ion affinity chromatography (IMAC) buffer A: 8 M Urea, 0.1 M Na_2HPO_4, 10 mM Tris–HCl, 10 mM reduced glutathione, pH 8.0.
6. IMAC buffer B: 8 M Urea, 0.1 M Na_2HPO_4, 10 mM Tris–HCl, 10 mM reduced glutathione, pH 4.5.
7. 0.5 M Ethylene glycol bis(2-aminoethyl ether)-*N*,*N*,*N*′*N*′-tetraacetic acid (EGTA), pH 8.0.
8. Desalting buffer: 6 M Urea, 0.1 M Tris–HCl, pH 7.5.
9. 50 mM Oxidized glutathione and stored in aliquots at –20°C.
10. Solutions for sepharose regeneration and preservation: 2 M NaCl; 1 M NaOH; molecular grade ethanol.
11. XK chromatography column (GE Healthcare).
12. HiPrep 26/10 desalting column (GE Healthcare).

2.4. High Performance Liquid Chromatography

1. HPLC buffer A: 0.1% trifluoroacetic acid (Supelco) in water.
2. HPLC buffer B: 0.1% trifluoroacetic acid in acetonitrille.
3. Protein C4 HPLC column: particle size 10 μm, inner diameter 22 mm, length 250 mm; column guard: particle size 12 μm, cartridge 10 mm (Vydac).
4. PES membrane disposable filter units (Nalgene).

2.5. Amyloid Fibril Formation (Manual Setup)

1. 0.5 M 2-(*N*-Morpholino)ethanesulfonic acid (MES) buffer, pH 6.0.
2. 10 mM Sodium acetate, pH 5.0.
3. 0.5 M Thiourea pH adjusted to 6.0.
4. 6 M Guanidine hydrochloride, pH adjusted to 6.0.
5. Dialysis tubing [Spectrapor, molecular weight cut-off (MWCO) 2,000] and clips.
6. 1 mM Thioflavin T (Molecular Probes) stock in water, stored in the dark at +4°C.
7. Delfia plate shaker (Perkin Elmer, Wellmix, or similar) with a microcentrifuge tube rack attached, Clay Adams Nutator mixer (model 1105, Becton Dickinson & Co).
8. Bath sonicator (Branson 2510, Bransonic, Danbury, CT).
9. Plastic tubes, 1.5 ml (Fisherbrand, Fisher Scientific)
10. Recombinant full-length PrP (see below).

2.6. Amyloid Fibril Formation (Semiautomated Setup)

In addition to the reagents described above (see Subheading 2.5):

1. Teflon spheres (3/32 in diameter, McMaster-Carr).
2. 96-Well flat bottom nontreated polystyrene assay plates (Corning Life Sciences).
3. Mylar Plate Sealers (Thermo Labsystems).
4. Microplate fluorescence reader equipped with 444-nm excitation and 485-nm emission filters.

2.7. Epifluorescence Microscopy

1. Inverted fluorescent microscope (Nikon Eclipse TE2000-U) equipped with the illumination system, sets of objectives, filters [excitation filter 485DF22, beam splitter 505DRLPO2, and emission filter 510LP (Omega Optical, Inc. Brattleboro, VT)], and a charge-coupled device (CCD) camera.
2. Immersion oil type FF (Cargille Laboratories, Cedar Grove, NJ).
3. Glass Coplin staining jar.
4. Microscope cover glass no. 1 (Fisher Scientific).

3. Methods

Researchers might face the following technical challenges during expression and purification of PrP:

1. Difficulties in achieving complete solubilization of PrP inclusion bodies.
2. Precipitation and irreversible binding of PrP to the IMAC matrix.

3. Copper-dependent self-cleavage of PrP.
4. Incomplete oxidative refolding of PrP.
5. Spontaneous formation of oxidative adducts.
6. Spontaneous methionine oxidation.

To minimize these problems and to achieve successful purification of PrP of high purity, the protocol described below need to be closely followed.

3.1. PrP Production

3.1.1. Transformation of Bacterial Cells

Chemical transformation of BL21Star (DE3) One Shot *E. coli* is based on the protocol described in the pET Directional TOPO expression Kits Instructional Manual (Invitrogen).

1. Thaw on ice one vial of cells.
2. Add 1 μl (20 ng) plasmid DNA into the vial of cells and mix by stirring gently with the pipette tip.
3. Incubate on ice for 30 min.
4. Heat-shock the cells for 30 s at 42°C.
5. Immediately transfer the tube on ice.
6. Add 250 μl of room temperature SOC medium.
7. Tape the tube on its side to the bottom of incubator and shake at 37°C at 200 rpm for 30 min.
8. Add the entire transformation reaction into 50-mL centrifuge tube containing 10 ml of LB supplemented with 100 μg/ml carbenicillin.
9. Shake at 37°C at 200 rpm for 3–5 h.
10. Add the entire volume into the 500-ml flask containing 90 ml of LB supplemented with 100 μg/ml carbenicillin.
11. Shake overnight at 37°C at 200 rpm.

3.1.2. Induction of PrP Expression

1. Supplement 1,080 ml autoclaved TB media with 120 ml filter-sterilized solution of phosphates (0.17 M KH_2PO_4 and 0.72 M K_2HPO_4) and 100 μg/ml carbenicillin. Mix and save 1 ml of resulting mixture as an absorbance reference for cell growth monitoring.
2. Add 60 ml overnight cell culture, mix, and divide equally between two baffled flasks (use sterile 1-L cylinder).
3. Incubate flasks with cell culture shaking at 37°C at 200 rpm until the absorbance at 600 nm reached 0.6. Dilute with fresh TB, if overgrown.
4. Induce expression by adding 1 mM IPTG.
5. Continue incubation for 4–5 h.

3.1.3. Cell Harvesting

1. To be able to determine cell pellet mass, weigh empty centrifuge bottles.
2. Divide bacterial culture between four 500-ml centrifuge bottles, centrifuge at 1,900 × *g* for 10 min at 4°C.
3. Discard supernatant, calculate cell pellet mass.
4. At this point, cells can be stored overnight at –20°C.

3.1.4. Cells Lysis and Isolation of Inclusion Bodies

1. Thoroughly resuspend the pellet in lysis buffer (8.7 ml of buffer per each gram of bacterial pellet) by vortex and pipetting up and down with 25-ml pipette.
2. Freeze at –80°C and thaw the cells at least one time to ensure cell lysis. At –80°C, cells freeze in about 10 min. Room temperature water bath is used to thaw the pellet quickly.
3. Pour cell lysate into a beaker, add 2 μl PMSF and 20 μl lysozyme per 1 ml lysis buffer, stir at room temperature for 20–40 min (see Note 3).
4. Add deoxycholic acid, 1 mg/ml, and stir for 20–30 min until the liquid becomes viscous.
5. Add DNase I to 5 μg/ml, stir for additional 30–45 min.
6. Divide the lysate between four 50-ml centrifuge tubes, centrifuge at 12,000 × *g* for 30 min at 4°C, decant the supernatant.
7. Thoroughly resuspend the pellet in 15 ml lysis buffer by vortex and pipetting up and down.
8. Repeat DNase I treatment: DNase I to 5 μg/ml to each centrifuge tube, incubate on rotating platform for 20 min.
9. Centrifuge at 12,000 × *g* for 30 min at 4°C, decant the supernatant.
10. Dilute lysis buffer with water 1:9. Thoroughly resuspend the pellet in 20 ml of diluted buffer. This step removes the excess of EDTA form the inclusion bodies to allow proper binding to Ni^{2+}-charged chromatography column.
11. Centrifuge at 12,000 × *g* for 20 min at 4°C, decant the supernatant. Resulting pellet contains recombinant PrP precipitated in the form of inclusion bodies, which can be stored frozen at –80°C for at least 1 month.

3.2. PrP Purification

3.2.1. Immobilized Metal Ion Affinity Chromatography

IMAC purification is performed using a XK chromatography column (GE Healthcare), packed with 8 mL of Chelating Sepharose Fast Flow. Loading the Sepharose with Ni ions and protein binding are performed in solution. The same Sepharose can be reused several times for purification of the same PrP variant (see Note 4). Desalting column is stored at 4°C; however, it should be equilibrated to room temperature before use.

Preparing Sepharose

1. Take the required aliquot of the Sepharose into a 50-ml centrifuge tube.
2. Let the Sepharose settle down by gravity and remove preservative solution.
3. To wash the Sepharose, add water to the top of the tube, cover the tube, and gently resuspend the Sepharose by inverting the tube several times. Let the Sepharose settle down (it takes about 20 min), remove water.
4. With the same procedure, wash with water again.
5. Remove water, charge the Sepharose by adding 2 ml 0.2 M $NiSO_4$.
6. Wash the excess of ions with water twice.
7. Elute the loosely bound ions, washing with acidic buffer, pH 3.0.
8. Wash two times with water.
9. Equilibrate the Sepharose by washing twice with IMAC buffer A. Keep the Sepharose under buffer until the protein is solubilized and ready for binding.

Protein Solubilization and Binding

1. Add 10 ml of IMAC buffer A to each tube of inclusion bodies (see Notes 2 and 5).
2. Thoroughly resuspend the pellet.
3. Incubate on rotating platform 1–1.5 h at room temperature.
4. Centrifuge at 12,000 × *g* for 15 min at 4°C.
5. Remove equilibration buffer from the Ni-charged Sepharose.
6. Add the supernatant containing solubilized recombinant PrP to the Sepharose.
7. Gently rotate the mixture of the Sepharose and the protein at room temperature allowing 30–40 min for binding of the protein.

IMAC and Desalting

1. Secure empty chromatography column on a holder nearby chromatographer.
2. Close column outlet and load the mixture of Sepharose and protein solution.
3. Open the outlet and drain the excess of liquid from the column, collecting it as IMAC flow-through for the analysis of binding efficiency (Figs. 1 and 2). Make sure not to drain the slurry completely: insert the adaptor and lock it above the Sepharose as soon as liquid front reaches the surface of the Sepharose.
4. Connect the column to the FPLC system (ÄKTA prime, GE Healthcare). Set flow rate to 2 ml/min and fraction size to 5 ml. Wash unbound proteins with IMAC buffer A until the UV readings from the chromatographer reach low plato (Fig 1, see Notes 4 and 5).

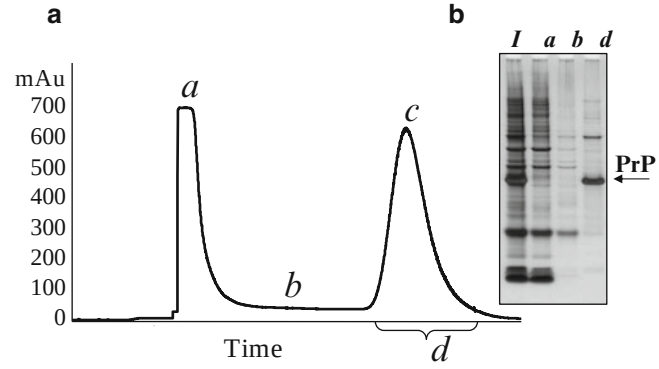

Fig. 1. Typical IMAC profile of mouse recombinant PrP purification. (**a**) IMAC profile. The peak of unbound proteins (stage *a*) typically reaches about 700 mAU. After this peak drops to the baseline (below 50 mAU, stage *b*), the IMAC buffer A (pH 8.0) is changed to the IMAC buffer B (pH 4.5). The PrP peak typically reaches approximately 600 mAU (stage *c*). Fractions with UV values above 50 mAU (stage *d*) are combined for subsequent purification. (**b**) Analysis of IMAC fractions in SDS-PAGE (10% bis-tris) following by silver staining. *I*—solubilized inclusion bodies; *a*, *b*, *d*—fractions collected at the stages *a*, *b*, and *d*, respectively.

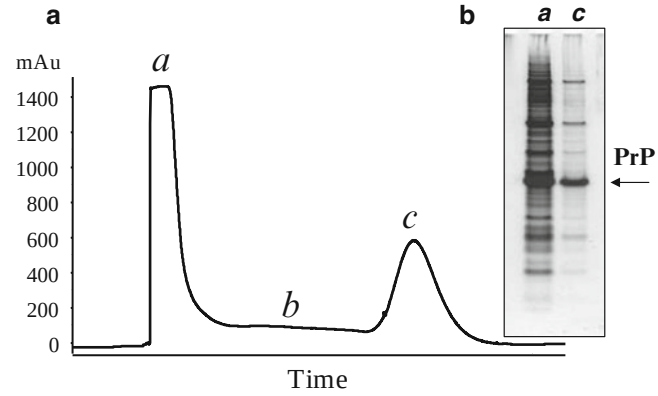

Fig. 2. Leakage of proteins from the IMAC column. (**a**) IMAC profile. Overloading of IMAC column results in higher than normal UV values of unbound proteins (>1,400 mAU, stage *a*) and subsequent baseline higher than 100 mAU (stage *b*). The height of the PrP peak remains at typical level of 600 mAU (stage *c*). (**b**) Analysis of IMAC fractions in SDS-PAGE (10% bis-tris) confirm the presence of high amount of PrP in the flow-trough (*lane a*).

5. Switch to the IMAC buffer B, pH 4.5, to start elution of PrP. Fractions with protein are collected into borosilicate glass (13×100-mm tubes, Fisher Scientific), containing EGTA; the final concentration of EGTA in each tube should be 5 mM after fraction is collected. Typical profile of IMAC purification is shown in Fig. 1.
6. Combine fractions containing PrP (see Fig. 1) in a 50-ml centrifuge tube. Typically, we collect 25 ml of protein solution, and proceed with desalting immediately.

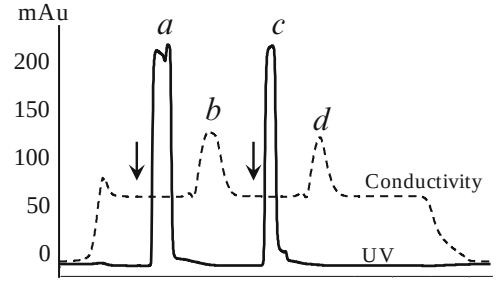

Fig. 3. Desalting profile. PrP collected after IMAC were divided into two parts and desalted using gel-filtration chromatography. The *arrows* mark the points of loading of PrP onto the desalting column. During desalting, the protein (peaks *a* and *c*) is separated from glutathione (peaks *b* and *d*).

7. To remove the Sepharose from the chromatography column, add water to the column, gently resuspend the slurry with the 25-ml pipette, and transfer the Sepharose with water to a new 50-ml tube for regeneration.
8. Attach HiPrep 26/10 desalting column to the FPLC system, wash out storage solution and equilibrate with desalting buffer: 6 M urea, 0.1 M Tris–HCl, pH 7.5 (see Note 6).
9. Desalting step is used to separate the protein from glutathione. Protein solution is loaded through the FPLC super loop. Because the total volume of the protein collected after IMAC exceeds column capacity (14 ml for HiPrep 26/10 desalting column), desalting is performed in two runs. First, 14 ml of the protein solution is loaded and desalted. Then, after the salt is washed out and the column is reequilibrated once more, the rest of the protein (~11 ml) is run through the column (Fig. 3).
10. Wash desalting column immediately after the last run. Wash with water until the conductivity is at the baseline level. Disconnect the column form the FPLC system and reconnect it upside down. Wash with 0.2 M NaOH until the conductivity is on high plato. Wash with water again. Finally, fill out the column with 20% ethanol, disconnect, close, and store at 4°C.
11. Combine the fractions containing recombinant PrP in a new 50-ml tube, mix. To estimate protein concentration (*C*), prepare 1:5 dilution of protein solution, measure absorbance at 280 nm and calculate the concentration using the following equation: $C\,(\mathrm{mg/mL}) = A280 \times 5 \times 0.37$ (for mouse PrP 23-230; 0.37 mg/ml = 1 o.e. at 280 nm). To minimize formation of dimmers during oxidative refolding of PrP, dilute PrP solution with the desalting buffer (6 M Urea, 0.1 M Tris–HCl, pH 7.5) to such extent that the concentration of PrP does not exceed 0.3 mg/ml.
12. Supplement the PrP solution with 5 mM EGTA and 0.2 mM oxidized glutathione, gently rotate at room temperature overnight (see Note 3).

Chelating Sepharose Regeneration

1. After the Sepharose is transferred from the chromatographer column to a 50-ml centrifuge tube, add water to the top of the tube, cover the tube, and gently resuspend the Sepharose by inverting the tube several times. Let the Sepharose settle down, remove water.
2. Wash with 2 M NaCl using the same procedure.
3. Wash with water three times.
4. Wash with 1 M NaOH.
5. Wash with water two times. When removing water after last wash, leave 2 ml above the Sepharose and add 2 ml of pure ethanol for preservation. Keep at 4°C.

3.2.2. High Pressure Liquid Chromatography

To perform C4 HPLC, we use Shimadzu (Columbia, MD) HPLC system operated with EZStart 7.3 SP1 software.

1. Prepare HPLC buffers A and B (1 l each).
2. Degas buffers A and B for 15–20 min by stirring under vacuum, and then keep under constant purging of helium.
3. Before connecting the column, wash the tubing and pumps of HPLC system with running buffers A and B at 5 ml/min for 10 min.
4. Connect the C4 column, equilibrate with buffer A.
5. If visible precipitation occurs after overnight oxidation, filter protein solution using disposable filter units with PES membrane (Nalgene Nunc).
6. To reduce urea concentration, dilute the protein solution with HPLC buffer A (1:2 v/v), and load onto C4 column (see Note 7).
7. Wash unbound proteins from the C4 column with HPLC buffer A at the flow rate of 5 ml/min; monitor UV absorbance at 220 and 280 nm. When the baseline is reached, start the gradient (see Note 8).
8. Using HPLC profile as guidance, manually collect PrP fractions into borosilicate glass tubes (Fisher). α-PrP is eluted in major peak between 52.5 and 54.5 min (Fig. 4). Slow gradient separates correctly folded α-PrP from PrP adducts.
9. By the end of the run, wash the column with HPLC buffer A until the baseline of UV absorbance is reached (see Note 9).
10. The quality of the purified protein is checked by SDS-PAGE (Fig. 4) and by mass spectroscopy (see Note 10).
11. Freeze collected fractions at −80°C. Lyophilize [we use FreeZone 2.5 Plus freeze dry system from Labconco (Kansas City, MO)]. The protein is stored as lyophilized powder at −20°C. Starting from 600 ml bacterial culture, purification typically results in 6–8 mg of pure PrP.

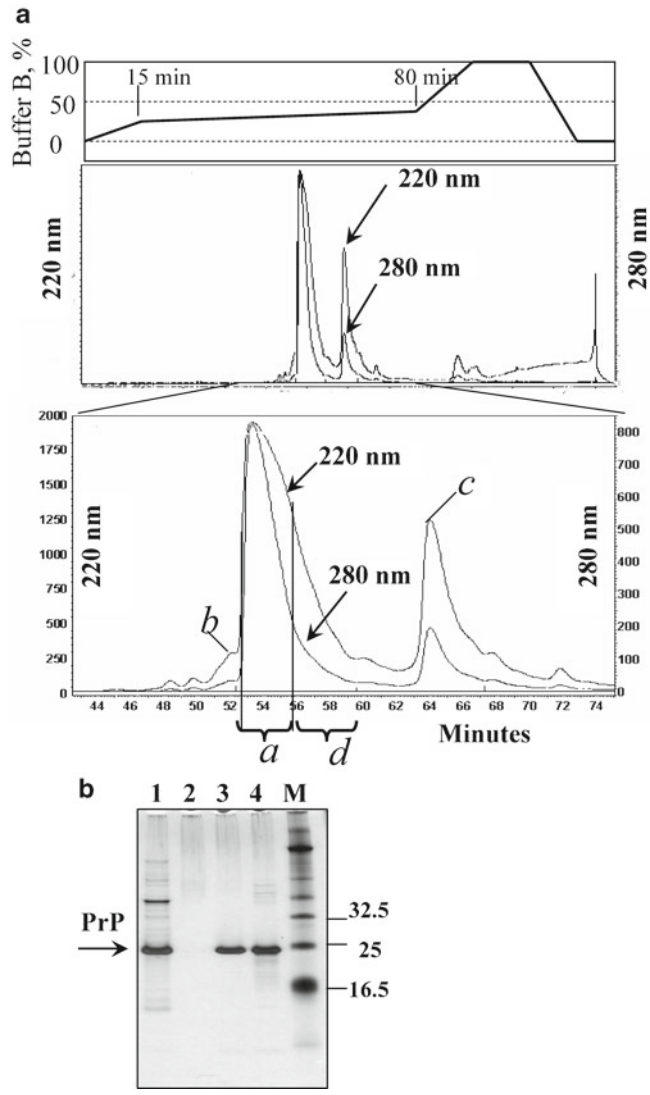

Fig. 4. Purification of PrP on C4 column. (**a**) Typical HPLC profile of elution of mouse recombinant PrP. Major peak contains pure PrP (peak *a*), it is separated from the peak containing PrP with oxidized methionines (peak *b*), from the peaks containing PrP with double glutathione adducts (peak *c*), and from other impurities. The right shoulder of the major HPLC peak (fractions *d* eluted at 56–60 min) is not collected; this shoulder may contain products of PrP degradation (*see lane 4* in **b**). (**b**) Analysis of HPLC fractions in SDS-PAGE following by silver staining: *lane 1*—PrP collected after IMAC and loaded onto C4 column; *lane 2*—HPLC flow-trough; *lane 3*—pure PrP collected from the major HPLC peak *a*; *lane 4*—right shoulder of the major peak (referred to as fraction *d*); *lane M*—molecular marker. *Lane 4* shows minor amounts of PrP degradation products that occurs due to self-cleavage (seen as a smear with Mw < 23 kDa). The extent of PrP degradation may vary from preparation to preparation (see Note 3).

3.3. Conversion of Full-Length PrP into Amyloid Fibrils in Manual Setup

Full-length PrP is capable of forming a variety of aggregated forms in vitro (7, 9, 13, 14). Formation of amyloid fibrils is highly dependent on the reaction conditions. Ideal reaction conditions for fibril formation combine neutral or slightly acidic pH (between 5.0 and 7.5) and moderate concentrations of denaturants such as guanidine hydrochloride (up to 2 M) or urea (up to 4 M). Possible complications during fibril formation include the inhibition of fibrillization by Cu^{2+} (13), copper-mediated and/or spontaneous N-terminal truncation of the protein (15–17), and side chain oxidation (14). To minimize these problems, copper ions are removed from the protein during purification, and 10 mM thiourea is added during fibril formation. Additional problem may arise if recombinant PrP used for conversion is of low purity. The conversion conditions described here and referred to as standard are: 2 M GdnHCl, pH 6. However, fibrillations can also be performed in the absence of GdnHCl or at concentrations lower than 2 M GdnHCl as previously described (18, 19).

1. Prepare stock solution of recombinant PrP (130 μM, 3 mg/ml) in 6 M GdnHCl, pH 6.0. This solution can be stored at −20°C for up to 1 week (see Note 11). Alternatively, the protein can be dissolved directly in the MES buffer (50 mM, pH 6) at lower concentration (0.5–1 mg/ml). This solution, however, cannot be stored and must be used for fibril formation immediately (within several hours).
2. To prepare 500 μl reaction (see Note 12), mix the following reagents in the conical plastic tube: water (273.3 μl), GdnHCl (6 M, 83.4 μl), MES buffer (0.5 M, pH 6.0, 50 μl), and thiourea (0.5 M, 10 μl). Then add stock solution of PrP in 6 M GdnHCl (3 mg/ml, 83.3 μl). Mix reagents gently, avoid introducing air bubbles.
3. If you are using previously formed fibrils as seeds, sonicate them for at least 10 s in the bath sonicator and add to the reaction mixture before PrP stock. Seeding capacity of fibrils decreases upon prolonged storage. Small amounts of seeds (as little as 0.1% of the amount of protein) are sufficient to significantly decrease the lag phase of conversion.
4. Incubate the tube with continuous shaking at 600 rpm using a plate shaker or rotation at 24 rpm using nutator mixer at 37°C (Fig. 5, Note 13).
5. Monitor the kinetics of fibril formation using a thioflavin T binding assay. For this assay, withdraw the aliquots during the incubation. Before taking aliquots, pipette the reaction mixture gently each time (strong pipetting might perturb the kinetics of fibril formation). Dilute each aliquot into 10 mM Na-acetate buffer (pH 5.0) to a final concentration of PrP of 0.3 μM, then add thioflavin T to a final concentration of 10 μM.

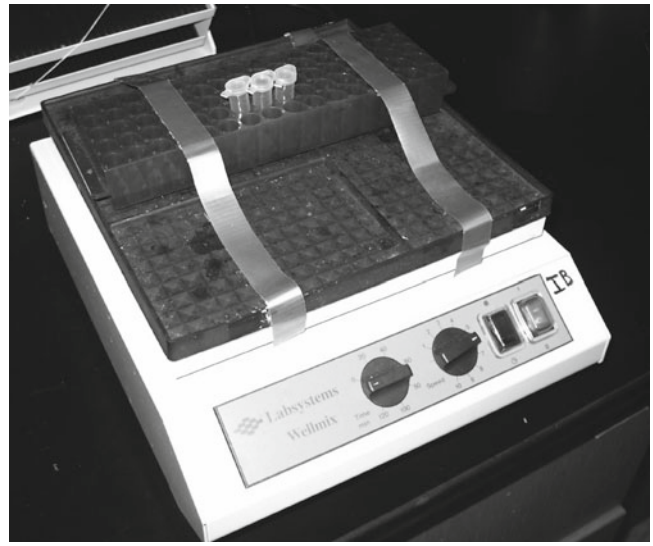

Fig. 5. Plate shaker with a microcentrifuge tube rack used for the conversion reaction. Place plastic tubes next to each other to prevent their rotation inside the rack during shaking.

Record three emission spectra (from 460 to 520 nm) for each time point in 0.4 cm rectangular cuvettes with excitation at 445 nm on a FluoroMax-3 fluorimeter (Jobin Yvon, Edison, NJ) keeping excitation and emission slits at 4 nm. Average the spectra and determine the fluorescence intensity at emission maximum (usually around 482 nm). Emission will remain low for a few hours or days, then start rising and eventually will rise 10–40-fold of the original baseline level (see Note 14).

6. After the fibril formation has reached plateau, the fibrils should be dialyzed for prolonged storage. Place the suspension of fibrils in the bag prepared from the dialysis tubing (MWCO 2,000) and dialyze against a large volume of 10 mM Na-acetate buffer (pH 5.0) with several buffer changes. Fibrils should be stored at +4°C. Prolonged storage of fibrils at room temperature or at higher pH may lead to their aggregation and copper-mediated protein self-cleavage. Freezing and thawing may cause fragmentation of fibrils into short pieces.

3.4. Conversion of Full-Length PrP into Amyloid Fibrils in Semiautomated Setup

1. Perform the conversion of PrP into amyloid fibrils in semiautomated setup at least in triplicate to ensure reproducibility. Add three Teflon spheres (3/32 in. diameter) per well of 96-well assay plate. Mix the following reagents in the conical plastic tube: water (268.3 μl), GdnHCl (6 M, 163.7 μl), MES buffer (0.5 M, pH 6.0, 50 μl), thioflavin T (1 mM, 5 μl), and

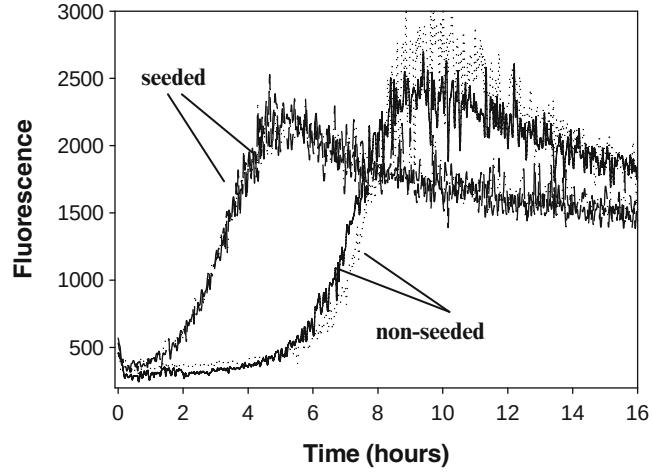

Fig. 6. Kinetics of fibril formation from PrP (1 μM) carried out in semiautomated format under standard solvent conditions. Two repeats for non-seeded and seeded conversion reactions are shown. After reaching a plato, the ThT fluorescence often shows a decline that appears to be due to sorption of fibrils to plate walls and partial aggregation of fibrils into clumps.

thiourea (0.5 M, 10 μl). Add stock solution of PrP in 6 M GdnHCl (3 mg/ml, 5 μl). After thorough mixing divide the reaction mixture between three wells of the 96-well plate (160 μl per well) and cover the plate with the plate sealer. If previously formed fibrils are used as seeds, they should be sonicated for at least 10 s in the bath sonicator and added to the reaction mixture before PrP stock.

2. Insert the 96-well plate into the microplate reader. Set up incubation at 37°C with shaking at 900 rpm (shaking diameter 1 mm) and fluorescence measurements every 5 or 10 min with excitation at 444 nm and emission at 485 nm (Fig. 6).
3. After the completion of the experiment, transfer the data to Origin (Origin Lab) and fit to the following equation:

$$F = \frac{A + (B + c't)}{[1 + \exp(k'(t_m - t))]}$$

where A is the initial level of thioflavin T fluorescence, B is the increase in thioflavin T fluorescence during conversion, k is rate constant of amyloid accumulation (per hour), t_m is the midpoint of conversion of PrP to amyloid, and c is an empirical parameter describing changes in fluorescence after fibril formation. The lag time (t_l) can be calculated as: $t_l = t_m - 2/k$.

3.5. Epifluorescence Microscopy

While ThT-fluorescence assay is convenient for measuring the kinetics of fibril formation, this assay, however, is not sufficient for providing a definite proof as to whether amyloid fibrils were formed in the reaction mixture. Relatively small (two- to threefolds) increase in ThT fluorescence may indicate the formation of nonfibrillar PrP isoforms such as soluble β-oligomers, which also bind ThT. Several techniques including electron microscopy and atomic force microscopy have been used for confirming the formation of fibrils; however, their application is laborious and requires costly equipment. In our experience, epifluorescence microscopy in the presence of ThT serves as a rapid and reliable test for the presence of the amyloid fibrils in the sample, for assessing their quality, size, aggregation status, and even growth rate (7, 8, 10, 13, 20). Here, we describe the experimental procedure for imaging amyloid fibrils using inverted fluorescence microscopy in the presence of ThT.

1. Deposit several cover glasses into staining jar clean them by sonicating it in isopropanol (1 min), then in acetone (1 min), and again isopropanol (1 min). Wash the cover glass with water and incubate it in the mixture of sulfuric acid (70%) and hydrogen peroxide (30%) for at least 1 h. Rinse with water several times. Store in water, and dry with compressed air before use.
2. Add 0.5 μl of suspension of PrP fibrils (0.5 mg/ml) in 10 mM acetate buffer (pH 5.0) to the same buffer (99.5 μl) containing 10 μM thioflavin T. Incubate the solution in the plastic tube at 25°C for 5 min.
3. Place 10–20 μl of the solution on the cover glass. Allow fibrils to sediment on the glass surface for 1–2 min. Examine the sample with an inverted fluorescence microscope (Nikon Eclipse TE2000-U) using 60× or 100× objective. The emission can be isolated from Rayleigh- and Raman-shifted light by a combination of filters: an excitation filter 485DF22, a beam splitter 505DRLPO2, and an emission filter 510LP (Omega Optical, Inc.). Digital images can be acquired using a CCD camera.
4. Shape and size of PrP fibrils vary depending on the conditions of their formation including shaking modes and purity of the protein (see Note 14). Under the standard conditions PrP yields long (>1 μm) and straight fibrils, if highly pure (Fig. 7a). Fibrils formed at higher pH (pH > 7.0) tend to aggregate into large clusters. Exposure of fibrils formed at pH < 6 to pH >6.5 or addition of salt induce aggregation into clumps of various size (Fig. 7b). Presence of impurities in the protein (substantially methionine oxidation or N-terminal truncation) can result in the formation of shorter fibrils (<1 μm) that often appear bent or very short, dot-like fibrils (Fig. 7c).

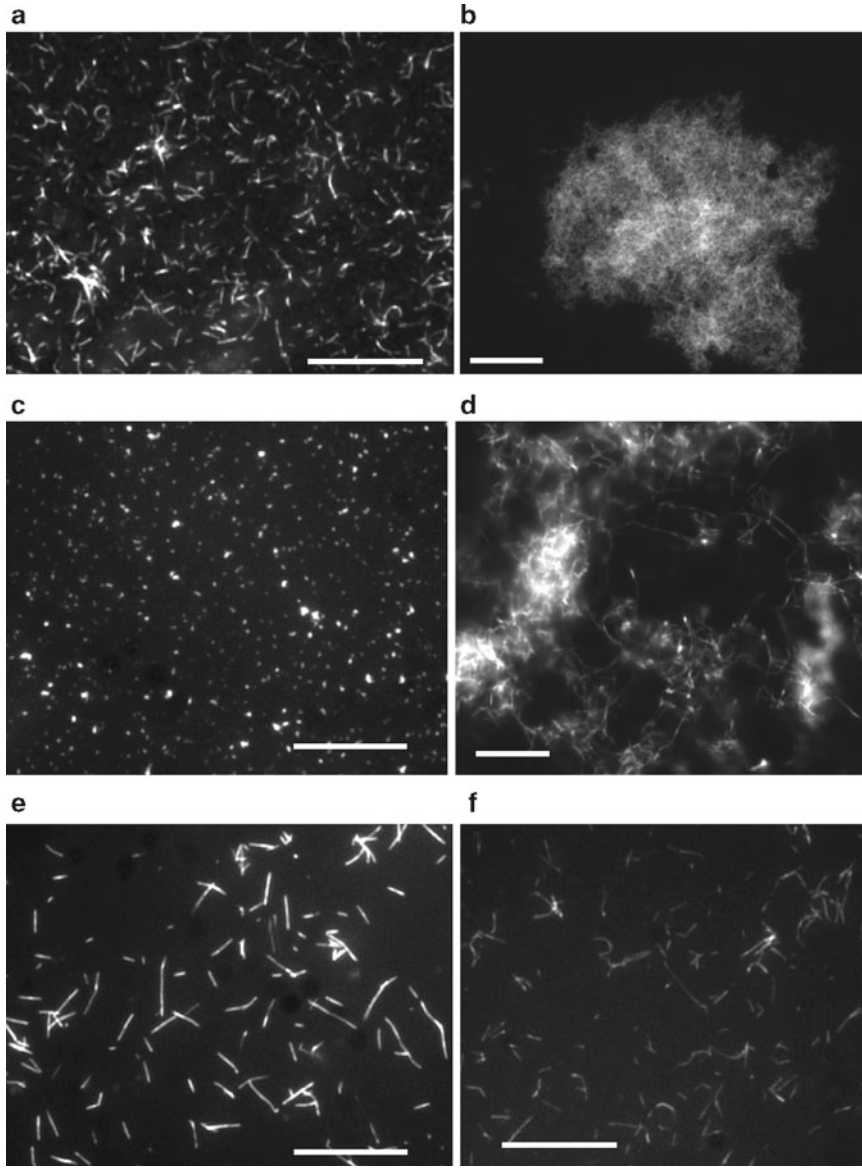

Fig. 7. Epifluorescence microscopy of PrP fibrils stained with thioflavin T. (**a**) Fibrils of mouse PrP prepared under standard conditions (shaking, pH 6). (**b**) Fibrils of mouse PrP prepared under standard conditions and incubated for 24 h in PBS, pH 7.2. (**c**) PrP (mouse) of insufficient purity or with substantial methionine oxidation converts into very short or dote-like fibrils under standard conditions. (**d**) Fibrils of mouse PrP prepared under standard conditions and digested with PK for 1 h at 37°C. (**e**) Fibrils of mouse PrP prepared under standard solvent conditions upon rotation. (**f**) Fibrils of Syrian Hamster PrP prepared under standard solvent conditions upon rotation. When stained with ThT, mouse fibrils show substantially brighter fluorescence than hamster fibrils. Scale bars = 10 μm.

4. Notes

1. Plasmids for the expression of mouse PrP 23-230 or Syrian hamster PrP 23-231 were cloned from mouse of Syrian hamster cDNA, respectively, as described (7, 14).
2. We have found convenient to grow bacteria in two flasks each containing 600 ml TB media. This typically results in total of 12 g bacterial pellet used for isolation of inclusion bodies. To prevent overloading of HPLC column, only one half of inclusion bodies should be used for IMAC. Another half is stored at −80°C.
3. Recombinant PrP is prone to copper-dependent self-cleavage (15, 16). Performing cell lysis steps at lower temperature could slow down degradation, however, would require prolonged incubation time. Therefore, the cell lysis steps are carried out at room temperature. EDTA and EGTA are added to the lysis buffer and during oxidative refolding, respectively, to minimize protein degradation.
4. Lack of Ni ions on the Sepharose may cause the leakage of protein during wash step. For better performance, recharge the column with Ni ions each time before reuse.
5. Loading the column with excessive amounts of protein (Fig. 2) or incomplete solubilization of inclusion bodies (Fig. 8) results in high UV readings during the wash with IMAC buffer A. To achieve proper solubilization of the protein, it is very important to prepare IMAC buffers A and B fresh, at the same day the IMAC purification is performed. Instead of keeping reduced glutathione in concentrated stock solution, we dissolved it directly in the IMAC buffers to the final concentration of 10 mM.

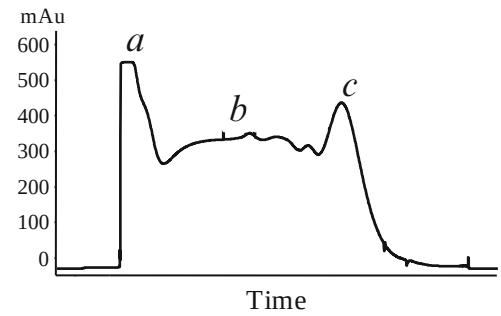

Fig. 8. IMAC profile of incompletely solubilized protein. Reduced glutathione degraded during the preparation of stock solution (see Note 5). As a result, recombinant PrP was incompletely solubilized and leaked from the Sepharose during the wash step. The peak of unbound proteins (stage *a*) was below 600 mAU; the UV values during the wash steps were above 300 mAU (stage *b*) and the yield of eluted PrP was reduced (stage *c*).

6. Make sure to follow recommendations on pressure limit and buffer compatibility for the specific column. Our desalting column cannot tolerate urea at the concentrations above 6 M, therefore, desalting buffer contains less urea than IMAC buffers. Depending on solution viscosity, flow rate needs to be adjusted during the run to keep pressure under the limit.
7. Because after overnight oxidation PrP solution contains urea, loading the protein onto C4 column requires pressure above Shimadzu HPLC system limits. To avoid high pressure, we dilute PrP solution threefold with buffer A and use external HPLC pump 2010 from Varian (Walnut Creek, CA) to load the protein. We wash the pump with water and with 20 ml of buffer A before loading PrP. We load protein solution at flow rate 5 ml/min and finish by loading 20 ml of HPLC buffer A, to ensure that no protein is left in the pump. After loading is completed, we disconnect and thoroughly wash the loading pump with water.
8. In our gradient method, the percentage of HPLC buffer B (0.1% trifluoracetic acid in acetonitrile) grows from 0 to 25% during the first 15 min (at flow rate 5 ml/min). Then, gentle gradient is applied (from 25 to 35% of buffer B in the next 65 min) to ensure efficient separation of PrP adducts (Fig. 4). Correctly folded, oxidized, γ-helical form of PrP is eluted between 52.5 and 54.5 min. Then, the percentage of buffer B grows from 35 to 100% in 15 min; the column is washed with 100% of buffer B for 15 min, and the gradient drops down to 0% within 10 min.
9. If the same C4 column is used for the purification of different PrP variants, running washing program with extended time of 100% acetonitrile will ensure the absence of cross-contamination. In our washing program, buffer B concentration grows from 0 to 100% within 20 min, remains constant 100% for 25 min, and then goes down to 0% during last 20 min. The run is finished by equilibration of the C4 column with buffer A for 25 min, which prepares the column for loading of new protein.
10. To perform mass spectroscopy, small amount of recombinant PrP (as a lyophilized powder) is dissolved in 20 μL of 1:1 water:methanol mixture containing 1% acetic acid. The solution is then analyzed on a Waters ZMD single quadrupole mass spectrometer operated in positive ion mode.
11. After PrP is purified, it is preferable to store the protein as a lyophilized powder at −20°C. Storage in 6 M GdnHCl at −20°C is possible for up to 1 week. However, prolonged storage at 6 M GdnHCl leads to the formation of the β-oligomeric nonfibrillar from. Prolonged storage (longer than 24 h) in solution at neutral pH and in the absence of denaturants is not advisable due to self-cleavage and nonspecific aggregation.

12. Fibril formation can proceed sluggishly if the volume of the solution in the tube is too low (<300 μL).
13. Make sure that the plastic tube fits tightly within the attached to the platform rack and does not rotate inside the rack during orbital shaking (Fig. 5). End-over-end rotation on nutator mixer or similar device can also be used as an alternative way for fibrillation reactions. However, structurally different types of fibrils are formed under different shaking/rotation modes even when identical solvent conditions are employed for fibrillation reactions (10, 21).
14. Exact value of thioflavin T fluorescence depends on several factors including purity of the protein and conditions of fibril formation. Differences in intensity of ThT fluorescence could be due to several factors including differences in ThT-binding affinity for fibrils prepared at different solvent conditions; different yield of fibrils formation; or different propensity of fibrils to aggregate into large clumps. The yield of ThT fluorescence of fibrils prepared under nonstandard conditions is often lower than that for standard fibrils. ThT fluorescence of fibrils prepared under different shaking modes or from different PrP variants (e.g., mouse vs. hamster PrP) can also vary (10) (Fig. 7e, f). Values of ThT fluorescence threefold or more above background usually indicate the presence of amyloid fibrils. In addition to ThT-fluorescence assay, fluorescence microscopy helps to analyze the yield and quality of fibrils (Fig. 7).

Acknowledgments

This work was supported by the National Institute of Health grant R01 NS045585.

References

1. Zahn, R., von Schroetter, C, and Wuthrich, K. (1997) Human prion protein expression in Escherichia coli and purified by high-affinity column refolding. *FEBS Letters* 417, 400–404.
2. Mehlhorn, I,. Groth, D., Stöckel, J et al. (1996) High-level expression and characterization of a purified 142-residue polypeptide of the prion protein. *Biochemistry* **35**, 5528–5537.
3. Rezaei, H., Marc, D., Choiset, Y. et al. (2000) High yield purification and physico-chemical properties of full-length recombinant allelic variants of sheep prion protein linked to scrapie susceptibility. *Eur J Biochem* **267**, 2833–2839.
4. Hornemann, S., Korth, C., Oesch, B. et al. (1997) Recombinant full-length murine prion protein, *m*PrP(23–231): purification and spectroscopic characterization. *FEBS Lett* **413**, 277–281.
5. Jackson GS, Hil AF, Joseph C et al. (1999) Multiple folding pathways for heterologously expressed human prion protein. *Biochim Biophys Acta* **1431**(1):1–13.
6. Yin, S.M., Zheng, Y., and Tien, P. (2003) On-column purification and refolding of

recombinant bovine prion protein: using its octarepeat sequences as a natural affinity tag. *Protein Expr Purif* **32**, 104–109.

7. Bocharova, O.V., Breydo, L., Parfenov, A.S., Salnikov, V.V., and Baskakov, I.V. (2005) In vitro conversion of full length mammalian prion protein produces amyloid form with physical property of PrPSc. *J Mol Biol* **346**, 645–659.
8. Baskakov, IV, and Bocharova, OV. (2005) In Vitro Conversion of Mammalian Prion Protein into Amyloid Fibrils Displays Unusual Features. *Biochemistry* **44**, 2339–2348.
9. Bocharova, O.V., Makarava, N., Breydo, L., Anderson, M., Salnikov, V.V., and Baskakov IV. (2006) Annealing PrP amyloid firbils at high temperature results in extension of a proteinase K resistant core. *J Biol Chem* **281**, 2373–2379.
10. Makarava, N., and Baskakov, I.V. (2008) The same primary structure of the prion protein yields two distinct self-propagating states. *J Biol Chem* **283**, 15988–15996.
11. Makarava, N., Kovacs, G.G., Bocharova, O.V. et al. (2010) Recombinant prion protein induces a new transmissible prion disease in wild type animals. *Acta Neuropathol* **119**, 177–187.
12. Novitskaya, V., Makarava, N., Bellon, A. et al. (2006) Probing the conformation of the prion protein within a single amyloid fibril using a novel immunoconformational assay. *J Biol Chem* **281**, 15536–15545.
13. Bocharova, O.V., Breydo, L., Salnikov, V.V., and Baskakov, IV. (2005) Cu(II) inhibits in vitro conversion of prion protein into amyloid fibrils. *Biochemistry* **44**, 6776–6787.
14. Breydo, L., Bocharova, O.V., Makarava, N., Salnikov, V.V., Anderson, M., and Baskakov, I.V. (2005) Methionine Oxidation Interferes with Conversion of the Prion Protein into the Fibrillar Proteinase K-Resistant Conformation. *Biochemistry* **44**, 15534–15543.
15. McMahon, H.E.M., Mange, A., Nishida, N., Creminon, C., Casanova, D., and Lehman, S. (2001) Cleavage of the Amino Terminus of the Prion Protein by Reactive Oxygen Species. *J Biol Chem* **276**, 2286–2291.
16. Mange, A., Beranger, F., Peoc'h, K., Onodera, T., Frobert, Y., and Lehmann, S. (2004) Alpha- and beta- cleavages of the amino-terminus of the cellular prion protein. *Biol Cell* **96**, 125–132.
17. Ostapchenko, V.G., Makarava, N., Savtchenko, R., and Baskakov, I.V. (2009) The polybasic N-terminal region of the prion protein controls the physical properties of both the cellular and fibrillar forms of PrP. *J Mol Biol* **383**, 1210–1224.
18. Sun, Y., Makarava, N., Lee, C.I., Laksanalamai, P., Robb, F.T, and Baskakov, I.V. (2008) Conformational stability of PrP amyloid firbils controls their smallest possible fragment size. *J Mol Biol* **376**, 1155–1167.
19. Almstedt, K., Nyström, S., Nilsson, K.P.R., and Hammarström. P. (2009) Amyloid fibrils of human prion protein are spun and woven from morphologically disordered aggregates. *Prion* **3**, 224–235.
20. Bocharova, O.V, Breydo, L., Salnikov, V.V., Gill, A.C, and Baskakov, IV. (2005) Synthetic prions generated *in vitro* are similar to a newly identified subpopulation of PrPSc from sporadic Creutzfeldt-Jakob Disease PrP^{Sc}. *Prot Science* **14**, 1222–1232.
21. Ostapchenko, V.G., Sawaya, M.R, Makarava, N et al. (2010) Two amyloid states of the prion protein display significantly different folding patterns. *J Mol Biol* **400**, 908–921.

Chapter 5

Featuring Amyloids with Fourier Transform Infrared and Circular Dichroism Spectroscopies

Miguel Calero and María Gasset

Abstract

Amyloids are fibrillar aggregates of proteins characterized by a basic scaffold consisting of cross β-sheet structure that can exert physiological or pathological effects. Both far-UV circular dichroism and Fourier transform infrared (FTIR) spectroscopies are techniques used for the fast analysis of protein secondary structure. Both techniques are complementary and preferentially used depending on the physical state of the analyte, the major secondary structure element and the relative abundance of given amino acids. Although there are special setups for working with films, circular dichroism is best suited for ideal diluted solutions of polypeptides exhibiting α-helix as major structural element and low content of aromatic residues. During the last decade, a related technique, linear dichroism, has been applied to study the orientation of protein subunits within amyloid oligomers or fibrils in solution. Alternatively, FTIR works best with concentrated solutions, solids and films, and resolves with accuracy the β-sheet composition, but it is affected by contributions of amide groups. The advent of new infrared techniques based on correlation analysis of time-dependent variations induced by external perturbations that generates two-dimensional IR maps has enabled to greatly increase spectral resolution and to extend its applicability to protein secondary structure characterization in a variety of physical environments. Within the amyloid field, conjunction of both spectroscopies has provided the first filter step for amyloid detection and has contributed to decipher the structural aspects of the amyloid formation mechanism.

Key words: Amyloids, Circular dichroism, Fourier transform infrared spectroscopy, 2D-FTIR, Linear dichroism, Secondary structure determination, β-Sheet content

Abbreviations

ATR	Attenuated total reflection
CD	Circular dichroism
CSA	(+)-10-Camphorsulfonic acid
D_2O	Deuterium oxide
DMSO	Dimethyl sulfoxide
EDTA	Ethylenediaminetetraacetic acid
IR	Infrared
FTIR	Fourier transform infrared spectroscopy
HEPES	4-(2-Hydroxyethyl)-1-piperazineethanesulfonic acid

Einar M. Sigurdsson et al. (eds.), *Amyloid Proteins: Methods and Protocols*, Methods in Molecular Biology, vol. 849,
DOI 10.1007/978-1-61779-551-0_5,

HFIP Hexafluoroisopropanol
HxD Hydrogen per deuterium exchange
LD Linear dichroism
TFA Trifluoroacetic acid
TFE Trifluoroethanol
UV Ultraviolet region

1. Introduction

Amyloids are a class of insoluble protein aggregates, which name comes from the early mistaken identification as starch based on their crude iodine staining. From a biophysical standpoint, the term amyloid refers to any polypeptide polymer maintained by a cross-β motif, despite its staining characteristics. This motif is minimally defined as a series of β-strands extended perpendicular to the fiber axis and joined by hydrogen bonds parallel to the fiber direction. While simple, this basic β-motif is highly flexible accommodating sheets, helices, and others β-folds for the protofilament (1–3). Supramolecularly, amyloids are largely heterogeneous, allowing ribbon shapes, helices with variable pitches, and multiple branching-derived morphologies. In addition, since amyloids are the final states of polymerization processes, they generally coexist with alternative assemblies which are both in-path and off-path intermediate species (4, 5). These alternative assemblies, as for instance the β-oligomers, can sustain essential functions emphasizing the importance of their differential characterization (6).

Circular dichroism (CD) and linear dichroism (LD) spectroscopies are forms of light absorption spectroscopy that measure the difference in absorbance polarized light as a function of the wavelength, rather than the commonly used absorbance of isotropic light (7). CD measures the difference in the absorbance of right- and left-circularly polarized light and provides the most convenient method to monitor protein secondary structure in solution (8–14). LD monitors the difference in absorption of light linearly polarized parallel and perpendicular to an orientation axis and provides information on relative orientations of subunits in protein oligomers and fibers, as well as protein orientation in an environment such as a membrane (7, 15). The chromophores responsible for the UV absorption bands in proteins (peptidic bond, aromatic amino acids, and disulfide bridges) also give rise to CD signals in the far-UV region (180–240 nm) that are dependent on the spatial arrangement of the peptide backbone and the environment of the peptide or protein (8). Hence, although different amyloidogenic proteins lack significant primary sequence similarity, the formation of their aggregates consistently involves an increase in β-sheet content, which is associated with fibrillar morphology. It has been shown that CD spectra ideally between 240 and approximately 180 nm

can be analyzed for the different secondary structural types achieving accuracies of 0.97 for α-helices, 0.75 for β-sheet, 0.50 for turns, and 0.89 for other structure types (9, 10, 16).

LD in the UV region (UV-LD) is sensitive to the spatial arrangement of protein chromophores, and it is best suited for the study of oriented protein polymers and represents one of the few techniques that provide information on the orientation of the subunits within an ordered array such as amyloid oligomers or fibers. UV-LD is typically employed in the analysis of flexible, long molecules such as DNA, and membrane and fibrous proteins that prove difficult to structurally determine by such methods as NMR and X-ray diffraction (7, 17–20).

Fourier transform infrared (FTIR) spectroscopy is an absorption spectroscopy in which the transitions detected are those arising from vibration modes of bonds involving heteroatoms (21–23). FTIR spectroscopy can be used to study proteins and peptides in any physical state (crystals, powder, thin film, and aqueous solutions), but the dominance of the IR signal by universal solvent H_2O represents a major practical problem. To overcome this limitation, different strategies have been developed: (1) mathematic algorithms for water signal subtraction, (2) replacement of H_2O with D_2O (HxD), and (3) use of thin hydrated films or solids. Among the nine characteristic bands of the peptide bond, the amide I (1,700–1,600 cm^{-1}) and II (1,600–1,500 cm^{-1}) bands are the major bands for conformation analysis. Particularly, about 80% of the intensity in the 1,700–1,600 cm^{-1} arises from the stretching of amide carbonyl group, whose vibration frequency depends on its involvement on hydrogen bonds and their geometry and thereof the secondary structure elements (21–23). The analysis of the amide I band (or I′ after HxD isotopic exchange) assumes that the experimental spectrum is the result of the convolution of the spectral signatures of pure secondary structure elements with a noise or broadening function (24, 25). The conjunction of the normal mode analysis with resolution-enhancement methods, as deconvolution or second derivative, and curve fitting routines allows identifying the vibration signatures of the different secondary structure elements and the quantification of their contribution (25–32).

In addition to the previous analytical strategy, the introduction of external perturbations (mechanical, thermal, chemical, etc.) to spread out the band congestion of the amide I spectrum into a second dimension correlation approaches (2D IR) have been implemented (33–37). Thus, correlation analysis of time-dependent variations in infrared spectra induced by external perturbations generates two-dimensional maps increasing the spectral resolution by spreading out peaks along the second dimension and revealing the order of the actual sequence of processes induced by the perturbation. This method provides a way to deconvolve amide bands into their secondary structure components, as well as to obtain the correlation of the interaction involving different elements

pertaining to the same or different types of molecules in the same sample. 2D-IR has been applied to the study of different key aspects of proteins, such as the identification of their secondary structure components, aggregation, dynamics, unfolding, protein–lipid interactions as well as amyloid formation (34–37).

2. Materials

2.1. Supplies

1. All buffers and solutions were freshly prepared using water provided by a Milli-Q system (18 MΩ/cm at 25°C, Millipore Corp., Bedford, MA).
2. D_2O and TFE were purchased from Sigma-Aldrich, and kept in a desiccator to prevent hydration.
3. Peptides were synthesized at the Peptide Synthesis Unit (Pompeu Fabra University) but can alternatively be purchased from different companies performing Custom Synthesis.

2.2. Instrumentation

1. Spectropolarimeter J-810 from Jasco for CD and LD analysis.
2. Polarimetric quartz cuvettes for CD from Hellma (Hellma GmbH & Co. KG, Germany).
3. FTIR spectrophotometer FTIR-670 Plus from Jasco.
4. CaF_2 or BaF_2 windows, Teflon spacers, and universal transmission cell holder, for FTIR transmission experiments.
5. Ge, ZnSe, or diamond crystals and ATR setup (mirrors for beam focusing and crystal holder) for ATR-FTIR experiments.

3. Methods

3.1. Basic Protocol for Analysis of Amyloids by Circular and Linear Dichroism in the Far-UV Region (190–250 nm)

CD and LD are closely related techniques with very similar methodological approaches. However, two important differences distinguish both techniques. First, CD spectroscopy uses circularly polarized light, whereas LD uses linearly polarized light. Thus, the information provided by these techniques are also different. UV-CD provides information on the composition of protein secondary structure motifs, while UV-LD provides information on the orientation of the subunits within an ordered array.

Second, opposite to CD, LD analysis requires that the molecules to be analyzed are oriented (otherwise, LD = 0). To induce molecular alignment, the most common method used for amyloid peptides is based on the use of flow alignment of elongated fibers within the flow direction in a laminar flow, or by a shear flow gradient produced by a spinning cylinder within a concentric sleeve, such as the Couette cell.

3.1.1. Sample Preparation

Cuvettes and Buffer Selection

Standard quartz cuvettes for far-UV CD analysis are made of high-grade quartz with transmission values of more than 80% over the spectral range (see Note 1). There are mainly two types: cylindrical (exposing to the beam a circular surface) and rectangular, having a 0.1–0.2 cm optical path (see Notes 2 and 3). For LD analysis of fibrous proteins such as amyloids, to produce a solution of flow-oriented molecules, special quartz cuvettes such as Couette flow cells (38) (see Note 4) or continuous flow cuvettes (17) are required. For both techniques, the selection of a cell type depends on a number of factors, mainly: protein concentration, amount of protein available, buffer used, and requirements for temperature control.

The buffer used for CD and LD measurements should be as optically transparent as possible in the far-UV region to avoid interference with protein CD signals. Best buffer with a wide pH range is potassium phosphate (10 mM), but some other suitable buffers for measurements down to 195 nm include: borate (20 mM), sodium cacodylate (20 mM), potassium acetate (20 mM), and HEPES (25 mM) (see Note 5). For accurately reaching short wavelengths (below 200 nm) needed for secondary structure estimation, it is recommended to avoid or keep at minimum the concentration of additives. Similarly, protein unfolding experiments performed by the addition of chaotropic agents, such us urea or guanidine–HCl cannot be followed by CD or LD below 205 nm, due to the strong absorbance of the reagents. Citrate, EDTA, or imidazole should not be used below 210 nm. Other buffers have to be tested before are used for sample preparation (see Note 6).

Protein/Peptide Solutions and Cuvettes Path Length

In general, before CD or LD analysis, protein or peptide solutions are equilibrated in the working buffer by dialysis at about 1–5 mg/ml (see Note 7). However, this procedure is unsuitable for highly amyloidogenic peptides that are prone to rapidly aggregate at those concentrations. For these peptides/proteins, more diluted solutions (below 0.15 mg/ml) are recommended (see Notes 3 and 8). However, more diluted solutions require the use of cuvettes with longer pathways, and caution should be exerted to avoid that the absorbance of the solution rises above 1.0 at any point of the spectra due to buffer interference (see Note 9).

To obtain quantitative information about secondary structure (see Subheading 3.1.3) is a primary requirement to know the exact protein concentration by suitable accurate methods such as UV-absorption readings, or preferably by quantitative amino acid analysis before and after spectra acquisition. By knowing the correct concentration of the protein, we will be able to optimize the signal-to-noise ratio and avoid artifacts due to improper measurement conditions (see Note 10).

3.1.2. Parameters and Data Acquisition of CD or LD Spectra

Several parameters directly affect spectral acquisition by altering the signal-to-noise ratio and have to be defined by the user before measuring to obtain a high-quality spectrum. Proper calibration of the energy level, wavelength accuracy, and CD or LD scale accuracy of spectropolarimeter will ensure also good and accurate data acquisition. As baseline is usually not straight in a CD experiment, it is important to perform a baseline correction by collecting a CD or LD spectrum of the solvent and subtracting it from the sample one. Following, a typical experimental setup for far-UV CD or LD (see Note 11) analysis that can be used as a guideline for choosing the appropriate conditions:

- Protein concentration: 0.15 mg/ml.
- Buffer: 10 mM potassium phosphate, pH 7.4.
- Cell: 1-mm cylindrical quartz cuvette (e.g., Hellma) for CD analysis or Couette-flow cell for LD analysis (see Note 4).
- Temperature: 20°C (adjust according to experimental requirements).
- Spectral range: 250–190 nm (250–200 nm, if buffer interference).
- Spectral bandwidth (or slit bandwidth): 1 nm (adjust for optimal signal to noise ratio) (see Note 12).
- Data resolution: 1 nm (usually, 0.2–1 nm).
- Instrument response time (or time constant): 1 s (indicates the time over which the instrument averages a data point) (see Note 13).
- Scan speed (speed of measurement): 50 nm/min (indicates the number of nanometers scanned per unit of time).
- Sensitivity: 50 millidegrees (set accordingly to the intensity of the sample signal).
- Accumulations: 10 (it refers to the number of spectra averaged) (see Note 14).

A basic protocol for CD data acquisition of a protein solution is described:

1. Prepare the sample by choosing adequate protein concentration, buffer and cell path.
2. Purged the system with nitrogen for at least 5 min before switching on the lamp. Leave the lamp on for 15 min before start measuring (see Note 15).
3. Set the acquisition parameters.
4. Acquire buffer spectrum. Check for interferences in the far-UV region.
5. Acquire sample spectrum.

6. Correct baseline by calculating sample-buffer difference spectrum.
7. Transform CD data (millidegrees) to mean residue ellipticity (degrees cm^2/dmol) or LD data to molar absorptivity (M^{-1}/cm) or Dichroic ratio spectra (see Note 16).
8. Use the appropriate software package for the analysis of far-UV CD or LD spectral data (see Subheading 3.1.3).

3.1.3. Analysis of Far-UV CD and LD Spectral Data

After the far-UV CD spectrum (250–190 nm) of a protein has been acquired and the baseline subtracted, the data can be analyzed for secondary structure composition. Several analytical algorithms for deconvolution of protein circular dichroism spectra are available and their suitability depends on the aim of the study (38–47) (see Notes 17 and 18). In amyloidogenic proteins, the quantification of β-sheet elements by deconvolution methods presents several inherent limitations and its accuracy is limited (around 0.75) (9, 10, 16). However, these algorithms are very reliable for monitoring changes in the conformation of proteins under different conditions such as denaturation studies, unfolding experiments, helix induction by TFA, etc. (see Note 19).

A convenient way for the analysis of protein CD spectra is the use of the on-line server DichroWeb ((http://dichroweb.cryst.bbk.ac.uk/html/home.shtml), hosted by the Department of Crystallography at Birkbeck College, University of London), which incorporates five respected and effective algorithms (Contin-LL, Selcon 3, CDSSTR, VARSLC, and K2d) to calculate protein secondary structure content (48) (see Note 20).

The analysis of experimental LD spectra poses an even more difficult challenge than CD spectra due to overlapping transitions that give raise to mixed LD signals and loss of signals. Recently, the development of web interface DichroCalc at the University of Nottingham (http://comp.chem.nottingham.ac.uk/dichrocalc/) has facilitated the access to assignments and calculations with access to PDB files for reference spectra calculations (49).

3.2. Basic Protocols for FTIR Analysis of Amyloids

3.2.1. Basic FTIR Setup Requirements

1. Amyloid source in noninterfering buffers for FTIR measurements (avoid components having amide groups) (see Note 21).
2. D_2O for HxD exchange.
3. For transmission measurements: CaF_2 or BaF_2 windows, Teflon spacers, and the universal transmission cell holder.
4. For ATR-FTIR: Ge, ZnSe, or diamond crystals and the ATR accessory (mirrors for beam focusing and crystal holder) (see Notes 22 and 23).
5. FTIR instrumentation. The main suppliers of FTIR spectrometers provided the specifications and accessories required for the use with biological samples (detectors and purge) (see Note 24).

6. Software for FTIR data analysis. The software for analysis can be supplied with the equipment and a curve fitting routine, acquired from Grams or Spectra-Calc (Galactic Industries), or obtained from specialists in the field. Two dimensional IR correlation analysis can be done with the free 2D-Shige program (http://sci-tech.ksc.kwansei.ac.jp/~ozaki/e_2D.htm; developed by S Morita and Y. Ozaki).

3.2.2. Preparation of Protein/Peptide Solutions

Prepare the sample by choosing appropriate protein concentration, buffer, and measuring mode:

1. Dialyze the peptide/protein of interest in a buffer free of amides and with low ionic strength (5 mM) or use an HFIP stock solution free from interfering substances (see Note 25).
2. For transmission, load 10–25 μL onto the window dried under N_2-stream. Repeat the process until ensuring >125 μg of protein. Add 25 μl D_2O and resuspend cautiously to avoid bubble formation, place the spacer (25–50 μm) and the upper window and seal the cell in its holder.
3. For ATR, load onto the crystal a protein solution volume enough to ensure >50 μg of protein and dry under N_2-stream. Once the cell is sealed, proceed to carry out the HxD exchange by passing D_2O-saturated N_2 (see Note 26).

3.2.3. Spectral Acquisition

FTIR spectrometers are supplied with several optimized default parameter sets. Set the acquisition parameters as follows: nominal resolution: 0.5 cm^{-1}, wavenumber range: 4,000–1,000 cm^{-1}, and number of scans: 1,000.

1. Acquire the background interferogram or spectrum using the same parameters that will be used for samples. Background interferogram is measured with no sample in the sample chamber and is stored automatically by the spectrometer. Subsequently, the absorbance spectra of samples will be obtained by rationing its interferogram with the background one to compensate the lamp energy peaks and CO_2 and H_2O bands.
2. Acquire the water vapor spectrum. Water vapor contribution appearing as spikes in the amide I band region must be subtracted before mathematical analysis to avoid undesired artifacts.
3. Acquire sample and buffer spectra. For two-dimensional analysis, define a perturbation to induce a spectral fluctuation in the IR spectra and collect the series of spectra. Perturbation can be thermal, time, concentration, etc.

3.2.4. Spectral Analysis

Spectral analysis requires a preliminary processing of the whole spectrum, for the subtraction of the buffer contribution and the correction of the water vapor noise. Before translating the information

Table 1
Significant vibrations of amino acid side chain overlapping the secondary structure signatures. Vibration from side chains in the 1,700–1,600 cm^{-1} can be very perturbing if the sequence under study is enriched in any of the amino acids with IR active side chains

Amino acid	Vibrating group	Wavenumber (cm^{-1})
Arg	$-CN_3H_5^+$	1,673/1,633
Lys	$-NH3^+$	1,629/1,526
Asn	$-C{=}O/-NH_2$	1,678/1,622
Gln	$-C{=}O/-NH_2$	1,670/1,610

contained in the spectrum into secondary structure, special caution with the sequence under study should be taken given possible overlaps (Table 1).

Secondary Structure Determination from the Amide I′ Band: Resolution Enhancement and Curve Fitting

1. Delimit the amide I′band (region between 1,700 and 1,600 cm^{-1}).
2. Using the appropriate program routine, perform a Fourier self-deconvolution of this region, choosing a resolution enhancement factor between 1.0 and 2.0 and a suitable smoothing factor. Alternatively, obtain the second derivative spectrum to maximized peak position. For some cases as in peptides involving two states or two populations, bands appeared resolved in the original spectra (Fig. 1).
3. Determine the number, position, amplitude, and width of the Lorentzian components appearing in the resolution enhanced spectra (normally from seven to nine components) using a curve-fit routine.
4. Use the previous set of Lorentzian as initial values and perform nonlinear least-squares fit to the original spectrum. Choose the Levenberg-Marquardt method, leave all the parameters free to vary and estimate the residual.
5. Assign the obtained bands to the secondary structure elements as described (50).

Two-Dimensional Correlation Analysis

1. Generate the file with a .csv format containing the series of the FTIR spectra that can be either the original or the Fourier self-deconvoluted.
2. Set a reference spectrum (generated an average or mean spectra) and calculate the synchronous and asynchronous 2D maps.

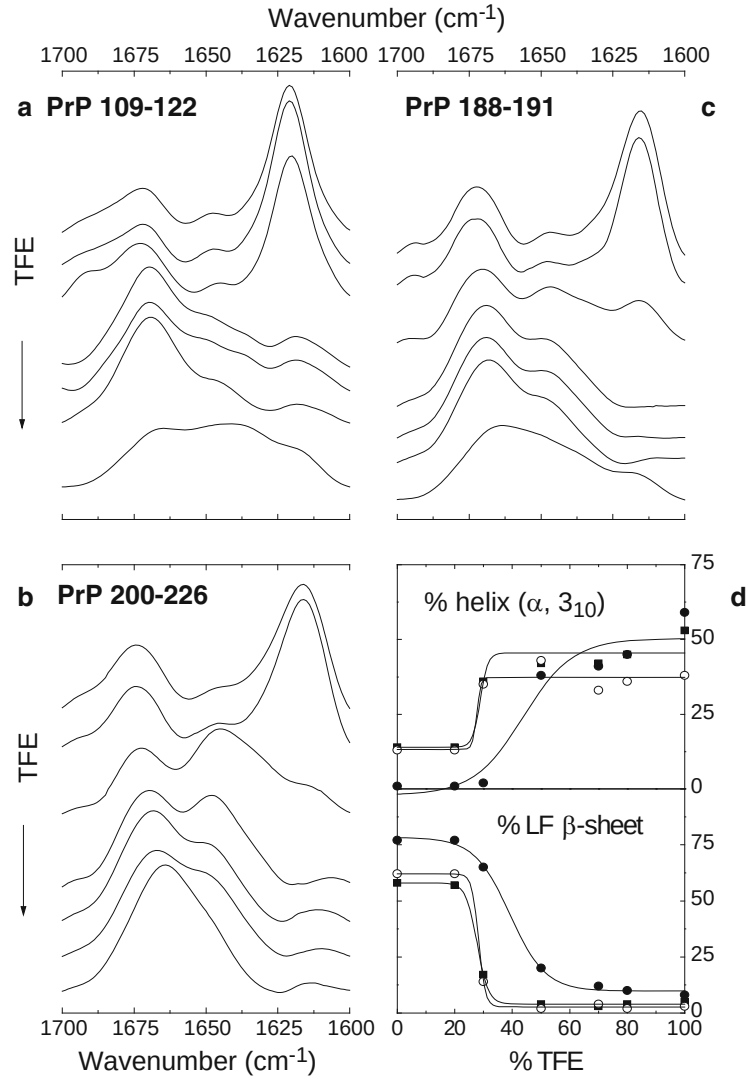

Fig. 1. Modulation of the secondary structure of amyloid forming sequences using TFE:H_2O mixtures. Changes in the amide I′ band of synthetic peptides corresponding to three different PrP regions: 109–122 (**a**), 200–226 (**b**), and 188–191 (**c**) as a function of the percentage of TFE in the solution. (**d**) Variation of the helical (*top panel*) and low frequency β-sheet (*bottom panel*) content with TFE content of the solvent for three different PrP regions: 109–122 (*solid circle*), 188–191 (*solid square*), and 200–226 (*open circle*). Helical content was obtained as the area of the bands occurring at the 1,662–1,645 cm^{-1} relative to the total amide I′ band area. For low frequency β-sheet, its content was obtained from the relative area of bands occurring in the 1,627–1,613 cm^{-1} referred to that of the total amide I′ band.

3. Visualize the 2D-IR maps using appropriate softwares such as *Origin* (Microcal Systems) to find the maximum and minimum intensities. For increasing the sensitivity, intensity values can be multiplied by 2 and draw 16–30 contour lines.

4. The synchronous 2D correlation spectrum informs on the simultaneous changes in spectral intensities measured at frequencies ν_1 and ν_2. In this spectrum, correlation peaks appear at both diagonal and off-diagonal peaks (auto-peaks and cross-peaks, respectively). Auto-peaks correspond to changes in intensity induced by the perturbation and they are always positive. The cross-peaks indicate in-phase relationships between two bands.
5. The asynchronous spectrum informs on sequential, or unsynchronized, changes in spectral intensities measured at ν_1 and ν_2. This spectrum has no auto-peaks, but cross-peaks located at off-diagonal positions. The cross-peaks will be positive if the change in ν_1 occurs earlier than that in ν_2, and negative in the opposite case.

4. Notes

1. Cuvettes made from quartz of the highest purity and homogeneity is recommended. Synthetic quartz produced from a silicon compound such as Quartz Suprasil from Heraeus Quarzglas GmbH is employed in the manufacture of QS Hellma cuvettes (www.hellma-worldwide.de) is a good option for far-UV CD cuvettes. Alternative, good quality cuvettes can be purchased from Spectrocell (www.spectrocell.com).
2. Cylindrical cuvettes, when sealed, offer the lowest birefringence and the best quality spectra, but offer limitations in titrations, parallel absorption measurements, and recovery. Rectangular cuvettes are more versatility and best suited for general applications.
3. Larger cells (0.5–10 mm) can be used if a low protein concentration is needed to avoid aggregation. The choice of width will be determined by the need to obtain an optimum total absorbance of the sample at the desired protein concentration.
4. Couette flow cells usually refer to special narrow-path cylindrical cells, where the sample solution is subjected to a viscous drag produced by two coaxial cylinders one of which is rotating, resulting in the orientation long-biomolecule chains. This type of cells is not generally commercially available and has to be custom-made for each specific spectropolarimeter. Recently some specific cells for Jasco spectropolarimeters, designed according to the work of Dafforn and collaborators (31), are sold by Kromatek (Kromatek, Essex, UK, http://www.kromatek.co.uk/).
5. To achieve the desired pH, prepare the proper ratios of the mono- and dibasic forms of potassium phosphate. Do not use

HCl to adjust pH or NaCl as a counter ion, since chloride ions will interfere with CD or LD in the lower UV. Instead use Na_2SO_4, KF, or NaF. For salt enrichment, KF and NaF are recommended for pH above 5, but fluoride salts should never be used below pH 5, because HF traces will damage the quartz cuvettes.

6. If the protein is dissolved in unsuitable buffer, it should be dialyzed against 10 mM potassium phosphate or other appropriate buffer.
7. This will ensure removal of contaminants and appropriated buffer conditions for analysis. As any additional protein or peptide will contribute to the CD signal, the protein to be studied should be as pure as possible, and the protein solution should contain only those chemicals required to maintain protein stability/solubility at the lowest concentrations possible.
8. Even in the absence of turbidity, soluble aggregates may cause light scattering and spectrum distortion, and therefore aggregation should be ruled out by performing the experiments at different concentrations of by using size exclusion chromatography before analysis.
9. A detailed description on how to define initial concentration for analysis is described elsewhere (50).
10. To improve the signal to noise ratio, particulate matter should be removed from the solution by filtering through a 0.2- or 0.45-μm filter or by centrifugation.
11. For LD analysis, spectropolarimeters have to be equipped with an LD mode.
12. Large slit bandwidth will give higher signal to noise ratios but will decrease resolution and distort the spectrum.
13. Signal to noise ratio increases with the square root of the time constant and this should be kept as large as possible.
14. Usually, obtaining a good quality spectrum requires more than 1 h, to avoid spectral drift it is better to run faster spectra and average them.
15. To prevent damage to the CD optics, caused by the ozone generated during the measurement, it is necessary to purge the instrument by flushing continuously with N_2 (99.999% pure) at a flow rate of 15–20 l/min.
16. CD is measured as *observed ellipticity* (θ) in millidegrees units. For secondary structure assessment, this value must be transformed into *mean residue ellipticity* ($(\theta)_{MRE}$) in degrees cm^2/dmol, by using the formula $(\Theta)_{MRE} = \theta\,(10 \times N \times c \times l)$, where θ is the observed ellipticity, N the number of amino acids of the protein, c the molar concentration of the protein, and l the cell path in cm. LD is measured as Molar Absorptivity in M^{-1}/cm

units or as a Dichroic ratio or reduced LD data derived from parallel and perpendicular absorption spectra.

17. As these methods rely on the comparison to reference structures in a residue molar basis, the analysis requires the protein concentration as an input parameter; and therefore the analyst must know precisely the concentration, molecular weight, and number of residues of the protein analyzed. Recently, mathematical methods relatively independent of concentration have been devised (51).
18. For the determination of protein conformation in solution, use SELCON, CDNN, or K2D algorithms. For determination of polypeptide conformation having a suitable polypeptide set of references, or estimation of relative changes (mutations, ligands, and perturbants), use LINCOMB. For evaluating the number of folding states giving rise to a set of spectra, use CCA or SVD algorithms.
19. Conformational shifts involving as few as ten amino acids may be readily detectable by CD spectroscopy.
20. Be aware that to use the server, an account must be obtained by signing up an on-line form or contacting the authors following the instructions provided.
21. Synthetic peptides can carry TFA traces that appear as a neat band at 1,672 cm^{-1}. To remove TFA, cycles of lyophilization and resuspension in 10 mM HCl has been shown satisfactory. Caution on the pH of the solution after buffer usage must be taken.
22. Barium fluorite should not be used at low pH. ZnSe should not be used with strong acids and alkalis, or complexing agents such as ammonia or EDTA. Ge has a high refractive index and it is mainly used for compounds with strong absorption bands. Diamond crystals are suited for a wide range of samples including acids, bases, and oxidizing agents; however, they present intrinsic absorption from 2,300 to 1,800 cm^{-1}.
23. To compensate for potential artifacts due to differential absorption of proteins on the surface of ATR, the FTIR spectrophotometer should have an ATR conversion mode that this effect.
24. Purging of the instrument with good quality dry air or oxygen-free nitrogen should be used to remove ambient moisture that will interfere with the analysis. Water vapor and carbon dioxide in air, as well as dust on mirrors of the spectrometer can generate intense infrared absorption bands. Loading the sample in the sample compartment involves opening the sample compartment; therefore it is important to allow the purging for 15 min before acquiring data.
25. A detailed description of sample preparation has been described elsewhere (50).

26. This is conveniently done by placing in the close sample compartment a shallow open container filled with D_2O under a N_2-stream.

Acknowledgments

This work was supported by grants from the Ministerio de Ciencia e Innovación (BFU2009-07971), Fundación CIEN-Fundación Reina Sofía and from the Fundación CIEN-ISCIII (MPY 1308/08).

References

1. Kelly, J. W. (1998) The alternative conformations of amyloidogenic proteins and their multi-step assembly pathways. *Curr Opin Struct Biol* **8**, 101–106.
2. Rochet, J. C. & Lansbury, P. T. Jr (2000) Amyloid fibrillogenesis: themes and variations. *Curr Opin Struct Biol* **10**, 60–68.
3. Sipe, J. D., Benson M. D., Buxbaum J. N., Ikeda S., Merlini G., Saraiva M. J., Westermark P. (2010) Amyloid fibril protein nomenclature: 2010 recommendations from the nomenclature committee of the International Society of Amyloidosis. *Amyloid* **17**, 101–104.
4. Pedersen, J. S., Andersen, C. B., Otzen D. E. (2010) Amyloid structure--one but not the same: the many levels of fibrillar polymorphism. *FEBS J.* **277**, 4591–4601.
5. Uversky, V. N. (2010). Mysterious oligomerization of the amyloidogenic proteins. *FEBS J.* **277**, 2940–2953.
6. Greenwald, J., Riek R. (2010). Biology of amyloid: structure, function, and regulation. *Structure* **18**, 1244–1260.
7. Dafforn T. R., Rodger A. (2004) Linear dichroism of biomolecules: which way is up? *Curr Opin Struct Biol.* **14**, 541–546.
8. Woody, R. W. (1972) The circular dichroism of aromatic polypeptides: theoretical studies of poly-L-phenylalanine and some para-substituted derivatives. *Biopolymers* **11**, 1149–1171.
9. Johnson, W. C. (1990) Protein secondary structure and circular dichroism: a practical guide. *Proteins* **7**, 205–214.
10. Woody, R. W. (1995) Circular dichroism. *Meth. Enzymol.* **246**, 34–71.
11. Greenfield, N. J. (2006) Using circular dichroism spectra to estimate protein secondary structure. *Nat Protoc.* **1**, 2876–2890.
12. Greenfield, N. J. (2006) Analysis of the kinetics of folding of proteins and peptides using circular dichroism. *Nat Protoc.* **1**, 2891–2899.
13. Bulheller B. M., Rodger A., Hirst J. D. (2007) Circular and linear dichroism of proteins. Phys *Chem Chem Phys.* **9**, 2020–2035
14. Whitmore L., Wallace B. A. (2008) Protein secondary structure analyses from circular dichroism spectroscopy: Methods and reference databases. *Biopolymers* **89**, 392–400.
15. Bulheller, B. M., Rodger, A., Hicks, M. R., Dafforn, T. R., Serpell, L. C., Marshall, K. E., Bromley, E. H., King, P. J., Channon, K. J., Woolfson, D. N., Hirst, J. D. (2009) Flow linear dichroism of some prototypical proteins. *J Am Chem Soc.* **131**, 13305–13314.
16. Manavalan, P. and Johnson, W. C. Jr. (1987) Variable selection method improves the prediction of protein secondary structure from circular dichroism spectra. *Anal. Biochem.* **167**, 76–85.
17. Adachi, R., Yamaguchi, K., Yagi, H., Sakurai, K., Naiki, H., Goto Y. (2007) Flow-induced alignment of amyloid protofilaments revealed by linear dichroism. *J Biol Chem.* **282**, 8978–8983.
18. Rodger, A., Marrington, R., Geeves, M. A., Hicks, M., de Alwis, L., Halsall, D. J., Dafforn, T. R. (2006) Looking at long molecules in solution: what happens when they are subjected to Couette flow? *Phys Chem Chem Phys.* **8**, 3161–3171.
19. Marrington, R., Dafforn, T. R., Halsall, D. J., Rodger, A. (2004) Micro-volume couette flow sample orientation for absorbance and fluorescence linear dichroism. *Biophys J.* **87**, 2002–2012.
20. Juárez, J., Taboada, P., Mosquera, V. (2009) Existence of different structural intermediates

on the fibrillation pathway of human serum albumin. *Biophys J.* **96**, 2353–2370.

21. Smith, B. C. (ed.) (1996) Fundamentals of Fourier Transform Infrared Spectroscopy. CRC Press, Boca Raton, Florida.
22. Miyazawa, T., Blout, E. R. (1961) The Infrared spectra of polypeptides in various conformations: amide I and II bands. *J Am Chem Soc* **83**, 712–719.
23. Krimm, S., Bandekar, J. (1986) Vibrational spectroscopy and conformation of peptides, polypeptides, and proteins. *Adv Protein Chem* **38**, 181–364.
24. Kauppinen, J. K., Moffatt, D. J., Mantsch, H. H. and Cameron, D. G. (1986)Fourier Self-Deconvolution: A Method for Resolving Intrinsically Overlapped Bands. *Appl. Spectrosc.* **35**, 271–276.
25. Yang, W. J., Griffiths, P. R., Byler, D. M. and Susi, H. (1985) Protein Conformation by Infrared Spectroscopy: Resolution Enhancement by Fourier Self Deconvolution. *Appl. Spectrosc.* **39**, 282–287.
26. Goormaghtigh, E., Cabiaux, V., and Ruysschaert, J. M. (1994) Determination of soluble and membrane protein structure by Fourier Transform Infrared Spectroscopy: I. Assignments and model compounds. *Subcell. Biochem.* **23**, 329–362.
27. Dousseau, F. and Pezolet, M. (1990) Determination of the Secondary Structure Content of Proteins in Aqueous Solutions from Their Amide I and Amide II Infrared Bands. Comparison between Classical and Partial Least-Squares Methods. *Biochemistry* **29**, 8771–8779.
28. Venyaminov S. Y., and Kalnin N. N. (1990) Quantitative IR spectrophotometry of peptide compounds in water (H2O) solutions. I. Spectral parameters of amino acid residue absorption bands. *Biopolymers* **30**, 1243–1257
29. Sarver, R. W., and Krueger, W. C. (1991) Protein Secondary Structure from Fourier Transform Infrared Spectroscopy: A Data Base Analysis. *Anal. Biochem.* **194**, 89–100.
30. Oberg K. A., Ruysschaert J. M., Goormaghtigh E. (2004) The optimization of protein secondary structure determination with infrared and circular dichroism spectra. *Eur J Biochem* **271**, 2937–2948.
31. Goormaghtigh, E., Gasper, R., Bénard, A., Goldsztein, A., Raussens, V. (2009) Protein secondary structure content in solution, films and tissues: redundancy and complementarity of the information content in circular dichroism, transmission and ATR FTIR spectra. *Biochim Biophys Acta.* **1794**, 1332–1343.
32. Hiramatsu, H., Kitagawa, T. (2005) FT-IR approaches on amyloid fibril structure. *Biochim Biophys Acta.* **1753**, 100–107.
33. Noda, I., Dowrey, A. E., Marcott, C., Story, G. M., Ozaki, Y. (2000). Generalized two-dimensional correlation spectroscopy. *Appl. Spectrosc.* **54**, 236A–248A.
34. Ganim, Z., Chung, H. S., Smith, A. W., Deflores, L. P., Jones, K. C., Tokmakoff, A. (2008) Amide I two-dimensional infrared spectroscopy of proteins. *Acc Chem Res.* **41**, 432–441.
35. Strasfeld, D. B., Ling, Y. L., Gupta, R., Raleigh, D. P., Zanni, M. T. (2009) Strategies for extracting structural information from 2D IR spectroscopy of amyloid: application to islet amyloid polypeptide. *J Phys Chem B.* **113**, 15679–15691.
36. Shim, S. H., Gupta, R., Ling, Y. L., Strasfeld, D. B., Raleigh, D. P., Zanni, M. T. (2009) Two-dimensional IR spectroscopy and isotope labeling defines the pathway of amyloid formation with residue-specific resolution. *Proc Natl Acad Sci USA.* **106**, 6614–6619.
37. Paquet, M. J., Laviolette, M., Pezolet, M., Auger, M. (2001). Two-dimensional infrared correlation spectroscopy study of the aggregation of cytochrome c in the presence of dimyristoylphosphatidylglycerol. *Biophys. J.* **81**, 305–312
38. Dafforn, T. R., Rajendra, J., Halsall, D. J., Serpell, L. C., Rodger, A. (2004). Protein fiber linear dichroism for structure determination and kinetics in a low-volume, low-wavelength couette flow cell. *Biophys J.* **86**, 404–410.
39. Greenfield, N., and Fasman, G. D. (1996) Computed circular dichroism spectra for the evaluation of protein conformation. *Biochemistry* **8**, 4108–4116.
40. Sreerema, N., and Woody, R.W. (1993) A self-consistent method for the analysis of protein secondary structure from circular dichroism. *Anal. Biochem.* **209**, 32–44.
41. Sreerema, N., Venyaminov, S. Y., and Woody, R. W. (1999) Estimation of the number of helical and strand segments in proteins using CD spectroscopy. *Protein Sci.* **8**, 370–380.
42. Provencher, S.W., and Glockner, J. (1981) E stimation of globular protein secondary structure from circular dichroism. *Biochemistry* **20**, 33–37.
43. Van Stokkum, I. H. M., Spoelder, H. J. W., Bloemendal, M., Van Grondelle, R., and Groen, F. C. A. (1990) Estimation of protein secondary structure and error analysis from CD spectra. *Anal. Biochem.* **191**, 110–118.
44. Compton, L. A., and Johnson, W. C., Jr. (1986) Analysis of protein circular dichroism spectra

for secondary structure using a simple matrix multiplication. *Anal. Biochem.* **155**, 155–167.

45. Manavalan, P., and Johnson, W. C., Jr. (1987) Variable selection method improves the prediction of protein secondary structure from circular dichroism spectra. *Anal. Biochem.* **167**, 76–85.
46. Sreerama, N., and Woody, R. W. (2000) Estimation of protein secondary structure from CD spectra: Comparison of CONTIN, SELCON and CDSSTR methods with an expanded reference set. *Anal. Biochem.* **287**, 252–260.
47. Andrade, M. A., Chacón, P., Merelo, J. J. and Morán, F. (1993) Evaluation of secondary structure of proteins from UV circular dichroism using an unsupervised learning neural network. *Prot. Engineering* **6**, 383–390.
48. Whitmore L., Wallace B. A. (2004) DICHROWEB, an online server for protein secondary structure analyses from circular dichroism spectroscopic data. *Nucleic Acids Res.* **32**, W668–673.
49. Bulheller B. M., Hirst J. D. (2009) DichroCalc--circular and linear dichroism online. *Bioinformatics* **25**, 539–540.
50. Calero, M., Gasset, M. (2005) Fourier transform infrared and circular dichroism spectroscopies for amyloid studies. *Methods Mol Biol.* **299**, 129–151.
51. McPhie, P. (2008) Concentration-independent estimation of protein secondary structure by circular dichroism: a comparison of methods. *Anal Biochem.* **375**, 379–381.

Chapter 6

Quasielastic Light Scattering Study of Amyloid β-Protein Fibrillogenesis

Aleksey Lomakin and David B. Teplow

Abstract

Quasielastic light scattering (QLS) spectroscopy is a noninvasive optical method for studying the dynamic properties of macromolecular solutions. Its most important application is the determination of diffusion coefficients, from which the sizes of particles in solution may be estimated. The technique thus is particularly useful for monitoring assembly (polymerization and aggregation) reactions without the need for removing aliquots from the assembly system or disrupting the assembly process in any other way. We discuss here two of the most important aspects of QLS: (1) measurement of the correlation function of the scattered light intensity and (2) the use of this correlation function to reconstruct the distribution of sizes of the scattering particles. The ability to monitor the temporal evolution of particle size provides a powerful tool for studying protein assembly. We illustrate here how QLS has been applied to elucidate features of the oligomerization and fibrillogenesis of the amyloid β-protein, Aβ, thought to be the causative agent of Alzheimer's disease.

Key words: Dynamic light scattering, Hydrodynamic radius, Aggregation, Fibrillogenesis, Amyloid, Alzheimer's disease

1. Introduction

Quasielastic light scattering (QLS), also known as dynamic light scattering (DLS), is an optical method for the determination of diffusion coefficients of particles in solution (1–3). The QLS method is rapid, sensitive, noninvasive, and quantitative. QLS measures the fluctuations in intensity of light scattered from a sample irradiated by a laser. These fluctuations contain information about the motion of the scattering particles, thus allowing determination of diffusion coefficients of the particles in the sample solution. The diffusion coefficients depend on particle size and shape and also are affected by inter-particle interactions. The ability to monitor the temporal evolution of these parameters makes

Einar M. Sigurdsson et al. (eds.), *Amyloid Proteins: Methods and Protocols*, Methods in Molecular Biology, vol. 849,
DOI 10.1007/978-1-61779-551-0_6,

QLS a useful tool for studying particle aggregation and, in particular, for monitoring protein assembly.

We discuss here the application of QLS to the study of protein assembly. Abnormal protein assembly is associated with a number of neurodegenerative diseases, including Alzheimer's, Huntington's, Parkinson's, and prion diseases (for a review, see (4)), as well as a variety of systemic amyloidoses (5). In each case, proteins that exist normally in a soluble, unaggregated state form oligomers and fibrils that cause cell and tissue injury, generally leading to death. QLS can monitor protein aggregation with high sensitivity and resolution (6), allowing determination of fundamental parameters of protein self-assembly, including rates of fibril nucleation and elongation, number of monomers in a fibril, fibril length, and activation energy for monomer addition. Importantly, the ability to determine these parameters enables structure-activity studies that suggest physical mechanisms responsible for sporadic and familial (mutation-induced) forms of AD (7) and other amyloidosis. This knowledge is critical for the conception and execution of knowledge-based therapeutic strategies.

2. General Principles of QLS

At a point of observation, the scattered electromagnetic field is a sum of electromagnetic waves scattered by all particles illuminated by the incident wave:

$$\mathbf{E} = \sum_k \mathbf{E}_k \exp(-i\omega t + i\mathbf{q}\cdot\mathbf{r}_k), \tag{1}$$

where E_k is the amplitude of the scattered wave produced by the kth particle located at position $\mathbf{r}_k$, and ω is the frequency of light, $\omega = c / \lambda_0$, where c is the speed of light and λ_0 is the wavelength of the incident light in a vacuum. The vector $\mathbf{q}$, called the "scattering vector," is a fundamental characteristic of any scattering process (Fig. 1). In a uniform medium, in which each point in space produces a wave with the same amplitude, the sum in Eq. 1 equals zero when $q \neq 0$ and the light only propagates in the forward direction, where $q = 0$. Scattering thus only occurs from medium inhomogeneities, such as those caused by solute particles or by density fluctuations in an otherwise uniform solvent.

The intensity I of the scattered light is proportional to the square of the amplitude of the electromagnetic field, that is:

$$I = A_0 \left| \sum_k \mathbf{E}_k \exp(i\mathbf{q}\cdot\mathbf{r}_k) \right|^2 . \tag{2}$$

Here A_0 is a coefficient that depends on the geometry of light collection. Equation 2 describes mathematically the interference

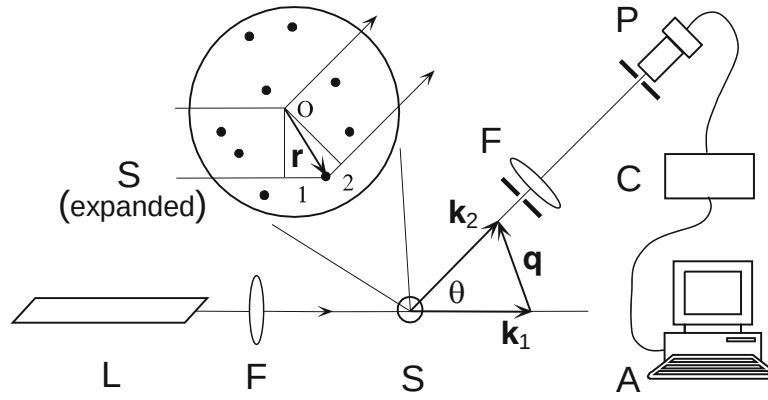

Fig. 1. Block scheme of the QLS setup. Laser (L); Focusing and collecting optics (may include optic fibers) (F); Sample cuvette (S); Photodetector (P); Correlator (C); data Analysis workstation (A). The scattering vector **q** (see expanded view of S): The path traveled by a wave scattered at the point with radius vector **r** differs from the path passing through the reference point 0 by two segments, 1 and 2, with lengths l_1 and l_2, respectively. The phase difference is $\Delta\varphi = k(l_1 + l_2)$, where $k = 2\pi n / \lambda_0$ is the absolute value of the wave vector and n is the refractive index of the scattering media. The segment l_1 is a projection of **r** on the wave vector $\mathbf{k}_1$ of the incident beam, i.e. $kl_1 = \mathbf{k}_1\mathbf{r}$. Similarly, $kl_2 = \mathbf{k}_2\mathbf{r}$, where $\mathbf{k}_2$ is a wave vector of the scattered light. Thus $\Delta\varphi = (\mathbf{k}_1 - \mathbf{k}_2)\mathbf{r}$. The vector $\mathbf{q} = \mathbf{k}_1 - \mathbf{k}_2$ is called the scattering vector. The absolute value of **q**, $q = 4\pi n / \lambda_0 \sin\theta / 2$, where θ is the angle of scattering.

pattern, or "speckles" produced by waves scattered by a set of scattering particles located at positions $\mathbf{r}_k$. As these particles move, the intensity varies with time around its average value, $I_0 = \sum I_k$, where $I_k = A_0 \mid \mathbf{E}_k \mid^2$ is the intensity of light scattered by the kth particle.

The intensity of scattering by an individual particle, I_k, is proportional to Δn^2, where Δn is the difference between the refractive index of the particle and that of the media. I_k also depends on particle mass and shape. Let us consider an aggregate composed of m monomers, each producing a scattered electromagnetic wave $\mathbf{E}_0$. If the size of the aggregate is small, so that each $\mathbf{q}\cdot\mathbf{r}_k$ in Eq. 2 is essentially the same, then for this aggregate $\mathbf{E}_k = m\mathbf{E}_0$. The intensity of the light scattered by the small aggregate thus is proportional to the square of its molecular weight. The quadratic dependence of scattering intensity on the mass of the scatterer is the basis for the optical determination of the molecular weight of macromolecules and for various turbidimetry and nephelometry techniques. If an aggregate is not small as compared to the light wavelength, the destructive interference of waves scattered from different points in the particle reduces the intensity of light scattering by a factor of $\mid \alpha \mid^2 < 1$, where $\alpha(\mathbf{q})$ is an averaged value of the $e^{i\mathbf{q}\cdot\mathbf{r}_k}$ for all monomers. After being averaged over all possible orientations of the particle relative to the scattering vector **q**, the factor $\mid \alpha \mid^2$, the "structure factor," is obtained. A table of expressions for the

structure factors for particles of various shapes can be found elsewhere (8). The structure factor depends on the absolute value of the scattering vector, $q = 4\pi n / \lambda_0 \times \sin(\theta/2)$ and thus defines the angular dependency of the intensity of scattered light. The measurements of this angular dependency can, therefore, be used to determine the size and shape of sufficiently large scattering particles.

In QLS, the photodetector registers the random temporal fluctuations of the intensity of the scattered light, $I(t)$. The resulting correlation function of the intensity fluctuations is computed according to Eq. 3:

$$G^{(2)}(\tau) = \langle I(t) I(t+\tau) \rangle, \tag{3}$$

in which the angular brackets denote an average over time t. One common approach to calculate $G^{(2)}(\tau)$ is to store the numbers of photons registered by the photodetector within short consecutive time intervals Δt. These photon counts represent instantaneous values of the scattered light intensity. According to Eq. 3, to obtain the correlation function $G^{(2)}(\tau)$ at $\tau = n\Delta t$, the average product of counts n intervals apart should be determined. Modern correlators simultaneously accumulate several hundred of these products without loss of information, with Δt in the nanosecond range.

The intensity of the scattered light fluctuates due to the motion of the scattering particles, in particular through their diffusion. According to Eq. 1, electromagnetic waves scattered by a pair of individual particles have, at the observation point, a phase difference $\mathbf{q}\cdot\Delta\mathbf{r}$, where $\Delta\mathbf{r}$ is the vector distance between particles. As the scattering particles move over distance $\Delta x \approx q^{-1}$, the phases for all pairs of particles change significantly and the intensity of the scattered light becomes independent of its initial value. Thus the correlation time of the intensity fluctuations, τ_c, is the time required for a particle to move a distance q^{-1}. The laws of diffusive motion stipulate that the mean square displacement of a particle with a diffusion coefficient D over time Δt is characterized by the relationship $\Delta x^2 = 2D\Delta t$. Thus for $\Delta x \approx q^{-1}$, $\tau_c \approx 1/Dq^2$. Mathematical analysis of light scattering by a solution of many small, noninteracting particles leads to the following expression for the intensity correlation function defined by Eq. 3:

$$G^{(2)}(\tau) = I_0^2 \left(1 + \gamma \left| g^{(1)}(\tau) \right|^2 \right) \tag{4}$$

Here I_0 is the average intensity of the detected light and γ is the efficiency factor, which depends on the size of the scattering volume and the angle in which scattered light is collected. The key element in Eq. 4 is the instrument-independent, normalized field correlation function $g^{(1)}(\tau)$. For a particle undergoing diffusive Brownian motion, the field correlation function is a pure

exponential, $g^{(1)}(\tau) = e^{-\tau/\tau_c}$, with the decay time $\tau_c = 1/Dq^2$, in accord with the above considerations. When many scattering particles are present,

$$g^{(1)}(\tau) = \frac{1}{I_0}\sum_k I_k e^{-D_k q^2 \tau}. \quad (5)$$

In a monodisperse system, when all scatterers are the same, Eq. 5 reduces to $g^{(1)}(\tau) = e^{-Dq^2\tau}$ allowing immediate determination of the diffusion coefficient D from the experimental data by fitting $g^{(1)}(\tau)$ with a single exponential function. For a spherical particle, the relation between its radius R_h and its diffusion coefficient D is given by the Stokes–Einstein (9) equation:

$$R_h = \frac{k_B T}{6\pi\eta D}. \quad (6)$$

Here k_B is the Boltzmann constant, T is the absolute temperature, and η is solution viscosity. For nonspherical particles, Eq. 6 defines the *apparent* hydrodynamic radius of the particle. The apparent hydrodynamic radius can be calculated numerically, and in some cases analytically, for a variety of particle shapes (10).

In polydisperse systems, i.e., where a variety of particles is present in the solution, the reconstruction of the size distribution of scattering particles from an experimentally measured correlation function is a complex mathematical problem. The difficulty stems from the fact that different distributions with similar smoothed, averaged characteristics can fit the experimental data equally well. The simplest approach to deal with this difficulty is to assume the functional form of the distribution a priori (single modal, bimodal, Gaussian, etc.). The parameters of the assumed distribution that lead to the best fit to the experimental data then can be determined. The value of this method depends on the validity of the assumed distribution. It has the potential to "confirm" any a priori assumption made, especially if excessive numbers of free parameters are used in the fitting procedure. In practice, typical QLS data allow reliable determination of no more than three independent parameters of the size distribution of the scattering particles.

The cumulant method, in contrast, is free from bias introduced by a priori assumptions. In this approach, the focus is not on the shape of the distribution but instead on its average characteristics, such as the moments of the distribution or closely related quantities called cumulants (11), which are derivatives of the logarithm of the correlation function $g^{(1)}(\tau)$ at $\tau = 0$. The first cumulant of the distribution, the initial slope of the normalized correlation function, gives the average diffusion coefficient $\bar{D}$. Indeed, using Eq. 5, it is straightforward to show that:

$$-\frac{d}{d\tau}\ln g^{(1)}(\tau)\Big|_{\tau=0} = \frac{1}{I_0}\sum_k I_k D_k q^2 \equiv \bar{D}q^2. \quad (7)$$

The second cumulant of the distribution, the dispersion $\overline{\Delta D^2}$, can be obtained from the curvature (second derivative) of the initial part of the correlation function. The typical QLS experiment allows determination of the first moment, $\bar{D}$, with better than ±1% accuracy. The second moment, i.e., the width of the distribution $\overline{\Delta D^2}$, can be determined with an accuracy of ±5–10%. The third moment, which characterizes the asymmetry of the distribution, usually can be estimated with an accuracy of only about ±100%.

A third method, the regularization approach, combines the best features of both of the previous methods. It assumes that the distribution is an arbitrary, but smooth, function and seeks a non-negative distribution producing the best fit to the experimental data. The requirement of smoothness precludes spikes in the distribution, allowing a unique solution to the minimization problem. The choice of the smoothness parameter is the most important part of the regularization method. A well-chosen value for the smoothness parameter produces stable, reproducible results in repetitive measurements of the same correlation function. If the magnitude of the smoothing is too great, the distribution, though stable, will lack details. Regularization analysis can resolve a bimodal distribution with two narrow peaks of equal intensity, if the diffusion coefficients corresponding to these peaks differ by more than a factor of ~2.5. Figure 2 illustrates how the smoothing parameter

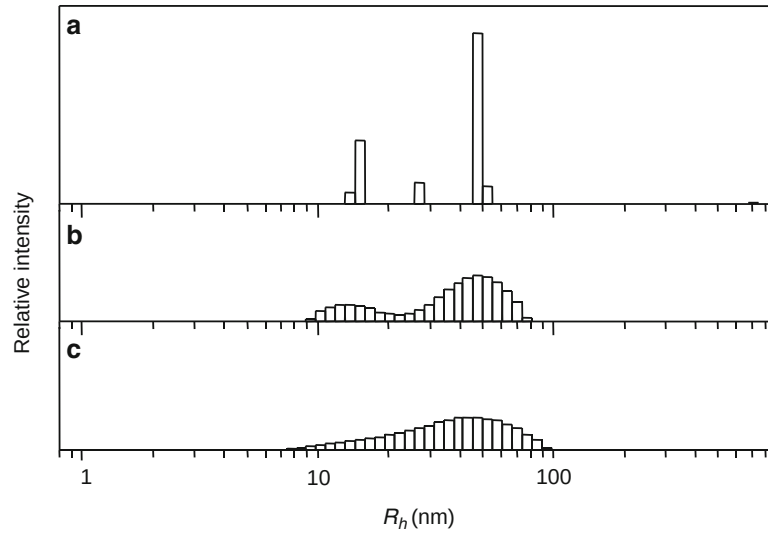

Fig. 2. Oligomer size distribution of Aβ. (**a**) A distribution computed with insufficient smoothing. Peaks positions in this distribution are not reliable, even though they provide the best fit to the experimental data. (**b**) A properly chosen regularization parameter allows observation of two populations, oligomers with hydrodynamic radii of 10–20 nm and their aggregates with average radius of ≈60 nm. This distribution is stable and does not vary significantly among measurements. The average deviation from the experimental data is only 0.5% larger than in (**a**). (**c**) An excessively smoothed distribution does not show separate oligomer and aggregate populations. This distribution is stable and also fits the experimental data well, with an average deviation only 3% more than in (**a**), but important details are not resolved.

choice can affect data interpretation. There are several regularization algorithms that differ in the specific mathematical implementation of the smoothness condition. One popular program is called CONTIN (12). We have developed and use the regularization procedure described in ref. (13). Our algorithm is also utilized in PrecisionDeconvolve software supplied with QLS instruments produced by Varian (USA) [formerly by Precision Detectors (USA)].

3. QLS Setup

A variety of QLS instruments is available commercially. Among the suppliers of QLS systems are ALV (Germany), Brookhaven Instruments (USA), Malvern Instruments (UK), and Wyatt Technology (USA). It is also possible to purchase the key elements of the QLS setup: laser, photodetector, and correlator separately and to build a custom system on an optical table using standard optical hardware. Our current QLS system uses a He–Ne laser (wavelength 633 nm and power 50 mW) from Coherent (USA) as a light source. The photodetector is an APT (avalanche photodiode) built into the PD4047 multitau correlator from Varian (USA). A 90° scattering geometry generally is used for monitoring the protein assembly.

There are several requirements that must be met to perform a successful QLS experiment. Conditioning of the incident laser beam is one important factor. The beam must produce a sufficient intensity of scattered light. If the photodetector count rate drops below 1 photocount per correlation time, the accuracy with which the correlation function can be measured decreases significantly. Conversely, an excessively intense incident beam may increase the temperature in the scattering volume. Because the diffusion coefficient is temperature-dependent, heating causes errors in its determination. To control for heating effects, especially when an accurate absolute measurement of scattering particle size is desired, one can do measurements at several intensities of the incident beam. The fluctuations in laser intensity make the factor I_0^2 in Eq. 4 dependent on delay time τ. This dependence affects the determination of $g^{(1)}(\tau)$, especially when the efficiency factor γ is small. At a given scattering angle, maximum scattering occurs in a plane perpendicular to the direction of the incident light polarization. Therefore, the incident beam should be polarized perpendicular to the plane formed by light source, sample, and photodetector. If the illuminating light is delivered via optical fiber, care should be taken to ensure that the vibrations of the fiber do no translate into significant fluctuations in the polarization of the incident beam.

To minimize the effect of stray light, the collecting optics is designed to pick up only light from a small collection volume

within the sample. The intersection of this volume and the volume illuminated by the incident beam is termed the "scattering volume." The scattering volume is an important factor in the QLS experiment. Reducing the scattering volume by focusing the incident beam, without significant loss of total scattering intensity, can be beneficial. Light from a smaller volume is coherent within a wider angle, allowing efficient collection of the scattered light from within a larger solid angle. If the light is collected within an angle wider than the coherence angle, averaging over several independently fluctuating speckles occurs. This reduces the efficiency factor γ in Eq. 4 and thereby only magnifies the effects of instability of the incident beam without improving the signal-to-noise ratio in the correlation function.

4. Large Aggregates and Intensity Spikes

As explained above, the intensity of scattering by an individual particle, I_k, is proportional the square of the molecular weight of the particle. For example, when dimer is formed it scatters twice as much as two monomers separately. When dense 1,000-particle aggregates (with a hydrodynamic radius about ten times that of a monomer) form, only 0.1%, by weight, of such aggregates produces the same scattering intensity as all the remaining monomers combined. The contribution of such an aggregate can be observed easily, which is one reason why the QLS method is well suited for detecting and studying the aggregation of particles in solution. However, these same considerations mean that even a small fraction of large impurities, for instance dust particles, can significantly affect light scattering. The easiest way to remove large impurities from solution is by filtration. Standard 0.22 μm filters are often too porous to be of use. We have found that 20 nm Anatop filters are satisfactory in most studies of protein aggregation. Centrifugation is another effective way to remove large impurities from the solution, provided that the sample is spun in the same sealed cuvette in which the QLS measurements will be done. Typical airborne dust can be pelleted in 30 min at $5{,}000 \times g$. However, "flaky" dust particles will not sediment by this procedure. A very useful, though cumbersome, method of sample purification is to utilize liquid chromatography to elute the desired fraction into a flow-through QLS cuvette (14).

During protein assembly in a closed system, the total amount of material does not change. Therefore, as the size of aggregates increases, the total particle number decreases. This often leads to a situation in which the number of aggregates, N, in the scattering volume is small. This can preclude accurate analysis of correlation

functions in QLS. Indeed, Eq. 4 for the intensity correlation function is applicable to the intensity fluctuations due to the temporal variations in the interference pattern produced by scattering particles as they move relative to each other. As Eq. 4 stipulates, $G^{(2)}(\tau) \sim I_0^2$. Equation 4 ignores intensity fluctuations caused by drifting of scattering particles into and out of the scattering volume. The relative fluctuation in the number of particles in the scattering volume is $N^{-1/2}$, the corresponding intensity fluctuations are I_0 / N, and the contribution of this effect in the intensity correlation function is therefore I_0^2/N. Thus, the relative magnitude of this contribution is proportional to $1/N$, and it may be ignored only when $N \gg 1$.

Fluctuations in the number of particles within the scattering volume can be measured using fluorescence correlation spectroscopy (FCS) (15). In FCS, the radiation is incoherent, factor γ in Eq. 4 is effectively zero, and only intensity fluctuations associated with position, orientation, or state of individual particles are measured. The FCS technique can be used to evaluate the size and concentration of particles in solution. However, in FCS, the intensity correlation function depends on the geometry of illumination and light collection and is difficult to analyze, especially in a multicomponent system.

In studies of systems in which aggregation occurs, it is important to recognize when the intensity fluctuations associated with the movement of individual particles through the scattering volume can significantly affect the analysis of the QLS data. This can be done by monitoring the scattered light intensity averaged over a relatively short time interval. In our measurements, we typically choose this time interval to be 1 s. Let us evaluate the expected "normal" QLS variations in the average intensity. The instantaneous relative amplitude of intensity fluctuations is given by factor γ in Eq. 4, and ideally can reach 100%. However, the correlation time of these fluctuations in the interference pattern is small. For example, a particle with a hydrodynamic radius of 15 nm in water at room temperature has, according to Eq. 6, a diffusion coefficient $D \approx 1.5 \times 10^{-11}$ m^2/s. For a He–Ne laser ($\lambda = 633$ nm) and a 90° scattering angle in water (the index of refraction $n = 1.33$), the scattering vector $q = 1.87 \times 10^{-7}$ m^{-1}. It is easy to estimate than that the intensity correlation time, $\tau = 1/(2Dq^2) \approx 10^{-4}$ s. For particles with smaller R_h, τ is proportionally smaller. The intensity averaged over 1 s thus includes at least 10^4 independent realizations of instant intensity each of no more than 100% in magnitude. We, therefore, expect typical average intensity fluctuations inherent for QLS to be less than 1%.

The same 1% level of fluctuations in the number of particles requires 10,000 particles ($N^{-1/2} = 0.01$) in the scattering volume. For comparison, for a 0.1 mM solution in a scattering volume of $10 \times 10 \times 10$ μm, we expect to have about 0.6×10^8 particles and

thus a practically negligible relative number of fluctuations of ≈10^{-4}. However, if in the process of aggregation, 0.1% of these monomers form 1,000-monomer aggregates, there will be only about 60 of these aggregates in the scattering volume and the relative intensity fluctuations will be 13%. The correlation function for these fluctuations depends on the size and geometry of the scattering volume. Under these circumstances, accurate determination of the sizes of particles in solution becomes difficult. Further increases in the size of aggregates and decreases in their numbers may eventually result in a situation in which most of the time there are no aggregates in the scattering volume. At rare time intervals, when an aggregate is inside the scattering volume, a large spike in intensity will be observed.

Figure 3 illustrates the manifestations of the aggregation process that leads to the formation of few large aggregates. The topmost panel shows data taken soon after sample preparation on May 13. We observe scattering from oligomers of R_H mostly between 15 and 30 nm, with some contributions from small particles, including monomers or dimers. The intensity fluctuations are "normal," i.e., below 1%. After 5 days of incubation, large 100 nm aggregates are formed. The contribution from the smaller 15–30 nm oligomers is still observable, but the scattering from monomers cannot now be detected. Intensity fluctuations have increased to about 10%, indicating that the number of large aggregates in the scattering volume is now small. After 14 days of incubation, very big aggregates are formed which now are too few to be found in the scattering volume all the time. Instead, they drift in and out of the scattering volume

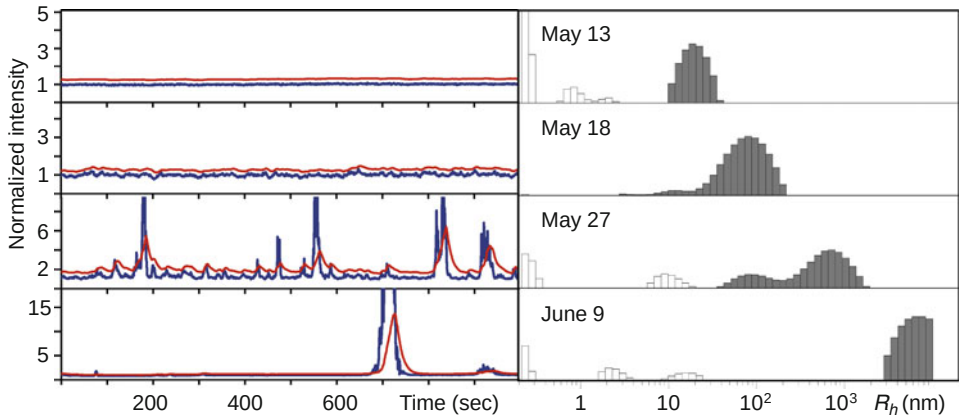

Fig. 3. Intensity spikes produced by large aggregates diffusing through a scattering volume. Normalized intensity fluctuations averaged over 1 s intervals during 1,000 s measurements (*left panels*) and the corresponding normalized size distributions (*right panels*) in an Aβ42 sample (concentration is 0.4 mM; data are from (16)). The panels show data immediately after sample preparation and then 5, 14, and 27 days later, from top to bottom. The date of measurements is shown in the distribution panels. In the *left panels*, the *blue lines* are intensity profiles and the *red lines* are intensity cutoff levels (see text). Note the changing scale in the normalized intensity and the fact that in the bottommost panel the main intensity spike is out of scale (it is actually >60 times the background intensity).

producing intensity spikes up to ten times the background scattering intensity from the sample. Finally, after about a month of incubation, very few very large aggregates are left in the solution. These aggregates produce huge intensity spikes when they occasionally enter the scattering volume.

When large aggregates are an integral part of a system and cannot be removed, or reform rapidly after filtration, "software dust filtering" can be done. This approach interrupts data accumulation during spikes in intensity caused by large particles passing through the scattering volume. Red lines in the intensity panels in Fig. 3 represent these intensity cutoff levels. When the intensity exceeds this level the data are discarded. In Fig. 3, the cutoff levels were set to be sliding average of the previous 10 s of measurements below the cutoff level. Some scattering from within intensity spikes was registered in this case to document the presence of large particles. If minimizing the effects of intensity spikes is desired, it can be beneficial to focus the laser beam to make the scattering volume as small as possible. Spikes in intensity associated with large particles in the scattering volume then become larger in intensity, but shorter in time and less frequent. This allows for better discrimination between these spikes and the regular intensity fluctuations.

Our in-house acquisition software can store correlator output every 0.1 s and later "replay" these measurements. This allows an effective exclusion of intensity spikes from the data analysis, leading to improvement in the quality of measurement of oligomer populations. Additionally, it is possible to obtain statistical information regarding spike frequency and intensity. This provides the means to quantify and to compare the process of formation of very large aggregates among different samples (17). It also is possible to determine the correlation function within the spikes. However, the interpretation of such correlation functions is very much dependent on the model adopted for the structure and dynamics of the aggregates.

5. QLS Monitoring of Fibril Assembly

The hydrodynamic radius of a small thin fibril with length L and diameter d, where $L >> d$ is approximately $R_h = L / \ln(L / 2d)$ (10). As fibrils grow in length, the diffusion of the fibril over distances of the order of q^{-1} becomes dependent on fibril orientation. The intensity of the scattering by a large fibril also depends on its orientation. As a result, the orientational diffusion of fibrils with length $L \geq q^{-1}$ ($q^{-1} \sim 100$ nm) plays an important role in QLS and produces a complex nonexponential correlation function even in monodisperse systems. These effects usually are subsumed into the definition of the apparent hydrodynamic radius of the fibril. In this

definition, the inverse average relaxation time of the multiexponential correlation function given by the left side of Eq. 7 is used to calculate the apparent diffusion coefficient, $\bar{D}$, which is then used in Eq. 6 to calculate R_h.

When the length of the fibril becomes comparable to the persistence length l_p (18), the effects of fibril flexibility must be taken into account. Flexibility adds even more complexity to the anisotropic diffusion and orientational dynamics of a fibril. Effects of flexibility on the correlation function have been discussed in detail by Maeda and Fujume (19). For the same length, a flexible fibril will have a smaller R_h than will a rigid one. Fibrils which are much longer than the persistence length form coils with apparent hydrodynamic radii of $R_h = 0.94\sqrt{l_p L}$. Fortunately, amyloid fibrils are rigid, thus their flexibility typically is not a factor in QLS experiments.

The most serious factor affecting the interpretation of QLS data on growing fibrils is fibril–fibril interaction. When the distance between fibrils is less than the fibril length (the "semidilute regime") fibrils cannot move perpendicular to their long axes because of caging by other fibrils. They only diffuse along their axes (20). The average distance between fibrils is $\sim N^{-1/3}$, where N is the number of fibrils in a unit volume, $N \approx \varphi / Ld^2$, and ϕ is the volume fraction occupied by fibrils. According to this estimate, $L \geq N^{-1/3}$ when $L \geq d / \sqrt{\varphi}$. Thus, regardless of the concentration, sufficiently long rigid fibrils always enter the semidilute regime. QLS on semidilute solutions of rods has been discussed by Zero and Pecora (21) and reviewed by Russo (22). Qualitatively, fibril–fibril interaction in a semidilute solution dramatically slows down diffusion of fibrils, and if unaccounted for, leads to gross overestimation of fibril length.

6. Amyloid β-Protein Self-Assembly

Amyloid β-protein (Aβ) fibrillogenesis plays a seminal role in the pathogenesis of Alzheimer's disease (4). QLS can be used to monitor quantitatively the temporal evolution of the fibril length distribution in solutions of synthetic Aβ, allowing determination of the rate constants for fibril nucleation and elongation (23, 24). Knowledge of these parameters allows modeling of the fibrillogenesis process and evaluation of the effect of chemical agents or solution condition on the process. Aβ fibrils have diameters $d \approx 6$–10 nm. At Aβ concentration $C = 0.1$ mM, Aβ fibrils occupy a volume fraction $\phi = 2 \times 10^{-3}$, and the semidilute regime in this solution occurs when fibrils are longer than 150 nm. This length is close to the estimated persistence length of Aβ fibrils (25) and is comparable to $q^{-1} \sim 100$ nm. These estimates imply that the

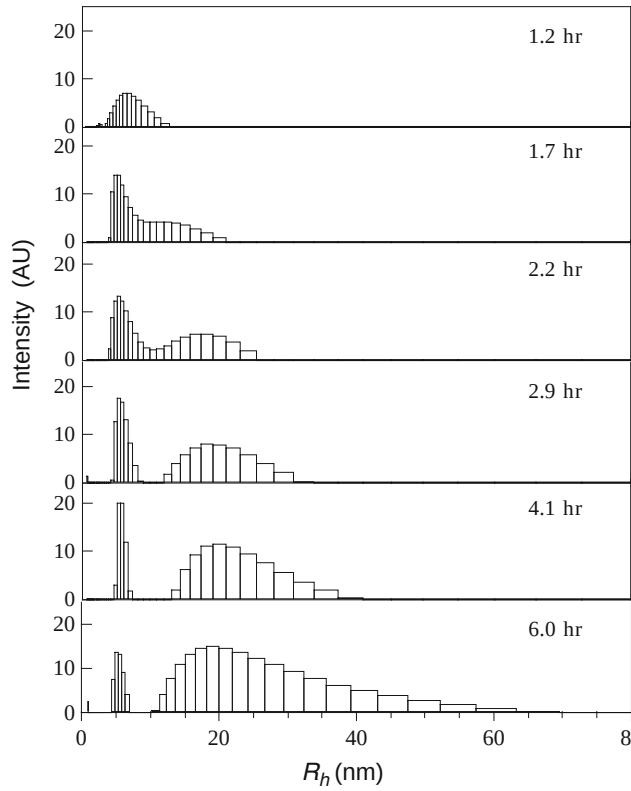

Fig. 4. Temporal evolution of the size distribution of the scattering particles in 0.25 mM solution of Aβ(1-40) in 0.1 N HCl. A freshly prepared and filtered sample contains particles with $R_h \sim 7$ nm. These particles were identified as micelles consisting of ~30 Aβ monomers (23, 26). As time progresses, a second distribution of larger particles emerges. These are Aβ fibrils that grow in size over time. Simultaneously, new fibrils are nucleated from micelles so that shorter fibrils are always present. Adapted from (27).

quantitative analysis of fibril assembly by QLS is most appropriate at the critical early stages of fibril assembly, when fibril length does not exceed 100–150 nm. At later stages, when solutions contain longer fibrils, structural information still can be obtained, but it is more qualitative in nature. Figure 4 shows an example of QLS monitoring of Aβ fibril nucleation and growth.

Hydrodynamic radii of fibrils can be converted into fibril lengths, and thus the elongation rate of the fibril can be determined. This is an extremely powerful capability. It enables quantitative study of fibril elongation reactions under different conditions, including alterations in peptide concentration, temperature, pH, ionic strength, or addition of cosolvents, thus providing insight into physical–chemical mechanisms underlying fibrillogenesis. Quantitative study of fibril growth also allows evaluation of the effects of chemical agents and changes in Aβ sequence that may facilitate or inhibit fibrillogenesis. As an example, Fig. 5 illustrates an experiment performed by dissolving HPLC-purified Aβ(1-40),

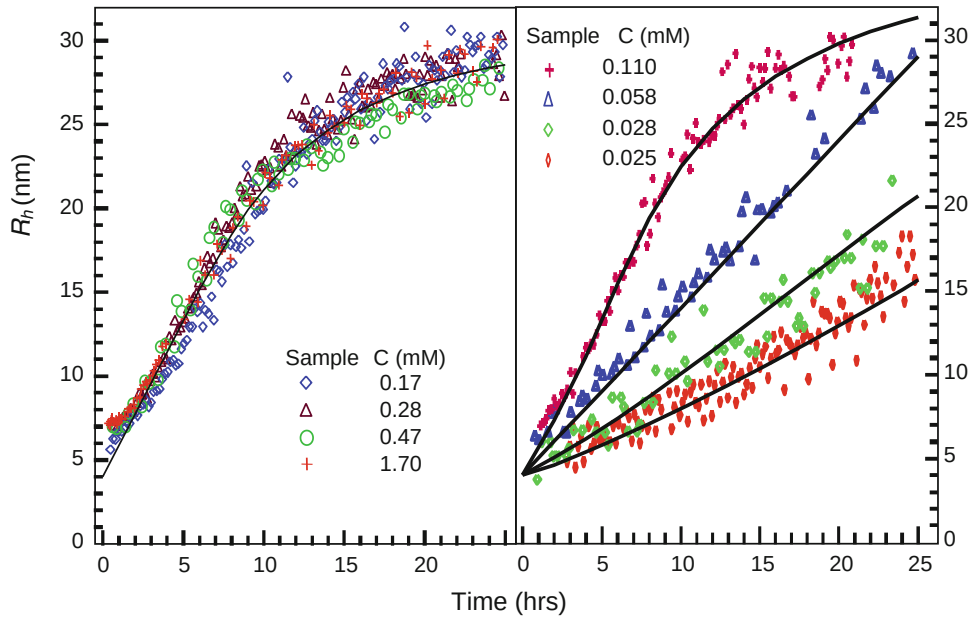

Fig. 5. Concentration dependence of Aβ fibrillogenesis. The *left panel* shows the temporal evolution of the average hydrodynamic radius R_h of scattering particles in solution with Aβ concentration above the critical micellar concentration (CMC; ~0.1 mM). An initial size of R_h ~ 7 nm observed at higher concentrations is due to the presence of micelles shown in Fig. 4. The *right panel* shows the evolution of average fibril size at concentrations at and below the CMC. *Solid lines* are eye guides. Adapted from (23).

at concentrations ranging from 25 μM to 1.7 mM, in 0.1 N HCl. For each concentration, ~200 μl of sample were placed in a 5 mm diameter glass test tube and then centrifuged at 5,000×*g* for 30 min to pellet dust particles and large aggregates. The tube then was placed into the QLS spectrometer and the intensity and correlation function of the scattered light measured periodically over the next 20–50 h. During the monitoring period, the sample remained at ~22°C. Figure 5 demonstrates that when Aβ concentration is above the critical concentration of approximately 0.1 mM, the temporal evolution of fibril is independent of concentration, indicating a constant elongation rate and a nucleation rate proportional to the total Aβ concentration. Below 0.1 mM, the elongation rate drops. The nucleation rate drops as well, resulting in fewer fibrils with larger average lengths (data not shown). These findings allowed us to conclude that, in these experiments, Aβ monomers form micelles at monomer concentration exceeding the CMC (23). As a result, the fibril elongation rate (~9 monomers/h) remains constant above the CMC. Moreover, these micelles serve as fibril nucleation centers (with a micelle-to-fibril conversion rate of 0.11/day). Thus the nucleation rate is proportional to the concentration of Aβ in excess of the CMC, and the rate drops dramatically when the total Aβ concentration is below the CMC.

Examples above from studies of Aβ fibrillogenesis illustrate the power of the quantitative capabilities of QLS to elucidate molecular mechanisms of fibrillogenesis reactions and guide development of fibrillogenesis inhibitors.

Acknowledgments

This work was supported by NIH grant AG027818 and the Jim Easton Consortium for Alzheimer's Drug Discovery and Biomarkers at UCLA.

References

1. Berne, B. J. and Pecora, R. (2000) Dynamic Light Scattering with Applications to Chemistry, Biology, and Physics, Dover.
2. Schmitz, K. S. (1990) An Introduction to Dynamic Light Scattering by Macromolecules. Academic Press, Boston.
3. Schärtl,W. (2007) Light Scattering from Polymer Solutions and Nanoparticle Dispersions. Springer, Berlin.
4. Herczenik, E. and Gebbink, F. B. G. (2008) FASEB J. 22: 2115–2133.
5. Sipe, J. D., Benson, M. D., Buxbaum, J. N., Ikeda, S.-I., Merlini, G., Saraiva, M. J. M., and Westermark, P. (2010) Amyloid 17: 101–104.
6. Lomakin, A., Benedek, G. B., and Teplow, D. B. (1999) Meth. Enzymol 309: 429–459.
7. Teplow, D. B., Lomakin, A., Benedek, G. B., Kirschner, D. A., and Walsh, D. M. (1997) in "Alzheimer's Disease: Biology, Diagnosis and Therapeutics", edited by K. Iqbal, B. Winblad, T. Nishimura, M. Takeda and H.M. Wisniewski) p. 313–321 John Wiley, New York.
8. Kerker, M. (1969) The Scattering of Light and other Electromagnetic Radiation. Academic Press, New York.
9. Einsten, A. (1905) Annalen der Physik und Chemie 17: 549–560.
10. de la Torre, J. G., and Bloomfield V. A. (1981) Quarterly Rev. Biophys. 14: 81–139.
11. Koppel, D. E. (1972) J. Chem. Phys. 57: 4814–4820.
12. Provencher, S. W. (1982) Comput. Phys. Commun. 27: 213–227.
13. Braginskaya, T. G., Dobitchin, P. D., Ivanova, M. A., Klyubin, V. V., Lomakin, A., Noskin, V. A., Shmelev G. E. and Tolpina, S. P. (1983) Physica Scripta 28: 73–79.
14. Walsh, D. M., Lomakin, A., Benedek, G. B., Condron, M. M., and Teplow, D. B. (1997) J. Biol. Chem. 272: 22364–22372.
15. Rigler, R., Elson, E. S. (Eds.) (2001) Fluorescence Correlation Spectroscopy, Theory and Applications, Springer, Berlin.
16. Maiti, P., Lomakin, A., Benedek, G. B., Bitan, G. (2010) Journal of Neurochemistry, 113: 1252–1262
17. Li, H., Monien, B. H., Lomakin, A., Zemel, R., Fradinger, E. A., Tan, M., Spring, S. M., Urbanc, B., Xie, C.-W., Benedek, G. B., Bitan, G. (2010) Biochemistry, 49: 6358–6364
18. Kratky, O. and Porod, G. (1949) Rec. Trav. Chim. 68: 1106–1122.
19. Maeda, T. and Fujume, S. (1984) Macromolecules 17: 1157–1167; Macromolecules 17: 2381–2391.
20. Doi, M. and Edwards, S. F. (1978) J. Chem. Soc. Faraday II 74: 1789–1802.
21. Zero, K. M. and Pecora, R. (1982) Macromolecules 15: 87–93.
22. Russo, P. S. (1993) in "Dynamic Light Scattering" (W. Brown, ed.), p. 512, Claredon Press, Oxford.
23. Lomakin, A., Chung, D. S., Benedek, G. B., Kirschner, D. A. and Teplow, D. B. (1996) Proc. Natl. Acad. Sci. USA 93: 1125–1129.
24. Lomakin, A., Teplow, D. B., Kirschner, D. A. and Benedek, G. B. (1997) Proc. Natl. Acad. Sci. USA 94: 7942–7947 .
25. Shen, C. L. and Murphy, R. M. (1995) Biophysical J. 69: 640–651.
26. Yong, W., Lomakin, A., Kirkitadze, M. D., Teplow, D. B., Chen, S.-H., and Benedek, G. B. (2002) Proc. Natl. Acad. Sci. USA 99: 150–154.
27. Kusumoto, Y., Lomakin, A., Teplow, D. B., and Benedek, G. B. (1998) Proc. Natl. Acad. Sci. USA 95: 12277–12282.

Chapter 7

Conformations of Microtubule-Associated Protein Tau Mapped by Fluorescence Resonance Energy Transfer

Sadasivam Jeganathan*, Subashchandrabose Chinnathambi*, Eva-Maria Mandelkow, and Eckhard Mandelkow

Abstract

The microtubule-associated protein Tau plays a physiological role of stabilizing neuronal microtubules by binding to their lateral surface. Tau belongs to the category of natively unfolded protein as it shows typical features of random coil, as analyzed by various biophysical techniques. In cells, it is subjected to several posttranslational modifications (e.g., phosphorylation, cleavage, ubiquitination, and glycosylation). In neurodegenerative diseases, Tau forms insoluble aggregates called paired helical filaments (PHFs). We have applied fluorescence resonance energy transfer (FRET) to examine the conformations of soluble Tau. We created a series of Tau mutants, each carrying one tryptophan and one cysteine (labeled by IEADANS). This made it possible to measure the distance between these FRET pairs placed in different domains of Tau. This approach enables one to analyze the global folding of soluble Tau and its alteration upon phosphorylation and denaturation.

Key words: Tau protein, Protein conformation, Alzheimer disease, Fluorescence resonance energy transfer, Aggregation

Abbreviations

CD	Circular dichroism
DTT	Dithiothreitol
FDTP-17	Frontotemporal dementia and parkinsonism linked to chromosome 17
FRET	Fluorescence resonance energy transfer
FTIR	Fourier transform infrared
GdnHCl	Guanidine hydrochloride
IAEDANS	5-(((2-Idoacetyl) amino) ethyl) amino) naphthalene-1-sulfonic acid
NMR	Nuclear magnetic resonance spectroscopy
PHFs	Paired helical filaments
SAXS	Small-angle X-ray scattering

* Sadasivam Jeganathan and Subashchandrabose Chinnathambi contributed equally.

Einar M. Sigurdsson et al. (eds.), *Amyloid Proteins: Methods and Protocols*, Methods in Molecular Biology, vol. 849,
DOI 10.1007/978-1-61779-551-0_7,

1. Introduction

Many human diseases involve the deposition of protein aggregates, either outside or inside cells (1). Some of the diseases affect the brain and are called neurodegenerative diseases (e.g., Alzheimer disease, Prion diseases, Parkinson disease, Huntington disease). In Alzheimer disease, the Aβ peptide aggregates to form extracellular plaques, the microtubule-associated protein Tau forms intracellular tangles, both of which ultimately result in neuronal toxicity and death. In principle, Tau is a highly soluble protein, and the reasons for its aggregation in neurons are not understood. In vitro, Tau aggregation can be induced by adding polyanions which compensate the positive charges on Tau (e.g., heparin, acidic peptides, nucleic acids, and arachidonic acid micelles (2–5). The polymerization kinetics can be followed by fluorescent dyes such as thioflavin S (ThS) (5). However, such dyes could potentially influence the conformations of the protein and its kinetics of aggregation. Therefore, there is a need to develop methods that are based on intrinsic reporters of protein structure.

In previous studies, we exploited the intrinsic fluorescence of single tryptophan residues inserted at selected sites to avoid possible complications due to added dyes (6, 7). Briefly, the fluorescence intensity and emission maximum change when the environment of the tryptophan changes during conformation changes or aggregation; moreover, the accessibility of the fluorophore to the solvent can be assessed by iodine-induced quenching. Using this approach, it was demonstrated that the repeat domain as a whole represents the core of paired helical filaments (PHFs), in agreement with data from limited proteolysis (8, 9). Finally, the intrinsic fluorescence approach revealed that assembled PHFs are surprisingly labile when initially formed, as judged by exposure to denaturants [guanidine hydrochloride (GdnHCl)]. This fact provides a justification for attempts to use Tau aggregation inhibitor compounds for reducing or preventing Tau pathology (10).

This example illustrated how methods based on intrinsic reporters can be used as tools to understand the conformation and aggregation properties of amyloidogenic self-assembling proteins such as Tau. In the present report, we describe another fluorescence technique, fluorescence (or "Förster") resonance energy transfer (FRET), which can be exploited specifically to map the conformational ensembles of soluble Tau (11, 12). This approach is based on the transfer of fluorescence energy from a donor to an acceptor within the protein, which is a measure of their distance. The approach is complementary to other biophysical methods to probe the size and conformations of Tau in solution, such as SAXS (13) and NMR (14).

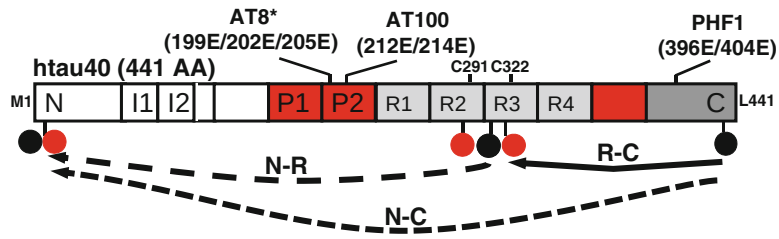

Fig. 1. Proteins and mutations. The diagram illustrates a set of single-tryptophan/single-cysteine Tau mutants created on the basis of the full-length isoform hTau40 (441 residues). The positions of tryptophan residues and IAEDANS (linked to cysteine) introduced in Tau in different paired combinations are indicated by *black* and *grey circles*. The natural cysteines of hTau40 occur at residues 291 and 322; one or both of the natural cysteine residues were mutated into alanine to generate mutants with single cysteines at residues 17, 291, or 322. FRET pairs for measuring the distance of the N-terminus to the repeat domain (N-R), repeats to C-terminus (R-C), and N-terminus to C-terminus (N-C) are indicated by *curved lines*. Adapted from ref. 11.

1.1. Tau Conformation Detected by FRET

The primary function of Tau (Fig. 1) is to stabilize axonal microtubules and thus modulate microtubule dynamics (15–17). The repeat domain in the C-terminal half of Tau together with the proline-rich flanking regions are important for the binding and assembly of microtubules, whereas the N-terminal domain projects away from the microtubule surface (18–20). Tau is a natively unfolded protein and does not contain a significant amount of secondary structure, as judged by several biophysical techniques including electron microscopy, X-ray diffraction, CD, FTIR, and fluorescence spectroscopy (21–23). However, even denatured proteins are expected to contain residual secondary structure elements (24, 25). In the case of full-length soluble Tau, the usual spectroscopic methods such as CD and FTIR failed to pick up the residual structure, because the signal is dominated by the random coil character. Nevertheless, two hexapeptide motifs in the repeat domains are known to undergo a conformational change from random coil to β-structure during aggregation (26, 27). Recent NMR analysis confirmed the presence of residual secondary structure elements in the repeat domain and elsewhere (14, 28).

Similarly, one may expect that there is some global conformation defined by interactions between the different domains of Tau that would not be detectable by the usual spectroscopic methods. Compelling support for this assumption comes from conformational antibodies that recognize discontinuous epitopes of Tau spaced widely apart in the sequence. Some of these antibodies react with Tau at an early stage of neurodegeneration, for example the Alz50 and MC1 antibodies which recognize an epitope formed by residues near the N-terminus (residues 7–9) and residues in the third repeat (313–322) (29, 30), antibody Tau-66 which recognizes elements upstream of the repeat domain and residues in repeat R3 (31, 32), antibody MN423 which reacts against a truncation site downstream

of the repeats (at E391) and residues within the repeat domain (33), and antibody SMI34 which reacts with an epitope that requires the repeat domain and one of the KSP motifs upstream or downstream from the repeats (34).

To examine such interactions between different domains of Tau, FRET analysis is a suitable spectroscopic method. FRET is the transfer of excited-state energy from a donor (D) to an acceptor (A) and results from long-range dipole–dipole interactions between them. If a protein contains a single donor and acceptor, then the distance between donor and acceptor can be estimated from the efficiency of energy transfer. The transfer efficiency can be determined by steady-state measurements of the donor emission in the presence and absence of the acceptor. Using the efficiency calculated and the knowledge of "Förster distance" R_o specific for the given donor and acceptor pair, the distance between donor and acceptor can be calculated using the Förster equation (see below).

To introduce FRET pairs, a protein is typically modified by covalent linkage of a donor and an acceptor. Because tryptophan residues have a fluorescence emission around 350 nm, they are often used as intrinsic donors. Full-length Tau does not contain any tryptophan residues but five tyrosine residues (at positions 19, 29, 198, 310, and 394) and one or two cysteines, depending on isoform, at positions 291 and 322 (Fig. 1). This feature of Tau enables one to make a conservative exchange of tyrosine to tryptophan at a selected position and chemical modification of one of the cysteines with linkage to a fluorophore without much perturbation of structure. A series of Tau constructs with a single tryptophan (acting as donor) and a single cysteine were created for FRET analysis. The cysteine residue was labeled with IAEDANS, a sulhydryl reactive dye acting as acceptor (Molecular Probes).

The analysis of FRET data of several mutants carrying tryptophan and IAEDANS in different domains of Tau (Fig. 1) suggested a complex interaction of both termini and the repeat domain (Fig. 2). In solution, Tau appears to be globally folded in a double sense, reminiscent of a "paperclip," whereby both the N- and C-terminal ends fold over into the vicinity of the repeat domain (Fig. 2) (12). We speculate that this folding is flexible and transient in soluble Tau (see Note 1) but may become more stable (and thus detectable by antibodies MC1 or Alz50) in pathologically folded Tau. Consistent with this, most Tau mutations found in familial frontotemporal dementia (FTDP-17) occur around the repeat domain, but some mutations lie toward the ends of the Tau molecule, e.g., R5L or R406W, compatible with the idea of a global hairpin folding of Tau. The recent analysis of full-length Tau by NMR confirmed the FRET observations of a double-hairpin folding (14).

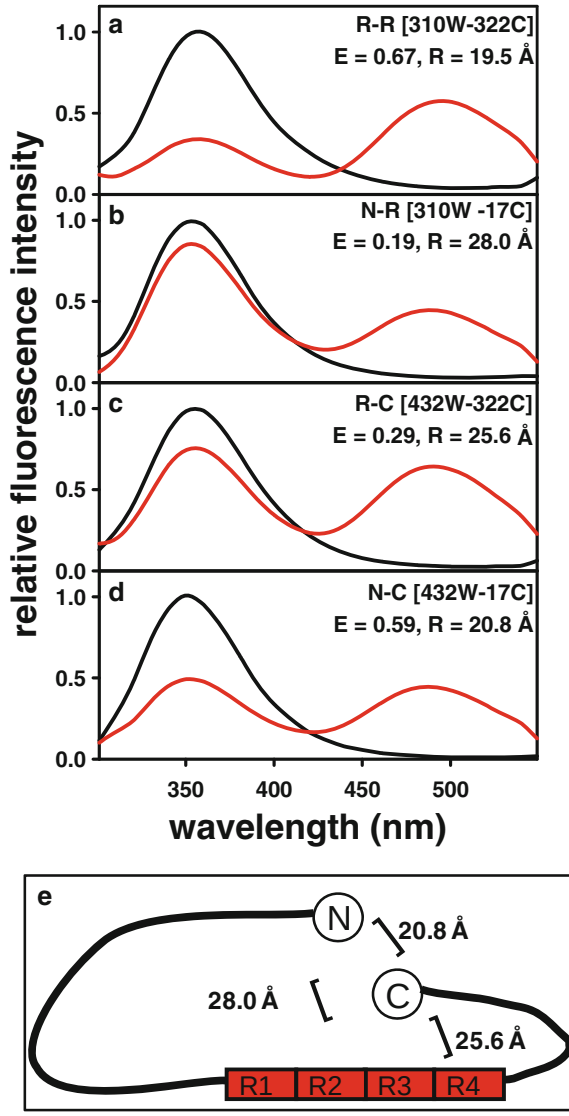

Fig. 2. Global folding of Tau revealed by FRET. All mutants contain one Trp (donor) and one Cys (for IAEDANS as acceptor) at the indicated positions. *Black curves* show emission scans (excitation at 290 nm) without IAEDANS, *red curves* with IAEDANS label, *arrows* indicate shifts in spectrum due to energy transfer from Trp to IAEDANS. (**a**) FRET pair 310W-322C, within repeat domain [R-R]: Fluorescence spectra of hTau40 mutant with tryptophan at position 310 and unlabeled cysteine at 322 (*black curve*), and with additional IAEDANS label at cysteine 322. Note that the tryptophan emission at 350 nm is decreased by ~70% after labeling of IAEDANS at 322, relative to the unlabelled protein, indicating a high efficiency of energy transfer (E=67%) and a small distance of the two residues in the repeat domain. (**b**) FRET pair 310W-17C [N-R]: Fluorescence spectra of mutant 310W-17C (*black*) and with additional IAEDANS at 17 (*red*). The tryptophan emission decreases only slightly from the unlabeled to the labeled mutant, indicating that the N-terminus Tau is further away from the repeat domain. (**c**) FRET pair 432W-322C [R-C]: Fluorescence spectra of hTau40 mutant with tryptophan at 432 and cysteine at 322, without (*black*) and with (*red*) labeling by IAEDANS. Note that the tryptophan emission at 350 nm is decreased ~30% in the IAEDANS-labeled protein, relative to unlabelled protein, indicating that the repeat domain is in the proximity of C-terminus. (**d**) FRET pair 432W-17C [N-C]: Fluorescence spectra of hTau40 mutant with tryptophan at 432 and cysteine at 17 (without or with IAEDANS). Note that FRET efficiency is ~60%, indicating the two termini of Tau are surprisingly close to each other. (**e**) The analysis of FRET distances of all the mutants mentioned above point to a paperclip-like folding of Tau. Adopted from ref. 12.

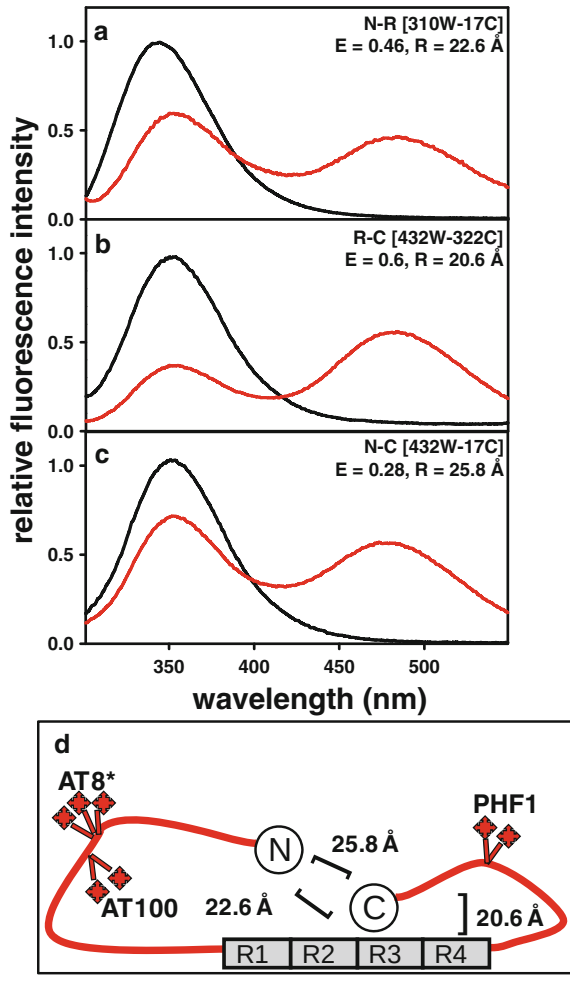

Fig. 3. FRET analysis of phospho-mimic mutants of Tau. In all cases, the epitopes of antibodies AT8 (S199, S202, and T205), AT100 (S212 and T214), and PHF1 (S396 and S404) are pseudo-phosphorylated by mutations to glutamic acid. (**a**) FRET pair 310W-17C [N-R]: Fluorescence spectra of the Tau mutant with Trp at residue 310, and Cys-IAEDANS at residue 17. Note that the FRET efficiency is increased to 45%, whereas unphosphorylated hTau40 N-R reaches only 20% (Fig. 2b). This indicates that the triple epitope pseudo-phosphorylation induces the N-terminus to come close to the repeats. (**b**) FRET pair 432W-322C [R-C]: Fluorescence spectra of the Tau mutant with tryptophan at residue 432 and Cys-IAEDANS at 322. Note that the FRET efficiency is increased to 60% relative to hTau40 R-C (30%) (Fig. 2c), indicating that the triple epitope pseudo-phosphorylation increases the proximity of the repeats and the C-terminal domain of Tau. (**c**) FRET pair 432W-17C [N-C]: Fluorescence spectra of the Tau mutant with tryptophan at residue 432 and Cys-IAEDANS at 17. Note that FRET efficiency is decreased to 30% relative to hTau40 N-C (60%) (Fig. 2d), indicating that the triple epitope pseudo-phosphorylation of both arms at the AT8*, AT100, and PHF1 epitopes causes the two termini to move apart. (**d**) Model of rearrangement of paperclip upon triple epitope pseudo-phosphorylation. The paperclip folding of Tau is altered in a way that both termini of Tau move into closer vicinity of repeat domain (N-R decreases from 28.0 to 22.6 Å, C-R decreases from 25.6 to 20.6 Å) but move apart from each other (N-C increases from 20.8 to 25.8 Å). Note that the distance values are only approximate because they represent averages of the flexible conformations of Tau. Adopted from ref. 12.

1.2. Tau Conformational Changes Induced by (Pseudo-) Phosphorylation

In normal physiological conditions, Tau is targeted by several kinases and can be phosphorylated at multiple sites. The results of phosphorylation vary depending on the phosphorylation site. For example, the phosphorylation at KXGS motifs in the repeat domains leads to a strong decrease of Tau-microtubule binding and to altered microtubule dynamics that is important for neurite outgrowth (35, 36). In pathological conditions, i.e., Alzheimer disease, Tau becomes abnormally phosphorylated at many sites, mostly at the repeat domain K*X*GS motifs and in the flanking domains (mainly SP or TP motifs). Certain antibodies including AT8, PHF1, and AT100 that react with phospho-epitopes of SP/TP sites are widely used as markers for Alzheimer Tau (37–39). To understand the effect of phosphorylation on global folding of Tau, we pursued the FRET approach with several Tau mutants carrying pseudo-phosphorylation sites (substitution of phosphorylatable serine or threonine residues by glutamic acid), corresponding to AT8 (S199, S202, and T205), AT100 (S212 and T214), and PHF1 (S396 and S404) epitopes combined with FRET pairs. We observed that the global folding is altered depending the position and combination of phosphorylation-mimicking sites (Fig. 3) (11). Notably, the combined pseudo-phosphorylation at three characteristic Alzheimer epitopes (antibodies AT8, AT100, and PHF1) leads to a compaction of the paperclip, bringing the terminal domains of Tau into closer vicinity of the repeat domain by ~6 Å, while increasing the distance between the terminal domains by ~5 Å (Fig. 3d). Consistent with this, the modification also leads to a strong increase of the reaction with conformation-dependent antibodies MC1 and Alz50, detected by immunoblotting (11).

1.3. "Unfolding of a Natively Unfolded Protein" by GdnHCl

The proximity of the repeat domain to the two ends of Tau pointed to a residual interaction within a mostly unfolded protein. To test the stability of such an interaction, the protein was denatured by GdnHCl and monitored by FRET. Protein denaturation is often used to probe the stability of a protein, and it can be expected that treatment with a denaturant such as GdnHCl may cause a considerable change in FRET distances between the Tau domains. As expected, the 310W-291C (IAEDANS) mutants regained its tryptophan donor emission intensity (i.e., lost FRET) with increasing concentration of GdnHCl, indicating that tryptophan and IAEDANS progressively move apart with increasing GdnHCl concentration (Fig. 4a). The FRET efficiency change is plotted in Fig. 4b for distances between different Tau domains. Within the repeat domain the changes were much smaller. This can be explained by noting that neither the initial state nor the fully denatured state may comply with the assumptions about the protein structure, which was derived by denaturing well-folded proteins (40, 41). On the other hand, even the chemically

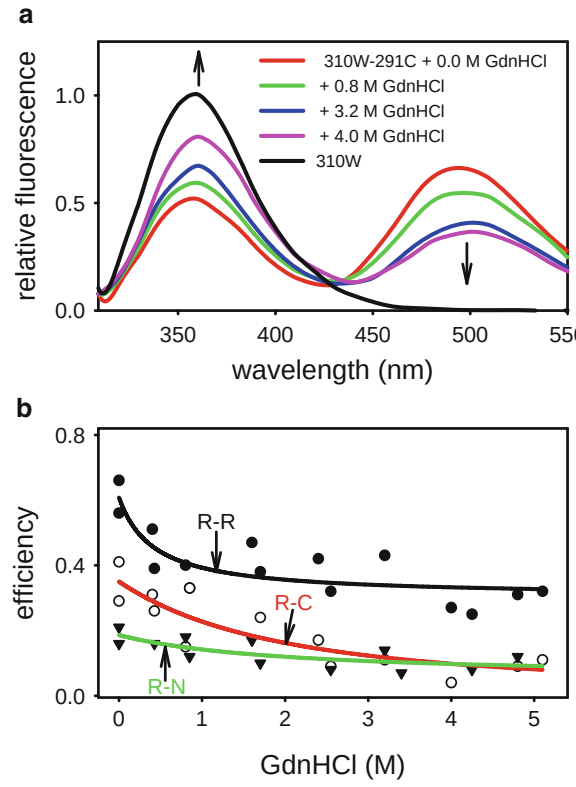

Fig. 4. Denaturation of Tau destroys folding and reduces FRET. (**a**) Fluorescence emission spectra of hTau40-310$_W$291$_{DANS}$ with increasing concentrations of GdnHCl. Note that with increasing GdnHCl concentration, the tryptophan emission of labeled hTau40-310$_W$291$_{DANS}$ approaches that of unlabeled one (*black line*), indicating the loss of FRET upon denaturant treatment. (**b**) Summary of efficiency of Tau FRET mutants against increasing GdnHCl concentration. The FRET efficiencies are plotted versus the GdnHCl concentrations (R-R = htau40-310$_W$291$_{DANS}$, R-C = htau40-432$_W$291$_{DANS}$, and N-R = htau40-18$_W$322$_{DANS}$). Note that the efficiency is diminished with increasing denaturant concentration, pointing to parting away of domains.

denatured state may differ significantly from a pure random coil model (25), especially in the presence of pronounced charge asymmetries (as is the case with Tau). A decrease in FRET efficiency was also observed upon GdnHCl treatment between the repeat domain and the C-terminal domain, with efficiencies dropping from ~0.3 to ~0.1 upon denaturation. In contrast, the disturbance of interactions between the N-terminus and the repeats upon denaturation was difficult to estimate, as the FRET efficiency of R-N mutants was ~0.1 in native conditions, too low for a reliable distance estimations.

2. Materials

2.1. Chemicals

1. Phosphate-buffered saline (PBS): 137 mM sodium chloride (NaCl), 3 mM potassium chloride (KCl), 10 mM disodium hydrogen phosphate (Na_2HPO_4), and 2 mM potassium dihydrogen phosphate (KH_2PO_4). To make 20× PBS, 160 g NaCl, 4 g KCl, 28.8 g Na_2HPO_4, and 4.8 g KH_2PO_4 dissolve and adjust to 1,000 ml with water, filter and store at room temperature.
2. 5-((((2-Iodoacetyl) amino) ethyl) amino) naphthalene-1-sulfonic acid (1,5-IAEDANS) (Molecular Probes, Eugene, Oregon, USA). Dissolve the fluorophore in dimethyl formamide (DMF) to 50 mM stock solution. Aliquot and store at –20°C (see Note 2).
3. GdnHCl. Make 8 M stock solution (76.42 g in 100 ml) in PBS.
4. Ammonium sulfate. Make 70% solution (47.2 g in 100 ml) in PBS.

2.2. Proteins

1. Create mutations by site-directed mutagenesis using the Quick Change Kit (Stratagene, California, USA) and the plasmid pNG2 (38), a derivative of pET-3b vector (42). Confirm the mutation by sequencing.
2. Express Tau or Tau mutants (Fig. 1) in *Escherichia coli* and purify as described earlier (43) with minor modifications (see Note 3).

3. Methods

3.1. Labeling of Proteins

1. Incubate Tau mutant protein (single tryptophan and single cysteine) diluted in 4 M GdnHCl/PBS buffer with 10 M excess of DTT for 10 min at 37°C (see Note 4).
2. Remove DTT by size exclusion chromatography (Fast Desalting column, Amersham Bioscience, Freiburg, Germany) (see Note 5).
3. Collect the eluting protein in fraction tubes containing an ~20 M excess of IAEDANS (see Note 6).
4. Alternatively use “solid state-based labeling” (44) as follows: Precipitate the Tau protein with 70% ammonium sulfate, wash the pellet thrice to get rid of residual DTT, dissolve the protein pellet with buffer-containing IAEDANS (see Note 7).

5. Allow reaction to proceed for ~2 h at room temperature or at 4°C overnight.
6. Dialyze the reaction mixture against PBS and remove residual IAEDANS by size exclusion chromatography.
7. Determine the concentration of protein and label using the molar extinction coefficient (see Note 8).

3.2. Fluorescence Spectroscopy Measurement

1. Perform all the steady-state fluorescence measurements at constant temperature, e.g., 25°C (see Note 9).
2. Allow the fluorescence lamp and temperature to stabilize after starting the instrument (follow instructions of spectrophotometer).
3. Excite the sample at 290 nm (excitation of the single Trp) (see Note 10).
4. Measure the blank (PBS).
5. Measure the samples and subtract blank signal.
6. Perform competition experiments to rule out FRET effects due to intermolecular fluorescence transfer. If the FRET were intramolecular, the emission intensity of tryptophan and IAEDANS would increase linearly for a series of protein concentrations and in contrast, if the FRET were intermolecular, the emission intensity would not be linear (see Note 11).
7. In case of denaturation experiments, corresponding blanks are measured, i.e., different GdnHCl concentration in PBS.

3.3. Calculation of FRET Efficiency

1. Plot the fluorescence intensity data files from measurements. Mark the maximum fluorescence intensity of an unlabeled Tau mutant protein (containing tryptophan and cysteine) at ~350 nm. Mark the maximum intensity of the same Tau mutant protein but labeled IAEDANS at its single cysteine residue at ~350 nm (see Note 12).
2. The energy transfer is calculated according to the equation: $E_{\mathrm{FRET}} = (1 - D_{\mathrm{A}} / D)(1 / f_{\mathrm{A}})$, where D_{A} is the fluorescence intensity of the donor in the presence of acceptor and D is the fluorescence intensity of the donor in the absence of acceptor and f_{A} is the fractional labeling with acceptor (see Note 13).
3. Calculate the distance R between donor and acceptor by the Förster equation, $E_{\mathrm{FRET}} = [1 + (R / R_{\mathrm{o}})^6]^{-1}$, where the Förster radius R_{o} is 22 Å for the Trp-IAEDANS pair (45, 46).
4. In denaturation experiments with GdnHCl, the efficiency is calculated from emission intensities of labeled and unlabeled proteins at the same GdnHCl concentration.

4. Notes

1. In general, the native state of a folded protein has a sharply defined distance distribution between a given pair of residues whose FRET efficiency can be translated into a well-defined separation. This does not hold for a natively unfolded protein such as Tau, which exists in solution as a mixture of random coil, residual secondary structure elements, and preferred conformational states, which are moreover heterogeneous and mobile. In unfolded proteins, the distance between a given FRET pair shows a wider distribution, and the apparent FRET reflects this heterogeneity (47).
2. We recommend to aliquot and store the IAEDANS stock solution at –20°C, which remains usable up to 3–6 months. If the labeling efficiency is diminishing with time, prepare fresh stock solution.
3. The purification of tryptophan-containing Tau mutant proteins is done by ammonium sulfate precipitation followed by ion exchange and gel filtration. This is to avoid boiling the cell lysate supernatant (which is classical way of Tau purification (43)) because treatment at high temperature would potentially diminish tryptophan fluorescence. Briefly, the cell lysate was precipitated with 25% $(NH)_2SO_4$ and centrifuged for 45 min at 127,000 × *g*. The supernatant was adjusted to 55% saturated $(NH)_2SO_4$ and after centrifugation for 45 min at 127,000 × *g*, the pellet was dissolved and dialyzed against ion exchange buffer.
4. The incubation of Tau mutants with DTT at 37°C for 10 min is sufficient to reduce cysteine for subsequent labeling. Long incubation results in the loss of reducing efficiency of DTT.
5. Amersham Biosciences has discontinued this type of desalting column, which is very convenient and quick for DTT removal by size exclusion. Alternatives are available (e.g., Zeba™ Desalt Spin Columns, 0.5 ml from PIERCE-Biotechnology, USA).
6. The labeling efficiency is better when we directly collect the protein fraction in a tube containing stock fluorophore solution.
7. We found the solid-state labeling method to be quick and efficient, resulting in slight better labeling efficiency.
8. The molar extinction coefficient at 280 nm wavelength of Tau mutants varies, $\in_{tau} = 10{,}800–12{,}100\ M^{-1}\ cm^{-1}$, depending on the different contents of aromatic residues in the isoforms and mutants of Tau. The amount of bound IAEDANS is determined by the absorption at 336 nm ($\in_{IAEDANS} = 6{,}100\ M^{-1}cm^{-1}$) (48). The protein concentration has to be corrected for the contribution of the IAEDANS at 280 nm, which we found about 20% of its absorbance at 336 nm. The stoichiometry is

then calculated and we typically obtained the labeling stoichiometry of 0.8–0.9.

9. Measurements were performed with a Spex Fluoromax spectrophotometer (Polytec, Waldbronn, Germany), using 3 × 3 mm quartz microcuvettes from Hellma (Mühlheim, Germany). This allows one to use a small sample volume of 20 µl. The experimental parameters are set as follows: excitation slit width = 4 nm, emission slit width = 6 nm, scans ranged from 300 to 550 nm, integration time = 0.25 s, and photomultiplier voltage = 950 V.
10. We excite the samples at 290 nm to avoid the contribution of tyrosine emission as the Tau mutants used contain four or five tyrosine residues but only one tryptophan. We typically measure tryptophan emission with protein concentrations of 2 or 4 µM.
11. In all the experiments, it is important to verify that the observed fluorescence (and FRET) is of intramolecular nature rather than due to intermolecular interactions. This can be checked by titration experiments, i.e., if the FRET were intramolecular, the emission intensity of tryptophan and IAEDANS would increase linearly for a series of protein concentrations. In contrast, if the FRET were intermolecular, the emission intensity would become nonlinear as the molecules in solution approach each other due to crowding. For this, we measured the fluorescence intensity of a Tau mutant with a concentration series ranging from 1 to 12 µM. In our conditions, we did not observe any indications of intermolecular interactions, i.e., the FRET efficiency of the protein remained unchanged with increasing concentration.
12. Tryptophan-containing Tau mutants, excited at 290 nm, show maximum emission intensity at ~350 nm. When labeled protein is excited, the tryptophan emission intensity is transferred to IAEDANS which has its maximum excitation at 336 nm and emits at a longer wavelength of ~490 nm.
13. The apparent efficiencies were normalized by f_A, the fractional labeling with acceptor (49).

Acknowledgments

We thank Bianca Scharnweber and Ilka Lindner for excellent technical assistance, and Dr. Jacek Biernat for advice and discussions on Tau mutations and purification. This project was supported in part by grants from the DFG, MPG (TPC project), V W Foundation (Protein Conformation project), and Breuer Foundation.

References

1. Chiti, F., and Dobson, C. M. (2006) Protein misfolding, functional amyloid, and human disease, *Annu Rev Biochem 75*, 333–366.
2. Goedert, M., Jakes, R., Spillantini, M. G., Hasegawa, M., Smith, M. J., and Crowther, R. A. (1996) Assembly of microtubule-associated protein tau into Alzheimer-like filaments induced by sulphated glycosaminoglycans, *Nature 383*, 550–553.
3. Kampers, T., Friedhoff, P., Biernat, J., Mandelkow, E. M., and Mandelkow, E. (1996) RNA stimulates aggregation of microtubule-associated protein tau into Alzheimer-like paired helical filaments, *FEBS letters 399*, 344–349.
4. Wilson, D. M., and Binder, L. I. (1995) Polymerization of microtubule-associated protein tau under near-physiological conditions, *The Journal of biological chemistry 270*, 24306–24314.
5. Friedhoff, P., Schneider, A., Mandelkow, E. M., and Mandelkow, E. (1998) Rapid assembly of Alzheimer-like paired helical filaments from microtubule-associated protein tau monitored by fluorescence in solution, *Biochemistry 37*, 10223–10230.
6. Li, L., von Bergen, M., Mandelkow, E. M., and Mandelkow, E. (2002) Structure, stability, and aggregation of paired helical filaments from tau protein and FTDP-17 mutants probed by tryptophan scanning mutagenesis, *J Biol Chem 277*, 41390–41400.
7. von Bergen, M., Li, L., and Mandelkow, E. (2005) Intrinsic fluorescent detection of tau conformation and aggregation, *Methods Mol Biol 299*, 175–184.
8. von Bergen, M., Barghorn, S., Muller, S. A., Pickhardt, M., Biernat, J., Mandelkow, E. M., Davies, P., Aebi, U., and Mandelkow, E. (2006) The core of tau-paired helical filaments studied by scanning transmission electron microscopy and limited proteolysis, *Biochemistry 45*, 6446–6457.
9. Jakes, R., Novak, M., Davison, M., and Wischik, C. M. (1991) Identification of 3- and 4-repeat tau isoforms within the PHF in Alzheimer's disease, *EMBO J 10*, 2725–2729.
10. Bulic, B., Pickhardt, M., Schmidt, B., Mandelkow, E. M., Waldmann, H., and Mandelkow, E. (2009) Development of tau aggregation inhibitors for Alzheimer's disease, *Angew Chem Int Ed Engl 48*, 1740–1752.
11. Jeganathan, S., Hascher, A., Chinnathambi, S., Biernat, J., Mandelkow, E. M., and Mandelkow, E. (2008) Proline-directed pseudo-phosphorylation at AT8 and PHF1 epitopes induces a compaction of the paperclip folding of Tau and generates a pathological (MC-1) conformation, *J Biol Chem 283*, 32066–32076.
12. Jeganathan, S., von Bergen, M., Brutlach, H., Steinhoff, H. J., and Mandelkow, E. (2006) Global hairpin folding of tau in solution, *Biochemistry 45*, 2283–2293.
13. Mylonas, E., Hascher, A., Bernado, P., Blackledge, M., Mandelkow, E., and Svergun, D. I. (2008) Domain conformation of tau protein studied by solution small-angle X-ray scattering, *Biochemistry 47*, 10345–10353.
14. Mukrasch, M. D., Bibow, S., Korukottu, J., Jeganathan, S., Biernat, J., Griesinger, C., Mandelkow, E., and Zweckstetter, M. (2009) Structural polymorphism of 441-residue tau at single residue resolution, *PLoS Biol 7*, e34.
15. Mandelkow, E., von Bergen, M., Biernat, J., and Mandelkow, E. M. (2007) Structural principles of tau and the paired helical filaments of Alzheimer's disease, *Brain Pathol 17*, 83–90.
16. Garcia, M. L., and Cleveland, D. W. (2001) Going new places using an old MAP: tau, microtubules and human neurodegenerative disease, *Curr Opin Cell Biol 13*, 41–48.
17. Goedert, M. (2004) Tau protein and neurodegeneration, *Semin Cell Dev Biol 15*, 45–49.
18. Hirokawa, N., Shiomura, Y., and Okabe, S. (1988) Tau proteins: the molecular structure and mode of binding on microtubules, *J Cell Biol 107*, 1449–1459.
19. Butner, K. A., and Kirschner, M. W. (1991) Tau protein binds to microtubules through a flexible array of distributed weak sites, *J Cell Biol 115*, 717–730.
20. Gustke, N., Trinczek, B., Biernat, J., Mandelkow, E. M., and Mandelkow, E. (1994) Domains of tau protein and interactions with microtubules, *Biochemistry 33*, 9511–9522.
21. Cleveland, D. W., Hwo, S. Y., and Kirschner, M. W. (1977) Physical and chemical properties of purified tau factor and the role of tau in microtubule assembly, *Journal of molecular biology 116*, 227–247.
22. Wille, H., Drewes, G., Biernat, J., Mandelkow, E. M., and Mandelkow, E. (1992) Alzheimer-like paired helical filaments and antiparallel dimers formed from microtubule-associated protein tau in vitro, *J Cell Biol 118*, 573–584.
23. Schweers, O., Schonbrunn-Hanebeck, E., Marx, A., and Mandelkow, E. (1994) Structural studies of tau protein and Alzheimer paired helical filaments show no evidence for beta-structure, *The Journal of biological chemistry 269*, 24290–24297.

24. Shortle, D., and Ackerman, M. S. (2001) Persistence of native-like topology in a denatured protein in 8 M urea, *Science 293*, 487–489.
25. Fitzkee, N. C., and Rose, G. D. (2004) Reassessing random-coil statistics in unfolded proteins, *Proc Natl Acad Sci USA 101*, 12497–12502.
26. von Bergen, M., Barghorn, S., Li, L., Marx, A., Biernat, J., Mandelkow, E. M., and Mandelkow, E. (2001) Mutations of tau protein in frontotemporal dementia promote aggregation of paired helical filaments by enhancing local beta-structure, *J Biol Chem 276*, 48165–48174.
27. von Bergen, M., Friedhoff, P., Biernat, J., Heberle, J., Mandelkow, E. M., and Mandelkow, E. (2000) Assembly of tau protein into Alzheimer paired helical filaments depends on a local sequence motif ((306)VQIVYK(311)) forming beta structure, *Proceedings of the National Academy of Sciences of the United States of America 97*, 5129–5134.
28. Mukrasch, M. D., Biernat, J., von Bergen, M., Griesinger, C., Mandelkow, E., and Zweckstetter, M. (2005) Sites of tau important for aggregation populate {beta}-structure and bind to microtubules and polyanions, *J Biol Chem 280*, 24978–24986.
29. Jicha, G. A., Bowser, R., Kazam, I. G., and Davies, P. (1997) Alz-50 and MC-1, a new monoclonal antibody raised to paired helical filaments, recognize conformational epitopes on recombinant tau, *J Neurosci Res 48*, 128–132.
30. Carmel, G., Mager, E. M., Binder, L. I., and Kuret, J. (1996) The structural basis of monoclonal antibody Alz50's selectivity for Alzheimer's disease pathology, *J Biol Chem 271*, 32789–32795.
31. Garcia-Sierra, F., Ghoshal, N., Quinn, B., Berry, R. W., and Binder, L. I. (2003) Conformational changes and truncation of tau protein during tangle evolution in Alzheimer's disease, *J Alzheimers Dis 5*, 65–77.
32. Ghoshal, N., Garcia-Sierra, F., Fu, Y., Beckett, L. A., Mufson, E. J., Kuret, J., Berry, R. W., and Binder, L. I. (2001) Tau-66: evidence for a novel tau conformation in Alzheimer's disease, *J Neurochem 77*, 1372–1385.
33. Skrabana, R., Kontsek, P., Mederlyova, A., Iqbal, K., and Novak, M. (2004) Folding of Alzheimer's core PHF subunit revealed by monoclonal antibody 423, *FEBS Lett 568*, 178–182.
34. Lichtenberg-Kraag, B., Mandelkow, E. M., Biernat, J., Steiner, B., Schroter, C., Gustke, N., Meyer, H. E., and Mandelkow, E. (1992) Phosphorylation-dependent epitopes of neurofilament antibodies on tau protein and relationship with Alzheimer tau, *Proc Natl Acad Sci USA 89*, 5384–5388.
35. Biernat, J., Wu, Y. Z., Timm, T., Zheng-Fischhofer, Q., Mandelkow, E., Meijer, L., and Mandelkow, E. M. (2002) Protein kinase MARK/PAR-1 is required for neurite outgrowth and establishment of neuronal polarity, *Mol Biol Cell 13*, 4013–4028.
36. Drewes, G., Ebneth, A., Preuss, U., Mandelkow, E. M., and Mandelkow, E. (1997) MARK, a novel family of protein kinases that phosphorylate microtubule-associated proteins and trigger microtubule disruption, *Cell 89*, 297–308.
37. Zheng-Fischhofer, Q., Biernat, J., Mandelkow, E. M., Illenberger, S., Godemann, R., and Mandelkow, E. (1998) Sequential phosphorylation of Tau by glycogen synthase kinase-3beta and protein kinase A at Thr212 and Ser214 generates the Alzheimer-specific epitope of antibody AT100 and requires a paired-helical-filament-like conformation, *Eur J Biochem 252*, 542–552.
38. Biernat, J., Mandelkow, E. M., Schroter, C., Lichtenberg-Kraag, B., Steiner, B., Berling, B., Meyer, H., Mercken, M., Vandermeeren, A., Goedert, M., and et al. (1992) The switch of tau protein to an Alzheimer-like state includes the phosphorylation of two serine-proline motifs upstream of the microtubule binding region, *EMBO J 11*, 1593–1597.
39. Otvos, L., Jr., Feiner, L., Lang, E., Szendrei, G. I., Goedert, M., and Lee, V. M. (1994) Monoclonal antibody PHF-1 recognizes tau protein phosphorylated at serine residues 396 and 404, *J Neurosci Res 39*, 669–673.
40. Krantz, B. A., Trivedi, A. D., Cunningham, K., Christensen, K. A., and Collier, R. J. (2004) Acid-induced unfolding of the amino-terminal domains of the lethal and edema factors of anthrax toxin, *J Mol Biol 344*, 739–756.
41. Navon, A., Ittah, V., Scheraga, H. A., and Haas, E. (2002) Formation of the hydrophobic core of ribonuclease A through sequential coordinated conformational transitions, *Biochemistry 41*, 14225–14231.
42. Studier, F. W., Rosenberg, A. H., Dunn, J. J., and Dubendorff, J. W. (1990) Use of T7 RNA polymerase to direct expression of cloned genes, *Methods Enzymol 185*, 60–89.
43. Barghorn, S., Biernat, J., and Mandelkow, E. (2005) Purification of recombinant tau protein and preparation of Alzheimer-paired helical filaments in vitro, *Methods Mol Biol 299*, 35–51.
44. Kim, Y., Ho, S. O., Gassman, N. R., Korlann, Y., Landorf, E. V., Collart, F. R., and Weiss, S. (2008) Efficient site-specific labeling of

proteins via cysteines, *Bioconjug Chem 19*, 786–791.

45. Wu, P., and Brand, L. (1994) Conformational flexibility in a staphylococcal nuclease mutant K45C from time-resolved resonance energy transfer measurements, *Biochemistry* **33**, 10457–10462.
46. Matsumoto, S., and Hammes, G. G. (1975) Fluorescence energy transfer between ligand binding sites on aspartate transcarbamylase, *Biochemistry 14*, 214–224.
47. Schuler, B., Lipman, E. A., and Eaton, W. A. (2002) Probing the free-energy surface for protein folding with single-molecule fluorescence spectroscopy, *Nature 419*, 743–747.
48. Hudson, E. N., and Weber, G. (1973) Synthesis and characterization of two fluorescent sulfhydryl reagents, *Biochemistry 12*, 4154–4161.
49. Li, G., Levitus, M., Bustamante, C., and Widom, J. (2005) Rapid spontaneous accessibility of nucleosomal DNA, *Nat Struct Mol Biol 12*, 46–53.

Chapter 8

Measuring the Kinetics of Amyloid Fibril Elongation Using Quartz Crystal Microbalances

Alexander K. Buell, Christopher M. Dobson, and Mark E. Welland

Abstract

Kinetic measurements of amyloid growth provide insight into the free energy landscape of this supramolecular process and are crucial in the search for potent inhibitors of the main disorders with which it is associated, including Alzheimer's and Parkinson's diseases and Type II diabetes. In recent years, a new class of surface-bound biosensor assays, e.g., those based on surface plasmon resonance (SPR) and the quartz crystal microbalance (QCM) have been established as extremely valuable tools for kinetic measurements of amyloid formation. Here we describe detailed protocols of how QCM techniques can be used to monitor the elongation of amyloid fibrils in real time and to study the influence of external factors on the kinetics of amyloid growth with unprecedented accuracy.

Key words: Amyloid disorders, Alzheimer's disease, Parkinson's disease, Quartz crystal microbalance, Biosensor, Kinetics, AFM, Surface attachment

1. Introduction

The study of the kinetics of amyloid formation and growth has attracted much attention in recent years, as a detailed understanding of the effect of external factors, such as temperature, ionic strength, or small molecules on the growth rates of amyloid fibrils provides fundamental insight into the free energy surfaces governing this process (1). In addition, in the light of the medical relevance of the amyloid form of proteins, the quest for potent inhibitors, the efficiency of which is primarily evaluated through their influence on the kinetics of amyloid formation, is a highly active field of research (see, e.g., ref. 2). Amyloid formation and growth kinetics from soluble precursor proteins have traditionally been studied in solution using either amyloidophilic dyes, such as Thioflavin T or spectroscopic techniques, such as FTIR or CD

Einar M. Sigurdsson et al. (eds.), *Amyloid Proteins: Methods and Protocols*, Methods in Molecular Biology, vol. 849,
DOI 10.1007/978-1-61779-551-0_8,

spectroscopy (3). However, in recent years, a new set of techniques has been developed by adapting pre-existing biosensing approaches for the measurement of amyloid growth, especially those based on surface plasmon resonance (SPR) (4, 5) and the quartz crystal microbalance (QCM) (1, 6, 7). In this chapter, we focus on the latter and describe how to apply this technique to obtain precise and reproducible kinetic data.

The principle of a QCM is that a piezoelectric quartz disc, coated with gold to form electrodes, is stimulated to vibrate at its resonant frequency via the application of a rapidly oscillating AC field, using the inverse piezoelectric effect. The resonant frequency is determined by, amongst other things, the total mass of the quartz crystal. When an analyte molecule attaches to the surface of the crystal, its mass increases and its resonant frequency decreases accordingly, as described by the Sauerbrey (8) equation:

$$\Delta f = -a\Delta m,$$

where Δf and Δm are the changes in resonant frequency and mass, respectively, and a is a proportionality factor that can be calculated from first principles for simple situations such as a thin rigid attached layer in contact with air or a vacuum (8). QCM can, however, also be applied in a liquid environment, and here an additional shift in resonant frequency arises from the coupling of the sensor surface to the liquid (9); in the case of a hydrophilic surface with sticky boundary conditions, some water is moved along with the oscillating crystal and increases the observed drop in frequency compared to the situation where the crystal is in contact with a vacuum. In addition, the friction that the crystal experiences in solution leads to a rapid decay of the vibrational motion. In the case where the material that is attached to the quartz crystal surface has viscoelastic properties, it is also possible to predict the induced shift in resonant frequency, if the viscosity and elasticity of the layer are known and if the layer is smooth and homogeneous (10, 11). In cases where the added material forms a rough layer, the induced frequency shift often has to be empirically calibrated, as we show, for example, in Subheading 3.6. Figure 1 illustrates the general principles of a QCM operating in liquid, and the effect of the attachment of additional material that increases the total mass of the crystal and the coupling to the liquid, leading to both a decrease in resonant frequency and a faster decay of the excited vibration.

Amyloid formation can be decomposed into at least three different sub-processes, namely the formation of seeds (nucleation), the growth of those seeds to form fibrils (elongation), and finally secondary nucleation processes (such as fibril fragmentation) that increase the number of fibrils and that depend on the number of existing fibrils (12). Each of these steps has a different mechanism and, therefore, represents the dynamics of the system in a different region of the global free energy surface. Traditional solution based

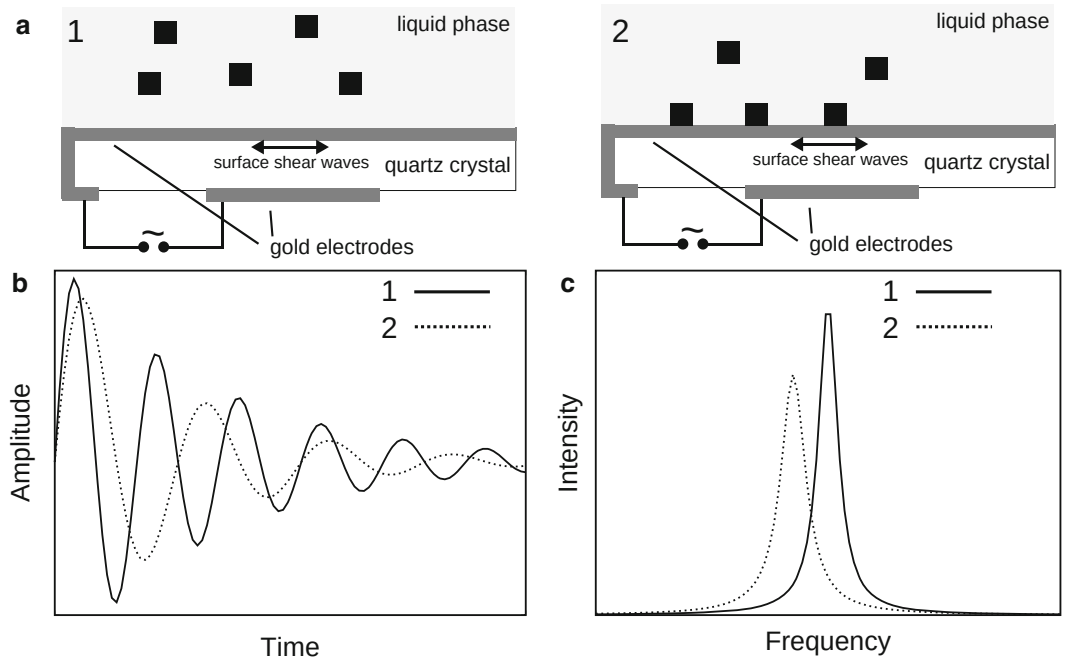

Fig. 1. Principle of a QCM operating in liquid. (**a**) A rapidly oscillating AC voltage is applied across a piezoelectric quartz disc and excites shear waves in the quartz crystal. The attachment of molecules from the solution phase is detected as an increase in mass. (**b**) The vibration of a quartz crystal immersed in liquid is characterized by a frequency and an exponential decay constant. The decay is due to the strong coupling between the liquid and the sensor surface. Additional mass attachment will lead to a decrease in resonant frequency and, if the attachment increases the coupling of the surface to the liquid, will lead to a more rapid exponential decay. (**c**) Schematic frequency spectra of the time domain record of (**b**). The decrease in resonant frequency and the increase in the full width at half maximum are recorded and represent the data that can be analysed to characterize the amount and structure of the attached material.

assays of amyloid kinetics are sensitive to all of the above-mentioned processes, especially in unseeded experiments. A unique strength of the QCM technique is that it is able to isolate the elongation step and allows its separate study. We will limit ourselves in this chapter to this particular application of QCM; it has been shown, however, that QCM can also be used to study the entire process of amyloid formation from the soluble precursor to the mature amyloid fibril (6, 7).

The study of the single step of fibril elongation is achieved via covalent, irreversible attachment of pre-grown amyloid seed fibrils to the surface of the QCM sensor, followed by passivation of the remaining exposed surface of the sensor (13). The growth of the fibrils, when brought into contact with a solution containing soluble amyloidogenic precursor molecules is then monitored via the change in resonant frequency of the QCM (1). This change in frequency upon elongation of the surface-bound seed fibrils has several origins. First, the increase in surface-bound mass (protein molecules and their associated water molecules). Second a change

in the coupling to the liquid; the elongation of the seeds increases the roughness of the surface and results in water being trapped between the fibrils, which leads to additional frequency shifts and therefore an overestimation of the attached mass (14). Third, the viscoelastic properties of the surface-bound fibrils (their finite rigidity) lead to an underestimation of the attached mass (11), as they will not be able to follow the oscillation of the QCM crystal perfectly. We will discuss the consequences and net result of these effects in more detail in Subheading 3.6.

The unique strength of these surface-bound kinetic techniques, of which QCM is a prominent representative, is the fact that the growth of a constant ensemble of seed fibrils can be probed repeatedly. Therefore, the growth rates upon incubation of the same seeds with different monomer solutions or under different conditions can be directly compared. Furthermore, the QCM sensor can be imaged with an atomic force microscope before and after the experiments. This procedure allows an estimation to be made of the number of seed fibrils that have contributed to the growth signal, as well as acting as a control for the absence of secondary pathways such as amorphous aggregation on the surface.

2. Materials

2.1. QCM Instrumentation: Basic Equipment and Accessories

We carried out our experiments with the QCM models D-300 and E4 from Q-Sense (Västra Frölunda, Sweden). These instruments allow the simultaneous monitoring of the resonant frequency and the dissipation of the vibrating crystal (QCM-D technology). The dissipation measurements are, however, not crucial for any of the applications presented in this chapter; therefore, any QCM with nanogram sensitivity is suitable. When we quote numerical values of frequency shifts in any of our examples, they are from experiments with the E4 microbalance and may vary for other systems.

The introduction of the buffer and protein solutions into the liquid cell in our experiments was accomplished either via a simple gravity flow system (D300) or via a peristaltic pump (E4). The QCM sensors we use are almost always gold-coated QSX 301 crystals (Q-Sense, Västra Frölunda, Sweden), with a fundamental shear mode resonant frequency of 5 MHz and a Sauerbrey mass sensitivity of 17.7 ng/Hz. The gold coating not only acts as an electrode but also allows irreversible covalent attachment via a gold sulphur bond to be achieved in a relatively straightforward manner. In addition, this type of sensor can be cleaned and reused multiple times.

2.2. Proteins

In our experience, the QCM is suitable for measuring amyloid elongation rates which span more than four orders of magnitude. This breadth of measurable elongation rates between the fastest

growing proteins we studied (Aβ 1–42 (15) and Ure 2p yeast prion) and the slowest (HEW lysozyme (16), bovine β-lactoglobulin) is possible because of the ability to vary the concentration of the protein solutions and of the extremely stable baseline of the QCM that can detect rates of frequency change as small as 3 Hz/h (for a 5 MHz crystal) or less, therefore enabling the most interesting amyloid systems to be studied with high accuracy. The more crucial factor in the general applicability of the QCM technique is the ability to produce in a reproducible manner well-defined seed fibril suspensions and their reliable attachment to a sensor surface (see Subheading 3 and (13)). In cases where the peptide or protein is readily available commercially (e.g., Aβ 1–42, hen lysozyme, bovine insulin), we used the lyophilized powder without further purification. However, in some cases (e.g., commercially available recombinantly produced human lysozyme), we found that dialysing the protein extensively prior to the kinetic experiments decreased the growth rate considerably (under otherwise identical conditions); this effect can be attributed to residual salts in the lyophilized commercial protein. Therefore, in all cases where the absolute aggregation rate needs to be accurately defined, dialysis or chromatographic separation of the precursor protein from any possible contaminant to achieve high levels of purity should be carried out. Recombinantly expressed protein should also be as highly purified as possible and salt free. In some cases, e.g., in the case of the commercially available Aβ (1–42) peptide (available as a trifluoroacetic acid (TFA) salt in most cases), specific procedures must be adopted (see Subheading 3) to ensure the absence of large oligomers and fibril seeds from the precursor solutions.

2.3. Chemicals

Apart from standard analytical solutions such as phosphate buffer and hydrochloric acid, which are used to provide conditions for reproducible amyloid formation rates other chemical treatment is needed in cases where the amyloid seed fibrils do not contain cysteine residues to allow covalent attachment to the gold surface. Indeed, most amyloidogenic peptides and proteins do not contain cysteine residues. For the well-established procedures for covalent attachment of fibrils to an activated self-assembled monolayer (SAM) (see, e.g., ref. 4), the required chemicals are mercaptoundecanoic acid (MUA), or a similar carboxy-terminated SAM forming molecule, 1-ethyl-3-(3-dimethylaminopropyl)carbodiimide hydrochloride (EDC), *N*-hydroxysuccinimide (NHS), and ethanolamine.

We recently reported a novel attachment strategy (13) that does not involve the attachment of the amyloid seeds to an activated SAM, but rather attaches a small sulphur-containing molecule to the seed fibrils, that in turn enables their covalent attachment to the gold. The chemical species required for this method are 2-imminothiolane ("Traut's reagent"), 2,2′-dithiobis(ethylamine) ("cystamine"), and methoxy-terminated PEG thiol (m-PEG thiol,

Polypure, Oslo, Norway). For Aβ (1–42) experiments, in particular, we recommend a chemical treatment of the commercially available peptide to disrupt any pre-existing aggregates. For this protocol (17), TFA of high purity and hexafluoroisopropanol (HFIP) are required. In addition, 7 M NaOH solution is used for the cleaning of the QCM sensors prior to reuse.

2.4. Further Requirements

Direct imaging of fibril functionalized surfaces is critical, especially in the initial stages of a study that involves the use of QCM methods to probe amyloid growth. AFM measurements should be used to confirm the successful production of seed fibrils as well as their attachment to the gold surface of the sensor. In this way, the starting point of the experiment can be easily verified, i.e., the number of seeds present on the sensor can be estimated. In addition, at the end of all experiments, the QCM sensor surface should be imaged again and the increase in length of the fibrils estimated, as well as ensuring the absence of amorphous aggregates or other off-pathway products.

Furthermore, a sensitive (to 0.1 mg) balance, a tabletop centrifuge, a heat plate with magnetic stirrer and a sonication probe (e.g., 500 W ultrasonic homogenizer, Cole Parmer, Hanwell, UK) are required. If reuse of the QCM sensors is desired, an ozone plasma cleaner (e.g., 172 nm Excimer Radiation System SUS-128, Ushio, Livingston, UK) is ideal; alternatively, the SAM can also be removed electrochemically. Here, only an electrical power supply that can deliver 2-V DC voltage is required. For the Aβ (1–42) preparation, a SpeedVac concentrator is also needed.

3. Methods

3.1. Seed Fibril Formation

In most cases where the kinetics of amyloid formation is the object of the study in question, conditions will be well established that enable the formation of appropriate seed fibrils. Therefore, we will not enter here into comprehensive details of the optimal conditions for fibril formation; instead we shall give examples of suitable conditions for three systems from our own work, involving bovine insulin, human α-synuclein, and human Aβ (1–42). The first example represents a globular protein that is widely used as a model system for studies of protein misfolding and aggregation. The second example is the natively unfolded 140-residue protein whose aggregation is associated with the formation of intracellular Lewy bodies in Parkinson's disease, and the third, the 42-residue fragment of the amyloid precursor protein whose aggregation results in extracellular amyloid plaques in Alzheimer's disease.

3.1.1. Insulin

Incubate a solution of 5 mg/ml (ca. 1 mM) of bovine insulin in HCl pH 2 (final pH not adjusted) at 60°C for 4 days, under con-

tinuous magnetic stirring. The solution will turn into a gel while the fibrils form (13).

3.1.2. α-Synuclein

Incubate a solution of 1.5 mg/ml (ca. 100 μM) human α-synuclein in PBS buffer at 37°C for 4 days under magnetic stirring (16). The stirring in this case is absolutely essential; no fibrils will form from highly purified protein solutions without stirring or shaking or other mechanical agitation, with stirring being the most efficient and preferable way.

3.1.3. Aβ (1–42)

Dissolve 0.5 mg commercially available Aβ (1–42) (TFA salt, e.g. from Bachem, Basel, Switzerland) without additional purification steps in 100 μl 10 mM NaOH solution. Divide into ten aliquots of 10 μl each, and store at −20°C. When a QCM sensor is to be prepared for a measurement, add 400 μl of 100 mM phosphate buffer pH 7.4 to each aliquot to be used. Mix well and incubate for 5 min. Then proceed without delay to "Sensor preparation". This protocol relies on the presence of oligomers and fibril seeds in the commercially available peptide and is, therefore, susceptible to a certain variability in terms of the mass and length distribution of fibrils obtained. Recently, a protocol has been established that enables the preparation of Aβ monomer and fibrils in a highly reliable and reproducible way (18) and which has potential to improve the control of the length distribution of seed fibrils attached to the QCM surface.

In most cases, the final fibril suspensions, or the resulting gels, can be stored at room temperature for months, especially the samples at acidic pH. In the case of α-synuclein and Aβ (1–42), however, the fibrils are stable only for a few days and, in addition, the proteins are prone to bacterial degradation, unless sodium azide is added. Fresh fibrils should, therefore, be grown every time a new set of experiments is performed.

The amyloid fibrils in these gels are up to several micrometres in length and the length distribution has to be greatly decreased to optimize the number of fibril ends on the QCM sensor to which the soluble protein molecules attach, and therefore to maximize the measured signal (1, 13). The required decrease in size distribution is achieved via ultrasonication. With the instrument we have been using, a minimum volume of 300 μl is required, as the sample will otherwise increase in temperature as a result of the energy that is dissipated in the sample. We routinely use cycles of 3 s sonication at 100 W and 3 s of recovery time for amyloid fibrils made from all proteins. The total number of sonication cycles necessary to obtain an average length of only a few hundred nanometres varies, however, quite strongly between the amyloid fibrils formed from different proteins, ranging from a single cycle for bovine β-lactoglobulin to 100 or more for bovine insulin. This variability is due to the differences in mechanical properties between fibrils consisting of different proteins. See Note 1 for details on the total sonication times recommended for amyloid fibrils from commonly used peptides and proteins.

3.2. Amyloid Fibril Activation

Two distinct strategies to attach the amyloid seed fibrils to the QCM sensor surface have been established. In the first, amyloid fibrils that are stable at neutral pH can be attached via standard amide coupling to an activated SAM (4, 5, 15). In the second, the fibrils can be directly attached to the gold surface, either via intrinsic sulphhydryl groups/disulphides (from cysteine residues in the protein) or via the attachment of small sulphur-containing molecules (cystamine and 2-imminothiolane) to side chains, a method that can be easily adapted to the desired pH value. We have described the latter approach in detail in ref. (13), as well as the difference between such a covalent attachment to gold and a purely non-covalent absorption of the fibrils onto the surface. Here we describe the procedures by means of two proteins as examples, α-synuclein and bovine PI3-SH3, for which amyloid fibrils are readily formed at neutral and acidic pH, respectively.

3.2.1. Attachment of Cystamine to PI3-SH3 at pH 2

For this protocol, non-sonicated fibrils must be used to facilitate the separation of the activated fibrils from excess reagent via centrifugation. The procedure is as follows:

1. Add 1 mg of EDC and 100 µl of a solution of 1 M cystamine to 300 µl of 1 mM PI3K-SH3 amyloid fibrils in HCl pH 2.
2. Mix thoroughly and make up to 2 ml with HCl pH 2.
3. Centrifuge for 1 h at 8,000 × *g* or more.
4. Remove the supernatant, make up to 2 ml with HCl pH 2 again and resuspend pellet.
5. Repeat centrifugation and resuspension a total of three times. Finally resuspend in 300 µl.
6. Sonicate for a total of 30 s under the conditions described above.

3.2.2. Attachment of 2-Imminothiolane to Human α-Synuclein at pH 7.4

In this case, the fibrils must be sonicated immediately prior to activation, as 2-imminothiolane (Traut's reagent) is only stable for a limited amount of time in its active form (13), and therefore the time delay between fibril activation and attachment to the surface needs to be minimized. The procedure is, therefore, to sonicate 300 µl of a 100 µM suspension of α-synuclein fibrils (in PBS) for a total of 5 min. Add 50 µl of a 1 mg/ml solution of Traut's reagent in water to the sonicated fibril solution. Incubate for 5 min, then proceed to the step described below as Subheading 3.3 without further delay.

3.3. Sensor Preparation

The principal aim of this step is to prepare a homogeneous seed fibril density on the sensor surface. The surface concentration of fibrils needs to be high enough that the growth of these fibrils generates a sufficiently strong, measurable change in resonant frequency of the QCM chip. This objective is obtained by incubating the surface with a concentrated suspension of sonicated fibrils.

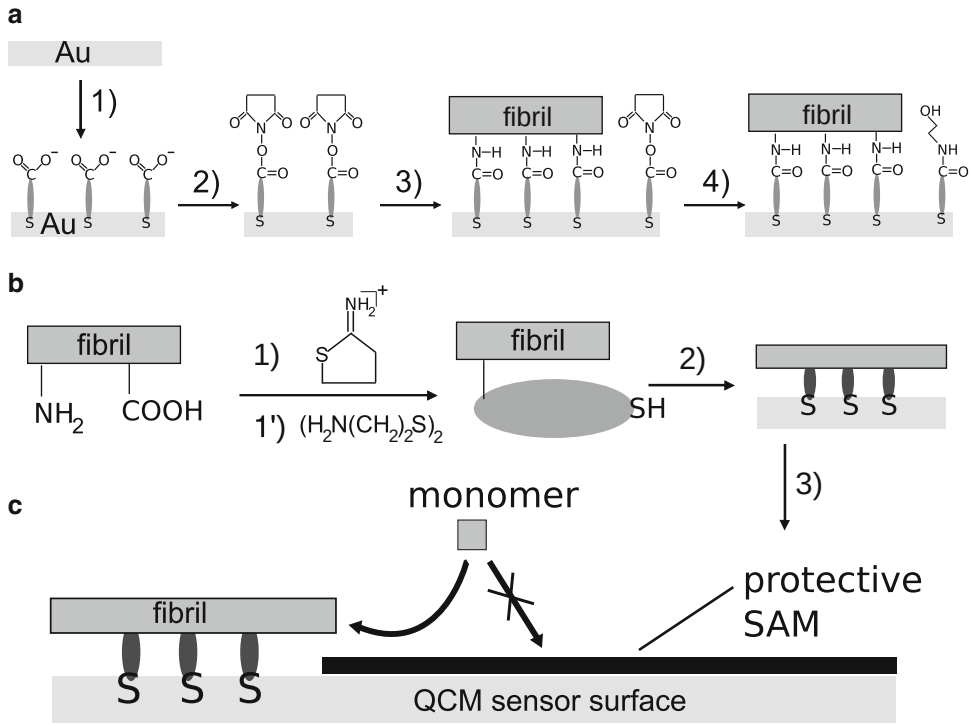

Fig. 2. Schematic illustration of the seed fibril attachment to a gold-coated QCM sensor. (**a**) Attachment of seed fibrils to a chemically activated SAM: (1) formation of SAM of mercaptoundecanoic acid (MUA), (2) activation of SAM with EDC and NHS to form reactive NHS esters, (3) coupling of the seed fibrils to the activated SAM, (4) passivation of the remaining activated MUA with ethanolamine; (**b**) attachment of chemically modified amyloid fibrils to a gold surface: coupling of Traut's reagent (1) or cystamine (1′) to the seed fibrils, (2) attachment of modified seeds to the gold surface, (3) passivation of the remaining exposed gold surface with an SAM; (**c**) QCM measurement where the surface-bound seeds are exposed to a solution of soluble amyloidogenic protein. The non-specific attachment of protein onto the surface is prevented by the SAM, and the attachment is uniquely directed onto the seeds.

The remaining sensor then has to be passivated in the cases where the fibrils are directly attached to the gold rather than to an SAM (13). We note here that it is important to incubate the QCM sensor with the fibril suspension outside the QCM cell. Not only does this procedure minimize the volume of fibril suspension needed for the surface preparation, but it also avoids the adsorption of amyloid fibrils in the flow system of the QCM.

As mentioned above, we can distinguish two attachment strategies, namely the reaction of seed fibrils with an activated SAM or the incubation of a bare gold surface with fibrils that have exposed sulphhydryl or disulphide groups. Examples of both types of attachment procedures will be given here and an illustrative summary is shown in Fig. 2.

In all cases where QCM experiments are performed with a protein not previously studied, or where the solution conditions are drastically changed, control experiments must be performed in

which no seed fibrils are attached to the surface of the QCM sensor, but the gold surface is only passivated by a SAM; when such a control sensor is brought into contact with a protein solution, no frequency shift should be observed. This control experiment is necessary to be able to attribute the observed frequency shift in experiments with surface-bound seed fibrils upon exposure to soluble protein entirely to the elongation of these fibrils, rather than at least in part to non-specific absorption of protein molecules to the surface.

3.3.1. Attachment of Aβ (1–42) Amyloid Fibrils to an SAM on a Gold Surface

This protocol follows a description in ref. 15 and is as follows. Incubate a gold-coated QCM sensor overnight in a solution of 1 mM MUA in absolute ethanol. Rinse the sensor with ethanol and dry with nitrogen and then incubate it for 20 min in a solution of 0.3 mg/ml 1-ethyl-3-(3-dimethylaminopropyl)carbodiimide (EDC) and 0.5 mg/ml NHS. Rinse with water and dry with nitrogen, and then add 100 µl of the fibril suspension onto the gold surface and leave for 5–10 min. Rinse surface with water, add 100 µl of a ca. 0.5 M solution of ethanolamine (pH adjusted with HCl to < 9) and incubate for 15 min. Rinse the surface again with water and insert into the microbalance (see Note 2).

3.3.2. Attachment of Insulin Fibrils to the Gold Surface of the QCM Sensor

Dilute the 5 mg/ml stock solution 1:20 into HCl at pH 2, sonicate for 10 min (under the conditions described above), and incubate the surface of a QCM sensor with 100 µl of the fibril suspension for 1 h. Rinse extensively with HCl at pH 2, then incubate the surface for 30 min with a solution of 1 vol.% of m-PEG thiol in HCl at pH 2. Then the surface is washed again with HCl at pH 2 and the sensor is inserted into the microbalance (see Note 2).

3.3.3. Attachment of Activated PI3K-SH3 and α-Synuclein Amyloid Fibrils to a Gold Surface

Add 100 µl of the activated and sonicated fibril suspension (see Subheading 3.2) onto a clean gold-coated QCM sensor. Incubate the sensor surface for 1 h in an atmosphere of 100% humidity (e.g., in a closed Petri dish with a few ml of water added). Rinse with HCl at pH 2 in the case of PI3K-SH3 and with PBS in the case of α-synuclein. In the case of the cystamine-activated fibrils, no further steps are required, as the remaining cystamine in the solution plays the role of an SAM forming molecule, and the sensor can be directly inserted into the microbalance (see Note 2). In the case of the α-synuclein activated with Traut's reagent, however, the formation of an SAM, as in the case of insulin described above, is required. It is carried out in an analogous manner, except that the mPEG thiol is dissolved in PBS at pH 7.4 instead of HCl at pH 2.

In general, it is useful to take AFM images of the QCM sensors after their initial preparation, to be able to define the length distribution and surface density of the attached seed fibrils. The images acquired at this point then provide the reference for images acquired after the experiment is complete. It is not necessary to carry out this procedure routinely, but for a new set of conditions it is indispensable.

It is possible to dry the sensor for the imaging process without interfering with the seeding capabilities of the surface-bound protein, although if the sensor surface is left dry for an extended period of time (hours to days), the seeding capability can eventually be lost.

3.4. Purification/ Treatment of Commercially Available Proteins and Peptides

When the amyloid formation reaction of commercially available protein (e.g., lysozyme, α-lactalbumin, and β-lactoglobulin) is studied and when absolute elongation rates are of interest, the soluble protein, even if reported to be of very high purity, might require dialysis against a large volume of water prior to the experiments, because of the possible presence of residual salts. The protein can be lyophilized again for convenient storage. If the growth rates (see Subheading 3.5) are indistinguishable between dialyzed and non-dialyzed protein, the dialysis step can be omitted.

To be able to use some highly aggregation prone systems, e.g., Aβ (1–42), for kinetic measurements, careful pre-treatment is needed to remove pre-existing aggregates and seeds that can induce rapid fibril formation when the peptide is dissolved in a buffer. To achieve this aim, various methods have been proposed in the literature, such as chemical treatment or size exclusion chromatography. In most cases, we used for Aβ (1–42) and its analogues the treatment with TFA and HFIP (17), as it yields good results on control QCM sensors, while being easy to carry out:

1. Dissolve 0.5 mg Aβ (1–42) in 500 μl of TFA, and sonicate for 30 s on ice with a probe sonicator (see above).
2. Flash freeze in liquid nitrogen and lyophilize over night.
3. Redissolve the peptide in 1 ml HFIP and incubate on ice for 15 min, as the dissolution can take some time.
4. Make aliquots of 50 μl and evaporate the HFIP in a speed vac. Store the aliquots (ca. 10 nmol) in a freezer.
5. Determine the exact amount of peptide per aliquot (amino acid analysis).

3.5. Measurements

Once the sensor is inserted into the liquid cell, the resonant frequency can be monitored and the establishment of a stable baseline can be followed. Changes in the temperature of the cell can lead to a large shift in the resonant frequency, despite the quartz crystal being specifically (AT) cut to minimize that dependency, because of the different thermal expansion coefficients of the quartz and the gold electrodes. The temperature at which the experiments are to be carried out should, therefore, be already established during the equilibration period.

To perform a measurement of the elongation rate of the surface-bound fibrils, they have to be brought into contact with a solution of soluble protein under conditions where amyloid growth

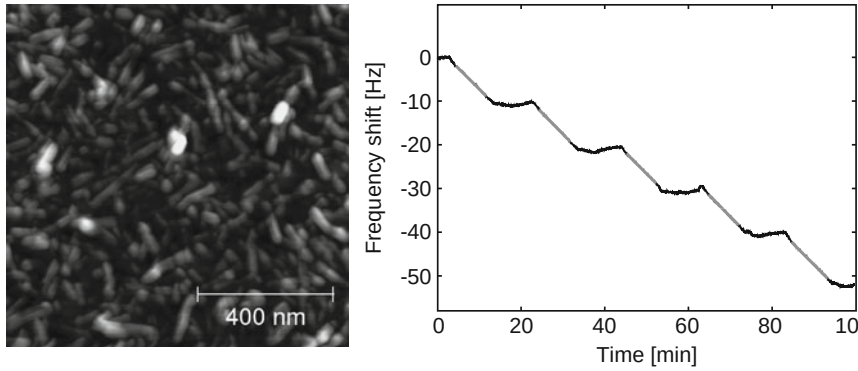

Fig. 3. The AFM image on the *left hand side* shows seed fibrils of the protein insulin attached to a QCM sensor surface, before the series of experiments shown on the *right hand side* of the figure were carried out. The surface number density is estimated to be 500 ± 200 μm^{-2}. On the *right hand side*, a typical QCM experiment, in this case a test of the intrinsic reproducibility is shown. The surface-bound seed fibrils are repeatedly exposed to a solution of 0.2 mg/ml insulin in HCl pH 2 at 40°C. The *grey lines* indicate the sections of the frequency trace (here the frequency overtone with $N = 5$, see main text for details) that were fitted with a linear function to extract the rates of frequency change. The average rate of the five repeats shown here is 0.96 ± 0.01 Hz/min.

is favourable; as an example, we describe a measurement of the elongation of insulin fibrils. As the surface-bound seed fibrils are brought into contact with a solution of 0.2 mg/ml insulin in HCl at pH 2 and 40°C, the resonant frequency will start to decrease linearly (see Fig. 3 and Note 3). The rate of change of frequency in this case is ca. 1 Hz/min, but in general can range from <0.05 to >20 Hz/min, therefore spanning several orders of magnitude, depending on the temperature, solution conditions, and the nature of the protein under study. The experiment is performed in the absence of flow, i.e. the pump or gravity flow is stopped once the liquid cell has been completely filled with protein solution. The change in frequency will cease when the insulin solution in the flow cell is replaced by HCl at pH 2. It is important to use the same buffer or other solution to dissolve the protein and to wash the liquid cell after each measurement (see Note 4). When very concentrated protein solutions are used, a shift in resonant frequency can be observed upon contact of the QCM sensor with the protein solution, due to the increased viscosity and density of the latter when compared with pure buffer. This shift is, however, reversible when the liquid cell is filled again with buffer.

The linearity in time of the decrease in resonant frequency greatly facilitates the analysis of the data (see below). To observe this linearity, significant depletion effects within the liquid cell, due to the addition of the soluble protein on the surface-bound seed fibrils, must not occur. This requirement arises because the fibril elongation rate is linearly dependent on the concentration of soluble protein over a wide concentration range, and, as this concentration decreases, so does the rate. It is, therefore, useful to carry out these QCM measurements under conditions where only a very

small fraction of the protein in the liquid cell is consumed, such that the concentration is effectively constant. In practical terms, this situation results for all except the most aggregation prone peptides and proteins where concentrations as low as 1 μM are used to obtain rates that are sufficiently slow to measure accurately (see Note 5).

A first experiment should always be a test of the reproducibility of the rate of frequency shift and therefore of the fibril elongation rate. This can be achieved by filling the liquid cell repeatedly with an identical protein solution (Fig. 3). The slopes of the change in resonant frequency can be expected to be identical to within less than 10%, due to the fact that the growth of the same, constant ensemble of fibril seeds is examined. In the example in Fig. 3, the observed rates of change in resonant frequency in five consecutive incubations are 0.96 ± 0.01 Hz/min. This exceptionally high reproducibility is a main strength of the biosensing approach and enables very small changes in aggregation rate to be detected (16).

If the total shift in frequency, and therefore the total increase in fibril mass reaches a certain threshold value, however, the sensor will not be sensitive to further addition of protein (see Note 5). This threshold value depends on the surface density of fibrils and on the specific protein contained within the fibrils and defines the "life time" of the sensor. Only within this "frequency-shift window", reliable and reproducible measurements can be carried out. The manifestation of this finite usability of a given sensor is the slow decrease in rate of frequency shift over time. The approximate time of onset of this decrease should be determined before a systematic study of the effects of changes in conditions is carried out.

Once this preliminary characterization has been carried out, a freshly prepared QCM sensor can be successively exposed to solutions of soluble protein and conditions such as temperature, ionic strength, the presence of small molecule compounds, and so on can be varied. This ability to carry out a series of experiments with the same fibrils enables a highly accurate study of the influence of such conditions on the fibril elongation rate, and therefore on the barriers that separate the soluble state of the protein on its energy landscape from the aggregated state. This characteristic enables in-depth studies of the mechanism of aggregation, as well as enabling a systematic and high throughput (due to the short duration of a single measurement) search for inhibitors of this process (15, 16).

At the end of one or a series of measurements, especially at the initial stages of a study, the sensor surface should be routinely imaged with an atomic force microscope (Fig. 3). Not only do these images allow an estimate of the average length increase of the surface-bound fibrils to be made (see Note 6) in cases where absolute elongation rates are required, but they can also be used, as mentioned above, to detect the presence of other aggregation products such as amorphous species, which can be induced by certain extrinsic factors, such as high ionic strength, and which can also give rise to a shift in resonant frequency if the aggregates attach to the surface.

3.6. Data Analysis

Two types of kinetic experiments designed to study amyloid fibril elongation are readily carried out using the QCM technique. In the first type, only relative changes of aggregation rate upon some change in conditions are of interest, e.g. a comparison of the fibril elongation rate in the presence and absence of an inhibitor. In the second type, the absolute rate of fibril elongation is needed, i.e. the number of protein molecules that add on to a single fibril end per time unit. For the first type of measurement, no knowledge of the total number of growing fibril ends on the QCM sensor surface is required (as long as it remains constant during the measurement), and the exact proportionality factor between the mass of added protein and the frequency shift do not have to be known. As long as it can be established that the decrease in resonant frequency is, within some range of the total frequency shift, proportional to the mass of added protein, and therefore to the total length increase of the surfac-bound seed fibrils, the rates of frequency change under different conditions can be directly compared.

QCM devices often allow for the fundamental resonant frequency, as well as several of its higher-order harmonics, to be monitored simultaneously. The fundamental frequency is most sensitive to perturbations, such as pressure and temperature changes, and is often not analysed. For surface-attached material of high rigidity, all the (normalized) frequency overtones ideally show the same shift. However, in the case of a rough, viscoelastic surface layer, there can be substantial deviations between the harmonics, as a result of, e.g., frequency-dependent viscoelastic properties of the attached material and different penetration depths of the different overtones of the shear wave into the attached layer. In such cases, the growth rate analysis should be carried out using either one particular frequency or an average of several overtones. The latter possibility can increase signal-to-noise ratio, and is possible because despite the fact that the different overtones show different mass sensitivity coefficients, the relative changes in rate upon changes in condition are in most cases extremely similar.

As mentioned above, experiments to measure growth rates are ideally carried out under conditions where no significant depletion of protein molecules in the liquid cell occurs during a measurement. In this case, the rate of change in frequency is very well approximated as a linear function of time and can be easily fitted to such a function. If a certain change in conditions leads to a faster rate of change in frequency, then it can be concluded that the rate of protein addition to the seed fibrils is enhanced and therefore that the given change in conditions promotes aggregation. The converse holds for inhibition giving rise to a decrease in the rate of frequency change.

3.6.1. Determination of Absolute Reaction Rates

However, the determination of absolute reaction rates in terms of microscopic rate constants requires knowledge about the number density of seed fibrils on the sensor surface and, in addition, the proportionality factor between the attached mass and the observed frequency

shift must be defined. We will describe below how these quantities can be estimated. Knowledge of these two quantities allows calculation of the absolute mass, and therefore of the total sum of protein molecules that have become attached to the fibril ends. At the same time, one has to bear in mind that this quantity will be an ensemble average, not least because amyloid fibrils may elongate via "stop and go" kinetics in which there may be pauses in between periods of rapid growth of individual fibrils (19). If these ensemble averages of absolute aggregation rates are analysed in the framework of an appropriate kinetic model, however, it is possible to determine key quantities such as the free energy barrier that separates the soluble protein from its fibrillar state (1, 20) and characteristic time scales involved in the attachment of a soluble protein molecule on a fibril end (20). Such information is key in the elucidation of the mechanism of amyloid formation.

3.6.2. Determination of the Seed Fibril Number Density on the Surface

This objective can be achieved by imaging of the surface with an AFM before or after the experiment (Fig. 3) and manual counting. The surface can be dried and simply imaged in air. In the case of high surface densities, it can, however, be challenging to obtain an accurate estimate of the number of density of seed fibrils. The fibril density should then be determined on several independent regions of the same sensor and the average value should be used.

3.6.3. Determination of the Proportionality Factor Between Attached Mass and Observed Frequency Shift

As mentioned in Subheading 1, due to the complex hydrodynamics of a network of surface-bound fibrils, it is not possible to interpret the frequency shift induced by the elongation of the fibrils in terms of a simple Sauerbrey (8) or Kelvin–Voigt (11) model. It is, therefore, necessary to determine empirically the proportionality coefficient between fibril length increase and frequency shift. Once this mass sensitivity coefficient has been determined, it can be assumed to be identical for similar experiments, involving amyloid fibrils made from the same protein.

Two methods for the calibration can be distinguished. The first is based on the determination of the length increase of amyloid fibrils by AFM imaging. The average length of amyloid fibrils is measured before and after a QCM experiment and the increase in length is correlated with the observed decrease in resonant frequency of the sensor during the experiment. In addition, the number of fibrils (see above) as well as their diameter and density needs to be known. The diameter can also be determined from AFM measurements, and the density can be assumed to be similar to that of a globular protein. From these data, the total mass of added fibrillar material can be estimated and compared to the frequency shift. Such calculation is illustrated in the following section. The second method, which we mention here only briefly, is based on the finding mentioned above that when low concentrations of soluble proteins are used in the case of highly aggregation prone peptides and proteins, depletion effects can be observed

provided that the volume of the liquid cell is sufficiently small. In these cases, effectively all the available protein in the liquid cell can be incorporated into the fibrils and the total observed frequency shift due to the addition of this protein on to the seed fibrils can be measured. The known amounts of protein (due to known concentrations and volumes) in contact with the seeds can then be correlated with the observed frequency shift.

3.6.4. Example Estimation of Mass Sensitivity Coefficient for E4 QCM Used to Probe Insulin Amyloid Growth

As an illustration of the principles detailed above, we carry through a calculation that allows us to estimate the microscopic rate constant of the insulin amyloid fibrils shown in Fig. 3. The average length increase per fibril is estimated from Fig. 4 to be 200 ± 100 nm. The number density of seed fibrils (Fig. 3) is estimated to be $500 \pm 200\ \mu m^{-2}$. The diameter of a fibril is 5 nm, and the density is assumed to be 1.2 g/cm^3, as for a globular protein. The active area of a QSX-301 sensor is 1 cm^2. Therefore, the observed frequency shift of ca. 50 Hz corresponds to between 70 and 500 ng of added fibrillar protein, yielding a mass sensitivity coefficient of between 1.4 and 10 ng/Hz. If this is compared to the Sauerbrey mass sensitivity of the sensor of 17.7 ng/Hz, it can be seen that an additional contribution to the frequency shift, not stemming from dry mass occurs. Using this range of mass sensitivity coefficients, we obtain a molecular rate constant for insulin fibril elongation of 1350–9630 $M^{-1}s^{-1}$ assuming growth occurs from one end only, or half these values if growth is symmetric. Such data can be used to calculate the free energy barriers that separate the soluble from the aggregated protein (20).

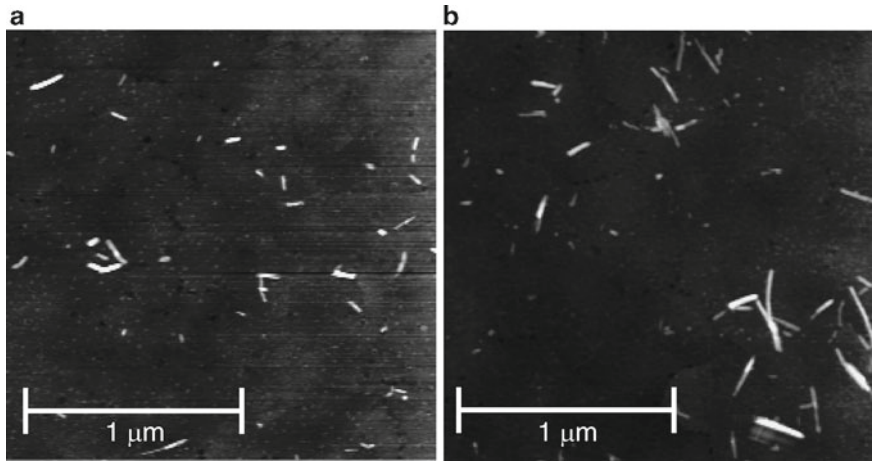

Fig. 4. These two AFM images were used to estimate the length increase that the surface-bound insulin seeds had undergone in the experiment shown in Fig. 3. Gold substrates had been prepared in a similar way to the QCM sensors, albeit with a much lower surface density, which greatly facilitates estimation of the length increase. For an actual QCM measurement, the elongation of surface-bound fibrils at such a low surface density would not give rise to a measurable signal. (**a**) At the beginning of the experiment. (**b**) After incubation for 1 h at 40°C with an insulin solution of 0.2 mg/ml in HCl pH 2. The average length increase is estimated to be 200 ± 100 nm.

3.7. Cleaning of QCM Sensors

In most cases, the gold-coated QCM sensors can be cleaned and reused (13). However, to remove the attached fibrils, relatively harsh conditions have to be applied. We found that heating the sensors to 80°C in 7 M NaOH solution removed >95% of the protein aggregates, as judged from AFM images taken after the cleaning process. When the sensor is reused for the same type of experiments, this level of cleanliness is sufficient. In cases where an SAM has been applied, it can be removed electrochemically by applying a voltage of −1 to −2 V against a gold counter electrode at neutral pH using any inert electrolyte, such as phosphate buffer. Even better results for the removal of the SAM (as judged from contact angle measurements) and residual protein material were obtained via UV/ozone cleaning with exposure times of 10 min, after which the sensors are ready for reuse.

4. Notes

1. The total sonication times used to achieve an appropriate length distribution under the conditions described above (see Subheading 3.1) are as follows: insulin: 10 min, PI3K-SH3: 30s, lysozyme: 15–30 s, insulin B-chain: 2 min, β-lactoglobulin: 3 s, α-lactalbumins: 15 s, α-synuclein: 5 min.
2. When the QCM sensor is inserted into the microbalance, the reverse of the chip (where no fibrils are attached and which is not in contact with the liquid during the experiment) needs to be dry. Otherwise, the baseline will not readily stabilize as a result of evaporation of the residual solution.
3. Often, the frequency shift is non-linear for the first few minutes of incubation of a freshly prepared sensor in contact with a protein solution. This instability is presumably due to a certain amount of non-specific absorption of soluble protein to the surface, despite the passivation of the surface with an SAM, as well as to lateral attachment of protein molecules to the seed fibrils. The extent to which this additional protein adsorption occurs depends strongly on the specific protein. The first contact of a new sensor with a protein solution should therefore always be repeated to check for the completion of this adsorption process that interferes with the signal associated with fibril elongation.
4. The resonant frequency of a QCM sensor in contact with liquid is also dependent on the density, viscosity and, in some cases, ionic strength of the solution involved. If any of these parameters is changed, a shift in resonant frequency will be observed, which is normally reversible when the solution is replaced by the previous solution. This effect can be important in cases, for

example, when the binding of small molecules to amyloid fibrils is being studied (15). The binding can lead to a shift in resonant frequency, but if different solvent conditions are needed to solubilise the small molecules, the shift induced by the change in solvent can be much larger than the shift induced by the binding and the latter can, therefore, be masked.

5. We have observed depletion effects in the case of the Yeast prion protein Ure 2 and for the peptide Aβ (1–42). In these cases, the concentration of soluble polypeptide was as low as 1 μM. Such low concentrations were required to slow down the growth rates sufficiently to prevent the seed fibrils on the sensor surface elongating at too high a rate. When the fibrils become too long, the sensor does not respond any more to the contact with soluble protein. This "saturation" is presumably due first to crowding of fibrils on the surface and second to the effect of their finite rigidity, leading to a loss of vibrational energy within the fibrillar layer.
6. In many cases, the surface density of fibrils on a QCM sensor will be too high to allow an easy estimation of the length increase via AFM imaging of the sensor surface. Such a high surface density might, however, be required to achieve a sufficiently high signal-to-noise ratio. In such cases, a gold substrate can be prepared with a much lower surface density of seeds than on the original QCM sensor and incubated with a monomer solution under identical conditions for the same amount of time. It is then much easier to estimate the length increase and correlate it with the observed frequency shift (Fig. 4).

Acknowledgments

We thank Duncan A. White and Evgenia G. Afanasieva for helpful comments on the manuscript. The authors acknowledge support from the EPSRC, the BBSRC, the Wellcome and Leverhulme Trusts, and the IRC in Nanotechnology. AKB acknowledges support through a Bye-Fellowship from Magdalene College, Cambridge.

References

1. T.P.J. Knowles, S.G.L. Devlin, S. Meehan, S. Auer, C.M. Dobson and M.E. Welland, Kinetics and thermodynamics of amyloid formation from direct measurements of fluctuations in fibril mass, *Proc Natl Acad Sci*, 2007, **104**, 10016–10021
2. B.Y. Feng, B.H. Toyama, H. Wille, D.W. Colby, S. R. Collins , B. C. H. May, S. B. Prusiner, J. Weissman and B.K. Shoichet, Small-molecule aggregates inhibit amyloid polymerization, *Nat Chem Biol*, 2008, **4**, 197–199
3. M.R. Nilsson. Techniques to study amyloid fibril formation in vitro, *Methods*, 2004, **34**, 151–160
4. W.-P. Hu, G.-L. Chang, S.-J. Chen and Y.-M. Kuo. Kinetic analysis of beta-amyloid peptide

aggregation induced by metal ions based on surface plasmon resonance biosensing, *J Neurosci Methods,* 2006, **154**, 190–197

5. S. Kawatake, Y. Nishimura, S. Sakaguchi, T. Iwaki, K. Doh-ura. Surface plasmon resonance analysis for the screening of anti-prion compounds, *Biol Pharm Bull*, 2006, **29**, 927–932
6. M. B. Hovgaard, M. Dong, D.E. Otzen, F. Besenbacher, Quartz crystal microbalance studies of multilayer glucagon fibrillation at the solid-liquid interface, *Biophys J*, 2007, **93**, 2162–2169
7. J.A. Kotarek, K.C. Johnson and M.A. Moss, Quartz crystal microbalance analysis of growth kinetics for aggregation intermediates of the amyloid-beta protein, *Anal Biochem*, 2008, 378, 15–24
8. G. Sauerbrey, Verwendung Von Schwingquarzen Zur Wägung Dünner Schichten Und Zur Mikrowägung, *Zeitschr f Physik,* 1959, 155, 206–222
9. K.K. Kanazawa and J.G. Gordon II, The oscillation frequency of a quartz resonator in contact with liquid, *Anal Chim Acta*, 1985, 175, 99–105
10. C.E. Reed, K.K. Kanazawa and J.H. Kaufman, Physical description of a viscoelastically loaded AT cut quartz resonator, *J Appl Phys*, 1990, 68, 1993–2001
11. M.V. Voinova, M. Rodahl, M. Johnson and B. Kasemo, Viscoelastic Acoustic Response of Layered Polymer Films at Fluid-solid Interfaces: Continuum Mechanics Approach, *Pysica Scripta*, 1999, 59, 391–396
12. T.P.J. Knowles, C.A. Waudby, G.L. Devlin, S.I.A. Cohen, A. Aguzzi, M. Vendruscolo, E.M. Terentjev, M.E. Welland and C.M. Dobson, An analytical solution to the kinetics of breakable filament assembly, *Science*, 2007, 326, 1533–1537
13. A.K. Buell, D.A. White, C. Meier, M.E. Welland, T.P.J. Knowles and C.M. Dobson, Surface attachment of protein fibrils via covalent modification strategies, *J Phys Chem B,* 2010, 114, 10925–10938
14. G. McHale and M.I. Newton, Surface roughness and interfacial slip boundary condition for quartz crystal microbalances, *J Appl Phys,* 2004, 95, 373–380
15. A.K. Buell, C.M. Dobson, T.P.J. Knowles, and M.E. Welland, Interactions between amyloidophilic dyes and their relevance to studies of amyloid inhibitors, *Biophys J,* 2010, 99(10), 3492–3497
16. D.A. White, A.K. Buell, T.P.J. Knowles, M.E. Welland and C.M. Dobson, Protein aggregation in crowded environments, *J Am Chem Soc*, 2010, 132, 5170–5175
17. C. Lendel, B. Bolognesi, A. Wahlström, C.M. Dobson and A. Gräslund, Detergent-like interaction of Congo red with the amyloid beta peptide, *Biochemistry*, 2010, 49, 1358–1360
18. D.M. Walsh, E. Thulin, A.M. Minogue, N. Gustavsson, E. Pang, D.B Teplow and S. Linse, A facile method for expression and purification of the Alzheimer's disease-associated amyloid beta-peptide, *FEBS J*, 2009, 1266–1281
19. J. Ferkinghoff-Borg, J. Fonslet, C. Beyschau Andersen, S. Krishna, S. Pigolotti, H. Yagi, Y. Goto, D. Otzen, M.H. Jensen, Stop-and-go kinetics in amyloid fibrillation, *Phys Rev E*, 2010, 82, 010901
20. A.K. Buell, J.R. Blundell, C.M. Dobson, M.E. Welland, E.M. Terentjev and T.P.J. Knowles, Frequency Factors in a Landscape Model of Filamentous Protein Aggregation, *Phys Rev Lett,* 2010, 104, 228101

Chapter 9

X-Ray Fibre Diffraction Studies of Amyloid Fibrils

Kyle L. Morris and Louise C. Serpell

Abstract

Amyloid fibrils are polymeric assemblies of normally soluble proteins or peptides. To investigate their structure, it is generally not possible to use conventional methods of crystallography and solution nuclear magnetic resonance. To examine the repeating crystalline structure along the fibre axis, X-ray fibre diffraction has been a useful tool. Here we discuss the methods by which amyloid-like fibrils may be prepared to form a sample suitable for structural analysis and describe how data may be collected and then analysed to arrive at a potential model structure.

Key words: Amyloid, Fibril, X-ray fibre diffraction, Texture, Assembly, Cross-beta

1. Introduction

Amyloid fibrils are formed by many different proteins and peptides. These highly ordered assemblies are associated with diseases such as Alzheimer's, Diabetes type 2, and the transmissible encephalopathies. Each disease is characterised by the ordered assembly of a particular protein or peptide (1). Amyloid fibrils are also utilised by different organisms in functional roles due to their impressive strength and stability (2).

Amyloidogenic peptides and proteins all assemble to form fibres that share similarities in their appearance by electron and atomic force microscopy and in their ability to bind amyloid-specific dyes, such as ThT and congo red. Figure 1 shows the typical morphology of amyloid fibres. X-ray fibre diffraction reveals a specific diffraction pattern known as the cross-β pattern, that is thought to arise from hydrogen-bonded β-strands running perpendicular to the fibre axis to form a series of β-sheet ribbons that extend along the fibre axis. This view is supported by evidence from cryo-electron microscopy (3), solid-state NMR (4, 5), and

Einar M. Sigurdsson et al. (eds.), *Amyloid Proteins: Methods and Protocols*, Methods in Molecular Biology, vol. 849,
DOI 10.1007/978-1-61779-551-0_9,

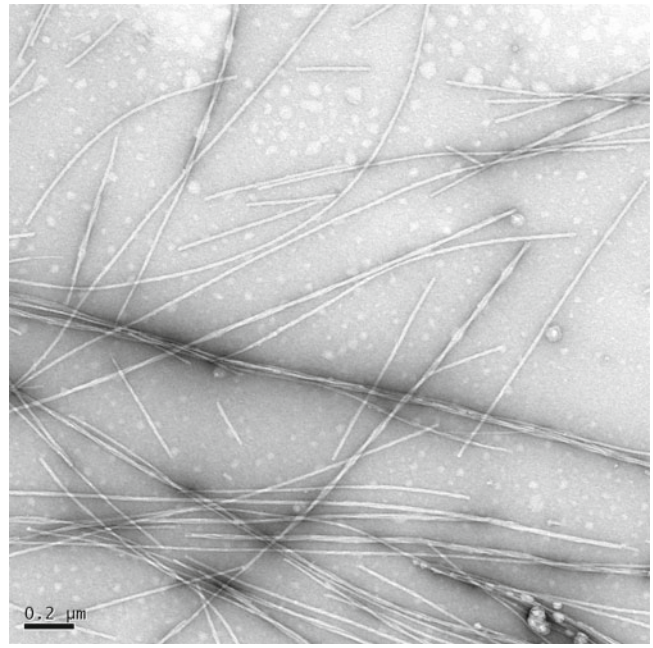

Fig. 1. The underlying amyloid structure predominantly extends in one direction creating fibrillar structures. Negative stain transmission electron microscopy is typically used to study fibre morphology and also rapidly identify features associated with amyloid fibres; fibres are of indeterminate length and ~10 nm in diameter.

EPR (6) and also by recent crystal structures of short amyloidogenic peptides (7). A typical cross-β diffraction pattern is shown in Fig. 2 and shows the characteristic 4.7–8 Å diffraction signal on the meridian of the pattern, corresponding to the distance between hydrogen-bonded β-strands and a more diffuse signal on the equator at a variable distance of 10–12 Å that arises from association of the sheets and is dependent on the size of side chains.

Recent work has revealed that despite the diversity in the sequences of precursor proteins, aggregation prone sequences can be predicted using algorithms that take into account specific characteristics such as charge, hydrophobicity, and beta-sheet propensity (8–10). However, these methods are not always able to exclusively predict ordered aggregation but taking into account the positions of side chains within a sequence has enabled the specific prediction of ordered amyloid-forming peptides (11, 12). In addition to hydrogen-bonded β-sheets, the specific architecture associated with amyloid formation is thought to arise from the interdigitation of side chains characterised as steric zippers (7, 12).

X-ray diffraction from fibres can be used to confirm the amyloidogenic and cross-β nature of assembling proteins or peptides,

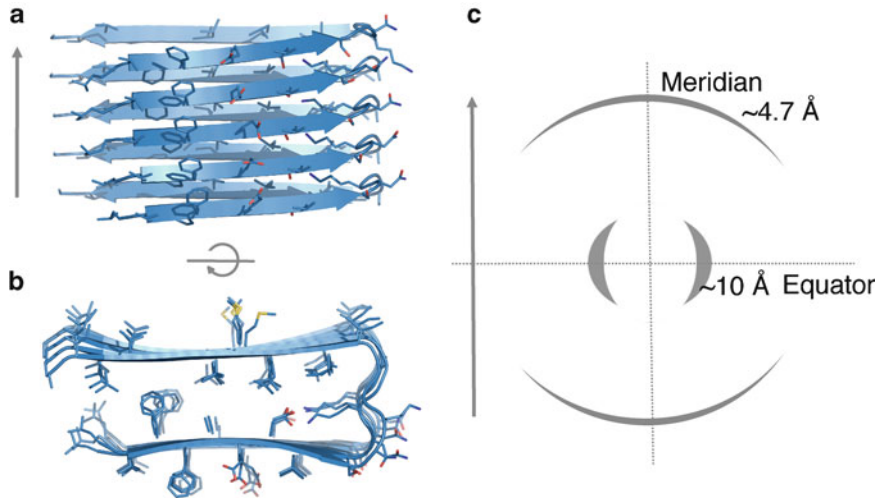

Fig. 2. The cross-β architecture and the typical fibre diffraction pattern exhibited by this arrangement using the model for Aβ(1–42) fibrils as an example (42). β-Strands are stacked perpendicular to the fibre axis (*arrow*) separated by 4.7–8 Å (**a**). β-Sheets run parallel to the fibre axis and are separated by 10–12 Å (**b**). This arrangement gives rise to a fibre diffraction pattern where the repetitive spacing along the fibre axis (*arrow*) is observed on the meridian and the repetitive spacing perpendicular to the fibre axis is observed on the equator.

either formed in vitro or isolated from tissue. More powerfully, this technique can be used to produce model structures to explain the association of peptides or proteins within an amyloid fibre. Here we describe the ways in which this technique can be used and the data can be analysed.

2. Materials

1. Protein fibres—high concentration in suitable low salt buffer or water.
2. Carbon-coated, electron microscope grids (AGAR Scientific, Stansted, UK).
3. 2% Uranyl acetate, 0.2 μm filtered.
4. Glass capillaries (Harvard Apparatus Ltd, Fircroft way, Edenbridge, Kent, UK), (1.5 mm OD × 1.17 ID borosilicate) to be filled with a wax plug.
5. 0.7-mm diameter X-ray glass capillaries (GLAS, W. Muller, D-13503, Berlin, Germany),
6. Goniometer (Hampton), X-ray set (in house).
7. Computer workstation running Mosflm/fit2d/fibrefix/CLEARER (latest version of java).

3. Methods

3.1. Preparation of Fibrils from Soluble Proteins or Peptides

Each protein or peptide that assembles to form amyloid fibrils will have a very specific set of conditions ideal for assembly. Conditions for assembly can be explored including variation in pH, temperature, ionic strength, and buffer (see Note 1). Concentration of peptide may often need to be high, although slow assembly may support formation of more ordered fibres that will be more amenable for structural analysis. Assessment of amyloid formation can be performed using well-established assays including thioflavin T fluorescence (13), congo-red staining (14), and turbidity (15).

3.2. Characterisation of Fibrils

Before X-ray diffraction samples are prepared, it is essential to investigate the morphology of fibres and the amount of fibrils that are formed in solution. Different proteins and peptides will form fibrils with differing efficiency, so it is not possible to predict an ideal starting solution concentration. Negative stain electron microscopy provides a rapid way to examine the fibrils, although atomic force microscopy is often used as alternative or to provide complementary information (see Note 2).

The fibrils should be long, straight, and unbranched (Fig. 1). An even covering and distribution of the fibrils on the grid is desirable to examine fibril morphology. Order and length directly affect fibril alignment; short fibrils are often difficult to align, whereas long fibrils and laterally associated fibrils are often successful. Amyloid fibres have been reported to adopt a range of morphologies at the macroscopic scale (16). These differences may give rise to inherent disorder in fibre alignments affecting fibre diffraction patterns and so morphology is an interesting and important feature to characterise.

3.2.1. Electron Microscopy

Grids may be prepared in the following way:

1. Holding a grid in a pair of fine forceps, place 4 µl of a protein/fibril solution on a glow-discharged, carbon or carbon/formvar coated, 400 mesh copper grid (available from TAAB or AGAR scientific) and incubate for 1 min. Blot away the excess using the edge of a piece of filter paper.
2. Wash twice with water (4 µl) (MilliQ filtered 0.2 µm) with 1-min incubations, blotting between each addition. Stain the grid twice by adding freshly filtered 2% uranyl acetate (4 µl), incubate for 1 min, and finally blot excess and allowing to air dry (see Note 3).
3. Examine grid using a transmission electron microscope at magnifications of over 20,000×.

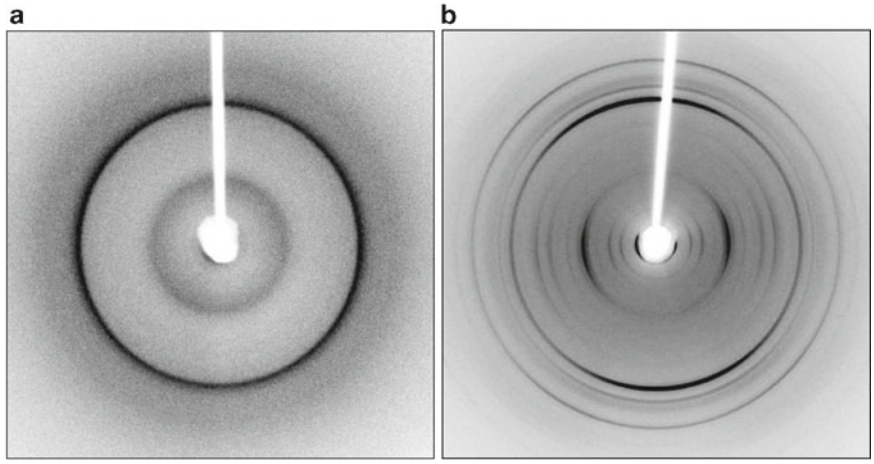

Fig. 3. Fibre diffraction from an un-oriented amyloid sample (**a**) and a well-oriented amyloid sample (5) (**b**). The un-orientated sample is characterised by complete radial averaging and only exhibits the reflections associated with inter- and intra β-sheet spacings. A well-oriented sample will typically contain much more information pertaining to repeating cell dimensions.

3.3. Preparation of Fibre Samples, Fibre, Mats, Discs: Importance of Texture

A sample of fibrils that has a high degree of alignment and order will likely give rise to more information in the resulting diffraction pattern. The diffraction pattern from a sample with no alignment will produce reflections that are entirely radially averaged (Fig. 3a) or appear as reflection rings, while a partial alignment will produce reflections arcs that are oriented on each axis of the pattern (17). A sample with a high degree of alignment will likely produce a pattern containing considerably more information (Fig. 3b) and reflections will be confined to distinct axes in the cross-β arrangement and possibly arranged on layer-lines. The information obtainable from X-ray fibre diffraction is dependent on alignment and this, in turn, may be dependent on the nature of the sample. A high concentration of long fibrils will be viscous and maybe very amenable to stretch frame alignment (18). However, samples that are short but laterally aggregated may be more successfully aligned by placing a solution in a capillary tube and allowing the solution to dry to form a disc. Where the degree and best method of alignment is sample dependent several methods should be attempted, each produces a sample with a different texture (defined as the arrangement of crystallites relative to one another (19)), these are shown in Fig. 4.

3.3.1. Stretch Frame Alignment

This method produces a bundle of fibrils whose fibre axes are ideally all parallel (Fig. 4a). This may be achieved by the drying of a fibril-containing solution between two capillaries mounted in a Petri dish or similar. Although not essential, a stretch frame apparatus (Fig. 5) may be used allowing the mounting of capillaries and their

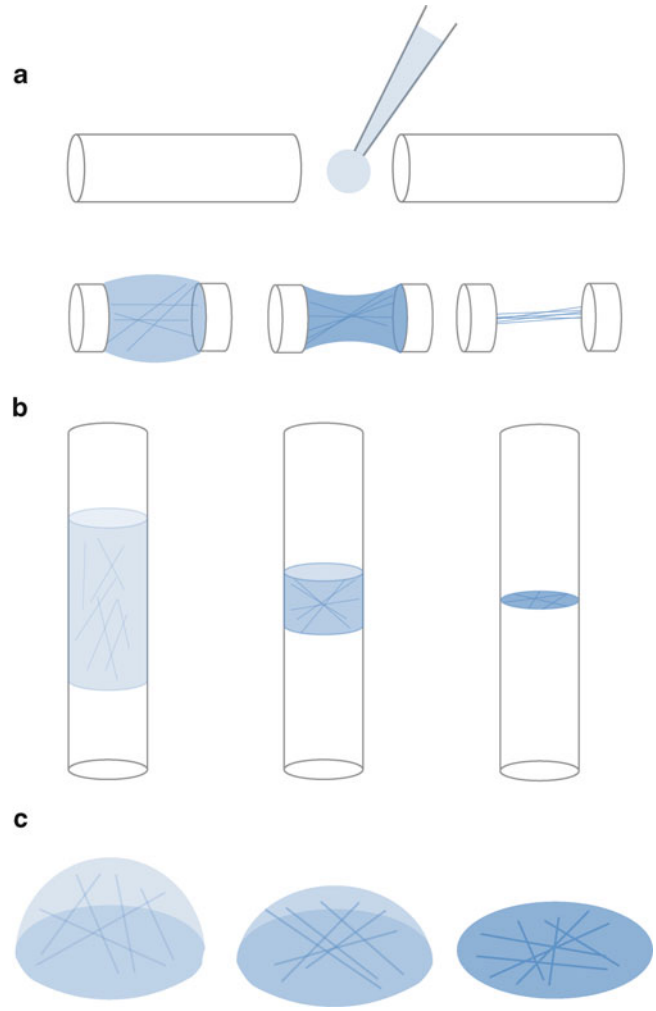

Fig. 4. Fibres in solution may be aligned by a number of methods and as solvent evaporates fibres naturally align into different textures. A solution suspended between two capillaries will produce a bundle of fibres with all fibre axes aligned (**a**), whereas solutions may be dried within capillaries (**b**) or on a surface (**c**) to produce a texture where fibre axes are at random orientations.

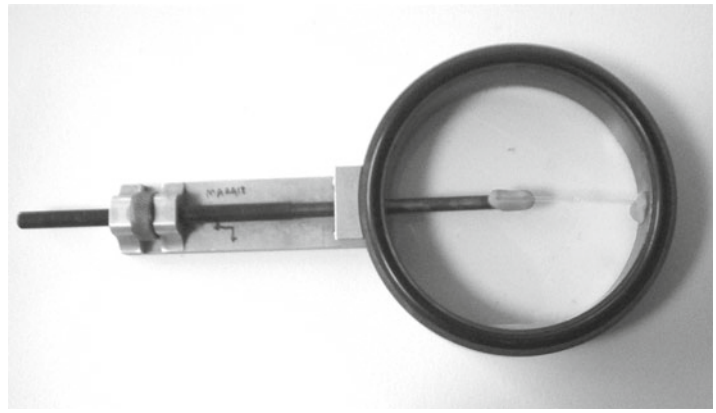

Fig. 5. The stretch frame apparatus used to improve the alignment of amyloid fibrils.

gradual separation during drying which may improve alignment. The method for stretch frame alignment is detailed below.

1. Borosilicate glass capillaries should be cut to a length of about 2–3 cm using a diamond pen and sealed. The capillaries should be sealed by dipping in liquid wax. If candle wax is melted to the correct temperature (~100°C), a small amount of wax will be drawn up by capillary action (1–2 mm). The wax surface should be flat for the fibril suspension to rest on.
2. Mount the sealed capillaries in the stretch frame or within a Petri dish using plasticine. They should be placed with a gap of about 0.5–2 mm. If fibrils are short, then the alignment may benefit from using a shorter gap.
3. Suspend a 10 µl droplet of solution between the two capillaries. Care should be taken that the solution makes contact with both wax ends but does not extend onto the glass.
4. Cover the Petri dish or stretch frame to prevent contamination from dust, allow the sample to evaporate and the fibrils align. Formation of a dried fibre sample can take hours to days depending on the temperature and humidity of the environment and the sample viscosity.

As the sample is aligning, the capillaries may be separated using the stretch frame to increase alignment. Altering the speed by which the sample dries may improve alignment. For example by incubating at lower temperatures or under humidity.

3.3.2. Alignment of Amyloid Fibrils in a Glass Capillary

The object of alignment in a glass capillary is to obtain a disc as shown in Fig. 4b. A glass capillary used for X-ray data collection with 0.7 mm diameter should be used. The use of siliconized capillary tubes (so that the meniscus is flat) can improve disc formation.

1. Using a 1-ml syringe fitted with a small piece of rubber tubing, fix to the wide end of the glass capillary and aspirate up about 2–3 cm of fibril solution/suspension (see Note 4).
2. Seal the end of the capillary using melted wax, leaving the top of the tube open for evaporation. Fix the capillary to a surface so that it stands vertical and allow to dry. To form a dry disc can take several weeks (see Notes 5 and 6).

3.3.3. Alignment of Fibrils as a "Mat" or Thin Film

The preparation of a mat or thin films may require a larger volume of protein than the previously described methods. The resulting sample should be a thin, flat film as shown in Fig. 4c. The sample can be dried onto a glass slide and then carefully lifted off. This method was used to prepare mats of polyamino acids by Fandrich and Dobson (20). However, it can be difficult to lift the material off the glass possibly due to the presence of short fibres and/or the sample being non-viscous. Other materials that can be used as a suitable surface to

make a film are parafilm or Teflon. This method is commonly used for polymer alignment and was also used to obtain diffraction patterns from PolyQ peptide by Perutz and co-workers (21).

The result should be a thin, flat film similar to the alignment produced inside a glass capillary (Fig. 4b). This can be mounted such that the X-ray beam passes parallel to the plane of the film. In the resulting sample, the fibre alignment is in the plane of the film, whereas diffraction through the face of the film will yield diffraction rings.

It is important that the different conditions for alignment and resulting sample texture are taken account of since they will have a direct effect on the nature of the diffraction pattern (see Note 7). A stretch frame alignment has a reasonably simple texture that can be used to determine repeating cell dimensions. Alternative textures are complicated by fibre axes being at alternative orientations relative to one another but may reveal additional structural information and are useful if stretch frame alignments are unsuccessful (see Note 8).

3.3.4. Examining the Sample

An indication of how well a sample has aligned can be obtained by examining the sample under cross-polarised light in a light microscope. The presence of birefringence can indicate that the fibres are aligned to some degree. This method was used by Kirschner and co-workers for examining the alignment of Aβ amyloid fibrils and allowed the authors to find that some peptides formed fibrils more amenable to alignment than others (22).

3.4. Hydration

Dehydration of amyloid samples has been suggested to have significant effects on the internal cross-β structure (23). The importance of the hydration state of fibrillar systems in fibre diffraction has been highlighted as a variable that should be controlled during fibre diffraction experiments and apparatus has been described for doing so (24). Hydration state can be controlled such that the fibril sample apparently better represents the solution structure but it is important to dry the alignment enough to introduce order and alignment.

3.5. Data Collection

Partially aligned fibre samples should be mounted onto a goniometer head and placed in the X-ray beam taking into account the orientation and direction of the fibres. The rotation axis will be around the fibre axis for a stretch frame aligned fibre. For discs the fibres tend to align across the diameter of the tube (Fig. 4b). A mat will have two distinct directions (parallel to the plane of the film and perpendicular to it) (Fig. 4c).

A diffraction pattern maybe collected using in-house X-ray equipment for protein crystallography or using synchrotron radiation. Exposure times would be expected to be from 1 s to 5 min depending on the quality of the sample (a well-aligned sample will diffract more strongly) and the intensity of the X-ray beam (see Note 9).

3.6. Data Analysis

Depending on the degree of fibre alignment, the diffraction pattern may contain rings, or many oriented diffraction signals. Measurements of signal positions can be performed using software accompanying the X-ray equipment or using mosflm (CCP4) (25) or other display programmes. If the pattern shows only the classical cross-β pattern, then further analysis is not useful. However, if a number of discrete signals are observed, then further processing can be performed.

Several fibre diffraction processing programmes are available. The CCP4 suite (25) has been designed for single crystal diffraction data; however, many of the components can be used for examination of diffraction data (e.g., Mosflm, imosflm, and Ipdisp). CCP13 (26) was developed as a collection of programmes designed to analyse high-quality fibre diffraction patterns.

Fit2d (www.esrf.fr/computing/expg/subgroups/data_analysis/FIT2D) has been developed for examining and analysing both small angle X-ray scattering data and fibre diffraction data.

Fxplor (www.molbio.vanderbilt.edu/fiber/software.html) is an extension of X-Plor, a programme useful for atomic model refinement (27) (additional details are given in a previous chapter (28)).

Recently, we have developed a programme that allows inspection and analysis of diffraction patterns called CLEARER (29). This programme is available free to academic users by contacting the corresponding author. In this chapter, we concentrate on the use of this particular tool. Further details can be found in ref. (29).

Initially, the diffraction pattern should be converted to a tiff file to enable it to be read into CLEARER. Once uploaded, the user must specify the diffraction settings including the pixel size (following conversion to tiff format), source wavelength, and sample to detector distance. The diffraction pattern can be rotated such that the meridian and equator are, respectively, vertical and horizontal and the pattern may be centred using the *Centring module*. This module compares intensity along the two main axes of the pattern that can be user specified. The *Radially Average module* outputs a graphical representation of reflection position and intensity at a user specified angle. This should be set along the two main axes (meridian and equator) and within this the *Peak Find module* can be used to automatically output reflection positions. The peak search width can be adjusted to change the sensitivity of the output where smaller search widths will be more sensitive to reflections that are close together. The *Zoom and Measure module* should be used to check the peak output by hand and then a list of signal positions can be verified in the equatorial and meridional directions. If a stretch frame aligned sample is well ordered and aligned, then the positions of the equatorial reflections are related to the *b* and *c* unit cell dimensions (Fig. 6). The equatorial reflections of the pattern are indexed by assigning [*hkl*] Miller indices

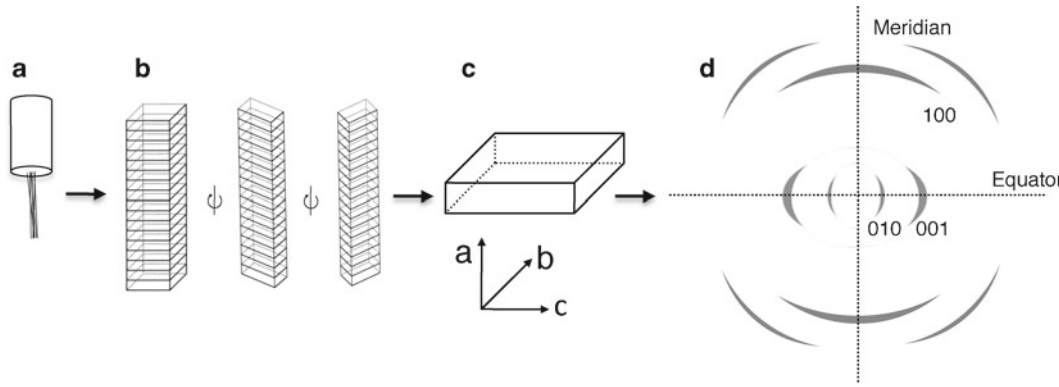

Fig. 6. The texture of a bundle of fibres (**a**) can be described as a collection of crystallites rotated around their long axis, giving rise to a cylindrically averaged sample (**b**). The repeating cell of a crystallite can be considered in isolation (**c**) as giving rise to many of the features of fibre diffraction from amyloid (**d**). The dimensions of this unit directly correspond to reflection positions in the resulting diffraction pattern as indicated by miller indices.

that describe the origin of each reflection. However because the sample is cylindrically averaged, reflections from the *b* and *c* dimensions are mixed and can also overlap and so manual pattern indexing can be problematic. Hence the signal position information can be input into the Unit Cell Optimisation module that allows the user to explore possible unit cell dimensions for the *b* and *c* dimensions based on indexing the input reflections. Since amyloid systems share a common β-strand spacing the largest *a* dimension will be 4.7–4.8 (or possibly 9.4–9.6 Å for an antiparallel β-sheet). Therefore, in most cases, this dimension is not explored and meridional signals are not input. The user must first specify an initial "guess" for a unit cell based on examining the strong signals found on the equator. A unit cell dimension cannot be smaller than the lowest resolution reflection. CLEARER calculates potential unit cell dimensions and predicts the reflection positions that would be produced by these cells; the predicted reflections are compared to the input reflections and the potential unit cells are scored on the agreement between the predicted and experimental signals. The top 20 matches are displayed based on this assessment and these should be inspected considering peptide precursor size and any available information including measurements obtained from other methods such as electron microscopy, AFM, or solid-state NMR.

3.7. Structural Modelling and Testing Using CLEARER

Models can be constructed using programmes such as Pymol (DeLano) or Insight II (Accelerys). Depending on the size of the unit cell, there are a number of potential arrangements that models can adopt, i.e., parallel/antiparallel β-sheets, face-to-face/face-to-back β-sheets, or up–up/up–down arrangements (7). The unit

cell models can be constructed and loaded into CLEARER, the fibre texture is constructed by CLEARER from user input settings (cell dimensions, crystallite size). The *Structure Chain Generator module* within CLEARER allows the constructed fibre texture to be examined to investigate whether clashing occurs in a particular cell size and to distinguish the fibre axis. Models can then be uploaded into the *Fibre Diffraction Simulation module* and the fibre diffraction pattern calculated using user input settings (fibre axis, beam orientation, X-ray source, and detector settings). The resulting simulated pattern can then be compared to the experimental pattern. Comparisons can be made in several ways. The *Zoom and Measure module* can be used to measure calculated diffraction signals and compared to those measured from experimental patterns; a module called *Layers* can be used to overlay calculated and experimental patterns to compare signal positions. Our preferred method is to compare a quadrant taken from the calculated pattern with the experimental pattern (Fig. 7) (5, 30, 31). This enables a comparison of signal positions and also of relative intensities. As described and shown in Fig. 6, the unit cell dimensions give rise to the signal positions, however, their relative intensities (and whether signals are observable) are modulated by the model structure. Therefore, this procedure allows an evaluation of the validity of a suggested unit cell and then the different possible structural arrangements within the cell. Multiple structures should be tested and information from other techniques to constrain modelling are useful to arrive at the best possible structural representation.

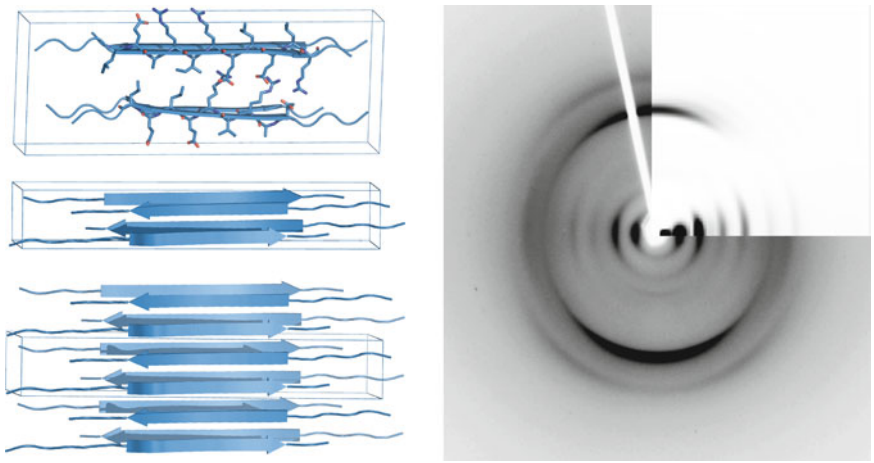

Fig. 7. A comparison of a simulated fibre diffraction pattern from an amyloid model based on the experimental pattern shown (38).

4. Conclusions

X-ray fibre diffraction has been used as a valuable method to analyse the repetitive and ordered nature of amyloid fibrils. Early work showed that amyloid fibrils derived from diseased tissue gave diffraction patterns (32) that shared similar characteristics to those obtained for cross-β silk from Lacewing egg stalks (33). A generic structure for amyloid arose from the X-ray diffraction analysis of amyloid fibrils composed of transthyretin (34) and other amyloid fibrils (35). More recently, X-ray diffraction has produced diffraction patterns with a large amount of information (36) that has enabled molecular models to be produced in which the association of side chains can be modelled (30, 37). The combination of X-ray fibre diffraction with other structural methods has been particularly useful for determining structural models (5, 38, 39). X-ray fibre diffraction has provided information regarding the repeating cross-β architecture of amyloid fibrils upon which other structural methods may build to produce a more complete structure of amyloid (40, 41).

5. Notes

1. Each protein/peptide requires different conditions for optimum amyloid fibril growth and morphology. Therefore, for each sample, conditions including protein/peptide concentration, buffer conditions, pH, and temperature should be explored to optimise the speed of amyloidogenesis to produce the most ordered amyloid fibrils suitable for structural analysis.
2. Each fibril solution can be imaged using electron microscopy (or atomic force microscopy). The method may need to be adapted if a high amount of salt is found in the fibril formation conditions and an additional wash step in the preparation of the grid may be added.
3. The uranyl acetate solution used for negative staining in electron microscopy is best left undisturbed prior to preparing grids where any uranyl acetate crystals will sediment out and not be transferred to the grid that is to be inspected. The uranyl acetate may also be filtered.
4. Samples aligned using the “stretch-frame” method are placed as a droplet of solution between two wax-tipped capillary tubes. The droplet must be held between the two tubes without running along the glass. If this does happen, the glass capillary should be replaced with a new dry one.

5. The wax-tipping process for capillaries to be used in fibril alignments can have variable results. A flat surface is ideal, whereas concave or convex surfaces can make drop suspension problematic and affect the quality of the final alignment.
6. In general slowing the alignment process appears to result in better aligned fibrils. The conditions under which this occurs can be explored, including temperature and humidity. Slowing evaporation by sealing the alignment in a Petri dish with parafilm is useful for slowing the alignment process.
7. Fibril alignments using capillaries become mounted to their surface naturally but mats/thin films must be mounted by hand. Using a Bunsen flame capillaries can be heated and stretched to have very fine tapered ends. When these ends are dipped in superglue they make an ideal surface for mounting mats/thin films, though care should be taken not contaminate the sample.
8. Diffraction patterns obtained from amyloid fibrils formed in solutions containing high salt concentrations may show rings with a spotted texture arising from crystallisation from the salt. This can, in some cases, obscure the protein diffraction. The salt crystals may be removed by careful washing of the fibrils (by centrifugation) prior to alignment (after ensuring the fibrils are stable), or alternatively by carefully washing the aligned sample.
9. Fibrils aligned by stretch frame should be cylindrically averaged. This can be assessed by collecting and comparing diffraction patterns at various rotations about the fibril axis.

References

1. Dobson, C. M. (2001) The structural basis of protein folding and its links with human disease, *Philos Trans R Soc Lond B Biol Sci* 356, 133–145.
2. Fowler, D. M., Koulov, A. V., Balch, W. E., and Kelly, J. W. (2007) Functional amyloid--from bacteria to humans, *Trends Biochem Sci* 32, 217–224.
3. Serpell, L., and Smith, J. (2000) Direct visualisation of the beta-sheet structure of synthetic Alzheimer's amyloid, *J Mol Biol.* 299, 225–231.
4. Petkova, A. T., Ishii, Y., Balbach, J. J., Antzutkin, O. N., Leapman, R. D., Delaglio, F., and Tycko, R. (2002) A structural model for Alzheimer's beta-amyloid fibrils based on experimental constraints from solid state NMR, *Proc Natl Acad Sci USA* 99, 16742–16747.
5. Madine, J., Jack, E., Stockley, P. G., Radford, S. E., Serpell, L. C., and Middleton, D. A. (2008) Structural insights into the polymorphism of amyloid-like fibrils formed by region 20–29 of amylin revealed by solid-state NMR and X-ray fiber diffraction, *Journal of the American Chemical Society* 130, 14990–15001.
6. Der-Sarkissian, A., Jao, C. C., Chen, J., and Langen, R. (2003) Structural organization of alpha-synuclein fibrils studied by site-directed spin labeling, *J Biol Chem* 278, 37530–37535.
7. Sawaya, M. R., Sambashivan, S., Nelson, R., Ivanova, M. I., Sievers, S. A., Apostol, M. I., Thompson, M. J., Balbirnie, M., Wiltzius, J. J., McFarlane, H. T., Madsen, A. O., Riekel, C., and Eisenberg, D. (2007) Atomic structures of

amyloid cross-beta spines reveal varied steric zippers, *Nature* 447, 453–457.

8. Lopez de la Paz, M., and Serrano, L. (2004) Sequence determinants of amyloid fibril formation, *Proc. Natl. Acad. Sci* 101, 87–92.
9. DuBay, K. F., Pawar, A. P., Chiti, F., Zurdo, J., Dobson, C. M., and Vendruscolo, M. (2004) Prediction of the absolute aggregation rates of amyloidogenic polypeptide chains, *J. Mol. Biol.* 341, 1317–1326.
10. Zibaee, S., Jakes, R., Fraser, G., Serpell, L. C., Crowther, R. A., and Goedert, M. (2007) Sequence Determinants for Amyloid Fibrillogenesis of Human alpha-Synuclein, *J. Mol. Biol.* 374, 454–464.
11. Maurer-Stroh, S., Debulpaep, M., Kuemmerer, N., de la Paz, M. L., Martins, I. C., Reumers, J., Morris, K. L., Copland, A., Serpell, L., Serrano, L., Schymkowitz, J. W., and Rousseau, F. (2010) Exploring the sequence determinants of amyloid structure using position-specific scoring matrices, *Nat. Methods* 7, 237–242.
12. Thompson, M. J., Sievers, S. A., Karanicolas, J., Ivanova, M. I., Baker, D., and Eisenberg, D. (2006) The 3D profile method for identifying fibril-forming segments of proteins, *Proc. Natl. Acad. Sci* 103, 4074–4078.
13. Naiki, H., and Nakakuki, K. (1996) First-order kinetic model of Alzheimer's beta-amyloid fibril extension in vitro, *Lab Invest* 74, 374–383.
14. Puchtler, H., and Sweat, F. (1965) Congo red as a stain for fluorescence microscopy of amyloid, *J Histochem Cytochem* 13, 693–694.
15. Wood, S. J., Maleeff, B., Hart, T., and Wetzel, R. (1996) Physical, morphological and functional differences between pH 5.8 and 7.4 aggregates of the Alzheimer's amyloid peptide Ab, *J. Mol. Biol.* 256, 870–877.
16. Jimenez, J. L., Nettleton, E. J., Bouchard, M., Robinson, C. V., Dobson, C. M., and Saibil, H. R. (2002) The protofilament structure of insulin amyloid fibrils, *Proc. Natl. Acad. Sci. USA* 99, 9196–9201.
17. Sikorski, P., Atkins, E. D., and Serpell, L. C. (2003) Structure and texture of fibrous crystals formed by Alzheimer's abeta(11–25) peptide fragment, *Structure* 11, 915–926.
18. Sunde, M., Serpell, L., Bartlam, M., Fraser, P., Pepys, M., and Blake, C. (1997) Common core structure of amyloid fibrils by synchrotron X-ray diffraction, *J. Mol. Biol.* 273, 729–739.
19. Alexander, L. E., p 21 of 582 (1969) *X-ray diffraction methods in polymer science*, 1st ed., Wiley-interscience.
20. Fandrich, M., and Dobson, C. M. (2002) The behaviour of polyamino acids reveals an inverse side chain effect in amyloid structure formation, *Embo J* 21, 5682–5690.
21. Perutz, M. F., Finch, J. T., Berriman, J., and Lesk, A. (2002) Amyloid fibers are water-filled nanotubes, *Proceedings of the National Academy of Sciences USA* 99, 5591–5595.
22. Malinchik, S. B., Inouye, H., Szumowski, K. E., and Kirschner, D. A. (1998) Structural analysis of Alzheimer's beta(1–40) amyloid: protofilament assembly of tubular fibrils, *Biophys. J.* 74, 537–545.
23. Maurstad, G., Prass, M., Serpell, L. C., and Sikorski, P. (2009) Dehydration stability of amyloid fibrils studied by AFM, *Eur. Biophys. J.* 38, 1135–1140.
24. Masters, C., Simms, G., Weinmann, N., Multhaup, G., McDonald, B., and Beyreuther, K. (1985) Amyloid Plaque Core Protein in Alzheimer Disease and Down Syndrome, *Proc Natl Acad Sci USA* 82, 4245–4249.
25. Winn, M. D. (2003) An overview of the CCP4 project in protein crystallography: an example of a collaborative project, *J Synchrotron Radiat* 10, 23–25.
26. Squire, J., AL-Khayat, H., Strunther, A., Cranshaw, J., Denny, R. C., Diakun, G., Dover, D., Forsyth, V. T., He, A., Knupp, C., Mant, G., Ganeshalingam, R., Rodman, M., Shotton, M., and Windle, A. H. (2003) New CCP13 Software and the Strategy Behind Further Developments: Stripping and Modelling of Fibre Diffraction Data, *Fibre Diffraction Review* 11, 7–19.
27. Wang, H., and Stubbs, G. (1993) Molecular dynamics in refinement against fiber diffraction data, *Acta Cryst* A49, 504–513.
28. Makin, O. S., and Serpell, L. C. (2005) X-ray diffraction studies of amyloid structure, in *Amyloid proteins: methods and protocols* (Sigurdsson, E. M., Ed.), pp 67–80, Humana press, Totowa, NJ.
29. Makin, O. S., Sikorski, P., and Serpell, L. C. (2007) CLEARER: a new tool for the analysis of X-ray fibre diffraction patterns and diffraction simulation from atomic structural models, *Appl. Cryst.* 40, 966–972.
30. Makin, O. S., Atkins, E., Sikorski, P., Johansson, J., and Serpell, L. C. (2005) Molecular basis for amyloid fibril formation and stability, *Proceedings of the National Academy of Sciences USA* 102, 315–320.
31. Jahn, T. R., Makin, O. S., Morris, K. L., Marshall, K. E., Tian, P., Sikorski, P., and Serpell, L. C. (2009) The common architecture of cross-beta amyloid, *J. Mol. Biol.* 395, 717–727.
32. Eanes, E. D., and Glenner, G. G. (1968) X-ray diffraction studies on amyloid filaments, *J Histochem Cytochem* 16, 673–677.

33. Geddes, A. J., Parker, K. D., Atkins, E. D., and Beighton, E. (1968) "Cross-beta" conformation in proteins, *J Mol Biol 32*, 343–358.
34. Blake, C., and Serpell, L. (1996) Synchrotron X-ray studies suggest that the core of the transthyretin amyloid fibril is a continuous beta-sheet helix, *Structure* 4, 989–998.
35. Sunde, M., Serpell, L. C., Bartlam, M., Fraser, P. E., Pepys, M. B., and Blake, C. C. (1997) Common core structure of amyloid fibrils by synchrotron X-ray diffraction, *J. Mol. Biol.* 273, 729–739.
36. Inouye, H., Fraser, P. E., and Kirschner, D. A. (1993) Structure of beta-crystallite assemblies formed by Alzheimer beta-amyloid protein analogues: analysis by x-ray diffraction, *Biophys. J.* 64, 502–519.
37. Sikorski, P., Atkins, E. D., and Serpell, L. C. (2003) Structure and texture of fibrous crystals formed by Alzheimer's abeta(11–25) peptide fragment, *Structure* 11, 915–926.
38. Steinmetz, M. O., Gattin, Z., Verel, R., Ciani, B., Stromer, T., Green, J. M., Tittmann, P., Schulze-Briese, C., Gross, H., van Gunsteren, W. F., Meier, B. H., Serpell, L. C., Muller, S. A., and Kammerer, R. A. (2008) Atomic models of de novo designed cc beta-Met amyloid-like fibrils, *J Mol Biol* 376, 898–912.
39. Madine, J., Copland, A., Serpell, L. C., and Middleton, D. A. (2009) Cross-beta spine architecture of fibrils formed by the amyloidogenic segment NFGSVQFV of medin from solid-state NMR and X-ray fiber diffraction measurements, *Biochemistry* 48, 3089–3099.
40. Jimenez, J. L., Nettleton, E. J., Bouchard, M., Robinson, C. V., Dobson, C. M., and Saibil, H. R. (2002) The protofilament structure of insulin amyloid fibrils, *Proc. Natl. Acad. Sci* 99, 9196–9201.
41. Petkova, A. T., Yau, W. M., and Tycko, R. (2006) Experimental constraints on quaternary structure in Alzheimer's beta-amyloid fibrils, *Biochemistry* 45, 498–512.
42. Luhrs, T., Ritter, C., Adrian, M., Riek-Loher, D., Bohrmann, B., Dobeli, H., Schubert, D., and Riek, R. (2005) 3D structure of Alzheimer's amyloid-beta(1–42) fibrils, *Proc. Natl. Acad. Sci* 102, 17342–17347.

Chapter 10

Structural Characterization of Prefibrillar Intermediates and Amyloid Fibrils by Small-Angle X-Ray Scattering

Annette Eva Langkilde and Bente Vestergaard

Abstract

Structural investigation of the species present during protein fibrillation is of tremendous importance, yet complicated by the equilibrium between species of very different sizes and life-times. Small-angle X-ray scattering may be applied to solve this problem, providing both information about the process (number of species present and volume fractions of individual species) and low-resolution three-dimensional shape reconstructions of individual species. Here, we describe in detail the challenges associated with the approach, exemplified using data from fibrillating insulin or α-synuclein samples.

Key words: SAXS, Structure, Amyloid fibril, Nucleus, Oligomer

1. Introduction

Protein fibrillation is often described as a nucleated polymerization, characterized by a lag-phase, an elongation phase, and a steady state, appearing as a characteristic S-shaped curve when following the process with fluorescent probes such as Thioflavin T (ThT). From a structural point of view, the native state dominates during the lag-phase but exists in equilibrium with partially un-/refolded states. The formation of an assumed oligomeric high-energy species (the critical nucleus) has been suggested to be the initiation point for the elongation, and during the elongation phase nonnative monomers or oligomers associate to this nucleus. Such a nucleus is per definition only present in solution in minute amounts, and only exists in equilibrium with multiple other native and nonnative protein structures. Likewise, during elongation, a decreasing amount of the native protein, an increasing amount of early fibrils, and an unknown amount of the nonnative building blocks coexist.

Einar M. Sigurdsson et al. (eds.), *Amyloid Proteins: Methods and Protocols*, Methods in Molecular Biology, vol. 849,
DOI 10.1007/978-1-61779-551-0_10,

A potential macroscopic heterogeneity of the final fibrils only adds to the structural complexity of the solutions, being most pronounced during the steady state. When also taking into account the differences in appearance of the individual species—both in terms of the length scales (Å to μm) and time frames (nano-second equilibriums to irreversibly formed aggregates)—this creates a tremendous challenge for structural investigation. Here, we describe a potential solution to the problem, by applying small-angle X-ray scattering (SAXS)-based structural analysis to the evolving mixtures of fibrillating protein solutions. The method was first applied by Vestergaard *et al.* (1) in a study of insulin fibrillation.

A transiently formed oligomeric species has, in several cases, been suggested to be the major source of cytotoxicity. Such a species may be on or off the fibrillogenesis pathway. Whether on- or off pathway, the oligomer exists in structural equilibrium with other native and nonnative species. This means that elucidation of the structural aspects of oligomeric species preferably should be performed without disturbing the associated structural equilibriums. If on pathway, the species would also represent the structural prerequisite of fibril formation, hence the smallest possible unit of the structural repeats that form the fibril core (i.e., structurally closely related to the critical nucleus).

A thermodynamic nucleus is only present in minute amounts at any time. A theory has been proposed that this species will accumulate in solution above the so-called supercritical concentration (2), defined as the concentration above which an increase no longer shortens the lag-phase. Hence, following this theory, the oligomeric nucleus (now termed the structural nucleus) may be studied above the supercritical concentration. Whether a structural nucleus is accumulating in solution, several structural species are present at any given time point during the fibrillation process, complicating structural analysis. As a consequence, most of the structural information currently available originates either from the endpoint of fibrillation, or from species that have been isolated from the solutions, hence from perturbed equilibriums (3).

SAXS, on the other hand, is uniquely suited for the study of the on-going process directly in solution. The method provides structural information from species in solution on a length scale from ~1 to 100 nm (i.e., comprising the lengths from native proteins to the typical length of the repeating units of mature fibrils), and the method is applicable with a virtually free choice of solutions, i.e., it is possible to apply the experimental conditions necessary for obtaining a particular fibrillation process, varying either the buffer composition or temperature. One important parameter, which in some cases, may be a limiting factor is that protein concentrations above 1 mg/ml typically are required (and for this type of data

analysis preferably above 5 mg/ml, see details below). This said the method can, in the best cases, provide both information about the course of the fibrillation process (number of species, volume fractions of individual species at different time points) and direct model-free (*ab initio*) three-dimensional low-resolution structural information about each species.

The method described here requires synchrotron radiation (see Note 1). Volumes of fibrillating sample are extracted at different time points of the fibrillation process and exposed for short time-intervals (hence represents a snap-shot of the evolving process) with synchrotron X-rays. For ideal solutions, SAXS data are strictly additive. This is very important for this application, since this enables a decomposition of the scattering data measured from mixtures, into scattering data originating from the individual species. In short:

$$I_{\text{total}} = aI_{\text{A}} + bI_{\text{B}} + cI_{\text{C}} + \cdots + nI_{N},$$

where I_{total} is the measured scattering curve at a given time point from the fibrillating sample (hence at most time points originating from a mixture of species), a is the volume fraction of species A at this given time point, and I_{A} is the scattering curve at any time from the isolated species A, etc. If only a limited number of the above parameters are unknown, the individual scattering components may be isolated. Roughly, the equation comes down to:

$$I_{\text{total}} = aI_{\text{native}} + bI_{\text{intermediate}} + cI_{\text{fibril}}.$$

Here, assuming that only one intermediate species is formed (e.g., the nonnative oligomeric species) and only one type of fibrils is formed (see Note 2). If measuring the scattering curve from the native state, prior to the onset of fibrillation and the fibrils during the steady state, only volume fractions and $I_{\text{intermediate}}$ are unknown. These parameters may be estimated, as described in detail below.

The final fibril scattering originates from species that are often micrometer long. Above, we mentioned that SAXS probes species in the size range 1–100 nm. Fibrils, however, may be regarded as beads on a string, with each bead being a repeating unit within the period of the twisting fibril (see Fig. 1). Scattering data from beads on a string may be represented by the scattering from one bead only, at angles corresponding to this length scale. Such a period most often is shorter than 100 nm, and hence may be probed by SAXS. Apart from the unique opportunity to extract structural information from individual components in equilibrium, the method thus also enables 3D structural elucidation of the mature fibrils, with no surface effects, no dehydration effects, and without perturbing any given equilibrium.

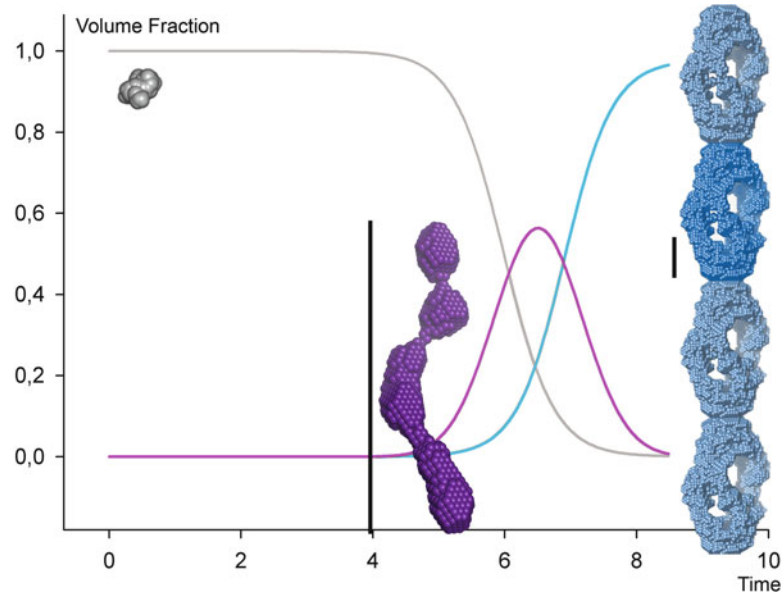

Fig. 1. The evolving equilibrium of fibrillating insulin. An idealized trace of the calculated volume fractions of insulin monomers (*gray*), intermediate oligomer (*purple*), and mature fibrils (*blue*) is shown versus time. Superimposed are the respective surface representation of a monomeric insulin molecule and *ab initio* models of the oligomer and fibril, respectively, shown in the same colors. A 200-Å length scale is shown next to the insulin oligomer and fibril repeating unit, respectively. Note that only one repeating unit is modeled (shown in more intense *blue* color). The intertwining fibril has been modeled by simple translation of individual repeats.

2. Materials

1. Protein or peptide for fibrillation.
2. Buffer solution, preferably exactly matching the conditions used for fibrillation. ThT, stock solution of approximately 1 mM. Prepare by dissolving ThT in H_2O, leave overnight, filter (0.22 μm), and determine the concentration by $A_{412\ nm}$ using $\varepsilon_{412} = 36{,}000\ M^{-1}/cm$. Store at 4°C protected from light. The solutions have limited stability (4) thus always check the concentration before use. Other fluorescent probes may be used.
3. Protein standard (e.g., bovine serum albumin, (BSA) at approximately 4 mg/ml). Often supplied by the beamline.
4. BSA buffer (50 mM HEPES, pH 7.4).
5. Fluorescence plate reader, clear bottom 96-well plates and sealing tape. For the use of ThT: $\lambda_{ex} = 450$ nm and $\lambda_{em} = 480$ nm (both with 10 nm bandpass).
6. Heat block for preheating samples/solvents and for maintaining the temperature of the 96-well plate when extracting samples for the SAXS measurements.

7. Synchrotron BioSAXS beamline.
8. If the samples have a tendency to align: A rod sonicator or Seed beads (Hampton) and Vortex equipment may be necessary.
9. Data evaluation software:
   (a) Fit2D (5) or SAXSview (6) for the evaluation of 2D images.
   (b) ATSAS package (7) for data evaluation, buffer subtraction, analysis, modeling, etc. In particular, the programs SVDplot and OLIGOMER (8) for decomposing the data.
   (c) PyMol (9) or similar to visualize models.

3. Methods

3.1. Sample/ Experiment Preparation

The experimental preparations must enable that the synchrotron experiment can be run as follows:

1. Samples are in a 96-well plate in a fluorescence plate reader, and sample buffers contain ThT. This way the course of the fibrillation is monitored for each individual sample, right until the point of extracting the sample for your X-ray exposures.
2. By pausing the plate reader, take out the 96-well plate, place it on a tempered surface (heating block, ice bath, etc., depending on experimental conditions). Release the covering film, extract a sample from the 96-well plate, return the 96-well plate to the plate reader as quickly as possible. Note the time and the last fluorescence value.
3. If necessary, homogenize the sample.
4. Load the sample into the X-ray sample cell and collect SAXS data from that sample.
5. Rinse the X-ray sample cell and collect SAXS data from a buffer.
6. Repeat from step 2.

To prepare for this type of experiment, one needs to consider three parts: (1) the sample, (2) the time course of the experiment, and (3) the beamline. The optimal (or possible) sample conditions depend highly on the specific beamline setup. Regardless of the system of interest, the following section lists several general issues to be aware of in the preparation phase.

1. To obtain a useful signal-to-noise ratio in the scattering data, the concentration of the fibrillating species should be above 5 mg/ml.

2. The timeframe of the fibrillation process should, if at all possible, be optimized via modifying the experimental conditions (see Note 3) where you have a stable starting point with a lag-phase of minimum 1 h (preferably more) to secure time for sample preparation and measurements of the process starting point (e.g., monomers). The optimal elongation phase depends on the beamline specifications (see below) and not least on the amount of beam time available, but most be long enough to secure that a number of measurements can be made. As a rule of thumb, *at least* six measurements during the lag-phase, eight measurements during the elongation phase, and six measurements during the steady state must be made. If possible, more measurements are highly desirable, in particular, during the elongation phase. The more the merrier.
3. The beamline must be suitable for this type of experiments. Before detailed optimization of the experimental conditions, it is necessary to communicate with the beamline scientist where the experiment will be performed. It is crucial to gather information on the following.
4. Time frame of one measurement (see Note 4).
5. Ask for q-range (which range of scattering angles can be measured, Note 5). In particular, the smallest angles near the beam stop hold crucial information on the overall size (of the fibril repeating unit).
6. How much sample is needed for each measurement (varies significantly, Note 6).
7. How are the samples loaded (automatic sample changers or not, Note 7).
8. Make sure (at the experiment day) to know when there are injections at the synchrotron. In some cases, these cause, as an absolute minimum, a pause in the measurements, thus they are important in the overall timing of the experiment. Avoid coinciding elongation phase and injection (except at beamlines on synchrotrons in a continuous top-up mode).

For optimizing conditions:

1. Given the above information, you can now calculate the shortest possible duration of the lag- and elongation phases (see Notes 4 and 7).
2. Applying a fluorescence plate reader, test different experimental parameters (see Note 3) until you are approximately within the demanded time course. All solvents and buffers should be filtered (0.22 μm). Use the sample volume pr. well that you anticipate applying on the beamline (see Note 6).
3. Establish the supercritical concentration of your protein/peptide in the above-mentioned buffer system.

4. Refine your experimental conditions to fit with the time course, while keeping the protein concentration at or above the supercritical concentration.
5. Before going to the beamline, learn as much as possible about your samples (see Notes 7 and 8).

3.2. Data Collection

As general remark, bring all materials from home. Do not rely on, e.g., Milli-Q water from the beamline to match the one from own lab, since any change may influence your prepared time course.

Before the main experiment:

1. If you have not tested for alignment in the cell prior to the experiment, do this before commencing the main experiment. Bring some "old," fully fibrillated samples and test loading and exposure prior to initiating your main experiment (see Note 7).
2. Measure standards (BSA, water, empty cell. Follow guidelines at the beamline!). Using the standards, (average) molecular mass (MM) of the scattering species can be calculated, based on the relative intensity of the forward scattering, $I(0)$. For the mature fibrils, it will not be possible to accurately determine the average MM from the forward scattering.
3. Make tests for potential radiation damage effects by making several exposures on the same sample (see Note 10). If possible, make this test both on (small-scale) start conditions, as some processes may be accelerated by the X-ray photons, and on mature fibril samples (prepared prior to the experiment).

The main experiment:

1. Do not forget to time your experiment relative to any injections or similar events that may give breaks in the measurement series.
2. Alternately measure buffer and protein/peptide.
3. Keep track of the timing of SAXS and ThT fluorescence signals. Clocks may differ on the different computers, and for later data analysis it is worthwhile keeping good notes on the timing of the various parts of the experiment.
4. Aim for collecting SAXS data from as many time points as possible, particularly immediately prior to, during, and immediately after the elongation phase.
5. Distribute measurements throughout the fibrillation process, hence keep an eye on the ThT values from the different wells (if possible, plot the fluorescence values of the samples immediately prior to measurement). Despite the prior tests and optimization, the process may behave differently when a larger batch is prepared for the data collection, thus take breaks or speed up (if possible) depending on the actual process.

6. It is important to secure measurements of the initial (e.g., monomers) structural state. If the process starts rapidly, the scattering may be measured on a sample prior to initiating fibrillation. If the fibrillation process cannot be controlled after dissolving the protein/peptide, a less optimal alternative is additional measurements at comparable experimental conditions that you have reason to believe corresponds to the same structural state (remember to use the corresponding buffers for those measurements).
7. Make sure to measure several samples also in the stationary phase of the fibrillation process. Even with a stable ThT signal, structural changes are quite possible (see Note 2).
8. During the experiment: Keep an eye on the sample loading (avoid bubbles in the sample chamber, imperfect positioning of the sample, etc.), and keep plotting the buffer-subtracted scattering curves and comparing buffer files (see Subheading 3.3 and Note 9).
9. During the experiment: make notes of any instances during the data collection. Injection, error messages, temperature variations, etc. Such information may be invaluable for understanding unexpected features later.
10. Before leaving the beamline ensure that you have (or know how to get) *all* the data, including potential individual repeated exposures and 2D images.

3.3. Data Evaluation

General guidelines and tutorials for SAXS data evaluation can be found online (e.g., BioIsis (10) and the Saxier forum (11)). Currently, there is significant development at the beamlines, meaning that several steps in the initial data evaluation are automated at a number of BioSAXS beamlines. However, extra caution must be taken for the fibrillating samples as they differ significantly from the systems normally studied at the BioSAXS beamlines.

1. Check all 2D images. Alignment of the sample will give rise to non-isotropic scattering (see Note 7 and Fig. 2) in which case the data cannot be used for decomposition of scattering components or modeling shape structures.
2. Check all buffers. They should superimpose without scaling; outliers should not be included (see Note 9).
3. Check repeated exposures. The individual curves should be identical (see Note 10).
4. Subtract scattering from the buffer (see Note 11).
5. Plot all buffer subtracted curves, check for outliers/cross-over, etc. (see Note 12 and Fig. 3).

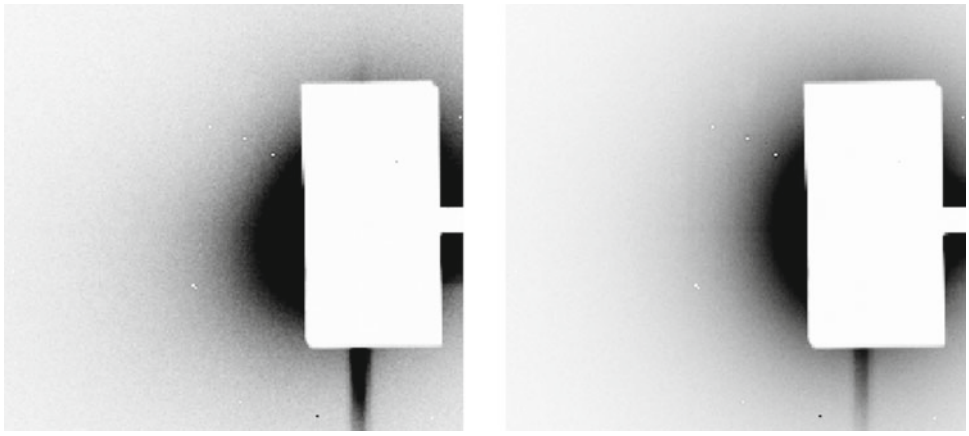

Fig. 2. Examples of 2D data files. 2D data files showing a sample with partial alignment (*left*) and a sample with randomly orientation of the particles (*right*) (see Note 7). The images are zoomed on the area close to the beamstop (*white box*). For the radial averaging a mask file is used to exclude the beamstop, areas with parasitic scattering, etc. The definition of the mask file and the radial averaging is typically done automatically at the beamline. The datafile is from a PILATUS pixel detector, installed at beamline X33 at EMBL-Hamburg/DESY.

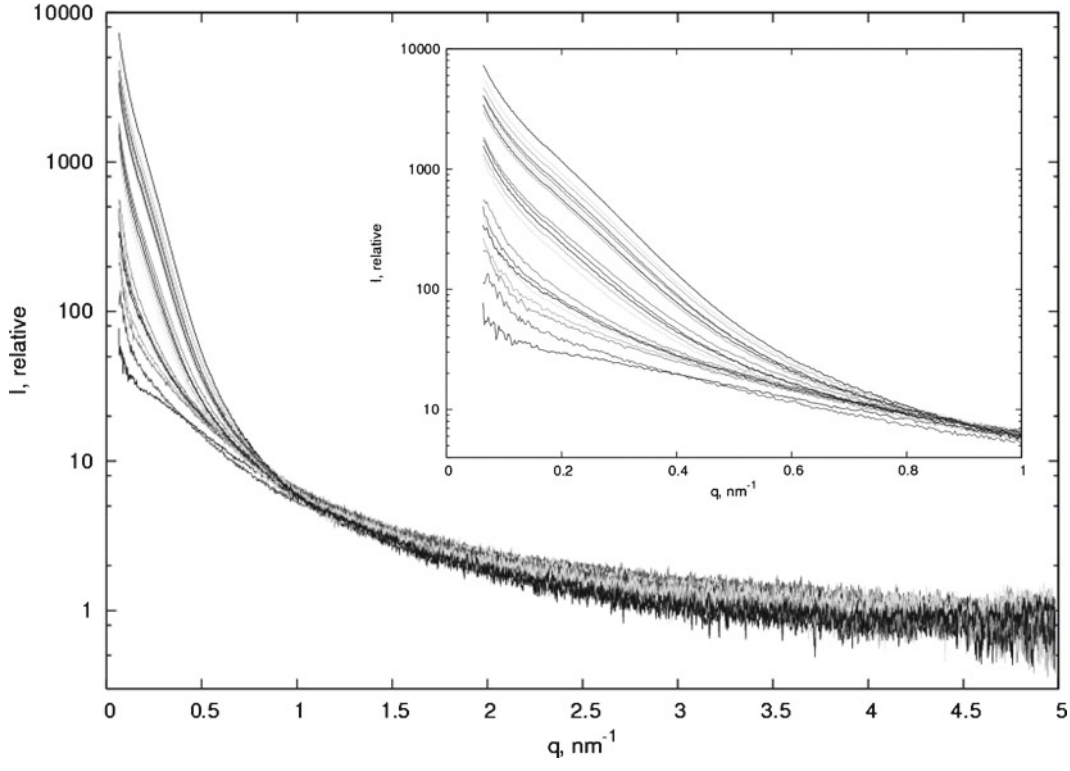

Fig. 3. Evident evolution of α-synuclein fibrillation. An example of how the structural changes during fibrillation are directly observable in the scattering data. Plotted are background-subtracted curves from samples of α-synuclein, taken from different time points in the fibrillation process. Scattering intensity is plotted versus q (see Note 5). The zoomed area emphasizes the significant changes occurring over time (lowest curve is early in the process, highest curve is the latest time point).

6. Inspect low-q data points. Estimate R_g and $I(0)$ as well as possible from the Guinier range and decide on emitting low-q data points for further data analyses (see Note 13).
7. The pair distance distribution function is determined by applying an indirect Fourier transformation (IFT). The maximum dimension D_{max} of the particle (or repeating unit of the fibril) is noted (see Note 14).
8. Plot R_g, $I(0)$, and D_{max} together with the fluorescence data against time. Look for trends or correlations, this will give indications as to when, and perhaps what, happens in the sample.
9. Estimate the minimal number of components contributing to the scattering (hence present in the samples) using singular value decomposition. Test with and without potential outliers in the input data pool, with and without late curves (since late repacking of the fibrils may complicate data decomposition), and with and without certain data ranges, and continue the evaluation until obtaining stable solutions (see Note 15).
10. Now decompose the data into the number of components that has been estimated above. We recommend the use of the program OLIGOMER (see Note 16). Be sure to continue this part of the data evaluation until you have a steady and consistent solution throughout the fibrillation process. Hence, there should not be significant differences in the residuals (or residuals + refined component) at different time points in the process. Do not average different signals.
11. Your final output will give you two significant results: firstly the volume fractions of individual components, hence information about the time course of the process. Secondly, the isolated scattering signal from the "unknown species," hence an in-process (on- or off pathway) species, which will have some relevance in understanding either the build-up of fibrils, the onset of fibrillation, or the structural basis of a potential cytotoxicity of a species involved with the given associated disease.
12. Evaluate your volume fractions. Do they make sense in relation to R_g, $I(0)$, D_{max} and the fluorescent signal?
13. Evaluate the basic parameters (Rg, $I(0)$, Dmax) of your isolated "unknown component." See above.

3.4. Modeling

Modeling based on fibrillating samples is not a simple task. With scattering data from a homogenous sample, *ab initio* shape reconstructions can be made, to give information of the particle overall shape. This is only applicable to scattering curves representing one species only, whether from a single measurement or decomposed data (see Note 17). The method is based on simulated annealing protocols, the theory behind the shape reconstruction and the programs is described elsewhere (12, 13). Scattering data cannot be

unambiguously analyzed, and the method implies the creation of several *ab initio* models, followed by spatial comparison of individual models and averaging of those agreeing (14).

1. The data range ($q_{min} - q_{max}$) to be used in the shape reconstructions must be determined (see Note 18). We recommend the inclusion of as large a q-range as possible in the IFT (see Note 14), subsequently varying q_{max} as an input parameter during modeling.
2. As a start, always make reconstructions from spherical search volumes, without symmetry or any assumed particle shape. Use the program Bodies (8) or the P(r) for support if choosing other shapes. Newly developed versions of the *ab initio* modeling programs (13) uses a dynamic search volume, but in general be careful with fibrillation data where default parameters are inadequate.
3. Calculate a number of *ab initio* models (see Note 19).
4. Create the averaged and filtered model. The filtered model should have the volume of an individual reconstruction (see Note 20).
5. Evaluate the reconstructions and models, based on the fits between the calculated scattering from the model and experimental data (Chi^2) and normalized spatial discrepancies (NSDs) of the individual superpositioned models. Visual inspection of individual fits and models is indispensable (see Note 21).
6. Based on the data analysis and the reconstructions (and possibly additional information) different search volumes, particle shapes and other input parameters can be tested until obtaining meaningful, consistent and well-fitting models (see Note 22).
7. An averaged model may be used as search volume for a subsequent refinement of the shape (see Note 20).

4. Final Remarks

The method described here may obviously be applied to other (nonfibrillating) systems involving equilibriums of different structural species evolving over time (or while varying other parameters). The method must be used with great care, constantly checking that results are meaningful and—very importantly—consistent for all measurements. If at all possible, include complementary information from any other type of data available. The method has been applied with success in our lab to several systems (1, 15, 16), but we have also encountered systems of greater complexity that we have not (yet) managed to decompose in a meaningful manner. Quite similar methodology has been applied in other laboratories, however with some important changes (17–19).

5. Notes

1. If using a less intense X-ray source (e.g., a rotating anode) exposure will be over longer time frames, which can compromise or complicate the procedure described here. When exposing over longer time frames, the resulting data from the evolving equilibrium will hence also be an average. Rotating anodes may however with advantage be used for more slowly developing processes (17).
2. More species may be present during the fibrillation process. Examples are a nonnative monomeric species (denoted $bI_{\text{intermediate\_1}}$ below) or repacked fibrils (e.g., lateral association of protofilaments) (denoted $dI_{\text{fibril\_2}}$ below). Hence the equation now comes to:

$$I_{\text{total}} = aI_{\text{native}} + bI_{\text{intermediate\_1}} + cI_{\text{intermediate\_2}} + dI_{\text{fibril\_1}} + dI_{\text{fibril\_2}}.$$

   The difficulty of isolating particular scattering signals from such a system is pronounced and can probably only be done if prior knowledge can be included. Yet another possible scenario is equilibrium between a monomeric nonnative species and the elongating fibrils. In such a case, the data may be fitted with a linear combination of an early measurement and a late measurement. This option must always be tested.
3. It is well known that all parameters of defined experimental conditions may influence your time course, i.e., you may vary buffer composition, temperature, shaking, volume, surface type, etc. until suitable conditions are defined. Here, note that everything in the solution contributes to the scattering signal. Hence, the signal from the protein rides on top of a scattering signal from the buffer. The more concentrated the buffer components, the less the relative protein signal. So—when possible—minimize the concentration and number of buffer components. As a rule of thumb, avoid more than 0.5 M salt and more than 5% of any buffer component. If in doubt, ask your beamline scientist in advance.

   For proper evaluation of the data, the signal from the buffer is measured without protein, and this signal is subtracted from the protein-sample signal. To get good resulting data on the fibrillating species, it is, therefore, of great importance to have a well-defined buffer such that you can measure the scattering signal from the *exact* same buffer as that of your protein sample. In the optimal scenario, the buffer is the very same solution as used for the sample, this is most easily obtained by dialysis of the protein sample, and using the dialysate as background buffer measurements. This is only possible if the protein remains native in the chosen buffer for a significant time, i.e.,

that fibrillation only starts when applying, e.g., a temperature change or similar.

When this is not possible, there are other options, albeit less optimal: either the protein/peptide is dissolved directly from powder into a defined buffer. In this case, consider if the protein/peptide powder has remains of salt, etc. which must be included in the background buffers. Alternatively, keep the protein/peptide in a buffer that ensures stable conditions (dialysis is recommended) and add the buffer component necessary to initiate fibrillation immediately prior to the experiment (e.g., a pH-change). Apply the exact same change to the background buffers.

Consider the temperature. If applying a plate reader without a cooler, the temperature may be stable only from ambient +5°C and above, but the ambient temperature at the beamline may differ from your home lab. Ask your beamline scientist. Also, the 96-well plates are shifted in and out of the plate reader multiple times during the experiment, thus a large difference between the ambient temperature and the temperature of the plate reader (fibrillation experiment), the bigger the risk of temperature-dependent variations in the ThT signals, and—even more serious—the bigger the risk of irregular variations in the fibrillation process.

4. Consult your beamline scientist (or the beamline home page). Make sure that it is explicit that you need to intervene with the sample loading between each protein measurement (because you need to extract your samples from the plate reader for each measurement). The calculated time must include: rinsing of the sample cell (sometimes automatic)—obtaining your sample from the plate reader—entering the sample area (most often this is in the beamline hutch)—loading your sample (also sometimes with an autosampler)—securing the sample area/hutch—exposing your sample with X-rays—storing the data files.

   Also, buffers and samples are measured alternately (i.e., buffer–sample–buffer–sample…), thus count two measurements per protein sample. Note that you may need additional time for loading of the fully fibrillated samples, due to the high viscosity of these samples. And finally, note that if you must sonicate/vortex/seed bead your fibril samples (see Notes 7 and 8), then add this time in your calculations for the last many samples (all samples beyond the lag-phase).

5. q is a momentum transfer of the scattering vector, defined as a function of the scattering angle: $q = 4\pi(\sin\theta)/\lambda$, where 2θ is the scattering angle and λ is the wavelength of the incoming X-rays. The available q-range is highly dependent on the beamline setup. As the fibrils are typically much larger than the average samples measured at the bioSAXS beamlines, it is important

to ask/check the actual q-range. In particular, if the low-q area is not optimized, very important data concerning the largest features of the fibril (i.e., the repeating unit) will not be recorded. Attempt obtaining data corresponding to real-space distances of >900 Å.

6. The X-ray sample cell has a defined (often 10–100 μl) volume. Automated sample changers have a safety margin, i.e., the volume needed may be larger. If using manual loading, inexperienced users tend to use significantly more than the X-ray sample cell volume. In particular, for the latest measurements of highly fibrillated samples, you must expect spending a larger volume because of the high viscosity.

   We recommend that all wells in the 96-well plate are filled with the same volumes (i.e., including considerations for viscosity, etc.). If needed, some material may be saved by calculating the filling of two X-ray sample cells per well in the 96-well plates in the beginning of the experiment, and one filling per well towards the end of the experiment. Note that this will influence the accuracy of your fluorescence measurements for the second filling in the early part of the experiment. Please note, finally, that if sonication, vortexing of the samples is necessary (see Note 7), then an even larger volume may be needed for late samples in particular.

7. High-viscosity samples cannot always be loaded automatically. If the automated sample changer can load the fibrillated samples, is it possible to frequently access the sample changer? Long tubing leading to the sample chamber may inflict unwanted alignment of the sample. Such alignment will be visible in the two-dimensional raw datafiles (prior to radial averaging). Non-isotropic scattering may be identified by visual inspection (e.g., using the plotting programs SAXSview or Fit2D) and will indicate alignment (see Fig. 2). Inconsistencies in the radially averaged curves (e.g., crossing of curves) may also indicate problems, in which case 2D images should be reinspected. We advice testing of fully fibrillated samples well in advance of the main experiment. If you have concluded that your fully fibrillated samples align in the sample cell, you must either establish alternative means of loading the sample (never do this without your beamline scientist!) or you must homogenize your sample prior to loading (we recommend vortexing or sonication, see Note 8). Note that the choice of homogenizing your sample prior to measurement has an effect on the time and sample volume needed for each measurement (see Notes 5 and 6).

8. The more you know about your system, the better. How reproducible is the time course of your fibrillation? How do you estimate as accurately as possible your protein concentration

before measuring SAXS data [the protein concentration is very important for correctly estimating the average molecular mass of the protein (and oligomers) in solution]. How viscous are your final fibrillated samples? How heterogeneous are your final samples? The latter two can be very important for the success of your SAXS data collection. Here we supply some concrete advice. AFM may indicate if your samples assemble heavily at a macroscopic level (lateral association, formation of "plates" of fibrils, etc.). You may also apply a rough test with diluted samples using DLS. If your DLS analysis does not provide an estimate of a frequently appearing size/very high heterogeneity, you may test the following means of homogenization [it has been shown numerous times that such a treatment only breaks the macroscopic arrangement of the fibrils, and not the fibril itself (at least not at a level corresponding to the repeating unit), but do check the effect on your sample.] (1) vortex your fibril with a seed-bead (normally applied in protein crystallography for the formation of seeds for crystallization). Retest with DLS to see if your sample appears more homogeneous. Alternatively (2) sonicate your sample with a fine rod-sonicator. Avoid foaming and heating of the sample, submerge your sample tube in ice, use brief sonication intervals and pauses.

9. Check that the repeated buffer measurements are stable, i.e., that the scattering signal from the buffers remain identical (plot and compare). If not, this could indicate that the sample cell is contaminated. It is very important to clean the sample cell. Data from a contaminated sample cell are useless. Alternative explanations for outliers: check snapshots (if available) of the sample cell for bubbles, or the logbook for notes explaining the outlier.
10. This is in principle often done as a standard procedure of the beamline, as several exposures can be averaged for improved signal-to-noise. Changing the exposure time may be relevant if repeated measurements result in diverging scattering curves.
11. Buffer subtraction may be done automatically by software at the beamline. If not, average the two buffer measurements (after checking that they are identical) flanking the sample measurement and subtract.
12. For any outlier go back, if possible, to snapshots of the sample cell or to your log-book. Look for bubbles, visible aggregation or other explanations noted in the log-book (injection, error messages, etc.). If there are no obvious faults with the sample and/or data, keep them in the data pool for now, but they may have to be excluded at a later stage (see Note 15).
13. The repeating unit of the fibrils is typically so large that there are not enough data points at the low angles to define a proper

Guinier range. Nevertheless, an estimate may be made, and evaluated from the Fourier transformation. Keep all data points at low angles, except if there is a potential direct noise from, e.g., parasitic scattering/data where the scattering was partly concealed by the beam stop.

14. Be meticulous in inspecting the fit of the calculated curve from the IFT to the experimental curve at low q, the fit should very closely follow the experimental data. Include low q data points as described (see Note 13). Include as much data as possible both at low and high q values, balancing the smooth pair distance distribution function and the fit. Automated IFT versions are underdevelopment and may be applied, but as for any other data evaluation, data from protein fibrillation is special, and care should be taken when applying automated procedures.
15. Cut as few low-q points as possible. In particular noisy data, low-q data may cause problems in the interpretation of the resulting eigenvalues and vectors as the "background" noise level will be higher. A stable solution is obtained when the number of eigenvalues that are significantly over noise level corresponds with the number of nonrandom eigenvectors. At the same time, this number should not be very sensitive to the inclusion or exclusion of one or a few data curves, a small change in the data range, etc. A few programs exist that will make this evaluation automatically, and at the same time decompose the data. We cannot at present recommend the use of these programs, since fibrillation scattering data are too complicated, and a careful consideration of the inclusion/exclusion of curves/data points is very much needed, hence can at present not be automated.
16. OLIGOMER (8) fits an experimental scattering curve by a linear combination of a number of input scattering curves:

$$I_{\text{exp}} = AI_{\text{a}} + BI_{\text{b}} + \cdots + NI_{n},$$

where I_{exp} is the observed scattering from the mixture of species; A, B, …, N are volume fractions of individual species a, b, …, n; In is the scattering of the nth species extrapolated to zero concentration; and n is the total number of species with an appropriate weight (volume fractions of the individual components, determined by a least squares fit). At any time point, hence for each experimental data curve the program produces the corresponding best fit and isolates residual scattering, which should be indistinguishable from the noise level of the data when an adequate description of the experimental data is obtained from the linear combination. To isolate the scattering from an oligomeric species, occurring during the

fibrillation process, data from the other species must be available (hence data from the starting structural state and the end structural state). If more species are present, the procedure can only be followed if good models of more species are available. Hence, the procedure has only been used by the authors with only one single completely unknown species present in solution. *Method a*: if a good atomic model is available of an oligomeric species, a theoretical scattering curve may be calculated based on such a model. Provide an input file with data from starting conditions, the model as the second component and the ending conditions as final component. Now isolate the calculated residuals, and add these to the second component, as the residuals would signify how different the solution scattering component is from the model. A special version of the program OLIGOMER is available from the program authors on request. This version differs from the original (available via ftp from EMBL-Hamburg), by automatically calculating the sum of the residual scattering and the second component in the input file. Repeat the procedure, now using the average (component 2 + residual) as an input second component. Check that residuals are not significantly above noise level. Finally average the scattering signal from (component 2 + residual) all experimental measurements where the volume fraction was significantly above 0. *Method b*: Although knowing beforehand (from your singular value decomposition) that you have three species in solution, if no adequate model is available for an oligomeric species, attempt decomposition of the data firstly into only two species. Now isolate the residual from the fit to all experimental files, and look for a trend in any strong signal. Average such signals, and attempt using this signal as a first estimate of the scattering curve from the second component. Continue as above.

17. If applying *ab initio* modeling using data from a heterogeneous sample, reconstructions will be build, but whatever the shape may resemble, the result will very likely be meaningless. The shape reconstruction method is based on the assumption that one species only gives rise to the data.
18. $q_{\min}$ can be estimated directly based on the primary data analyses: for standard globular particles, include all points that satisfy the Guinier approximation. For samples including fibrils, the Guinier approximation is not satisfied. Here, we recommend to include all data points with the exception of points that are obviously flawed by, e.g., parasitic scattering. $q_{\max}$ may be estimated as the point to which the scatterer represents a shape with a well-defined boundary (i.e., the contrast between the scattering length density of the particle and the solvent is well-defined). This may often be evaluated by the Porod law, i.e.,

exclude points beyond the q value where the data drops with q^{-4} dependency. Alternatively a rule of thumb is that $q \times R_g \leq 7–8$. Several ranges may be tested during the reconstructions as one of the parameters to vary.

19. In the beginning, while still varying and testing different input parameters of the modeling process, five reconstructions may be enough. For the final optimized models, 10–20 reconstructions are recommended as a minimum.
20. The program DAMAVER (14) is most often run in a batch mode, where individual subprograms are called sequentially with default settings. In the default setting, the number of dummy atoms will be too low and should manually be varied to the maximum possible number. For refinement, we recommend that all dummy atoms of the averaged model are included in the damstart.pdb.
21. Chi^2 values depend on the error estimates of the data, thus can be used for internal comparison of different reconstructions, but only with difficulty among different datasets. Visual inspection of the fits is very important. NDSs below 0.9 are recommended. Visual inspection of both the individual constructions and the averaged and filtered models is necessary. For the mature fibrils: remember that you have modeled the repeating unit (repeated like beads on a string). Hence, if your data evaluation makes sense, it should be possible to build a full fibril model by adding repeating units (translated along the length axis and potentially rotated).
22. If the fibril is a very rod-like structure, the cross-section may be inspected (by IFT) which will assist in choosing a suitable start volume. Also, for the fibrils in particular, changing parameters such as the dummy atom radius, number of nodes, speed of the simulated annealing, peripheral penalty weight, etc. may improve the model.

Acknowledgments

The experiences gathered in this chapter were not collected overnight, thus we would like to thank our colleagues and collaborators for significant discussions and help. In particular, from the University of Copenhagen: Minna Grønning, Marco van de Weert, and Vito Foderá. From EMBL, Hamburg: Dmitri I. Svergun, Manfred Roessle and the rest of BioSAXS group for valuable help with programs and for being very helpful beamline contacts (which, as stated many times above, is of great importance during this kind of experiments). Likewise, we are grateful for interest and kind support from Novo Nordisk A/S. We greatly acknowledge

plenty beamtime at beamline X33 (EMBL-Hamburg/DESY), without which the development of the methodology described here would not have been possible. We also appreciate funding from The Lundbeck Foundation, the Danish Council for Independent Research | Medical Sciences, and DanScatt.

References

1. Vestergaard B, Groenning M, Roessle M et al (2007) A Helical Structural Nucleus Is the Primary Elongating Unit of Insulin Amyloid Fibrils. PLoS Biol 5:e134
2. Powers ET, Powers DL (2006) The kinetics of nucleated polymerizations at high concentrations: amyloid fibril formation near and above the supercritical concentration. Biophys J 91:122–132
3. Langkilde AE, Vestergaard B (2009) Methods for structural characterization of prefibrillar intermediates and amyloid fibril. FEBS lett 583:2600–2609
4. Foderà V, Groenning M, Vetri V et al (2008) Thioflavin T Hydroxylation at Basic pH and Its Effect on Amyloid Fibril Detection. J Phys Chem B 112:15174–15181
5. Hammersley A. Fit2D. http://www.esrf.eu/computing/scientific/FIT2D/
6. Franke D. Saxsview. http://saxsview.sourceforge.net/
7. Konarev PV, Petoukhov MV, Volkov VV, Svergun DI (2006) ATSAS 2.1, a program package for small-angle scattering data analysis. J Appl Cryst 39:277–286
8. Konarev PV, Volkov VV, Sokolova AV et al (2003) PRIMUS: a Windows PC-based system for small-angle scattering data analysis. J Appl Cryst 36:1277–1282
9. The PyMOL Molecular Graphics System, Version 1.3, Schrödinger, LLC
10. BioISIS tutorial http://bioisis.net/tutorial
11. SAXIER forum www.saxier.org/forum/
12. Svergun DI (1999) Restoring low resolution structure of biological macromolecules from solution scattering using simulated annealing. Biophys J. 76:2879–2886
13. Franke D, Svergun DI (2009) DAMMIF, a program for rapid ab-initio shape determination in small-angle scattering. J Appl Cryst 42:342–346
14. Volkov VV, Svergun DI (2003). Uniqueness of ab-initio shape determination in small-angle scattering. J Appl Cryst 36:860–864
15. Giehm L, Svergun DI, Otzen DE, Vestergaard B (2011) Low-resolution structure of a vesicle disrupting α-synuclein oligomer that accumulates during fibrillation. PNAS 108: 3246–3251
16. Groenning M et al (2011) manuscript in prep.
17. Oliveira CL, Behrens MA, Pedersen JS et al (2009) A SAXS study of glucagon fibrillation. J Mol Biol 387:147–61
18. Martel A, Burghammer M, Davies RJ et al (2008) Silk Fiber Assembly Studied by Synchrotron Radiation SAXS/WAXS and Raman Spectroscopy. J Am Chem Soc 130:17070–17074
19. Nayak A, Sorci M, Krueger S, Belfort G. (2009) A universal pathway for amyloid nucleus and precursor formation for insulin. Proteins 74:556–565

Chapter 11

Atomic Force Fluorescence Microscopy in the Characterization of Amyloid Fibril Assembly and Oligomeric Intermediates

Valeriy Ostapchenko, Maria Gasset, and Ilia V. Baskakov

Abstract

Atomic force microscopy (AFM) has become a conventional tool for elucidation of the molecular mechanisms of protein aggregation and, specifically, for analysis of assembly pathways, architecture, aggregation state, and heterogeneity of oligomeric intermediates or mature fibrils. AFM imaging provides useful information about particle dimensions, shape, and substructure with nanometer resolution. Conventional AFM methods have been very helpful in the analysis of polymorphic assemblies formed in vitro from homogeneous proteins or peptides. However, AFM imaging on its own provides limited insight into conformation or composition of assemblies produced in the complex environment of a cell, or prepared from a mixture of proteins as a result of cross-seeding. In these cases, its combination with fluorescence microscopy (AFFM) increases its resolution.

Key words: Amyloids, Assembly, Atomic force microscopy, Atomic force fluorescence microscopy, Immunofluorescence, Oligomers

Abbreviations

AFM Atomic force microscopy
AFFM Atomic force fluorescence microscopy

1. Introduction

Atomic force microscopy (AFM) was evolved from STM to overcome its drawbacks that limited its use to the study of conducting or semiconducting materials and generalize its applications to the study of the surface properties of materials (1). Despite its name, AFM does not provide atomic resolution and mostly it does not measure atomic forces but interfacial. AFM images the topographic,

Einar M. Sigurdsson et al. (eds.), *Amyloid Proteins: Methods and Protocols*, Methods in Molecular Biology, vol. 849,
DOI 10.1007/978-1-61779-551-0_11,

chemical, mechanical, and electrical properties of surfaces (interfaces). Basically, it consists of a sharp microtip attached to a cantilever which is scanned across the surface of a sample. The deflection of this cantilever is monitored using a laser and a four-quadrant photodiode and is used to build the surface image.

Of the different modes of work, given the softness of biological material and the shear force involved in contact, the analysis of peptide and protein assemblies is mainly performed using intermittent-contact (tapping) or dynamic force working mode (DFM or AC-AFM). In this mode, a stiff cantilever is oscillated closer to the sample than in noncontact mode. Part of the oscillation extends into the repulsive regime, so the tip intermittently touches (or "taps") the surface improving lateral resolution by abolishing dragging and avoiding damaging of the sample.

AFM imaging provides useful information about particle's dimensions, shape, and substructure at a nanometer resolution. Conventional AFM methods have been very helpful in the analysis of fibrils formed in vitro from homogeneous proteins or peptides (1–4). In theory, AFM imaging using commercial AFM instruments can provide up to 10^{-10} m resolution. However, due to the tip convolution and finite width, the resolution is limited to a few nanometer (Fig. 1). Considering that the length of amyloid fibrils is in the range of 10–10,000 nm and their lateral dimension is between 3 and 30 nm, the precision of AFM measurements is usually sufficient to probe filament substructure of amyloid fibrils (1).

However, AFM imaging on its own provides limited insight into conformation or composition of fibrils produced in complex environments, or prepared from a mixture of proteins as a result of cross-seeding. For these cases, combination of AFM with fluorescence microscopy (will be referred to as AFFM) increases the resolution of the composition and conformation of individual fibrils (5, 6). The analysis of fibril composition addresses the question of

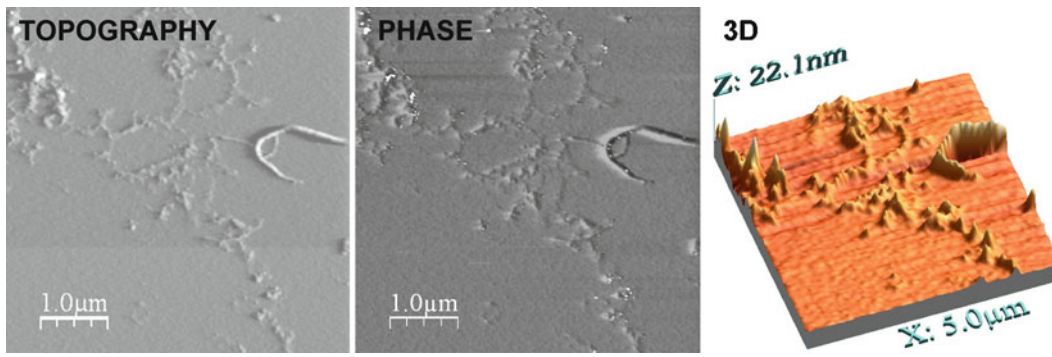

Fig. 1. Schematic diagram illustrating the information contained in an intermittent-noncontact AFM scan of protein fibrils. Topography and Phase imaging layers of aggregates formed using a 1:1 mixture of rHaPrP wt and rHaPrP M206S-M213S under native conditions (9). 3D profile of the aggregates constructed with WSxM 5.0 after equalization and flattening.

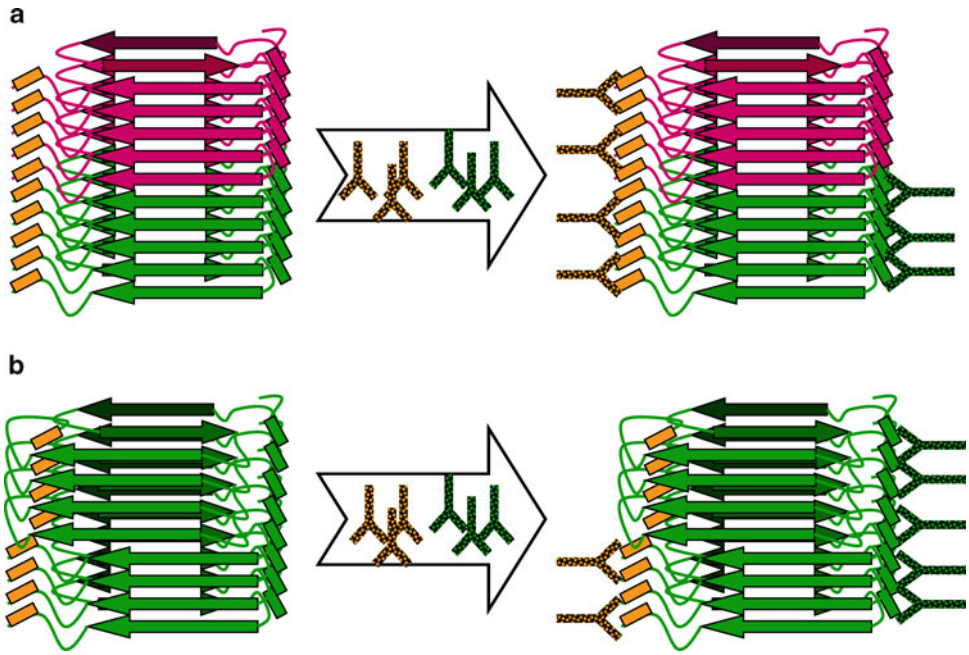

Fig. 2. Schematic diagram illustrating analysis of fibril composition or conformation using double immunostaining. (**a**) Analysis of fibril composition. Amyloid fibrils produced from two homologous proteins (*green* and *red*) are treated with a pair of antibodies. Antibodies should be selected using the following rules: one antibody used in a pair (*yellow*) should recognize either one or both proteins, whereas another antibody (*green*) should be specific to only one protein, epitopes to both antibodies should be immunoreactive in fibrillar form. (**b**) Analysis of conformational switching within individual fibils. Amyloid fibrils are treated with a pair of antibodies which are selected using the following rules: the epitope to one antibody used in a pair (*green*) should be immunoreactive in both amyloid states, whereas the epitope to the second antibody (*yellow*) should be immunoreactive in only one amyloid state.

whether individual amyloid fibrils are made of identical/homologous or heterologous polypeptides. The procedure involves coimmunostaining using a pair of antibodies specific to the proteins of interest (5). This method requires the epitopes recognized by both antibodies to be exposed on fibrillar surface and to be immunoreactive (Fig. 2a). Information obtained by this approach is important for elucidating the mechanisms of cross-seeding or cross-talk between homologous or non-related amyloidogenic proteins or peptides.

Analysis of fibril conformation addresses the question of whether the structure of β-spine is uniform within individual fibrils or switches between alternative conformations (7). The procedure involves coimmunostaining using a pair of antibodies specific to two different epitopes within the same polypeptide chain (Fig. 2b). To perform this assay, both epitopes have to be immunorective in one amyloid state, whereas only one epitope should maintain immunoreactivity in alternative amyloid state. This approach can be applied for elucidating molecular mechanisms of prion or amyloid strain evolution, adaptation, or modification (6, 7). While the

experimental protocols described in the current chapter were optimized for the analysis of composition or conformation of fibrils prepared from mammalian prion protein (PrP), these procedures can be adopted for the analysis of fibrils formed by non-prion proteins if appropriate sets of antibodies are available.

The current chapter describes the routine AFM imaging mode (AC-AFM) and introduces a new approach that relies on AFM and fluorescence microcopy coimaging (AFFM).

2. Materials

All the solutions must be made using ultrapure water (e.g., Milli Q) and ACS quality reagents.

2.1. Protein and/or Peptide Fibrils

Recombinant prion protein purified and converted into amyloid fibrils as described previously (5, 6, 8).

2.2. Mica Surface and Its Preparation

1. Unmodified AFM-grade mica 1 cm × 1 cm pieces (Novascan).
2. Magnetized-stainless steel coin-like sample holders (15-mm diameter, 3-mm height).
3. Stick the mica pieces on the top of the holder using double-sided scotch paper.
4. Clean covered containers for preservation (35-mm diameter dishes allow their independent storage).

2.3. Cover Glasses and Its Preparation

5. Two separate hoods for handling organic solvents and oxidants, respectively.
6. 100% Isopropanol.
7. 100% Acetone.
8. Sulfuric acid/hydrogen peroxide cleaning solution: 70% sulfuric acid; 10% hydrogen peroxide; 20% water (Prepare immediately before use by pouring 98% sulfuric acid over 30% hydrogen peroxide solution and gentle mixing of the solution. Proceed with care as the mixing of these solutions generates heat).
9. 25-mm Square premium cover glasses (0.13–0.17 mm thin, Fisher Scientific).
10. Cover glass coplin staining jar (Wheaton Science Products).
11. Ultrasonic cleaner (Branson Ultrasonics).

2.4. Double Immunostaining of Recombinant PrP Fibrils

1. 5 μg/ml solutions of recombinant Syrian hamster PrP R-fibrils seeded with S-fibrils, in 5 mM sodium acetate, pH 5.0, prepared according to Makarava and Baskakov (see ref. 6, 8, Note 1).
2. Tris-buffered saline (TBS) solution, containing 50 mM Tris and 0.15 M NaCl, pH 7.5.

3. TBST (TBS with 0.25% Triton X-100).
4. TBST–HS (TBST with 5% horse serum and 0.02% sodium azide).
5. TBST–BSA (TBST with 1% bovine serum albumin and 0.02% sodium azide).
6. Primary antibodies: anti-PrP human R2 and anti-PrP mouse AG4 antibody solutions, both stored in 20% Glycerol at –20°C (see Note 2).
7. Secondary antibodies: goat anti-human IgG, labeled with Alexa-546, and goat anti-mouse IgG, labeled with Alexa-488, both stored at 4°C (see Note 3).

2.5. Atomic Force Fluorescence Microscopy

1. Atomic force microscope with 10-μm scanner (Pico LE AFM system, Agilent).
2. Inverted light microscope (Eclipse TE2000-U, Nikon, Japan) equipped with an oil-immersion objective (1.3 aperture Plan Fluor ×100, Nikon, Japan), a CCD camera (CoolSnap HQ, Photometrics, Tucson, AZ) and filter sets for Alexa-488 (ET GFP) and Alexa 546 (ET DsRED) fluorescent imaging (Chroma Technology).
3. Dark room equipped with a vibration isolation system/table (Veeco) and preferably isolated or distanced from the sources of loud sounds.
4. AFM probes for intermittent (tapping/noncontact) mode with resonant frequency ~300 kHz, elastic constant ~40 N/m, and tip diameter ~7 nm.
5. Software to obtain and treat the images. For the setup above besides the software supplied with the instrumentation (V++ for the inverted microscope, Pico Scan for the AFM microscope), we use WCIF ImageJ, which can provide RGB merging of fluorescence images as well as generic (size, crop, alignment) treatment of AFM images. For specific AFM analysis, we used the free software WSxM 5.0 (http://www.nanotec.es).

3. Methods

Unless stated otherwise, all the operations are done at room temperature (20–25°C). The whole experiment takes one to a few days, depending on the quality of fibril samples and AFM probes and the necessity to adjust immunostaining and AFM scanning procedures. It is first recommended to check separately the quality of fibrils by both atomic force and fluorescence imaging beforehand.

3.1. Sample Preparation

3.1.1. Sample Preparation on Mica Surfaces for AFM

1. Stick the mica pieces on the top of the holder using double-sided scotch paper.
2. Immediately before use, exfoliate the mica surface adhering the sticky side of scotch paper and pulling up.
3. Deposit the protein solution (typically 10 µl of 5–10 µg/ml protein fibrils) on the mica and allow it to incubate for 10 min in a dust-free atmosphere (covered) for adsorption (see Note 4).
4. Wash extensively the surface with Milli Q water and aspirate the excess with filter paper avoiding touching the surface.
5. Dry them with compressed air/N_2 immediately before use.

3.1.2. Sample Preparation on Glass Surfaces for AFFM

AFFM Cover Glass Pretreatment

It is important to provide additional cleaning even to precleaned cover glasses. The following procedure significantly decreases the background in fluorescence images, improves image contrast, and facilitates focus handling. Steps involving organic solvents and sulfuric acid should be performed under separate hoods using standard precautions (nitrile gloves, lab robes, eye glasses):

1. Place cover glasses separately in glass jars. Be sure that all the jars are intact and their caps sit tight on them.
2. Fill the jars with isopropanol until it covers glasses. Place the jars in the ultrasonic bath and sonicate for 2 min. Take the jars out, collect isopropanol.
3. Repeat step 2 with acetone instead of isopropanol.
4. Repeat step 2.
5. Wash the jars with cover glasses with ultrapure water 5–7 times.
6. Pour freshly prepared sulfuric acid/hydrogen peroxide solution in the jars to cover the glasses. Incubate for 1 h under the hood. Draw the solution off the jars to a special waste bottle.
7. Repeat step 5. Store the cleaned cover glasses in the jars at 4°C. Dry them with the compressed air/N_2 immediately before use.

Double Immunostaining on Glass Surfaces

The following procedure for double immunostaining was designed to discriminate between two conformational states of full-length PrP amyloid fibrils: S and R states (8). Mouse IgG AG4, which binds to both R- and S-states, was used in a pair with R2 antibody (epitope 225–231), which binds only to S-state (8). The same procedure with minor modifications can be employed for analyzing fibrils produced from non-prion proteins for which panels of appropriate antibodies are available. If a choice of antibodies is limited, amyloid-specific fluorescent dyes (such as thioflavin T) can be used instead of one antibody in pair with a specific antibody (5).

Follow the recommended storage conditions for all antibodies. If stored frozen, antibody solutions should be divided into aliquots. All operations with Alexa-labeled antibodies should be done

minimizing light exposure. Used solutions of primary antibodies can be stored for a few days at 4°C for repeated use.

1. Spread 50 µl of fibril solutions on freshly dried cover glasses. Incubate for 5 min for fibrils to get attached to the glass surface (see Note 4).
2. Wash gently with Milli Q water. Cover the glass surface with TBS until proceeding with antibody staining.
3. Prepare 1:500 dilution of anti-PrP human Fab R2 in TBST–HS. Apply 250 µl of this solution to cover glasses. Incubate for 1 h at room temperature.
4. Wash with 3 × 300 µl TBST by gentle pipetting.
5. Prepare 1:1,000 dilution of anti-PrP mouse IgG AG4 in TBST–HS. Apply 250 µl of this solution to cover glasses. Incubate for 1 h at room temperature (see Note 5).
6. Repeat step 4.
7. Wash with 300 µl TBST–BSA for 10 min.
8. Prepare the mix of anti-human IgG (H+L) Alexa 546 (red) and anti-mouse IgG (H+L) Alexa 488 (green), both diluted 1:700 in TBST–BSA. Apply 250 µl of this solution to cover glasses. Incubate for 1 h at room temperature.
9. Repeat step 4.
10. Wash with 300 µl TBS for 10 min or store with TBS at 4°C overnight.
11. Wash with Milli Q water and dry on bench top or with low force N_2 before AFFM imaging.

3.2. Imaging

3.2.1. Basic AFM Imaging Procedure

1. Assemble and adjust the AFM scanner. Following the user manual provided with each equipment, insert the cantilever and center the laser on it, and proceed to adjust the detector.
2. Determine the resonant frequency of the tip.
3. Fix the sample in the sample holder and mount the scanner, so the sample surface is approximately 200 µm apart from the tip.
4. Adjust scanning parameters (tapping at 99.9% of resonant frequency, scanning speed 1 line/s, scan square size of about 5 µm) and start the approach.
5. Scanning will provide three imaging layers: topography, amplitude, and phase. The three layers should be coherent, but topography and phase can differ.
6. Export images for analysis with any free software as WSxM 5.0 (http://www.nanotec.es).

3.2.2. AFFM Imaging

In general, AFM operations on inverted microscope sample holder do not differ from those on a standalone AFM microscope. All the operations with the AFM scanner placed on the inverted

microscope sample holder should be done with the additional care as the objective and cover glass movements can destroy the AFM probe (see Note 6).

1. Assemble the AFM scanner in this case fixing the sample cover glass in the sample holder and proceed to adjust scanning parameters. Withdraw the tip to 200 μm above the sample surface.
2. Transfer the AFM scanner with the sample to the inverted microscope sample holder. Approach the sample cover glass with the microscope objective at the minimal pace and carefully focus on fibrils.
3. Move the sample vertically from the microscope objective and toward AFM probe so the distance between the AFM probe and the sample surface is approximately 20 μm. After the sample surface approached the AFM probe and moved from the inverted microscope objective, refocus the fluorescence microscope again with the AFM laser turned off.
4. Turn on the AFM laser. Reposition the inverted microscope sample holder horizontally so that the AFM probe tip is pointing to the center of the CCD camera viewing field. Using fluorescence microscope, take an image of laser diffraction on AFM probe cantilever (Fig. 3). The image of laser diffraction will help to align the fibril fluorescence image with AFM images.

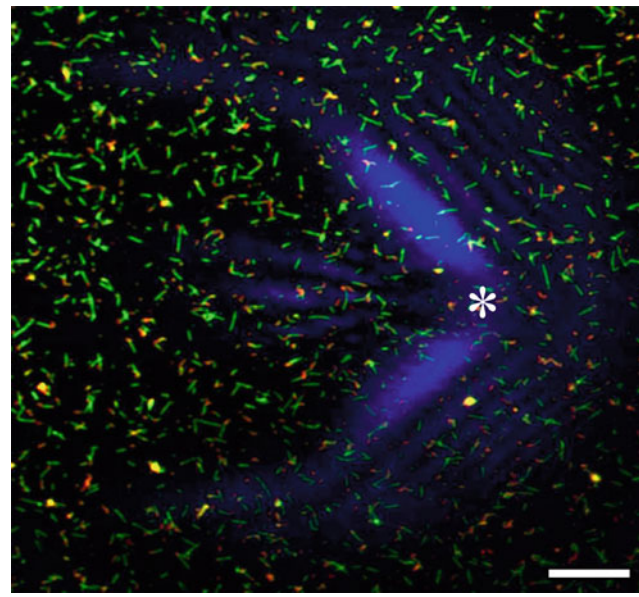

Fig. 3. Aligning fluorescence and AFM field of views. Fluorescence microscopy image of hybrid mouse-hamster PrP fibrils recoded in two channels (*red* and *green*) using corresponding filter stets and a diffraction image of AFM laser on a probe cantilever that was registered by fluorescence microscope without a filter. The *asterisk* marks the spot on the fluorescence field of view that corresponding to the AFM tip facilitating subsequent manual alignment of AFM and fluorescence images. Bar length is 5 μm.

5. Turn off the AFM laser. Using appropriate filter sets (ET-GFP for AG4 staining, ET DsRED for R2 staining), record fluorescence images from the same field of view (see Note 7).
6. Slightly withdraw the objective so it still touches the sample through the oil drop.
7. Turn on the AFM laser. Approach the sample with the AFM probe. Scan 10 × 10-μm field.
8. (optional) If higher resolution images are needed, zoom into a smaller scan size, adjust scanning parameters (lower scanning speed, higher integral gain, smaller servo amplitude, etc.), scan again (see Note 8).
9. Withdraw the sample from the AFM probe to distance 20 μm. Turn off the AFM laser.
10. Focus the inverted microscope again. Move the sample approximately 10 μm horizontally in any direction using fluorescence live-time imaging to control the moving process.
11. Repeat steps 6–10 several times to collect a combined AFM image of 20–30-μm side square.
12. Move the sample horizontally to obtain a different inverted microscope viewing field. Repeat steps 5 and 11.
13. Withdraw the AFM probe from the sample. Withdraw the objective from the sample. Transfer the AFM scanner with the sample to its holder. If needed, replace the sample cover glass with the next one and repeat the procedure.
14. Match fluorescence and AFM images (see Note 9) (Fig. 4).

4. Notes

1. If you are going to apply AFFM to preparations of amyloid fibrils other than used here, check the sample for the presence of standalone fibrils in sufficient quantity (e.g., by ThT fluorescence, negative staining electron microscopy).
2. Carefully plan the pair of primary antibodies to use in double immunostaining. Be sure that they are of different origin, so the secondary antibodies distinguish between the primary ones. If antibodies recognize epitopes, which are in close proximity to each other, you might encounter interference. In this case, changing the sequence of immunostaining could sometime help to resolve this problem.
3. Make sure that the spectral characteristics of filters in your fluorescence microscope match those of fluorescent dyes with which the secondary antibodies are labeled.

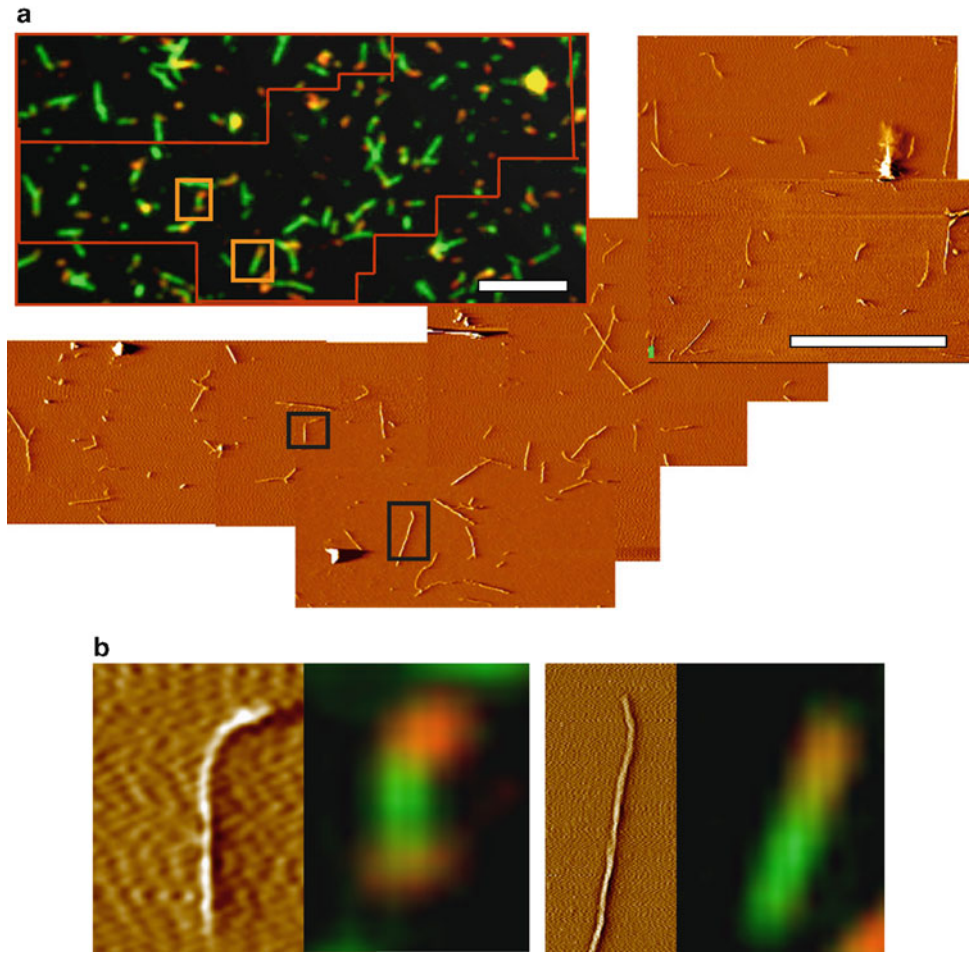

Fig. 4. Matching of fluorescence and AFM imaging. (**a**) Hybrid hamster-mouse PrP fibrils were stained with two anti-PrP antibodies: hamster-specific (*red*) and antibodies that recognize both hamster and mouse PrPs (*green*). The matching of fluorescence and AFM images was performed manually. The area corresponding to several AFM scans is marked by a *red line* in the fluorescence field of view. (**b**) Examples of individual hybrid hamster-mouse fibrils imaged by AFFM. Bar length is 5 μm.

4. Attachment efficiency depends on both the assembly features and the surface and it must be empirically determined for each system. Some types of amyloid fibrils attach poorly to glass surface. To overcome this problem, a cross-linking step can be employed. Optimize conditions for cross-linking with care; be aware that cross-linking might interfere with the epitope immunoreactivity.
5. Read notes II and III. In case you need only single antibody staining, omit the step involving treatment with the second primary antibody. Second antibody staining can be replaced by the staining with small fluorescent molecules (such as thioflavin T).
6. Approaching and withdrawal of the objective can slightly move the sample cover glass when the oil drop connects them. Move

the objective slowly with the AFM tip withdrawn from the surface by at least 20 μm. Do not forget to turn on the laser every time you approach the sample with AFM tips.

7. It is desirable to use high-quality filter sets (such as ET series from Chroma) as they considerably increase resolution and contrast of fluorescence images.
8. Follow generic AFM imaging improvement methods which can be found in AFM system manual or specialized internet sites such as http://www.afmuniversity.org. Thermal or mechanical drift happens often in such systems and is especially noticeable at small scan areas. It can be counteracted using the software supplied with the AFM system (Pico Scan in this case).
9. User-friendly freeware WCIF ImageJ can be used to merge RGB images. Matching of AFM and fluorescence images can be done manually either on a PC display or using printed images. Because the square size of a single AFM field of view is 10×10 μm or less, whereas the square size of a single fluorescence field of view is 60×60 μm, several AFM scan images can fit within a single fluorescence image.

Acknowledgments

This work was supported in parts by the National Institute of Health (grant R01 NS045585 to I.V.B), the Spanish MICINN (BFU2009—07971 to MG), and the Fundación CIEN (to MG).

References

1. Anderson, M., Bocharova, OV, Makarava, N., Breydo, L., Salnikov, VV, and Baskakov IV. (2006) Polymorphysm and Ultrastructural Organization of Prion Protein Amyloid Fibrils: An Insight from High Resolution Atomic Force Microscopy. *J Mol Biol* **358**, 580–596.
2. Jansen, R., Dzwolak, W., and Winter, R. (2005) Amyloidogenic Self-Assembly of Insulin Aggregates Probed by High Resolution Atomic Force Microscopy. *Biophys J* **88**, 1344–1353.
3. Zhu, M., Han, S., Zhou, F., Carter, SA, and Fink, AL. (2004) Annular olgomeric amyloid intermediates observed by in situ atomic force microscopy. *J Biol Chem* **279**, 24452–24459.
4. Chamberlain, AK, MacPhee, CE., Zurdo, J. et al. (2000) Ultrastructural Organization of Amyloid Fibrils by Atomic Force Miscroscopy. *Biophys J* **79**, 3282–3293.
5. Makarava, N., Lee, CI, Ostapchenko, VG, and Baskakov IV. (2007) Highly promiscuous nature of prion polymerization. J Biol Chem **282**, 36704–36713.
6. Makarava, N., Ostapchenko, VG., Savtchenko, R., and Baskakov, IV. (2009) Conformational switching within individual amyloid fibrils. *J Biol Chem* **28**, 14386–14395.
7. Baskakov, IV. (2009) Switching in amyloid structure within individual fibrils: implication for strain adaptation, species barrier and strain classification. *FEBS Lett* **583**, 2618–2622.
8. Makarava, N., and Baskakov, IV. (2008) The same primary structure of the prion protein yields two distinct self-propagating states. *J Biol Chem* **283**, 15988–15996.
9. Lisa, S., Meli, M., Cabello, G., Gabizon, R., Colombo, G., and Gasset, M. (2010) The structural intolerance of the PrP α-fold for polar substitution of the helix-3 methionines. *Cell. Mol. Life Sci.* **67**, 2825–2838

Chapter 12

Investigating Fibrillar Aggregates of Tau Protein by Atomic Force Microscopy

Susanne Wegmann, Daniel J. Muller, and Eckhard Mandelkow

Abstract

Atomic force microscopy (AFM) has been used in numerous studies to visualize and analyze the structure and conformation of biological samples, from single molecules to biopolymers to cells. The possibility to analyze native samples without fixation, staining and in physiological buffer conditions, combined with the sub-nanometer resolution, makes AFM a versatile tool for the analysis of protein aggregation and amyloid structures. Here, we describe the application of AFM to study fibrillar Tau protein aggregates.

Key words: Amyloid, Atomic force microscopy, Paired helical filaments, Protein aggregation, Fibers, Oscillation mode, Tau protein, Alzheimer disease

1. Introduction

The formation of amyloid fibers is a common feature of various pathogenic human protein aggregation diseases. Accordingly, the characterization of the structure, the function, and the assembly mechanism of these protein aggregates has a long history (reviewed in ref. 1). In the 1850s, Rudolph Virchow created the term "amyloid" (=starch-like) for aggregates found in brain plaques that can be stained with iodine-containing reagents (2). Up to now, many amyloidoses in various human diseases were characterized by histochemical staining methods (3, 4). In 1907 (5), Alois Alzheimer discovered changes in the brain of patients who suffered from an obscure form of dementia [Alzheimer disease (AD)]. From the 1960s onwards, high-resolution electron microscopy (EM) images of amyloid fibers—extracted postmortem from AD patient brains or assembled in vitro—revealed the structure of A-beta amyloid fibers and showed the existence of protofibrils. X-ray analysis of

Einar M. Sigurdsson et al. (eds.), *Amyloid Proteins: Methods and Protocols*, Methods in Molecular Biology, vol. 849,
DOI 10.1007/978-1-61779-551-0_12,

A-beta fibers revealed the building principle of amyloid fibers, where subunits are stacked axially and are arranged in a cross-beta conformation. The beta-strands have an axial separation of ~0.47 nm, which gives rise to a characteristic meriodional reflection in the X-ray pattern that is diagnostic of most amyloid fibers (6–10).

In Alzheimer disease, there are two types of pathological fibers. Extracellular fibers that are composed of A-beta coalesce into "amyloid plaques," intracellular fibers composed of Tau protein coalesce into "neurofibrillary tangles." The A-beta fibers readily revealed their "amyloid" character by the 0.47 nm X-ray reflection (11). In contrast, there was a protracted debate about the structure of Tau fibers that showed very low information in their X-ray pattern. This problem originated from the "natively unfolded" nature of Tau with very little secondary structure and a hydrophilic character that normally prevents its aggregation (12). We now know that one or two short hexapeptide motifs in Tau are responsible for aggregation, even though they represent only a minute fraction of the protein sequence (13). In appropriate conditions, these short sequences in Tau aggregate into fibers with a fibril core exposing cross-beta structure with a 0.47 nm reflection, as seen by X-ray and electron diffraction (14, 15). Thus, Tau fibers may also be regarded as "amyloid" in a broader sense, even though most of the protein remains unfolded after aggregation (see below). Recent NMR results revealed that the fingerprint of this beta-structure is transiently present even in soluble Tau (16).

By EM, most Tau fibers from AD brain have a twisted appearance with an apparent groove along the fiber axis and were hence termed "paired helical filaments" (PHFs, Fig. 1) (17). It was suggested that two protofibrils (diameter ~12 nm) twist around each other giving the PHFs a periodicity of ~80 nm (18). However, clear evidence that one PHF contains two single protofibrils was lacking. For example, neither the splaying apart of protofilaments, nor the extension of one protofilament over the other at the ends of fibers was observed. Thus, the "paired helical" nature of PHFs remained a matter of debate, and an alternative "twisted fiber" structure was proposed as well (18–22).

The substructure of Alzheimer fibers received renewed attention with the advent of high resolution scanning probe microscopes. In the late 1980s, the scanning probe technique "atomic force microscopy (AFM)" was developed by Binning, Quate, and Gerber (23). Originally designed to detect an organic surface topographies in sub-nanoscopic resolution in vacuum or air, AFM was soon applied to biological samples such as DNA (24) and protein assemblies (25, 26) in aqueous conditions. Nowadays, AFM is commonly used to image a wide variety of biological samples, from single proteins in the nanoscopic range (27, 28) to cells and tissues in the range of micrometers (29–31). AFM has been applied to elucidate the structure of fibrillar assemblies from various amyloidogenic

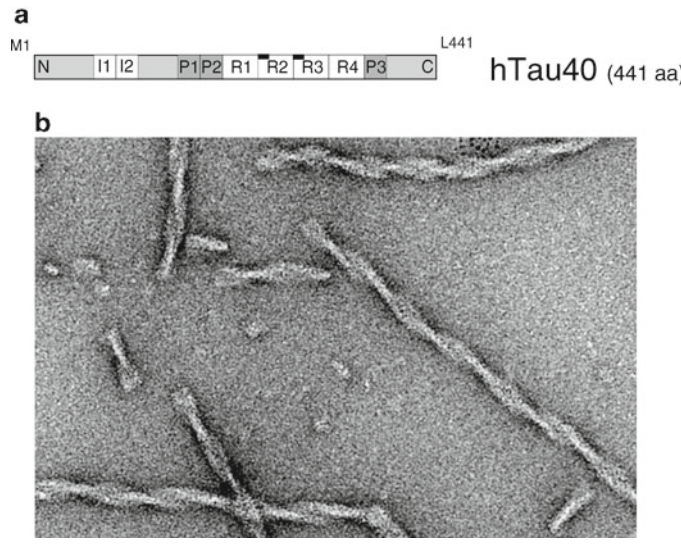

Fig. 1. Human Tau protein and its fibrillar assemblies. (**a**) Survey of hTau40, the longest human Tau isoform (441 aa). (**b**) EM image of regularly twisted, uniform fibers assembled from hTau40 in vitro, termed PHFs.

proteins including A-beta (32), alpha-synuclein (33), prion protein (34), and Tau protein (35). In the case of Tau, AFM images revealed a considerable structural polymorphism of Tau fibers (36, 37) instead of uniform PHF population. A "two-protofibril-model" for PHFs was derived from EM images (19) and supported by some AFM imaging experiments (20, 35). In contrast, results obtained from other EM (18, 38, 39) and AFM (21, 22, 40) imaging experiments of Tau fibers described PHFs as flat ribbons that twisted around their longitudinal axis. This model is supported by our recent finding that Tau fibers fragment into single "pearl-chains" of small fragments connected by thin thread-like structures (37).

Additionally, the ongoing discussion on the conformation of the N- and C-terminal domains of Tau molecules in the aggregated state was advanced by the application of AFM. While it seems clear that the fiber core resembles a stack of Tau repeat regions (41), the conformation of the unstructured termini of the Tau molecules in the fibers is imagined as a "fuzzy coat" protruding from the fibers. Comparing the AFM height of fibers from full-length Tau with fibers from a Tau repeat region construct revealed only a minor difference of 2–3 nm. The long termini (~250 aa) escape the AFM stylus during scanning and remain almost "invisible." The fuzzy coat is thus appropriately described as a "soft polymer brush" of medium density.

For high-resolution imaging of macromolecular protein assemblies like amyloid fibers, oscillation mode (also "tapping mode," "dynamic mode," and "jumping mode") AFM imaging proved to be best suited (42, 43). In this imaging mode, the AFM stylus is

oscillated vertically near its resonance frequency, while the sample surface is scanned in the horizontal *x*–*y*-plane. In contrast to imaging in constant force mode (also termed "contact mode"), where samples need a lateral fixation on the supporting surface to prevent their displacement, the oscillation of the cantilever during scanning largely reduces lateral interaction forces between the AFM stylus and sample and does not require any treatment of the sample. Oscillation mode AFM is thus especially suitable for imaging fragile, non-fixed molecular assemblies with a high aspect ratio. Thereby, a vertical resolution of ~0.1–0.2 nm and a lateral resolution of ~1.0–5.0 nm can be achieved, even with stylus diameters around ~10 nm. The resolution limit for amyloid fibers imaged with the AFM largely depends on the fiber softness and stability, both of which can be manipulated by cross-linking of the proteins with aldehydes which stiffens the fibers.

Furthermore, a controlled local increase in scanning force can be used to mechanically break and unravel non-fixed Tau fibers with the AFM stylus on the mica surface (37). Scanning the same surface region again can then reveal the subunits (diameter ~10 nm) of single Tau fibers and help to interpret the fiber integrity (Fig. 4).

In this chapter, we provide detailed information on how to image fibrillar assemblies of Tau proteins in oscillation mode AFM to achieve high-resolution, artifact-free AFM topographs that can be used for reliable analysis of structural parameters such as fiber height, width, and twist periodicity (Fig. 3c, d). We also describe how targeted mechanical fragmentation of single fibers can be used to analyze the substructure of Tau fibers. The protocol can also be used as a guideline for AFM imaging of other protein assemblies.

2. Materials

2.1. Muscovite (Mica) Surfaces

1. Magnetic steel disks (diameter 12 mm; Ted Pella, Inc., Redding, CA, USA).
2. Teflon sheets of 0.2-mm thickness (Maag Technic AG, Birsfelden, Switzerland).
3. Muscovite (mica) sheets (Mica House, Calcutta, India).
4. "Punch and die" set (Precision Brand Products, Inc., IL, USA).
5. Ethanol, p.a. ≥98% (v/v).
6. Precision Wipes from Kimtech-Science™ (Kimberley-Clark professional, Neenah, WI, USA).
7. Loctite 406 superglue (KVT Koenig, Dietikon, Switzerland).
8. Two-component epoxy glue Araldit rapid (Tesa AG, Bergdietikon, Switzerland).
9. Scotch tape.

2.2. Buffers

For buffer preparations, use ultrapure water (18 MΩ/cm at 25°C) and per analysis (p.a.) grade reagents only. All buffers should be prepared freshly before each experiment. All buffers should be sterile filtered before use (pore size 0.1 μm).

1. Adsorption buffer: PBS (137 mM NaCl, 8 mM NH_2PO_4, 2.7 mM KCl, 1.5 mM KH_2PO_4) adjusted to pH 7.4.
2. Imaging buffer: 10 mM Tris–HCl, 50 mM KCl adjusted to pH 7.4.
3. Sterile syringes 5–30 ml (e.g., BD Syringe Luer-Lok™ tip from Becton-Dickinson & Co, Franklin Lakes, NJ, USA).
4. Sterile syringe driven filter unit, Millex-VV pore size 0.1 μm (Millipore, Carrigtwohill, Ireland).
5. Glutaraldehyde solution [50% (w/v) in water] (Fluka Biochemica, Steinheim, Germany).

2.3. Tau Protein Fibers

Recombinant expression of human Tau proteins, protein purification, and assembling into fibers was performed according to ref. 44. Briefly, Tau was expressed in *Escherichia coli*, pre-purified by boiling in high salt concentration buffer, and purified by ion exchange chromatography. The assembling of Tau proteins into fibers was facilitated by the incubation of 50 μM Tau proteins in PBS pH 7.4 containing 2 mM DTT at 37°C for various times. Mature fibers were stored at 4°C in PBS pH 7.4 containing 1 mM DTT.

2.4. AFM and Cantilevers

1. Nanoscope III (Di-Veeco, Santa Barbara, California, USA) equipped with a piezo scanner allowing a *x*,*y*-scan size of ~100 μm and a *z*-range of ~4 μm (J-scanner, Di-Veeco, Santa Barbara, California, USA).
2. Triangular cantilevers (length ~100 μm; gold-coated backside) carrying sharpened pyramidal Si_3N_4 styluses and having nominal spring constants $k \approx 0.32$ N/m (NPS series, Di-Veeco, Santa Barbara, California, USA).
3. Commercially available oscillation mode quartz glass fluid cell (Di-Veeco, Santa Barbara, California, USA) for acoustically driven oscillation of the mounted cantilever.

3. Methods

To obtain AFM topographs of a quality sufficient for proper analysis, all steps during surface and sample preparation have to be carried out with extreme care and purity. Any buffer or surface contamination will prevent well-resolved images and cause stylus (or tip) artifacts.

3.1. Mica Surface Preparation

1. Choose a sheet of mica (thickness ~0.5 mm) that appears to be flat and has no obvious cracks and air inclusions (see Note 1).
2. Use the punch set to cut out muscovite disks (diameter ~5–10 mm) and Teflon disks (diameter ~15 mm).
3. The top of the steel disks and backside of the Teflon is wiped with ethanol and glued onto each other using a drop of Loctite 406.
4. Clean the Teflon surface on the steel disk with ethanol.
5. Use scotch tape to cleave off the bottom layer(s) of a mica disk and glue it onto the Teflon surface using two component epoxy (see Note 2).
6. Let the glue dry over night at room temperature under ambient conditions.
7. Muscovite surfaces can be stored at room temperature under ambient conditions until used in an AFM experiment.

3.2. Sample Preparation and Adsorption

1. Remove the upper layer(s) of a muscovite support by stripping off with scotch tape (see Note 3; Fig. 2).

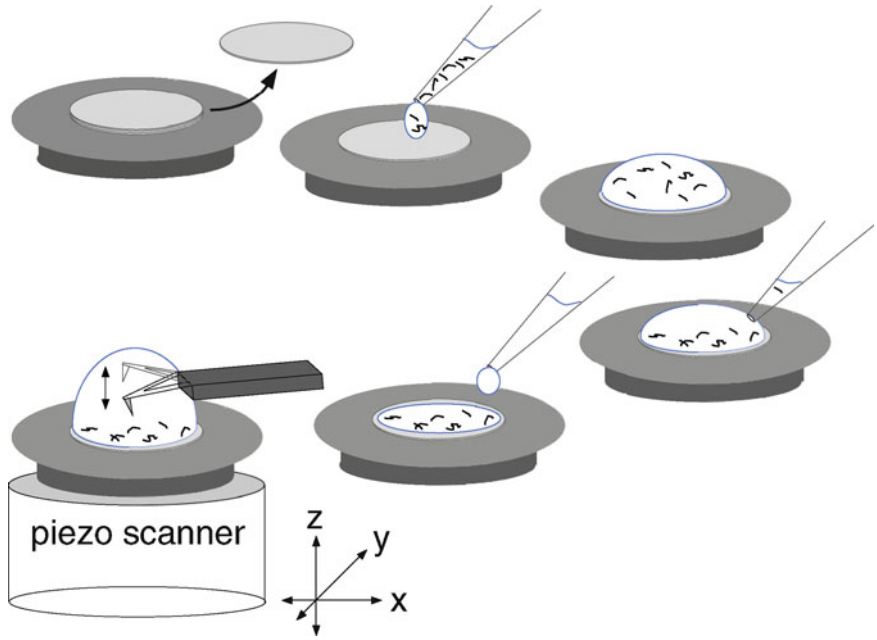

Fig. 2. Sample immobilization for AFM imaging of Tau fibers. A stable and ultraflat supporting surface that is necessary for high-resolution AFM imaging consists of the following components (from *bottom* to *top*) a steel disk (*dark grey*) that can later be mounted on the magnetic piezo scanner, a sheet of thin Teflon (*medium grey*), tightly glued to the steel disk, that prevents spreading and draining of the sample/buffer, a thin piece of mica (*light grey*) with a diameter of ~6 mm glued to the Teflon surface with two component epoxy. To immobilize Tau fibers on a clean mica surface, the upper layers of the mica are stripped off using scotch tape and Tau fiber sample solution (~30 μl; 1–2 μM) is pipetted onto the freshly cleaved mica. Adsorption of the fibers is allowed by incubation at room temperature for ~10 min. Next, the drop of sample is removed and replaced by pure imaging buffer. After mounting the supporting steel disk now carrying the adsorbed fibers on the magnetic piezo scanner, the fibers can be imaged in oscillation mode.

2. Immediately place a drop of ~30 μl imaging buffer on the freshly cleaved muscovite disk to prevent contamination of the surface.
3. Place the steel disk on the AFM piezo element.
4. Mount the cantilever in the clean oscillation mode glass fluid cell.
5. Fill the fluid cell with imaging buffer and mount it in the AFM head.
6. Place the AFM head on the sample.
7. Image the surface in constant force mode to check the purity off buffer and supporting surface (see Note 4).
8. If the muscovite surface appears clean, dilute the Tau fiber sample in adsorption buffer to a final concentration of ~1–2 μM and final volume of ~30 μl.
9. Replace imaging buffer on muscovite surface by ~30 μl Tau fiber sample (see Note 5).
10. Incubate for 10–20 min at room temperature (see Note 6).
11. Carefully exchange the drop of Tau sample against fresh imaging buffer using a pipette; repeat 3–5 times to remove non-adsorbed proteins.

3.3. Glutaraldehyde Fixation of Fibers

If necessary, fibers adsorbed to the mica surface can be hardened by cross-linking with glutaraldehyde (45).

1. Adsorb fibers on mica and exchange adsorption against imaging buffer as described above.
2. Exchange imaging buffer against ~30 μl imaging buffer containing 0.5% (w/v) glutaraldehyde and incubated for 30–60 s.
3. Replace glutaraldehyde containing buffer by 30 μl imaging buffer for at least five times.
4. Cross-linked Tau fibers are imaged in imaging buffer in the same way as non-fixed ones in oscillation mode AFM imaging.

3.4. Oscillation Mode AFM Imaging

All AFM scanning is performed in buffer solution and under ambient temperature and pressure conditions.

1. Place the AFM head with fluid cell and cantilever on the sample.
2. Allow for thermal equilibration at room temperature for ~10–20 min.
3. The initial approach of the cantilever to the surface is performed in constant force mode with a relative setpoint of ~1 V and the scan size set to 0 nm to avoid scanning of the sample in constant force mode.
4. Retract the cantilever ~50 μm from the surface.

5. Choose oscillation frequency and drive amplitude for oscillation mode imaging using the in-built auto-tuning procedure: Perform a frequency sweep between 0 and 30 kHz to find the first resonance peak of the cantilever, typically between 8.5 and 10 kHz. Choose the operating frequency where the cantilever oscillation amplitude is 95%. Set the drive amplitude to achieve a target amplitude of ~1 V.
6. Approach the surface in oscillation mode using an amplitude setpoint of ~60% of the target amplitude; before verify the following parameters: piezo scanner *z*-range set to maximum (~4 μm), set *x*- and *y*-offset to zero, set feedback gains to default, and set scan size to 0 nm to prevent immediate start of the scanning process what may cause stylus contamination (see Note 7) and sample destruction.
7. Bring the cantilever into weak contact with the surface by putting the amplitude setpoint just below the target amplitude.
8. Start scanning the sample with a scan rate of ~1 Hz and a scan size of ~15 μm to generate a low-resolution overview image. Adjust the instrument feedback while scanning your sample with lowest possible force (=highest amplitude setpoint that brings the cantilever in contact with the surface) to give the best height contrast without oscillations (see Note 8). The resolution is enhanced by step-wise zooming into surface areas showing deposited Tau fibers. At scan sizes ~3 μm (Fig. 3a), the fiber morphology, persistence length, and large periodicity (gray arrows in Fig. 3a) of Tau fibers become measurable. The fiber height (=thickness) and structural details like the stack periodicity (white arrows in Fig. 3b) can be analyzed when reaching a scan size of ~1 μm (see Note 9).
9. Topographies are recorded at a resolution of 512 by 512 pixel (or higher) in two channels in parallel that show trace and retrace scanning direction of both height and error in amplitude. This helps to judge the stylus induced sample deformation (see Note 10).
10. To achieve minimal imaging forces between AFM stylus and sample, amplitude setpoint and feedback gains are adjusted and optimized manually during scanning to compensate for thermal drift of the cantilever. In this way, a reliable tracking of the surface without sample deformation, and a good contrast in height signal (see Note 11) can be attained.
11. For controlled destruction of non-fixed fibers deposited on mica, the force acting between AFM stylus and sample is locally increased (Fig. 4). After recording an image of the surface region of interest at minimal force (as described above), the same region is scanned again whereby the amplitude setpoint is lowered during 1–5 scan lines at the scan position where

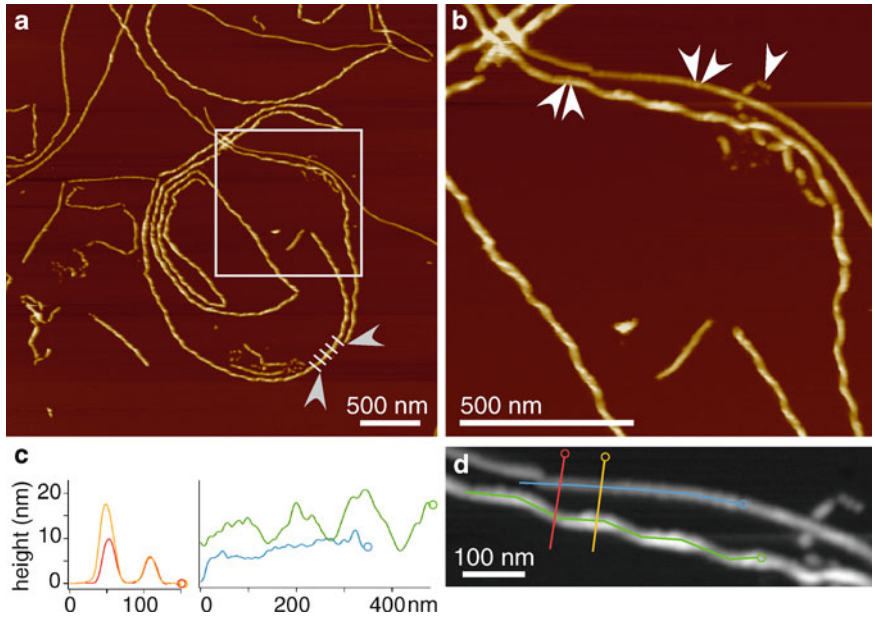

Fig. 3. Oscillation mode AFM images of hTau40 fibers on mica surface. (**a**) Fibers prepared from hTau40 were diluted in adsorption buffer (PBS) to a final concentration of 2 μM, then adsorbed to freshly cleaved mica for 10 min at room temperature, and imaged in oscillation mode (scan rate ~1 Hz; amplitude setpoint ~0.8 V). At a scan size of 3,700 nm and an image size of 512 × 512 pixels, the fiber morphology, persistence length, and their twist periodicity (*grey arrows*) can be analyzed. The *grey square* indicates the area at which the zoom in (**b**) was taken. (**b**) Keeping the same image size (512 × 512 pixels) as in the overview scan in (**a**), the resolution of the AFM scan increases after zooming into the area of interest (*grey square* in **a**). At the new scan size of ~1,250 nm, the substructure of the fibers (*white arrows*) becomes visible. (**c**) Analysis of fiber height is measured from cross-sections through the fibers (*red* and yellow curves), the topography along the fiber backbone (*green* and *blue curve*) reveals a ~120 nm twist periodicity (distance of large peaks in *green curve*) and ~17 nm stack periodicity (distance of sub-peaks in *green* and *blue* trace) in hTau40 fibers (37). (**d**) Colored lines indicate the position of cross-sections (*yellow* and *red lines*) for height measurements and the path tracked for backbone topography, both as shown in (**c**). The full-range color scale from *black* to *white* corresponds to a height of 25 nm.

mechanical manipulation of the sample should be achieved. Decreasing the amplitude setpoint by 0.05–0.2 V (see Notes 12–14) usually breaks and "unzips" the fibers into their subunits. To see the result of the mechanical perturbation, the same surface region is imaged again applying minimal scanning force.

4. Notes

1. For high-resolution topographs of Tau fibers, ultra-flat muscovite surfaces are necessary; this means that the mica surface should be bent ≤15 nm over an area of 200 μm^2.
2. For gluing mica disks on the Teflon use only a small drop of epoxy glue, just enough to spread under the entire mica disk. In this way, the cleaving of the upper mica layers before sample

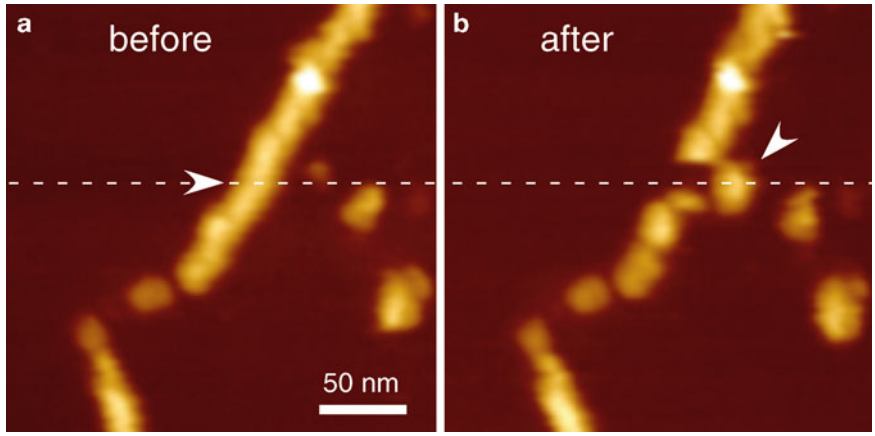

Fig. 4. Mechanical dissection of hTau40 fibers induced by the AFM stylus reveals 10–20 nm building blocks. (**a**) High-resolution topograph of an hTau40 fiber adsorbed onto mica and imaged in AFM oscillation mode applying minimal scanning force (scan rate ~1 Hz; amplitude setpoint ~0.8 V). In the next step, the same area was scanned again whereby the scanning force was locally increased for ~2 scan lines (white dashed line; amplitude setpoint ~0.7 V). (**b**) Scanning the same surface region again with minimal force (amplitude setpoint ~0.8 V) reveals the displacement of a single fiber subunit (white arrow) at the position where the increased scanning force was applied. The full-range color scale from black to white corresponds to a height of 25 nm.

adsorption remains possible and the contact of the glue to buffer and sample solution during the experiment is avoided.

3. To achieve a clean mica layer for your experiments, make sure to cleave the entire mica surface by checking the stripped off layer sticking on the scotch tape.
4. When checking the purity of the buffer, any feature on the freshly cleaved mica surface is considered to be a contamination. If your surface is contaminated at this point, cleave the mica and try with fresh buffer or filtered nanopure water again to sort out the source of contamination.
5. Always leave a thin layer of liquid on the supporting mica when replacing/exchanging the buffer. Once the mica surface runs dry you have to cleave your mica again!
6. Adsorption of samples onto the negatively charged mica is driven by physiosorption that depends on attractive and repulsive forces between the mica surface and the sample, mainly electrostatic forces (46). Thus, the amount of deposited fibers can be tuned by the concentration of fibers in the sample solution, the time given for adsorption, and the ion concentration and pH of the adsorption buffer. Surface charges that are exposed to the buffer become compensated by mono- and divalent ions in the electrolyte solution and the Debye length of charged surfaces in solution decreases. This effect can be

used to diminish repulsive forces between a specimen and the mica surface (47) and can help to adsorb negatively charged specimens to mica surfaces.

7. Biological material that sticks to the cantilever stylus can result in stylus shape-related imaging artifacts that lead to misinterpretation of AFM images (48). To give two examples (1) a stylus that has an extra protrusion would lead to a double image of each feature in the sample, a so-called double-stylus image; (2) the contamination of a sharp stylus can increase the stylus radius, prohibit the interaction of the stylus with small features of the sample, and generate a blurred, so-called blunt-stylus image. Since commercial AFM styluses often have a shape and radius different form the nominal one, similar artifacts can also occur when using clean cantilevers. To circumvent misinterpretations in AFM topographs, imaging experiments should be reproduced using several cantilevers from different manufacturing batches. It may help to use structures of known shape and dimensions as internal standards that can be compared to the specimen of interest.
8. The faster the feedback system of the AFM instrument, the better is the height tracking of the imaged surface. However, too high feedback gains and fast scanning can lead to oscillations, which usually appear as periodic features or stripes in the AFM image. Acoustic noise and minute vibrations are also sources of oscillations and other image artifacts in AFM imaging. Therefore, efficient vibration isolation, e.g., provided by an active damping table or a heavy supporting platform mounted on bungees, is essential to achieve AFM topographs of high quality. Acoustic shielding of the instrument is to be provided by a glass bell or a commercially available noise isolation hood.
9. The resolution of AFM topographs is very different in the two dimensions: The resolution in the vertical *z*-direction is given by the cantilever bending, and height differences can be detected with subnanometer precision. In the lateral *x*,*y*-plane, the resolution is largely influenced by the AFM stylus shape. A pyramidal shape of the AFM stylus prevents a true tracking of the sample edges and leads to broadening of the imaged features. For a sample on the surface, the apparent width in the AFM topograph overestimates its true width, a phenomenon called stylus(or tip) convolution. This issue should be kept in mind when comparing fiber dimensions from AFM images with dimensions measured in EM where the width is detected very precisely but no height information is provided. However, the spatial distances between different features in AFM images can again be detected with high precision, limited by the ratio of scan size to recorded pixels.

10. The height of Tau fibers is usually determined from cross-sections through the position of interest (Fig. 3c, d). The fiber periodicity can be derived from the peak distances in the topography of the fiber backbone (Fig. 3c, d). Tracking the fiber path over a long distance and calculating the mean bending angle gives access to the bending and the persistence length of the fibers.
11. If the force acting between AFM stylus and sample becomes to high, unintentional deformation and displacement of the sample in the direction of scanning can occur. This issue becomes especially crucial when dealing with non-fixed soft biological macromolecules that have a large aspect (height:width) ratio. Deviations occurring in images of simultaneously recorded trace and retrace scanning directions indicate such deformation scanning artifacts. If this is the case, one needs to increase the amplitude setpoint, reduce the scanning speed or adjust the imaging buffer salt concentration (49).
12. The force exhibited by the AFM stylus to the sample during imaging in buffer may compress the hydrated sample, thus decrease its measured height. Additionally, attractive and repulsive electrostatic forces that act between the negatively charged Si_3N_4 AFM stylus and the sample surface locally influence the tracking of the sample surface and influence the height measured from AFM topographs (50). These electrostatic effects on the measured height can be minimized by proper adjustment of pH and electrolyte concentration in the imaging buffer (51).
13. In constant force mode, the sum of the forces acting on the AFM stylus is derived directly from the cantilever deflection. In oscillation mode, the amplitude of the oscillating cantilever is recorded and adjusted, and sample stiffness and stylus-sample interaction forces can largely influence the oscillation amplitude and make it a complex issue to determine the actually exerted force and real height of the sample (52, 53). To obtain the real height of a biological sample, its height in oscillation mode AFM topographs is related to the known height of a reference structure with similar height imaged under the same conditions. Nanoparticles and beads or other biological samples, e.g., purple membrane (43), can be used as so-called internal standards.
14. The decrease in amplitude setpoint (=increase in scanning force) needed for unraveling a fiber depends on the fiber stability, which is influenced by buffer conditions and type of fiber, and the sharpness of the AFM stylus. Thus, several approaches in the same experimental setup may be necessary to induce fiber unzipping without uncontrolled scratching and destruction of the sample. The actual force that is applied to the fibers can be estimated from a cross-correlation of the amplitude setpoint, the deflection sensitivity of the AFM, and the cantilever spring constant.

Acknowledgments

This work was supported by the Max-Planck-Society (program on "Toxic Protein Conformation," to DM and EM), the Volkswagen Foundation (program "Conformation of Biological Molecules," to EM), the BMBF program on Degenerative Diseases (KNDD, to EM), and the Deutsche Forschungsgemeinschaft (GK1401 at TU Dresden, to DM and SW). We are grateful to Eva-Maria Mandelkow and Subash Chinnathambi for their advice and contributions to Tau biochemistry and aggregation.

References

1. Sipe, J. D., Cohen, A. S. (2000) Review: history of the amyloid fibril. *J. Struct. Biol.* **130**, 88–98.
2. Virchow, R. (1854) Ueber eine im Gehirn und Rückenmark des Menschen aufgefundene Substanz mit der chemischen Reaction der Cellulose. *Virchow Arch. Path. Anat. Phys.* **6**, 135–138.
3. Elghetany, M. T., Saleem, A. (1988) Methods for staining amyloid in tissues: a review. *Stain Technol.* **63**, 201–212.
4. Picken, M. M. (2010) Amyloidosis-where are we now and where are we heading? *Arch. Pathol. Lab. Med.* **134**, 545–551.
5. Alzheimer, A. (1907) Ueber eine eigenartige Erkrankung der Hirnrinde. *Allg. Zeitschrift f. Psychiatrie u. Psychisch-gerichtliche Medizin* **64**, 146–148.
6. Antzutkin, O. N., Leapman, R. D., Balbach, J. J. and Tycko, R. (2002) Supramolecular structural constraints on Alzheimer's beta-amyloid fibrils from electron microscopy and solid-state nuclear magnetic resonance. *Biochemistry* **41**, 15436–15450.
7. Eanes, E. D., Glenner, G. G. (1968) X-ray diffraction studies on amyloid filaments. *J. Histochem. Cytochem.* **16**, 673–677.
8. Luhrs, T., Ritter, C., Adrian, M., Riek-Loher, D., Bohrmann, B., Döbeli, H., Schubert, D., Riek, R. (2005) 3D structure of Alzheimer's amyloid-beta(1–42) fibrils. *Proc. Natl. Acad. Sci. USA* **102**, 17342–17347.
9. Nelson, R., Sawaya, M. R., Balbirnie, M., Madsen, A. Ø., Riekel, C., Grothe, R., Eisenberg, D. (2005) Structure of the cross-beta spine of amyloid-like fibrils. *Nature* **435**, 773–778.
10. Serpell L. C. (2000) Alzheimer's amyloid fibrils: structure and assembly. *Biochim. Biophys. Acta* **1502**, 16–30.
11. Glenner, G. G., Eanes, E. D., Bladen, H. A., Linke R. P., Termine, J. D. (1974) Beta-pleated sheet fibrils. A comparison of native amyloid with synthetic protein fibrils. *J. Histochem. Cytochem.* **22**, 1141–1158.
12. Schweers, O., Schonbrunn-Hanebeck, E., Marx, A., Mandelkow, E. (1994) Structural studies of tau protein and Alzheimer paired helical filaments show no evidence for beta-structure. *J. Biol. Chem.* **269**, 24290–24297.
13. von Bergen, M., Friedhoff, P., Biernat, J., Heberle, J., Mandelkow, E. M., Mandelkow, E. (2000) Assembly of tau protein into Alzheimer paired helical filaments depends on a local sequence motif ((306)VQIVYK(311)) forming beta structure. *Proc. Natl. Acad. Sci. USA* **97**, 5129–5134.
14. Barghorn, S., Davies, P., Mandelkow, E. (2004) Tau paired helical filaments from Alzheimer's disease brain and assembled in vitro are based on beta-structure in the core domain. *Biochemistry* **43**, 1694–1703.
15. Berriman, J., Serpell, L. C., Oberg, K. A., Fink, A. L., Goedert, M., Crowther, R. A. (2003) Tau filaments from human brain and from in vitro assembly of recombinant protein show cross-beta structure. *Proc. Natl. Acad. Sci. USA* **100**, 9034–9038.
16. Mukrasch, M. D., Bibow, S., Korukottu, J., Jeganathan, S., Biernat, J., Griesinger, C., Mandelkow, E., Zweckstetter, M. (2009) Structural polymorphism of 441-residue tau at single residue resolution. *PLoS Biol.* **7**, e34.
17. Kidd, M. (1963) Paired helical filaments in electron microscopy of Alzheimer's disease. *Nature* **197**, 192–193.
18. Crowther, R. A. (1991) Straight and paired helical filaments in Alzheimer disease have a common structural unit. *Proc. Natl. Acad. Sci. USA* **88**, 2288–2292.

19. Ksiezak-Reding, H., Wall, J. S. (2005) Characterization of paired helical filaments by scanning transmission electron microscopy. *Microsc. Res. Tech.* **67**, 126–140.
20. Moreno-Herrero, F., Valpuesta, J. M., Perez, M., Colchero, J., Barö, A. M., Avila, J., Montejo De Garcini, E. (2001) Characterization by atomic force microscopy and cryoelectron microscopy of tau polymers assembled in Alzheimer's disease. *J. Alzheimers Dis.* **3**, 443–451.
21. Pollanen, M. S., Markiewicz, P., Bergeron, C., Goh, M. C. (1994) Twisted ribbon structure of paired helical filaments revealed by atomic force microscopy. *Am. J. Pathol.* **144**, 869–873.
22. Pollanen, M. S., Markiewicz, P., Goh, M. C. (1997) Paired helical filaments are twisted ribbons composed of two parallel and aligned components: image reconstruction and modeling of filament structure using atomic force microscopy. *J. Neuropathol. Exp. Neurol.* **56**, 79–85.
23. Binnig, G., Quate, C. F., Gerber, C. (1986) Atomic force microscope. *Phys Rev Lett.* **56**, 930–933.
24. Hansma, H. G., Bezanilla, M., Zenhausern, F., Adrian, M., Sinsheimer, R. L. (1993) Atomic force microscopy of DNA in aqueous solutions. *Nucleic Acids Res.* **21**, 505–512.
25. Guthold, M., Bezanilla, M., Erie, D. A., Jenkins, B., Hansma, H. G., Bustamante, C. (1994) Following the assembly of RNA polymerase-DNA complexes in aqueous solutions with the scanning force microscope. *Proc. Natl. Acad. Sci. USA* **91**, 12927–12931.
26. Engel, A., Schoenenberger, C. A., Muller, D. J. (1997) High resolution imaging of native biological sample surfaces using scanning probe microscopy. *Curr. Opin. Struct. Biol.* **7**, 279–284.
27. Muller, D. J., Schabert, F. A., Buldt, G., Engel, A. (1995) Imaging purple membranes in aqueous solutions at sub-nanometer resolution by atomic force microscopy. *Biophys. J.* **68**, 1681–1686.
28. Yu, J., Bippes, C. A., Hand, G. M., Muller, D. J., Sosinsky, G. E. (2007) Aminosulfonate modulated pH-induced conformational changes in connexin26 hemichannels. *J. Biol. Chem.* **282**, 8895–8904.
29. Franz, C. M., Muller, D. J. (2005) Analyzing focal adhesion structure by atomic force microscopy. *J. Cell. Sci.* **118**, 5315–5323.
30. Wegmann, S., Miesbauer, M., Winklhofer, K. F., Tatzelt, J., Muller, D. J. (2008) Observing fibrillar assemblies on scrapie-infected cells. *Pflugers Arch.* **456**, 83–93.
31. Liu, S., Wang, Y. (2010) Application of AFM in microbiology: a review. *Scanning* **32**, 61–73.
32. Harper, J. D., Lieber, C. M., Lansbury, P. T., Jr. (1997) Atomic force microscopic imaging of seeded fibril formation and fibril branching by the Alzheimer's disease amyloid-beta protein. *Chem. Biol.* **4**, 951–959.
33. Conway, K. A., Harper, J. D., Lansbury, P. T., Jr. (2000) Fibrils formed in vitro from alpha-synuclein and two mutant forms linked to Parkinson's disease are typical amyloid. *Biochemistry* **39**, 2552–2563.
34. Anderson, M., Bocharova, O. V., Makarava, N., Breydo, L., Salnikov, V. V., Baskakov, I. V. (2006) Polymorphism and ultrastructural organization of prion protein amyloid fibrils: an insight from high resolution atomic force microscopy. *J. Mol. Biol.* **358**, 580–596.
35. Moreno-Herrero, F., Perez, M., Baro, A. M., Avila, J. (2004) Characterization by atomic force microscopy of Alzheimer paired helical filaments under physiological conditions. *Biophys. J.* **86**, 517–525.
36. Frost, B., Ollesch, J., Wille, H., Diamond, M. I. (2009) Conformational diversity of wild-type Tau fibrils specified by templated conformation change. *J. Biol. Chem.* **284**, 3546–3551.
37. Wegmann, S., Jung, Y. J., Chinnathambi, S., Mandelkow, E. M., Mandelkow, E., Muller, D. J. (2010) Human Tau isoforms assemble into ribbon-like fibrils that display polymorphic structure and stability. *J. Biol. Chem.* **285**, 27302–27313.
38. Ruben, G. C., Novak, M., Edwards, P. C., Iqbal, K. (2005) Alzheimer paired helical filaments (PHFs) studied by high-resolution TEM: what can vertical Pt-C replication tell us about the organization of the pronase-digested PHF core? *Microsc. Res. Tech.* **67**, 196–209.
39. Wischik, C. M., Novak, M., Edwards, P. C., Klug, A., Tichelaar, W., Crowther, R. A. (1988) Structural characterization of the core of the paired helical filament of Alzheimer disease. *Proc. Natl. Acad. Sci. USA* **85**, 4884–4888.
40. Pollanen, M. S., Markiewicz, P., Goh, M. C., Bergeron, C. (1995) Alzheimer paired helical filaments: a comparison with the twisted ribbon model. *Acta Neuropathol.* **90**, 194–197.
41. von Bergen, M., Barghorn, S., Biernat J., Mandelkow, E. M., Mandelkow, E. (2005) Tau aggregation is driven by a transition from random coil to beta sheet structure. *Biochim. Biophys. Acta* **1739**, 158–166.
42. Elie-Caille, C., Severin, F., Helenius, J., Howard, J., Muller, D. J., Hyman, A. A. (2007) Straight GDP-tubulin protofilaments form in the presence of taxol. *Curr. Biol.* **17**, 1765–1770.
43. Erler, A., Wegmann, S., Elie-Caille, C., Bradshaw, C. R., Maresca, M., Seidel, R., Habermann, B., Muller, D. J., Stewart, A. F. (2009) Conformational adaptability of Redbeta during DNA annealing and implications for its

structural relationship with Rad52. *J. Mol. Biol.* **391**, 586–598.

44. Barghorn, S., Biernat, J., Mandelkow, E. (2005) Purification of recombinant tau protein and preparation of Alzheimer-paired helical filaments in vitro. *Methods Mol. Biol.* **299**, 35–51.
45. Hopwood, D. (1972) Theoretical and practical aspects of glutaraldehyde fixation. *Histochem. J.* **4**, 267–303.
46. Nakanishi, K., Sakiyama, T., Imamura, K. (2001) On the adsorption of proteins on solid surfaces, a common but very complicated phenomenon. *J. Biosci. Bioeng.* **91**, 233–244.
47. Tadmor, R., Hernandez-Zapata, E., Chen, N., Pincus,P., Israelachvili, J. (2002) Debye Length and Double-Layer Forces in Polyelectrolyte Solutions. *Macromolecules* **35**, 2380–2388.
48. Ricci, D., Braga, P. C. (2004) Recognizing and avoiding artifacts in AFM imaging. *Methods Mol. Biol.* **242**, 25–37.
49. Muller, D. J., Fotiadis, D., Scheuring, S., Müller, S. A., Engel, A. (1999) Electrostatically balanced subnanometer imaging of biological specimens by atomic force microscope. *Biophys. J.* **76**, 1101–1111.
50. Butt, H. J. (1991) Electrostatic interaction in atomic force microscopy. *Biophys. J.* **60**, 777–785.
51. Muller, D. J., Engel, A. (1997) The height of biomolecules measured with the atomic force microscope depends on electrostatic interactions. *Biophys. J.* **73**, 1633–1644.
52. Das, S., Sreeram, P. A., Raychaudhuri, A. K. (2007) Effects of nonlinear forces on dynamic mode atomic force microscopy and spectroscopy. *J. Nanosci. Nanotechnol.* **7**, 2167–2171.
53. Legleiter, J. (2009) The effect of drive frequency and set point amplitude on tapping forces in atomic force microscopy: simulation and experiment. *Nanotechnology* **20**, 245703.

Chapter 13

Structural Studies of Amyloids by Quenched Hydrogen–Deuterium Exchange by NMR

Marçal Vilar, Lei Wang, and Roland Riek

Abstract

The elucidation of the structure of amyloid fibrils and related aggregates is an important step towards understanding the pathogenesis of diseases such as Alzheimer's and Parkinson's, which feature protein misfolding and/or aggregation. However, the large size and poor solubility of amyloid-like fibrils make them resistant to high-resolution structure determination. Here, we describe the use of hydrogen–deuterium exchange coupled with NMR as an indirect strategy to determine the folding regions of amyloid-forming proteins at residue level resolution.

Key words: Amyloid fibrils, H/D exchange, NMR, Aβ, α-synuclein

1. Introduction

Despite great interest and substantial efforts from various research communities, deriving high-resolution structures of amyloid fibrils remains a challenging problem, due to the insolubility and non-crystalline nature of the fibrils. An array of experimental methods, such as electron microscopy, fiber diffraction, solid-state nuclear magnetic resonance (NMR), hydrogen–deuterium exchange, electron paramagnetic resonance spectroscopy, and biochemical approaches, have been explored to study these aggregates, yielding considerable amount of information about the fibril conformation (1). A defining characteristic of amyloid fibrils is the presence of the cross-β structural motif, originally revealed by X-ray fiber diffraction (2–5), in which ribbon-like β-sheets, extending over the length of the fibril, are formed by β-strands that run nearly perpendicular to the long axis of the fibril, with backbone hydrogen bonds that run nearly parallel to the long axis. Recent studies on

Einar M. Sigurdsson et al. (eds.), *Amyloid Proteins: Methods and Protocols*, Methods in Molecular Biology, vol. 849,
DOI 10.1007/978-1-61779-551-0_13,

fibrous microcrystals formed by short peptides as well as solid-state NMR spectroscopy of both amyloid peptides and proteins (6–11) have confirmed the structural details of the cross-β spine of fibrils (12). However, X-ray crystallography of amyloid microcrystals appears to be limited to short peptides, and high-resolution structure determination of amyloid proteins by solid-state NMR is still challenging. Here, we describe a method using hydrogen/deuterium (H/D) exchange detected by solution NMR spectroscopy to study the structural and dynamic properties of amyloid fibrils in an aqueous environment. H/D exchange monitored by NMR has been used for decades to identify backbone amide protons involved in protective secondary structure within globular proteins at single-residue resolution. The use of NMR and H/D exchange in the study of amyloid proteins was originally developed by the groups of Dr. Goto in Japan with the β2-microglobulin amyloid (8) and by Dr. Alesandrescu in the USA with the study of cold shock protein A (13). Although H/D exchange measurements do not provide specific geometric constraints on molecular structures, they do offer valuable information about the nature and extent of the structural rearrangements that proteins with stable native folds undergo upon conversion to an amyloid form, and about the presence and location of peptide segments in the amyloid entity that are involved in stable secondary structure elements. During past years, several groups, including ours, have described the H/D exchange monitored by NMR from different amyloid fibrils such as β-2 microglobulin, transthyretin, HET-s, α-synuclein, the Aβ peptide, the mammalian prion protein, as well as other aggregates such as bacterial inclusion bodies or temperature-induced aggregates (14–18).

It is the purpose of this chapter to describe the application, procedure of measurements, and analysis of quenched H/D exchange NMR of protein aggregates.

2. Materials

Prepare all solutions with ultrapure water and analytical grade reagents. Diligently follow all waste disposal regulations when disposing material.

1. Protein or peptide for amyloid fibril formation, isotopically labeled for NMR spectroscopy.
2. Liquid nitrogen (see Note 1).
3. 99.9% Deuterated dimethylsulfoxide—d_6 (DMSO) and NMR tubes (see Note 2).
4. Long Pasteur pipettes (see Note 3).
5. Deuterated trifluoroacetic acid (TFA) (see Note 4).
6. 99.9% D_2O.

3. Methods

3.1. H/D Exchange Determination by NMR Spectroscopy

The intrinsic exchange rate constant of hydrogen in an exposed amide group is described as:

$$k_{\text{int}} = k_{\text{w}} + k_{\text{acid}}[\text{H}^+] + k_{\text{base}}[\text{OH}^-], \quad (1)$$

where k_{int}, k_{w}, k_{acid}, and k_{base} are the observed rate constants for exchange, the spontaneous rate constant in water, and the acid and base catalyzed second-order rate constants, respectively. The exchange reaction is highly dependent on the pH of the solution and it is catalyzed by both acids and bases. The exchange rate changes by a factor of 10 per pH unit, and the minimal exchange rate is around pH 2.6 in a water environment and around pH 5.0 in DMSO (19). k_{int} of a backbone amide of an amino acid residue is both dependent on the residue side chain type and the side chain of its N-terminal neighboring residue, and hence the k_{int} of an amide of a given residue is different, depending on its position in the protein sequence. On top of the sequence-dependent exchange rate, the 3D structure of the protein determines the exchange rate of the amide. Hence, in a folded protein, the exchange of amide protons is usually slower than in an intrinsically disordered protein due to the formation of hydrogen bonds within secondary or tertiary structural elements or by the amides spatial location inside the globular tertiary structure of the protein. This slower exchange is described by the protection factor, P, which is calculated as the ratio between the observed exchange rate, k_{ex}, and the intrinsic exchange rate, k_{int} (k_{int} is the intrinsic exchange rate expected if the hydrogen is positioned in an intrinsically disordered or flexible oligo/polypeptide chain):

$$P = \frac{k_{\text{int}}}{k_{\text{ex}}}. \quad (2)$$

Following standard measurements on short peptides k_{int} was determined and can be now extracted from a spreadsheet with the input values of pH, temperature, and the amino acid sequence (20), while k_{ex} must be experimentally measured (*see* http: //HX2.Med.Upenn.edu/).

There are two main techniques to measure slow exchange rates by NMR. The standard method is to quickly exchange the buffer in which the protein is dissolved from H_2O to D_2O (or vice versa) followed by the measurement of a time-resolved series of amide-resolved NMR spectra (which is typically a [^{15}N,^{1}H]-HMQC experiment using ^{15}N-labeled protein). The exchange from an H_2O to D_2O buffer can be done for example on an exchange column (such as the PD10 column) or by protein lyophilization followed by the addition of the D_2O buffer. Progress of the H/D exchange

reaction can be observed as a decrease in the peak intensity/volume in the spectra, and the exchange rate constants can be obtained from nonlinear least-square fitting of the decay of the cross-peak intensity as a function of exchange-time to the single exponential function:

$$I(t) = I(0)\exp(-k_{ex}t), \tag{3}$$

where t is the exchange time, $I(0)$ and $I(t)$ are peak intensities at time zero and time t, respectively, and k_{ex} is the exchange rate constant. This approach allows the measurement of the H/D exchange within one protein sample with a resolution of several minutes per experiment (note: faster acquisition is also possible if necessary (21)). An alternative approach is to exchange the buffer from H_2O to D_2O and after a given exchange time, the exchange is quenched by placing the protein in an aprotic solvent such as DMSO. This procedure prevents further exchange in the aprotic solvent due to the lack of exchangeable hydrogens. Now, the NMR experiment is measured. It is evident that this approach requires for each exchange time point a new sample; but under some circumstances, it enables also the measurement of exchange in otherwise not accessible systems such as protein aggregates as discussed below.

3.2. Amyloid Fibril Solubilization: Advantages of DMSO

Protein aggregates are usually composed of an intermolecular cross-β-sheet structure forming a supramolecular assembly composed of numerous protein molecules; and therefore, only the quenched H/D exchange method is appropriate. According to Alexandrescu (13), to be applicable to protein aggregates such as amyloid fibrils, a quenched hydrogen exchange experiment must satisfy at least two requirements. First, the aggregates need to be dissolved to unfolded liquid state NMR-detectable monomers. Second, the H/D exchange must be sufficiently slow under the dissolving conditions for NMR detection. Actually, the intrinsic H/D exchange in the dissolving buffer should be much slower than the time of an NMR experiment, because otherwise, it shadows the exchange of interest, which is the one of the protein aggregates.

Let us discuss the first requirement. Although the aggregates are generally very stable under aqueous conditions, they can be dissolved into monomeric protein molecules with several organic solvents. DMSO together with TFA is shown to be an excellent *solubilization* agent for protein aggregates. Other organic solvents used to dissolve β2-microglobulin amyloid fibrils are also ethanol (EtOH), 2,2,2-trifluoroethanol (TFE), and 1,1,1,3,3,3-hexafluoro-2-propanol (HFIP) by Hirota-Nakaoka et al. (22). Their results showed that, although HFIP and TFE dissolve amyloid fibrils, the effects are not complete, yielding amorphous aggregates. In contrast, DMSO dissolved amyloid fibrils of β2-m completely without such adverse effects, although high concentration of DSMO is required.

Next, the second important requirement, the intrinsic exchange in the organic solvent is discussed in detail. The nature of the experiments described here is to determine the amount of H/D exchange that has occurred at each exchangeable position in the peptide or protein, when the peptide is resident in the aggregate. Thus, to obtain interpretable NMR spectra allowing an evaluation of the degree of deuterium incorporation during an exchange time, it is necessary to perform the analysis indirectly on the dissolved monomeric peptide obtained by dissolving fibrils in a suitable solvent. To obtain an accurate H/D exchange map of the aggregate once the aggregates are dissolved, the continued exchange of protons/deuterons between the dissolved fibril and the bulk solvent should be either eliminated or significantly reduced. Zhang and collaborators (19) examined the H/D exchange rate constant of different peptides in DMSO. They found that the exchange rates in DMSO were about 100 times slower than in aqueous buffer with strong dependency on residual water. Exchange is thus sufficiently slow to detect amide protons in unfolded polypeptides that would otherwise be completely exchanged during the course of NMR measurements in D_2O. In conclusion, DMSO has been proved to be an excellent solvent to dissociate the protein aggregates. This includes aggregates of β2-microglobulin, Aβ(1–42), α-synuclein, HET-S prion, inclusion bodies, and other types of aggregates (8, 14–18, 22).

The basic idea of the DMSO-quenched H/D exchange method described above is that the H/D exchange rate can be significantly slowed down in the presence of a very high concentration of DMSO, which has no exchangeable hydrogen. Ideally, if a partially deuterated protein sample, which has been subjected to H/D exchange under aqueous conditions, is dissolved in 100% DMSO, further exchange in this pure organic solvent would be completely "frozen." In practice, however, this does not work for the following reasons. First, it is very difficult to avoid any contamination of water molecules in DMSO, as it is a highly hygroscopic solvent. Second, it is not possible to strictly control the pH of the sample, which is necessary to keep the intrinsic exchange rate to a minimum. Third, even if it is possible to remove any contamination of water in DMSO, undesired exchange reactions from one amide site to another may occur. This possible "flip-flop" between amide hydrogens could disturb the obtained experimental results. Because the total amount of water molecules is very low in the DMSO-quenched H/D exchange method, it is very sensitive to contamination by H_2O. Therefore, H_2O contamination should be avoided as much as possible when performing the experiment.

Although the exchange rates greatly decrease around 100 times in the presence of 95% (v/v) DMSO, further nonnegligible exchange does still occur as highlighted above. To eliminate the effect of exchange in the DMSO-quenching buffer, we measured

a series of 80 fast HMQC (3 min each) and the intensities of each peak are plotted versus the experimental time. In this manner, we can extrapolate the value of the intensities of amide proton at time zero of the measurement.

A solvent completely lacking exchangeable protons is ideal, because that should completely inhibit back exchange with the solvent. However, in practical terms, because water cannot be completely excluded when fibrils are dissolved in polar, aprotic solvents, some water contamination is likely to be observed. In those conditions, residues that display slow exchange in the fibrils and residues that have high-intrinsic exchange rates in DMSO will both yield intense peaks in the [^{15}N,^{1}H] correlation spectrum. To distinguish those residues that have a fast intrinsic exchange in DMSO, 0.5 M H_2O and 0.5 M D_2O were added to the sample, and a second series of 80 2D spectra were measured. Residues showing a 50% decrease in the intensity in comparison to the one showed in the first spectrum have a fast intrinsic exchange during the acquisition time in DMSO and should, therefore, be discarded from the analysis (Fig. 1).

3.3. Quenched H/D Exchange Analysis

Each NMR sample has a minimal volume of 250 μL and contains at least 0.1 mM of dissolved monomeric protein, assuming the NMR instrument is equipped with a cryogenic probe. Otherwise, the protein concentration should be at least 0.3 mM. To monitor the change of peak intensities during H/D exchange, six or more NMR samples are needed.

3.4. Procedure and Data Analysis

1. Prepare amyloid fibrils or other protein aggregates using specific protocols as established in the literature. Usually, a high concentration of protein will be necessary, and the buffer, temperature, and mode of agitation should be optimized to form highly homogeneous fibrils. Make sure that the fibril formation process is finished. This can be monitored by time-resolved fluorescence spectroscopy of the amyloid-specific dye thioflavin-T, electron microscopy of the amyloid fibrils, as well as the amount of soluble protein in the supernatant (see Note 5). The amyloid fibril formation process may usually take from several hours to several weeks.
2. Centrifuge the protein aggregate, discard the supernatant, and incubate the fibrils into the same buffer as in step 1, but with the use of deuterated compounds such as D_2O or/and Tris–DCl (pH 7.0). To remove remaining H_2O if necessary repeat the procedure again by centrifugation of the protein aggregate, discarding the supernatant and incubating the fibrils with the deuterated buffer. Take the fibril samples at different time points between several minutes to several months following an exponential distribution (Fig. 2). Typically, we prepare around ten samples.

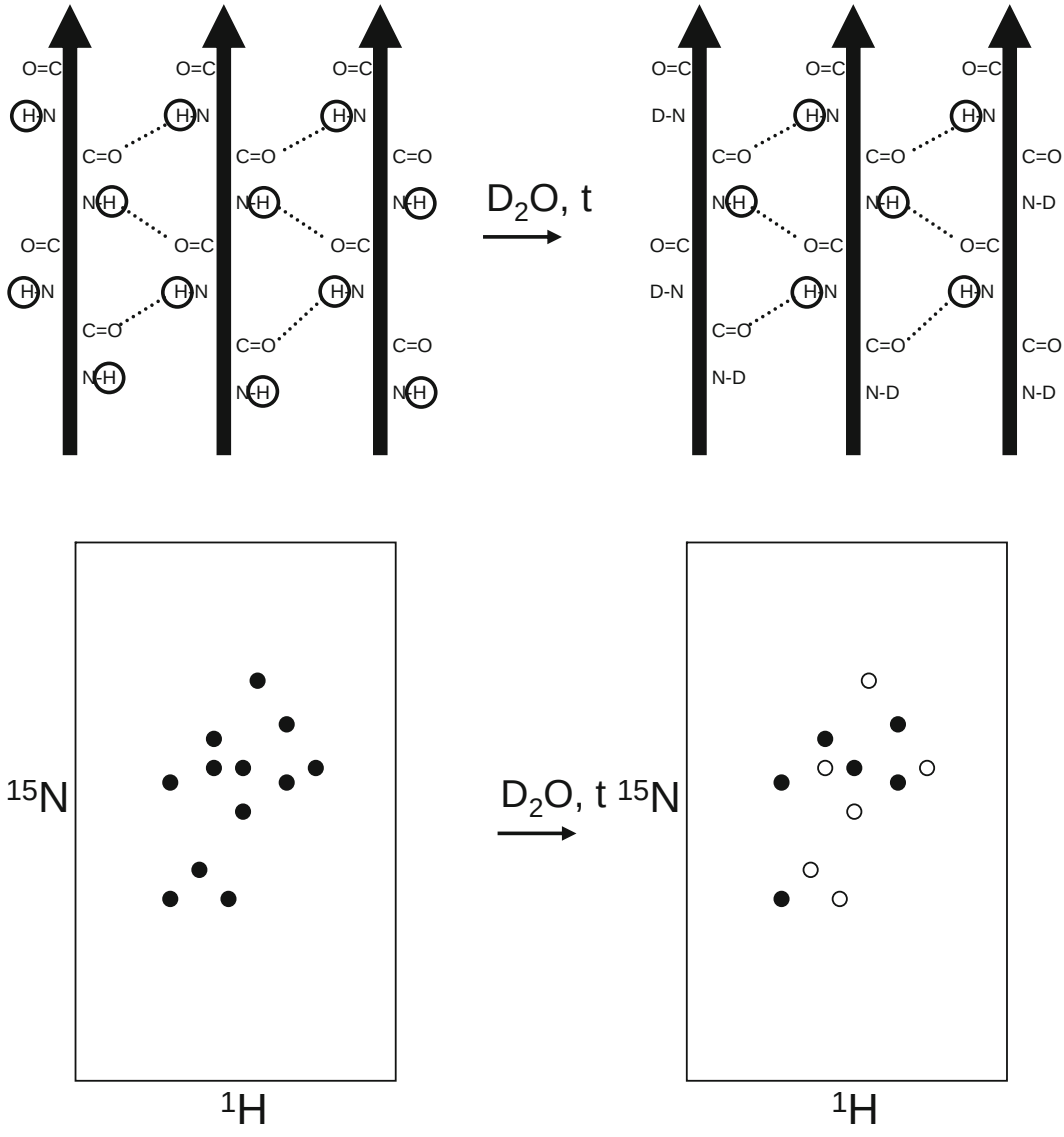

Fig. 1. Scheme of the H/D exchange procedure. Amyloid fibrils form a cross-β structure, with the hydrogen bonds parallel to the long fibril axis. *Circled* are the amide protons susceptible to exchange with the solvent. Those protons are visible in the 2D NMR spectrum below. Upon incubation with D_2O, the amide protons freely accessible, exchange very fast with the deuterium of the solvent. Instead, amide protons making the hydrogen bonds of the β-sheets inside the fibrils structure, exchange much slower. Upon recording the NMR spectra, the peaks corresponding to those protons have reduced intensity or even disappear. After each time point, the fibrils are solubilized in DMSO and a two-dimensional spectrum is recorded. The exchange constant of each residue is calculated from the fitting of the peak intensity, and the time of D_2O incubation of the fibrils to the monoexponential decay equation $I(t) = I(0)\exp(-k_{ex}t)$ (see text for details).

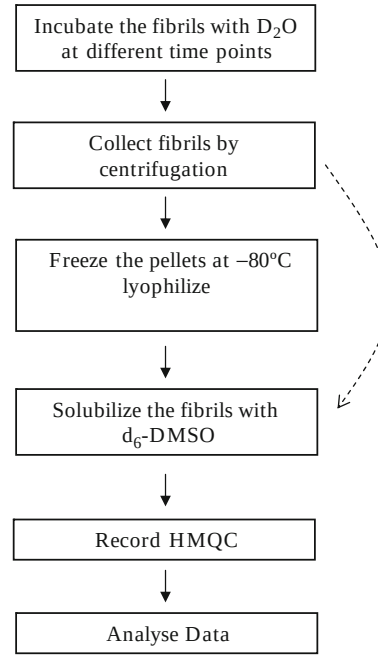

Fig. 2. Flowchart showing the standard protocol described.

3. After each time point, the protein aggregates are centrifuged to pellet the aggregates (see Note 6) and the supernatant is removed (see Note 7).
4. The pelleted protein aggregates are rapidly frozen in liquid nitrogen to stop the exchange (see Note 8).
5. Prepare the NMR instrument with a reference sample (see Note 9).
6. To dissociate the exchanged fibrils into monomers, the frozen pellet is resuspended in a mixture of DMSO/TFA (see Note 10).
7. The solution is transferred immediately to the NMR tube with a long Pasteur pipette and the tube is brought to the NMR spectrometer (see Note 11).
8. Start recording the NMR experiments. Measure first a 1D ^{1}H spectrum, followed by a series of [^{15}N,^{1}H]-HMQC experiments. Typical measuring time per experiment is 2–10 min. At the end, measure again a 1D ^{1}H spectrum (see Note 12).
9. Add 0.5 M H_2O and 0.5 M D_2O and measure again a series of [^{15}N,^{1}H]-HMQC experiments (see Note 13). This series of experiment may be repeated after each time point only if necessary (see Note 14).

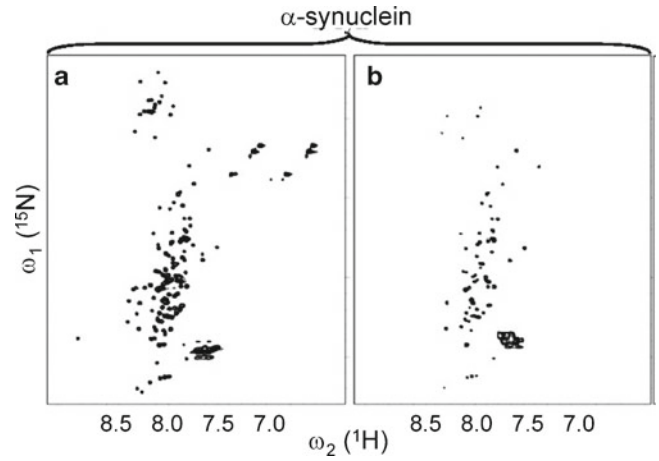

Fig. 3. Fast [^{15}N,^{1}H]-HMQC-spectra of solubilized ^{15}N-labeled α-synuclein in d_6-DMSO containing 0.1% d_1-TFA, corresponding to fully protonated (**a**) and 1 h exchanged amyloid fibrils of α-synuclein (**b**). Many cross-peaks are lost on H/D exchange for 1 h. The figure was taken from Vilar et al. (16) with permission. Copyright (2008) National Academy of Sciences, USA.

10. Transformation of the [^{15}N,^{1}H]-HMQC spectra as a pseudo 3D having in the third dimension the axis of H/D exchange time is suggested. This procedure guarantees identical transformation parameters including noise levels and base line corrections. Alternatively, the [^{15}N,^{1}H]-HMQC experiments are transformed individually. Fig. 3 shows the [^{15}N,^{1}H]-HMQC spectra of α-synuclein core fibrils at exchange times $t=0$ and $t=1$ h, respectively.
11. The individual cross peaks of the [^{15}N,^{1}H]-HMQC in the DMSO buffer must be assigned for a residue-specific analysis of the H/D exchange rates. For this purpose, a ^{13}C,^{15}N-labeled sample must be prepared following steps 1–8 of the recipe above without changing the sample into a D_2O buffer. The following NMR experiments are suggested to be measured: As a reference, a [^{15}N,^{1}H]-HMQC spectrum. For the sequential assignment, a 3D HNCA (23) (or 3D HNCACB) experiment and a 3D HN(COCA)NH (24) experiment are required. The latter experiment makes use of the dispersion along the ^{15}N frequency and the small rotational correlation time of the molecule in DMSO. Sequential assignment is then obtained following strategies described in Cavanagh et al. (25).
12. Each residue is analyzed by a single- or biexponential decay fit of the corresponding cross-peak intensities. Figure 4 shows the analysis of three residues of α-synuclein fibrils (see Note 14).

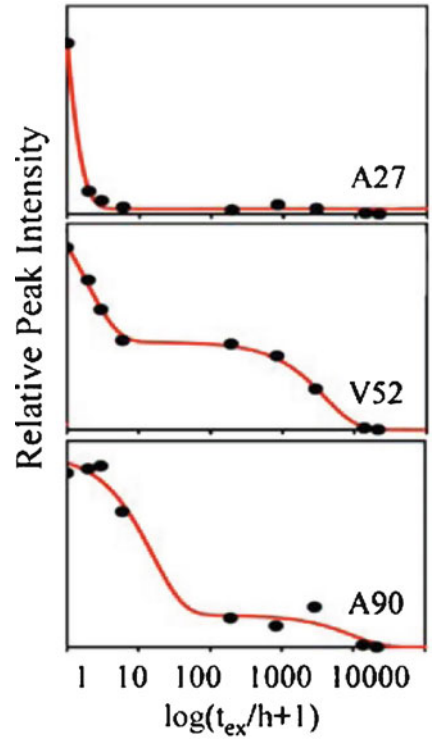

Fig. 4. Detailed H/D exchange analysis and side-chain solvent accessibility of α-synuclein fibrils. H/D exchange curves for three amide moieties. The peak volumes versus logarithm of the exchange time are shown. Data points are shown as *spheres*. Smooth *lines* represent a superposition of two monoexponential fits of the raw data. The figure was taken from Vilar et al. (16) with permission. Copyright (2008) National Academy of Sciences, USA.

4. Notes

1. Liquid nitrogen can cause terrible burns due to the death of living tissue caused by the extreme cold. Hand protection and goggles (not safety glasses) are to be worn when dispensing and handling liquid nitrogen.
2. DMSO by itself has low toxicity. However, glove selection is important when working with DMSO. Thick rubber gloves are recommended. Nitrile gloves, which are commonly used in chemical laboratories, have been found to dissolve rapidly with exposure to DMSO. Because DMSO easily penetrates the skin, substances dissolved in DMSO may be quickly absorbed.
3. The use of very long Pasteur glass pipettes facilitates the transfer of the solution to the bottom of the NMR tubes, without losing solution in the walls of the NMR tubes and avoiding the need of centrifuging the NMR tubes to bring down the solution.

4. TFA cause severe burns to the skin, eyes, mucous membranes, and other exposed tissues because of its strong acidity and fast tissue penetration. Special precautions and protective clothing, including rubber gloves and face masks, should be worn when handling it. The best treatment for spills on the skin is immediate and continuous flooding with water on the affected area.
5. Depending on the protein of interest, the protocol to obtain amyloid fibrils is different. The fibrils should be very homogeneous. It has been suggested nucleation of the solution with tiny amounts of fibrils to obtain highly homogenous amyloid fibrils. Protein concentration, pH, buffer composition, incubation temperature, speed agitation and even the plastic formulation of the tubes affect the formation and homogeneity of the fibrils.
6. Pelleting the fibrils is simple because they are big, but centrifuging at high speed, namely $100{,}000 \times g$ also pulls down small oligomers that could increase the heterogeneity of the sample. For instance, for our α-synuclein experiments, we used only $24{,}000 \times g$ for a period of 3 min.
7. The pellet should be as dry as possible. However, the lack of (heavy) water may result in problems to dissolve the aggregates in the DMSO/TFA mixture and hence a certain amount of water must be present in the pellet for some of the aggregates. In such a case (e.g., HET-s fibrils), we weight the pellet to make sure that we have always the same amount of remaining D_2O present in the pellet.
8. The pelleted fibrils are stored at −80°C. In the case of Aβ peptide, we resuspended the pellet with D_2O and after freezing the pellet was lyophilized. Lyophilized Aβ peptide was kept in powder and easily dissociated in the next step. However, HET-s and α-synuclein fibrils were practically insoluble with various DMSO/TFA mixtures upon freeze-drying. Hence, the pelleted fibrils were stored at −80°C without freeze-drying. Alternatively, in the case of bacterial inclusion bodies after H/D exchange, they were pelleted right before each NMR measurement and dissolved in the DMSO/TFA mixture without freezing or freeze-drying.
9. To avoid a delay in the acquisition of the data, it is recommended to adjust the NMR spectrometer, such as setting up the NMR parameters, finding the lock and shimming, with a reference sample tube that contains a similar concentration of protein aggregates dissolved in the optimized d_6-DMSO–TFA solution as the one to be measured
10. Depending on the aggregates of interest, different concentrations of TFA are required. In our hands, Aβ requires DMSO containing 0.1% TFA followed by a dilution by a factor of 10 with DMSO (18). In the cases of α-synuclein and HET-S

DMSO with 0.1% TFA is required, while for HET-S the pellet must be wet, hence a small amount of (heavy) water must be present in the buffer. In the cases of bacterial inclusion bodies and heat-induced aggregates, DMSO containing 0.03–0.05% TFA is enough to dissolve them. We also find that sonication during the solubilization procedure may help to dissolve the aggregates. It is important to note that the amount of TFA concentration needed appears to be related to the amount of protein to be dissolved, as well as to the size of the protein. Although we have been always successful with the DMSO/TFA buffer approach, please do not forget that other aprotic solvents may also be used.

The buffer conditions are critical since, on one hand, the DMSO buffer must contain sufficient TFA or/and (heavy) water to ensure a dissolving of the aggregate into NMR-observable monomers, and on the other hand as little as possible TFA or/and (heavy) water should be present in the buffer because these additive enhance the intrinsic H/D exchange in DMSO. This optimization step is critical and needs to be, in part, measured on the NMR spectrometer. The latter also serves for the optimization of the best signal dispersion and line-width of the amide peaks, which is also indicative of a good dissociation of the fibrils into monomers. In rare cases, broad NMR spectra were observed, indicative of aggregate formation in DMSO. The addition of more TFA usually helped to solve this potential problem.

11. Be as fast as possible and record the time it takes between adding the DMSO/TFA buffer and the acquisition of the NMR experiments. This time is required for the data processing (see below). Depending on the preparation procedure, about 5–20 min is usually needed in our hands.

12. The measurements of the 1D ^{1}H spectra have two purposes. First, the comparison between the two spectra will show that during the NMR measurements no additional material is dissolved from remaining aggregates. If the methyl region of the two 1D spectra is identical, the aggregates will be dissolved almost completely before the NMR measurements. This is important for an accurate determination of the exchange rates and optimization of the sample condition is required otherwise. Second, the first 1D ^{1}H NMR spectrum is used to quantify the amount of solubilized material using the methyl part of the spectrum. By comparison of the 1D ^{1}H NMR spectra of the individual exchange time points, the exact relative amount of sample dissolved can be measured.

    It is possible to measure a normal [^{15}N,^{1}H]-HMQC experiment (26). If a [^{15}N,^{1}H]-HMQC of type SOFAST is measured as suggested by Lührs and collaborators (18), higher signal to noise per measurement time is obtained because of the shorter

interscan delay. It is anticipated to obtain sufficient signal to noise within 2–10 min measuring time. This requires also protein concentration in the order of 0.2 mM when measured on an instrument with a cryoprobe. However, since the remaining H_2O water content influence the ^1H relaxation time in the latter experiment the water content of the DMSO solvent must be controlled (step 2). Furthermore, in the comparison between the experiments measured before (step 8) and after the addition of 0.5 M H_2O/0.5 M D_2O (step 9), an overall signal intensity change may occur.

If the residual (heavy) water content and the TFA concentration required to dissolve the fibrils can be kept very low, the intrinsic exchange in DMSO is so slow that only the first HMQC experiment at each exchange time point is required to determine the H/D exchange rate of individual amide moieties within the protein aggregate. This greatly simplifies the following analysis.

13. The second series of [^{15}N,^1H]-HMQC experiments are used to determine the intrinsic exchange in the DMSO/TFA mixture. A fast increase of the signal in the first of these [^{15}N,^1H]-HMQC experiments indicates fast intrinsic exchange in the DMSO buffer excluding these residues for any evaluation.
14. The spectra were analyzed using the program PROSA (27) and a specially written Visual Basic program in combination with Microsoft Excel. Overall, our procedure yielded precise exchange rates for 88% of the amino acid residues in the sequence of Aβ(1–42) (18) and 96% of the amino acid in the core of the α-synuclein (16).

Acknowledgments

MV is funded by the MPY-1413-09 intramural grant from the Spanish Institute of Health Carlos III and by BFU2010-15276 grant from Spanish MICINN.

References

1. Tycko, R. (2000) Solid-state NMR as a probe of amyloid fibril structure. *Curr. Opin. Chem. Biol.* **4**, 500–506.
2. Cohen, A. S., and Calkins, E. (1959) Electron microscopic observations on a fibrous component in amyloid of diverse origins. *Nature* **183**, 1202–1203.
3. Eanes, E. D., Glenner, G. G. (1968) X-ray diffraction studies on amyloid filaments. *J. Histochem. Cytochem.* **16**, 673–677.
4. Sipe, J.D., Cohen, A. S. (2000) Review: history of the amyloid fibril. *J. Struct. Biol.* **130**, 88–98.
5. Sunde, M., Serpell, L. C., Bartlam, M., Fraser, P. E., Pepys, M. B., Blake, C. C. (1997) Common core structure of amyloid fibrils by synchrotron X-ray diffraction. *J. Mol. Biol.* **273**, 729–39.
6. Shewmaker, F., Wickner, R. B., Tycko, R. (2006) Amyloid of the prion domain of Sup35p has an in-register parallel beta-sheet structure. *Proc. Natl. Acad. Sci. USA.* **103**, 19754–19759.

7. van der Wel, P. C., Lewandowski, J. R., Griffin, R. G. (2007) Solid-state NMR study of amyloid nanocrystals and fibrils formed by the peptide GNNQQNY from yeast prion protein Sup35p. *J. Am. Chem. Soc.* **129**, 5117–5130.
8. Hoshino, M., Katou, H., Hagihara, Y., Hasegawa, K., Naiki, H., Goto, Y. (2002) Mapping the core of the beta(2)-microglobulin amyloid fibril by H/D exchange. *Nat. Struct. Biol.* **9**, 332–336.
9. Wasmer, C., Lange, A., Van Melckebeke, H., Siemer, A. B., Riek, R., Meier, B. H. (2008) Amyloid fibrils of the HET-s(218–289) prion form a beta solenoid with a triangular hydrophobic core. *Science* **319**, 1523–1526.
10. Castellani, F., van Rossum, B., Diehl, A., Schubert, M., Rehbein, K., Oschkinat, H. (2002) Structure of a protein determined by solid-state magic-angle-spinning NMR spectroscopy. *Nature* **420**, 98–102.
11. Heise, H., Hoyer, W., Becker, S., Andronesi, O. C., Riedel, D., Baldus, M. (2005) Molecular-level secondary structure, polymorphism, and dynamics of full-length alpha-synuclein fibrils studied by solid-state NMR. *Proc. Natl. Acad. Sci. USA.* **102**, 15871–15876.
12. Nelson, R., Sawaya, M. R., Balbirnie, M., Madsen, A. Ø., Riekel, C., Grothe, R., Eisenberg, D. (2005) Structure of the cross-beta spine of amyloid-like fibrils. *Nature* **435**, 773–778.
13. Alexandrescu, A. T. (2001) An NMR-based quenched hydrogen exchange investigation of model amyloid fibrils formed by cold shock protein A. *Pac. Symp. Biocomput* 67–78.
14. Wang, L., Schubert, D., Sawaya, M. R., Eisenberg, D., Riek, R. (2010) Multidimensional structure-activity relationship of a protein in its aggregated states. *Angew. Chem. Int. Ed. Engl.* **49**, 3904–3908.
15. Wang, L., Maji, S. K., Sawaya, M. R., Eisenberg, D, Riek, R. (2008) Bacterial inclusion bodies contain amyloid-like structure. *PLoS Biol.* **6**:e195.
16. Vilar, M., Chou, H. T., Lührs, T., Maji, S. K., Riek-Loher, D., Verel, R., Manning, G., Stahlberg, H., Riek, R. (2008) The fold of alpha-synuclein fibrils. *Proc. Natl. Acad. Sci. USA.* **105**, 8637–8642.
17. Ritter, C., Maddelein, M. L., Siemer, A. B., Lührs, T., Ernst, M., Meier, B. H., Saupe, S. J., Riek, R. (2005) Correlation of structural elements and infectivity of the HET-s prion. *Nature* **435**, 844–848.
18. Lührs, T., Ritter, C., Adrian, M., Riek-Loher, D., Bohrmann, B., Döbeli, H., Schubert, D., Riek, R. (2005) 3D structure of Alzheimer's amyloid-beta(1–42) fibrils. *Proc. Natl. Acad. Sci. USA.* **102**, 17342–17347.
19. Zhang, Y. Z., Paterson, Y., Roder, H. (1995) Rapid amide proton exchange rates in peptides and proteins measured by solvent quenching and two-dimensional NMR. *Protein Sci.* 4, 804–814.
20. Englander, S. W. (http://HX2.Med.Upenn.edu/).
21. Gal, M., Kern, T., Schanda, P., Frydman, L., Brutscher, B. (2009) An improved ultrafast 2D NMR experiment: towards atom-resolved real-time studies of protein kinetics at multi-Hz rates. *J. Biomol. NMR* **43**, 1–10.
22. Hirota-Nakaoka, N., Hasegawa, K., Naiki, H., Goto, Y. (2003) Dissolution of beta2-microglobulin amyloid fibrils by dimethylsulfoxide. *J. Biochem.* **134**, 159–64.
23. Grzesiek, S. and Bax, A. (1992) Improved 3D Triple-Resonance NMR Techniques Applied to a 31-kDa Protein. *J. Magn. Reson.* **96**, 432–440.
24. Bracken, C., Palmer, A. G. 3rd, and Cavanagh, J. (1997) (H)N(COCA)NH and HN(COCA)NH experiments for 1H-15N backbone assignments in 13C/15N-labeled proteins. *J. Biomol. NMR* **9**, 94–100.
25. Cavanagh, J., Fairbrother, W. J., Palmer, A. G. 3rd, Rance, M., Skelton, N. J. (2007) Protein NMR spectroscopy : principles and practice. 2. Academic Press; San Diego.
26. Griffey, R. H., Poulter, C. D., Bax, A., Hawkins, B. L., Yamaizumi, Z., Nishimura, S. (1983) Multiple quantum two-dimensional 1H--15N nuclear magnetic resonance spectroscopy: chemical shift correlation maps for exchangeable imino protons of Escherichia coli tRNAMetf in water. *Proc Natl Acad Sci USA.* **80**, 5895–5897.
27. Güntert, P., Dötsch, V., Wider, G., and Wüthrich, K. (1992). Processing of Multi-Dimensional NMR Data with the New Software PROSA. *J. Biomol. NMR* **2**, 619–629.

Chapter 14

Cyclic Amplification of Prion Protein Misfolding

Marcelo A. Barria, Dennisse Gonzalez-Romero, and Claudio Soto

Abstract

Protein misfolding cyclic amplification (PMCA) is a technique that takes advantage of the nucleation-dependent prion replication process to accelerate the conversion of PrP^{C} into PrP^{Sc} in the test tube. PMCA uses ultrasound waves to fragment the PrP^{Sc} polymers, increasing the amount of seeds present in the infected sample without affecting their ability to act as conversion nuclei. Over the past 5 years, PMCA has become an invaluable technique to study diverse aspects of prions. The PMCA technology has been used by several groups to understand the molecular mechanism of prion replication, the cellular factors involved in prion propagation, the intriguing phenomena of prion strains and species barriers, to detect PrP^{Sc} in tissues and biological fluids, and to screen for inhibitors against prion replication. In this chapter, we describe a detailed protocol of the PMCA technique, highlighting some of the important technical aspects to obtain a successful and reproducible application of the technology.

Key words: Prions, Creutzfeldt–Jakob disease, Bovine spongiform encephalopathy, Scrapie, Protein misfolding cyclic amplification

1. Introduction

1.1. Prion Diseases and the Infectious Agent

Transmissible spongiform encephalopathies (TSEs), also known as prion diseases, are fatal and infectious neurodegenerative disorders that affect both human and animals (1). In these diseases, a long incubation period, in which the infectious agent starts its replication in the target organs, is followed by a brief and fatal clinical phase (2). Creutzfeld–Jakob disease (CJD) in humans and scrapie, bovine spongiform encephalopathy (BSE), and chronic wasting disease (CWD) in animals are the most common forms of TSE (3). Although TSE are rare, their unique mechanism of transmission and the concerns generated by the transmission of the cattle disease into humans has put prions in the spotlight (4). In addition, due to the lack of early presymptomatic diagnosis, there is a tremendous

Einar M. Sigurdsson et al. (eds.), *Amyloid Proteins: Methods and Protocols*, Methods in Molecular Biology, vol. 849,
DOI 10.1007/978-1-61779-551-0_14,

risk of iatrogenic transmission of vCJD from human to human, a route that has already produced thousands of deaths in other human prion diseases, such as kuru and iatrogenic CJD (5). Finally, it is not yet clear whether the disease in sheep (scrapie) and in deer (CWD) can be transmitted to human beings. Although, there seem to be a species barrier protecting humans from these animal infections, this phenomenon is not yet completely understood, especially in the case of CWD. The latter is worrisome, because the number of CWD cases has been dramatically increasing recently in the USA (6).

The nature of the infectious agent in TSE has been the center of passionate controversy (7, 8). The most accepted hypothesis proposes that PrP^{Sc} is the sole component of the infectious agent and that its propagation does not involve nucleic acid (9). PrP^{Sc} is a posttranslationally modified version of the normal host protein, PrP^{C}. Chemical differences have not been detected to distinguish these two PrP isoforms and the conversion seems to involve a conformational change whereby the misfolded protein is organized in β-sheet-rich aggregates. This structural change confers new biochemical properties to the misfolded protein: insolubility in nondenaturing detergents and partial resistance against digestion with proteinase K (10, 11). The hypothesis that PrP^{Sc} is the active component of the infectious agent associated to TSE remained controversial for decades, but recent exciting studies demonstrating the generation of infectious material from purified prion protein in vitro by protein misfolding cyclic amplification (PMCA) have settled all doubts regarding the validity of the prion hypothesis (12).

1.2. The Mechanism of Prion Replication

According to the protein-only hypothesis, PrP^{Sc} propagates itself by an autocatalytic reaction (10). The mechanism by which PrP^{Sc} propagates the disease in vivo has been a subject of intense investigation. At the time of infection, the proportion of PrP^{Sc} inoculated is very low compared with endogenous PrP^{C}. However, by the time animals develop the clinical signs, the amount of PrP^{Sc} in brain is very high. This finding suggests that PrP^{Sc} replicates in vivo at expenses of the normal protein. The notion that endogenous PrP^{C} is involved in the development of infection is supported by the findings that PrP knockout animals are resistant to infection (13). These findings suggest that infectious PrP^{Sc} is capable of inducing the conversion of host PrP^{C}, resulting in the autocatalytic formation of PrP^{Sc}.

PrP^{Sc} has been described as an oligomer of variable size that can even form large fibrillar aggregates, resembling amyloid fibrils observed in Alzheimer's disease and other amyloid-related disorders (14, 15). The comparison of prion conversion with the process of amyloidosis provides a model for the transition of PrP^{C} to PrP^{Sc}, in which the pathological protein may act as a seed to

recruit molecules of partially misfolded PrP^{C}, stabilizing the misfolding by incorporation into the oligomer (14, 16). Thus, the PrP^{Sc} oligomer is elongated at the ends as new molecules of PrP^{C} are converted and incorporated. The kinetics of such nucleated conformational conversion is limited by the number of seeds present in the sample (14, 16). This rate-limiting process might explain in part the long period of time needed in vivo to generate a concentration of PrP^{Sc} high enough to trigger neurodegeneration.

1.3. Protein Misfolding Cyclic Amplification: Rationale and Applications

Based on the nucleation/polymerization model, we have described a strategy that mimics in vitro the PrP^{Sc} conversion process that takes place in vivo and that amplifies in an exponential fashion minute quantities of PrP^{Sc} present in a sample (17). This system is called PMCA, and consists of cycles of accelerated prion replication. Each cycle is composed of two phases. During the first phase, the sample containing minute amounts of PrP^{Sc} and an excess of PrP^{C} are incubated to induce growing of PrP^{Sc} polymers. In the second phase, the sample is subjected to sonication to break down the polymers, multiplying the number of nuclei (18). After each cycle the number of seeds increases in an exponential fashion. PMCA is conceptually analogous to DNA amplification by PCR. In both systems, a template grows at expenses of a substrate in a cyclic reaction, combining growing and multiplication of the template units.

We have previously reported proof-of-concept experiments in which the technology was applied to replicate the misfolded protein from diverse species (17, 19). The newly generated protein exhibits the same biochemical, biological, and structural properties as brain-derived PrP^{Sc} and strikingly it is infectious to wild-type animals, producing a disease with similar characteristics as the illness produced by brain-isolated prions (20). The technology has been automated, leading to a dramatic increase on efficiency of amplification. Indeed, one round of 144 PMCA cycles results in a 6,000-fold increase of sensitivity of detection (21), whereas two and seven of successive PMCA rounds result in ten million and three billion folds amplification (22). Moreover, our results demonstrate that PMCA is capable to detect as little as a single molecule of oligomeric infectious PrP^{Sc} (22). PMCA enables to generate millions infectious units starting with the equivalent to one PrP^{Sc} oligomer, that is way below the infectivity threshold (22). These data demonstrate that PMCA has a similar power of amplification as PCR techniques used to amplify DNA and open a great promise for development of a highly sensitive detection of PrP^{Sc} and for understanding the molecular basis of prion replication. Indeed, we have demonstrated that after amplification we can detect PrP^{Sc} in blood of hamsters experimentally infected with scrapie during both the symptomatic (21) and presymptomatic phases (23), as well as in urine.

The PMCA technology has been used by several groups to understand the molecular mechanism of prion replication, the

effect of cellular components, to detect PrP^{Sc} in tissues and biological fluids, and to screen for inhibitors against prion replication (24–58). There are now more than 50 publications successfully using the technology from more than ten different groups. Of particular interest are the studies by Supattapone and colleagues who have been able to produce prion replication in vitro by PMCA using purified PrP^{C} and PrP^{Sc} with the sole addition of synthetic polyanions (25, 59). Recently, Caughey and colleagues were able to optimize PMCA using recombinant bacterial PrP^{C} (42). This advance is important since it provides a much easier source for PrP^{C} than mammalian brain homogenate and enables labeling of the protein in several ways for structural and biochemical studies. Finally, in a recent milestone study, Ma and colleagues were able to generate bona fide infectious material from recombinant PrP with the sole addition of RNA and lipids as catalyzers (57). This study constitutes one of the strongest evidences in favor of the prion hypothesis.

PMCA allows the faithful replication of prion strains in many different species of prions, indicating that all the elements required for strain determination are enciphered in the folding of PrP^{Sc} (60). Furthermore, the related phenomena of species barrier, strain adaptation, and molecular memory were also reproduced in vitro by PMCA (61–63), suggesting again that they are dependent purely on PrP^{Sc} replication. When PrP^{C} from one species is used to replicate prions from a different species, new strains are generated, pointing to an extremely high flexibility of PrP. Finally, PMCA allows to reproduce the spontaneous generation of prions, which happen in the sporadic forms of prion disease (59, 64).

2. Materials

PMCA have been applied successfully to a variety of brain samples from different species, including human, cow, sheep, cervid, mink, mouse, and hamster (19). In the following sections, we describe the equipment required, the technical considerations, and the standard parameters that afford an optimal amplification of PrP^{Sc}.

2.1. Equipment

1. Sonicator Misonix S3000 or S4000.
2. Tube holder and cover for PMCA. Part # 444 Misonix.
3. Potter-Elvehjem Tissue Grinders 15 or 30 ml.
4. Refrigerated centrifuge (Eppendorf model 5810R).
5. Ultra low freezer So-Low Model u-8525 (Thermo Fisher Scientific).
6. Pipettes (serological and micropipttes).

7. Incubator (Shel Lab).
8. Thermomixer Eppendorf (Cat No. 022670107).
9. Eppendorf Adaptor plate for 96×02 ml PCR tubes (Cat No. 022670581).

2.2. Biological Samples

1. Normal brain homogenate (NBH).
2. Infectious material homogenate (IMH).

2.3. Solutions, Reagents, and Buffers

1. Triton X-100, Sigma-Aldrich, Cat No. T8787-100 ml.
2. EDTA 0.5 M, Promega, Cat No. V4231.
3. Complete Protease Inhibitor Cocktail Tablets (PI), Roche, Cat No. 11697498001.
4. Proteinase K (PK), Sigma-Aldrich, Cat No. P2308-25 mg.
5. PBS 1×, Cellgro, Cat No. 21-040-CV.
6. Sampler buffer, Invitrogen Cat No. NP0007.
7. Conversion Buffer: 150 mM NaCl, 1% Triton X-100, 1× Protease Inhibitor Cocktail in PBS 1× (see Note 1).
8. Solution PK 1 µg/µl in PBS.
9. Phenylmethanesulfonyl fluoride (PMSF) 50 mM, Sigma, Cat No. P7626.

3. Methods

3.1. Preparation of Normal Brain Homogenate

1. Extract brain immediately after death (see Note 2). Using the tissue grinder homogenate 1.0 g of normal brain in chilled conversion buffer to finally obtain a 10% (w/v) solution. Work with the tissue grinder buried on ice to keep the homogenate at low temperature.
2. Centrifuge the homogenate sample at 3,000×*g* for 40 s in a refrigerated centrifuge (4°C) (see Note 3). This step is necessary to remove tissue debris.
3. Carefully remove the tube from the centrifuge. Avoid mixing supernatant and pellet.
4. Save the supernatant and discard the pellet. Make aliquots of the supernatant in 1.5 ml microcentrifuge tubes. Quick-freeze the aliquots in liquid nitrogen and store at –80°C until use (see Note 4).

3.2. Preparation of Infectious Material Homogenate

It is possible to use as infectious material any tissue homogenate or biological fluid suspected to contain prions. Prepare infectious material following the same protocol used for the preparation of NBH, except that quick freezing is not so critical for the IMH.

For some tissues or fluids, especially those containing large amounts of blood, it is necessary to perform a step to remove inhibitors of PMCA reaction (65). For this purpose, we recommend to add 1 volume of 20% sarkosyl, incubate for 10 min at room temperature, and centrifuge at 100,000 × *g* for 1 h at 4°C. Supernatants are discarded and pellets resuspended into 2 volumes of 10% sarkosyl. The centrifugation process is repeated and pellets resuspended directly in 10% NBH prepared in conversion buffer. Following this protocol, PrP^{Sc} is recovered with a yield higher than 90%. We do not recommend using precipitation with phosphotungstic acid or immunoprecipitation with anti-PrP antibodies, since both of these procedures interfere with PMCA.

3.3. Preparations of Serially Diluted Samples for PMCA

1. Take and thaw an aliquot of NBH and IMH.
2. Mix carefully 11 µl of infectious brain homogenate with 99 µl of NBH in 0.2 ml PCR tubes (Nunc, Cat No. 265643) (see Note 5) to prepare a standard PMCA dilution (Fig. 1).
3. Take 11 µl from the first PMCA dilution and transfer to the second tube ($d \times 10^{-3}$) (Fig. 1). Pipette up and down to mix both homogenates.
4. Continue with the serial dilution (1/10 up to the dilution of interest) using NBH and the previous seeded dilution $d \times 10^{-4}$, $d \times 10^{-5}$, etc. as an inoculum (Fig. 1).

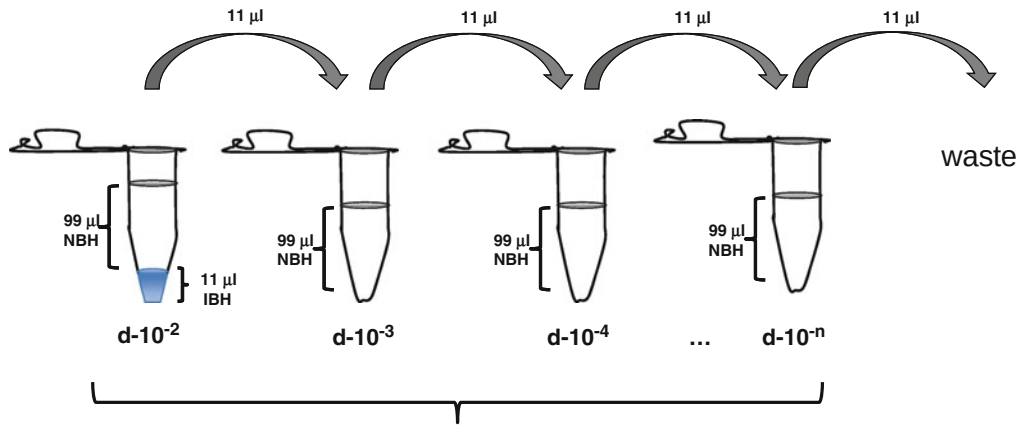

Fig. 1. Diagram depicting serial dilution of infected brain in normal brain homogenate. The first dilution (1:100 with respect to the brain) will contain 1 volume of 10% infected brain homogenate (source of PrP^{Sc} seeds) and 9 volumes of normal brain homogenate (source of PrP^{C} substrate); the second tube is a ×10 dilution of the previous mix (1:1,000 dilution with respect to the brain); the third tube is a ×100 dilution of the first tube; etc. Note that all tubes should end up with the same final volume (99 µl). From each tube 19 µl are removed and kept frozen for the non-amplified control. Thus the final reaction volume is 80 µl.

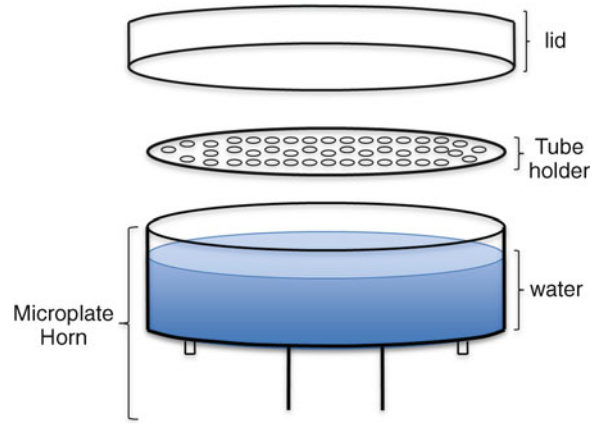

Fig. 2. Diagram of tube-adapted for Misonix sonicator. PMCA tubes are hanged from the tube holder allowing their partial immersion in water. An acrylic cover is put on top of the tubes to keep them in place during the sonication.

5. Take 19 µl from the serially diluted samples (called "Frozen" samples) and freeze immediately. This is the control for non-amplified reaction.
6. Mix carefully the samples before to incubate/sonicate in the sonicator.

3.4. Automatic Cyclic Amplification

The sonication step in the PMCA technique is a key element to increase the efficiency and decrease the time used in the conversion of the PrP^{C} into the abnormal form of the prion protein. The aim of the sonication is to fragment the PrP^{Sc} aggregates to increase the amount of seeds present in the infected sample without affecting their ability to act as conversion nucleus. The microplate horn and the tube holder (Fig. 2) offer an alternative of indirect sonication and function as a high-intensity ultrasound water baths capable to process a group of samples at the same time (see Note 6).

1. Connect the Misonix generator S3000 or 4000 to the convertor/microplate horn.
2. Put the convertor/microplate horn in the sound enclosure box provided by Misonix (see Note 7).
3. Put the system (convertor/microplate horn/sound enclosure box) inside of an incubator previously set at 37°C. Kept the temperature constant during the whole process.
4. Set carefully the parameters of sonication for the cyclic amplification. For the sonicator S3000 or S4000, use the amplitude necessary to obtain potency between 200 and 300 W (see Note 8).
5. Use 20 s as a pulse *on* time and 29 min 40 s a pulse *off* time for the setting of the sonicator. The efficiency of the NBH used as substrate decreases over time and the decrease is not the same

for distinct strains. The optimal duration of the PMCA rounds are usually between 24 and 72 h of incubation/sonication (see Note 9).

6. Add between 180 and 200 ml of clear tap water to the microplate horn (see Fig. 2). In our experience, it is not necessary to recirculate the water, but it is important to check that the temperature does not increase over 45°C at any point during PMCA.
7. Put the samples in the PMCA tube holder and dipped into the water. Check carefully that the level of water is not in touch with the tube holder.
8. Keep the samples amplifying for 24–72 h (see Note 9).

3.5. PrP^{Sc} Detection

To detect the PrP^{Sc} product after amplification, it is possible to use any assay designed for this purpose, including western blot, ELISA, conformational-dependent immunoassay (CDI), etc. In our studies, we traditionally use western blots after proteinase K (PK) digestion to remove the remaining PrP^{C} from the samples. Western blot is a widely used methodology in the field and has the advantage over some of the other assays that it is possible to distinguish PrP^{C} from PrP^{Sc} by the molecular weight of the product after proteolytic digestion (see Note 10). Following is the protocol we use.

1. Take 19 µl of each sample and incubate with 1 µl of 1 µg/µl Proteinase K for 1 h at 45°C and 450 rpm in a Thermomixer (see Notes 10 and 11).
2. After PK treatment centrifuge the samples at 3,000 × *g* for 10 s.
3. Stop the reaction adding 2 µl of 50 mM PMSF and 8 µl of 4× Sampler buffer, Invitrogen.
4. Heat the tubes for 10 min at 100°C.
5. Centrifuge the heated samples at 3,000 × *g* for 10 s to bring down the condensate.
6. Load the samples into an 4–12% acrylamide gel for SDS-PAGE.
7. Run the electrophoresis at 70 V for 30 min until the samples enter to the staking gel and then continue at 135 V for 1 h and 30 min.
8. Proteins are electrotransferred to a Hybond-ECL nitrocellulose membrane (GE Healthcare) using 800 mA constant for 1 h.
9. Block the membrane with blocking solution for 1 h.
10. Incubate the blocked membrane for 1 h with an appropriate anti-PrP antibody such as 3F4 (Covance) diluted in 1× PBS with 0.05% Tween 20 (PBST).
11. Rinse three times (10 min each time) with 1× PBST (washing buffer).
12. Add Sheep Anti-Mouse IgG Horseradish Peroxidase (GE Healthcare) and incubate for 1 h.

13. Rinse the membrane three times for 10 min each with washing buffer to eliminate excess of secondary antibody.
14. Develop the membrane with a luminescent peroxidase substrate like the ECL-Plus from GE Healthcare.
15. Expose the membrane to a photographic film or to other gel documentation system. Digitalize the image for future analysis.
16. Amplification rate should be calculated by comparing the last dilutions giving similar reactivity (intermediate intensity) between frozen and amplified samples (Fig. 3). Do not compare signal intensities to estimate amplification rate, because this can produce highly misleading results.

3.6. Recommendations to Avoid the Possibility of Cross-contamination

Because of the high power of amplification of PMCA, special care should be taken to prevent as much as possible cross-contamination. In addition, because PMCA enables, the de novo generation of PrP^{Sc} (without preexisting PrP^{Sc}) under defined set of conditions (64), it is very important to reduce any potential source of contamination that could complicate interpretation of these results. Following is a list of precautions recommended to minimize the possibility of cross-contamination.

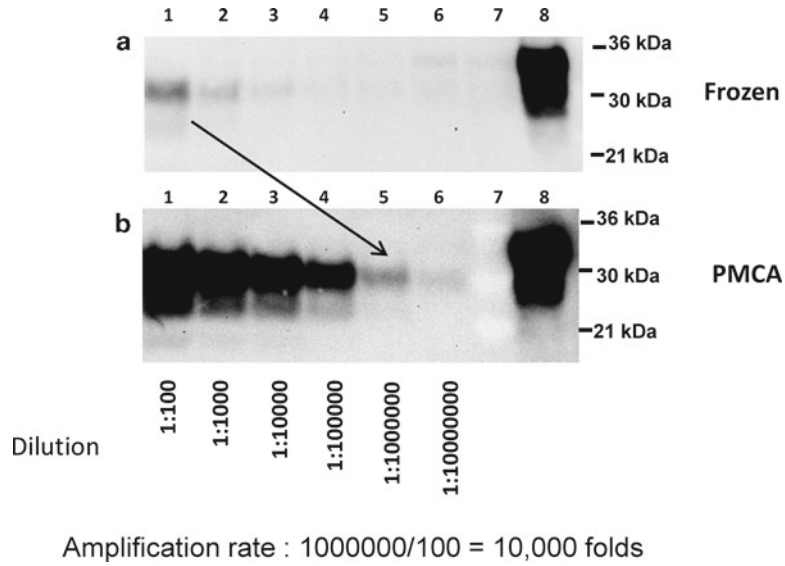

Fig. 3. Example of PrP^{Sc} amplification by PMCA. Serial dilutions of infected brain homogenate were frozen (**a**) or subjected to one round of 96 PMCA cycles (**b**). Samples were PK-digested (except *lane 8* the NBH control), western blotted, and detected with an anti-PrP antibody. An initial dilution of 1×10^{-2} (*lane 1*, **a**) has an equivalent reactivity to a dilution 1×10^{-6} after PMCA (*lane 5*, **b**). Therefore, the estimated amplification rate in this experiment is 10,000-fold. *Lanes 1–6*: Serial dilution of infected sample. *Lane 7*: molecular weight marker. *Line 8*: non-digested normal brain homogenate.

1. Work under similar conditions used to manipulate sterile material (double gloves, biosafety cabinet, change tips every time, avoid spills, keep neatly clean bench, clean frequently bench, pipettes, and other materials with NaOH).
2. Use only recommended tubes. Discard tubes that open during the experiment or have higher or lower volume of buffer (see Note 5).
3. Change water and clean sonicator cup with NaOH after each experiment.
4. Do not mix prions from different sources in one sonicator.
5. If attempting to detect PrP^{Sc} with very high sensitivity (e.g., in blood samples), do not manipulate simultaneously samples with high quantity of infectious material.
6. Do not do more than seven rounds of serial PMCA, except when propagating large quantities of infectious material.
7. Always include a large number of controls (NBH without PrP^{Sc}) to assess false positives in each experiment. These samples should be amplified and serially diluted in parallel with the experimental samples. In case a control sample results positive using standard PMCA conditions (i.e., not set for de novo formation of PrP^{Sc}) (64), discard the entire experiment and clean the machine with NaOH.
8. For safety conditions, filter tips should be used for liquid handling, and tissue homogenization should be performed in a closed container inside a biosafety hood to avoid the spread of infectious material.
9. Avoid working with easily convertible PrP^{C} substrates (e.g., Bank voles).

4. Notes

1. Composition of the conversion buffer has been established and optimized following exhaustive studies and we have found that even small changes may dramatically affect the efficiency of the amplification process. Particular attention has to be put in adding the right amount of Triton X-100, which owing to it viscosity is difficult to pipette accurately. A recent improvement in PMCA efficiency described by Baskakov and colleagues consists on adding Teflon beads to the tubes before starting PMCA cycles (66). Addition of beads improve efficiency of amplification and reduce inter-sample variability, most likely by helping the homogenous dispersion of the ultrasound waves in the tube.

2. For the preparation of NBH, animals should be perfused with PBS plus 5 mM EDTA to remove as much as possible the amount of blood that can interfere with PMCA. Brains have to be taken in the shortest possible time after death. In case animal perfusion is not possible, we recommend washing the fresh tissue immediately with cold PBS + 5 mM EDTA to remove as much blood as possible and add EDTA to the conversion buffer.
3. A high centrifugal force is not recommended because it might remove important membrane components implicated in $PrP^{C} \rightarrow PrP^{Sc}$ conversion.
4. Frequent freezing–thawing of the NBH reduces significantly the amplification. Store the stock in aliquots and use them once. Discard the remaining of the unused material.
5. It is very important to use thin-walled 0.2 ml PCR tubes to obtain the most effective penetration of ultrasound waves. However, care should be taken in that tubes should not crack or open during the procedure. This happens with tubes from some manufacturers. In case the tube is open or the volume is significantly higher or smaller than expected, these samples should be discarded.
6. The Misonix sonicator was not designed to hold tubes, so a tube holder was manufactured (Fig. 2). Although the holder can be devised to hold around 100 tubes or more, we have found that PMCA efficiency is best if the holder is not filled more than 50% capacity with tubes. This is probably because each tube attenuates to some extent the effect of the ultrasound waves.
7. Do not close the sound enclosure box. This will increase substantially the temperature of the microplate horn.
8. Different strains require different settings for optimal amplification. In our hands, for example, the 263K strain has optimal amplification using potency around 215–230 W.
9. Different strains also require distinct time for refreshing the substrate, because the decrease in the efficiency of the NBH substrate decreases differently for distinct strains. For optimal amplification of 263 K, we use 48 h and for variant CJD 24 h as a total time in each round of cyclic amplification.
10. The conditions for proteinase K digestion (concentration and temperature) are different for each prion strain and have to be carefully chosen. The critical issue is to make sure that no PrP^{C} remains undigested after PK treatment, because it is a common mistake to confuse incomplete digestion of PrP^{C} with false-positive PrP^{Sc} formation. When PrP is detected by western blotting, it is easy to distinguish incomplete PrP^{C} digestion from bona fide PrP^{Sc}, because the latter exhibit a

switch on molecular weight due to the removal of the first ~90 amino acids. To assure complete digestion, especially following extended incubations, a higher concentration of PK may be required to digest increasingly larger aggregates. Addition of up to 0.05% SDS in the buffer used for the PK treatment may also help. Digestions using temperatures of between 42 and 64°C and with shaking at 350–450 rpm are also recommended.

11. Aliquots of PK are stored frozen at –20°C and in the interests of reproducibility any thawed, unused enzyme is discarded at the end of the experiment.

Acknowledgments

This work was supported in part by R01 NS049173 grant from NIH.

References

1. Prusiner, S.B. (1991) Molecular biology of prion diseases. *Science* **252**, 1515–1522.
2. Roos, R., Gajdusek, D.C. and Gibbs, C.J., Jr. (1973) The clinical characteristics of transmissible Creutzfeldt-Jakob disease. *Brain* **96**, 1–20.
3. Collinge, J. (2001) Prion diseases of humans and animals: their causes and molecular basis. *Annu Rev Neurosci* **24**, 519–550.
4. Soto, C. and Saborio, G.P. (2001) Prions: Disease propagation and disease therapy by conformational transmission. *Trends Mol Med* **7**, 109–114.
5. Brown, P., Preece, M., Brandel, J.P., Sato, T., McShane, L. and Zerr, I. (2000) Iatrogenic Creutzfeldt-Jakob disease at the millennium. *Neurol* **55**, 1075–1081.
6. Sigurdson, C.J. and Aguzzi, A. (2006) Chronic wasting disease. *Biochim Biophys Acta* **1772**, 610–618.
7. Aguzzi, A. and Polymenidou, M. (2004) Mammalian prion biology: one century of evolving concepts. *Cell* **116**, 313–327.
8. Soto, C. and Castilla, J. (2004) The controversial protein-only hypothesis of prion propagation. *Nat Med* **10**, S63-S67.
9. Prusiner, S.B. (1998) Prions. *Proc Natl Acad Sci USA* 95, 13363–13383.
10. Cohen, F.E. and Prusiner, S.B. (1998) Pathologic conformations of prion proteins. *Annu Rev Biochem* **67**, 793–819.
11. Baldwin, M.A., Cohen, F.E. and Prusiner, S.B. (1995) Prion protein isoforms, a convergence of biological and structural investigations. *J Biol Chem* **270**, 19197–19200.
12. Soto, C. (2011) Prion Hypothesis: The end of the Controversy? *Trends Biochem Sci* **36**, 151–158.
13. Bueler, H., Aguzzi, A., Sailer, A., Greiner, R.A., Autenried, P., Aguet, M., et al. (1993) Mice devoid of PrP are resistant to Scrapie. *Cell* **73**, 1339–1347.
14. Caughey, B., Kocisko, D.A., Raymond, G.J. and Lansbury, P.T., Jr. (1995) Aggregates of scrapie-associated prion protein induce the cell-free conversion of protease-sensitive prion protein to the protease-resistance state. *Chem Biol* **2**, 807–817.
15. Ghetti, B., Piccardo, P., Frangione, B., Bugiani, O., Giaccone, G., Young, K., et al. (1996) Prion protein amyloidosis. *Brain Pathol* **6**, 127–145.
16. Jarrett, J.T. and Lansbury, P.T., Jr. (1993) Seeding "one-dimensional crystallization" of amyloid: a pathogenic mechanism in Alzheimer's disease and scrapie? *Cell* **73**, 1055–1058.
17. Saborio, G.P., Permanne, B. and Soto, C. (2001) Sensitive detection of pathological prion protein by cyclic amplification of protein misfolding. *Nature* **411**, 810–813.
18. Soto, C., Saborio, G.P. and Anderes, L. (2002) Cyclic amplification of protein misfolding:

application to prion- related disorders and beyond. *Trends Neurosci* **25**, 390–394.

19. Soto, C., Anderes, L., Suardi, S., Cardone, F., Castilla, J., Frossard, M.J., et al. (2005) Presymptomatic detection of prions by cyclic amplification of protein misfolding. *FEBS Lett* **579**, 638–642.
20. Castilla, J., Saá, P., Hetz, C. and Soto, C. (2005) In vitro generation of infectious scrapie prions. *Cell* **121**, 195–206.
21. Castilla, J., Saa, P. and Soto, C. (2005) Detection of prions in blood. *Nat Med* 11, 982–985.
22. Saa, P., Castilla, J. and Soto, C. (2006) Ultra-efficient replication of infectious prions by automated protein misfolding cyclic amplification. *J Biol Chem* **281**, 35245–35252.
23. Saa, P., Castilla, J. and Soto, C. (2006) Presymptomatic detection of prions in blood. *Science* **313**, 92–94.
24. Lucassen, R., Nishina, K. and Supattapone, S. (2003) In vitro amplification of protease-resistant prion protein requires free sulfhydryl groups. *Biochemistry* **42**, 4127–4135.
25. Deleault, N.R., Lucassen, R.W. and Supattapone, S. (2003) RNA molecules stimulate prion protein conversion. *Nature* **425**, 717–720.
26. Nishina, K., Deleault, N.R., Lucassen, R.W. and Supattapone, S. (2004) In vitro prion protein conversion in detergent-solubilized membranes. *Biochemistry* **43**, 2613–2621.
27. Nishina, K., Jenks, S. and Supattapone, S. (2004) Ionic strength and transition metals control PrPSc protease resistance and conversion-inducing activity. *J Biol Chem* **279**, 40788–40794.
28. Deleault, N.R., Geoghegan, J.C., Nishina, K., Kascsak, R., Williamson, R.A. and Supattapone, S. (2005) Protease-resistant prion protein amplification reconstituted with partially purified substrates and synthetic polyanions. *J Biol Chem* **280**, 26873–26879.
29. Orem, N.R., Geoghegan, J.C., Deleault, N.R., Kascsak, R. and Supattapone, S. (2006) Copper (II) ions potently inhibit purified PrPres amplification. *J Neurochem* **96**, 1409–1415.
30. Bieschke, J., Weber, P., Sarafoff, N., Beekes, M., Giese, A. and Kretzschmar, H. (2004) Autocatalytic self-propagation of misfolded prion protein. *Proc Natl Acad Sci USA* **101**, 12207–12211.
31. Piening, N., Weber, P., Giese, A. and Kretzschmar, H. (2005) Breakage of PrP aggregates is essential for efficient autocatalytic propagation of misfolded prion protein. *Biochem Biophys Res Commun* **326**, 339–343.
32. Sarafoff, N.I., Bieschke, J., Giese, A., Weber, P., Bertsch, U. and Kretzschmar, H.A. (2005) Automated PrPres amplification using indirect sonication. *J Biochem Biophys Methods* **63**, 213–221.
33. Barret, A., Tagliavini, F., Forloni, G., Bate, C., Salmona, M., Colombo, L., et al. (2003) Evaluation of quinacrine treatment for prion diseases. *J Virol* **77**, 8462–8469.
34. Jones, M., Peden, A.H., Prowse, C.V., Groner, A., Manson, J.C., Turner, M.L., et al. (2007) In vitro amplification and detection of variant Creutzfeldt-Jakob disease PrPSc. *J Pathol* **213**, 21–26.
35. Kim, N.H., Choi, J.K., Jeong, B.H., Kim, J.I., Kwon, M.S., Carp, R.I., et al. (2005) Effect of transition metals (Mn, Cu, Fe) and deoxycholic acid (DA) on the conversion of PrPC to PrPres. *FASEB J* **19**, 783–785.
36. Kurt, T.D., Perrott, M.R., Wilusz, C.J., Wilusz, J., Supattapone, S., Telling, G.C., et al. (2007) Efficient in vitro amplification of chronic wasting disease PrPres. *J Virol* **81**, 9605–9608.
37. Murayama, Y., Yoshioka, M., Yokoyama, T., Iwamaru, Y., Imamura, M., Masujin, K., et al. (2006) Efficient in vitro amplification of a mouse-adapted scrapie prion protein. *Neurosci Lett* **413**, 270–273.
38. Seidel, B., Thomzig, A., Buschmann, A., Groschup, M.H., Peters, R., Beekes, M., et al. (2007) Scrapie Agent (Strain 263K) can transmit disease via the oral route after persistence in soil over years. *PLoS ONE* **2**, e435.
39. Haley, N.J., Seelig, D.M., Zabel, M.D., Telling, G.C. and Hoover, E.A. (2009) Detection of CWD prions in urine and saliva of deer by transgenic mouse bioassay. *PLoS ONE* **4**, e4848.
40. Mays, C.E., Titlow, W., Seward, T., Telling, G.C. and Ryou, C. (2009) Enhancement of protein misfolding cyclic amplification by using concentrated cellular prion protein source. *Biochem Biophys Res Commun* **388**, 306–310.
41. Shi, S., Dong, C.F., Wang, G.R., Wang, X., An, R., Chen, J.M., et al. (2009) PrP(Sc) of scrapie 263K propagates efficiently in spleen and muscle tissues with protein misfolding cyclic amplification. *Virus Res* **141**, 26–33.
42. Atarashi, R., Moore, R.A., Sim, V.L., Hughson, A.G., Dorward, D.W., Onwubiko, H.A., et al. (2007) Ultrasensitive detection of scrapie prion protein using seeded conversion of recombinant prion protein. *Nat Methods* **4**, 645–650.
43. Geoghegan, J.C., Valdes, P.A., Orem, N.R., Deleault, N.R., Williamson, R.A., Harris, B.T.,

et al. (2007) Selective incorporation of polyanionic molecules into hamster prions. *J Biol Chem* **282**, 36341–36353.

44. Haley, N.J., Mathiason, C.K., Zabel, M.D., Telling, G.C. and Hoover, E.A. (2009) Detection of sub-clinical CWD infection in conventional test-negative deer long after oral exposure to urine and feces from CWD+ deer. *PLoS ONE* **4**, e7990.
45. Jones, M., Peden, A.H., Yull, H., Wight, D., Bishop, M.T., Prowse, C.V., et al. (2009) Human platelets as a substrate source for the in vitro amplification of the abnormal prion protein (PrP) associated with variant Creutzfeldt-Jakob disease. *Transfusion* **49**, 376–384.
46. Kim, J.I., Surewicz, K., Gambetti, P. and Surewicz, W.K. (2009) The role of glycophosphatidylinositol anchor in the amplification of the scrapie isoform of prion protein in vitro. *FEBS Lett* **583**, 3671–3675.
47. Kurt, T.D., Telling, G.C., Zabel, M.D. and Hoover, E.A. (2009) Trans-species amplification of PrP(CWD) and correlation with rigid loop 170N. *Virology* **387**, 235–243.
48. Mays, C.E. and Ryou, C. (2010) Plasminogen stimulates propagation of protease-resistant prion protein in vitro. *FASEB J* **24**, 5102–5112.
49. Murayama, Y., Yoshioka, M., Horii, H., Takata, M., Yokoyama, T., Sudo, T., et al. (2006) Protein misfolding cyclic amplification as a rapid test for assessment of prion inactivation. *Biochem Biophys Res Commun* **348**, 758–762.
50. Murayama, Y., Yoshioka, M., Masujin, K., Okada, H., Iwamaru, Y., Imamura, M., et al. (2010) Sulfated dextrans enhance in vitro amplification of bovine spongiform encephalopathy PrP(Sc) and enable ultrasensitive detection of bovine PrP(Sc). *PLoS One* **5**, e13152.
51. Pastrana, M.A., Sajnani, G., Onisko, B., Castilla, J., Morales, R., Soto, C., et al. (2006) Isolation and Characterization of a Proteinase K-Sensitive PrP(Sc) Fraction. *Biochemistry* **45**, 15710–15717.
52. Shi, S., Dong, C.F., Tian, C., Zhou, R.M., Xu, K., Zhang, B.Y., et al. (2009) The propagation of hamster-adapted scrapie PrPSc can be enhanced by reduced pyridine nucleotide in vitro. *FEBS J* **276**, 1536–1545.
53. Shikiya, R.A., Ayers, J.I., Schutt, C.R., Kincaid, A.E. and Bartz, J.C. (2010) Coinfecting prion strains compete for a limiting cellular resource. *J Virol* **84**, 5706–5714.
54. Suyama, K., Yoshioka, M., Akagawa, M., Murayama, Y., Horii, H., Takata, M., et al. (2007) Prion inactivation by the Maillard reaction. *Biochem Biophys Res Commun* **356**, 245–248.
55. Tattum, M.H., Jones, S., Pal, S., Collinge, J. and Jackson, G.S. (2010) Discrimination between prion-infected and normal blood samples by protein misfolding cyclic amplification. *Transfusion* **50**, 996–1002.
56. Thorne, L. and Terry, L.A. (2008) In vitro amplification of PrPSc derived from the brain and blood of sheep infected with scrapie. *J Gen Virol* **89**, 3177–3184.
57. Wang, F., Wang, X., Yuan, C.-G. and Ma, J. (2010) Generating a Prion with Bacterially Expressed Recombinant Prion Protein. *Science* 327, 1132–1135.
58. Weber, P., Giese, A., Piening, N., Mitteregger, G., Thomzig, A., Beekes, M., et al. (2007) Generation of genuine prion infectivity by serial PMCA. *Vet Microbiol* **123**, 346–357.
59. Deleault, N.R., Harris, B.T., Rees, J.R. and Supattapone, S. (2007) Formation of native prions from minimal components in vitro. *Proc Natl Acad Sci USA* **104**, 9741–9746.
60. Castilla, J., Morales, R., Saa, P., Barria, M., Gambetti, P. and Soto, C. (2008) Cell-free propagation of prion strains. *EMBO J* **27**, 2557–2566.
61. Castilla, J., Gonzalez-Romero, D., Saa, P., Morales, R., De Castro, J. and Soto, C. (2008) Crossing the species barrier by PrP(Sc) replication in vitro generates unique infectious prions. *Cell* **134**, 757–768.
62. Green, K.M., Castilla, J., Seward, T.S., Napier, D.L., Jewell, J.E., Soto, C., et al. (2008) Accelerated high fidelity prion amplification within and across prion species barriers. *PLoS Pathog* 4, e1000139.
63. Meyerett, C., Michel, B., Pulford, B., Spraker, T.R., Nichols, T.A., Johnson, T., et al. (2008) In vitro strain adaptation of CWD prions by serial protein misfolding cyclic amplification. *Virology* **382**, 267–276.
64. Barria, M.A., Mukherjee, A., Gonzalez-Romero, D., Morales, R. and Soto, C. (2009) De novo generation of infectious prions in vitro produces a new disease phenotype. *PLoS Pathog* **5**, e1000421.
65. Chen, B., Morales, R., Barria, M.A. and Soto, C. (2010) Estimating prion concentration in fluids and tissues by quantitative PMCA. *Nat Methods* **7**, 519–520.
66. Gonzalez-Montalban, N. *et al.* (2011) Highly efficient protein misfolding cyclic amplification. *PLoS Pathog* **7**, e1001277.

Chapter 15

Search for Amyloid-Binding Proteins by Affinity Chromatography

Miguel Calero, Agueda Rostagno, and Jorge Ghiso

Abstract

'Amyloid binging proteins' is a generic term used to designate proteins that interact with different forms of amyloidogenic peptides or proteins and that, as a result, may modulate their physiological and pathological functions by altering solubility, transport, clearance, degradation, and fibril formation. We describe a simple affinity chromatography protocol to isolate and characterize amyloid-binding proteins based on the use of sequential elution steps that may provide further information on the type of binding interaction. As an example, we depict the application of this protocol to the study of Alzheimer's amyloid β (Aβ) peptide-binding proteins derived from human plasma. Biochemical analysis of the proteins eluted under different conditions identified serum amyloid P component (SAP) and apolipoprotein J (clusterin) as the main plasma Aβ-binding proteins while various apolipoproteins (apoA-IV, apoE, and apoA-I), as well as albumin (HSA) and fibulin were identified as minor contributors.

Key words: Affinity chromatography, Alzheimer disease, Amyloid peptides, Amyloid-binding proteins

Abbreviations

ACT	α1-Antichymotrypsin
AD	Alzheimer's disease
apoA-I	Apolipoprotein A-I
apoA-IV	Apolipoprotein A-IV
apoE	Apolipoprotein E
apoJ	Apolipoprotein J (clusterin)
CAPS	3-Cyclohexilamino-1-propanesulphonic acid
CNBr	Cyanogen bromide
ELISA	Enzyme-linked immunosorbent assay
HSA	Human serum albumin
NHS	*N*-hydroxysuccinimide
SAP	Serum amyloid P component
Vn	Vitronectin

Einar M. Sigurdsson et al. (eds.), *Amyloid Proteins: Methods and Protocols*, Methods in Molecular Biology, vol. 849,
DOI 10.1007/978-1-61779-551-0_15,

1. Introduction

Amyloid-binding protein is a generic term used to group together a heterogeneous collection of proteins that interact with different structural assemblies (monomeric, oligomeric, and fibrillar) of amyloidogenic peptides or proteins. These interactions have been described to modulate physiological and pathological functions of the respective amyloid subunits by altering their solubility, transport, clearance, degradation, and fibril formation.

Extensive immunohistochemical analysis have demonstrated that, *in vivo*, complex mixtures of unrelated molecules, collectively referred in the field as amyloid-associated proteins, colocalize with all types of amyloid deposits albeit not being a structural part of the final fibril (reviewed in ref. 1). Serum amyloid P component (SAP), α1-antichymotrypsin (ACT), apolipoprotein E (apoE), apolipoprotein J (apoJ) or clusterin, complement components, vitronectin, glycosaminoglycans, interleukins, and extracellular matrix proteins are among the many amyloid-associated components so far described coexisting with all forms of cerebral and systemic amyloidosis (2–11). To the moment, it is still unclear whether these molecules are innocent bystanders or whether their presence is related to the mechanism of amyloidogenesis. Several lines of investigation favor the latter notion, at least for some of them. For example, apoE and SAP have been found in all amyloid light chain (AL) fibrillar deposits, whereas their presence could not be demonstrated in the nonfibrillar Congo red negative immunoglobulin deposits in cases of light chain deposition disease (12, 13). Similar findings have been reported in cerebral forms of amyloidosis in which SAP and activation-derived products of the complement system are present in amyloid deposits but consistently absent in nonfibrillar preamyloid lesions (8, 12). Mice knockout for either SAP or apoE exhibit fewer amyloid lesions and delay in their onset although neither SAP nor apoE gene ablation prevents the formation of amyloid deposits (14, 15).

Most of the published reports dealing with amyloid-binding proteins are limited to those found associated with amyloid β (Aβ), the major constituent of the fibrils deposited into senile plaques and cerebral blood vessels of patients with Alzheimer's disease (AD) (16). Aβ extracted from senile plaques of AD patients is mainly 42–43 amino acids long (17), while vascular amyloid is two residues shorter at the C-terminus (18). A soluble form of Aβ (sAβ), homologous to the amyloid protein extracted from cerebrovascular lesions (19), has also been identified in culture media supernatants from untransfected and β amyloid precursor protein (βAPP)-transfected cells, as well as in cerebrospinal fluid (CSF), plasma, urine and brain parenchyma from normal subjects and AD

patients (19–23). Notably, several proteins have been shown to interact with sAβ in physiological fluids (24–26) and in vitro experiments have demonstrated that the presence of plasma or CSF prevents the fibril formation of synthetic peptides homologous to sAβ (27, 28), likely reflecting the result of the peptide's interaction with the biological fluid components. In this sense, many of the amyloid-associated proteins have also the ability to modulate the formation of Aβ fibrils *in vitro*. Some of them (e.g., complement component C1q, apoE4, SAP, ACT) enhance Aβ fibril formation (27, 29–32), while others (e.g., apoJ) contribute to the peptide solubility precluding fibrillogenesis *in vitro* (11, 33). In the latter, this protecting effect has been proposed to contribute to the enhanced production of slowly sedimenting Aβ-derived diffusible ligands (ADDLs) highly toxic to neurons in culture at nanomolar concentrations (34).

The present work describes a simple methodology to identify amyloid-binding proteins by using affinity chromatography (see Note 1). This methodology is readily applicable to the study of different amyloidogenic proteins and their respective interactions with components of different physiological fluids. As an example, we describe the application of this protocol to the study of human plasma proteins with Aβ-binding properties by affinity chromatography using sequential elution with buffers of different characteristics. Detailed biochemical analysis and quantitation of the proteins eluted in the different fractions indicated that SAP and apoJ (clusterin) are the main plasma Aβ-binding proteins, while other minor components were identified as apoA-IV, apoE, and apoA-I, as well as HSA and fibulin (see Fig. 1). The distribution of these proteins within the different elution protocols is indicative of the distinct nature of the physicochemical interactions involved.

2. Materials

2.1. Reagents

1. Plasma samples were obtained from normal healthy subjects (age 25–40 years) after 12 h fast with adequate understanding and written consent of subjects.
2. Peptide DAEFRHDSGYEVHHQKLVFFAEDVGSNKGA IIGLMVVGGV ($A\beta_{1-40}$), homologous to residues 672–711 of βPP_{770} was synthesized at W.M. Keck facility at Yale University using tBOC (*N-tert*-butyloxycarbonyl) chemistry.
3. All buffers and solutions were freshly prepared using water provided by a Milli-Q system (18 MΩ/cm at 25°C, Millipore Corp., Bedford, MA). All reagents were of the highest purity available and were purchased from Sigma-Aldrich, unless otherwise noted.

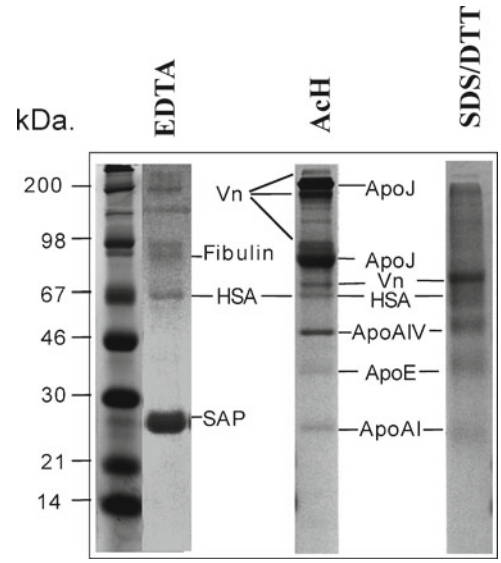

Fig. 1. Binding of human plasma proteins to an Aβ-affinity matrix. Normal human plasma was incubated for 3 h at room temperature with $A\beta_{1-40}$ affinity matrix equilibrated in TBS containing physiological concentrations of Ca^{2+}. After extensive washing to eliminate non-specific binding, bound proteins were eluted from the Aβ-matrix sequentially with 10 mM EDTA (EDTA), 2 M NaCl, 1% (v/v) Triton X-100, 1 M acetic acid (AcH), and 5%/1 M SDS/DTT (SDS/DTT). Aliquots of the eluted fractions were separated on 10% tris-tricine SDS-PAGE, transferred to PVDF and the membranes stained with Coomassie Blue. The identity of the eluted components, determined by amino-terminal amino acid sequence, is indicated. Affinity chromatography of normal human serum revealed an array of Aβ-binding proteins that interact with immobilized Aβ. The major Ca^{2+}-dependent binding component observed in the EDTA eluate corresponded to amyloid P component (SAP), while other minor bands were also observed and identified as albumin and fibulin. Under acidic conditions (AcH elution), we observed the presence of two major bands corresponding to apoJ (monomer and dimer), several vitronectin isoforms, as well as other minor bands identified as apolipoprotein A-IV, apolipoprotein A-I, apolipoprotein E, and albumin (see Note 11). Under denaturing conditions (SDS/DTT fraction), we observed the elution of vitronectin, apoE, apoA-IV, apoA-I, and albumin (HSA).

4. *Specific buffers.*
   (a) Tris-buffered saline (TBS):10 mM Tris–HCl, 150 mM NaCl, pH 7.4.
   (b) TBS-Ca: TBS containing 2.5 mM $CaCl_2$.
   (c) TBS-E: TBS containing 10 mM EDTA.
   (d) TBS-HS: TBS containing 2 M NaCl.
   (e) TBS-T: TBS containing 1% Triton X-100 (v/v).
   (f) AcH: Acetic acid 1 M solution. Prepare by adding 57.5 ml of glacial acetic acid (Sigma-Aldrich, # 537020) to 942.5 ml of Milli-Q water to obtain 1 l of 1 M acetic acid solution, pH ~2.2. Do not adjust the pH.
   (g) SDS/DTT buffer: 5% SDS and 1 M DTT in TBS buffer.

5. *Other reagents.*
   (a) CNBr-activated Sepharose 4B (GE HealthCare, # 17-0430-01).
   (b) CAPS (3-cyclohexylamino-1-propanesulphonic acid) transfer buffer: 10 mM CAPS, 10% methanol. Prepare 1 l of 10× CAPS stock (100 mM CAPS) by adding 22.13 g of CAPS (Sigma-Aldrich, #C2632) to 950 ml of Milli-Q water, adjust to pH and complete volume to 1 l. Prepare CAPS transfer buffer (1×) with 100 ml of CAPS 10× solution, 100 ml of methanol, and 800 ml of Milli-Q water.
   (c) DC Protein Assay (Bio-Rad, #500-0111).
   (d) Tricine Sample Buffer (Bio-Rad #161-0739).

2.2. Instrumentation

1. Peristaltic pump. Single channel laboratory peristaltic pump for use in liquid chromatography (GE-Healthcare, #18-1110-91).
2. Fraction Collector (GE-Healthcare, #18-1177-40).
3. Spectrophotometer UV-Vis.
4. Polystyrene 20-ml volume chromatographic columns including upper bed supports, end caps, tip closures (Econo-Pac Chromatography Columns, Bio-Rad #732-1010).
5. Appropriate column holders and clamps for attaching columns and tubing to the system.

3. Methods

3.1. Immobilization of Amyloid β Peptides to Chromatography Medium

3.1.1. Selection of Affinity Matrix Support and Coupling Chemistry

The nature of the affinity matrix support (solid support onto which ligand is immobilized) is an important factor that has to be considered when planning an affinity chromatography experiment. Detailed discussion on how to select an appropriate matrix is discussed in depth elsewhere (35). For the particular case of coupling hydrophobic amyloidogenic peptides, it is very important to select a hydrophilic, non-charged supports that minimize nonspecific hydrophobic and ionic interactions (see Note 2).

Depending on the nature of the peptide or protein to be coupled (amino acid composition, presence of carbohydrates, sulphydril groups, etc.) and the aim of the experiment, different chemistries can be used for coupling the ligand to the chromatographic media (35). Activated chromatography media with carboxyl esters such as *N*-hydroxysuccinimide (NHS) or cyanogen bromide (CNBr) represent two of most convenient methods for covalent binding of short peptides. Both NHS or CNBr moieties react with free primary amino groups from peptides or proteins to form stable covalent links, most typically through lysine side chains. In this protocol,

we used CNBr-activated Sepharose (GE HealthCare) for binding of Aβ peptides.

CNBr-activated Sepharose 4B is a commercially available preactivated medium for immobilization of ligands containing primary amines with a very high coupling efficiency. It provides a very convenient way to immobilize proteins and peptides. The coupling reaction is spontaneous, rapid and easy to carry out (see Note 3). Buffers containing primary amines (e.g., Tris and glycine) should not be used for coupling reactions.

3.1.2. Ligand Preparation and Coupling

Amyloid peptides have an intrinsic tendency to oligomerize and aggregate. Therefore, proper handling of peptide solutions is a key aspect to be controlled to obtain an affinity matrix with a defined ligand composition. For this protocol, we aimed at coupling to the matrix support $A\beta_{1-40}$ peptide mainly as monomers or small oligomers. Coupling of the peptide to CNBr-activated Sepharose was performed following the manufacture's instruction with one important exception regarding the coupling buffer where the ligand is dissolved. In brief, 2.3 μmol (10 mg) of $A\beta_{1-40}$ peptide was slowly dissolved in 20 ml of 0.1 M carbonate/bicarbonate buffer, pH 9.0 without NaCl. After centrifugation at 16,000 × *g* at 4°C, this peptide solution was allowed to interact with 2 ml of activated Sepharose matrix for 16 h at 4°C on a rotating wheel. After washing, any remaining active groups were blocked by washing with 0.1 M Tris–HCl buffer, pH 8.0.

The $A\beta_{1-40}$ peptide coupled affinity matrix (2 ml) was packed into a polystyrene chromatographic column (Bio-Rad #732-1010) and washed extensively by three cycles of alternating pH with 0.1 M acetic acid/sodium acetate, pH 4.0 containing 0.5 M NaCl, and 0.1 M Tris–HCl, pH 8 containing 0.5 M NaCl.

3.2. Affinity Chromatography with Sequential Elution

This procedure can be performed in an FPLC system, or conveniently in an in-house chromatography system composed of a column containing the packed affinity media, a peristaltic pump to provide flow circulation, a fraction collector, and a UV-Vis spectrophotometer for later analysis of fractions.

3.2.1. Protocol for Affinity Chromatography with Sequential Elution

1. Equilibrate the affinity matrix by flowing 10 volumes of TBS-Ca (see Note 4). For a bed volume of 2 ml, use at least 20 ml of TBS-Ca.
2. Drain remaining TBS-Ca buffer, stop the flow, and load the sample of interest into the column (see Notes 5 and 6). Connect the exit tubing to the top of the column and recirculate the sample through the column with a slow flow (0.2 ml/min) for 1 h at 37°C, 3 h at room temperature, 16 h at 4°C, or any other suitable setting (see Note 7).
3. Collect the pass-through sample in one single fraction that contains unbound proteins.

4. Remove additional unbound material by extensive washing with at least 10 bed volumes of TBS-Ca, or until the absorbance of the eluent at 280 nm is negligible.
5. Elute Ca^{2+}-dependent binding proteins with TBS-E. Carefully add 5 volumes of TBS-E to the drained ligand matrix, restart the flow and take fractions of about one-forth of the bed volume (see Note 8).
6. Wash EDTA excess with 5 volumes of TBS.
7. Elute electrostatically bound proteins with TBS-HS. Carefully add to the drained matrix bed 5 volumes of TBS-HS, restart the flow and take fractions of about one-forth of the bed volume.
8. Wash salt excess with 5 volumes of TBS.
9. Elute hydrophobically bound proteins with TBS-T. Carefully add 5 volumes of TBS-T to the drained matrix bed, restart the flow and take fractions of about one-forth of the bed volume.
10. Wash Triton X-100 detergent with 5 volumes of TBS.
11. Elute pH-dependent binding proteins bound proteins with 1 M acetic acid (AcH). Carefully add 5 volumes of AcH to the drained matrix bed, restart the flow, and take fractions of about one-forth of the bed volume.
12. Wash AcH with 5 volumes of TBS.
13. Analyze remaining bound proteins by taking a small aliquot of affinity matrix and elute by boiling the sample for 5 min in the presence of 5% SDS and 1 M DTT in TBS (SDS/DTT buffer) (see Note 9).
14. To determine the fractions containing the eluted proteins at the different steps, read the absorbance at 280 nm of each fraction against a blank reference buffer, or by a suitable protein quantitation method such as the Bio-Rad DC Protein Assay (Bio-Rad, #500-0111) (see Note 8).
15. Pool fractions containing protein for each elution step, dialyze extensively against 50 mM ammonium bicarbonate, and store at –80°C until used.

3.3. Downstream Analysis

3.3.1. Identification

Proteins bound to the affinity column and eluted with different buffers could be easily identified via either amino acid sequence or mass spectrometry analysis. To obtain rapid *N-terminal sequence* data without the need of complex and time-consuming fractionation procedures (e.g., high performance liquid chromatography separation of the individual components of the eluate), electrophoretic methodology usually provides enough resolution and sufficient amount of material to successfully carry out protein identification. Samples are separated on 10% tris-tricine SDS-PAGE and transferred to polyvinylidene difluoride membranes (Immobilon P, Millipore, Mildford, MA) using CAPS (3-cyclohexylamino-1-propanesulphonic acid) pH 11, containing 10% methanol. After transfer, the membrane

is stained with Coomassie Blue (see Note 10) to visualize the components of the mixture, procedure that in our example render a series of components of different molecular mass (see Fig. 1). The protein bands are excised from the membrane and used directly to obtain N-terminal sequence (in our example, proteins were identified on a 477 A protein sequencer, Applied Biosystems, Foster City, CA). An alternative identification methodology that has greater sensitivity is *mass spectrometry*, an approach highly recommended for samples with low abundance components. The technique, matrix-assisted laser desorption/ionization time-of-flight (MALDI-TOF), requires an additional step in the sample preparation; samples separated on SDS-PAGE are stained with mass spectrometry compatible Silver stain (SilverQuest, InVitrogen) following the manufacturer's guidelines. Bands are excised from the gel, subjected to proteolytic degradation with TPCK-trypsin and the resulting peptide mix resolved in the mass spectrometer using the protocols recommended by the manufacturer. Searching the mass data against a database of tryptic peptides will allow the identification of the unknown components (36).

3.3.2. Data Validation

Further validation of the data obtained via N-terminal sequence or mass spectrometry can be obtained via *Western blot analysis* of the different eluates using specific antibodies for the identified proteins. The technique is highly sensitive and will provide direct visualization of each of the specific components of the sample. The use of complementary *immunohistochemical* techniques will provide additional confirmation of the topographical location of the identified amyloid-binding proteins in the tissue deposits.

4. Notes

1. Affinity chromatography is one of the most powerful chromatographic methods for purification of specific molecules from a complex mixture based on the interaction with the affinity matrix. Sequential elution may allow purifying proteins that interact by different mechanism, providing further information on the type of binding interaction.
2. Sepharose from GE-HealthCare and Affigel from Bio-Rad are agarose-derived matrices that fulfill these criteria. Cellulose or synthetic supports such as polyacrylamide beads, Sephacryl, or Ultragel are also good options. Hydrophobic polystyrene beads and negatively charged silica supports are not generally recommended for this purpose.
3. This type of attachment presents also some drawbacks, including partial leaking of ligands, and potential steric hindrance due to the absence of linker. Additionally, attachment of ligands

through free primary amino groups may alter their interaction with other proteins.

4. A regular flow from 0.2 to 0.5 ml/min is recommended for most applications.
5. Do not allow to matrix to get dry at any point during the procedure, because this will adversely affect the performance of the column.
6. Viscous samples, such as plasma and serum, should be diluted at least 1:1 with TBS-Ca. Additionally, before loading the sample into the column, samples should be centrifuged for 15 min at >4,000 × *g*, or filtered through a 0.23-μm filter to remove debris.
7. Incubation at 37°C mimics physiological conditions; however, for labile proteins this setup may result unsuitable. Adjust temperature and time for binding according to experimental needs. In the experiment depicted in this work (see Fig. 1), 2 ml of the $A\beta_{1-40}$ peptide matrix was allowed to interact with 10 ml of normal plasma for 3 h at room temperature with continuous recirculation.
8. For a ligand matrix bed volume of 2 ml, take 0.5 ml fractions. The bulk of protein should elute within the last two fractions of the first bed volume.
9. Since this procedure may render the affinity matrix unusable, it is important that you analyze only a small fraction (20–50 μl) by this procedure. The rest of the affinity matrix can be reused several times with optimal performance, provided proper care of column has been taken. For general cleaning and regeneration, wash the column with 3 volumes of alternating high pH (0.1 M Tris–HCl, 0.5 M NaCl, pH 8.5) and low pH (0.1 M sodium acetate, 0.5 M NaCl, pH 4.5) buffers. To remove precipitated or denatured substances, wash with 2 column volumes of 6 M guanidine hydrochloride, and wash immediately with 5 column volumes of TBS or other suitable buffer. To remove hydrophobically bound substances, wash with 3 column volumes of 70% ethanol or 1% Triton X-100, and immediately with 5 column volumes of TBS. For storage, keep the column at 4°C in 20% ethanol at neutral pH.
10. Use the high-quality reagents for the preparation of the Coomassie Blue staining and distaining solutions. Use 1% acetic acid as fixative in the solutions instead of 5–10% commonly used in Coomassie Blue staining standard protocols to facilitate downstream analysis by N-terminal sequencing.
11. In some Aβ-affinity chromatography experiments, we have found a significant presence of IgG (0–10%) in the Triton X-100 and acetic acid fractions. This fact may be associated to a specific interaction of bound apoJ with IgG molecules (37).

Acknowledgments

This work was supported by grants from the Fundación CIEN-ISCIII (MPY 1308/08) and CIBERNED to MC and from the National Institutes of Health NS051715 to AR and AG030539 to JG.

References

1. Ghiso, J., and Frangione, B. (2002) Amyloidosis and Alzheimer's disease. *Adv. Drug Delivery Rev.* **54**, 1539–1551.
2. Coria, F., Castano, E., Prelli, F., Larrondo-Lillo, M., van Duinen, S., Shelanski, M. L et al. (1988) Isolation and characterization of amyloid P component from Alzheimer's disease and other types of cerebral amyloidosis. *Lab. Invest.* **58**, 454–458.
3. Kalaria, R. N., Galloway, P. G., and Perry, G. (1991) Widespread serum amyloid P immunoreactivity in cortical amyloid deposits and the neurofibrillary pathology of Alzheimer's disease and other degenerative disorders. *Neuropathol. Appl. Neurobiol.* **17**, 189–201.
4. Namba, Y., Tomonaga, M., Kawasaki, H., Otomo, E., and Ikeda, K. (1991) Apolipoprotein E immunoreactivity in cerebral amyloid deposits and neurofibrillary tangles in Alzheimer's disease and kuru plaque amyloid in Creutzfeldt-Jakob disease. *Brain Res.* **541**, 163–166.
5. Wisniewski, T., and Frangione, B. (1992) Apolipoprotein E: a pathological chaperone protein in patients with cerebral and systemic amyloid. *Neurosci Lett.* **135**, 235–238.
6. Yamada, T., Kakihara, T., Gejyo, F., and Okada, M. (1994) A monoclonal antibody recognizing apolipoprotein E peptides in systemic amyloid deposits. *Ann. Clin. Lab. Sci.* **24**, 243–249.
7. Kindy, M. S., King, A. R., Perry, G., de Beer, M. C., and de Beer, F. C. (1995) Association of apolipoprotein E with murine amyloid A protein amyloid. *Lab Invest* **73**, 469–475.
8. Rostagno, A., and Ghiso, J. (2003) Amyloidosis. In M Aminoff and R Daroff, eds. *Encyclopedia of neurological sciences.* **1,** pp. 129–135. Academic Press, San Diego.
9. Ghiso, J., Rostagno, A., Tomidokoro, Y., Lashley, T., Holton, J., et al. (2005) Familial British and Danish dementias. In JD Sipe, ed., *Amyloid proteins. The beta sheet conformation and disease.* **2,** pp. 515–526. Wiley-VCH Verlag GmbH & Co. KGaA, Weinheim, Germany.
10. Rostagno, A., Tomidokoro, Y., Lashley, T., Ng, D., Plant, G., et al. (2005) Chromosome 13 dementias. *Cell Mol Life Sci.* **62**, 1814–25.
11. Veerhuis, R., Boshuizen, R. S., and Familian, A. (2005) Amyloid associated proteins in Alzheimer's and prion disease. *Curr. Drug Targets CNS & Neurological Dis.* **4**, 235–248.
12. Gallo, G., Picken, M., Frangione, B., and Buxbaum, J. N. (1988) Nonamyloidotic monoclonal immunoglobulin deposits lack amyloid P component. *Mod. Pathol.* **1**, 453–456.
13. Gallo, G., Wisniewski, T., Choi-Miura, N. H., Ghiso, J., and Frangione, B. (1994) Potential role of apolipoprotein-E in fibrillogenesis. *Am. J. Pathology* **145**, 526–530.
14. Botto, M., Hawkins, P. N., Bickerstaff, M. C. M., Herbert, J., Bygrave, A. E., et al. (1997) Amyloid deposition is delayed in mice with targeted deletion of serum amyloid P component. *Nature Med.* **3**, 855–859.
15. Holtzman, D. M., Bales, K. R., Wu, S., Bhat, P., Parsadanian, M., et al. (1999) Expression of human apolipoprotein E reduces amyloid-beta deposition in a mouse model of Alzheimer's disease. *J. Clin. Invest.* **103**, R15–R21.
16. Glenner, G. G., Wong, C. W. (1984) Alzheimer's disease: initial report of the purification and characterization of a novel cerebrovascular amyloid protein. *Biochem Biophys Res Commun* **120**, 885–890.
17. Masters, C. L., Multhaup, G., Simms, G., Pottgiesser, J., Martins, R. N., Beyreuther, K. (1985) Neuronal origin of a cerebral amyloid: neurofibrillary tangles of Alzheimer's disease contain the same protein as the amyloid of plaque cores and blood vessels. *EMBO J.* **4**, 2757–2763.
18. Prelli, F., Castano, E. M., Glenner, G. G., and Frangione, B. (1988) Differences between vascular and plaque core amyloid in Alzheimer's disease. *J. Neurochem.* **51**, 648–651.
19. Seubert, P., Vigo-Pelfrey, C., Esch, F., Lee, M., Dovey, H., Davis, D. et al (1992) Isolation and

quantitation of soluble Alzheimer's β-peptide from bilogical fluids. *Nature* **359**, 325–327.

20. Shoji, M., Golde, T. E., Ghiso, J., Cheung, T. T., Estus S., Shaffer, L. M. et al. (1992) Production of the Alzheimer amyloid beta protein by normal proteolytic processing. *Science* **258**, 126–129.
21. Haass, C., Koo, E. H., Mellon, A., Hung, A. Y., Selkoe, D. J. (1992) Targeting of cell-surface beta-amyloid precursor protein to lysosomes: alternative processing into amyloid-bearing fragments. *Nature* **357**, 500–503.
22. Ghiso, J., Calero, M., Matsubara, E., Governale, S., Chuba, J., Beavis, R, et al. (1997) Alzheimer's soluble amyloid beta is a normal component of human urine. *FEBS Lett.* **408**, 105–108.
23. Tabaton, M., Nunzi, M. G., Xue, R., Usiak, M., Autilio-Gambetti, L., Gambetti, P. (1994) Soluble amyloid beta-protein is a marker of Alzheimer amyloid in brain but not in cerebrospinal fluid. *Biochem Biophys Res Commun.* **200**, 1598–1603.
24. Golabek, A., Marques, M. A., Lalowski, M., Wisniewski, T. (1995). Amyloid β binding proteins in vitro and in normal human cerebrospinal fluid. *Neuroscience Lett.* **191**, 79–82.
25. Ghiso, J., Matsubara, E., Koudinov, A., Choi-Miura, N. H., Tomita, M., Wisniewski, et al. (1993) The cerebrospinal-fluid soluble form of Alzheimer's amyloid beta is complexed to SP-40,40 (apolipoprotein J), an inhibitor of the complement membrane-attack complex. *Biochem J.* **293**, 27–30.
26. LaDu, M. J., Lukens, J. R., Reardon, C. A., Getz, G. S. (1997) Association of human, rat, and rabbit apolipoprotein E with beta-amyloid. *J Neurosci Res.* **49**, 9–18.
27. Wisniewski, T., Castaño, E. M., Golabek, A. A., Vogel, T., and Frangione, B. (1993) Acceleration of Alzheimer's fibril formation by apolipoprotein E in vitro. *Am. J. Pathology* **145**, 1030–1035.
28. Wegiel, J., Chauhan, A., Wisniewski, H.M., Nowakowski, J., Wang, K.C., Le Vine, H. (1996) Promotion of synthetic amyloid beta-peptide fibrillization by cell culture media and cessation of fibrillization by serum. *Neurosci. Lett.* **211**, 151–154.
29. LaDu, M. J., Falduto, M. T., Manelli, A. M., Reardon, C. A., Getz, G. S., and Frail, D. E. (1994) Isoform-specific binding of apolipoprotein E to beta-amyloid. *J. Biol. Chem.* **269**, 23403–23406.
30. Ma, J., Yee, A., Brewer, H. B., Jr., Das, S. and Potter, H. (1994) Amyloid-associated proteins alpha 1-antichymotrypsin and apolipoprotein E promote assembly of Alzheimer beta-protein into filaments. *Nature*, **392**, 92–94.
31. Webster, S., O'Barr, S., and Rogers, J. (1994) Enhanced aggregation and β structure of amyloid β peptide after coincubation with C1q. *J. Neurosci. Res.* **39**, 448–456.
32. Tennent, G. A., Lovat, L. B., and Pepys, M. B. (1995) Serum amyloid P component prevents proteolysis of the amyloid fibrils of Alzheimer's disease and systemic amyloidosis. *Proc. Natl. Acad. Sci. USA*, **92**, 4299–4303.
33. Matsubara, E., Soto, C., Governale, S., Frangione, B., and Ghiso, J. (1996) Apolipoprotein J and Alzheimer's amyloid beta solubility. *Biochem J.*, **316**, 671–679.
34. Lambert, M. P., Barlow, A. K., Chromy, B. A., Edwards, C., Freed, R., et al. (1998) Diffusible, nonfibrillar ligands derived from Aβ1–42 are potent central nervous system neurotoxins. *Proc. Natl. Acad. Sci. USA*, **95**, 6448–6453.
35. Urh, M., Simpson, D., Zhao, K. (2009) Affinity chromatography: general methods. *Methods Enzymol.* **463**, 417–438.
36. Ovodenko, B., Rostagno, A., Neubert, T. A., Shetty, V., Thomas, S., et al. (2007) Proteomic analysis of exfoliation deposits. *Invest. Ophthalmol. Vis. Sci.*, **48**, 1447–1457.
37. Wilson, M. R., Easterbrook-Smith, S. B. (1992) Clusterin binds by a multivalent mechanism to the Fc and Fab regions of IgG. *Biochim. Biophys. Acta* **1159**, 319–326.

Part II

Cell Culture Models and Assays

Chapter 16

Establishing the Links Between Aβ Aggregation and Cytotoxicity In Vitro Using Biophysical Approaches

Asad Jan and Hilal A. Lashuel

Abstract

Aggregation and fibril formation of the amyloid-β (Aβ) peptides play a pivotal role in the pathogenesis of Alzheimer's disease (AD). The missing links on the pathway to Aβ oligomerization, fibril formation, and neurotoxicity in AD remain the identity of the toxic Aβ species and mechanism(s) of their toxicity. Such information is crucial for the development of mechanism-based therapeutics to treat AD and tools to diagnose and/or monitor the disease progression. Herein, we describe a simple approach that combines standard biophysical methods with cell biology assays to correlate the aggregation state of Aβ peptides with their cytotoxicity in vitro. The individual assays are well-established, commonly used, rely on easily accessible materials and can be performed within 24 h.

Key words: Alzheimer's disease, Amyloid-β, Oligomers, Toxicity

1. Introduction

Alzheimer's disease (AD) is the most common cause of debilitating dementia in elderly worldwide. Despite significant advances in the understanding of the mechanisms of Aβ production and aggregation in vitro, translating this knowledge in a clear mechanistic understanding of the pathogenesis of AD and effective clinical therapies remain challenging. Circumstantial evidence, principally derived from neuropathology, molecular genetics, animal models of AD, cell culture studies, and biophysics indicate that the aggregation and fibril formation of amyloid-β (Aβ) peptides play central role in AD pathogenesis (1, 2). Aβ peptides are produced as a consequence of sequential proteolytic processing of the amyloid precursor protein (APP) by β- and γ-secretase activities. APP cleavage by γ-secretase results in production of Aβ peptides of various chain lengths, principally composed of 40 and 42 amino acid

Einar M. Sigurdsson et al. (eds.), *Amyloid Proteins: Methods and Protocols*, Methods in Molecular Biology, vol. 849,
DOI 10.1007/978-1-61779-551-0_16,

residues (Aβ40 and Aβ42), which densely populate the core of the neuritic plaques in AD neuropathology (3). During the in vitro fibril formation of Aβ peptides, various nonfibrillar aggregates of diverse morphologies and heterogeneous size distributions, collectively known as the soluble oligomers, have been observed. Some of the well-characterized Aβ oligomer species include protofibrils (4), Aβ-derived diffusible ligands (ADDLs) (5), annular oligomers (6), and the low molecular weight oligomers (7).

Several independent lines of evidence indicate that the soluble oligomers and/or the process of oligomerization (8–10), rather than plaque-associated fibrils, are the primary cause of neurodegeneration in AD: (1) Soluble Aβ, rather than total (soluble and insoluble) Aβ, levels correlate better with AD progression (11, 12); (2) Significant functional deficits in the memory performance tasks are observed in the APP transgenic animals long before the emergence of amyloid plaques (13, 14); (3) Soluble Aβ oligomer preparations, upon intracerebral infusion, induce transient memory deficits in experimental animals (15); (4) Rare mutations in the APP gene [e.g., arctic mutation (E22G)], which enhance Aβ oligomerization without altering the total Aβ levels, are associated with the development of familial AD (16); (5) Aβ oligomer and protofibril preparations alter neuronal metabolism (17), induce changes in neuronal electrophysiology (18) and lead to neurotoxicity towards cultured neurons (10, 17, 19). Therefore, inhibiting Aβ oligomerization, by attenuating its production and/or promoting the clearance of toxic Aβ oligomers from brain, has emerged as potential therapeutic strategies for treating AD (20).

Cultured primary neurons and/or cell lines provide easy and economic means of investigating the role of Aβ aggregation state and the mechanism of Aβ toxicity, and also as valuable tools for the screening of the inhibitors of Aβ toxicity in vitro. This chapter describes simple, inexpensive, and reproducible methods which would allow the investigators to assess the toxicity of Aβ preparations (soluble or insoluble) and correlating Aβ aggregation/fibrillization with its cytotoxicity. The general outline is provided in Fig. 1. Briefly, cultured cells are treated with purified Aβ preparations (monomers, protofibrils, and fibrils) or crude preparations containing mixtures of heterogeneous Aβ species. For detailed protocols on the preparation of these species, the reader is referred to our previous work (10, 21). At desired intervals, cell viability is determined by the MTT (3-(4,5-dimethylthiazol-2-yl)-2,5-diphenyltetrazolium bromide) reduction assay. In the case of primary neurons, subtle changes in neuronal viability can also be quantified using immunostaining for neuronal nuclei (NeuN) (8) or via quantification of the loss of neuronal processes (19, 21). In addition, media aliquots of Aβ-treated cultured cells can be used to investigate the cytotoxicity and the aggregation state of Aβ simultaneously. Quantitative cytotoxicity information can be obtained by performing

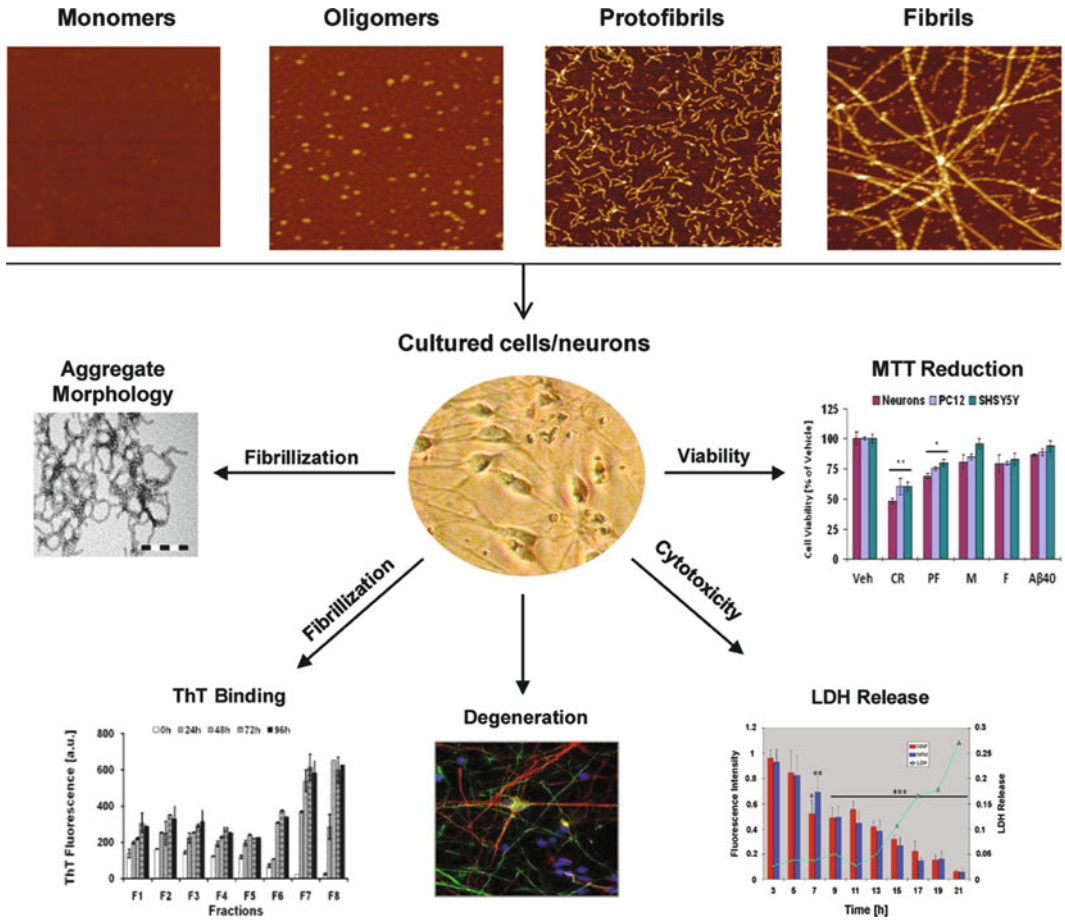

Fig. 1. Overview of the methods used to correlate Aβ aggregation with cytotoxicity in vitro. Cultured cells (primary neurons and/or cell lines) are treated with the desired concentration(s) of the purified or crude Aβ preparations (21). At selected intervals, cell viability can be assessed by the MTT reduction assay. In the case of neuronal cultures, immunostaining for neuronal nuclei (NeuN) (8) or neuronal processes (19) can also be used. The culture medium can be assayed for cytotoxicity using the LDH release method. In addition, Aβ aggregation and fibrillization can be monitored by ThT dye binding and TEM analysis of the culture medium and allow for the correlation of the Aβ aggregation with the relative cytotoxicity (the MTT graph and the LDH release graphs are reprinted with copyright permission (10, 19)). Labels in the MTT graph: cultured primary neurons, PC12 and SHSY5Y cells were treated with different Aβ preparations (10 μM total Aβ) or the buffer vehicle and cell viability was assessed by the MTT reduction assay (*Veh* buffer vehicle, *CR* crude Aβ42 preparations, *PF* Aβ42 protofibrils, *M* Aβ42 monomers, *Aβ40* Aβ40 monomers) (10). Labels in the LDH graph: cultured primary neurons were treated with Aβ40-arctic (E22G) monomers (20 μM total Aβ) and cell viability was assessed over time by the LDH release in the culture medium and quantitative immunocytochemistry for the microtubule-associated protein (MAP) and neurofilament-M (NF-M) (19).

the lactate dehydrogenase (LDH) release assay using the cell culture medium. Finally, a direct link between the extent of cytotoxicity and Aβ aggregation state can be established by combining these assays with methods that allow monitoring of Aβ aggregation in the cultured media, e.g., dye [Thioflavin T (ThT)] binding and negative-staining transmission electron microscopy (TEM).

This approach will allow the researchers to closely monitor changes in the quaternary structure of Aβ under cell culture

conditions, formation of oligomers and fibrils during the duration of the experiment, and most importantly, directly correlate Aβ aggregation state(s) with relative cytotoxicity. The knowledge gathered from such studies is indispensable for the identification of the critical stages (aggregation states) on the Aβ amyloid formation pathway which underlie Aβ cytotoxicity and help design the intervention strategies. Herein, we describe the use of MTT reduction and the LDH release assays for quantifying Aβ toxicity toward cultured PC12 cells. Detailed methods for culturing primary neurons, including immunostaining and measuring cell viability by relevant assays, have been described elsewhere (8, 21).

1.1. MTT Reduction Assay

MTT [3-(4,5-dimethylthiazol-2-yl)-2,5-diphenyltetrazolium bromide] belongs to the group of tetrazolium salts which, upon endocytosis by the cells, is reduced to the insoluble formazan crystals principally by the activity of the mitochondrial respiratory chain enzymes (22). In addition, certain enzymes in cytoplasm, endosomes/lysosomes, and plasma membrane have also been implicated in the metabolism of MTT into the formazan (23). Metabolically active and viable cells can reduce the MTT in short durations of time, e.g., 30 min, into purple formazan products the formation of which can be monitored spectrophotmetrically (Fig. 2) (23). It is one of the most commonly used assays to monitor cytotoxicity of various drugs, synthetic polymers, and amyloid proteins (17, 24, 25). Numerous research groups have shown that Aβ preparations containing monomers, oligomers, or fibrils consistently impair the ability of cultured neurons or other cells to metabolize MTT (9, 17, 26). The simple nature of the assay and

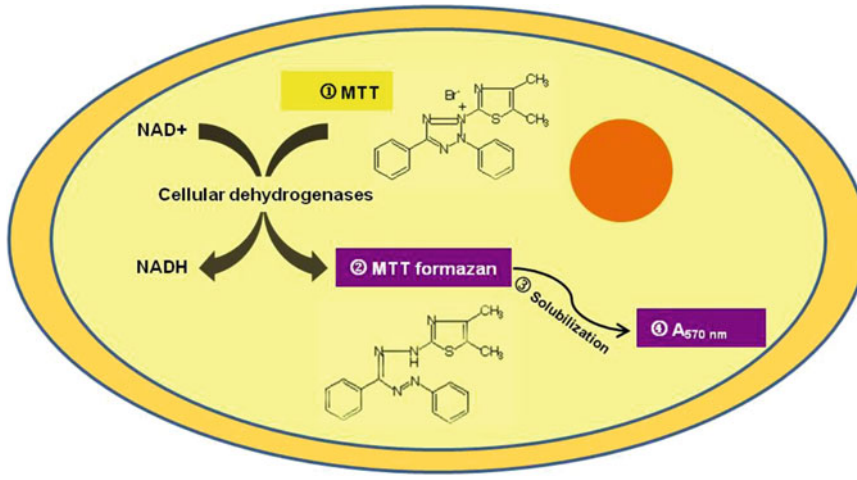

Fig. 2. Principle of the MTT assay. MTT is internalized by the cells and reduced by the action of various cellular dehydrogenases, principally in mitochondria, into the purple formazan product. The crystals of formazan are solubilized and the absorbance (570 nm) of the resulting solution provides a measure of the cellular viability.

the lack of requirements for expensive instrumentation make it a convenient choice for assessing the relative toxicity of Aβ preparations and also for the evaluation of the Aβ aggregation inhibitors in rescuing the survival of Aβ-treated cells.

Although it is very easy to perform, some shortcomings of the assay are worth mentioning: (1) the assay does not differentiate between cell death and metabolic stress (27); (2) the readout is semiquantitative, i.e., a decrease in MTT reduction does not correlate with number of dead cells in a linear fashion (27); (3) different cell types metabolize MTT, and related tetrazolium dyes, to differential extent, i.e., the assay readout is influenced by the metabolic phenotype of the cells (28); and (4) it has also been suggested that amyloidogenic proteins interfere with crystallization of MTT formazan in a manner such that the extent of cytotoxicity is overestimated (9). Therefore, it is highly recommended that MTT reduction assay be used in conjunction with some other biochemical and/or immunocytochemical means of assessing the cell viability, e.g., LDH release assay (see below) and/or, in the case of neurons, staining for the loss of neuronal processes.

1.2. LDH Release Assay

LDH is an oxidoreductase enzyme present in the cytoplasm of a wide variety of cells and catalyzes the interconversion of pyruvate and lactate, coupled to the concomitant interconversion of NADH and NAD^+ (29, 30). Cell membrane disruption, during various physiological or pathological processes, leads to the release of the enzyme in extracellular milieu (e.g., cell culture medium). Hence, if appropriate substrates are added to the culture medium, the levels of LDH release, and therefore the extent of cell membrane damage, can be quantified (Fig. 3). LDH release is also a commonly used assay for investigating the biosafety of drugs and for assessing the cytotoxicity of the amyloidogenic proteins including Aβ (31, 32).

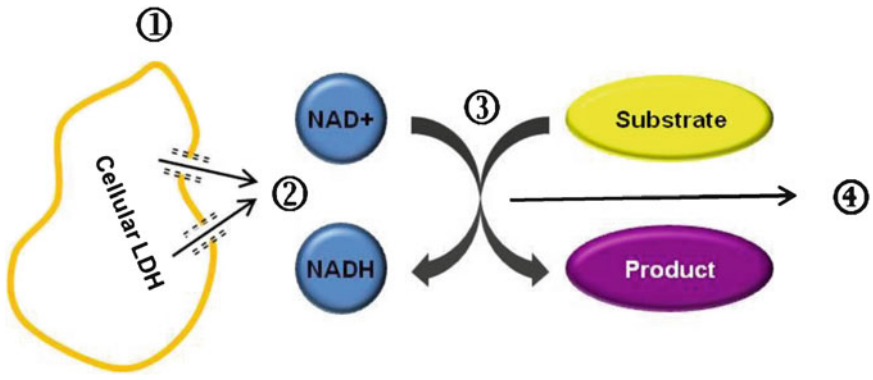

Fig. 3. Principle of the LDH release assay. Upon ① membrane disruption/cell damage, ② the cytosolic LDH is released into the extracellular milieu/tissue culture medium. In the presence of appropriate substrates and cofactors, ③ the enzyme activity results in ④ the formation of colorimetric/fluorescent products. The latter can be quantified and indicate the extent of cytotoxicity.

Interestingly, it has been observed that in neuronal cultures exposed to Aβ oligomers, loss of neuronal processes precedes the rise in LDH release. The latter observations suggest that Aβ oligomer toxicity is mediated by multiple mechanisms and the neurodegeneration commences long before the frank death of neurons (9, 10, 18, 19).

In contrast to the MTT reduction assay, the amount of LDH release provides a more reliable measure of the number of dead/damaged cells (33). However, it is also known that different cell types have differential LDH content and/or the kinetics of the LDH release is not identical (34); therefore, correlation of the assay readout to the extent of cell death between different cell types cannot be accurately determined. Nevertheless, the combined application of the two assays (MTT and LDH) provides valuable information regarding both the early and the late events associated with Aβ cytotoxicity.

1.3. Negative-Staining TEM

Electron microscopy (EM)-based approaches have played important role in our current understanding of the mechanism of amyloid formation of nearly all amyloidogenic proteins, and also in elucidating the structural basis of amyloid toxicity. As early as 1960s, these approaches facilitated the detailed structural characterization of amyloid aggregates associated with neuropathological lesions in AD brains (35). In addition, EM methods have also played important role in the discovery and structural characterization of various Aβ oligomers, including protofibrils, which precede the emergence of fibrils during the aggregation of Aβ peptides (4, 17). The latter findings significantly changed the paradigm of understanding the interrelation of the process of amyloid formation and associated neurodegeneration, and ushered the notion of toxic oligomer/protofibril hypothesis (36). Although, the toxicity of plaque-associated fibrillar aggregates is not ruled out, this hypothesis points toward soluble Aβ oligomers as neurotoxins in AD and stipulates that the Aβ oligomers trigger a complex series of the cellular and molecular events culminating in the development of AD (36). A detailed description of various EM-based methods and their utility in studying amyloid aggregation can be found elsewhere (21, 37).

Herein, we describe the methods and use of the negative-staining EM on the cell culture media aliquots to study Aβ aggregation under cell culture conditions, and directly establish the correlation of the aggregate structure with their respective cytotoxicity in neuronal and nonneuronal cell culture systems. In brief, cell culture medium aliquots are deposited on carbon-coated formvar film attached to an EM grid, followed by the staining with a dilute solution of a heavy salt (uranyl acetate, uranyl formate etc.). The latter help enhance the contrast in the images by their ability to scatter electrons in the incident electron beam. Although, a convenient and simple method, the quality of the information obtained by negative-staining EM is limited by certain factors such as: (1) limited resolution capability (≈2.5 nm) of the technique, (2) drying of the

surface causes flattening of the aggregate structures, (3) the aggregates may differ in their adsorption to the grid surface, (4) image artifacts can be induced by uneven staining of the sample (this could be addressed by preparing multiple grids of the sample), and (5) most importantly, it is not a quantitative method. Therefore, it is suggested that information about the characterization of amyloid aggregates should be complimented by other standard biophysical assays, e.g., Thioflavin-T (ThT) dye binding and solubility analysis by the size exclusion chromatography (6, 8).

1.4. Thioflavin-T Dye Binding

Thioflavin-T (4-(3,6-dimethyl-1,3-benzothiazol-3-ium-2-yl)-*N*,*N*-dimethylaniline chloride), and its homologue Thioflavin-S, is a benzothiazole salt and belongs to the so-called amyloid-specific dyes. The thioflavin dyes undergo red shift in their emission spectrum upon binding to amyloid plaques in amyloid laden tissue sections (38, 39). In vitro, thioflavin dyes bind to the ordered amyloid aggregates such as fibrils and protofibrils of diverse proteins, e.g., Aβ (8, 17), α-synuclein (40), but not to the low molecular weight oligomers (2–12 mers) or monomers (8, 17). The specificity of the dyes for binding to the amyloid structures has been proposed to be based on the presence of the cross-strand ladders, characteristic arrangements of side chains, present in β-sheet-rich structures, and formation of channels along the β-sheet surfaces which allow for the binding of linear thioflavin dyes (Fig. 4) (41). Although very simple and inexpensive method, ThT binding per se does not always provide a quantitative measure of the amount of amyloid aggregates, e.g., a small amount of fibrils in Aβ preparations can result in high-ThT values. Also, extensive fibrillization, and intertwining of the fibrils, may reduce the accessibility of ThT dyes towards the binding sites thus erroneously decreasing the ThT readout. Nevertheless, changes in ThT binding in kinetic assays is a reliable indicator of the metastability in amyloid aggregates and, if used in combination with cytotoxicity assays, is a reliable correlate of extent of cytotoxicity with amyloid aggregation.

2. Materials

1. Human wild-type (wt) synthetic Aβ42 and Aβ40 from a suitable commercial source (e.g., W.M. Keck Facility, Yale University, New Haven, CT, USA).
2. Trizma® hydrochloride solution (Tris–HCl) 1 M (Sigma, cat. no. T2663).
3. Uranyl acetate (UA) (Electron Microscopy Sciences, cat. no. 22400).
4. Formvar-coated TEM grids (Electron Microscopy Sciences, cat. no. FCF200-Cu-50).

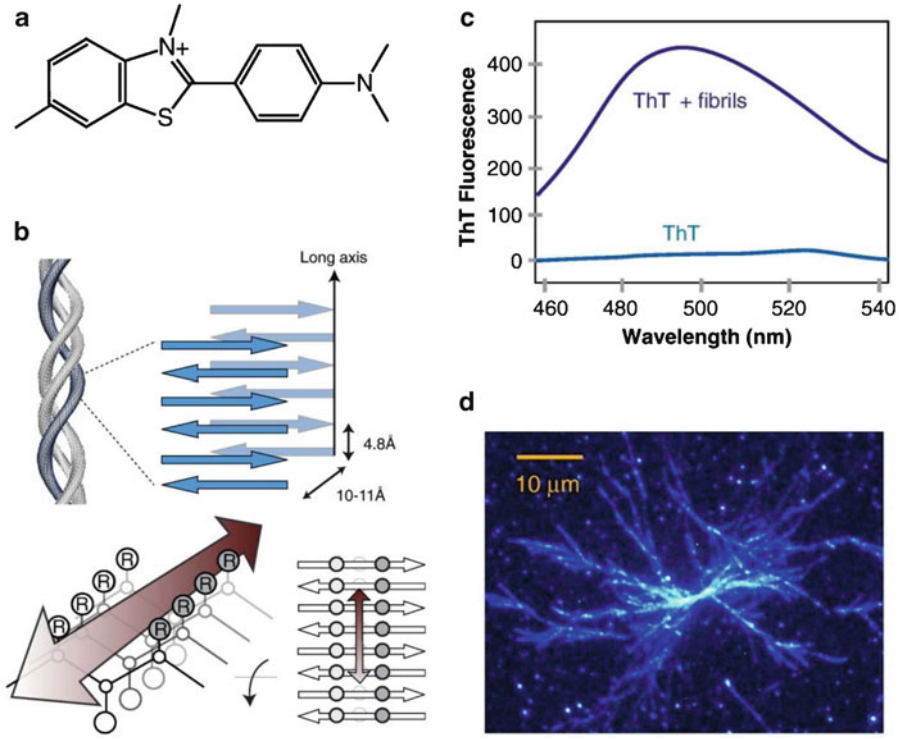

Fig. 4. Mechanism of ThT binding to the amyloid aggregates. (**a**) Structure of ThT. (**b**) Cross-β structure of amyloid fibrils, formed from layers of laminated β-sheets. ThT is proposed to bind along surface side-chain grooves running parallel to the long axis of the β-sheet. (**c**) Characteristic increase in ThT fluorescence upon binding to amyloid fibrils. (**d**) TIRF microscopy image of branched glucagon fibrils stained with ThT (Images (**a–c**) are reprinted with copyright permission (41). The TIRF image (**d**) is reprinted with copyright permission (42)).

5. Grid storage box (Electron Microscopy Sciences, cat. no. 71140).
6. High Precision Ultrafine tweezers (Electron Microscopy Sciences, cat. no. 78318-3X).
7. Thioflavin-T (ThT) (Sigma, cat. no. T3516).
8. Glycine (Sigma, cat. no. 50046).
9. Sterile microtubes (e.g., Eppendorf cat. no. Z606340).
10. Dulbecco's Modified Eagle's Medium (DMEM) (Invitrogen, cat. no. 41966-029).
11. DMEM (Invitrogen, cat. no. 21063-029).
12. Recombinant insulin (Invitrogen, cat. no. 12585014).
13. Phosphate-buffered saline (PBS; GIBCO, cat. no. 10010-015).
14. Fetal bovine serum (FBS; GIBCO, cat. no. 10101145).
15. Penicillin–streptomycin (Pen–Strep, 100×; GIBCO, cat. no. 15140-122).
16. LDH cytotoxicity assay kit (Sigma, cat. no. TOX7).
17. MTT (3-(4,5-Dimethylthiazol-2-yl)-2,5-diphenyltetrazolium bromide) (Sigma, cat. no. M5655). Prepare 5 mg/ml MTT

stock solution in sterile PBS and filter through 0.22-μm syringe-driven filter units (TPP, cat. no. 99722). The stock solution should be aliquoted in sterile microtubes (1 ml/tube) and frozen at –20°C.

18. 96-Well, transparent bottom, cell culture plates (BD Falcon, cat. no. 353072).
19. 384-Well plates, black (Nunc, cat. no. 262260).
20. Dimethyl sulfoxide (DMSO) (Sigma, cat. no. D4540).
21. 1 N Hydrochloric acid solution (Sigma, cat. no. H9892).
22. Microplate reader (e.g., Safire 2, TECAN).
23. Poly-L-Lysine (PLL) 0.01% solution (Sigma, cat. no. P4832).
24. Rat pheochromocytoma (PC12) cells: PC12 cells are commercially available (e.g., ATCC, cat. no. CRL-1721) and should be grown in DMEM (Invitrogen, cat. no. 41966-029) supplemented with 1% Pen–Strep and 10% FBS (5% horse-serum, in addition to 10% FBS, during early passages) in 75-cm^2 culture flasks (37°C; ambient humidity; 5% CO_2). It is recommended that the cells should be split before they reach complete confluence (twice/week), to record the number of passages and to keep some frozen stocks of the cells.

3. Methods

3.1. Preparation of Crude Aβ Preparations, Purified Monomers, Protofibrils, and Fibrils

Detailed methods for the preparation and characterization of the crude Aβ preparations, containing heterogeneous Aβ aggregation states and monomers, or defined Aβ species including monomers, protofibrils, and fibrils have been described previously (8, 21).

3.2. Toxicity of Aβ Preparations in PC12 Cell Cultures

1. Plate PC12 cells in 96-well, transparent bottom, culture plates previously coated with 0.01% PLL (30,000 cells/well/200 μl) in the culture medium consisting of phenol red-free DMEM medium (Invitrogen, cat. no. 21063-029) supplemented with 1% Pen–Strep and 2 μM recombinant insulin. The cells should be grown in culture plates for at least 24 h (37°C; ambient humidity; 5% CO_2), and should be treated with Aβ preparation within 24–48 h after plating (see Note 1).
2. Dilute the Aβ preparations (Subheading 3.1) in the culture medium at twice the final concentration(s) desired to be tested (see Note 2). For example, if the desired test Aβ concentration is 10 μM, dilute the Aβ preparations to 20 μM in appropriate volume of the culture medium.
3. Remove 100 μl of the culture medium from each condition and control well and discard into a waste container.

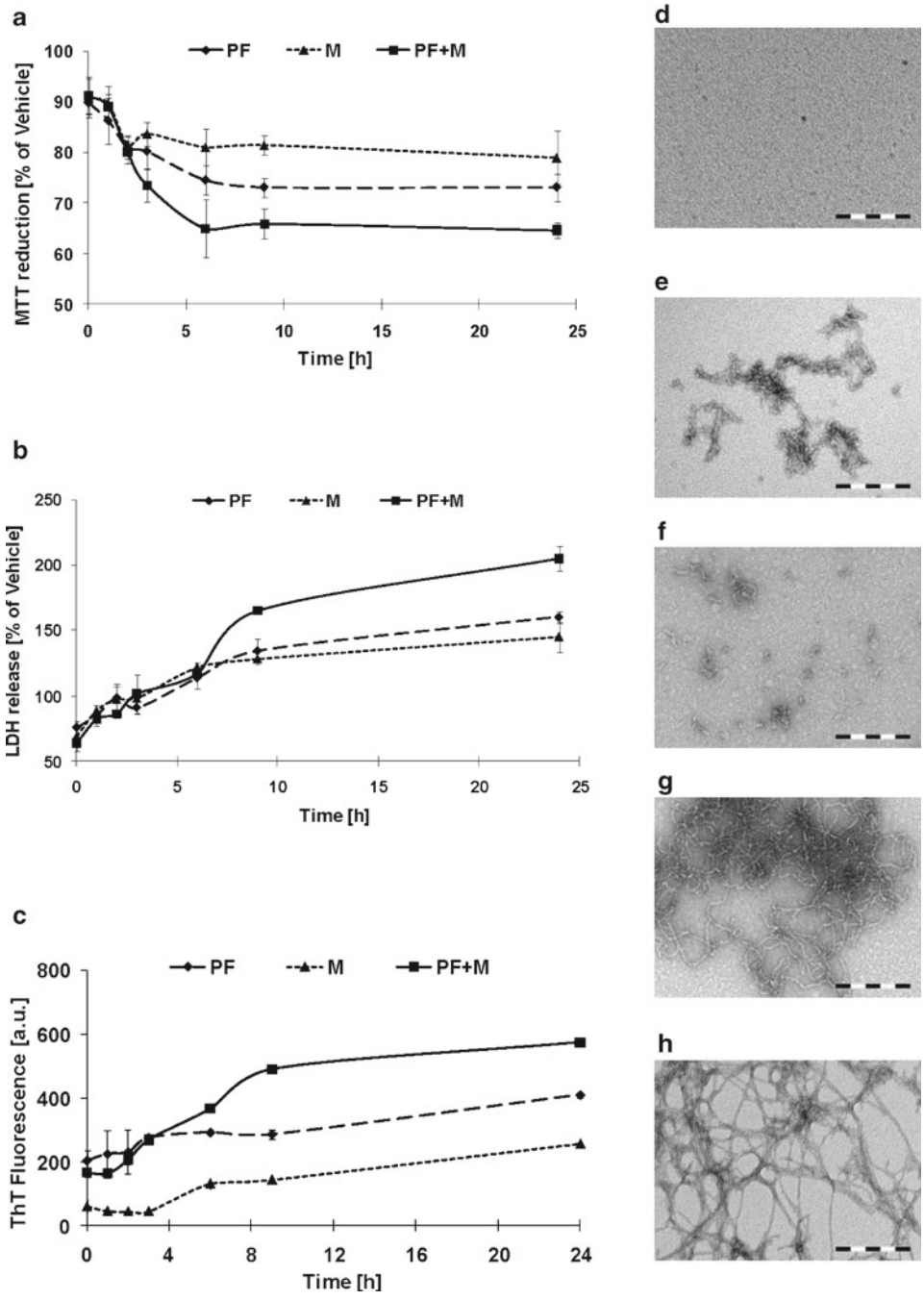

Fig. 5. Fibrillization and relative toxicities of the soluble Aβ42 preparations. Cultured PC12 cells were treated with purified Aβ42 preparations (*M* monomers, *PF* protofibrils, 1:1 molar mixtures of the monomers and protofibrils, i.e., 5 μM of each). The final Aβ concentration was ≈10 μM. (**a**) MTT reduction over time. Aβ42 protofibrils and mixtures of Aβ42 protofibrils with Aβ42 monomers significantly inhibit MTT reduction. In addition, the MTT reduction is significantly impaired with 6–9 h of Aβ42 treatment. The values are expressed as percentage of the buffer control (the error bars represent s.d. in at least six replicate conditions). (**b**) LDH release. Mixture of Aβ42 protofibrils and Aβ42 monomers cause early and robust increase in the LDH release as compared to the monomers, protofibrils, and fibrils alone. The values are expressed as percentage of the buffer control (the error bars represent s.d. in at least six replicate conditions). (**c**) ThT binding. Mixture of Aβ42 protofibrils and Aβ42 monomers fibrillize faster and to a greater extent than the monomers or protofibrils alone.

4. Add 100 μl of culture medium containing Aβ preparations, prepared in Subheading 3.2, step 2 to each condition well. To establish statistical significance, across different conditions and across different experiments, at least 4–6 wells should be treated with each Aβ preparation.
5. Include medium only treated and buffer sample (prepared in identical fashion as the Aβ preparations in step 2) treated cells as controls. If performing a time course study, the controls should be included for each time point.
6. At desired intervals (e.g., every hour), carefully remove 150 μl of the culture medium, without touching the well bottom, into sterile microtubes and label accordingly. The removed medium will be used for assays outlined below (Subheadings 3.4–3.6).
7. Carefully remove the rest of the medium and discard.

3.3. MTT Reduction Assay

1. Wash the cells by adding 200 μl of sterile PBS (room temperature) into each well and remove carefully without disturbing the cells in the bottom of the wells. Perform the PBS wash 2–3 times and discard into a waste container.
2. Add 100 μl of the fresh culture medium containing 5% (vol./vol.) MTT dye solution to each well and place the cells back in the incubator for 2–4 h (see Note 3).
3. Carefully remove the culture medium and discard into a waste container. Then, add 100 μl of the 100% DMSO to each well (see Note 3).
4. Solubilize the cells by careful pipetting and transfer the contents into empty wells of another 96-well plate. Transfer the latter plate to a 4°C chamber for storage not exceeding 24 h.
5. Repeat steps 1–4 above at each desired time point and collect the cell lysates. In order to avoid differential evaporation across the culture plates, add 200 μl of sterile water to each empty well before placing the plate back in the incubator.
6. Warm the plate containing the cell lysate collected from each time point above, to 20–25°C [room temperature (RT)] by simply leaving the plate on a desk for 15 min.

Fig. 5. (continued) The *error bars* represent s.d. in at least six replicate conditions (a.u. = arbitrary units). (**d**–**k**) Representative images obtained by negative-staining TEM of the culture medium. (**d**, **e**) Aβ42 monomers at time 0 and 24 h respectively; (**f**, **g**) Aβ42 protofibrils at time 0 and 24 h respectively; (**h**) Equimolar mixtures of Aβ42 monomers and protofibrils and (**k**) Aβ40 monomers at 24 h (*scale bar* = 200 nm). These data show that an ongoing process of Aβ oligomerization and fibrillization, rather than discrete Aβ species (monomers, protofibrils, or fibrils), critically impairs cell viability (9, 10). In other words, dynamics of the protofibril–monomers interactions and the resultant growth of the protofibrils into fibrils is more important determinant of Aβ toxicity than relatively stable protofibril species (8, 10). This hypothesis is also supported by the observations that enhancing the kinetic stability of Aβ42 protofibrils by adding Aβ40 monomers significantly reduces their toxicity toward cultured neurons (8). Similarly, small molecules that stabilize Aβ protofibrils in vitro have also been shown to improve behavioral performance in APP transgenic mice (43).

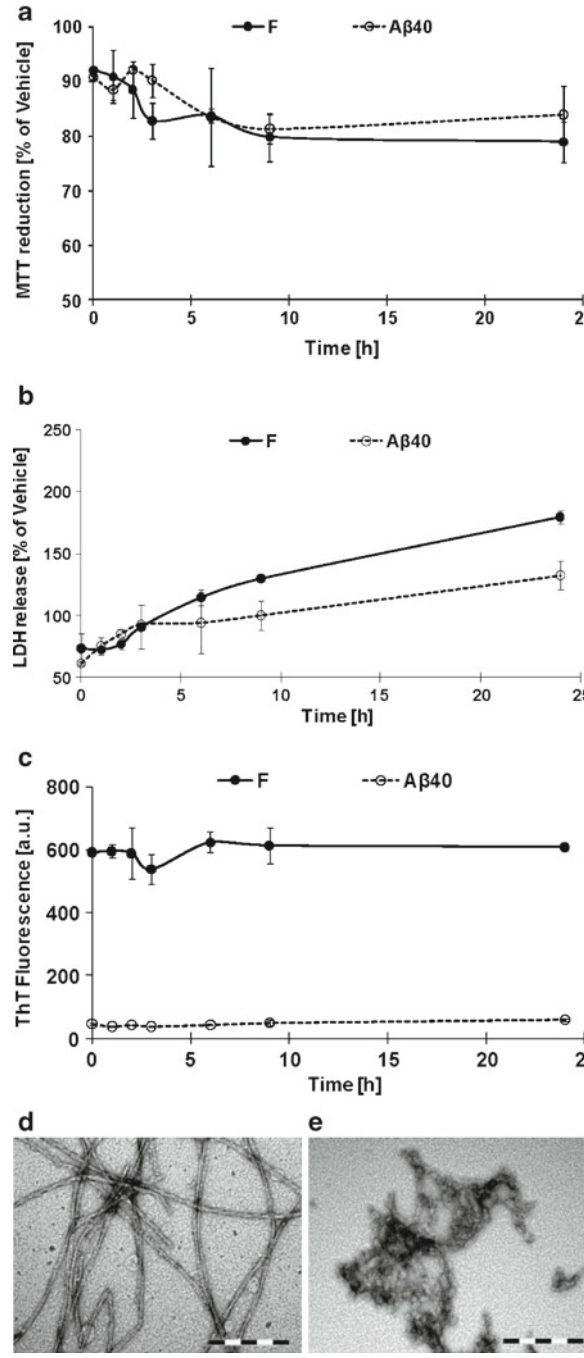

Fig. 6. Fibrillization and relative toxicities of Aβ40 monomers and Aβ42 fibrils. Cultured PC12 cells were treated with Aβ40 monomers and Aβ42 fibrils. The final Aβ concentration was ≈10 μM. (**a**) MTT reduction over time. Both Aβ40 monomers and Aβ42 fibrils cause slight, but insignificant, reduction in MTT metabolism by the cultured cells. The values are expressed as percentage of the buffer control (the *error bars* represent s.d. in at least six replicate conditions). (**b**) LDH release. Aβ42 fibrils cause relatively greater release of the cellular LDH as compared to Aβ40 monomers (the *error bars* represent s.d. in at least six replicate conditions). (**c**) ThT binding. The ThT binding by Aβ40 monomers remains relatively unchanged over time suggesting lack of fibril formation. The *error bars* represent s.d. in at least six replicate conditions (a.u. = arbitrary units). (**d**, **e**) Representative images obtained by negative-staining TEM of the culture medium. (**d**) Aβ42 fibrils and (**e**) Aβ40 after 24 h (*scale bar* = 200 nm).

7. Record the absorbance at 570 nm using a microplate reader. Use a wavelength in the range of 630–750 nm (e.g., 690 nm) as a reference wavelength to account for the plate background, cell debris, nonspecific absorbance etc.
8. Plot the data in a suitable software (Figs. 5a and 6a).

3.4. LDH Release Assay

1. Prepare LDH assay mixture according to the manufacturer's recommendations (Sigma, cat. no. TOX7).
2. Vortex the tubes containing culture medium removed in Subheading 3.2, step 6 from each test and control condition.
3. Separately add 50 µl of each test sample in empty wells of a transparent 96-well plate.
4. Add 100 µl of the LDH assay mixture to each well.
5. Include the culture medium as a control sample.
6. Incubate the plate at 37°C for 20–30 min. Protect from light.
7. To stop the reaction, add 15 µl of 1 N HCl to each well.
8. Record the absorbance at 490 nm using a microplate reader. Use a wavelength in the range of 630–750 nm (e.g., 690 nm) as a reference wavelength to account for the plate background, cell debris, nonspecific absorbance etc.
9. Plot the data in a suitable software (Figs. 5b and 6b).

3.5. Thioflavin-T Assay

1. Vortex the tubes containing culture medium removed in Subheading 3.2, step 6 from each test and control condition.
2. Mix 80 µl of the culture medium with 10 µl of 100 µM ThT (see Note 4) and 10 µl of 500 mM glycine–NaOH pH 8.5 in corresponding wells of a Nunc 384 black well plate (see Note 5). Each sample should be assayed in at least duplicates.
3. Acquire ThT fluorescence values in a suitable fluorescence microplate reader using an excitation wavelength 450 nm and emission wavelength 485 nm (see Note 6).
4. Plot the data in a suitable software (see Figs. 5c and 6c).

3.6. Transmission Electron Microscopy

1. Vortex the tubes containing culture medium removed in Subheading 3.2, step 6 from each test and control condition.
2. On a formvar-coated TEM grid, apply 2–10 µl of one of the samples and let the droplet settle for ~60 s (see Note 7).
3. Then, using a blotting paper gently wick the edge of the sample grid and remove excess solution.
4. Apply a 10 µl droplet of negative-staining solution (e.g., 2% wt/vol. UA) and let it settle for ~60 s on the grid surface (see Note 8).
5. Remove the excess solution as in step 3 above.

6. Using a fine vacuum probe, gently vacuum dry the grid from the edges. Sample grids not examined immediately can be stored in a storage box in a dry place (e.g., a desiccating chamber).
7. Acquire images on a CM10 TEM (or equivalent TEM), equipped with a CCD camera, operated at an acceleration voltage of 80–100 kV (Figs. 5d–h and 6d, e).

4. Notes

1. Other cell lines of neural origin (e.g., human neuroblastoma SHSY5Y cells) and/or primary neurons can be used as well. For culturing primary neurons, see the methods described elsewhere (21).
2. Excessive dilution of Aβ samples can be avoided by preparing the Aβ stock samples in supplemented 10× DMEM (e.g., Sigma, cat. no. D2429) (10) or modified 100× neurobasal medium (21).
3. Alternatively, commercially available kits can also be used with appropriate modifications to the procedure (e.g., Promega, cat. no. G4000).
4. A 100 μM stock solution of ThT can be prepared as follows: Dissolve 0.32 mg of ThT in 10 ml of ultrapure H_2O and vortex until a particulate-free solution is achieved. Filter the solution using a 0.22-μm PES syringe filter. Aliquot the volume needed for the day (Subheading 3.5, step 2) and store the rest at 4°C. The solution can be stored at 4°C for 2–3 months. The presence of precipitates warrants immediate disposal. Protect from light by wrapping the tube in aluminum foil. To prepare 500 mM glycine–NaOH pH 8.5 solution, dissolve 376 mg of glycine in 10 ml of ultrapure H_2O until clear. Bring the pH to 8.5 by drop by drop addition of 1 N NaOH and continuous mixing. Filter the solution with a 0.22-μm PES syringe filter and store at 4°C. Remove the volume needed for the day (Subheading 3.5, step 2), and store the rest at 4°C for up to 2–3 months. Presence of precipitates warrants immediate disposal.
5. The described step is optimized for final concentration of Aβ ≤ 10 μM, ThT:Aβ ratio ≥ 1 and final glycine–NaOH concentration being 50 mM. The step can be modified to accommodate different concentrations of Aβ. For example: For a sample of 50 μM Aβ, either dilute the sample with normal culture medium to 10 μM and proceed as above or use 70 mM glycine–NaOH stock solution (20 μl Aβ + 70 μl glycine–NaOH + 10 μl ThT (100 μM).

6. In addition to the excitation and emission wavelengths, adjust the settings of the fluorometer as follows: (1) number of reads (5–10); (2) plate (Nunc 384-well black); (3) Z-height (middle of the well); (4) integration time (100 ms); and (5) reading interval (10 × 10 ms).
7. To reduce the TEM grid surface contamination and hydrophobicity, it is recommended to apply the glow discharge the grids prior to the sample application.
8. A 2% wt/vol. UA stock solution can be prepared as follows: Dissolve 200 mg of UA in 10 ml of ultrapure H_2O and vortex until a particulate-free solution is achieved. Filter the solution using a syringe-driven 0.22-μm PES filter and store at 4°C. The solution should be prepared as needed and can be stored at 4°C for 1 month. Dispose of the solution as per institutional regulations. Wear gloves while handling.

Acknowledgments

This work was supported by the Swiss Federal Institute of Technology Lausanne (EPFL) and grants from the Swiss National Foundation (Grant# 310000-110027). The authors thank AC Immune (S.A.), Lausanne, Switzerland for financially supporting Asad Jan. We also thank Prof. Andrea Pfeifer, Dr. Andreas Muhs, and Dr. Oskar Adolfsson from AC Immune (S.A.), Lausanne Switzerland for thoughtful discussions.

References

1. Selkoe, D. J. (1991) Amyloid protein and Alzheimer's disease, *Sci.Am.* **265**, 68–66, 78.
2. Hardy, J. A., and Higgins, G. A. (1992) Alzheimer's disease: the amyloid cascade hypothesis, *Science* **256**, 184–185.
3. Selkoe, D. J. (2001) Alzheimer's disease: genes, proteins, and therapy, *Physiol Rev* **81**, 741–766.
4. Walsh, D. M., Lomakin, A., Benedek, G. B., Condron, M. M., and Teplow, D. B. (1997) Amyloid beta-protein fibrillogenesis. Detection of a protofibrillar intermediate, *J Biol Chem* **272**, 22364–22372.
5. Lambert, M. P., Barlow, A. K., Chromy, B. A., Edwards, C., Freed, R., Liosatos, M., Morgan, T. E., Rozovsky, I., Trommer, B., Viola, K. L., Wals, P., Zhang, C., Finch, C. E., Krafft, G. A., and Klein, W. L. (1998) Diffusible, nonfibrillar ligands derived from Abeta1–42 are potent central nervous system neurotoxins, *Proc.Natl. Acad.Sci.U.S.A* **95**, 6448–6453.
6. Lashuel, H. A., Hartley, D. M., Petre, B. M., Wall, J. S., Simon, M. N., Walz, T., and Lansbury, P. T., Jr. (2003) Mixtures of wild-type and a pathogenic (E22G) form of Abeta40 in vitro accumulate protofibrils, including amyloid pores, *J.Mol.Biol.* **332**, 795–808.
7. Bitan, G., Kirkitadze, M. D., Lomakin, A., Vollers, S. S., Benedek, G. B., and Teplow, D. B. (2003) Amyloid beta -protein (Abeta) assembly: Abeta 40 and Abeta 42 oligomerize through distinct pathways, *Proc.Natl.Acad.Sci. USA* **100**, 330–335.
8. Jan, A., Gokce, O., Luthi-Carter, R., and Lashuel, H. A. (2008) The ratio of monomeric to aggregated forms of Abeta40 and Abeta42 is an important determinant of amyloid-beta aggregation, fibrillogenesis, and toxicity, *J Biol Chem* **283**, 28176–28189.
9. Wogulis, M., Wright, S., Cunningham, D., Chilcote, T., Powell, K., and Rydel, R. E. (2005) Nucleation-dependent polymerization is an

essential component of amyloid-mediated neuronal cell death, *J Neurosci* **25**, 1071–1080.

10. Jan, A., Adolfsson, O., Allaman, I., Buccarello, A. L., Magistretti, P. J., Pfeifer, A., Muhs, A., and Lashuel, H. A. (2010) A{beta}42 neurotoxicity is mediated by ongoing nucleated polymerization process rather than by discrete A{beta}42 species, *J Biol Chem* **286**, 8585–8596.
11. Lemere, C. A., Blusztajn, J. K., Yamaguchi, H., Wisniewski, T., Saido, T. C., and Selkoe, D. J. (1996) Sequence of deposition of heterogeneous amyloid beta-peptides and APO E in Down syndrome: implications for initial events in amyloid plaque formation, *Neurobiol Dis* **3**, 16–32.
12. McLean, C. A., Cherny, R. A., Fraser, F. W., Fuller, S. J., Smith, M. J., Beyreuther, K., Bush, A. I., and Masters, C. L. (1999) Soluble pool of Abeta amyloid as a determinant of severity of neurodegeneration in Alzheimer's disease, *Ann.Neurol.* **46**, 860–866.
13. Moechars, D., Dewachter, I., Lorent, K., Reverse, D., Baekelandt, V., Naidu, A., Tesseur, I., Spittaels, K., Haute, C. V., Checler, F., Godaux, E., Cordell, B., and Van Leuven, F. (1999) Early phenotypic changes in transgenic mice that overexpress different mutants of amyloid precursor protein in brain, *J Biol Chem* **274**, 6483–6492.
14. Holcomb, L., Gordon, M. N., McGowan, E., Yu, X., Benkovic, S., Jantzen, P., Wright, K., Saad, I., Mueller, R., Morgan, D., Sanders, S., Zehr, C., O'Campo, K., Hardy, J., Prada, C. M., Eckman, C., Younkin, S., Hsiao, K., and Duff, K. (1998) Accelerated Alzheimer-type phenotype in transgenic mice carrying both mutant amyloid precursor protein and presenilin 1 transgenes, *Nat.Med.* **4**, 97–100.
15. Walsh, D. M., Klyubin, I., Fadeeva, J. V., Cullen, W. K., Anwyl, R., Wolfe, M. S., Rowan, M. J., and Selkoe, D. J. (2002) Naturally secreted oligomers of amyloid beta protein potently inhibit hippocampal long-term potentiation in vivo, *Nature* **416**, 535–539.
16. Nilsberth, C., Westlind-Danielsson, A., Eckman, C. B., Condron, M. M., Axelman, K., Forsell, C., Stenh, C., Luthman, J., Teplow, D. B., Younkin, S. G., Naslund, J., and Lannfelt, L. (2001) The 'Arctic' APP mutation (E693G) causes Alzheimer's disease by enhanced Abeta protofibril formation, *Nat Neurosci* **4**, 887–893.
17. Walsh, D. M., Hartley, D. M., Kusumoto, Y., Fezoui, Y., Condron, M. M., Lomakin, A., Benedek, G. B., Selkoe, D. J., and Teplow, D. B. (1999) Amyloid beta-protein fibrillogenesis. Structure and biological activity of protofibrillar intermediates, *J.Biol.Chem.* **274**, 25945–25952.
18. Hartley, D. M., Walsh, D. M., Ye, C. P., Diehl, T., Vasquez, S., Vassilev, P. M., Teplow, D. B., and Selkoe, D. J. (1999) Protofibrillar intermediates of amyloid beta-protein induce acute electrophysiological changes and progressive neurotoxicity in cortical neurons, *J.Neurosci.* **19**, 8876–8884.
19. Whalen, B. M., Selkoe, D. J., and Hartley, D. M. (2005) Small non-fibrillar assemblies of amyloid beta-protein bearing the Arctic mutation induce rapid neuritic degeneration, *Neurobiol Dis* **20**, 254–266.
20. Mucke, L. (2009) Neuroscience: Alzheimer's disease, *Nature* **461**, 895–897.
21. Jan, A., Hartley, D. M., and Lashuel, H. A. (2010) Preparation and characterization of toxic A[beta] aggregates for structural and functional studies in Alzheimer's disease research, *Nat. Protocols* **5**, 1186–1209.
22. Mosmann, T. (1983) Rapid colorimetric assay for cellular growth and survival: application to proliferation and cytotoxicity assays, *J Immunol Methods* **65**, 55–63.
23. Berridge, M. V., Herst, P. M., and Tan, A. S. (2005) Tetrazolium dyes as tools in cell biology: new insights into their cellular reduction, *Biotechnol Annu Rev* **11**, 127–152.
24. Wu, B., Zhu, J. S., Zhang, Y., Shen, W. M., and Zhang, Q. (2008) Predictive value of MTT assay as an in vitro chemosensitivity testing for gastric cancer: one institution's experience, *World J Gastroenterol* **14**, 3064–3068.
25. Mueller, H., Kassack, M. U., and Wiese, M. (2004) Comparison of the usefulness of the MTT, ATP, and calcein assays to predict the potency of cytotoxic agents in various human cancer cell lines, *J Biomol Screen* **9**, 506–515.
26. Chromy, B. A., Nowak, R. J., Lambert, M. P., Viola, K. L., Chang, L., Velasco, P. T., Jones, B. W., Fernandez, S. J., Lacor, P. N., Horowitz, P., Finch, C. E., Krafft, G. A., and Klein, W. L. (2003) Self-assembly of Abeta(1–42) into globular neurotoxins, *Biochemistry* **42**, 12749–12760.
27. Green, P. S., Perez, E. J., Calloway, T., and Simpkins, J. W. (2000) Estradiol attenuation of beta-amyloid-induced toxicity: a comparison o, *J Neurocytol* **29**, 419–423.
28. Janjic, D., and Wollheim, C. B. (1992) Islet cell metabolism is reflected by the MTT (tetrazolium) colorimetric assay, *Diabetologia* **35**, 482–485.
29. Decker, T., and Lohmann-Matthes, M. L. (1988) A quick and simple method for the quantitation of lactate dehydrogenase release in measurements of cellular cytotoxicity and tumor necrosis factor (TNF) activity, *J Immunol Methods* **115**, 61–69.

30. Lappalainen, K., Jaaskelainen, I., Syrjanen, K., Urtti, A., and Syrjanen, S. (1994) Comparison of cell proliferation and toxicity assays using two cationic liposomes, *Pharm Res* **11**, 1127–1131.

31. Jurisic, V. (2003) Estimation of cell membrane alteration after drug treatment by LDH release, *Blood* **101**, 2894; author reply 2895.

32. Kehrer, G., Blech, M., Kallerhoff, M., and Bretschneider, H. J. (1989) Urinary LDH-release for evaluation of postischemic renal function, *Klin Wochenschr* **67**, 477–485.

33. Lobner, D. (2000) Comparison of the LDH and MTT assays for quantifying cell death: validity for neuronal apoptosis?, *J Neurosci Methods* **96**, 147–152.

34. Legrand, C., Bour, J. M., Jacob, C., Capiaumont, J., Martial, A., Marc, A., Wudtke, M., Kretzmer, G., Demangel, C., Duval, D., and et al. (1992) Lactate dehydrogenase (LDH) activity of the cultured eukaryotic cells as marker of the number of dead cells in the medium [corrected], *J Biotechnol* **25**, 231–243.

35. Terry, R. D., Gonatas, N. K., and Weiss, M. (1964) Ultrastructural Studies in Alzheimer's Presenile Dementia, *Am J Pathol* **44**, 269–297.

36. Haass, C., and Selkoe, D. J. (2007) Soluble protein oligomers in neurodegeneration: lessons from the Alzheimer's amyloid beta-peptide, *Nat Rev Mol Cell Biol* **8**, 101–112.

37. Lashuel, H. A., and Wall, J. S. (2005) Molecular electron microscopy approaches to elucidating the mechanisms of protein fibrillogenesis, *Methods Mol Biol* **299**, 81–101.

38. Maezawa, I., Hong, H. S., Liu, R., Wu, C. Y., Cheng, R. H., Kung, M. P., Kung, H. F., Lam, K. S., Oddo, S., Laferla, F. M., and Jin, L. W. (2008) Congo red and thioflavin-T analogs detect Abeta oligomers, *J Neurochem* **104**, 457–468.

39. Yamamoto, T., and Hirano, A. (1986) A comparative study of modified Bielschowsky, Bodian and thioflavin S stains on Alzheimer's neurofibrillary tangles, *Neuropathol Appl Neurobiol* **12**, 3–9.

40. Uversky, V. N., Li, J., Souillac, P., Millett, I. S., Doniach, S., Jakes, R., Goedert, M., and Fink, A. L. (2002) Biophysical properties of the synucleins and their propensities to fibrillate: inhibition of alpha-synuclein assembly by beta- and gamma-synucleins, *J Biol Chem* **277**, 11970–11978.

41. Biancalana, M., and Koide, S. (2010) Molecular mechanism of Thioflavin-T binding to amyloid fibrils, *Biochim Biophys Acta* **1804**, 1405–1412.

42. Andersen, C. B., Yagi, H., Manno, M., Martorana, V., Ban, T., Christiansen, G., Otzen, D. E., Goto, Y., and Rischel, C. (2009) Branching in amyloid fibril growth, *Biophys J* **96**, 1529–1536.

43. Hawkes, C. A., Deng, L. H., Shaw, J. E., Nitz, M., and McLaurin, J. (2010) Small molecule beta-amyloid inhibitors that stabilize protofibrillar structures in vitro improve cognition and pathology in a mouse model of Alzheimer's disease, *Eur J Neurosci* **31**, 203–213.

Chapter 17

Preparation of Cultured Human Vascular Cells

Ingvar H. Olafsson, Dadi Th. Vilhjalmsson, and Finnbogi R. Thormodsson

Abstract

Cerebral amyloid angiopathy (CAA) results from amyloid accumulation within arteries of the cerebral cortex and leptomeninges. This condition is age-related, especially prevalent in Alzheimer's disease (AD), and the main feature of certain hereditary disorders (i.e., HCHWA-I). The vascular smooth muscle cells (VSMCs) appear to play a vital role in the development of CAA, which makes them well suited as an experimental model to study the disease and screen for possible remedies. We describe two different methods for isolating and culturing human VSMCs. First, using the human umbilical cord as an easy source of robust cells, and secondly, using brain tissue that provides the proper cerebral VSMCs, but is more problematic to work with. The umbilical cord also provides human umbilical vascular endothelial cells (HUVECs), useful primary cells for vascular research. Finally, the maintenance, preservation, and characterization of the isolated vascular cells are described.

Key words: Amyloid, Cell culture, Human, Cystatin C, Human umbilical vascular endothelial cells, Vascular smooth muscle cells, Umbilical cord, Cerebral amyloid angiopathy, HCHWA-I, Immunostaining, Leptomeninges, Cerebral blood vessels

1. Introduction

The accumulation of amyloid within cerebral vascular walls is the central feature of cerebral amyloid angiopathy (CAA) and is found associated with over 90% of brains from patients with Alzheimer's disease. Similarly, CAA is found in Down's syndrome, few other cerebrovascular maladies and otherwise unaffected aging brains (1). Apart from those principally sporadic CAAs, an increasing number of rare familial conditions have been identified (2), two of which are hereditary cerebral hemorrhage with amyloidosis-Dutch type (HCHWA-D) (3) and Icelandic type (HCHWA-I), also known as hereditary cystatin C amyloid angiopathy (HCCAA) (4, 5).

Einar M. Sigurdsson et al. (eds.), *Amyloid Proteins: Methods and Protocols*, Methods in Molecular Biology, vol. 849,
DOI 10.1007/978-1-61779-551-0_17,

The amyloid fibrils accumulate in the media of the vessel walls eventually replacing the vascular smooth muscle cells (VSMCs) suggesting a causal relationship between the muscle cells and the amyloid (6, 7). The VSMC might be the source or a partial source of the amyloid material and subsequently the victims of its accumulation. In an effort to study different aspects of this interaction, several research groups have established cellular models, utilizing VSMC from various sources. Cerebral VSMC from aged dogs have served as a model for Alzheimer's CAA to study their ability to produce amyloid-β protein (Aβ) (8), human VSMCs have been used to establish the toxic effects of the Aβ (9) and we are using cerebral VSMC for studying HCHWA-I (10). Here we present methods to obtain human VSMC from two distinct sources. The umbilical cord which is a good source of robust VSMC and human brain leptomeningal tissue containing the small arteries that play central role in the pathology of CAA. This umbilical cord also produces human umbilical vascular endothelial cells (HUVECs), an important cell culture model for studying vascular function and pathology.

2. Materials

2.1. Special Equipment and Supplies

1. Autoclave.
2. Inverted microscope.
3. Laminar flow cabinet (clean hood).
4. CO_2 Incubator.
5. Water bath at 37°C.
6. Centrifuge for 12–15-ml tubes.
7. Dissecting microscope (optional).
8. Fluorescence microscope.
9. Automated cell counter or hemocytometer.
10. Sterile scalpels.
11. For the umbilical cord: Two sets of sterile blunt needles with a valve (see Note 1) and straight 5"–7" hemostatic forceps.
12. For the brain: Sterile microdissecting forceps and scissors.
13. Disposable sterile syringes, 25 and 50 ml.
14. Syringe filter 0.2 μm.
15. Sterilized 250-ml glass beakers.
16. Disposable sterile centrifuge tubes, 12–15 and 50 ml.
17. Glass coverslips, 22 × 22 mm, cleaned in acid (see Subheading 3.3.4).

18. Glass beaker, 500 ml.
19. Disposable plastic Petri dishes about 55 cm^2.
20. Disposable 9-cm^2 culture dishes or 25-cm^2 flasks (see Note 2).

2.2. Reagents

1. Hanks balanced salt solution (HBSS).
2. HBSS w/o Ca^{2+} & Mg^{2+}.
3. Sterile saline solution (150 mM NaCl).
4. Chymotrypsin solution (0.2 mg/ml): Dissolve 8 mg α-Chymotrypsine (type II at ≥40 U/mg, Sigma C-4129) in 40 ml of Ca^{2+} and Mg^{2+}-free HBSS and sterilize by using a syringe and a 0.2-μm ultra syringe filter. Make fresh each time.
5. Collagenase solution (0.4 mg/ml): Dissolve 16 mg collagenase (type IA at ≥125 U/mg, Sigma C-2674) in 40 ml Ca^{2+} and Mg^{2+}-free HBSS and filter sterilize as above. Make fresh each time.
6. Dulbecco's Modified Eagle's Medium (DMEM) w/ GLUTAMAXI™ (Invitrogen 31966-021).
7. Fetal bovine serum (FBS).
8. Endothelial cell growth supplement (ECGS) (Sigma E-2759). Reconstitute the contents (15 mg) of the vial in 3 ml of HBSS, filter sterilize, and keep frozen at –20°C in 400 μl aliquots.
9. Penicillin/streptomycin solution (5,000 U/5,000 μg).
10. Culture medium for umbilical VSMC: Place 4 ml of FBS into 50 ml disposable centrifuge tube, add 400 μl of penicillin/streptomycin, and fill to the 40 ml mark with DMEM. Make fresh each time.
11. Culture medium for umbilical vascular endothelial cells (HUVEC): Place 8 ml of FBS into 50 ml disposable centrifuge tube, add 400 μl of penicillin/streptomycin, 1 ml of 1 M HEPES solution, 400 μl reconstituted ECGS, and fill to the 40 ml mark with Medium 199 w/GLUTAMAXI (Invitrogen/Gibco 41150-020). Make fresh each time (see Note 3).
12. Enzyme solution for cerebral VSMC: Place 10 ml of DMEM in a sterile centrifuge tube and add 0.1 ml of penicillin/streptomycin solution along with 150 μl of 1 M HEPES buffer solution. Weigh 10 mg of Protease (Dispase) (at ~0.4 U/mg, Sigma P-3417) and 20 mg of Collagenase (type IA, Sigma C-2674) and add to the tube. Mix the enzyme solution thoroughly and filter sterilize.
13. Insulin-like growth factor-I (IGF-I) (Sigma I-3769). Prepare a stock solution by reconstituting the 50 μg of IGF-I in 100 μl of 0.1 M sterile filtered acetic acid (228 μl glacial acetic acid in 40 ml water). In this form, it will keep for maximum of 3 months in the refrigerator but for an extended period in the freezer. Since repeated freezing and thawing is not recommended it should be frozen in working aliquots.

14. Hydrocortisone (Sigma H-0135). Hydrocortisone stock solution is prepared by dissolving 1 mg hydrocortisone in 1.0 ml absolute ethanol and adding 19 ml DMEM. Keep frozen in working aliquots.
15. Culture medium for cerebral VSMC: Place 4 ml of FBS into a 50 ml sterile centrifuge tube and fill to 40 ml with DMEM. Then add 0.4 ml of the penicillin/streptomycin solution, 40 μl of the hydrocortisone solution and 4 μl of the insulin-like growth factor solution. Make fresh each time (see Note 3).
16. Phosphate-buffered saline (PBS): $NaH_2PO_4 \cdot H_2O$ 3.1 g; Na_2HPO_4 (anhydrous) 10.9 g; NaCl 9.0 g; Fill to 1 l with distilled water. The pH should be 7.4 (adjust with 1 N HCl or 1 N NaOH if needed). Autoclave or sterilize by filtration before use. Will keep for 1 month at 4°C.
17. PBSA: Add 0.5 g bovine serum albumin (BSA) to 50 ml PBS. Make fresh and sterilize by filtration before use.
18. Trypsin–EDTA (0.25% trypsin, 1 mM EDTA), sterile.
19. Blocking solution: For each culture dish you need: PBSA 1 ml; normal goat serum (NGS) 50 μl; 20% Triton X-100 in PBS 5 μl.
20. Trypan blue stain, 0.4%.
21. Dimethyl sulfoxide (DMSO).
22. Nitric acid.
23. Hydrochloric acid.
24. Methanol at –20°C.
25. Monoclonal anti-α-smooth muscle actin (Sigma A-2547).
26. Alexa Fluor 546 goat anti-mouse IgG (Molecular Probes A-1018).
27. Vectrashield mounting medium with DAPI (Vector H-1200).
28. Clear nail polish.

3. Methods

This section describes methods for isolating human VSMC from two different sources. Cells from umbilical cord are relatively easy to work with and more readily available. These cells may often be adequate as experimental paradigm to tackle various questions related to CAA. Moreover, the procedure also provides HUVECs. We also describe a method for extracting VSMC from human brain tissue that are more difficult to isolate and adequate tissue samples more difficult to secure, but represent the SMC cells directly involved in CAA.

3.1. Vascular Cells Extracted from Umbilical Cord

Culture of pure endothelial cells is obtained by stripping away the endothelial lining from the blood vessel lumen prior to the smooth muscle cell extraction. Chymotrypsin detaches the endothelial cells without penetrating the collagen-rich basal lamina leaving the smooth muscle cells intact (11). Digestion with collagenase will subsequently yield a culture of smooth muscle cells with degree of purity that rests solely on the success of the previous endothelial removal. The following method is limited to one umbilical cord, but in practice we usually harvest cells from few cords in each session.

3.1.1. Preparing the Umbilical Cord

1. Start the procedure by taking all the necessary reagents out of the freezer or refrigerator and place in the clean hood. Then fill a 250-ml glass beaker with sterilized saline and secure in the 37°C water bath. While things are warming up the umbilical cord is fetched.
2. Cut the umbilical cord from the placenta that was placed in a plastic bag and transported on ice to the laboratory.
3. Rinse the cord thoroughly in running tap water, making sure that no water enters the blood vessels and do one final wash with sterile saline.
4. Wipe the cord with a clean paper towel. Now, all subsequent work is performed on a clean surface using only sterile material and instruments, starting by cutting few centimeters from each end of the cord with a sterile scalpel.
5. Thread a blunt needle, attached to a valve, into one of the two arteries (see Note 4), and seal with hemostatic forceps (Fig. 1a).
6. Attach a saline filled 50-ml syringe to the valve and rinse the blood vessel clean of all blood. The other end of the same blood vessel is fitted in the same way with a blunt needle plus a valve and now the umbilical cord is ready for the enzymatic treatment.

3.1.2. Digestion

1. Close the valve at one end of the umbilical cord and attach a syringe with the chymotrypsin solution to the other end. Subsequently, the blood vessel is filled with the enzyme solution under enough pressure to balloon the cord (Fig. 1b), but without breaking the seal. Remove the syringe after closing the valve.
2. Place the cord in the saline-filled beaker in the 37°C water bath, arranging the hemostatic forceps across the beaker to secure the cord (Fig. 1c).
3. Leave to incubate for 20 min and then decant the enzyme solution through one of the valves into sterile 12–15-ml centrifuge tubes and sediment the cells at 140 × *g* for 5 min in the centrifuge (see Note 5). Continue under Subheading 3.1.3.
4. Fill the blood vessel twice with HBSS and squeeze out the liquid to wash away any residual endothelial cells.

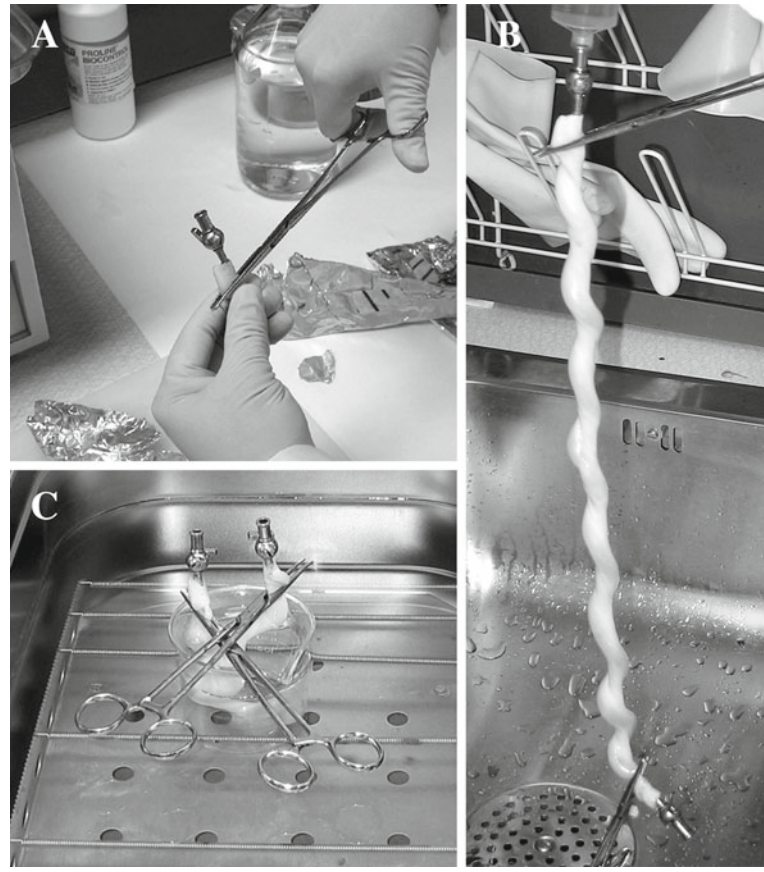

Fig. 1. (**a**) Thread a blunt-ended needle, fitted with a valve, into one of the arteries and seal with hemostatic forceps. (**b**) Fill a blood vessel of the cord to its full capacity with the enzyme solution. (**c**) The hemostatic forceps are used to secure the cord by crossing them on *top* of the saline-filled beaker. The saline solution in the beaker is maintained at 37°C in the water bath.

5. Now, fill the blood vessel with the collagenase solution and placed in the 37°C saline, as described above, and incubate for 10 min.
6. Decant the enzyme solution containing the smooth muscle cells into sterile 12–15-ml centrifuge tubes and sediment the cells at 140×*g* for 5 min in the centrifuge. Continue under Subheading 3.1.4.

3.1.3. Culturing the Umbilical Vascular Endothelial Cells

1. Discard the supernatant and resuspend the cells in 3 ml of the umbilical vascular endothelial cell culture medium prepared as described above (Subheading 2.2, item 11).
2. Transfer the cell suspension into one 25-cm^2 culture flask and add 3 ml of prepared culture medium to make a total of 6 ml (see Note 6). If the cells are being prepared for microscopic evaluation, place acid treated coverslip (22×22 mm) into each

of three disposable 9-cm^2 culture dishes, and put 1 ml of the cell suspension, along with 2 ml of the prepared culture medium, in each dish (see Notes 6 and 7).

3. Place the cells in the CO_2 incubator, set at 37°C and 5% CO_2.

3.1.4. Culturing the Umbilical VSMC

1. Discard the supernatant and resuspend the cells in 3 ml of the umbilical VSMC culture medium prepared as described above (Subheading 2.2, item 10).
2. Transfer the cell suspension into one 25-cm^2 culture flask and add 3 ml of prepared culture medium to make a total of 6 ml (see Note 6). If the cells are being prepared for microscopic evaluation, place acid treated coverslip (22×22 mm) into each of three disposable 9-cm^2 culture dishes, and put 1 ml of the cell suspension, along with 2 ml of the prepared culture medium, in each dish (see Notes 6 and 7).
3. Placed the cells in the CO_2 incubator, set at 37°C and 5% CO_2.

3.1.5. Maintaining the Cells

On the second day in culture change the medium to remove any cell debris. Wash the cells once with HBSS before adding the fresh culture medium. The umbilical VSMC will loose the typical smooth muscle phenotype in few days and enter a fibroblast-like synthetic state and commence exponential growth reaching confluence in the second week. If the cells will be passed on to produce more cells in subcultures they are not allowed to be become fully confluent and then proceed as described in Subheading 3.3.1. However, if the cells are being prepared for staining, or other experimental procedure, grow them to full confluence and for the last 2 days exchange the culture media with serum-free media (prepare the media as before, but omitting the FBC). This should return them to the spindle shape contractile phenotype (Fig. 2).

3.2. VSMCs Isolated from Human Brain Tissue

For isolation and culturing of human cerebral VSMC, we use a method outlined by Van Nostrand et al. (12) and present it here as we have come to apply it.

3.2.1. Set Up

Prior to fetching the tissue sample, autoclaved fine instruments (forceps and scissors), arrange a tray for crushed ice under a dissecting microscope (with practice we find it possible to forgo the microscope), and prepare the protease/collagenase solution (Subheading 2.2, item 10) aseptically in the laminar hood and place it on ice.

3.2.2. Preparation and Digestion of the Sample

Brain sample should be as fresh as possible, either from autopsy few hours postmortem or from surgical brain operation. Make sure that the sample is from the cortical surface containing mostly leptomeningal tissue.

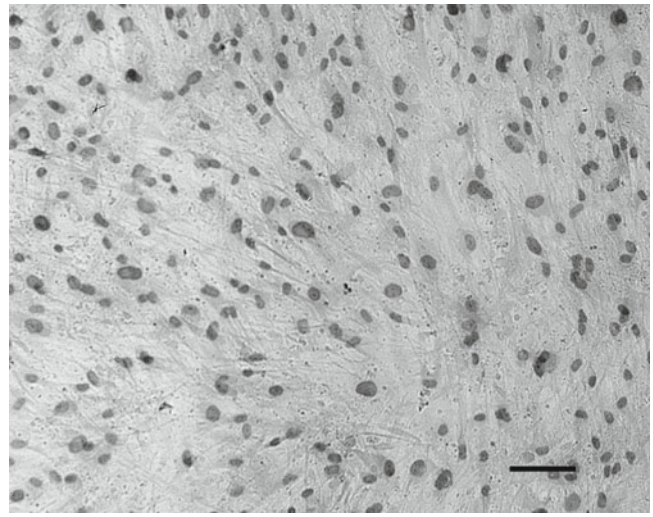

Fig. 2. Confluent culture of H&E-stained vascular smooth muscle cells. *Bar* = 100 μm.

1. Place the sample aseptically into a bottle of cold sterile HBSS and transport on ice to the tissue culture facility.
2. Transfer the tissue sample into a sterile Petri dish containing ice cold HBSS and peel the leptomeninges from the residual cortical tissue. Move 1–2 cm^2-meningal tissue to another HBSS-filled Petri dish and place it on crushed ice under the microscope.
3. Take fine forceps in each hand and tease the meningal tissue apart to free the blood vessels from the supporting tissue. This is the most critical part of the procedure requiring both patience and great care.
4. Transfer the fragments of blood vessels to the cold enzyme solution and cut the larger ones into smaller pieces with fine scissors.
5. Incubate the tube on ice for 90 min to ensure that the enzymes penetrate the tissue fragments before they are activated at elevated temperature.
6. Transfer the tube to the 37°C water bath and incubate for additional 2 h to digest the tissue.
7. While the sample is incubating, prepare the culture medium as described in Subheading 2.2, item 13.

3.2.3. Culturing the Cells

1. Following the incubation at 37°C, triturate the tissue fragments by vigorously pipetting up and down to brake up the tissue and liberate the cells.
2. Transfer the tube to a centrifuge and pull down the tissue debris at 140 × *g* for 5 min.

3. Discard the supernatant and suspend the tissue pellet in 1 ml of the prepared culture medium. Triturate again by pulling the mixture few times into the pipette tip.
4. Place the tissue suspension in 25-cm^2 culture flask (see Note 8), making the final volume 6 ml by adding prepared culture medium. Alternatively, seed the cells into a dish with a coverslip as described in Subheading 3.1.3 (see Note 7).
5. Finally, the place flasks in the incubator at 37°C and 5% CO_2.

3.2.4. Maintaining the Cells

The same procedure applies as in Subheading 3.1.4, except that these cells are usually not as vigorous with slower growth rate.

3.3. Miscellaneous Techniques

3.3.1. Subcultures of the Cells

When the cells are close to confluence they can be split into subcultures, which are also referred to as passing the cells. It is our experience that 1:3 splitting ratio suites the VSMCs well that is one culture is divided into three, but if needed they can easily be stretched into four cultures.

1. Warm the trypsin–EDTA solution to 37°C in the incubator, 3 ml for each flask of culture being split.
2. Transfer the culture flasks from the incubator to the laminar hood and discard the medium.
3. Wash the cells once in Ca^{2+} and Mg^{2+}-free HBSS and place 3 ml of the diluted trypsin solution into each flask.
4. After 30 s, decant the trypsin–EDTA and incubate the flasks at 37°C for 5–15 min or till the cells start to round up. Remove from the incubator at regular intervals to monitor the process, using the inverted microscope and help the cells to detach by tapping the flask gently on the tabletop. Trypsin causes cellular damage; so keep the time of exposure to a minimum (see also Note 9).
5. When most of the cells have rounded up, add 1-ml culture medium to the flask. Squirt the medium a few times down the culture surface of the flask, held at an angle, to pry the cells loose.
6. Dilute the cell suspension further with 2 ml of medium and divide them by transferring 1 ml to each of three new flasks. Finally, add 5 ml of medium to each flask to make the final volume 6 ml.
7. Place the flasks into the CO_2 incubator at 37°C.

3.3.2. Cell Counting

The cells need to be counted to determine the cell seeding density. Recently, we have started using automatic cell counters, such as the Countess® from Invitrogen (or the new TC10™ from Bio-Rad with auto-focusing) and find them both convenient and reliable (Fig. 3a). However, the classic way is using a hemocytometer.

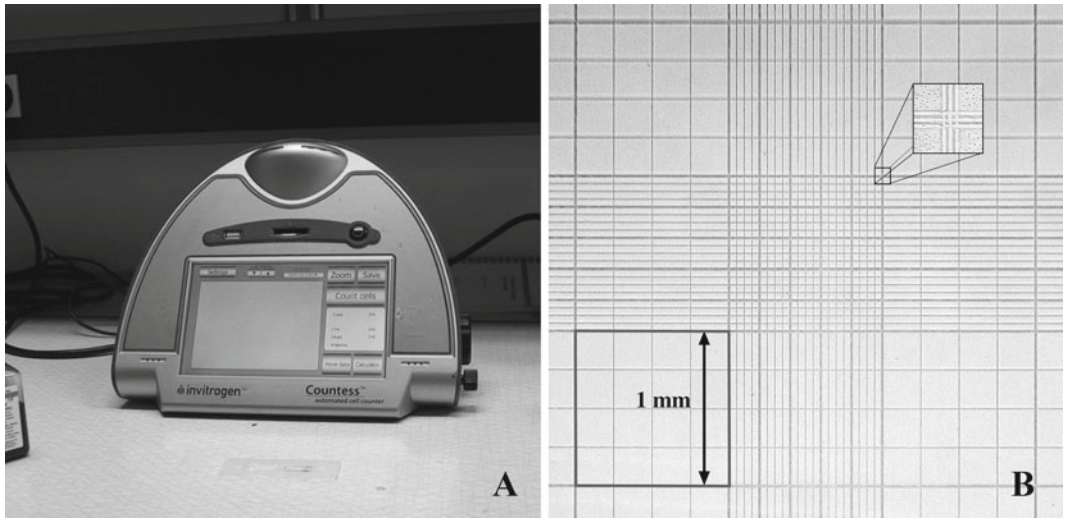

Fig. 3. (**a**) The automatic cell counter Countess® from Invitrogen that we use. (**b**) The *grid lines* in one of the two chambers of a standard hemocytometer. Count the cells in the center and the four corner 1 × 1 mm square. Do not count any cells touching the *middle* of the *triple line* (see *insert*) at the *bottom* and *right* of each *square*.

1. Start by putting 0.5 ml of 0.4% Trypan blue solution into a small tube along with 0.3 ml of HBSS and then add 0.2 ml of the cell suspension (dilution factor = 5) and mix carefully (see Note 9). Keep in mind that Trypan blue is harmful and protective gloves should be worn.
2. Clean the hemocytometer thoroughly with alcohol and put the coverslip in place on top of it to cover the two chambers.
3. Transfer a small amount of the cell mixture by a pipette tip to the edge of the coverslip and allow the chambers to fill by capillary action, making sure that they do not over- or under fill.
4. Count all the cells in the center 1 mm by 1-mm square and the four corner squares (Fig. 3b) in both chambers, ten squares in all. Cells that stain blue are either dead or not viable and are counted separately as such. Cells that touch the middle line of the triple lines at the top and on the left side of each square are not counted.

Since each square represents 0.1 mm^3 (approximatly10^{-4} ml), the number of cells per milliliter is calculated by:

$$\text{Cells per ml} = \text{the average count per square} \cdot \text{dilution factor} \cdot 10^4.$$

Best accuracy is acquired if each square contains between 20 and 50 cells. Adjust by chancing the dilution factor if needed.

3.3.3. Freezing and Thawing the Cells

Instead of passing the cells right away, it is possible to freeze them and use them later.

1. Detach the cells by trypsin, as described in Subheading 3.3.1, and suspend them in 3 ml of freezing solution, made up of 95% FCS and 5% DMSO, instead of culture medium. Caution: do not let DMSO come in contact with any part of you (it will penetrate many types of gloves).
2. Split the 3 ml of cell suspension between three 1.5-ml freezing tubes.
3. Freeze the cells in a –70°C freezer. To slow down the freezing rate, to the optimal –1°C/min, the tubes can be fitted into a close Styrofoam cube with a 2-cm wall thickness on each side.
4. Next day, the tubes are transported to liquid nitrogen, where they will keep for a long time.

When the cells are needed, thaw them rapidly.

1. Place the tube into a bucket containing 37°C water and cover with a lid. Protective goggles and gloves must be worn since the tubes can explode if liquid nitrogen is trapped inside.
2. Transfer the cell suspension to a culture flask and add 5 ml of medium slowly, drop by drop over 1 min.
3. Place the flask into the CO_2 incubator at 37°C.

3.3.4. Cleaning Coverslips with Acid

New coverslips may have a film of grease that will interfere with their binding capacity and cause background fluorescence.

1. Mix 200 ml nitric acid to 100 ml hydrochloric acid in a glass beaker. Caution: Concentrated acids are harmful. Use gloves and safety glasses and handle with great care in a chemical fume hood.
2. Place few coverslips at time in the acid mixture and let sit for about 2 h with intermittent swirling.
3. Pour out the acid into a waste container.
4. Wash the coverslips thoroughly in running tap water.
5. Store the coverslips in 70% ethanol.
6. Air dry each coverslip in the hood prior to use.

3.3.5. Immunostaining the Cells

The cells can be immunostained with a host of different antibodies. As an example we describe staining for a smooth muscle actin that serves to confirm the smooth muscle phenotype of the cells.

1. Discard the culture medium and wash the cells once in few milliliter of cold PBS.
2. After pouring off the washing solution, fix the cells in few milliliter of –20°C methanol for 10 min.

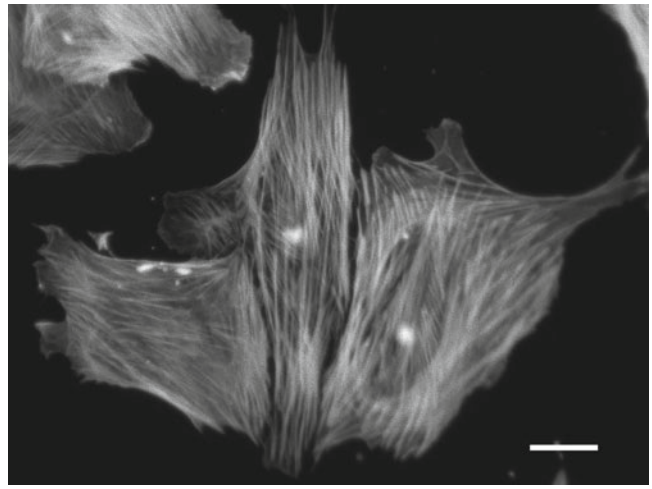

Fig. 4. Three vascular smooth muscle cells grouped together in a culture, immunostained with anti-α-smooth muscle actin. *Bar* = 10 μm.

3. Remove the methanol and wash the cells three times in PBS for 5 min each time and then once in PBSA.
4. To block unspecific staining add, 1 ml of blocking solution to each 9 cm^2 culture dish and incubate for 30 min at room temperature.
5. Dilute the primary antibody 1:400 by adding 2.5 μl mouse anti-α-smooth muscle actin to 1 ml PBSA.
6. Remove the blocking solution and add the diluted antibody, without washing the cells, and incubate at room temperature for 30 min or over night at 4°C (see Note 10).
7. Then wash the cells three times with PBSA for 5 min each time and add the secondary antibody at appropriate dilution. We use Alexa Fluor 546 goat anti-mouse at 1:500 dilution and incubate for 30 min in the dark.
8. Wash off excess secondary antibody by two 5 min washes in PBSA and one with PBS.
9. Take the coverslip with the stained cells out of the culture dish with forceps and shake excess wetness from the cells. The cell free side and edges of the coverslip are dried with a paper towel.
10. Place the coverslip on a table edge, put one drop of the mounting medium on the center and lower a reversed microscope slide on top of it. Try to let the coverslip attach without introducing any air bubbles.
11. Allow the mounting medium to harden for 15 min in the dark and then the cells are ready for the microscope (Fig. 4).

The mounted slides can be kept for later use at 4°C and protected from the light. It is advisable to seal the edges of the coverslip with clear nail polish to protect the sample from drying. The mounting medium will slow the fading of the fluorescence intensity making the stained slides usable for several weeks for most fluorescent reagents.

4. Notes

1. In our laboratory, we have old reusable 16 gauge 1.5" needles with a 2-mm ball to make the end blunt. A valve with a Luer lock is attached at the inlet end. We have not been able to find this item in any catalog but as an alternative, various blunt needles and valves can be locked together with Luer fittings. George Tiemann & Co. carries a valve with female Luer to male Luer needle lock (160-7021) and an appropriate straight ball pointed 18 gauge, 1.5" long needle, with a 2.25-mm ball (160-8904) or 16 gauge, 3" long needle, with a 3.0-mm ball (160-8908). Roboz has 16G, 2" needles with 3-mm ball, reusable (FN-7923) or disposable (FN-9918). Similar needles can also be obtained from Fine Science Tools.
2. We prefer Nunclon™Δ T-25 flasks with filter cap (Thermo Scientific/Nunc, 136196). The cells attach to this surface without any problem. If attachment is a problem there are various methods of coating the surface such as gelatin, poly-lysine, or collagen. Gelatin solution from Sigma (G-1393) is easy to use and several vendors carry precoded culture vessels.
3. Few suppliers carry special medium kits that enhance cell growth and allow the cells to grow at low serum concentration. For endothelial cells, Lonza has Clonetics® Endothelial Cell System and Invitrogen/Gibco has Low Serum Growth Supplement Kit. We have used the Clonetics® system with good results. Correspondingly, special culturing systems exist for VSMC. Invitrogen/Gibco has Medium 231 (M-231-500) that when used with a mixture of growth factors (SMGF, cat. # S-007-25) makes up a complete culture environment. Lonza offers the Clonetics® SmGM®-2 Smooth Muscle Growth Medium-2.
4. We occasionally use the large central vein, since it is more accessible and easier to work with. However, the arteries are richer in VSMC and there might be additional reasons for preferring cells of that origin. As an extra bonus there are two of them and we have succeeded in harvesting both in the same cord.

5. The force applied to a sample within a centrifuge is called relative centrifugal force (RCF) or g. This can be calculated in the following way: $g = \mathrm{RCF} = 0.00001118 \times r \times N^2$, where g is the relative centrifugal force, r is the rotational radius (cm), and N is the rotating speed (revolutions per minute, r/min). Many centrifuges can display RCF or come with a table that converts RCF to rpm for a given rotor.
6. Seeding densities of smooth muscle cells are extremely important and should be between 7,000 and 70,000 cells/cm^2. With too few cells they will go through too many population doublings and exceed their ability to return to the contractile phenotype before reaching confluence. To determine the proper dilution the cells are counted in an automated cell counter or a hemocytometer (see Subheading 3.3.2).
7. If the cells in the primary culture will in due course be prepared for light microscopic evaluation, then we grow them on glass coverslips and proceed as explained in Subheading 3.3.5. However, since the cells are usually passed few times before they are utilized for experiments, a better choice is the 25-cm^2 culture flask. In the final passing the cells are seeded on a coverslip as described.
8. As explained in Note 3, minimum-seeding density is crucial for a successful culture. However, the digested leptomeningal sample contains tissue fragments along with the liberated cells, making counting difficult. We bypass this problem by seeding them in a limited area, usually only one culture flask per digested sample. As soon as the cells have attached, the debris is washed away by changing the medium.
9. The smooth muscle cells tend to clump together, especially cells from confluent cultures. This makes them more difficult to count and for that reason it is important to trypsinize completely and then try to disperse the cells well in the trypan blue cell suspension by thorough mixing. But keep in mind that trypsin is harmful to the cells.
10. Double immunostaining can be performed by adding a second polyclonal antibody in appropriate dilution and incubating along with the anti-α-actin monoclonal antibody. A suitable secondary antibody is then used along with the anti-mouse Alexa Fluor 546, such as Alexa Fluor 488. The mounting medium that we employ contains DAPI nuclear stain for triple staining cells in a microscope with the right filter set.

Acknowledgments

We would like to thank The Icelandic Research Council and Heilavernd (The Icelandic HCHWA-I Foundation) for their support.

References

1. Vinters, H. V. (1987) Cerebral amyloid angiopathy: A critical review. *Stroke* **18**, 311–324.
2. Revesz, T., Holton, J. L., Lashley, T., Plant, G., Rostagno, A., Ghiso, J., and Frangione, B. (2002) Sporadic and familial cerebral amyloid angiopathies. *Brain Pathol* **12**, 343–357.
3. Levy, E., Carman, M. D., Fernandez-Madrid, I. J., Power, M. D., Lieberburg, I., van Duinen, S. G., Bots, G. T., Luyendijk, W., and Frangione, B. (1990) Mutation of the Alzheimer's disease amyloid gene in hereditary cerebral hemorrhage, Dutch type. *Science* **248**, 1124–1126.
4. Gudmundsson, G., Hallgrimsson, J., Jonasson, T. A., and Bjarnason, O. (1972) Hereditary cerebral hemorrhage with amyloidosis. *Brain* **95**, 387–404.
5. Bjarnadottir, M., Nilsson, C., Lindstrom, V., Westman, A., Davidsson, P., Thormodsson, F., Blondal, H., Gudmundsson, G., and Grubb, A. (2001) The cerebral hemorrhage-producing cystatin C variant (L68Q) in extracellular fluids. *Amyloid: Int. J. Exp. Clin. Invest.* **8**, 1–10.
6. Wisniewski, H. M., Fraçkowiak, J., Zòltowska, A., and Kim, K. S. (1994) Vascular ß-amyloid in Alzheimer's disease angiopathy is produced by proliferating and degenerating smooth muscle cells. *Amyloid: Int. J. Exp. Clin. Invest.* **1**, 8–16.
7. Wang, Z. Z., Jensson, O., Thorsteinsson, L., and Vinters, H. V. (1997) Microvascular degeneration in hereditary cystatin C amyloid angiopathy of the brain. *APMIS* **105**, 41–47.
8. Wisniewski, H. M., Frackowiak, J., and Mazur-Kolecka, B. (1995) In vitro production of β-amyloid in smooth muscle cells isolated from amyloid angiopathy-affected vessels. *Neuroscience Letters* **183**, 120–123.
9. Van Nostrand, W. E., Davis-Salinas, J., and Saporito-Irwin, S. M. (1996) Amyloid beta-protein induces the cerebrovascular cellular pathology of Alzheimer's disease and related disorders. *Ann N Y Acad Sci* 777, 297–302.
10. Vilhjalmsson, D. T., Blondal, H., and Thormodsson, F. R. (2007) Solubilized cystatin C amyloid is cytotoxic to cultured human cerebrovascular smooth muscle cells. *Experimental and Molecular Pathology* **83**, 357–360.
11. Mulder, A. B., Blom, N. R., Smit, J. W., Ruiters, M. H., van der Meer, J., Halie, M. R., and Bom, V. J. (1995) Basal tissue factor expression in endothelial cell cultures is caused by contaminating smooth muscle cells. Reduction by using chymotrypsin instead of collagenase, *Thromb. Res.* **80**, 399–411.
12. Van Nostrand, W. E., Rozemuller, A. J. M., Chung, R., Cotman, C. W., and Saporito-Irwin, S. M. (1994) Amyloid ß-protein precursor in cultured leptomeningeal smooth muscle cells, *Amyloid: Int. J. Exp. Clin. Invest.* **1**, 1–7.

Chapter 18

Murine Cerebrovascular Cells as a Cell Culture Model for Cerebral Amyloid Angiopathy: Isolation of Smooth Muscle and Endothelial Cells from Mouse Brain

Sebastien A. Gauthier, Susmita Sahoo, Sonia S. Jung, and Efrat Levy

Abstract

The use of murine cerebrovascular endothelial and smooth muscle cells has not been widely employed as a cell culture model for the investigation of cellular mechanisms involved in cerebral amyloid angiopathy (CAA). Difficulties in isolation and propagation of murine cerebrovascular cells and insufficient yields for molecular and cell culture studies have deterred investigators from using mice as a source for cerebrovascular cells in culture. Instead, cerebrovascular cells from larger mammals are preferred and several methods describing the isolation of endothelial and smooth muscle cells from human, canine, rat, and guinea pig have been published. In recent years, several transgenic mouse lines showing CAA pathology have been established; consequently murine cerebrovascular cells derived from these animals can serve as a key cellular model to study CAA. Here, we describe a procedure for isolating murine microvessels that yields healthy smooth muscle and endothelial cell populations and produce sufficient material for experimental purposes. Murine smooth muscle cells isolated using this protocol exhibit the classic "hill and valley" morphology and are immunoreactive for the smooth muscle cell marker α-actin. Endothelial cells display a "cobblestone" pattern phenotype and show the characteristic immunostaining for the von Willebrand factor and the factor VIII-related antigen. In addition, we describe methods designed to preserve these cells by storage in liquid nitrogen and reestablishing viable cell cultures. Finally, we compare our methods with protocols designed to isolate and maintain human cerebrovascular cell cultures.

Key words: Cerebral blood vessels, Cerebrovascular cells, Smooth muscle cells, Endothelial cells, Cerebral amyloid angiopathy

1. Introduction

In cerebral amyloid angiopathy (CAA), the deposition of amyloid proteins in the cerebral vasculature destabilizes the integrity of the blood vessel wall. It triggers degeneration of smooth muscle and endothelial cells and can lead to hemorrhagic stroke and death (reviewed in refs. 1, 2). A variety of proteins form the amyloid

Einar M. Sigurdsson et al. (eds.), *Amyloid Proteins: Methods and Protocols*, Methods in Molecular Biology, vol. 849,
DOI 10.1007/978-1-61779-551-0_18,

deposited in cerebral vasculature of patients with different forms of CAA. CAA is a common pathological hallmark of Alzheimer's disease (AD) caused by the deposition of amyloid β (Aβ), and population-based studies demonstrate that having both CAA and AD contributes to substantially worse cognitive performance than AD alone (3, 4). Familial forms of cerebral vascular Aβ amyloid deposition have mutations within the amyloid β precursor protein gene (APP), resulting in amino acid substitutions within Aβ. The first mutation was described in a family with hereditary cerebral hemorrhage with amyloidosis of the Dutch type (HCHWA-D) (5). Additional APP mutations associated with CAA were described in patients with familial AD (FAD) (6, 7). While Aβ is the most common amyloid forming peptide in the brain, other proteins can form cerebrovascular amyloid. In HCHWA of the Icelandic type (HCHWA-I) (8), also known as hereditary cystatin C amyloid angiopathy (HCCAA) (9), the deposited protein is a variant form of cystatin C (10, 11). The amyloid proteins deposited in the cerebral vasculature of patients with familial British and Danish dementias are ABri and ADan, respectively (12, 13). Gelsolin forms amyloid angiopathy in familial amyloidosis of the Finnish type (14). Mouse models of these diseases have been generated, each developing some of the symptoms of CAA pathology (15–21). In vitro studies using cerebrovascular cells isolated from these mice are crucial for the investigation of the mechanisms involved in the degeneration of cerebrovascular cells.

Previous studies on cerebrovascular smooth muscle cells from human brain obtained at autopsy (22, 23), canine (24–26), rat (27–29), and other large animals (30, 31) have been reported. However, these brain tissues may not be easily available to many researchers and the published methods used to obtain smooth muscle cells vary with the source of tissues. Overall, the technical challenges associated with the isolation and the propagation of murine cerebrovascular cells along with insufficient yields for molecular and cell culture studies have deterred investigators from using mice as a source of brain tissues for culturing cerebrovascular cells (32).

Here we describe a method for the isolation and propagation of cerebrovascular cells from murine brain tissues. Gentle enzymatic digestion and filtration through a glass bead column are used to collect cerebral microvessels that can produce either smooth muscle cells or endothelial cells depending on the culture medium. With this method, one round of cerebrovascular cell isolation from the brain of two to four adult mice of about 4 months of age can generate healthy smooth muscle and endothelial cells in high yield that can be maintained in culture for up to 15–20 passages for either immediate use or storage in liquid nitrogen for future use.

2. Materials

1. Murine brain tissue of 2–4 mice of about 4 months of age.
2. 70% Ethanol.
3. Sterile scalpels, forceps, tweezers, scissors.
4. 1× Sterile phosphate-buffered saline (PBS) without calcium and magnesium (Invitrogen, Piscataway, NJ, 10010-049).
5. 1× Sterile Hanks' Balanced Salt Solution (HBSS; Invitrogen/Gibco, 14175-145).
6. Fetal bovine serum (FBS), heat-inactivated (VWR-Mediatech, Batavia, IL, 45000-736).
7. Dulbecco's Modified Eagle's Medium (DMEM; Sigma-Aldrich, St. Louis, MO, D5671).
8. Penicillin base, 10,000 U/ml, and streptomycin base, 10,000 μg/ml (Invitrogen/Gibco, 15140-122).
9. GlutaMAX™, 200 mM (Invitrogen/Gibco, 35050-061).
10. Nonessential amino acids, 10 mM (Invitrogen/Gibco, 11140-050).
11. *N*-2-Hydroxyethylpiperazine-*N*′-2-ethane sulfonic acid (HEPES), pH 7.5, 1 M (Cellgro, Manassas, VA, 25-060-CI). Prepare a solution of 20 mM HEPES in DMEM. Store at 4°C.
12. DNase, Type I (Sigma-Aldrich, DN25). Prepare a 10 mg/ml stock solution in PBS, filter sterilize through a 0.22-μm membrane filter, aliquot and store at −20°C.
13. Endothelial cell growth supplement (ECGS) from bovine neural tissue (Sigma-Aldrich, E2759). Prepare stock solution of 3 mg/ml in sterile PBS and filter sterilize through a 0.22-μm membrane filter, aliquot and store at −20°C.
14. Prepare complete culture medium for culturing microvessels and smooth muscle cells: DMEM containing 10% FBS, 2 mM GlutaMAX™, 100 U/ml penicillin, 100 μg/ml streptomycin, 0.1 mM nonessential amino acids, and 50 μg/ml DNase I. Store at 4°C. Keep the medium at room temperature before starting the procedure.
15. Collagen (Invitrogen, A10483-01). Prepare a 0.167 mg/ml solution in ddH_2O to coat glass coverslips.
16. Heparin (Sigma, H-3933).
17. L-glutamine (Invitrogen/Gibco, 25030-081).
18. Sodium pyruvate (Invitrogen, 11360-070).
19. Prepare complete culture medium for culturing endothelial cells: High-glucose DMEM lacking Phenol red (Invitrogen/

Gibco, 31053-036) containing 20% FBS, 100 U/ml penicillin, 100 µg/ml streptomycin, 0.1 mM nonessential amino acids, 100 µg/ml Heparin, 100 µg/ml ECGS, 2 mM L-glutamine, 1× sodium pyruvate, and 25 mM HEPES. Store at 4°C. Keep the medium at room temperature before starting the procedure.

20. Collagenase/dispase (Roche Diagnostics, Indianapolis, IN, 1097113). Prepare a 100 mg/ml stock in ddH_2O, dilute with PBS to a concentration of 10 mg/ml. Sterilize through a 0.22-µm membrane filter, aliquot and store at –20°C. Prepare 0.05% collagenase/dispase in DMEM before starting the procedure. Store at room temperature.
21. 0.5 M EDTA, pH 8.0, sterile (Invitrogen, 15575-020). Prepare a fresh 5 mM EDTA solution in 20 mM HEPES in DMEM. Store on ice before use.
22. Dextran (Sigma-Aldrich, D3759). Prepare a fresh 17% dextran solution in 20 mM HEPES in DMEM. Sterilize through a 0.22-µm membrane filter unit and store on ice before use.
23. Trypsin, 2.5% (Invitrogen/Gibco, 15090-046). Keep at –20°C. Dilute 1:10 in HBSS and warm up to 37°C before use.
24. Poly-D-lysine (Sigma-Aldrich, P7886). Prepare a stock solution of 1 mg/ml poly-D-lysine in ddH_2O. Sterilize through a 0.22-µm membrane filter, aliquot, and store at –20°C. Prepare a 20 µg/ml solution in ddH_2O to coat glass slides.
25. Albumin, bovine, Fraction V (BSA) (Sigma-Aldrich, A7906). Prepare a 5% BSA solution in PBS to use as blocking solution for immunocytochemistry.
26. Cell culture grade dimethyl sulfoxide (DMSO) (Sigma, D2650).
27. Tissue culture dishes, 35 mm (BD-Falcon, Franklin Lakes, NJ, 353001).
28. Tissue culture dishes, 60 mm (BD-Falcon, 353002).
29. Tissue culture dishes, 100 mm (BD-Falcon, 353003).
30. 12-Well culture plates (BD-Falcon, 353043).
31. Vented tissue culture flasks, 75 cm^2 (BD-Falcon, 353136).
32. 50 ml Oak Ridge polycarbonate tubes (Thermo Fisher Scientific/Nalgene, Rochester, NY, 3118-0050). Sterilize by autoclaving.
33. 70-µm Nylon cell strainer (BD-Falcon, 352350).
34. 50-ml Conical tubes (BD-Falcon, 352098).
35. 1-ml Screw cap CryoTube™ Vials (Nunc, Denmark, 368632).
36. 2-Butanol (Sigma-Aldrich, 236691). Keep at room temperature.

37. 5100 Cryo 1°C Freezing Container (Thermo Fisher Scientific/Nalgene, 5100-0001). Fill the container with 2-butanol and store at –20°C before starting the procedure of freezing smooth muscle cells.
38. Glass beads, 425–600 μm, acid-washed (Sigma-Aldrich, G8772). Autoclave the glass beads in a small beaker. When ready to use, transfer the beads into a 70-μm nylon cell strainer and wash twice with sterile PBS and twice with complete culture medium.
39. 8-Well glass chamber slides (ThermoScientific/Lab-Tek II, Rochester, NY, 154534).
40. Gel/Mount (Biomeda, Foster City, CA, M01).
41. Cover slips (Fisher Scientific, Suwanee, GA).
42. Methanol, 100%, chilled at –20°C.
43. Anti-α smooth muscle actin antibody (Sigma-Aldrich, A2547).
44. Anti-human von Willebrand factor (Factor VIII-related antigen) antibody (Sigma-Aldrich, F3520).
45. Sheep anti-mouse Ig, fluorescein-linked whole antibody (Amersham Biosciences, Piscataway, NJ, N1031).
46. Texas Red anti-rabbit IgG (H+L) antibody (Vector Laboratories, Burlingame, CA, TI-1000).
47. Dynabeads® Sheep anti-Rat IgG (Invitrogen/Dynal, 110.35) at a concentration of 4×10^8 beads/ml.
48. Purified Rat anti-Mouse CD31/PECAM-1 antibody (Pharmingen, 553369) at 0.5 mg/ml.
49. Magnetic separator for 1.5-ml tubes (Invitrogen, K1585-01).
50. Buffer 1: PBS (without Ca and Mg), 0.1% BSA, and 2 mM EDTA, pH 7.4.

3. Methods

The following protocols describe the isolation of microvessels from mouse brain tissues (Subheading 3.1), the propagation of smooth muscle cells (Subheading 3.2), and endothelial cells (Subheading 3.3), a method to identify both types of cerebrovascular cells (Subheading 3.4), and a method to store smooth muscle cells in liquid nitrogen (Subheading 3.5). We recommend isolating cerebral microvessels from the brains of at least two age- and gender-matched mice to obtain a good yield of cerebral microvessels. All steps must be performed in a sterile environment including the removal of the mouse brain. All solutions should be filtered through a 0.22-μm membrane filter.

3.1. Isolation of Mouse Brain and Microvessels

1. Sacrifice a mouse by a method approved by your animal care committee.
2. In a laminar flow hood, wet the fur of the mouse with 70% ethanol around the neck/head area and decapitate the animal.
3. Remove the mouse brain from the skull and place it in a 100-mm cell culture dish filled with ice-cold 20 mM HEPES in DMEM (see Note 1).
4. Repeat the procedure for the other animals.
5. Transfer the brains to the lid of the dish and finely mince them (to about 1-mm cubes) with a sterile scalpel in a few drops of ice-cold 20 mM HEPES in DMEM.
6. Transfer the brain bits with a sterile bulb pipette in a conical tube containing ice-cold 20 mM HEPES in DMEM.
7. Centrifuge the tissue for 5 min at 500 × *g* at room temperature.
8. Discard the supernatant and resuspend the tissue in 0.05% collagenase/dispase in 20 mM HEPES in DMEM kept at room temperature (5 ml per brain) (see Notes 2 and 3).
9. Digest the tissue for 45 min at room temperature. Gently pipette the brain bits solution every 5 min to help dissociate the tissue.
10. Stop the digestion by adding an equal volume (5 ml per brain) of ice-cold 5 mM EDTA in 20 mM HEPES in DMEM (final EDTA concentration is 2.5 mM) (see Note 4).
11. Centrifuge for 10 min at 1,000 × *g* at room temperature.
12. Discard the supernatant and resuspend the tissue in 17% dextran in 20 mM HEPES in DMEM (10 ml per brain, up to 40 ml for four brains) and transfer the solution to a sterile polycarbonate tube (high-speed centrifuge grade) (see Note 5).
13. Ultracentrifuge at 10,000 × *g* for 30 min at 4°C using a fixed-angle rotor (e.g., Sorvall centrifuge RC2-B, Rotor no. SS34).
14. Remove the supernatant and the fatty layer under vacuum (the red pellet contains cerebrovascular vessels and microvessels).
15. Resuspend the red pellet in 10-ml complete culture medium (10% FBS, 2 mM L-glutamine, 100 U/ml penicillin, 100 µg/ml streptomycin, 0.1 mM nonessential amino-acids, and 50 µg/ml DNase I) at room temperature.
16. Transfer autoclaved glass beads into a 70-µm nylon cell strainer and fit the strainer into a 50-ml conical tube (see Note 6).
17. Wash sterile glass beads with sterile PBS twice and complete culture medium twice.
18. Pour the vessel suspension over the sterile glass beads.
19. Transfer the strainer to a new 50-ml tube.
20. Pass the flow-through over the beads.

21. Repeat four to five times to collect most of the microvessels on the glass beads.
22. Transfer the glass beads to a sterile 100-mm tissue culture dish containing 15 ml of complete culture medium at room temperature.
23. Gently shake the dish to separate the microvessels from the beads.
24. Collect free microvessels in solution with a sterile pipette and transfer into a 50-ml conical tube.
25. Add 15 ml of complete culture medium to the dish to rinse the glass beads.
26. Gently shake the dish to separate the vessels from the beads and transfer the free microvessels in solution into a 50-ml conical tube.
27. Repeat up to four more times to collect as many microvessels as possible (fill two 50-ml conical tube).
28. Centrifuge at 1,000 × *g* for 12 min at room temperature.
29. Discard the supernatant.
30. Use the pellet for isolating smooth muscle cells (Subheading 3.2) or endothelial cells (Subheading 3.3).

3.2. Propagation of Smooth Muscle Cells

1. Resuspend the pellet with vessels from step 30 (Subheading 3.1) above in complete culture medium supplemented with 0.05% collagenases/dispase (combine all the resuspended pellets together if multiple tubes were used after Subheading 3.1, step 27) and incubate for 2.5–3 h in a 37°C water bath. Gently pipette the solution up and down every 15 min, taking care not to introduce bubbles into the solution.
2. Add an equal volume of ice-cold complete culture medium supplemented with 5 mM EDTA (final EDTA concentration is 2.5 mM).
3. Centrifuge at 1,000 × *g* for 12 min at room temperature.
4. Discard the supernatant.
5. Resuspend the pellet in 3 ml of complete culture medium kept at 37°C.
6. Plate 1.5 ml of the microvessels suspension in two wells of a sterile 12-well cell culture plate. Incubate the cells at 37°C and 5% CO_2 in a humidified environment.
7. Change the growth medium once the microvessels have settled down at the bottom of the wells (this takes 2–3 days).
8. Change the medium every 3–4 days until the cell population is confluent (it takes 1–2 weeks). Then, harvest the smooth muscle cells with 0.25% trypsin and transfer them into one 35-mm cell culture dish (1:1.23 surface ratio).

9. Change the medium every 3–4 days until the cell population is confluent. Harvest the smooth muscle cells with 0.25% trypsin and transfer them into two 35-mm cell culture dishes (1:2 surface ratio).
10. Change the medium every 3–4 days until the cell population is confluent. Harvest the smooth muscle cells with 0.25% trypsin and transfer them into one 60-mm cell culture dish (1:1.5 surface ratio).
11. Change the medium every 3–4 days until the cell population is confluent. Harvest the smooth muscle cells with 0.25% trypsin and transfer them into two 60-mm cell culture dishes (1:2 surface ratio).
12. Change the medium every 3–4 days until the cell population is confluent. Harvest the smooth muscle cells with 0.25% trypsin and transfer them into one 100-mm cell culture dish or a 75-cm^2 cell culture flask (1:1.35 surface ratio) (see Note 7).
13. Passage the smooth muscle cell culture every 7–10 days using 0.25% trypsin (see Notes 8–10).

3.3. Propagation of Endothelial Cells

In this protocol, the CD31 harboring endothelial cells are first selectively attached to anti-CD31 antibody-bound magnetized beads (see Note 11). The cell-magnetized beads complex is then isolated using a magnet to yield purified endothelial cell cultures.

3.3.1. Preparation of Anti-mouse CD31 Dynabeads

1. Mix well the Dynabeads Sheep Anti-Rat IgG suspension and pipette in at least 500 µl in a 1.5-ml microfuge tube.
2. Place tube on magnetic separator and leave for 1 min.
3. Remove the supernatant without disturbing the beads pellet, add 1 ml of buffer 1, mix well, and place on a magnetic separator for 1 min. Repeat this washing step three times.
4. Resuspend the beads to the original 500 µl volume with buffer 1.
5. Add 5 µl of purified rat anti-mouse CD31/PECAM-1 antibody for each 100 µl of beads.
6. Incubate overnight on a rotator at 4°C (or 2 h at room temperature).
7. Wash well to remove unbound antibody by repeating steps 2 and 3 four times.
8. Resuspend beads to the original volume of 500 µl in buffer 1 to maintain the concentration at 4×10^8 beads/ml.
9. Store beads at 4°C and use within 1–2 weeks.

3.3.2. Cell Sorting

1. Add 15 µl of the Dynabead-conjugated anti-mouse CD31 antibody per 1 ml of the cell suspension (from Subheading 3.1, step 30).

2. Incubate on a rotator at room temperature for 15 min.
3. Mount on a magnetic separator, and leave for 1 min.
4. Remove supernatant without disturbing the beads pellet. The bead-bound cells should look foamy if there is a good yield of selected cells.
5. Remove the tube from the magnetic separator and resuspend bead-bound cells in 1-ml endothelial cell complete culture medium by vigorous trituration to break up clumps (clumps potentially contain contaminating cells).
6. Place the tube on magnetic separator and leave for 1 min.
7. Remove the supernatant without disturbing the beads pellet and resuspend in endothelial cell complete culture medium and plate bead-bound cells in two wells of a 12-wells collagen/fibronectin-coated culture plate.
8. The next day, rinse the wells three times with endothelial cell complete culture medium to remove any loosely adherent cells and add new endothelial cell complete culture medium.

3.3.3. Cell Propagation

1. Change 50% of the growth medium every other day because endothelial cells secrete factors necessary for their growth, and transfer when the cell population is nearly confluent.
2. Split cells 1:3 onto collagen/fibronectin-coated plates when they reach 80–90% confluence. Do not allow cells to remain confluent for more than a day or two as small numbers of non-endothelial cells such as fibroblasts or smooth muscle cells will continue to divide and further contaminate the culture.

3.4. Immunocytochemistry for the Identification of Cell Types

1. From a nearly confluent cell population, split the cerebrovascular cells into a 10-μg/ml poly-D-lysine-coated glass chamber slide.
2. When the cerebrovascular cell population reaches 70% confluence, gently wash the cells three times with filter-sterilized PBS to remove traces of growth medium.
3. Fix the cells in 100% methanol chilled at –20°C for 15 min at room temperature.
4. Block the fixed cells with a 5% BSA solution in PBS for 1 h at room temperature.
5. Wash the cells three times with PBS.
6. Apply the cell-specific primary antibody. Use the anti-α smooth muscle actin (for identifying smooth muscle cells) or the anti-von Willebrand factor (for identifying endothelial cells) antibodies at a 1:200 dilution in 5% BSA in PBS.
7. Incubate for 1 h at room temperature.
8. Wash the cells three times with PBS.

9. Apply the fluorescently labeled secondary antibodies at a 1:100 dilution in 5% BSA in PBS.
10. Incubate for 1 h at room temperature.
11. Wash the cells three times with PBS.
12. Mount cover slip with Gel/Mount and examine the slide using a fluorescence microscope.

3.5. Long-Term Storage of Smooth Muscle Cells

1. Use a nearly confluent cell population from four 75-cm^2 flasks to prepare 5 ml of cell suspension to be stored in five cryovials in liquid nitrogen.
2. Wash the cells twice with 5 ml of HBSS per flask.
3. Add 1 ml of 0.25% trypsin to each flask.
4. Wait 30–60 s for the cells to detach from the bottom of the flask (tap the sides of the flask to help detach the cells).
5. Add 9 ml of complete culture medium and wash the bottom of the flask to collect all the cells.
6. Transfer the cells into a 50-ml polypropylene conical tube.
7. Centrifuge at 300 × *g* for 5 min at room temperature.
8. Resuspend the cells in 4.5 ml of either 50/50% FBS/complete culture medium (without antibiotics) or 100% FBS.
9. Add 0.5 ml of cell culture grade DMSO to the cell suspension slowly, mix gently.
10. Aliquot the cell suspension in CryoTubes vials (1 ml per tube, five tubes).
11. Transfer the CryoTubes into a butyl alcohol tube bath kept at –20°C.
12. Transfer the tube bath into a –80°C freezer and keep at –80°C for 4–24 h, and then transfer the CryoTubes into liquid nitrogen for long-term storage.
13. To start a smooth muscle cell culture, remove one CryoTube from the liquid nitrogen and release the pressure inside the tube by slightly opening the cap.
14. Quickly thaw the cells in the CryoTube in a 37°C water bath.
15. Transfer the cells into a 75-cm^2 flask containing 10 ml of complete medium.
16. Incubate the cells at 37°C and 5% CO_2 in a humidified environment.
17. Change the medium after the cells have settled down at the bottom of the flask.
18. Incubate the cells for at least 48 h after thawing before splitting them.

4. Notes

1. Vessels adhere to glass and therefore, plastic disposables should be used at all steps. Glass beakers, Pasteur pipettes, etc. should be avoided.
2. Higher concentrations of collagenase/dispase are used in the isolation of smooth muscle cells from rat and human brains. For example, it has been reported that for the isolation of rat cerebral vessels 0.1% collagenase/dispase is used for 1 h at 37°C (27–29) and for human brains 0.5% collagenase/dispase at 4°C for 2 h followed by 37°C for 1.5 h (33). These higher concentrations have been shown to be too harsh for mouse brains resulting in lower yields.
3. Elastase and hyaluronidase are often used in isolation methods in addition to collagenase/dispase (27–29, 34).
4. Collagenase/dispase is not inhibited by serum. Use 2.5 mM EDTA or EGTA (final concentration) to stop the enzymatic reaction.
5. The percentage of dextran varies in the literature. A 13–15% dextran solution is used for isolating microvessels from rat brains (27–29) and a 15% dextran solution for human brain tissue (35), we recommend a higher dextran concentration (at least 17%) for isolating microvessel from murine brains.
6. If the separation of the vessel population based on size is preferred, a nylon cell strainer without the glass beads can be used. While leptomeninges and large cortical vessels do not pass through the 70-μm nylon cell strainer, smaller cortical vessels pass through it (34).
7. At this point, the smooth muscle cells culture has been passaged five times. We recommend passaging the cells two more times (1:2 surface ratio) up to passage 7 to get four 75-cm^2 cell culture flasks before using the cells for long-term storage in liquid nitrogen or for experiments.
8. Murine smooth muscle cells require several weeks (more than 3 weeks) before a suitable doubling time is reached for experimental purposes. The doubling time is very long in the early passages and the split ratio should be 1:2. In later passages, the doubling time shortens and a split ratio of 1:4 can be used.
9. The choice of the source of smooth muscle cells should be made with great consideration. Human cerebrovascular smooth muscle cells behave very differently from those obtained from human umbilical artery, and this could have a great effect on the outcome of the experiments. For example, human umbilical

artery smooth muscle cells produce free radicals in response to Aβ treatment, whereas human adult smooth muscle cells do not (36).

10. Experiments performed on smooth muscle cells often require incubation of the cells in serum-free medium. For example, treatment of human smooth muscle cells with Aβ is done in the absence of serum (33). Furthermore, serum contains high levels of cystatin C, and therefore, for the purpose of investigating its effects on murine smooth muscle cells, cystatin C is reconstituted in medium without serum. Murine smooth muscle cells, however, do not survive in the absence of serum. Therefore, we have successfully used Opti-MEM I Reduced Serum Media (Invitrogen, 51985-034) containing 2 mM L-glutamine, 100 U/ml penicillin, 100 μg/ml streptomycin, and 0.1 mM nonessential amino acids. Cells are viable up to 3–4 days in this medium in the presence or absence of cystatin C. After 4 days, smooth muscle cell morphology changes dramatically as cells start to degenerate.
11. Anti-CD31 antibody-coated Dynabeads are used only in the first cell sorting of endothelial cells. Their use in later sorts is hindered by mouse CD31 sensitivity to trypsin digestion. A second purification step of the endothelial cells from other cell types can be included by using CD102/ICAM2 antibody (Pharmingen # 553325) at 1 mg/ml and magnetic beads.

Acknowledgments

This work was supported by grants from the NINDS (NS42029), NIA (AG017617), and the Alzheimer's Association (IIRG-07-59699).

References

1. Kalaria, R. N. (2001) Advances in molecular genetics and pathology of cerebrovascular disorders. *Trends Neurosci* **24**, 392–400.
2. Vinters, H. V. (1987) Cerebral amyloid angiopathy. A critical review. *Stroke* **18**, 311–324.
3. Greenberg, S. (2002) Cerebral amyloid angiopathy and dementia - Two amyloids are worse than one. *Neurology* **58**, 1587–1588.
4. Pfeifer, L. A., White, L. R., Ross, G. W., Petrovitch, H., and Launer, L. J. (2002) Cerebral amyloid angiopathy and cognitive function: the HAAS autopsy study, *Neurology* **58**. 1629–1634.
5. Levy, E., Carman, M. D., Fernandez-Madrid, I. J., Power, M. D., Lieberburg, I., van Duinen, S. G., Bots, G. T. A. M., Luyendijk, W., and Frangione, B. (1990) Mutation of the Alzheimer's disease amyloid gene in hereditary cerebral hemorrhage, Dutch type. *Science* **248**, 1124–1126.
6. Grabowski, T. J., Cho, H. S., Vonsattel, J. P., Rebeck, G. W., and Greenberg, S. M. (2001) Novel amyloid precursor protein mutation in an Iowa family with dementia and severe cerebral amyloid angiopathy. *Ann Neurol* **49**, 697–705.
7. Tsubuki, S., Takaki, Y., and Saido, T. C. (2003) Dutch, Flemish, Italian, and Arctic mutations of APP and resistance of Aβ to physiologically relevant proteolytic degradation. *Lancet* **361**, 1957–1958.

8. Gudmundsson, G., Hallgrimsson, J., Jonasson, T. A., and Bjarnason, O. (1972) Hereditary cerebral haemorrhage with amyloidosis. *Brain* **95**, 387–404.
9. Olafsson, I., Thorsteinsson, L., and Jensson, O. (1996) The molecular pathology of hereditary cystatin C amyloid angiopathy causing brain hemorrhage. *Brain Pathol* **6**, 121–126.
10. Cohen, D. H., Feiner, H., Jensson, O., and Frangione, B. (1983) Amyloid fibril in hereditary cerebral hemorrhage with amyloidosis (HCHWA) is related to the gastroenteropancreatic neuroendocrine protein, γ trace. *J Exp Med* **158**, 623–628.
11. Ghiso, J., Jensson, O., and Frangione, B. (1986) Amyloid fibrils in hereditary cerebral hemorrhage with amyloidosis of Icelandic type is a variant of γ-trace basic protein (cystatin C). *Proc Natl Acad Sci USA* **83**, 2974–2978.
12. Vidal, R., Frangione, B., Rostagno, A., Mead, S., Revesz, T., Plant, G., and Ghiso, J. (1999) A stop-codon mutation in the BRI gene associated with familial British dementia. *Nature* **399**, 776–781.
13. Vidal, R., Revesz, T., Rostagno, A., Kim, E., Holton, J. L., Bek, T., Bojsen-Moller, M., Braendgaard, H., Plant, G., Ghiso, J., and Frangione, B. (2000) A decamer duplication in the 3′ region of the BRI gene originates an amyloid peptide that is associated with dementia in a Danish kindred. *Proc Natl Acad Sci USA* **97**, 4920–4925.
14. Kiuru, S., Salonen, O., and Haltia, M. (1999) Gelsolin-related spinal and cerebral amyloid angiopathy. *Ann Neurol* **45**, 305–311.
15. Sturchler-Pierrat, C., Abramowski, D., Duke, M., Wiederhold, K. H., Mistl, C., Rothacher, S., Ledermann, B., Burki, K., Frey, P., Paganetti, P. A., Waridel, C., Calhoun, M. E., Jucker, M., Probst, A., Staufenbiel, M., and Sommer, B. (1997) Two amyloid precursor protein transgenic mouse models with Alzheimer disease-like pathology. *Proc Natl Acad Sci USA* **94**, 13287–13292.
16. Calhoun, M. E., Burgermeister, P., Phinney, A. L., Stalder, M., Tolnay, M., Wiederhold, K. H., Abramowski, D., Sturchler-Pierrat, C., Sommer, B., Staufenbiel, M., and Jucker, M. (1999) Neuronal overexpression of mutant amyloid precursor protein results in prominent deposition of cerebrovascular amyloid. *Proc Natl Acad Sci USA* **96**, 14088–14093.
17. Winkler, D. T., Bondolfi, L., Herzig, M. C., Jann, L., Calhoun, M. E., Wiederhold, K. H., Tolnay, M., Staufenbiel, M., and Jucker, M. (2001) Spontaneous hemorrhagic stroke in a mouse model of cerebral amyloid angiopathy. *J Neurosci* **21**, 1619–1627.
18. Herzig, M. C., Eisele, Y. S., Staufenbiel, M., and Jucker, M. (2009) E22Q-mutant Aβ peptide (AβDutch) increases vascular but reduces parenchymal Aβ deposition. *Am J Pathol* **174**, 722–726.
19. Kumar-Singh, S. (2009) Hereditary and sporadic forms of Aβ-cerebrovascular amyloidosis and relevant transgenic mouse models. *Int J Mol Sci* **10**, 1872–1895.
20. Pawlik, M., Sastre, M., Calero, M., Mathews, P. M., Schmidt, S. D., Nixon, R. A., and Levy, E. (2004) Overexpression of human cystatin C in transgenic mice does not affect levels of endogenous brain amyloid β peptide. *J Mol Neurosci* **22**, 13–18.
21. Vidal, R., Barbeito, A. G., Miravalle, L., and Ghetti, B. (2009) Cerebral amyloid angiopathy and parenchymal amyloid deposition in transgenic mice expressing the Danish mutant form of human BRI2. *Brain Pathol* **19**, 58–68.
22. Vinters, H. V., Reave, S., Costello, P., Girvin, J. P., and Moore, S. A. (1987) Isolation and culture of cells derived from human cerebral microvessels. *Cell Tissue Res* **249**, 657–667.
23. Vinters, H. V. (1987) Cerebral amyloid angiopathy. A critical review. *Stroke* **18**, 311–324.
24. Frackowiak, J., Mazur-Kolecka, B., Wisniewski, H. M., Potempska, A., Carroll, R. T., Emmerling, M. R., and Kim, K. S. (1995) Secretion and accumulation of Alzheimer's β-protein by cultured vascular smooth muscle cells from old and young dogs. *Brain Research* **676**, 225–230.
25. Mazur-Kolecka, B., Frackowiak, J., Krzeslowska, J., Ramakrishna, N., Haske, T., Emmerling, M. R., Zhang, W., Kim, K. S., and Wisniewski, H. M. (1999) Apolipoprotein E alters metabolism of AβPP in cells engaged in β-amyloidosis. *Journal of Neuropathology and Experimental Neurology* **58**, 288–295.
26. Mazur-Kolecka, B., Frackowiak, J., and Wisniewski, H. M. (1995) Apolipoproteins E3 and E4 induce, and transthyretin prevents accumulation of the Alzheimer's β-amyloid peptide in cultured vascular smooth muscle cells. *Brain Research* **698**, 217–222.
27. Diglio, C. A., Grammas, P., Giacomelli, F., and Wiener, J. (1982) Primary culture of rat cerebral microvascular endothelial cells. Isolation, growth, and characterization. *Lab Invest* **46**, 554–563.
28. Diglio, C. A., Grammas, P., Giacomelli, F., and Wiener, J. (1986) Rat cerebral microvascular smooth muscle cells in culture. *J Cell Physiol* **129**, 131–141.
29. Diglio, C. A., Liu, W., Grammas, P., Giacomelli, F., and Wiener, J. (1993) Isolation and

characterization of cerebral resistance vessel endothelium in culture. *Tissue Cell* **25**, 833–846.

30. Reisner, A., Olson, J. J., Yang, J., Assietti, R., Klemm, J. M., and Girard, P. R. (1995) Isolation and culture of bovine intracranial arterial endothelial cells. *Neurosurgery* **36**, 806–812; discussion 813.
31. Seidel, M. F., Simard, J. M., Hunter, S. F., and Campbell, G. A. (1991) Isolation of arteriolar microvessels and culture of smooth muscle cells from cerebral cortex of guinea pig. *Cell Tissue Res* **265**, 579–587.
32. Tontsch, U., and Bauer, H. C. (1989) Isolation, characterization, and long-term cultivation of porcine and murine cerebral capillary endothelial cells. *Microvasc Res* **37**, 148–161.
33. Van Nostrand, W. E., Rozemuller, A. J. M., Chung, R., Cotman, C. W., and Saporito-Irwin, S. M. (1994) Amyloid β-protein precursor in cultured leptomeningeal smooth muscle cells. *Int.J.Exp.Clin.Invest.* **1**, 1–7.
34. Frackowiak, J., Miller, D. L., Potempska, A., Sukontasup, T., and Mazur-Kolecka, B. (2003) Secretion and accumulation of Aβ by brain vascular smooth muscle cells from AβPP-Swedish transgenic mice. *J Neuropathol Exp Neurol* **62**, 685–696.
35. Grammas, P., Roher, A. E., and Ball, M. J. (1991) Decreased α-adrenergic receptors at the blood-brain barrier in Alzheimer's disease, in *Alzheimer's Disease: Basic Mechanisms, Diagnosis and Therapeutic Strategies* (Iqbal, K., McLachlan, D. R. C., Winblad, B., and Wisnieski, H. M., Eds.), pp 129–136, John Wiley & Sons Ltd., New York.
36. Jung, S. S., and Van Nostrand, W. E. (2002) Aβ does not induce oxidative stress in human cerebrovascular smooth muscle cells. *Neuroreport* **13**, 1309–1312.

Chapter 19

In Vitro Assays Measuring Protection by Proteins such as Cystatin C of Primary Cortical Neuronal and Smooth Muscle Cells

Sebastien A. Gauthier, Belen Tizon, Susmita Sahoo, and Efrat Levy

Abstract

Neuronal cell culture models have been used to demonstrate the protective effects of cystatin C against a variety of insults, including the toxicity induced by oligomeric and fibrillar amyloid β (Aβ). Here, we describe assays quantifying cystatin C protective effects against cytotoxicity induced by nutrient deprivation, oxidative stress, or cytotoxic forms of Aβ. Three methods for the evaluation of either cell death or cell survival are described: measurement of metabolic activity, cell death, and cell division. The cell culture models used are murine primary cortical neurons and murine primary cerebral smooth muscle cells. The effects of exogenously applied cystatin C are studied by comparing the viability of nonstressed control, stressed control, and cystatin C-treated stressed cells. The effect of endogenous level of cystatin C expression is studied by comparing stressed primary cells isolated from brains of cystatin C transgenic, cystatin C knockout, and wild-type mice.

Key words: Amyloid β, Cell death, Cell survival, Cerebrovascular cells, Cortical neurons, Cystatin C, Primary cell culture, Protection assays, Stress-induced cytotoxicity

1. Introduction

Recent studies suggest that the secretory cysteine protease inhibitor cystatin C plays a protective role against Alzheimer disease (AD) pathogenesis by inhibiting Aβ aggregation (1–4) and by protecting against Aβ cytotoxicity as demonstrated in vitro using murine primary cortical neuronal cultures treated with either Aβ fibrils or oligomers (5). In addition, other studies have shown that cystatin C protects primary cortical neurons against a variety of toxicities, including oxidative stress (6). These studies suggest that the higher levels of cystatin C observed in vivo following brain insults, including epilepsy (7), ischemia (8), and stroke (9), serve as a protective

Einar M. Sigurdsson et al. (eds.), *Amyloid Proteins: Methods and Protocols*, Methods in Molecular Biology, vol. 849,
DOI 10.1007/978-1-61779-551-0_19,

mechanism against cell death. The data obtained demonstrate that primary cortical neuronal culture is a reliable tool to study the protective roles of proteins such as cystatin C. Here, we describe protocols designed to measure the protection effect of exogenously applied as well as endogenously expressed protein, using cystatin C as an example. Murine primary cortical neurons and primary cerebral smooth muscle cell cultures are treated with nutrient deprivation, oxidative stress, or Aβ cytotoxic peptides. These methods can be adapted to other cell types, such as fibroblasts or cell lines, treated with a variety of stressors, including staurosporine, colchicine, and hydrogen peroxide (6), to measure the protective effects of proteins. In our studies, we have been using cells derived from cystatin C knockout mice (10) to study the effect of exact concentrations of extracellularly added cystatin C. Further, to study the effect of different concentrations of endogenously expressed cystatin C, we compare cells derived from transgenic mice overexpressing cystatin C (11) and wild-type mice to cells derived from cystatin C knockout mice (10). We describe assays to measure cellular metabolic activity, cell death and survival, and cell division to characterize the cytotoxic effects of the stressors and the protective effects of cystatin C. Depending on the goal of the study, a suitable cytotoxicity (membrane permeability assay), viability (measurement of cellular activity), or proliferation assays should be used.

2. Materials

2.1. Supplies/Reagents Used for All Protocols

1. Sterile 12-mm round glass coverslips (Fisher Scientific, Pittsburgh, PA, 12-545-83).
2. Sterile 24-well cell culture plates (BD-Falcon, Franklin Lakes, NJ, 353047).
3. Sterile 96-well cell culture plates (BD-Falcon, 353072).
4. Cell culture incubator at 37°C, 5% CO_2, with a humidified environment.
5. 50-ml Conical tubes (BD-Falcon, no. 352098).
6. Dulbecco's Modified Eagle's Medium (DMEM; Sigma-Aldrich, St. Louis, MO, D5671).
7. Fetal bovine serum (FBS), heat-inactivated (VWR-Mediatech, Batavia, IL, 45000-736).
8. Penicillin (10,000 U/ml) and streptomycin (10,000 μg/ml) stock solutions (Invitrogen/Gibco, Piscataway, NJ, 15140-122).
9. L-Glutamine (GlutaMAX™), 200 mM (Invitrogen/Gibco, 35050-061).
10. Nonessential amino acids, 10 mM (Invitrogen/Gibco, 11140-050).

11. DNase, Type I (Sigma-Aldrich, no. DN25). Prepare a 10 mg/ml stock solution in PBS, filter sterilize through a 0.22-μm membrane filter, aliquot and store at −20°C.
12. 1× Sterile Hanks' Balanced Salt Solution (HBSS; Invitrogen/Gibco, 14175-145).
13. 1× Sterile Dulbecco's phosphate-buffered saline (PBS) without calcium and magnesium (Invitrogen, Piscataway, NJ, 10010-049).
14. Neurobasal medium (1×) without Phenol Red (Invitrogen/Gibco, 12348-017).
15. B27 serum-free supplement (50×) (Invitrogen/Gibco, 17504-044) (see Note 1).
16. Cell culture grade 16% paraformaldehyde (EMS, Hatfield, PA, 15710).
17. Hemocytometer for cell counting.
18. GlutaMAX™, 200 mM (Invitrogen/Gibco, 35050-061).

2.2. Supplies/Reagents Used for Cell Cultures

1. Complete medium for culturing smooth muscle cells: DMEM containing 10% FBS, 2 mM GlutaMAX, 100 U/ml penicillin, 100 μg/ml streptomycin, 0.1 mM nonessential amino acids, and 50 μg/ml DNase I. Store at 4°C for up to 6 months. Warm up the medium to 37°C before use.
2. Complete medium freshly prepared for culturing primary cortical neurons: Neurobasal medium containing 1× B27, 0.5 mM GlutaMAX™, 100 U/ml penicillin, 100 μg/ml streptomycin. Store at 4°C. Warm up the medium to 37°C before use.
3. Complete medium without FBS for culturing smooth muscle cells under nutrient deprivation stress: DMEM containing 2 mM GlutaMAX™, 100 U/ml penicillin, 100 μg/ml streptomycin, 0.1 mM nonessential amino acids, and 50 μg/ml DNase I. Store at 4°C. Warm up the medium to 37°C before use.
4. Complete medium without B27 for culturing primary cortical neurons under oxidative stress: Neurobasal containing 0.5 mM GlutaMAX™, 100 U/ml penicillin, 100 μg/ml streptomycin. Store at 4°C. Warm up the medium to 37°C before use (see Note 1).
5. Trypsin, 2.5% (Invitrogen/Gibco, 15050-065). Keep at −20°C. Dilute 1:10 in HBSS and warm up to 37°C before use.
6. Human urinary cystatin C (EMD/Calbiochem, Gibbstown, NJ, 240896). Keep at 4°C. The preparation of cystatin C for in vitro studies is as previously described (5, 6). Resuspend cystatin C in basic medium (DMEM for smooth muscle cells/neurobasal for primary cortical neurons) at a stock concentration of 100–500 ng/μl. Keep at −20°C. Add the required volume of the cystatin C stock solution to the cell culture medium at the same time the stress treatment is applied (use a

1:20 dilution factor or less). The final cystatin C concentrations should range from 2 to 20 ng/μl, (or 0.15–1.5 μM), corresponding to the range of physiological cystatin C concentrations measured in human fluids in vivo (12, 13).

2.3. Supplies/Reagents for Studies Using Smooth Muscle Cell Cultures

1. Cerebral smooth muscle cell culture grown in complete smooth muscle cell medium. A protocol describing the isolation of primary murine cerebral smooth muscle cells from brain microvessels of mice is published in this issue of "Amyloid Proteins, Methods and Protocols" (Gauthier, S. A., Sahoo, S., Jung, S. S. and Levy, E. Murine cerebrovascular cells as a cell culture model for cerebral amyloid angiopathy. Isolation of smooth muscle and endothelial cells from mouse brain).

2.4. Supplies/Reagents for Studies Using Primary Cortical Neuronal Cultures

1. Poly-D-lysine (PDL, 1 mg/ml, Millipore, Billerica, MA, A-003-E). Aliquot in 1.5-ml tubes. Store at –20°C. Prepare a fresh 0.1 mg/ml PDL solution in sterile double-distilled water.
2. PDL-coated 96-well cell culture plate, 24-well cell culture plate, or 15-mm glass coverslips. Prepare 1 day before primary cortical neurons are harvested. Fill the wells of the 96-well and 24-well cell culture plates with 100 and 500 μl, respectively, with the 0.1 mg/ml PDL solution. 15-mm Glass coverslips can be coated on one side at the bottom of a well in a 24-well cell culture plate filled with 500 μl of the 0.1 mg/ml PDL solution. Incubate at 37°C overnight in a humidified environment. Wash the wells and coverslips once with sterile double-distilled water. Air dry the cell culture plate and coverslips in a sterile cell culture hood. Keep the cell culture plate and coverslips at 37°C before use.
3. Saline solution I (8.1 g/l NaCl, 0.4 g/l KCl, 0.15 g/l Na_2HPO_4, 0.15 g/l KH_2PO_4, 4 g/l dextrose, pH 7.2).
4. A protocol describing the isolation of primary cortical neurons was previously described (5, 6).

2.5. Supplies/Reagents for Measuring Metabolic Activity in Cell Culture (MTS Assay)

1. CellTiter 96® AQueous One Solution Cell Proliferation Assay (MTS) (Promega, Madison, WI, G3580). Store at –20°C. Warm up to 37°C before use.
2. Cell plate reader and corresponding analysis software (e.g., SpectraMax with SoftmaxPro, Molecular devices, Sunnyvale, CA).

2.6. Supplies/Reagents for Hoechst/Propidium Iodide Staining

1. Hoechst 2495 (Sigma-Aldrich, 654434). Prepare a 200 μg/ml solution in HBSS. Store at 4°C in the dark.
2. Propidium iodide (PI, Sigma-Aldrich, P4170). Prepare a 1 mg/ml solution in HBSS. Store at 4°C in the dark.

3. Prepare a fresh Hoechst (0.4 μg/ml)/PI (7.5 μg/ml) solution by mixing 20 μl of the Hoechst solution and 75 μl of the PI solution in 10 ml of HBSS. Keep at 4°C.
4. Fresh 4% paraformaldehyde solution in PBS. Keep at room temperature until use.
5. 50% Glycerol solution in PBS. Keep at 4°C. Warm up to room temperature before use.
6. Aqueous mounting medium with antifading agents (Biomeda, Foster City, CA, M01).

2.7. Supplies/Reagents for Fluorescein Diacetate/Propidium Iodide Staining

1. Fluorescein diacetate (FD, Sigma, F7378). Prepare a fresh 15 mg/ml solution in DMSO. Keep at room temperature in the dark.
2. Propidium iodide (PI, Sigma, P4170). Prepare a 1 mg/ml solution in HBSS. Keep at 4°C in the dark.
3. Cell culture grade dimethyl sulphoxide (DMSO) (Sigma-Aldrich, D2650).
4. Prepare a fresh 1:10 dilution of the FD stock solution in 60% DMSO/40% DMEM. Keep at room temperature.
5. Prepare a fresh working FD/PI solution by adding 500 μl of the 1:10 diluted FD solution in 50 ml of DMEM containing 230 μl of the PI solution. Keep at room temperature.

2.8. Supplies/Reagents for 5-Bromo-2′-Deoxyuridine Staining

1. Prepare a 10 mM 5-bromo-2′-deoxyuridine (BrdU, Sigma, B9285) stock solution in PBS. Sterilize using 0.2-μm filter and store at −20°C. Dilute to 10 μM with culture medium before use.
2. Fresh 4% formaldehyde in PBS. Keep at room temperature.
3. 16-Well CultureWell chambered coverglass slides (Grace Bio-Labs, Bend, OR, C37000).
4. HCl diluted to 1 and 2 M in double-distilled water.
5. Borate buffer 0.1 M, pH 8.5.
6. Tween 20, 0.05% in PBS.
7. FITC-conjugated anti-BrdU monoclonal antibody (BD Pharmingen, San Diego, CA, 556028).
8. Gel mount (Biomeda, Foster City, CA, M01).

3. Methods

The following protocols describe the preparation (Subheadings 3.1 and 3.2) and the treatment of murine smooth muscle cells and primary cortical neuronal cultures with stressors including nutrition deprivation, oxidative stress, and Aβ fibrils and oligomers in the

absence or presence of cystatin C (Subheading 3.3). We are using cells derived from cystatin C knockout mice (10) to study the effect of exact concentrations of the protein added extracellularly and to eliminate any effect of the endogenous cystatin C expressed and secreted by wild-type cells. To study the effect of different concentrations of endogenously expressed cystatin C, we are comparing cells expressing different levels of cystatin C: homozygous transgenic mice overexpressing cystatin C (11), wild-type mice, and cystatin C knockout mice (10). The assays described below (Subheading 3.4) measure the cytotoxic effects of the stressors and the protective effect of cystatin C on cellular metabolic activity (Subheading 3.4.1), cell survival rate (Subheading 3.4.2), and cell division rate (Subheading 3.4.3), comparing cells under non-stressed, stressed, and stressed/treated with cystatin C conditions.

3.1. Preparation of Smooth Muscle Cell Cultures

Murine cerebrovascular smooth muscle cells (see Gauthier, S. A., Sahoo, S., Jung, S. S. and Levy, E. Murine cerebrovascular cells as a cell culture model for cerebral amyloid angiopathy. Isolation of smooth muscle and endothelial cells from mouse brain, in this issue of "Amyloid Proteins, Methods and Protocols") are used at passages 7–20. The cells grown in a 100-mm cell culture dish in 10 ml of complete smooth muscle cell medium are harvested when 90% confluent (see Note 2) with 0.25% trypsin and suspended in 1-ml complete smooth muscle cell medium. The cells are counted, diluted, and seeded in appropriate number in the required culture wells/coverslips (see Note 3) in the corresponding volume of media (see Table 1). This yields a 50–70% confluent smooth muscle cell culture after 24 h incubation at 37°C, 5% CO_2, in a humidified environment (see Note 4). Cell seeding can be adjusted based on the length of the protection assay (see Note 5).

3.2. Preparation of Primary Cortical Neuronal Cultures

We designed this protocol using day 5 murine primary cortical neuronal cultures harvested from the brains of E16 mouse pups using the protocol described by Tizon et al. (6). The neurons are seeded on PDL-coated 96-well cell culture plate, 24-well cell

Table 1
Surface area of the cell culture, number of cells to be plated, and the volume of smooth muscle cell suspension that would yield a 50–70% confluence after 24 h incubation

	Surface area (cm^2)	Number of cells	Volume (μl)
96-Well plate	0.32	10,000	100
12-mm Coverslip	1.13	35,000	350
24-Well plate	2	60,000	600

culture plate, or 12-mm glass coverslips at a 10^5 cells/cm^2 density. Incubate the cell cultures at 37°C, 5% CO_2, in a humidified environment for 5 days in complete primary cortical neuronal medium, changing 50% of the medium at day 3.

3.3. Stress Treatment and Use of Extracellular Cystatin C in Protection Assays

In this protocol, cerebral smooth muscle cell or primary cortical neuronal cultures are treated with cellular stresses to slow down cell growth and proliferation and to induce cell death. The cystatin C protective effects on these stressed cells is measured by comparing cell survival rate between stressed cultures incubated with cystatin C and control stressed cell cultures. Smooth muscle cell cultures under nutrient deprivation are grown in complete medium without FBS, and primary cortical neuronal cultures under oxidative stress are grown in complete medium without B27 (see Note 1). Studies of cystatin C protection from other cytotoxic factors, such as the microtubule-depolymerizing agent colchicine (0.5 μM), the apoptotic agent staurosporine (100 nM), and H_2O_2 (10 μm) are described in Tizon et al. (6) and from oligomeric (20–30 μM) and fibrillar (20–30 μM) Aβ are described in Tizon et al. (5). In the experiments to study the effect of endogenous levels of cystatin C, smooth muscle cells or neurons expressing different levels of cystatin C (transgenic, wild type, and knockout) grow in either complete medium or in stressed medium (without serum or B27 supplement).

We designed this protocol to yield a 60–70% cell survival at the end of the 24 h long stress treatment in stressed cell cultures compared to nonstressed cell culture controls (see Note 5). This provides safe experimental conditions to observe and measure the protective effects of cystatin C. We strongly recommend that nonstressed cell culture controls will be set up in all protection assays to measure cell death in stressed cell culture controls and to verify that the stress treatment actually slows down cell growth and proliferation, and induces cell death.

1. Wash the cell cultures prepared in Subheadings 3.1 and 3.2 twice with HBSS (smooth muscle cells) or basal Neurobasal medium (primary cortical neurons).
2. Add corresponding complete medium to either smooth muscle cells or primary cortical neurons, and add stress-inducing medium (complete smooth muscle medium without FBS/complete primary cortical medium without B27) or complete medium supplemented with Aβ fibrils/oligomers to the stressed cell cultures. Add 100 μl in each well of a 96-well cell culture plate; 500 μl in each well of a 24-well cell culture plate; 500 μl in each well of a 24-well cell culture plate containing a 12-mm coverslip.
3. Add cystatin C to the designated wells at different concentrations to study concentration dependence of the effect.

4. Incubate the cell culture plates at 37°C, 5% CO_2, in a humidified environment for 24 h.
5. Perform one of the protection assays described in Subheading 3.4.

3.4. Measurement of Cystatin C Protective Effects on Stressed Cell Cultures

Cell culture growth rate depends on the cell type, genotype, and passage. In addition, the nature of the stressor used may play a role in the overall health of the cells and in the incubation time the cell culture can sustain. For these reasons, we recommend to perform preliminary studies to monitor the health of the stressed cell cultures, experiment with different stressors, concentrations of stressors, and length of treatment. We recommend to set up a stress treatment protocol (incubation time, starting number of cells/cell population confluence) to yield a 60–70% cell survival rate in stressed cell culture controls for every cell type/genotype/stressor used before any protection assay is performed. Here we describe three assays used to measure the effects of cystatin C on smooth muscle cells and primary cortical neuronal cultures under 24 h nutrient deprivation and oxidative stress, respectively.

3.4.1. Measurement of Cellular Metabolic Activity (MTS Assay)

The tetrazolium compound MTS is metabolized into formazan by metabolically active cells and the levels of formazan in the medium reflect the number of live cells in the culture. This protection assay should include multiple replicates (at least 4) per condition and the proper controls (nonstressed and stressed cell cultures) (see Note 6). We recommend using cell cultures grown in 96-well culture plates to minimize the amount of MTS solution used for the assay and to accommodate large number of different controls and replicates. It should be noted that alternative methods are available for measuring cellular viability. Similar to MTS, XTT and WST-1 reagents measure cell viability based on the mitochondrial enzyme in live cells that reduce XTT/WST-1 and determine the live cell number using standard microplate readers. Further, ATP quantification is a rapid and sensitive method to assess viability using ATP quantification reagents containing luciferase enzyme and luciferin substrate.

1. Add 20 μl of MTS solution to 100 μl medium in each well and incubate at 37°C, 5% CO_2, in a humidified environment in the dark.
2. Gently shake the plate and record the absorbance at 490 nm with a plate reader every hour for 3–4 h. Keep the plate at 37°C, 5% CO_2, in a humidified environment and in the dark.

Baseline absorbance at 490 nm should be measured in cell-free complete medium. Subtract the baseline absorbance from the measured absorbance for all conditions. We use nonstressed cell culture absorbance reading as reference. Lower absorbance at 490 nm indicates a higher cell death rate and higher absorbance for cystatin

C-treated stressed cell cultures compared with the absorbance in the stressed cell culture controls shows a cystatin C protective effect against the stressor used in the experiment (5, 6).

3.4.2. Measurement of Cell Survival Rate (Live/Dead Staining)

We use the Hoechst/Propidium iodide (PI) staining to count the number of dead cells (PI-stained, red, excitation wavelength 488 nm) and the total cell number (Hoechst stained cells, blue, excitation wavelength 350 nm). The cell survival rate is determined by dividing the total number of live cells [(Hoechst-stained cells) – (PI-stained cells)] by the total cell number (Hoechst-stained cells). As an alternative, we substitute Hoechst staining with the nonfluorescent Fluorescein analog Fluorescein diacetate (FD) (14) that stains live cells only because live cells internalize and cleave FD into the green fluorescent Fluorescein. With this method, the cell survival rate is calculated by dividing the number of live cells (FD-stained cells) by the total number of cells [(FD-stained cells) plus (PI-stained cells)]. These techniques are used on cells grown on 12-mm coverslips (Hoechst/PI staining) or in 24-well cell culture plates (FD/PI staining).

We take pictures of at least 10 fields containing about 50 cells each (use a 4× magnifying lens for smooth muscle cells and use a 10–20× magnifying lens for primary cortical neurons, avoid the edge of the coverslip). Count the number of live and number of dead cells per field and calculate the average survival rates. Use the cell survival rate measured for nonstressed cell culture controls as reference.

Hoechst/Propidium Iodide Staining

1. Wash the cells twice with HBSS or saline solution I at room temperature.
2. Add 200 µl of the Hoechst/PI solution to each coverslip. Make sure the coverslip is entirely submerged.
3. Incubate for 5–10 min at room temperature in the dark (see Note 7). Keep the cells in the dark for the rest of the procedure.
4. Wash the cells twice with HBSS or saline solution I at room temperature.
5. Fix the cells in 200 µl of 4% paraformaldehyde in PBS for 30 min at room temperature.
6. Wash the cells twice with PBS.
7. Wash the coverslips with 50% glycerol in PBS.
8. Mount the coverslips on microscope slides with Gel Mount.
9. Store the Hoechst/PI-stained cells in the dark at 4°C.

Fluorescein Diacetate/ Propidium Iodide Staining

1. Wash the cells twice with HBSS at room temperature.
2. Add 1 ml of the FD/PI solution to each well.
3. Incubate for 5–10 min at room temperature in the dark (see Note 7). Keep the cells in the dark for the rest of the procedure.

4. Wash the cells twice with HBSS at room temperature.
5. Immediately observe and count the FD/PI-stained cells using a fluorescent microscope (see Note 8).

3.4.3. Measurement of Cell Division

The halogenated pyrimidine bromodeoxyuridine (BrdU) is incorporated into duplicating DNA helix instead of thymidine during the S-phase of the cell cycle. BrdU is commonly used to stain the nucleus of cells undergoing mitotic division (15). Here, we use this staining technique to quantify the effect of cystatin C on the number of dividing cells in stressed smooth muscle cell cultures. The cell division rate is the ratio of the number of dividing cells, labeled with BrdU, to the total number of cells, stained with Hoechst.

We take pictures of at least 10 fields containing about 50 cells each (use a 4× magnifying lens and avoid the edge of the coverslip). Count the number of BrdU-stained nuclei and the total number of cells per field and calculate the average cell division rate. Use the division rate measured for nonstressed cell culture controls as reference.

1. Plate smooth muscle cells (about 50,000 cells) in 16-well chamber slides, and grow for about 6 h to 20–30% confluence.
2. Wash the cells three times with HBSS, and incubate them in serum containing or lacking medium and different concentrations of cystatin C for 20 h at 37°C, 5% CO_2, in a humidified environment.
3. Add BrdU to a final concentration of 10 μM and incubate for 20 h at 37°C, 5% CO_2, in a humidified environment.
4. Aspirate the medium gently with a pipette. Avoid vacuum because cells are lightly attached to the glass chamber slides as compared to plastic wells.
5. Wash the cells three times by dipping the slides very gently in PBS.
6. Fix the cells with 4% formaldehyde in PBS for 30 min and permeabilize them in 0.2% Triton-X for 5 min, at room temperature.
7. Wash the cells three times with PBS.
8. Denature the DNA by dipping the slides in 1 M HCl on ice for 10 min, then in 2 M HCl for 10 min at room temperature, and in 2 M HCl at 37°C for 1 h.
9. Neutralize the slides by washing three times in 0.1 M borate buffer pH 8.5.
10. Wash the cells three times with PBS containing 0.05% Tween 20.
11. For immunostaining, cells are blocked by incubating in PBS containing 0.05% Tween 20 and 2% BSA at 37°C for 1 h.

12. Incubate the cells with FITC-conjugated anti-BrdU monoclonal antibody overnight at 4°C.
13. Wash the cells three times with PBS containing 0.05% Tween 20 and 1% BSA for at least 45 min.
14. Stain with Hoechst diluted to 0.4 mg/ml in PBS for 30 min in the dark.
15. Wash well in PBS, mount with Gel mount.
16. Count the BrdU-stained nuclei and Hoechst-stained cells to calculate the cell division rate (see Notes 9 and 10).

4. Notes

1. The B27 growth supplement contains compounds with antioxidant activities (16). Primary cortical neuronal cultures incubated in complete medium lacking B27 are grown under oxidative stress.
2. The confluence of a smooth muscle cell culture is measured as the area of the well covered by the cells.
3. Murine primary cortical neurons should always be seeded in PDL-coated cell culture plates or on PDL-coated glass coverslips as described in Subheading 2.2. Smooth muscle cells grow in noncoated cell culture plates. While these cells can be plated on collagen-coated glass coverslips (0.167 mg/ml collagen solution in sterile ddH_2O, air dry overnight under a closed cell culture hood), collagen can play a protective role and should be avoided.
4. We recommend seeding smooth muscle cells to yield a 50–70% confluent cell culture 24 h later. This allows the smooth muscle cell culture to grow without reaching 100% confluence during the standard 24 h long stress treatment that follows.
5. Adjust the volume of cell suspension (and thus the number of cells) used for seeding for shorter or longer stress treatment durations.
6. Washing the cell cultures with PBS, HBSS, or saline solution I before incubation in stress treatment or before starting a protection assay can damage the cell cultures and skew the results of the assay. To minimize the detrimental effects of these washing steps, we strongly recommend setting up multiple replicates for each condition. In addition, for assays using cell cultures grown in 96-well plates, we recommend to empty and fill eight wells at a time with a multichannel pipettes (instead of using vacuum to remove medium and washing solution) while tilting the plate to remove as much fluid as possible without

drying up the cell cultures. Finally, regardless of the technique used to wash the cell cultures, it is very important to avoid scratching the bottom of the well to avoid disturbing the cell layer.

7. Propidium iodide is cytotoxic and therefore intensively PI-stained cell cultures will show false-positive PI-stained cells that died because of long exposure to PI.
8. Fluorescein green fluorescence fades with time and therefore FD/PI-stained cell cultures should be observed immediately after the staining protocol is completed. For this reason, we recommend staining only one or two cell culture wells at a time and take pictures of the cells. This would guarantee that the intensity of the FD staining remains high to facilitate live cell counting.
9. The cell numbers from the stained nuclei can be counted manually or digitally with the help of cell counting software such as ImageJ. However, care must be taken to count the nuclei in a clumped area, or in the area of uneven staining, which is better counted manually. Therefore, it is important to keep the initial cell numbers low, and mixing the cell suspension well, before plating, especially in fast growing cell lines.
10. Colorimetric BrdU assays are available for 96-well plates (Calbiochem, EMD, QIA58), using HRP-tagged anti-BrdU antibodies instead of fluorescence-tagged antibodies that can be read in a plate reader. However, we found this method to be less sensitive as compared to the immunofluorescence staining method.

Acknowledgments

This work was supported by grants from the NIA (AG017617) and the Alzheimer's Association (IIRG-07-59699).

References

1. Sastre, M., Calero, M., Pawlik, M., Mathews, P. M., Kumar, A., Danilov, V., Schmidt, S. D., Nixon, R. A., Frangione, B., and Levy, E. (2004) Binding of cystatin C to Alzheimer's amyloid β inhibits amyloid fibril formation. *Neurobiol Aging* **25**, 1033–1043.
2. Kaeser, S. A., Herzig, M. C., Coomaraswamy, J., Kilger, E., Selenica, M. L., Winkler, D. T., Staufenbiel, M., Levy, E., Grubb, A., and Jucker, M. (2007) Cystatin C modulates cerebral β-amyloidosis. *Nat Genet* **39**, 1437–1439.
3. Mi, W., Pawlik, M., Sastre, M., Jung, S. S., Radvinsky, D. S., Klein, A. M., Sommer, J., Schmidt, S. D., Nixon, R. A., Mathews, P. M., and Levy, E. (2007) Cystatin C inhibits amyloid-β deposition in Alzheimer's disease mouse models. *Nat Genet* **39**, 1440–1442.
4. Selenica, M. L., Wang, X., Ostergaard-Pedersen, L., Westlind-Danielsson, A., and Grubb, A. (2007) Cystatin C reduces the in vitro formation of soluble Aβ1-42 oligomers and protofibrils. *Scand J Clin Lab Invest* **67**, 179–190.

5. Tizon, B., Ribe, E. M., Mi, W., Troy, C. M., and Levy, E. (2010) Cystatin C protects neuronal cells from amyloid β-induced toxicity. *J Alzheimers Dis* **19**, 665–894.
6. Tizon, B., Sahoo, S., Yu, H., Gauthier, S., Kumar, A. R., Mohan, P., Figliola, M., Pawlik, M., Grubb, A., Uchiyama, Y., Bandyopadhyay, S., Cuervo, A. M., Nixon, R. A., and Levy, E. (2010) Induction of autophagy by cystatin C: a mechanism that protects murine primary cortical neurons and neuronal cell lines. *PLoS One* **5**, e9819.
7. Deng, A., Irizarry, M. C., Nitsch, R. M., Growdon, J. H., and Rebeck, G. W. (2001) Elevation of cystatin C in susceptible neurons in alzheimer's disease. *Am J Pathol* **159**, 1061–1068.
8. Palm, D. E., Knuckey, N. W., Primiano, M. J., Spangenberger, A. G., and Johanson, C. E. (1995) Cystatin C, a protease inhibitor, in degenerating rat hippocampal neurons following transient forebrain ischemia. *Brain Res* **691**, 1–8.
9. Pirttila, T. J., and Pitkanen, A. (2006) Cystatin C expression is increased in the hippocampus following photothrombotic stroke in rat. *Neurosci Lett* **395**, 108–113.
10. Huh, C. G., Hakansson, K., Nathanson, C. M., Thorgeirsson, U. P., Jonsson, N., Grubb, A., Abrahamson, M., and Karlsson, S. (1999) Decreased metastatic spread in mice homozygous for a null allele of the cystatin C protease inhibitor gene. *Mol Pathol* **52**, 332–340.
11. Pawlik, M., Sastre, M., Calero, M., Mathews, P. M., Schmidt, S. D., Nixon, R. A., and Levy, E. (2004) Overexpression of human cystatin C in transgenic mice does not affect levels of endogenous brain amyloid β peptide. *J Mol Neurosci* **22**, 13–18.
12. Abrahamson, M., Barrett, A. J., Salvesen, G., and Grubb, A. O. (1986) Isolation of six cysteine proteinase inhibitors from human urine. Their physicochemical and enzyme kinetic properties and concentrations in biological fluids. *J Biol Chem* **261**, 11282–11289.
13. Yamada, T., Mukaiyama, I., Miyake, N., and Igari, J. (2002) Measurement of cystatin C in cerebrospinal fluid. *Rinsho Byori* **50**, 613–617.
14. Jones, K. H., and Senft, J. A. (1985) An improved method to determine cell viability by simultaneous staining with fluorescein diacetate-propidium iodide. *J Histochem Cytochem* **33**, 77–79.
15. Soames, A. R., Lavender, D., Foster, J. R., Williams, S. M., and Wheeldon, E. B. (1994) Image analysis of bromodeoxyuridine (BrdU) staining for measurement of S-phase in rat and mouse liver. *J Histochem Cytochem* **42**, 939–944.
16. Perry, S., Norman, J., Litzburg, A., and Gelbard, H. (2004) Antioxidants are required during the early critical period, but not later, for neuronal survival. *J Neurosci Res* **78**, 485–492.

Chapter 20

Study of Neurotoxic Intracellular Calcium Signalling Triggered by Amyloids

Carlos Villalobos, Erica Caballero, Sara Sanz-Blasco, and Lucía Núñez

Abstract

Neurotoxicity in Alzheimer's disease (AD) is associated to dishomeostasis of intracellular Ca^{2+} induced by amyloid β peptide (Aβ) species. Understanding of the effects of Aβ on intracellular Ca^{2+} homeostasis requires preparation of the different Aβ assemblies including oligomers and fibrils and the testing of their effects on cytosolic and mitochondrial Ca^{2+} in neurons. Procedures for cerebellar granule cell culture, preparation of Aβ species as well as fluorescence and bioluminescence imaging of cytosolic and mitochondrial Ca^{2+} in neurons are described.

Key words: Amyloid β peptide, Oligomers, Calcium, Bioluminescence imaging, Aequorin, Alzheimer's disease

1. Introduction

Alzheimer's disease (AD) is an aging-related neurodegenerative disorder associated to excess of amyloid β peptide (Aβ) production, an aberrant cleavage product of the amyloid precursor protein. AD has been also related to dis-homeostasis of intracellular Ca^{2+}, an elusive issue that remains controversial (1, 2). Aβ species in AD brains are made of polypeptides of several lengths that may show different assemblies from monomers, dimers, or other oligomers to the large fibrils forming macroscopic amyloid plaques, the hallmarks of AD (3). Aβ species are toxic to neurons and contribute largely to neurodegeneration in AD. The mechanism of neurotoxicity is under intense scrutiny and might differ among the several species (4, 5). Recent data show that $Aβ_{1–42}$ oligomers, the most likely neurotoxin in AD, but not fibrils, induce dramatic increases in cytosolic and mitochondrial Ca^{2+} concentrations in primary

Einar M. Sigurdsson et al. (eds.), *Amyloid Proteins: Methods and Protocols*, Methods in Molecular Biology, vol. 849,
DOI 10.1007/978-1-61779-551-0_20,

neurons that contribute to neurotoxicity (6). Here, we describe in detail the procedures for studying neurotoxic intracellular calcium signalling triggered by amyloids including neuron cell culture, preparation of different $A\beta_{1-42}$ species including oligomers and fibrils as well as the methodology to investigate the effects of these species on cytosolic and mitochondrial Ca^{2+} in single neurons by fluorescence imaging of fura2-loaded cells and bioluminescence imaging of cells expressing aequorin targeted to mitochondria.

2. Materials

2.1. Cell Preparation, Culture, and Transfection

1. HEPES-buffered saline (HBS) contains 145 mM NaCl, 5 mM KCl,1 mM $MgCl_2$, 1 mM $CaCl_2$, 10 mM glucose, 10 mM sodium-HEPES, pH 7.4 (MEC 1X).
2. Ham's F12 nutrient mixture is made solving (powder) Dulbecco's Modified Eagle's Medium (DMEM, Sigma-Aldrich Ref. 7777-10X1L) in 900 ml of double-distilled, sterile water. Then, 6 g HEPES and 336 mg $NaHCO_3$ are added to the mix. The solution is stirred and the pH adjusted to 7.42 using 4 N NaOH. Sterile water is added to a final volume of 1 l. Solution is then filtered in sterile conditions using Nalgene filters (Nalgene Labwere, Roskilde, Denmark) and saturated with CO_2 in sterile conditions before use.
3. Hank's medium is prepared mixing 85 ml of HBSS medium (Gibco Ref. 041-04170) with 15 ml of 4% bovine serum albumin (BSA, prepared previously solving 4 g of BSA in 100 ml of HBSS).
4. Solutions for cell dissociation: Dispase II (neutral protease) from *Bacillus polymyxa*, grade II (Roche).
5. Culture medium is made of DMEM (Gibco Ref. 41966-029) containing 4,500 mg/l glucose and 2 mM L-glutamine, fetal bovine serum (FBS, 10%), horse serum (HS, 5%), penicillin 100 U/ml, and streptomycin 100 µg/ml. All these items are from Invitrogen, Barcelona, Spain.
6. Sato's medium (7) is made of DMEM (Gibco Ref. 41966-029) containing also 0.5% HS, 5 µg/ml insulin, 100 µg/ml BSA, 16 µg/ml putrescine, 30 nM Se^{2+}, 60 ng/ml progesterone, 0.4 µg/ml tiroxine, 0.3 µg/ml tri-iodotironine, and 5 mg/ml holo-transferrin.
7. Poly-L-lysine-coated coverslips are prepared by placing 12-mm glass sterilized coverslips into a 0.01 mg/ml solution of poly-L-lysine (Sigma-Aldrich, Madrid, Spain). Treat for 15 min and then wash the coverslips twice with water and air-dry for 30–60 min under sterile conditions.

8. Multidish four wells for 12-mm glass coverslips are from Nunc (Ref. 176740), Rochester, NY, USA.
9. Amaxa Nucleofector and solution kit for neurons (Lonza Cologne, Germany).

2.2. Preparation of Amyloid β Peptide Species

Amyloid β peptide (1-42) is from Bachem AG (Bubendorf, Switzerland).

Solvents HCl and hexafluoroisopropanol (HFIP) are from Sigma-Aldrich.

Dimethyl sulfoxide (DMSO, Sigma-Aldrich).

DMEM F12 without phenol red (Gibco, Ref. 21041-025).

DMEM without phenol red (Lonza, Ref. 12-917F).

Speed Vac SPD111V (Thermo Electron Corporation, Marietta, OH, USA).

2.3. Fluorescence and Bioluminescence Imaging

1. HBS containing 145 mM NaCl, 5 mM KCl,1 mM $MgCl_2$, 1 mM $CaCl_2$, 10 mM glucose, 10 mM sodium-HEPES, pH 7.4.
2. Fura2/AM (Invitrogen, F1201, 1 mg). Stock solutions are made in DMSO at a concentration of 2 mM and stored at –20°C.
3. Digitonin (Sigma-Aldrich, D5628) dissolved at 100 μM in HBS containing 10 mM $CaCl_2$ instead 1 mM. Stock solution can be prepared at 10 mM in DMSO.
4. mGA plasmid. The mGA probe contain a mutated, low-affinity aequorin targeted to mitochondria and a GFP sequence to help select transfected neurons for bioluminescence imaging (8).
5. Coelenterazine *n* (Invitrogen, Ref. C6776). Stock solution is dissolved in methanol at 200 μM, aliquoted in 30 μl portions in Eppendorf tubes in ice and gassed briefly with N_2 before closing the tubes. Wrap with aluminum foil and store at –80°C for up to 6 months.
6. Zeiss Axiovert S100 TV (Carl Zeiss, Inc., Gottingen, Germany) inverted microscope equipped with a Zeiss Fluar 40x, 1.3 NA oil objective, a Xenon XBO75 fluorescence excitation lamp or a XCITE illumination system (EXFO, Ontario, Canada), a excitation filter wheel (Sutter Instrument Company, Novato, CA, USA) with band pass filters for fura2 excitation (340 and 380 nm) and a fura2 dichroic mirror.
7. ORCA ER fluorescence camera (Hamamatsu) mounted in the frontal or the lateral port of the microscope and handled by the Hamamatsu Aquacosmos software.
8. Hamamatsu VIM photon-counting ICCD camera (C2400-35) mounted in the bottom port of the microscope. Argus Image

Processor and M4314 image intensifier controller (Hamamatsu) are handled by the Aquacosmos software.

9. Cell perfusion system for living cells mounted in a PH-3 thermostated platform for open 12-mm glass coverslips using an 8-line gravity-driven perfusion system equipped with pinch valves (VC-8 valve controller) and solutions heated using an SH-27B inline heating system. All the above components are from Warner Instruments, Hamden, CT, USA.
10. Home-made, light-proof box covering the imaging set up. Size is about $100 \times 100 \times 100$ cm. They are also available from commercial sources (see Hamamatsu Photonics, Hamamatsu, Japan).

3. Methods

3.1. Neuron Cell Culture

1. Cerebellar granule cells are obtained from 5 to 7-day-old Wistar rat pups as reported previously (9). Animals are sacrificed by decapitation and the head is quickly washed in fresh HBS medium devoid of Ca^{2+} and glucose.
2. The skull is open to extract the brain that is washed quickly with Ham's F12 medium before dissecting the cerebellum.
3. Meninges are carefully removed and cerebellum is then washed with Hank's medium without Ca^{2+} or Mg^{2+} at 4°C.
4. Cerebellum is then cut in small pieces (about 2 mm) and incubated with Hank's medium without Ca^{2+} or Mg^{2+} but containing now dispase II (5 mg/ml) for 30 min at 37°C with discontinuous stirring every 5–10 min.
5. Tissue pieces are then dispersed using a silanized Pasteur pipette.
6. Dispersed tissue is allowed to rest to help debris removal. Supernatant-containing dispersed cells is placed into centrifuge tubes containing 7 ml of DMEM and cell suspension is then centrifuged at $200 \times g$ for 5 min.
7. The cell pellet is suspended in 1 ml of DMEM and then centrifuged again. Supernatant is removed and the new pellet is suspended again in 1 ml of DMEM containing now 10% horse serum.
8. At this point, cell density is estimated using a Neubauer counting chamber and medium is added to get a cell density of 1×10^6 cells/ml. At this point, 60 µl drops of cell suspension are plated on 12-mm glass coverslips previously coated with poli-L-lysine (0.01 mg/ml) and located inside the four wells multidish plaque. Cells are allowed to attach to the coverslips inside a cell incubator (37°C, 10% CO_2) for about 1 h.

9. Once cells are attached, 500 µl of DMEM containing 4,500 mg/ml glucose, 10% FBS, 5% horse serum, and antibiotics (penicillin, 100 U/ml and streptomicine, 100 µg/ml) are added to the four wells.
10. After 24 h, plating medium was exchanged for Sato's medium (7) containing 5% HS to avoid excess proliferation of glia (9). Cells are kept in the incubator for 3–5 days before imaging experiments.

3.2. Preparation of Aβ Oligomers and Fibrils

1. Preparation of $A\beta_{1-42}$ assemblies is carried out as described by Klein (10). $A\beta_{1-42}$ (Bachem AG) is initially dissolved to 1 mM in hexafluoroisopropanol and aliquoted in sterile, non-siliconated microcentrifuge tubes. The peptide was incubated 60 min at room temperature and then in ice for 5–10 min.
2. The eppendorf containing the peptide solution is maintained open overnight to allow evaporation of HFIP.
3. Hexafluoroisopropanol (HFIP) is then fully removed under vacuum in a speed vac. (10 min), and the peptide film was stored desiccated at −80°C.
4. For the aggregation protocol, the peptide was first solved in dry DMSO at a concentration of 5 mM and treated differently for preparation of oligomers and fibrils (Fig. 1).
5. For preparation of oligomers, DMEM without phenol red was added to bring the peptide to a final concentration of 100 µM and incubated at 4°C for 24 h. The preparation was then centrifuged at 14,000 × *g* for 10 min at 4°C to remove insoluble aggregates (protofibrils and fibrils) and the supernatants containing soluble $A\beta_{1-42}$ oligomers were transferred to clean tubes and stored at −20°C (see Note 1).
6. For preparation of fibrils, the peptide resuspended in DMSO at 5 mM concentration was diluted in 10 mM HCl to bring the peptide to a final concentration of 100 µM and incubated at 37°C for 24 h (see Note 1).

3.3. Fluorescence Imaging of Cytosolic Ca^{2+}

1. Coverslips containing cultured cerebellar granule cells were washed with HBS medium and incubated in the dark in the same medium containing 4 µM fura2/AM (11) for 60–90 min at room temperature.
2. Coverslips are then placed on a Warner PH-3 thermostated platform for open 12-mm glass coverslips (total volume about 500 µl) on the stage of an inverted microscope (Zeiss Axiovert S100 TV) and perfused continuously with heated (37°C) HBS using a Warner 8-line gravity-driven perfusion system equipped with pinch valves (Warner VC-8 valve controller) and a Warner SH-27B inline heating system (see Note 2).

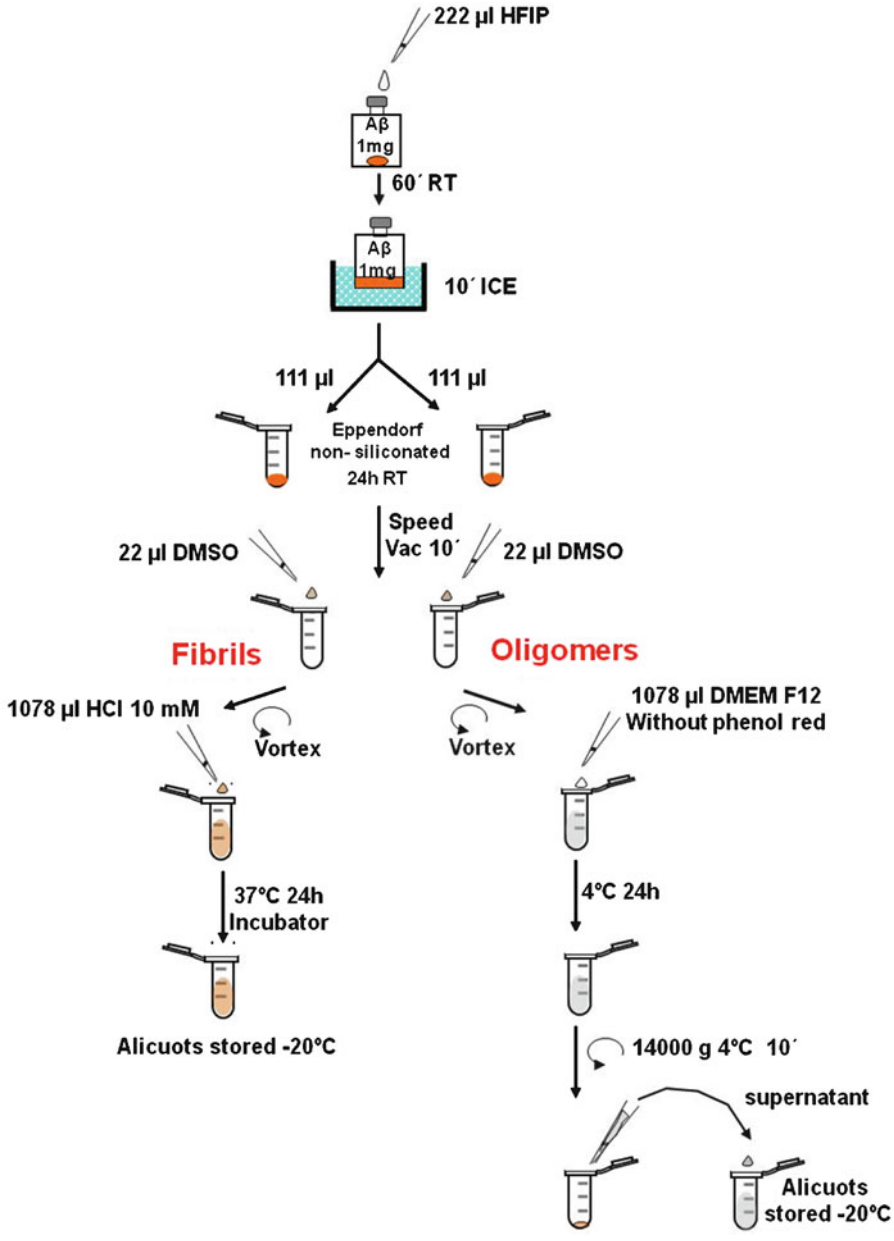

Fig. 1. Preparation of Aβ oligomers and fibrils. $A\beta_{1-42}$ (Bachem AG, 1 mg) was dissolved at 1 mM in hexafluoroisopropanol (HFIP) and incubated first 60 min at RT and then 10 min in ice. Then, the peptide was incubated overnight with the eppendorf's cup open. HFIP was removed under vacuum in a speed vac., (10 min); the peptide film can be stored desiccated at –20°C at this point. The peptide film is solved in DMSO at 5 mM and treated differently for preparation of oligomers (*right*) and fibrils (*left*). For oligomers (*right*), DMEM F-12 without phenol red is added to bring the peptide to 100 µM and incubated at 4°C for 24 h. Then, preparation is centrifuged (14,000 × *g*, 10 min, 4°C) and the supernatant-containing $A\beta_{1-42}$ oligomers is transferred to clean non-siliconated, eppendorf tubes and stored at –20°C until use. For fibrils (*left*), the peptide (5 mM) in DMSO is solved in 10 mM HCl to bring the peptide to a final concentration of 100 µM and incubated at 37°C for 24 h. Then, samples are stored at –20°C.

3. Cells are epi-illuminated alternately at 340 and 380 nm using band pass filters located on the excitation filter wheel. Light emitted above 520 nm at both excitation lights was filtered by the fura-2 dichroic mirror, collected every 5–10 s with a 40×, 1.4 NA, oil objective and recorded with the Hamamatsu Orca ER camera (Fig. 2).

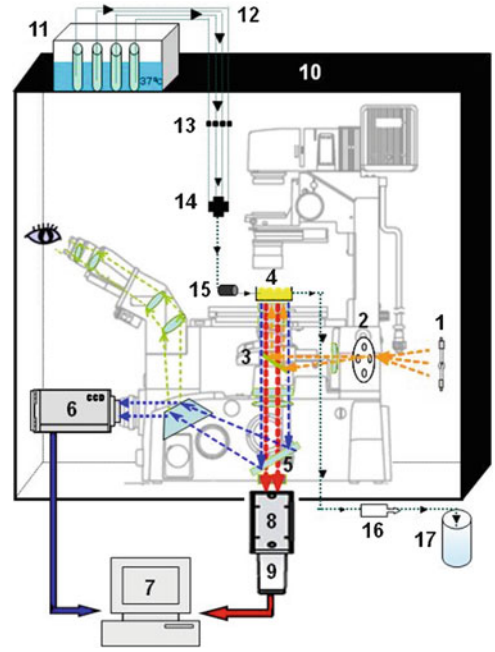

Fig. 2. Equipment for imaging of cytosolic and mitochondrial calcium. The system set up for imaging is built on an inverted microscope (Zeiss Axiovert S100 TV). For fluorescence excitation, a X-cite excitation lamp (1) provides excitation light that passes through filters (340 and 380 nm) contained in a filter wheel (2) and reflected by a dichroic mirror (3) before illuminating cells located in the heated stage of the microscope (4). Fura2 fluorescence (>520 nm) is collected by a Zeiss Fluar 40x, 1.3 NA oil objective, passes through the dichoric mirror (3) but is reflected by a further mirror (5) before being captured by a frontal or lateral-port located, Hamamatsu Orca ER digital camera (6) handled by the camera controller and the aquacosmos software in a computer system (7). For bioluminescence imaging, photonic emissions coming from the living cells pass through the least possible optic devices (dichroic mirror is removed from the pathway) including only an analyzer lens and a tube lent. Light travels through the microscope's bottom port via adaptor without lent and reaches the Hamamatsu C2400-35 ICCD intensifier (8) controlled by the M431 image intensifier controller, before is captured by a Hamamatsu CCD video camera (9). Signal goes through an Argus image processor and a JVC RGB monitor and is finally processed by the same computer system (7). The entire microscope must be covered by a light-proof box (10) to avoid light interference. Cells are perfused using a gravity-fed system (Warner). Solutions are prewarmed at 37°C (11) and driven through silicon tubes (12) by a valve-controlled perfusion system (13). All tubes converge by a manifold system (14) into one silicon tube that goes through an on-line heating system (15) before getting to the stage. Medium is continuously removed by another silicon tube attached on the platform and aspirated by vacuum pump (16) to the waste bottle (17).

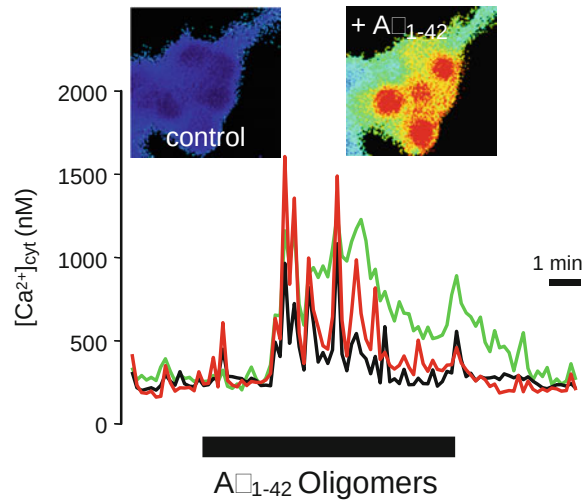

Fig. 3. $A\beta_{1-42}$ oligomers elicit increases in cytosolic Ca^{2+} in neurons. Cerebellar granule cells were cultured, loaded with fura2 and subjected to fura2 imaging. Pictures show pseudocolor images (Ratio 340/380) of granule cells before (*left*) and after stimulation with $A\beta_{1-42}$ oligomers. Warmer colors reflect increased cytosolic Ca^{2+} concentration. Recordings show cytosolic Ca^{2+} concentrations taken every 5 s in three individual cells. Perfused $A\beta_{1-42}$ oligomers increase cytosolic Ca^{2+} concentrations in all three neurons.

4. A background image is also captured at both excitation wavelengths with the shutter closed. During recordings, cells are perfused either with heated (37°C) control HBS or HBS containing test substances at a flow of 5 ml/min. This flow ensures that the medium bathing the cells is exchanged about ten times in less than 1 min.
5. At the end of the recording period, the complete sequences of images taken at 340 and 380 nm excitation light are stored in the computer for further analysis.
6. Using the Aquacosmos software, background images are subtracted and the resulting images are ratioed pixel by pixel to obtain a sequence of ratio images. Ratio images are coded in pseudocolor to better appreciate changes in Ca^{2+} concentrations. Perfusion of cerebellar granule cells with oligomers prepared from $A\beta_{1-42}$ induced rather dramatic increases in these ratios (Fig. 3), whereas no effect is induced by fibrils (data not shown).
7. For quantitative analysis of individual cells, regions of interest (ROIs) are drawn on individual cells and all ratio values corresponding to all pixels within each ROI are averaged for each image resulting in a recording of ratio values for individual ROIs (cells).
8. Recorded ratio values are converted into Ca^{2+} concentration values using the algorithm developed by Grynkiewicz et al. (11) (see Note 3).

3.4. Bioluminescence Imaging of Mitochondrial Ca^{2+}

1. Coverslips containing cerebellar granule cells are transfected with the mGA plasmid (see Note 4) using a Nucleofector II® device and the VPG-1003 transfection kit (Amaxa Biosystems, Cologne, Germany). Neurons are cultured for 24 h after transfection to allow efficient expression and targeting of the probe.
2. The coverslips containing the cells expressing the apoaequorins are transferred to a 4-well plate containing 0.20 ml of HBS. Then, 1 μl of coelenterazine *n* is added and gently mixed. Finally, the plate is incubated for 1–2 h at room temperature in the dark.
3. Bioluminescence imaging was carried out as described previously (12, 13). Coverslips are placed on the stage of the bioluminescence microscope (Zeiss Axioverti S100 TV) into a perfusion chamber thermostated to 37°C and perfused continuously with prewarmed HBS at a rate of 5 ml/ml. The cells are examined for GFP fluorescence using the FITC filters and the microscopic field selected. A typical field may contain 4-8 transfected cells. A GFP fluorescence image (Fig. 4) is captured with the help of the Hamamatsu C2400-35 ICCD camera with the sensitivity set to a minimum (0) and located in the bottom port of the microscope (see Note 5).
4. After turning off the excitation lamp, a bright field image of the same cells is captured using the same camera.
5. Microscope light was turned off and the dark-box doors closed for complete darkness (see Note 6). Sensitivity of the intensifier is then set to maximum (12) and photonic emission images are captured with the Hamamatsu VIM photon-counting camera handled with an Argus-20 image processor and integrated every 10 s periods (Fig. 4). Total counts per region of interest may range between 2×10^3 and 2×10^5 for different cells. Background photonic emissions in regions of interest of similar size in nonexpressing cells are typically about 1 ± 1 count per second per typical cell area (about 2,000 pixels).
6. Cells are perfused at selected periods with Aβ species at an estimated concentration of 1 μM by using the perfusion system. Alternatively, Aβ species can be provided as drops using an automatic pipette.
7. Before ending the experiment, cells are perfused with HBS containing 0.1 mM digitonin and 10 mM $CaCl_2$ to permeate the cells and release all the remaining aequorin counts. These photonic emissions must be added up to estimate the total photonic emissions, a value required for calibration in Ca^{2+} concentrations. Emission of all residual counts may take 2–5 min from the time of lysis. The experiment is finished once aequorin photonic emissions cease.

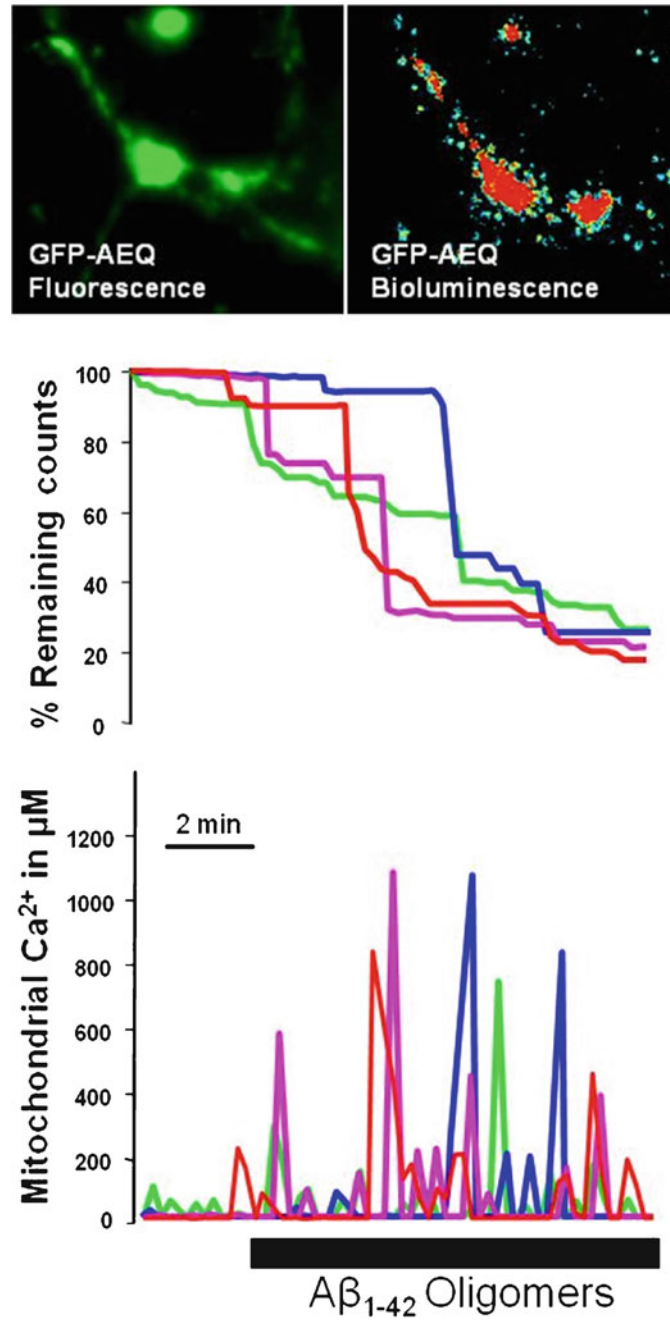

Fig. 4. $A\beta_{1-42}$ oligomers induce mitochondrial Ca^{2+} overload in neurons. Cerebellar granule cells were transfected with the low-affinity, mitochondria-targeted aequorin fused to GFP, incubated with 1 µM coelenterazine *n* and subjected to bioluminescence imaging of $[Ca^{2+}]_{mit}$. Pictures show the fluorescence (*top*, GFP fluorescence) and accumulated photonic emissions (*bottom*, Aequorin Bioluminescence) images of representative microscopic fields. Luminescence intensity is coded in pseudocolor. Top recordings show the release of photonic emissions (expressed as % of remaining counts) during recording in four individual cells. Perfusion with $A\beta_{1-42}$ oligomers (but no fibrils) released photonic emissions (thus, decreasing the % of remaining counts). Those values were used to calculate mitochondrial Ca^{2+} concentrations (*bottom* recordings). $A\beta_{1-42}$ oligomers promoted increases in mitochondrial Ca^{2+} concentrations that reached even the mM level as previously reported (6).

8. Bioluminescence images are finally stored in the computer with the bright field and fluorescence images captured before photon-counting imaging.
9. Regions of interest (ROIs) are selected with the help of the Aquacosmos software by drawing circles around infected cells according to the fluorescence and bright field images captured at the beginning of the experiment (see Note 7). The same ROIs are pasted on every image of the sequence. Total photonic emissions in every ROI are computed with the Aquacosmos software to obtain the luminescence emission value (L) for each cell at each point in time. A few ROIs are drawn in regions devoid of cells to compute background luminescence.
10. All the photonic emissions in the bioluminescence images, including the obtained after digitonin permeabilization, are added up using the Aquacosmos software to obtain a bioluminescence image containing all the photonic emissions. The size of the ROI is adjusted to the area in which photons are emitted from each individual cell, which is usually somewhat larger than the size of the cell. Cells with overlapping of photonic emissions are excluded from the analysis.
11. The luminescence values for every ROI at each time value (L) are computed and exported to a worksheet. Background luminescence is subtracted from each L value. For every ROI, the total luminescence, Total(L) was computed by adding up the values of all the images. Then, the following values were computed for every time point (t):
    - L: Luminescence emission at time t
    - $\mathrm{Sum}(L) = \Sigma L$ values from $t = 0$ to t
    - L_{TOTAL}: Total luminescence remaining at time $t = \mathrm{Total}(L) - \mathrm{Sum}(L)$
    - % Remaining luminescence: $100 \times L_{\mathrm{TOTAL}} / \mathrm{Total}(L)$
    - L / L_{TOTAL}
    - $[Ca^{2+}]$ using the following algorithm:

$$[Ca^{2+}]\,(\text{in M units}) = \frac{R + (R \times K_{\mathrm{TR}}) + 1}{K_{\mathrm{R}} - (R \times K_{\mathrm{R}})},$$

where $R = \left(\dfrac{L}{L_{\mathrm{TOTAL}} \times \lambda}\right)^{(1/n)}$,

where L is the luminescence emitted at the time of measurement and L_{TOTAL} is the addition of the counts present in the tissue at that time, estimated by integrating all the counts from the time of measurement until the release of all the residual luminescence by lysis at the end of the experiment. Calculations were made using the constant values published elsewhere (14).

4. Notes

1. Characterization of amyloid β preparations is beyond the scope of this chapter. However, the characterization is required to confirm the species that are present in each preparation, their purity and actual concentrations. This characterization is not simple and may require a combination of several approaches including electron microscopy, amino acid analysis, PAGE-SDS, and silver staining (6).
2. Perfusion is very helpful during imaging not only to add and remove easily and quickly test solutions to the cell chamber but also to keep physiological conditions (37°C, or even CO_2 if required) thanks to the in-line heating system. Perfusion of expensive test solutions such as Aβ species may be, however, cost limiting. In those cases where perfusion is not available or convenient, Aβ can be provided by carefully adding a 250 µl drop of 2×, Aβ-containing solution, to a half-filled chamber (about 250 µl) and making a quick mix of solutions. In this case, it is best to keep the heating system off and make the experiment at room temperature to avoid changes in the composition of saline due to evaporation.
3. Binding of Ca^{2+} to fura2 changes fura2 fluorescence according to the law of mass action (11):

$$[Ca^{2+}]=K_d \frac{F_{max}-F}{F-F_{min}},$$

where K_d is the dissociation constant of the fura2–Ca^{2+} complex (224 nM at 37°C), F is the fluorescence emission for each $[Ca^{2+}]$, F_{max} is the fluorescence emission when fura2 is saturated with Ca^{2+}, and F_{min} is fluorescence emission when fura2 is free of Ca^{2+}. If we apply the above algorithm to both wavelengths and do the ratio, then we obtain the following algorithm:

$$[Ca^{2+}]=K_d \beta \frac{R_{max}-R}{R-R_{min}},$$

where R is the ratio of fluorescence recordings obtained after exciting at 340 and 380 nm for a given $[Ca^{2+}]$, R_{max} is the same ratio when fura2 is saturated with Ca^{2+}, and R_{min} is the same ratio when fura2 is free of Ca^{2+}. Finally, β is the ratio of F_{max}/F_{min} at 380 nm. This algorithm allows estimation of $[Ca^{2+}]$ knowing the R values at any point in time. R_{max}, R_{min}, and β values can be determined experimentally using fura2 solutions in the presence of saturating concentrations of Ca^{2+} (HBS containing

1 mM Ca^{2+}) and in the absence of Ca^{2+} free medium (HBS without added Ca^{2+} and containing 5 mM EGTA).

4. The use of the fusion protein GFP–aequorin in the mGA plasmid has many advantages over the native aequorin. It allows direct visualization of the expressed protein under the fluorescence microscope which is very convenient particularly when transfection efficiency is low. In addition, the protein is more stable, and it gives a higher quantum yield (8).
5. The same set up for fluorescence imaging can be used for bioluminescence imaging. We have the fluorescence camera placed in the lateral port and the photon-counting camera in the bottom port. This configuration avoids loosing of aequorin photonic emissions when the system is used in the bioluminescence imaging mode. Before photon counting, a GFP fluorescence image of GFP and aequorin-transfected cells is captured with the bottom-port located, photon-counting camera and the sensitivity gain set to a minimum. Then, the dichroic-containing box located in the light pathway is removed, the excitation light turned off, the dark-box doors are closed and the sensitivity gain is set to a maximum before starting bioluminescence imaging.
6. Photon-counting cameras are extremely sensitive to any contaminating light. Accordingly, any light source inside the dark box must be turned off during photon counting. Putative light sources such as leads of different operators, even if they are outside the dark box, must be turned off. Some motorized microscopes have internal leads that may produce a light leak to the camera.
7. Calibration of the recorded signals is dependent of the total amount of photonic emissions, including those released after cell permeabilization. If cell density is excessive or the amount of light emitted by some individual cells is too high, overlap between photonic emissions from different cells may happen and this could influence the calculations of Ca^{2+} concentrations. This can be avoided by optimizing expression efficiency and/or by plating the cells at a proper density.

Acknowledgments

Financial support from Spain's Ministerio de Educación y Ciencia (BFU2009-08967), Instituto de Salud Carlos III (PI07/0766), and Junta de Castilla y León (CSI12A08 and VA270A11-2) are gratefully acknowledged.

References

1. Berridge, M. J. (2010) Calcium hypothesis of Alzheimer's disease. *Pflugers Arch.* **459**, 441–449.
2. Foskett, K., Bacskai, B., Kuchibhotla, K., Fagan, T., Bezprozvanny, I., Moyer, J., Stutzmann, B., Green, K., Villalobos, C., Michno, K., Goussakov, I., Atwood, C., Rybalchenko, V., Chakroborty, S. (2009) Alzheimer research forum live discussion: calcium in AD pathogenesis. *J. Alzheimers Dis.* **16**, 909–917.
3. Haass, C., Selkoe, D. J. (2007) Soluble protein oligomers in neurodegeneration: lessons from the Alzheimer's amyloid beta-peptide. *Nat. Rev. Mol. Cell Biol.* **8**, 101–112.
4. Dahlgren, K. N., Manelli, A. M., Stine, W. B. Jr, Baker, L. K., Krafft, G. A., LaDu, M. J. (2002) Oligomeric and fibrillar species of amyloid-beta peptides differentially affect neuronal viability. *J. Biol. Chem.* **277**, 32046–32053.
5. Deshpande, A., Mina, E., Glabe, C., Busciglio, J. (2006) Different conformations of amyloid beta induce neurotoxicity by distinct mechanisms in human cortical neurons. *J. Neurosci.* **26**, 6011–6018.
6. Sanz-Blasco, S., Valero, R. A., Rodríguez-Crespo, I., Villalobos, C., Núñez, L. (2008) Mitochondrial Ca^{2+} overload underlies Aβ oligomers neurotoxicity providing an unexpected mechanism of neuroprotection by NSAIDs. *PLoS ONE* **3**(7): e2718
7. Bottestein, J.E., Sato, G. H. (1979) Growth of a rat neuroblastoma cell line in serum-free supplemented medium. *Proc. Natl. Acad. Sci. USA* **76**, 514–517.
8. Rogers, K. L., Stinnakre, J., Agulhon, C., Jublot, D., Shorte, S. L., Kremer, E. J., Brûlet, P. (2005) Visualization of local Ca^{2+} dynamics with genetically encoded bioluminescent reporters. *Eur. J. Neurosci.* **21**, 597–610.
9. Núñez, L., Sánchez, A., Fonteriz, R. I., García-Sancho, J. (1996) Mechanisms for synchronous calcium oscillations in cultured rat cerebellar neurons. *Eur. J. Neurosci.* **8**, 192–201.
10. Klein, W. L. (2002) Abeta toxicity in Alzheimer's disease: globular oligomers (ADDLs) as new vaccine and drug targets. *Neurochem. Int.* **41**, 345–352.
11. Grynkiewicz, G., Poenie, M., Tsien, R. Y. (1985) A new generation of Ca^{2+} indicators with greatly improved fluorescence properties. *J. Biol. Chem.* **260**, 3440–3450.
12. Villalobos, C., Núñez, L., Chamero, P., Alonso, M. T., García-Sancho, J. (2001) Mitochondrial $[Ca^{2+}]$ oscillations driven by local high $[Ca^{2+}]$ domains generated by spontaneous electric activity. *J. Biol. Chem.* **276**, 40293–40297.
13. Núñez, L., Senovilla, L., Sanz-Blasco, S. I., Chamero, P., Alonso, M. T., Villalobos, C., García-Sancho, J. (2007) Bioluminescence imaging of mitochondrial calcium in sympathetic neurons from adult rat dorsal root ganglion. *J. Physiol.* **580**, 385–395.
14. Villalobos, C., Alonso, M. T., García-Sancho, J. (2009) Bioluminescence imaging of calcium oscillations inside intracellular organelles. *Methods Mol. Biol.* **574**, 203–214.

Chapter 21

Bacterial Amyloids

Yizhou Zhou, Luz P. Blanco, Daniel R. Smith, and Matthew R. Chapman

Abstract

Many bacteria can assemble functional amyloid fibers on their cell surface. The majority of bacterial amyloids contribute to biofilm or other community behaviors where cells interact with a surface or with another cell. Bacterial amyloids, like all functional amyloids, share structural and biochemical properties with disease-associated eukaryotic amyloids. The general ability of amyloids to bind amyloid-specific dyes, such as Congo red, and their resistance to denaturation have provided useful tools for scoring and quantifying bacterial amyloid formation. Here, we present basic approaches to study bacterial amyloids by focusing on the well-studied curli amyloid fibers expressed by *Enterobacteriaceae*. These methods exploit the specific tinctorial and biophysical properties of amyloids. The methods described here are straightforward and can be easily applied by any modern molecular biology lab for the study of other bacterial amyloids.

Key words: Bacterial amyloids, Curli, Congo red dye, Western blot analysis, Plug western blot analysis, Overlay assay, Interbacterial complementation

1. Introduction

Amyloids are traditionally associated with protein misfolding and neurodegenerative diseases including Alzheimer's disease, Parkinson's disease, and Creutzfeldt-Jacob disease (1–3). However, a rapidly growing class of "functional amyloids" has recently been described, which indicates that the amyloid fold can be utilized by all walks of cellular life for a variety of functions (4–6). So far, most functional amyloids in bacteria perform physiological tasks on the cell surface including biofilm formation, adhesion, invasion of host cells, and host–pathogen interactions (7–14). For example, curli generated by *Escherichia coli* and *Salmonella spp.* (15, 16), chaplins formed by *Streptomyces spp.* (6, 17), and TasA fibers produced by *Bacillus subtilis* (11) are all functional amyloids utilized by microbes to promote interbacterial interactions. Unlike disease-associated

Einar M. Sigurdsson et al. (eds.), *Amyloid Proteins: Methods and Protocols*, Methods in Molecular Biology, vol. 849,
DOI 10.1007/978-1-61779-551-0_21,

eukaryotic amyloids, functional bacterial amyloids are assembled by highly regulated biosynthetic pathways (4). Bacterial amyloids exhibit the structural and biochemical properties of amyloids. Like all amyloids, functional amyloids bind dyes such as Congo red (CR) and Thioflavin T (6, 11, 15, 18). The structural analysis of bacterial amyloid fibers indicates a beta-sheet-rich secondary structure (11, 15, 17, 19). Amyloid fibers are also extraordinarily stable and resistant to SDS denaturation and Protease K digestion (17, 20, 21). These properties provide a toolbox for research on bacterial amyloids. Here we use curli, one of the best-characterized bacterial amyloids as an example to describe a few basic approaches to study bacterial amyloids.

Curli are extracellular amyloid fibers produced by many species of *E. coli* and *Salmonella spp.* strains (16, 22, 23). Purified curli fibers bind CR and induce a spectral red shift in absorbance (15). Colonies of curliated *E. coli* K-12 stain red on agar plates containing CR, whereas curli defective mutants are nonstained (15). Once CR interacts with curli, it also produces a bright red fluorescence that can be quantified with an excitation wavelength of 485 nm and an emission wavelength of 612 nm.

Curli fibers are composed of two structural components: the major curlin subunit CsgA (csg: curli-specific gene) and the minor subunit CsgB. The secretion of CsgA and CsgB requires the outer membrane lipoprotein CsgG and the periplasmic accessory factors CsgE and CsgF (4). Once incorporated into curli fibers, CsgA and CsgB are no longer soluble by SDS denaturation treatment (15). CsgB functions as a nucleator by templating the polymerization of CsgA in vivo. Without CsgB, CsgA proteins are secreted to the extracellular space in an SDS-soluble, unstructured form that can be detected in the agar (24, 25).

In this chapter, we describe basic approaches for analyzing the presence and/or integrity of curli fibers under physiological conditions. The CR-based assays described here are amendable to high-throughput screens that assess curli production. CR indicator plates can be used to screen for curli defective mutants and to identify genes important for curli regulation and assembly (26, 27). Western blot analysis of whole cell lysate is also useful to sort factors involved in curli amyloidogenesis (28–30). Curli produced by wild-type *E. coli* are cell associated and insoluble in SDS-sample buffer with boiling. Treatment of whole cell lysates with formic acid (FA) or hexafluoro-2-propanol (HFIP) dissociates the curli fibers into monomores of the major subunit CsgA. After chemical denaturation, CsgA can mobilize into an SDS–PAGE gel and can be identified as a band that migrates at about 17.5 kDa using anti-CsgA antibodies (15). We will also detail how a "plug" western blot assay can be used to differentiate between curli subunits that are unpolymerized from those that are cell-associated and polymerized

(15, 25, 29). Finally, the overlay assay and interbacterial complementation provide ways to test CsgA polymerization templated by CsgB in vivo on the bacterial surface. Freshly purified CsgA or CsgA secreted by a *csgB* mutant assembles on a *csgA* mutant that presents CsgB on the cell surface. The assays also help to identify the interacting domains of CsgA and CsgB responsible for the nucleation process. These assays can be carried out using common equipment and can be adapted to study other bacterial amyloids.

2. Materials

Prepare all the solutions and media using ultrapure water. Prepare and store the reagents at room temperature (RT) unless otherwise indicated. Add antibiotics to media if needed.

2.1. Standard Growth Media for E. coli Curli Induction

1. Luria-Bertani (LB) agar plates: dissolve 5 g/L yeast extract, 10 g/L bacto tryptone, and 10 g/L sodium chloride in water.
2. YESCA agar plates: YESCA agar is used to induce curli production. Dissolve 1 g/L yeast extract, 10 g/L casamino acids, and 20 g/L agar in water. Pour 25 mL per Petri dish to make normal YESCA plates. For thin YESCA plates used in plug western blots, pour only 15 mL per Petri dish (see Note 1).

2.2. Congo Red Assays

1. For quantitative CR biochemical assays, one will need a Spectra max M2 plate reader (or equivalent) and opaque flat-bottom polystyrene 96-well plates for CR fluorescence quantification.
2. CR stock solution (10 mg/mL): dissolve 1 g CR in 100 mL water and filter sterilize. Store at 4°C (see Note 2).
3. Brilliant Blue G250 stock solution (10 mg/mL): dissolve 1 g Brilliant Blue G250 dye in 100 mL water and filter sterilize. Store at 4°C (see Note 3).
4. YESCA CR plates: dissolve 1 g/L yeast extract, 10 g/L casamino acids, and 20 g/L agar in water. After autoclave, add 5 mL CR stock and 100 µl Brilliant blue stock to make a final concentration of 50 µg/mL CR and 1 µg/mL Brilliant blue.
5. 50 mM Potassium phosphate buffer (KPi), pH 7.2: dissolve 28.9 mmol KH_2PO_4 and 21.1 mmol K_2HPO_4 into pure water. Dilute to 1 L and filter sterilize.

2.3. Western Blot Analysis

1. In this experiment, you will need Pasteur pipettes with 8 mm diameter, Whatman filter paper, polyvinylidene difluoride (PVDF) and nitrocellulose (0.2 µM) membranes, protein

electrophoresis apparatus, semidry and wet transfer apparatus, chemiluminescent substrates, and autoradiography cassettes.

2. 50 mM KPi, pH 7.2.
3. HFIP or FA (see Note 4).
4. 2× SDS sample buffer: mix 1 mL 1.25 M Tris pH 6.8, 1 mL β-mercaptoethanol, 200 μL 1% bromophenol blue, 2 mL glycerol, 6 mL 10% SDS, and 10 mL water. Bring the final volume up to 20 mL.
5. 15-Well SDS–polyacrylamide gel: 15% separating gel and 3% stacking gel.
6. SDS running buffer: dissolve 30.27 g Tris base, 144.1 g glycine, and 10 g SDS into 1 L water to make a 10× stock. Dilute the stocking buffer by 10× into water to make 1× running buffer.
7. Semidry transfer buffer: dissolve 30.3 g Tris base, 7.5 g glycine, and 0.386 g dithiothreitol (DTT) in 1 L water to make a 10× stock solution. Mix 100 mL 10× stock buffer, 20 mL methanol, and 70 mL water to make 1 L of 1× semidry transfer buffer.
8. Wet transfer buffer: dissolve 5.53 g CAPS in a mixture of 100 mL methanol and 900 mL water. Use NaOH pellets to adjust the pH to 11.2 (see Note 5).
9. Tris-buffered saline–Tween-20 (TBS-T): dissolve 160 g NaCl, 4 g KCl, and 60 g Tris in water and adjust pH to 7.5 with HCl. Add 20 mL Tween-20 and add water to make a 1 L 20× stock. Dilute the stock in water to make 1× TBS-T buffer. Store the 20× stocking buffer and 1× buffer at 4°C.
10. Blocking solution: dissolve 1% dry fat-free milk and 1% BSA in 1× TBS-T buffer.
11. CsgA antibody (Proteintech, Chicago, IL) was raised in rabbits against purified CsgA proteins. CsgB antibody (Proteintech, Chicago, IL) was raised in rabbits against a peptide fragment of the second repeating units of CsgB. Save the antibodies at –20°C. Dilute antibodies by 1:10,000 for CsgA and 1:7,000 for CsgB into blocking solution for primary probing (see Note 6).
12. Anti-rabbit secondary antibody: peroxidase antibody produced in goat. Store the antibody at –20°C. Dilute the antibody by 1:7,000 into blocking solution before use.

2.4. CsgA Purification and Overlay Assay

1. For CsgA purification as described here, you will need 0.22-μm polyethersulfone bottle-top filters, nickel–nitrilotriacetic acid agarose (Ni-NTA), sephadex G-25, BCA protein assay kit, Kontes 2.5 × 10 cm, and 1 × 30 cm glass columns, Nalgene powder funnel (150 mm with 2.5 cm spout), disposable polypropylene columns, 30 kDa centrifugal filter units, spin desalting columns and 0.02-μm Anotop filters (Whatman).

2. LSR12/pMC1/pMC3: LSR12 is a complete curli deletion mutant of *E. coli* C600 (31). pMC1 was made by cloning CsgG into the *Nco*I and *Bam*HI sites of pTRC99. pMC3 was made by cloning full-length C-terminal His_6-tagged CsgA into the *Nde*I and *Eco*RI sites of pHL3 (15, 31).
3. NEB C2566/pNH11 (30): The plasmid pNH11 was made by cloning C-terminal His_6-tagged CsgA without the Sec signal sequence into the pET11d vector.
4. Isopropyl β-d-1-thiogalactopyranoside stock (1 M): dissolve 4.76 g IPTG powder into 20 mL water and filter sterilize. Make 1 mL aliquots in 1.5-mL microcentrifuge tubes. Store at −20°C.
5. Guanidine hydrochloride (8 M): Dissolve 764.2 GdnHCl into 1 L 50 mM KPi. Adjust the pH to 7.2 with NaOH and bring up the final volume to 1 L.
6. 50 mM KPi, pH 7.2. Store at 4°C.
7. 100 mM Imidazole in 50 mM KPi, pH 7.2: dissolve 6.8 g imidazole into 1 L 10 mM KPi and filter sterilize. Store at 4°C.
8. 12.5 mM Imidazole in 50 mM KPi, pH 7.2: dissolve 0.85 g imidazole into 1 L 50 mM KPi and filter sterilize. Store at 4°C.
9. 125 mM imidazole in 50 mM KPi, pH 7.2: dissolve 8.51 g imidazole into 1 L 50 mM KPi and filter sterilize. Store at 4°C.

3. Methods

3.1. Congo Red Assays

Curliated bacteria stain red when grown on plates amended with CR. Therefore, it is easy to differentiate curli-producing strains from curli defective strains by assessing the colony color on plates containing CR (15).

3.1.1. CR Staining of Bacterial Colonies (Fig. 1a)

1. Streak *E. coli* strains from −80°C frozen stock onto an LB plate and grow at 37°C overnight.
2. Pick single colonies, streak out on a YESCA CR agar plate (see Note 7).
3. Grow bacteria at 26°C for 2 days to induce curli production (see Note 8).
4. Check the color of colonies on the YESCA CR plate. Curliated bacteria stain red on YESCA CR agar, while curli defective mutants are usually pink or white (see Note 9).

3.1.2. Congo Red Fluorescence (see Notes 7 and 9)

(a) Quantification of CR fluorescence by post-CR staining (Fig. 1b, c).

1. Streak *E. coli* strains from −80°C frozen stock to an LB plate and grow at 37°C overnight.

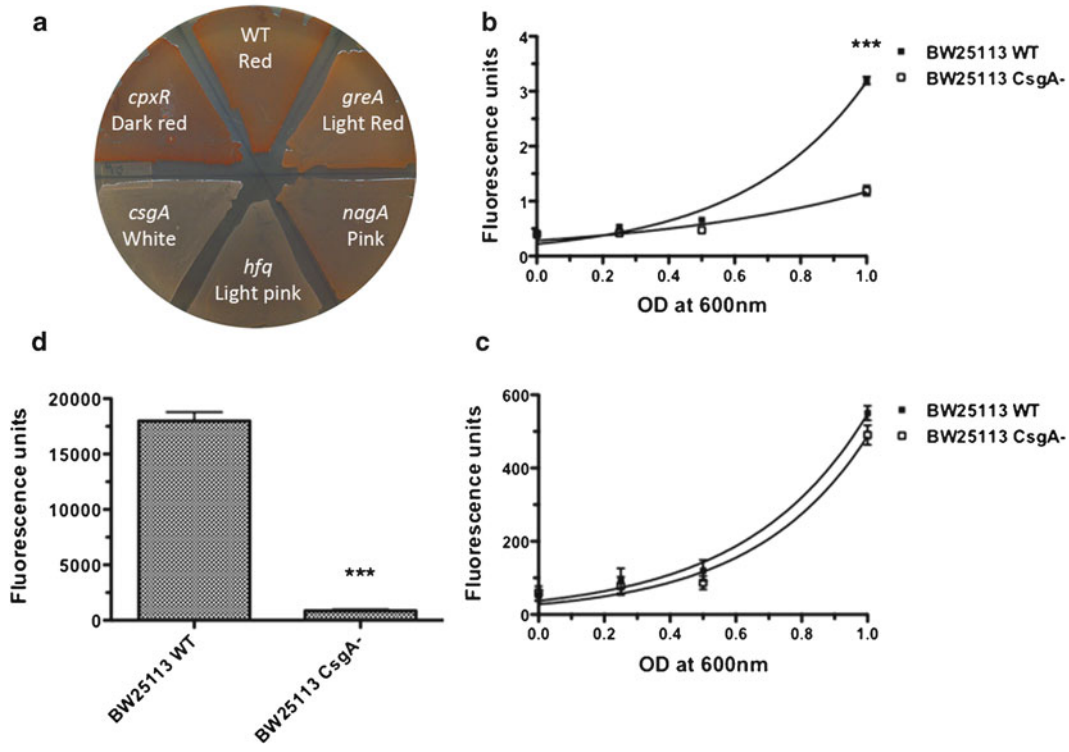

Fig. 1. CR staining and fluorescence quantification. (**a**) Use of CR staining to screen for curli mutants. Colonies of the wild-type *E. coli* stained *red* on the YESCA CR agar plate, while the curli defective mutant, *csgA,* remained *white*. Curli mutants (36) showed *dark red*, *pink,* or *light pink* color on the YESCA CR plate. (**b–d**) Measurements of the fluorescence associated with bacteria for CR (Em/Ex: 485/612 nm). BW25113 wild-type and the *csgA* deletion mutant strains were recovered from YESCA plates after 48 h of growth at 26°C and resuspended in 1 mL of 50 mM KPi (pH 7.2) containing 0.5 μg/mL CR or 4.5 μg/mL DAPI. After wash, serial base two dilutions are prepared and the fluorescence was measured in a 96-well plates by triplicate. As a reference, 100 μL of 50 mM KPi were used. (**b**) Comparison of CR fluorescence of curli producing wild-type and curli deficient *csgA* strains. Nonlinear (exponential fit): $R^2 = 0.970$ and 0.778 for BW25113 and *csgA,* respectively. (**c**) To show that the BW25113 *csgA* mutant was present in the same amount as the wild-type BW25113 strain, bacteria were post-labeled with the unspecific DNA 4′,6-diamidino-2-phenylindole (DAPI) fluorochrome and the DAPI fluorescence is measured (Em/Ex: 350/460 nm). Nonlinear (exponential fit): $R^2 = 0.865$ and 0.867 for BW25113 and *csgA,* respectively. (**d**) Quantification of CR fluorescence for bacteria prestained on YESCA CR plates. The CR fluorescence of the wild-type strain was significantly higher (around three times) compared with the BW25113 *csgA* mutant. ***$p < 0.0001$ using student's *t* test. Error bars: average SEM of at least six wells per sample. The plate reader used in this determination was an Infinite 200 with the Tecan-I application and automatic optimization of the gain.

2. Inoculate single colonies in LB liquid broth and grow at 37°C overnight with shaking.
3. Spot 4 μL drops of overnight cultures on an YESCA agar plate without CR. Incubate the plate at 26°C for 48 h to induce curli production.
4. Recover bacteria cells from the YESCA plate and suspend them in 1 mL 50 mM KPi. Adjust the optical density at 600 nm to 1 U in 1 mL of 50 mM KPi.

5. Centrifuge bacteria at 16,000 × *g* for 1.5 min and resuspend them in 1 mL 50 mM KPi containing 0.5 μg/mL CR. Incubate at RT with shaking for 20 min.
6. Wash bacterial cells by centrifugation and resuspend them in 1 mL of 50 mM KPi buffer.
7. Prepare serial dilutions of bacterial suspension. Load 100 μL of each sample onto a 96-well opaque plate. Measure the CR fluorescence using a Spectra max M2 plate reader. Set the excitation wavelength at 485 nm and the emission at 612 nm (see Note 10). Use 100 μL of KPi as the blank.

(b) Quantification of CR fluorescence for bacteria prestained on YESCA CR plates (Fig. 1d).

1. Spot 4 μL of overnight bacterial culture on the YESCA CR plate. Incubate the plate at 26°C for 48 h.
2. Recover bacteria from the YESCA CR plate. Wash them in 50 mM KPi by centrifugation at 16,000 × *g* for 1.5 min and resuspend them in 1 mL 50 mM KPi. Adjust the cell density to $1OD_{600}$/mL.
3. Load 100 μL bacteria suspensions onto a 96-well plate reader. Measure the CR fluorescence with a Spectra max M2 plate reader as described above.

3.1.3. Interbacterial Complementation (see Note 11)

Unpolymerized CsgA secreted out by an *E. coli csgB* mutant assemble into amyloid fibers on the surface of an adjacent *E. coli csgA* mutant that is expressing the nucleator protein CsgB, a process called interbacterial complementation Fig. 2a (15). Interbacterial complementation provides a tool for analyzing the nucleation process during curli assembly. In this section, we define the *E. coli csgB* mutant that secretes out unpolymerized CsgA as the donor strain and the *csgA* mutant that expresses CsgB on the cell surface as the recipient strain.

1. To test the ability of *E. coli* mutants to nucleate CsgA secreted by the donor, streak out the donor from the top of the YESCA CR plate to the bottom and then streak the putative acceptor strains perpendicularly across the donor streak. Use an *E. coli csgA* mutant as a positive control. Incubate the plate at 26°C for 48 h. Bacteria that are able to accept CsgA from the donor and convert them to curli fibers stain red on CR plate when cross-streaked.
2. To analyze the secretion of CsgA or the properties of CsgA protein variants, streak out the recipient from the top of the YESCA CR plate to the bottom and cross-streak the putative donor strains perpendicularly over the recipient. Use an *E. coli csgB* mutant as the positive control. Incubate the plate at 26°C for 48 h. Bacteria donating functional CsgA stain red after cross-streaked over the recipient (see Notes 12 and 13).

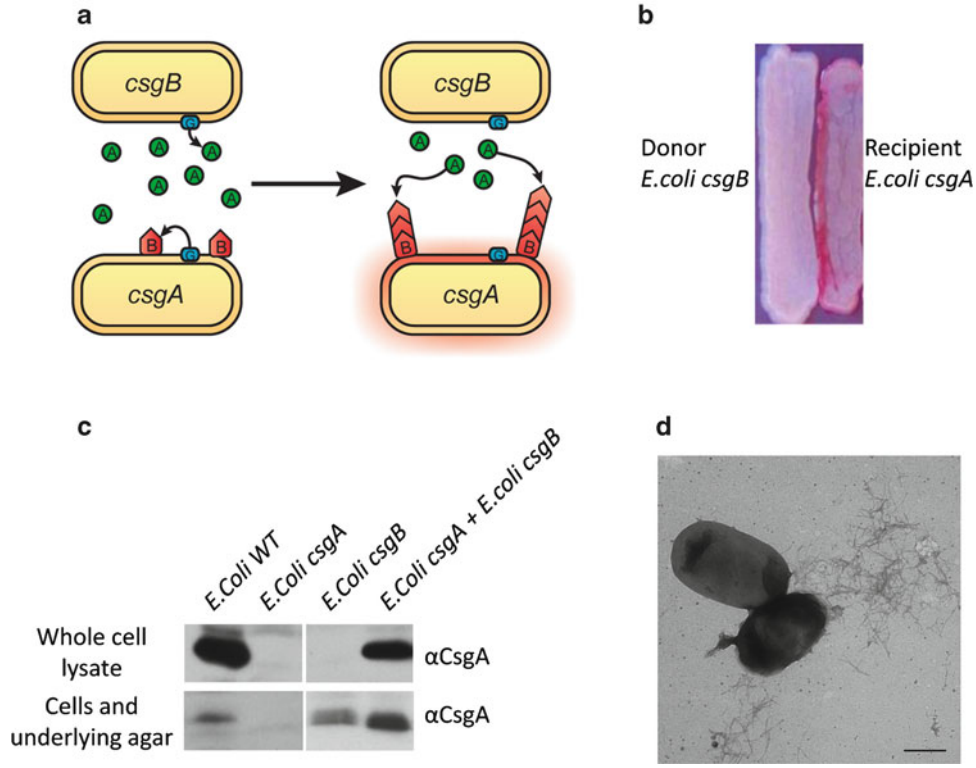

Fig. 2. Interbacterial complementation between an *E. coli csgA* mutant and a *csgB* mutant. (**a**) A schematic presentation of interbacterial complementation. A *csgB* mutant (the donor) secretes soluble CsgA into the media, which assembles into curli fibers on the cell surface of an adjacent *csgA* mutant (the recipient) expressing CsgB. (**b**) A *csgA* mutant and a *csgB* mutant were streaked adjacent to each other on the YESCA CR plate and incubated at 26°C for 48 h. Colonies of the *csgA* mutant facing to the *csgB* mutant stained *red*. (**c**) Western blot analysis was used to detect formation of intercellular curli fibers between an *E. coli csgA* mutant and a *csgB* mutant. Overnight cultures of *csgA* and *csgB* mutants were mixed in a 1:1 ratio and spotted onto a YESCA plate and a thin YESCA plate, respectively. Whole cell lysates and the plugs were collected for western analysis. A wild-type *E. coli*, a *csgA* and a *csgB* mutant were used as controls. All of the samples were treated with HFIP and probed with anti-CsgA antibody. (**d**) A mixed culture of *E. coli csgA* and *csgB* mutants was spotted onto YESCA plate and grown for 48 h. Curli were detected by EM. Scar bar equals to 500 nm.

3.2. Western Blot Analysis of the Whole Cell Lysate (Fig. 3)

Western blotting provides another way to study curli assembly. Curli fibers are resistant to SDS. HFIP/FA treatment of curli releases monomeric CsgA and CsgB that mobilize into the SDS–PAGE and can be probed by anti-CsgA or anti-CsgB antibodies, respectively.

1. Grow *E. coli* strains on the YESCA agar plate at 26°C for 48 h.
2. Scrape off bacteria cells from the YESCA agar using a sterile inoculating loop and suspend them in 1 mL 50 mM KPi. Normalize cells by optical cell density at 600 nm to $1OD_{600}$/mL.
3. Transfer 150 μL of normalized cell suspension into each of two new tubes per strain under analysis, one for HFIP/FA treatment and the other for the SDS only control.

4. Spin down bacteria cells at 16,000 × *g* for 3 min and remove the supernatant. Cell-associated curli fibers and protein aggregates should pellet.
5. To depolymerize curli fibers into monomers, resuspend one of the duplicate pellets in 70 μL 100% HFIP or FA briefly (see Note 14).
6. Immediately dry samples in a Speedvac at 45°C for 30 min (see Note 14).
7. Resuspend all pellets in 150 μL 2× SDS loading buffer. FA-treated samples may contain residual acid turning the sample buffer yellow. Adjust the pH by the addition of 1 μL at a time of 5 N NaOH until the loading buffer turns blue again. Boil samples at 95°C for 10 min (see Note 15).
8. Run 5–7 μL of each samples on a 15% SDS–polyacrylamide gel at 25 mA per gel.
9. Semidry transfer: Use for CsgA western blotting. After electrophoresis, transfer proteins from the SDS–polyacrylamide gel to a PVDF membrane by semidry transfer system. Each blotting stack should be made of three sheets of Whatman paper, the gel, a PVDF membrane followed by another three sheets of Whatman paper. The PVDF membrane needs to be pretreated with methanol, water, and transfer buffer. Transfer for 20 min at 10 V (see Note 16).
10. Wet transfer: Use for CsgB, which does not efficiently transfer using the semidry transfer system, probably due to its high pI. Use a similar blotting stack as it is for the semidry transfer, except use a nitrocellulose membrane instead of PVDF and use the wet transfer buffer, pH 11.2. Transfer in a wet transfer system for at 50 V for 3 h or 12 V overnight at 4°C (see Note 16).
11. Block the western blot with blocking solution for at least 1 h at RT or at 4°C overnight.
12. Probe the western blots with 1:10,000 diluted anti-CsgA or 1:7,000 diluted anti-CsgB polyclonal antibodies in blocking buffer at RT for 1 h (see Note 6).
13. Wash the blot with TBS-T and then probe with anti-rabbit secondary antibody at a dilution of 1:10,000 in blocking buffer at RT for 1 h.
14. Develop blot with chemiluminescent substrates.

3.3. Plug Western Blot Analysis (Fig. 3)

Western blotting of whole cell lysate is a powerful tool to study cell-associated fibers. However, it has its drawbacks. If no CsgA is detected by FA/HFIP treatment, it is possible that CsgA or CsgA mutants are secreted into the agar in an unpolymerized form. It is also likely that non-cell-associated fibers are formed in the agar, or

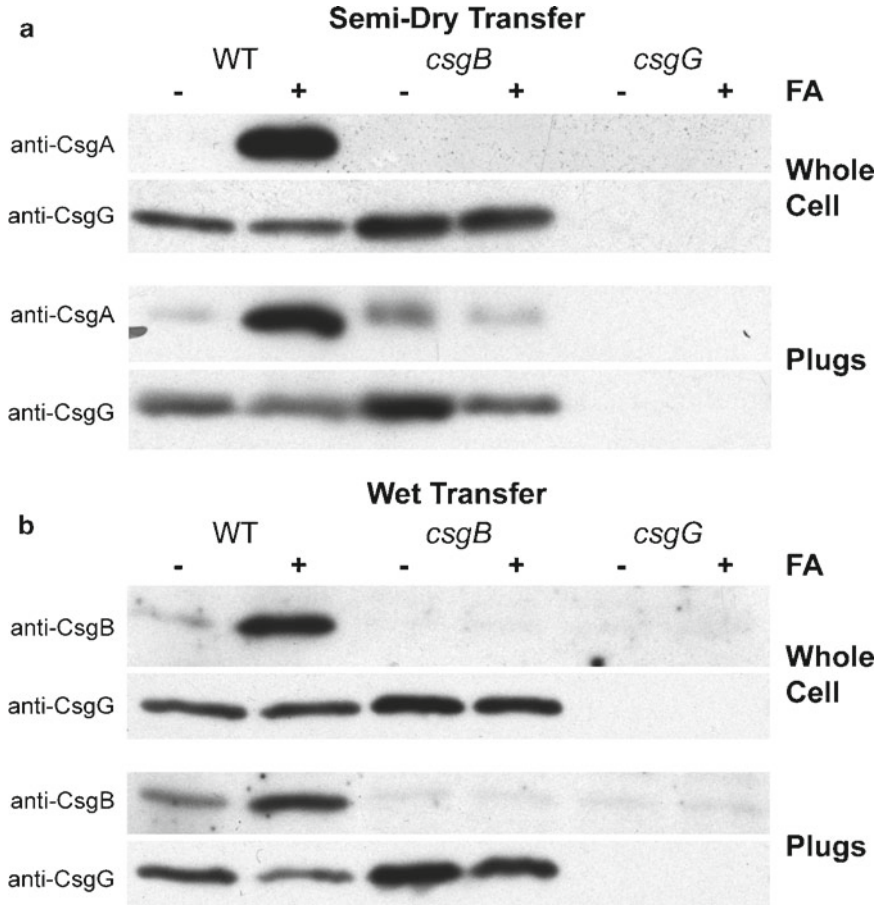

Fig. 3. Western blot analysis of whole cell lysates and agar plugs. (**a**) Western blots of whole cell extracts and plugs of *E. coli* strains (36) that were transferred onto PVDF membranes and probed with polyclonal anti-CsgA antibodies. The *csgB* mutant strain did not produce curli fibers and soluble secreted CsgA was found in the agar plug. (**b**) Western blots of whole cell and plugs of *E. coli* strains (36) that were transferred onto nitrocellulose membranes and probed with polyclonal anti-CsgB antibodies. A strain lacking CsgG results in no CsgA or CsgB in whole cells or in the agar analysis.

CsgA is not expressed or is degraded. The plug western blot analysis provides an approach to distinguish between those possibilities.

1. Inoculate single colonies of *E. coli* strains to LB liquid broth and grow at 37°C overnight with shaking.
2. Equilibrate the overnight cultures by OD_{600}.
3. Spot 4 μL of normalized cultures onto a thin YESCA agar plate.
4. Grow bacteria on the thin YESCA plate at 26°C for 48 h.
5. Use the wide end of a Pasteur pipette as a cookie cutter-like tool to remove an 8-mm circular plug including the bacteria and the underlying agar. Collect 2 plugs for each strain: one for HFIP/FA treatment and the other as an SDS only control. Put each plug into a 1.5-mL microcentrifuge tube.

6. For the HFIP/FA treatment group, suspend the plug in 100 μL HFIP or FA and briefly vortex. Dry the samples in a Speedvac at 45°C for 40 min, and then resuspend the pellets with 2× SDS loading buffer.
7. For the nontreated plugs, suspend plugs in 150 μL 2× SDS loading buffer.
8. Sonicate both HFIP/FA-treated samples and nontreated samples in a water-bath sonicator for 3 min (see Note 17).
9. Adjust the sample pH to neutral by 1 or 2 μL of 5 N NaOH if the SDS loading buffer turns yellow. Heat the samples at 95°C for 10 min before loading onto a 15% SDS–polyacrylamide gel (see Note 15).
10. Electrophorese the samples, transfer proteins to a PVDF membrane for detecting CsgA or nitrocellulose for detecting CsgB, probe, and develop the blot as described in Subheading 3.2.

3.4. CsgA Purification and Overlay Assay

There are two CsgA purification schemes in the published literature (see Note 18). In one of the approaches, both CsgA and CsgG are overexpressed in the absence of all other curli proteins. CsgA is secreted into the supernatant and is collected and purified by nickel affinity chromatography (15, 31). In an alternative purification method, CsgA without the Sec signal sequence can be purified from the cytoplasm using a denaturing protocol (10). C-terminal His_6-tagged CsgA is referred as "CsgA" in this section.

3.4.1. CsgA Purified from Cell Supernatants (see Note 19)

Perform the purification in a 4°C cold room or a 4°C fridge. Store the columns and buffers at 4°C unless otherwise stated.

1. Start an overnight culture of LSR12/pMC1/pMC3 in 25 mL LB-Amp-Cm per 1 L of desired prep at 37°C.
2. Dilute the overnight culture into 1 L LB-Amp-Cm and incubate with shaking at 37°C to OD_{600} of ~1.0.
3. Induce with 0.25 mM IPTG and incubate with shaking for 45 min at 37°C.
4. Centrifuge the culture at 10,000 × *g* for 15 min at 4°C. Collect the supernatant.
5. Shift purification to 4°C.
6. Filter the supernatant over a 0.22-μm polyethersulfone bottle-top filter (see Note 20).
7. Prepare a column with 4 mL of Ni-NTA bead volume. Wash the column with 4 bed volumes (BV) of 50 mM KPi, pH 7.2.
8. Flow the filtrates over the column set to the maximum flow rate (see Note 21).
9. Wash the column with 10BV of 50 mM KPi, pH 7.2.

10. Elute the protein off the column with 2BV of 100 mM imidazole in 50 mM KPi, pH 7.2. Adjust the flow rate to 20 drops/min. Collect elutes in 1 mL fractions and store in microcentrifuge tubes.
11. Combine fractions containing CsgA as measured by BCA in a 15-mL conical tube.
12. Equilibrate a Sephadex G-25 gel filtration column with 25 mL 50 mM KPi, pH 7.2.
13. Load 3–4 mL of protein onto the column. Elute 1 mL fractions into microcentrifuge tubes using 50 mM KPi, pH 7.2. Measure the protein concentration of each fraction by UV_{280} or BCA assay. Combine the fractions that contain most of CsgA proteins, filter through a 0.02-μm Anotop filter, and measure the final concentration. Store on ice (see Notes 22 and 23).

3.4.2. CsgA Purified from Cell Lysates (see Note 19)

1. Start an overnight culture of NEB C2566/pNH11 in 10 mL LB Amp-Kan-Cm per 500 mL of desired prep at 37°C.
2. Dilute the overnight culture into 500 mL LB-Amp and incubate with shaking at 37°C to an OD_{600} of ~1.0.
3. Induce with 0.5 mM IPTG and incubate for 1 h at 37°C.
4. Collect bacteria by centrifugation at 5,000 × *g* for 20 min and discard the supernatant. The pellet can be stored at −80°C for future use.
5. Lyse bacterial cells by adding 50 mL 8 M GdnHCl to the pellet and incubate at 4°C overnight with stirring.
6. Centrifuge the GdnHCl bacterial suspension at 10,000 × *g* for 20 min to remove the insoluble portion of the lysate.
7. Incubate the resulting supernatant with Ni-NTA resin for 1 h at RT with rocking.
8. Load the supernatant with Ni-NTA onto a disposable polypropylene column.
9. Wash the beads with 10BV 50 mM KPi, pH 7.2 followed by 3BV 12.5 mM imidazole in 50 mM KPi, pH 7.2 to remove nonspecific bound proteins.
10. Elute the protein off the column with 6BV 125 μM imidazole in 50 mM KPi, pH 7.2. Collect 1 mL of elutes for each fraction in 1.5-mL microcentrifuge tubes. Store fractions on ice (see Note 22).
11. Measure the protein concentration from each fraction by BCA assay. Combine the fractions with proteins and load onto a 30 kDa centrifugal filter unites. Centrifuge at 7,500 × *g* for 10 min (see Note 24). The bottom part of the filter units contains CsgA monomers.

12. Prewash a spin desalting column with 50 mM KPi by centrifugation at 1,000 × *g* for 2 min. Collect proteins from the bottom part of the 30 kDa filter units and load onto the desalting column. Centrifuge at 1,000 × *g* for 2 min (see Note 24).
13. Store purified protein on ice (see Note 22). Measure protein concentration by BCA assay or UV_{280}.

3.4.3. Overlay Assay

Soluble amyloid proteins polymerize into amyloid fibers and this polymerization can be accelerated by its own fibers, a process known as seeding. The polymerization and seeding can be monitored in vitro by Thioflavin T fluorescence or EM. The overlay assay provides a mechanism to test the assembly of bacterial amyloids directly on the cell surface. It can be used to determine the amyloidogenic domains of bacterial amyloid proteins (28).

1. Spread a lawn of 50 μL desired bacterial suspension on the YESCA plate by sterile inoculation loop and incubate for 2 days at 26°C. Use *E. coli* K-12 *csgA* and *csgBA* mutant as the positive control and negative control, respectively.
2. Drip 10 μL of freshly purified CsgA on the bacterial lawn. Incubate at RT for 10 min.
3. Stain the plate with 10 mL of 0.5 mg/mL CR at RT for 5 min then wash with 50 mM KPi, pH 7.2.
4. Observe the CR stain at the spot where CsgA proteins were spotted. *csgA* mutant with CsgA proteins should strain red, while *csgBA* mutant with CsgA proteins will remain white (Fig. 4a). Assembly of curli fibers on bacterial surfaces can also be verified by electron microscopy (EM) (Fig. 4b, c).

4. Notes

1. Other than YESCA agar, T-agar (16), colonization factor antigen (CFA) agar (20), and LB agar without salt (32) are also used to induce curli production of *Salmonella spp.* and *E. coli*. LB agar with no salt contains 5 g/L yeast extract, 10 g/L bacto tryptone, and 1.5% agar.
2. Mix CR with water by stirring for at least an hour. Make sure CR is completely dissolved before filter sterilizing.
3. Brilliant blue is used to increase the color contrast of colonies on CR agar.
4. HFIP is a strong solvent that disaggregates curli subunits and does not result in acid hydrolysis. FA is also used to disassociate curli subunits. FA and HFIP are corrosive and cause burns. They evaporate at room temperature. Store FA and HFIP in a

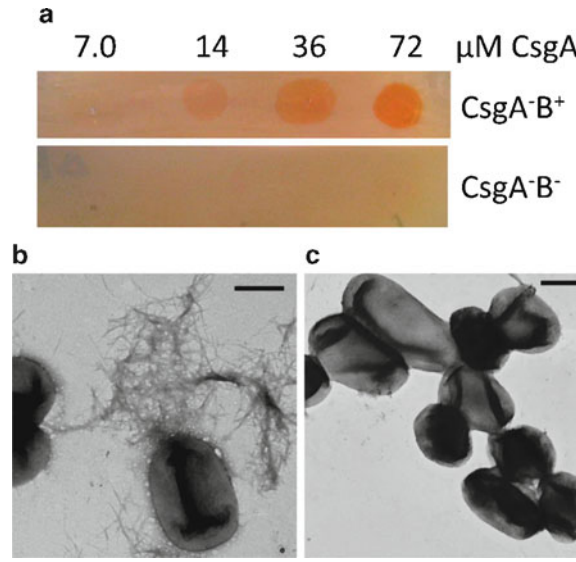

Fig. 4. Purified CsgA assembles into curli fibers on CsgB expressing cells. (Figure adapted from Wang et al. (29)) (**a**) CR staining of CsgA⁻B⁺ and CsgA⁻B⁻ overlaid with different concentrations of freshly purified CsgA. Only CsgA⁻B⁺ cells with CsgA proteins stained *red*. (**b**) Negative-stain EM of CsgA⁻B⁺ overlaid with freshly purified CsgA. Fibers were observed on the bacterial surface. Scar bar equals to 500 nm. (**c**) Negative-stain EM of CsgA⁻B⁻ overlaid with purified CsgA. No fibers were detected. Scar bar equals to 500 nm.

cool, well-ventilated place. Always use them under a chemical fume hood and wear appropriate protective equipment.

5. Here we use high-pH CAPS buffer because the CsgB protein has a high pI and cannot be transferred efficiently with normal buffer.
6. 1:10,000 dilution rate of anti-CsgA antibody or 1:7,000–1:10,000 of anti-CsgB antibody gives good signal for western blotting. High concentration of antibody is not recommended as it may cause nonspecific binding. The anti-CsgA antibody also binds to an unknown nonspecific protein that migrates at around 40 kDa on SDS–PAGE.
7. For CR staining and fluorescence quantification, it is recommended to grow a curliated wild-type strain as a positive control and curli defective mutant such as a *csgA* mutant or a *csgB* mutant as a negative control.
8. Temperature and incubation time are important factors for CR assays. Most of the *E. coli* K-12 and *Salmonella spp*. lab strains produce curli at 26°C, whereas some clinical isolates produce curli at 37°C (33, 34). Although *E. coli* K-12 lab strains grown at 37°C do not produce curli, they may eventually take up CR and stain red. Incubation for longer than 2 days may also make bacteria take up or bind CR.

9. Most *E. coli* K-12 isolates have CR phenotypes that are completely dependent on curli fiber production. However, many bacterial strains can produce cellulose or other extracellular polysaccharides that bind to CR. The corresponding curli defective mutants of those strains may form pink, smooth colonies on YESCA CR plates.

   CR is able to interact and emit fluorescence with cellulose. Therefore, multiple approaches are recommended for the study of amyloids produced by bacteria with complex surface structures.

10. A wavelength scan of CR fluorescence is required to determine the ideal excitation and emission wavelength for CR quantification for the analysis of other bacterial amyloids.

11. Some bacteria do not participate in interbacterial complementation. Interbacterial complementation is not detected between *S. enterica serovar Enteritidis 3b csgA* and *csgB* mutants, probably due to the lipopolysaccharide *O* polysaccharide (35).

12. The curli mutants of cellulose-positive bacteria are pink on the YESCA CR agar, which makes the detection of interbacterial complementation difficult by CR staining. As an alternative, a mixture of desired bacteria can be collected and the intercellular curli formation can be assessed by EM or western blot analysis as mentioned in Subheadings 3.2 and 3.3 (Fig. 2c, d).

13. Another way to test interbacterial complementation is to streak the donor or recipient on the YESCA plate and, then make a parallel streak 3 mm away from the first streak. Incubate the plate at 26°C for 48 h (Fig. 2b). The recipient cells facing to donor stain red if intercellular curli are formed.

14. FA is capable of hydrolyzing proteins including curli subunits. Long treatment with FA may result in target protein loss. Speed-dry samples immediately after the FA treatment or use HFIP instead.

15. Make sure that samples are thoroughly dried after speed-vac step. If there is still liquid FA or HFIP left in the tube after 30 min in the Speedvac, dry the sample for longer. The remaining FA in bacterial pellets or plugs lowers the pH and turns the SDS-sample buffer yellow. The low pH of samples affects electrophoresis and boiling low pH sample increases the chance of acid hydrolysis. It is recommended to adjust the pH of sample buffer back to around pH 7 before loading samples onto SDS–PAGE.

16. We use the semidry transfer apparatus from FisherBiotech and a wet transfer system from Biorad. The voltage and transfer time may vary for different transfer systems.

17. We found that water bath sonication makes the results for the plug assay more consistent, probably by breaking up large chunks of dried agar.

18. Both CsgA purification approaches have advantages and drawbacks. Purification of CsgA from bacterial supernatant does not required denaturation of the target protein. However, the whole process is time consuming and typically takes 2 days. The denaturing method takes only half a day, but the final yield is typically lower. CsgA proteins purified by both methods have the same biochemical properties and form fibers with same morphologies and with similar kinetics.
19. Collect ~100 μL of sample during each of the purification steps (e.g., the load, the wash, and elutes) and store on ice. Run an SDS–PAGE of the samples after purification to make sure that the protein is pure. Also, an expression test is required for new expression strains to make sure that protein is expressed in the tested conditions.
20. To remove bacteria that remain in the supernatant after centrifugation, filter the supernatant through the 0.22-μm filter. Filtered supernatant can be stored at 4°C overnight. However, longer storage is not recommended.
21. Depending on the column size and the particulates in the supernatant, it can take upwards of 10 h to gravity flow 1 L of supernatant through the nickel affinity column. Use of high-flow Ni-NTA and addition of a powder funnel on top of the column both greatly accelerate the loading process.
22. Purified CsgA forms fibers at RT in 1–2 h, so it is important to keep the protein on ice to slow the aggregation process. Start the overlay assay immediately after the purification. CsgA cannot be stored at −20°C or −80°C because CsgA precipitates out of solution during the thawing process.
23. To purify CsgA from cell supernatants under denaturing conditions, equilibrate the Ni-NTA gel with 5BV 8 M GdHCl in 10 mM KPi, pH 7.2 at RT after supernatant binding and washing with 5BV 10 mM KPi, pH 7.2. Elute with 3BV 8 M GdHCl in 50 mM KPi, pH 2. Use BCA assay or UV_{280} to detect and pool CsgA-containing fractions, which can be stored at RT for several days. Desalt using Sephadex G-25 at RT using cold columns and 4°C 50 mM KPi, pH 7.2.
24. Check the manuals that accompany the 30 kDa centrifuge units and desalting columns. The speed and time for centrifugation may vary from product to product.

Acknowledgments

We thank members of the Chapman laboratory for helpful discussions and review of this manuscript. This work was supported by the National Institutes of Health Grant AI073847.

References

1. Cooper, G. J., Willis, A. C., Clark, A., Turner, R. C., Sim, R. B., and Reid, K. B. (1987) Purification and characterization of a peptide from amyloid-rich pancreases of type 2 diabetic patients, *Proc Natl Acad Sci USA 84*, 8628–8632.
2. Glenner, G. G., and Wong, C. W. (1984) Alzheimer's disease: initial report of the purification and characterization of a novel cerebrovascular amyloid protein, *Biochem Biophys Res Commun 120*, 885–890.
3. Prusiner, S. B. (1996) Molecular biology and pathogenesis of prion diseases, *Trends Biochem Sci 21*, 482–487.
4. Barnhart, M. M., and Chapman, M. R. (2006) Curli biogenesis and function, *Annu Rev Microbiol 60*, 131–147.
5. Gebbink, M. F., Claessen, D., Bouma, B., Dijkhuizen, L., and Wosten, H. A. (2005) Amyloids--a functional coat for microorganisms, *Nat Rev Microbiol 3*, 333–341.
6. Elliot, M. A., Karoonuthaisiri, N., Huang, J., Bibb, M. J., Cohen, S. N., Kao, C. M., and Buttner, M. J. (2003) The chaplins: a family of hydrophobic cell-surface proteins involved in aerial mycelium formation in Streptomyces coelicolor, *Genes Dev 17*, 1727–1740.
7. Tukel, C., Nishimori, J. H., Wilson, R. P., Winter, M. G., Keestra, A. M., van Putten, J. P., and Baumler, A. J. (2010) Toll-like receptors 1 and 2 cooperatively mediate immune responses to curli, a common amyloid from enterobacterial biofilms, *Cell Microbiol.*
8. Gophna, U., Barlev, M., Seijffers, R., Oelschlager, T. A., Hacker, J., and Ron, E. Z. (2001) Curli fibers mediate internalization of Escherichia coli by eukaryotic cells, *Infect Immun 69*, 2659–2665.
9. Austin, J. W., Sanders, G., Kay, W. W., and Collinson, S. K. (1998) Thin aggregative fimbriae enhance Salmonella enteritidis biofilm formation, *FEMS Microbiol Lett 162*, 295–301.
10. Cegelski, L., Pinkner, J. S., Hammer, N. D., Cusumano, C. K., Hung, C. S., Chorell, E., Aberg, V., Walker, J. N., Seed, P. C., Almqvist, F., Chapman, M. R., and Hultgren, S. J. (2009) Small-molecule inhibitors target Escherichia coli amyloid biogenesis and biofilm formation, *Nat Chem Biol 5*, 913–919.
11. Romero, D., Aguilar, C., Losick, R., and Kolter, R. (2010) Amyloid fibers provide structural integrity to Bacillus subtilis biofilms, *Proc Natl Acad Sci USA 107*, 2230–2234.
12. Vidal O, L. R., Prigent-Combaret C, Dorel C, Hooreman M, Lejeune P. (1998) Isolation of an Escherichia coli K-12 mutant strain able to form biofilms on inert surfaces: involvement of a new ompR allele that increases curli expression, *J Bacteriol 180*, 2442–2449.
13. Johansson, C., Nilsson, T., Olsen, A., and Wick, M. J. (2001) The influence of curli, a MHC-I-binding bacterial surface structure, on macrophage-T cell interactions, *FEMS Immunol Med Microbiol 30*, 21–29.
14. Tükel C, R. M., Humphries AD, Wilson RP, Andrews-Polymenis HL, Gull T, Figueiredo JF, Wong MH, Michelsen KS, Akçelik M, Adams LG, Bäumler AJ. (2005) CsgA is a pathogen-associated molecular pattern of Salmonella enterica serotype Typhimurium that is recognized by Toll-like receptor 2, *Mol Microbiol 58*, 289–304.
15. Chapman, M. R., Robinson, L. S., Pinkner, J. S., Roth, R., Heuser, J., Hammar, M., Normark, S., and Hultgren, S. J. (2002) Role of Escherichia coli curli operons in directing amyloid fiber formation, *Science 295*, 851–855.
16. Collinson, S. K., Emody, L., Muller, K. H., Trust, T. J., and Kay, W. W. (1991) Purification and characterization of thin, aggregative fimbriae from Salmonella enteritidis, *J Bacteriol 173*, 4773–4781.
17. Claessen, D., Rink, R., de Jong, W., Siebring, J., de Vreugd, P., Boersma, F. G., Dijkhuizen, L., and Wosten, H. A. (2003) A novel class of secreted hydrophobic proteins is involved in aerial hyphae formation in Streptomyces coelicolor by forming amyloid-like fibrils, *Genes Dev 17*, 1714–1726.
18. de Jong W, W. H., Dijkhuizen L, Claessen D. (2009) Attachment of Streptomyces coelicolor is mediated by amyloidal fimbriae that are anchored to the cell surface via cellulose, *Mol Microbiol 73*, 1128–1140.
19. Shewmaker F, M. R., Thurber KR, McPhie P, Dyda F, Tycko R, Wickner RB. (2009) The functional curli amyloid is not based on in-register parallel beta-sheet structure, *J Biol Chem 284*, 25065–25076.
20. Collinson, S. K., Doig, P. C., Doran, J. L., Clouthier, S., Trust, T. J., and Kay, W. W. (1993) Thin, aggregative fimbriae mediate binding of Salmonella enteritidis to fibronectin, *J Bacteriol 175*, 12–18.
21. Collinson, S. K., Parker, J. M., Hodges, R. S., and Kay, W. W. (1999) Structural predictions of AgfA, the insoluble fimbrial subunit of Salmonella thin aggregative fimbriae, *J Mol Biol 290*, 741–756.
22. Zogaj, X., Bokranz, W., Nimtz, M., and Romling, U. (2003) Production of cellulose and curli fimbriae by members of the family

Enterobacteriaceae isolated from the human gastrointestinal tract, *Infect Immun 71*, 4151–4158.

23. Olsen, A., Jonsson, A., and Normark, S. (1989) Fibronectin binding mediated by a novel class of surface organelles on Escherichia coli, *Nature 338*, 652–655.
24. Loferer, H., Hammar, M., and Normark, S. (1997) Availability of the fibre subunit CsgA and the nucleator protein CsgB during assembly of fibronectin-binding curli is limited by the intracellular concentration of the novel lipoprotein CsgG, *Mol Microbiol 26*, 11–23.
25. Hammer, N. D., Schmidt, J. C., and Chapman, M. R. (2007) The curli nucleator protein, CsgB, contains an amyloidogenic domain that directs CsgA polymerization, *Proc Natl Acad Sci USA 104*, 12494–12499.
26. Hammar M, A. A., Bian Z, Olsén A, Normark S. (1995) Expression of two csg operons is required for production of fibronectin- and congo red-binding curli polymers in Escherichia coli K-12., *Mol Microbiol 18*, 661–670.
27. Weiss-Muszkat, M., Shakh, D., Zhou, Y., Pinto, R., Belausov, E., Chapman, M. R., and Sela, S. (2010) Biofilm formation by and multicellular behavior of Escherichia coli O55:H7, an atypical enteropathogenic strain, *Appl Environ Microbiol 76*, 1545–1554.
28. Wang, X., and Chapman, M. R. (2008) Sequence determinants of bacterial amyloid formation, *J Mol Biol 380*, 570–580.
29. Wang, X., Hammer, N. D., and Chapman, M. R. (2008) The molecular basis of functional bacterial amyloid polymerization and nucleation, *J Biol Chem 283*, 21530–21539.
30. Wang, X., Zhou, Y., Ren, J. J., Hammer, N. D., and Chapman, M. R. (2010) Gatekeeper residues in the major curlin subunit modulate bacterial amyloid fiber biogenesis, *Proc Natl Acad Sci USA 107*, 163–168.
31. Wang, X., Smith, D. R., Jones, J. W., and Chapman, M. R. (2007) In vitro polymerization of a functional Escherichia coli amyloid protein, *J Biol Chem 282*, 3713–3719.
32. Werner Bokranz, X. W., Helmut Tschäpe and Ute Römling. (2005) Expression of cellulose and curli fimbriae by Escherichia coli isolated from the gastrointestinal tract, *J Med Microbiol 54*, 1171–1182.
33. Kikuchi, T., Mizunoe, Y., Takade, A., Naito, S., and Yoshida, S. (2005) Curli fibers are required for development of biofilm architecture in Escherichia coli K-12 and enhance bacterial adherence to human uroepithelial cells, *Microbiol Immunol 49*, 875–884.
34. Bian, Z., Brauner, A., Li, Y., and Normark, S. (2000) Expression of and cytokine activation by Escherichia coli curli fibers in human sepsis, *J Infect Dis 181*, 602–612.
35. White AP, G. D., Collinson SK, Banser PA, Kay WW. (2003) Extracellular polysaccharides associated with thin aggregative fimbriae of Salmonella enterica serovar enteritidis, *J Bacteriol 185*, 5398–5407.
36. Baba, T., Ara, T., Hasegawa, M., Takai, Y., Okumura, Y., Baba, M., Datsenko, K. A., Tomita, M., Wanner, B. L., and Mori, H. (2006) Construction of Escherichia coli K-12 in-frame, single-gene knockout mutants: the Keio collection, *Mol Syst Biol 2*, 2006–0008.

Chapter 22

Study of Amyloids Using Yeast

Reed B. Wickner, Dmitry Kryndushkin, Frank Shewmaker, Ryan McGlinchey, and Herman K. Edskes

Abstract

We detail some of the genetic, biochemical, and physical methods useful in studying amyloids in yeast, particularly the yeast prions. These methods include cytoduction (cytoplasmic mixing), infection of cells with prion amyloids, use of green fluorescent protein fusions with amyloid-forming proteins for cytology, protein purification and amyloid formation, and electron microscopy of filaments.

Key words: Protein transformation, Cytoduction, Mass per length, Electron diffraction

Abbreviations

USA	Ureidosuccinic acid
SD	Synthetic dextrose (medium)
SC-Ade	Synthetic complete minus adenine (medium)
YPAD	Yeast extract peptone adenine dextrose (medium)
YPG	Yeast extract peptone glycerol (medium)
GFP	Green fluorescent protein
NiNTA	Nickel column
TCA	Trichloroacetic acid
TEM	Transmission electron microscopy
TMV	Tobacco mosaic virus

1. Introduction

Saccharomyces cerevisiae has been a useful model organism in such fields as the cell cycle, regulation of transcription, protein trafficking and cell biology, primarily because of its ease of genetic manipulation. This is no less so in the area of amyloid studies. The endogenous yeast amyloids described to date include prions, infectious proteins (Table 1), and some cell wall proteins (1). Amyloids

Einar M. Sigurdsson et al. (eds.), *Amyloid Proteins: Methods and Protocols*, Methods in Molecular Biology, vol. 849,
DOI 10.1007/978-1-61779-551-0_22,

Table 1
Prions of *Saccharomyces cerevisiae* and *Podospora anserina*

Prion	Protein	Normal function	Pathology	Reference
[URE3]	Ure2	Nitrogen catabolite repression	Slow growth; NCR stuck in "on" position	(11)
[*PSI*+]	Sup35	Translation termination	Translation termination read-through	(11)
[*PIN*+]	Rnq1	Unknown	Rare seeding of other prions	(22)
[β]	Prb1	Vacuolar protease B	A normal nonamyloid prion: active form of Prb1p	(98)
[*SWI*$^+$]	Swi1	Chromatin remodeling complex subunit	Unable to use ethanol, galactose, sucrose; mating type switch – deficient	(26)
[*OCT*$^+$]	Cyc8	Transcription repressor subunit	Reduced fermentation	(27)
[*MOT*$^+$]	Mot3	Transcription factor		(29)
[*ISP*$^+$]	Sfp1	Transcription factor for ribosome components	Translational antisuppression	(99)
[Het-s]	HET-s	Prion functions in heterokaryon incompatibility and in a meiotic drive system		(19)

of humans and a fungal prion have also been studied using the yeast system. Accordingly, the emphasis of this chapter is on genetic, biochemical, cell biological, and physical methods particularly useful in the study of yeast prions and other amyloids studied in yeast. We limit our description of these methods to those aspects which have been most useful in studying yeast prions, citing more detailed expositions in the literature. Volumes on yeast genetic methods (2–4) and on amyloids and prions (5, 6) are useful, and Masison has edited a volume of *Methods* on "Identification, analysis and characterization of fungal prions" which covers some of this territory (7). We also outline some useful physical methods, pointing the reader to more extensive and authoritative descriptions.

2. How to Identify a New Prion

Several approaches have been used to find new prions. The first two yeast prions found were nonchromosomal genetic elements, [URE3] (8, 9) and [PSI+] (10), which were found to have three properties that could not be explained as a nucleic acid replicon, but which were expected of a prion (11).

2.1. Genetic Criteria for a Yeast Prion

2.1.1. Reversible Curability

Various nucleic acids may be cured by certain treatments: mitochondrial DNA is eliminated by growth on ethidium bromide (12) and the L-A and M dsRNA viruses are cured by growth at 42°C (13, 14), but once cured these elements will not arise again de novo. In contrast, the prions [URE3] and [PSI+] can be cured by growth in the presence of millimolar concentrations of guanidine HCl and high osmotic strength medium, respectively (11, 15), but having been cured, they can arise again de novo in the cured strain (11, 16).

2.1.2. Overproduction of the Prion Protein Induces Prion Formation

The more prion protein available, the more likely that a conversion event will occur, and having occurred, it should take over the population of molecules because it is fundamentally a positive feedback event (11). Overproduction of Ure2p induces [URE3] formation (11) and overproduction of Sup35p induces [PSI+] (17). This is best done with transient overproduction, using a *GAL1* (galactose-induced) or *CUP1* (copper-induced) promoter and showing that the appearance of the infectious genetic element (prion) is induced de novo at increased frequency.

2.1.3. Phenotypes of Prion and Gene Encoding the Prion Protein

The phenotype of *ure2* mutants is similar to that due to carrying the [URE3] prion, and *ure2* is required for [URE3] prion propagation (9, 11). This is easily understood if [URE3] is a prion of Ure2p, but incomprehensible otherwise (11). Likewise, for the similarity of phenotype of *sup35* mutants and the [PSI+] prion and *SUP35* being required for [PSI+] prion propagation (11).

2.2. How to Find Prion Candidates

Like [URE3] and [PSI+], the [Het-s] prion was long known as a nonchromosomal gene (18), but using the same genetic criteria as for the former prions, along with biochemical evidence of aggregation, [Het-s] was shown to be a prion of the HET-s protein (19).

[PIN+] was found as a nonchromosomal genetic element necessary for the induction of [PSI+] by overexpression of Sup35p (20). Later, evidence that Rnq1p could be heritably aggregated was presented (21), and finally, Rnq1p was identified as the prion protein underlying [PIN+] (22). However, it was shown that overproduction of many proteins could have a Pin-like effect, allowing induction of [PSI+] by overproduction of Sup35p, and all of these proteins had Q/N-rich domains (22, 23), similar to the prion domains of Ure2p (24) and Sup35p (25). Although the Pin effect did not require these proteins to be in a prion form, they became candidates for prions nonetheless, and Swi1p (26) and Cyc8p (27) were shown to be capable of prion formation, by the genetic criteria above.

[MOT3+] was identified as a prion of Mot3p, a transcription regulator, by screening a group of proteins having Q/N-rich domains by fusing the domains to the nonprion part of *SUP35* (29).

There are now quite a few yeast amyloid-based prions to use as a guide to which other proteins might also be prions. Ross et al. showed that, at least for Ure2p and Sup35p, the amino acid

composition is more important than the sequence of the prion domain in determining prion-forming ability (30, 31). Now an algorithm that correlates amino acid composition with prion-forming ability promises to detect further yeast prions (32).

2.3. Manifestations of a Prion Domain: Prion-Inducing, Prion Propagation, Interference

There are a variety of properties of prions that could be used to screen for new prions, but which do not constitute evidence for a prion. Aggregation is certainly a prion property, but any overproduced protein may aggregate and not be a prion. All of the amyloid-based prions form amyloid in vitro, but it has been suggested that any protein can be induced to form amyloid under some condition (33). Of course, not all aggregation is amyloid: proteins may aggregate as a consequence of oxidation or denaturation without forming the ordered filamentous structure that is amyloid. The prion domain of a prion protein can propagate the prion in the absence of the remainder of the protein (25, 34). In addition, prion domains, when overproduced, are particularly good inducers of formation of the corresponding prion (24, 35). However, as exemplified by the Pin phenomenon described by Derkatch and Liebman (20, 22), not all proteins whose overproduction induces a prion is a prion domain. Overproduction of parts of a prion protein may also specifically interfere with the propagation of the corresponding prion (36).

3. Genetic Methods for Studying Yeast Prions

3.1. Materials

1. Replicaplating blocks, velveteens, and dissecting needles (Cora Styles Needles 'N Blocks, CS@CoraStyles.com), 1/8"×6" wooden applicator sticks (sterilize in large glass tubes for streaking for single colonies).
2. Sources of strains, knock-out mutants, plasmids, libraries (www.atcc.org, www.openbiosystems.com; most yeast workers make their strains and plasmids freely available).
3. General yeast genetic and prion methods (7, 37).
4. Chemicals: G418, hygromycin B, zymolyase.

3.2. Prion Phenotypes

Many yeast prions produce a phenotype that reflects deficiency of the normal active form of the prion protein. Others have a phenotype reflecting an activity of the prion amyloid.

3.2.1. [URE3] Phenotypes

Ure2p is a negative regulator of transcription of genes encoding enzymes and transporters for the utilization of poor nitrogen sources (38, 39). When Ure2p becomes an amyloid prion, it loses activity and the expression of these nitrogen catabolism genes is stuck in the "on" position (8, 11). The gene most strongly

regulated by Ure2p is *DAL5*, encoding allantoate/ureidosuccinate permease (40, 41). Since the product of Ura2p (aspartate transcarbamylase) is ureidosuccinate, the [URE3] prion, by inactivating Ure2p, derepresses *DAL5* transcription and makes *ura2* cells able to grow on ureidosuccinate (USA) in place of uracil in spite of the presence of a good nitrogen source, such as ammonia.

3.2.2. Materials

1. Strains: 3687 (*MAT***a** *kar1 leu2 ura2 his-* [URE3]) (11), 1065 (ura2/ura2 [ure-o] diploid).
2. Media: SD (Synthetic Dextrose): 6.7 g/l yeast nitrogen base without amino acids (Difco), 20 g/l dextrose, 20 g/l agar.
3. L-Ureidosuccinate (L-carbamoylaspartic acid).

3.2.3. Procedures

Ureidosuccinate Uptake Test

1. In place of uracil, spread 1 ml of 1 mg/ml ureidosuccinate on a slightly dry SD plate along with the other supplements needed by the strain(s) being tested (see Note 1).
2. Place small streaks of the strains to be tested (including control [URE3] and [ure-o] strains) on the plate or replica plate colonies. Leave at least 3 mm between streaks to prevent cross-feeding.
3. After 2 days at 30°C, check for growth (see Note 2).

DAL5:ADE2 Fusion Gene Test

In place of the USA uptake test, a *DAL5:ADE2* fusion allows using adenine prototrophy in spite of the presence of a good nitrogen source (ammonia) as a measure of Ure2p activity. The red–white color assay (see the [P*SI*+] assay below) may be used to assess *DAL5* transcription and hence the presence of [URE3]. In this construct, 500 bp upstream of the *ADE2* open reading frame is replaced by 568 bp of the *DAL5* promoter (42). This test has the advantage that there is no significant cross-feeding, and the red–white colony color assay avoids replica plating. The results of the *DAL5::ADE2*-based assay are not necessarily exactly the same as the USA uptake test, perhaps as a result of different turnover numbers of the Ade2p and Dal5p, but there is a general consistency of results.

Uracil Secretion Test

The presence of [URE3] can be checked also in prototrophic strains. A lawn of ~10^6 diploid *ura2/ura2* cells are seeded on an SD plate having 100 µg/ml of ureidosuccinate, and small streaks of the strains to be tested are made. A [URE3] strain will take up an excess of USA, convert it to uracil, and secrete it from the cells, producing a halo of growth of the lawn around the patch of the [URE3] strain. The use of 30 µg/ml ureidosuccinate in the USA uptake assay reduces the amount of cross-feeding, but does not entirely eliminate it.

1. In place of uracil, spread 1 ml of 3 mg/ml ureidosuccinate on a slightly dry SD plate along with a lawn of ~10^6 cells of a *MAT***a**/*MAT*α *ura2/ura2* diploid strain.

2. When the plate is dry, make small streaks of the strains to be tested along with [URE3] and [ure-o] controls.
3. After ~2 days at 30°C, examine plates looking for a halo of growth of the lawn around the strain to be tested.

3.2.4. [PSI] Phenotype

The assay for [PSI+], developed by Cox (10), is a general nonsense-suppression assay. Sup35p encodes a subunit of the translation termination factor (Sup45p is the other subunit). In [PSI+] cells, most of the Sup35p is tied up in amyloid filaments and cannot efficiently terminate translation. Frequent read-through of premature termination codons is assessed using the nonsense mutation *ade2-1* and the weak serine-inserting suppressor *SUQ5*, or just the easily suppressed *ade1-14* mutation. Mutants in *ade1* and *ade2*, when grown on adenine-limiting media, accumulate a precursor (phosphoribosyl–aminoimidazole) that gradually converts to a red pigment. The intensity of the red color is an indirect indicator of the fraction of soluble Sup35p. Cells lacking the prion [[psi–]] are bright red, while [PSI+] cells are a shade of pink or white. Note that the loss of respiratory capacity, due to mutation of the mitochondrial DNA or a nuclear *pet* gene, greatly reduces the accumulation of the red pigment. In addition, mutations earlier in the adenine pathway prevent the accumulation of the precursor, and so are white. The red pigment is toxic, so these mutations are selected over time. A high level of adenine in the medium represses the adenine biosynthetic pathway and makes colonies be white. Plates of 1/2 YPD (below) contain enough adenine to allow growth of [psi–] cells, but not enough to repress adenine biosynthesis. These plates are often used for visualizing the [PSI+] or [psi–] state of a strain. Yeast grow best at 30°C, but the color develops better by leaving the plates at room temperature for a few days after colonies have grown.

Strains: 74-D694 (*MAT***a** *ade1-14 ura3-52 leu2-2,112 his3-200 trp1-289* [p*si*–] [*PIN*$^+$)] (43), 5V-H19 (*MAT***a** *ura3-52 leu2 ade2-1 SUQ5 can1-100* [P*SI*+]).

Media: 1/2YPD: 5 g/l yeast extract, 20 g/l peptone, 20 g/l dextrose, 20 g/l agar.

Synthetic complete minus adenine (SC-Ade) (37).

3.3. Cytoduction

Infectivity is a central defining feature of a prion. In yeast, as in other organisms, vertical transmission – from parents to offspring – is distinguished from horizontal transmission – from one individual to a neighbor. Horizontal transmission of yeast plasmids and viruses is only known via the cell mating process. No infectious element is known to leave one cell and enter another. The same is true for prions.

Laboratory yeast strains are generally haploid. Yeast has two mating types, **a** and alpha, controlled by a single locus on chromosome III. Mixing two haploid strains of opposite type on rich medium, results in mating with cell fusion occurring within a few

hours. Normally diploids are formed which will grow and remain diploid. Meiosis is induced by transfer to 1% potassium acetate medium containing a small amount of required nutrients (if any). Having a *kar1* mutation in one (or both) of the mating strains prevents the nuclear fusion (karyogamy) step that is part of the mating process and follows cell fusion (44). The *kar1* cells then mate, fusing their cytoplasms, but not their nuclei. At the next cell division, the nuclei separate into separate daughter cells, each of which gets a mixture of the cytoplasms of the two parents. This is fundamentally a symmetrical process, but one is usually interested in the transfer of cytoplasm from strain A to strain B. The transfer of cytoplasm is indicated by showing the transfer of some known cytoplasmic genetic element present in strain A but not in B, usually the mitochondrial genome (mitDNA or ρ), or occasionally the killer trait, determined by M_1 dsRNA. Strain B is cured of mitochondrial DNA by growth to single colonies on rich plates containing 30 μg/ml ethidium bromide. The now ρ° strain B is then grown on rich dextrose medium to dilute out any remaining ethidium.

3.4. Cytoduction Procedure

1. About 50 μl of strain A (a large dab from a plate) is mixed with about 25 μl of strain B (a smaller dab) in ~100 μl of water. The exact amount of cells is not critical, but having a roughly twofold excess of donor (strain A) over recipient (strain B) is desirable to insure that all strain B cells mate. Also, having a high cell density insures cells find a mate quickly.
2. The suspension is placed on a slightly dry YPAD plate and allowed to dry, so that the cells are brought into contact, insuring rapid mating. The plate is placed at 30°C for ~7 h.
3. The mating mixture is then streaked for single colonies on media selecting against growth of the donor strain A. The colonies formed will include diploids (few because of the *kar1* mutation), unmated recipient strain B (few because of the modest excess of strain A in the mating mixture), and cytoductants (having the nuclear markers of the recipient strain B and the mitochondrial genome (as shown by ability to grow on a carbon source such as glycerol that requires respiration for its utilization)). Alternatively, one can use recessive selectable markers, such as *can1* (canavanine-resistance) or *cyh2* (cycloheximide-resistance), in the recipient to select against diploids and donors.
4. Replica plate colonies to YPG (only diploids and cytoductants will grow), media selective for diploids, and a plate that scores for the phenotype of the prion. Cytoductants are those colonies that grow on YPG but not on the plate selective for diploids.

Sample Cytoduction: *MAT*a *leu2 ura2* [URE3] $\rho^+ \rightarrow$ *MAT*α *his3 ura2* [ure-o] ρ° (see Note 3). Streak cytoduction mix on synthetic complete—Leu plates. When colonies are grown, replica

plate to YPG, SD + uracil, and SD + his + USA (30 μg/ml). Clones growing on YPG but not SD + uracil are cytoductants, and their acquisition of [URE3] is indicated by their growth on SD + his + USA.

3.5. Curing Prions with Guanidine

Guanidine hydrochloride, at concentrations of 1–5 mM is a surprisingly specific inhibitor of Hsp104 (45–48), and growth to single colonies on rich medium in the presence of ~3 mM guanidine is routinely used to cure yeast prions. If an *ADE2* reporter is being used, then growth on 1/2 YPD with guanidine allows direct detection of cured colonies. [PIN+] is slightly resistant to curing by guanidine (49). The kinetics of guanidine curing have been used to measure prion seed number (50).

4. Fluorescent Proteins and Yeast Expression Vectors

The *S. cerevisiae* prion proteins capable of forming amyloid in vitro also form aggregates in vivo, which are readily detected by fluorescence microscopy. Immunofluorescence has been used in yeast (51) but its application has been mostly limited to the study of yeast prion proteins in mammalian cells (52–55). In yeast, prion-forming proteins have been tagged with variants of green fluorescent protein (derived from Aequorea Victoria jellyfish), although monomeric red fluorescent protein (derived from Discosoma coral; (56)) has also been used. Green fluorescent protein with enhanced brightness and containing codons optimized for expression in yeast has been created (57). Using this yeast optimized green fluorescent protein, variants emitting in the cyan and yellow spectral regions have been engineered (58). Plasmids have been created that allow the fusion of a fluorescent protein tag to open reading frames in *S. cerevisiae* (Yeast Resource Center http://depts.washington.edu/yeastrc/pages/plasmids.html; (58)). However, most experiments have utilized yeast expression vectors containing prion-forming domains fused to fluorescent proteins. Sup35p prion formation has also been studied by embedding green fluorescent protein between the N and M domains (59, 60). A collection of yeast vectors can be found at Stanford Genomic Resources (http://genome-www.stanford.edu/vectordb/vector_pages/Yeast.html). Vectors used to study aggregates utilize a centromeric origin of replication ensuring the presence of 1-2 plasmids per cell. The use of a high copy 2 μm origin of replication, results in artificial differences in expression levels between cells. The expression of the fusion proteins can be directed by the native promoter of the prion-forming protein or by inducible promoters such as *GAL1* and *CUP1*.

For another measure of the presence of [PSI+], a glutathione synthetase ORF containing a UGA stop codon was placed directly

upstream of red fluorescent protein. Only in the presence of [PSI+] will the GST-DsRed fusion protein be formed (60). A nuclear localization signal engineered upstream of red fluorescent protein but separated from it by a stop codon allows more sensitive detection as the fluorescence signal concentrates in the nucleus (61).

4.1. Microscopy and Sample Preparation

Yeast cells expressing fluorescent proteins can be observed using a standard fluorescence microscope with the appropriate filter sets using 60× or 100× objective lenses. However, a confocal microscope is often used to reduce light scattering from out of focus aggregates. An alternative is to use a microscope equipped with an ApoTome. To minimize movement of the yeast cells, it is important to place them at relatively high concentration (clearly turbid) in a minimal volume (2 μl) on a microscope slide. Slightly tapping the cover slip with a pipette tip after it has been applied but before the slide is placed on the microscope also reduces movement of the cells. To further reduce movement microscope slides can be coated with poly L-lysine or the lectin concanavalin A, which both bind the yeast cell wall. Cover slips cleaned by soaking in 1 M NaOH and rinsed with distilled water can be coated with a 2 mg/ml solution of concanavalin A for 10 min. The slips are air dried, rinsed with distilled water and left to dry again. To firmly immobilize yeast cells an agarose pad can be applied to the microscope slide. If needed, nutrients can be added to the agarose as yeast nitrogen-based media has no autofluorescence. The pads are prepared by placing two strips of Scotch Tape on either end of a microscope slide. 30 μl 1% SeaPlaque GTG Agarose is pipetted on a warm taped slide and a second slide is placed immediately on top. The slides are place on a metal block that has been cooled in ice. After a minute, gentle pressure is applied to separate the two slides with a sliding motion. The agarose pad will stick to the warmer top slide. For long-term observations, yeast cells can be grown in Lab-Tek™ Chamber Slides (Thermo Fisher Scientific) which allow for direct microscopic observation. To prevent the cells from moving in the chamber during observation the chambers can be coated with concanavalin A as described earlier. Unbound cells are washed away with media prior to microscopic observation. To study prion aggregates by fluorescence microscopy, yeast cells do not need to be fixed.

4.2. Microscopic Observations

In the absence of prions, fusion of prion-forming domains to fluorescent proteins results in a diffuse signal present throughout most of the yeast cell. However, in prion-containing cells, the fluorescence signal is punctate. As has been shown for [PSI] and [URE3] there can be one or multiple foci in a cell (36, 62). However, care has to be taken as expression of some fusion cures cells of the prion. In addition, overexpression of some fusions results in aggregate formation without the presence of the prion (36, 63). Expression of the NM domain of Sup35 fused to green fluorescent protein in [psi−] cells gives a diffuse fluorescence signal. However, continued

expression of this fusion protein results in the formation of ring and line-shaped aggregates (64). Daughter cells that bud from these ring and line-containing mother cells will contain punctate fluorescence signals (65). It should be noted that not all the cells in a population contain aggregates visible by fluorescence microscopy, although they all contain the prion. Moreover, foci observed after transient expression of Sup35-GFP disappear after the induction is stopped without the fusion protein being degraded (61). Nevertheless, the presence of fluorescent puncta in a substantial number of cells in the population is indicative of the presence of the prion. It has been shown by electron microscopy that a large filamentous network formed by Ure2p is present in cells that contain [URE3] (66). A similar filamentous network, formed by Sup35p, has been observed in [PSI+]-containing cells (67). In this later, case the puncta observed by fluorescence microscopy corresponded to the filamentous network observed by electron microscopy.

When two prions are present within a cell the individual prion-forming proteins have been labeled with cyan and yellow emitting variants of green fluorescent protein. The aggregates formed by the two prion proteins can be found in different parts of the cell or can colocalize (68, 69). Likewise, the association of prions with other proteins has been studied using green fluorescent protein and red fluorescent protein (70, 71).

To measure prion aggregate size in live yeast cells fluorescence recovery after photobleaching [FRAP] and fluorescence correlation spectroscopy [FCS] have been used. The former measures the recovery rate of the fluorescence signal after a limited region of the cell has been photobleached. The latter measures fluorescence intensity fluctuations in a small cell volume. FRAP analysis showed that a yeast mutant that weakens the [PSI+] phenotype also results in the presence of larger prion aggregates (59). Using a modified FRAP technique in which a whole budding daughter cell is photobleached (fluorescence loss in photobleaching; FLIP), it was observed that a weaker [PSI+] variant forms larger aggregates than a strong [PSI+] variant (72). Increase in aggregate size has also been observed after the inhibition of Hsp104 (73–75). FCS measurements indicated that in addition to large fluorescence foci Sup35NM-GFP molecules also form smaller diffusible aggregates in [PSI+] cells. These smaller diffusible aggregates are also present in the newly forming buds (61).

5. Protein Expression, Purification, Amyloid Formation, and Proteinase K Treatment

A huge advantage in using yeast prions to study amyloid is that the biologically active amyloid state can be produced in vitro from recombinant yeast proteins. Yeast prion proteins can be produced using *E. coli* expression systems, and once purified, these proteins

will readily form infectious amyloid after incubation in common laboratory buffers. This enables the production of large quantities of prion amyloid and greatly facilitates the biophysical characterization of the biologically relevant state. A combination of methods such as Proteinase K digestion coupled with LC-MS (liquid chromatography mass spectrometry) has aided in defining the amyloid core associated with many disease-related amyloids. This will be discussed below.

5.1. Materials

5.1.1. His-Tagged Protein Expression/Purification and Amyloid Formation

1. BL21(DE3)* chemically competent cells (see Note 4).
2. SDS-PAGE + reagents (commercially available).
3. Plasmid containing gene of interest, e.g., pET21(a).
4. Luria broth (LB) media.
5. Antibiotic (e.g., Ampicillin).
6. Isopropyl-beta-D-thiogalactopyranoside (IPTG).
7. Ni-NTA Agarose.
8. Polypropylene columns (5 ml).
9. Lysis buffer (8 M GuHCl, 10 mM imidazole, 0.1 M phosphate buffer, pH 7.4, 0.1 M NaCl, protease inhibitors (e.g., Complete™).
10. Wash buffer (8 M GuHCl, 20 mM imidazole, 0.1 M phosphate buffer, pH 7.4, 0.1 M NaCl).
11. Elution buffer (8 M GuHCl, 250 mM imidazole, 0.1 M phosphate buffer, pH 7.4, 0.1 M NaCl).
12. Slide-A-Lyzer Dialysis Cassette (3–20 K MW cut-off, 3–12 ml) (Thermo Scientific).
13. Fibrilization buffer (100 mM phosphate buffer, pH 7.4, 0.1 M NaCl). The best buffer to induce fiber formation will vary with the protein.

5.1.2. Proteinase K Digestion and LC-MS (Mass-Spec)

1. Proteinase K (Merck).
2. Fibrilization buffer (100 mM phosphate buffer, pH 7.4, 0.1 M NaCl).
3. Trichloroacetic acid (TCA).
4. Acetic acid (5%)/water (95%).

5.2. Methods

5.2.1. His-Tagged Protein Expression/Purification and Amyloid Formation

Protein Expression

1. Refer to manufacturer's protocol for transformation guidelines.
2. Select for cells containing plasmid of interest by plating (25–100 μl) on selection media (LB agar + antibiotic) using a sterile spreader and incubate overnight at 37°C.
3. Inoculate 10 ml aliquots of LB broth containing the antibiotic required to maintain the expression plasmid with single colonies

from the transformation. Shake at 220–250 rpm at 37°C overnight.

4. The next morning, harvest culture by spinning at 4,000 rpm for 10 min and resuspend pellet in fresh LB (10 ml). Add resuspended culture to 1 L LB (1% v/v) and incubate at 37°C with agitation on an orbital shaker (220–250 rpm) (see Note 5).
5. Monitor cell growth (OD_{600}) and add IPTG (1.0 mM) when cells reach an OD_{600} of approx. 0.5. Continue incubating for a further 4 h at 37°C with agitation. The values for IPTG concentration and induction time are starting values only and may require optimization depending on the gene expressed.
6. Check protein expression by SDS-PAGE. Pipette 20 μl of the induced cultures (and uninduced control) into clean microcentrifuge tubes. Add 20 μl of 2× SDS gel sample buffer to each microcentrifuge tube. Heat tubes to 95°C for 5 min. Load the associated noninduced (control) and induced sample in adjacent lanes for analysis by SDS-PAGE. Stain the protein gel with Coomassie® Brilliant blue stain. Check that the protein of interest has expressed before proceeding.

Protein Purification

1. Harvest cells by centrifugation at 10,000 ×*g* for 20 min and wash cell pellet with 100 mM phosphate buffer, pH 7.4. Resuspend pellet vigorously in lysis buffer (40 ml) and incubate at 4°C for 1 h with gentle agitation.
2. Spin cell suspension at 30,000 rpm for 45 min and retain lysate (contains his-tagged protein). Add 4 ml NiNTA to 40 ml lysate and gently agitate at 4°C for 2 h. Pour lysate over polypropylene column (5 ml) and wash NiNTA with 10 column volumes of wash buffer. Elute bound protein with 10 ml elution buffer.
3. Filter purified protein through YM-100 filter unit (molecular weight cutoff 100 kDa), and exchange into fibrilization buffer using a dialysis cassette. Incubate overnight at RT.

Amyloid Formation

1. For amyloid formation, incubate dialyzed protein at RT for several days with gentle agitation. A typical concentration for amyloid formation is 1.0 mg/ml.
2. Spin amyloid solution at 50,000 rpm for 45 min at 10°C and retain pellet.

5.2.2. Proteinase K Digestion and LC-MS

1. Prepare serial dilutions of proteinase K in 100 mM phosphate buffer, pH 7.4. A typical concentration range is 1–100 μg/ml.
2. Add 0.5 mg amyloid to serial dilutions of proteinase K giving a final volume of 1.0 ml and incubate overnight at RT with gentle agitation.
3. Terminate reaction by adding 4% (v/v) TCA. Lyophilize sample by freeze-drying or speed-vac.

4. Resuspend lyophilized material in 285 µl dH_2O and 15 µl acetic acid (5% v/v) for LC-MS analysis.
5. For LC-MS analysis, 100 µl of sample is injected onto a C18 column running at 0.2 ml/min.
6. A long gradient of 95 min is used to obtain good peptide separation. Buffer A consists of 98% water, 2% acetonitrile, 0.1% acetic acid, and 0.01% TFA. Buffer B contains 80% acetonitrile, 20% water, 0.09% acetic acid, and 0.01% TFA.
7. After analysis; the MS data reveals average masses corresponding to peptide fragments generated after Proteinase K digestion, which can be used along with the known protein sequence to identify the sequence of these fragments. Software from ExPASY proteomics tools can be used to analyze the data.

6. Protein Transformation

The prion hypothesis implies that a single protein can misfold into multiple distinct infectious forms, which can be maintained during cell proliferation. The direct proof of this hypothesis can be made by protein transformation, e.g., by introducing in vitro prepared prion aggregates into living organisms that would result in stable prion propagation. This was first achieved for the [Het-s] prion of *Podospora anserina* (77) and was then developed for [*PSI*+] (78, 79) and applied successfully for other known yeast prions. Remarkably, the introduction of Sup35p amyloid aggregates of different structures led to appearance of different prion variants in yeast cells, suggesting that the prion strain phenomenon results from conformational variations in the underlying amyloid structure. Here, we present a protein transformation protocol based on the original technique of Tanaka et al. (79) as modified by us (42).

6.1. Materials and Equipment

1. YPD medium (1% yeast extract, 2% bactopeptone, and 2% dextrose); autoclave before use.
2. Buffer A (25 mM Tris–HCl, pH 7.4, 150 mM NaCl, 1 mM dithiothreitol, 10 mM phenyl methyl sulphonyl fluoride (PMSF), and 1× complete protease inhibitor cocktail).
3. Glass beads (0.5 mm diameter, Biospec products).
4. Vortex Genie 2 (Daigger) to break yeast cells.
5. BCA reagent (Pierce, Rockford, IL).
6. Branson Sonifier 250 (Branson Scientific) or Sonic Dismembrator (Fisher Scientific) at lower settings (10–20% intensity).
7. 20% Triton X-100 solution.
8. 30% (w/v) Sucrose solution in buffer A.

9. 1 M lithium acetate with 1× complete protease inhibitor cocktail.
10. Optima L-90K ultracentrifuge equipped with SW55 rotor (Beckman Coulter).
11. Buffer B (5 mM potassium phosphate buffer, 150 mM NaCl).
12. ST buffer (1 M sorbitol, 10 mM Tris–HCl, pH 7.5).
13. STC buffer (1 M sorbitol, 10 mM Tris–HCl, 10 mM $CaCl_2$, pH 7.5).
14. PTC buffer (20% (w/v) polyethylene glycol (PEG) 8000 (MP Biomedicals), 10 mM Tris–HCl, 10 mM $CaCl_2$, pH 7.5).
15. SOS buffer (1 M sorbitol, 7 mM $CaCl_2$, 0.25% yeast extract, 0.5% peptone).
16. Lyticase (10 U/ml in 20% glycerol).
17. Salmon sperm DNA (2 mg/ml).
18. Plasmid pRS425 (0.5 mg/ml) or another yeast plasmid for initial clone selection.
19. Sorbitol agar medium (1× complete amino acid mix lacking leucine and adenine (see 20), 0.67% yeast nitrogen base, 2% glucose, 2.5% agar, 1 M sorbitol). May contain either 5 mg/l adenine (full amount) or 0.1 mg/l adenine (limited amount for prion selection: for –LEU–0.02ADE plates).
20. 10× Complete amino acid mix, per liter, autoclave before use (200 mg methionine, 500 mg tyrosine, 500 mg isoleucine, 500 mg phenylalanine, 1,000 mg glutamic acid, 2,000 mg threonine, 1,000 mg aspartic acid, 1,500 mg valine, 4,000 mg serine, 200 mg arginine, 200 mg histidine, 300 mg lysine, 300 mg tryptophan, and 200 mg uracil). Alternatively, complete synthetic dropout mix [–LEU] can be used (US Biological).
21. LEU-ADE plates (1× complete amino acid mix lacking leucine and adenine, 0.67% Yeast nitrogen base, 2% glucose, 2% agar).
22. ½ YPD medium (0.5% yeast extract, 2% bactopeptone, 2% dextrose, and 2% agar) (Quality Biologics).

6.2. Methods

6.2.1. Preparation of Prion Material

Both crude cellular extracts of prion-containing cells and amyloid fibrils formed by yeast prion proteins in vitro can be used for prion protein transformation. Preparation of amyloid fibers is described in Subheading 4. To obtain yeast extracts suitable for transformation, grow [PRION+] yeast cells in liquid YPD medium to optical density at 600 nm (OD_{600}) of 1.5. After harvesting by centrifugation (5,000×*g*, 5 min) wash yeast cells with buffer A. Mix 1 volume of yeast cell pellet with 2 volumes of buffer A and 2 volumes of glass beads. Vortex tubes at top speed for a total of 4 min with

cooling on ice for 30 s after each minute to break the cells. Remove cell debris by centrifugation at 5,000 × *g* for 10 min (see Note 6). Protein levels can be measured at this stage with BCA reagent according to manufacturer's protocol. Sonicate protein extracts on ice for 10–20 s at lower settings (10–20% intensity) before use for protein transformation.

Partial purification of prion aggregates can significantly improve transformation efficiency. To this end, treat protein extracts with 0.5% Triton X-100 for 5 min on ice, spin at 5,000 × *g* for 10 min, layer the supernatant on the top of a 0.5 ml 30% sucrose pad prepared in buffer A and do ultracentrifugation at 150,000 × *g* for 45 min (SW55 rotor, Beckman). Resuspend the pellet with 1 M lithium acetate with 1× complete protease inhibitor cocktail, incubate on ice for 30 min with gentle agitation and spin again through a 0.5 ml 30% sucrose pad at 150,000 × *g* for 45 min. Resuspend the pellet with buffer B, determine protein concentration with BCA reagent, sonicate on ice for 10–20 s at lower settings (10–20% intensity) immediately before use for protein transformation.

6.2.2. Protein Transformation

Although the technique was reported to be general and has been successfully applied for most known yeast prions, we observed that the efficiency of protein transformation is greatly dependent on yeast strain background. Since the factors that determine the success are not clear, one may need to compare available strains experimentally. We recommend 74D-694 [p*si*–] (43) for Sup35 prion transformation and BY241 [ure-o] (42) for Ure2 prion transformation. In contrast to de novo prion induction, the transformation efficiency does not depend on the presence of the [P*IN*+] prion (79). To select "competent" yeast cells that have taken up prion aggregates, a yeast vector is usually used during the transformation procedure together with the protein preparation.

Grow yeast strains in 50 ml YPD at 30°C with constant shaking at 250 rpm to OD_{600} of 0.6; spin cells at 1,500 × *g* for 5 min at room temperature, and wash twice with 25 ml ST buffer. Resuspend cells in 5 ml ST buffer, add 10 µl lyticase (10 U/ml), and incubate for 40 min at 30°C while shaking at 200 rpm to digest the yeast cell wall (see Note 2). Pellet spheroplasts at 250 g for 5 min at room temperature, wash twice with 10 ml ST buffer, and then resuspend in 0.5 ml STC buffer (see Note 3). Mix a 100 µl portion of the spheroplast suspension with 5 µl of salmon sperm DNA (ssDNA), 1 µl of 0.5 mg/ml selectable plasmid (pRS425), and 5–10 µl solution containing prion particles, either in vitro-formed filaments or from cell extracts (see Note 6). The final protein concentration of amyloid fibers should be about 5 µM or 0.2 mg/ml total protein for yeast prion extracts. Incubate the mixture for 10 min at room temperature and then induce fusion by the addition of 900 µl PTC buffer. Mix gently and incubate for 20 min at room temperature. Collect spheroplasts by centrifuga-

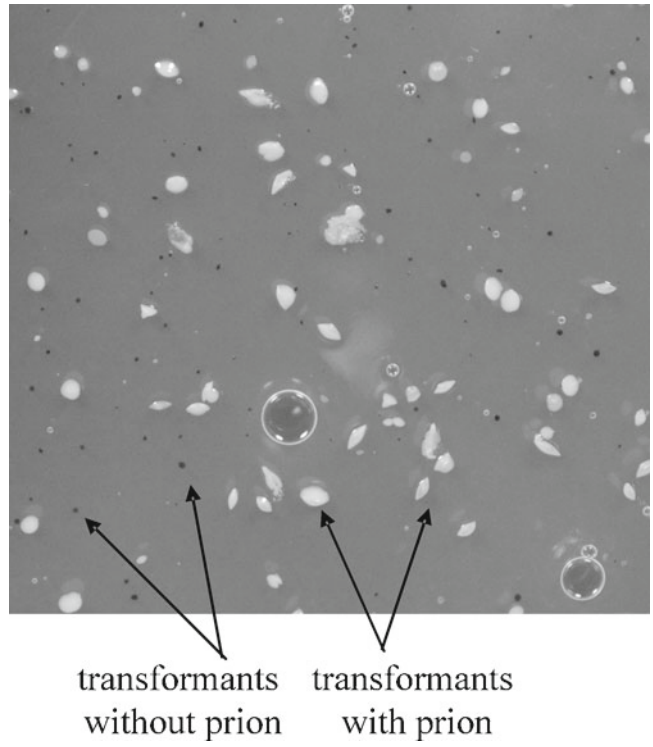

Fig. 1. Strain 74D-694 [p*si*–] was transformed with amyloid fibrils formed in vitro from recombinant Sup35 prion protein mixed with pRS425 (carrying *LEU2*). Transformants were selected on –Leu plates containing 2% of the normal amount of adenine. [P*SI+*] transformants are large, Ade+ and *white*, while [p*si–]* transformants are small, Ade- and *red.*

tion at 500 × *g* for 5 min at room temperature, resuspend in 200 µl SOS buffer and incubated for 30 min at 30°C.

Gently mix the transformation reactions with 10 ml liquid sorbitol agar medium at 50°C (see Note 6) and immediately pour onto Petri plates with 20 ml of solidified sorbitol agar medium, selective for the presence of the plasmid (e.g., –LEU) and (optional) for the prion state (–LEU + 0.02 ADE) (see Note 6). Incubate plates at 30°C for 5–7 days (Fig. 1). Colonies can be picked from agar using sterile toothpicks and streaked to single colonies on –LEU-ADE plates or ½ YPD plates to detect and verify [PRION+] appearance (see Note 6). To determine the efficiency of transformation, the number of growing transformants on –LEU + 0.02 ADE plates (that can grow further on –LEU-ADE plates) should be divided by the number of transformants on –LEU plates.

7. SDS Treatment and SDD-AGE

Amyloid-based yeast prions form high molecular weight complexes in vivo, which consist of a prion protein and associated proteins (80,

81). The interaction between prion protein molecules is strong enough to resist the treatment with the strong anionic detergent sodium dodecyl sulfate (SDS) at room temperature (82, 83). The insolubility in SDS distinguishes prion polymers from the majority of protein–protein complexes in a yeast lysate and allows their purification and analysis. Importantly, SDS treatment does not reduce, but instead modestly improves the infectivity of prion material extracted from yeast lysates (for infectivity assay, see Subheading 6.2.2) (83), providing the evidence that SDS does not disrupt the intrinsic prion structure. Purification of SDS-resistant prion polymers from yeast cell lysates is done by ultracentrifugation and was described in detail in ref. 84. Moreover, high molecular weight prion polymers can be analyzed by semidenaturing detergent–agarose gel electrophoresis (SDD–AGE) (82, 83). This technique is widely used to provide an alternative confirmation for the presence of a prion in yeast cells; in addition, different prion variants can be distinguished by different migration in agarose gels (82, 85). This method can be applied to characterize different amyloids (83, 86) and for large-scale screening for new prions (29).

8. Electron Microscopy

A combination of methods in electron microscopy and solid-state NMR has made possible the unraveling of the structural elements that underlie infectious amyloid.

8.1. Materials

8.1.1. Transmission Electron Microscopy

1. Negative Stain: 1–2% uranyl acetate in water (filtered, and protected from light to prevent precipitation).
2. Sample Support: Carbon-coated copper grids (commercially available).

8.1.2. Electron Diffraction

1. Diffraction/atomic spacing control: Thallous chloride crystals (Electron Microscopy Sciences).
2. Sample Support: Carbon-coated copper grids.

8.1.3. Mass-per-Length Measurements by Tilted-Beam TEM

1. Internal mass standard: Tobacco mosaic virus.
2. Sample Support: Ultra-thin carbon-coated copper grids.

8.2. Methods

8.2.1. Transmission Electron Microscopy Using Negatively Stained Amyloid

1. Prepare serial dilutions of amyloid samples in water or the same buffer that is used during fibrillization. A typical concentration range is 0.01–1.0 mg/ml.
2. Apply approximately 10 µl of each amyloid sample to a carbon-coated copper mesh grid (Fig. 2a). (carbon-coated grids are sometimes glow-discharged to increase their hydrophilicity, (87)).

3. After 2–3 min, use absorbent paper to blot off the sample from the grid and quickly add 10 µl of water to the grid surface.
4. Immediately blot the water away with absorbent paper and quickly add 10 µl of 1–2% uranyl acetate negative stain to the grid.
5. After 1–2 min, blot away the stain with absorbent paper and leave the grid to air dry for a few minutes. Once the grid is completely dry it is ready for examination by TEM or can be stored for subsequent examination.
6. Negatively stained amyloid samples are generally visualized with the electron microscope operating at 80 kV.

8.2.2. Electron Diffraction

1. To achieve strong electron diffraction from amyloid, a greater amount of sample is usually used than would be for a negatively stained sample viewed by TEM. As described above, first prepare samples with negative stain and check for concentrations of the amyloid that yield larger aggregates or a thin film of amyloid on the grid surface. Incubation time can also be increased to get more sample adherence to the grid surface.
2. Once the desired concentration and incubation time is determined, prepare the grid as would be done for negative staining, but without adding the stain.
3. At low magnification, find a region of the grid that clearly contains sample aggregates.
4. Put the EM in diffraction mode and use the smallest condenser aperture and remove the objective aperture.
5. Minimize the beam dose to avoid destroying the amyloid sample; use low intensity and heating settings, and reduce beam spot size.
6. Use the pointer to block the center of the beam before putting CCD camera in (Fig. 2c, d).
7. Adjust camera settings to quickly acquire images before electron diffraction diminishes (biological samples are damaged by the electron beam).
8. Scan grid for strong electron diffraction signal (Fig. 2c).
9. After recording an electron diffraction signal, the microscope can be set to regular mode to visualize diffracting species, although resolution is lower due to the lack of negative stain.
10. Diffraction distances and atomic spacing will ultimately be calibrated using the electron diffraction of a known crystal, such as thallous chloride, under identical conditions (Fig. 2d). Before checking the diffraction of the amyloid sample, it may be easier to adjust the initial settings using a grid with thallous

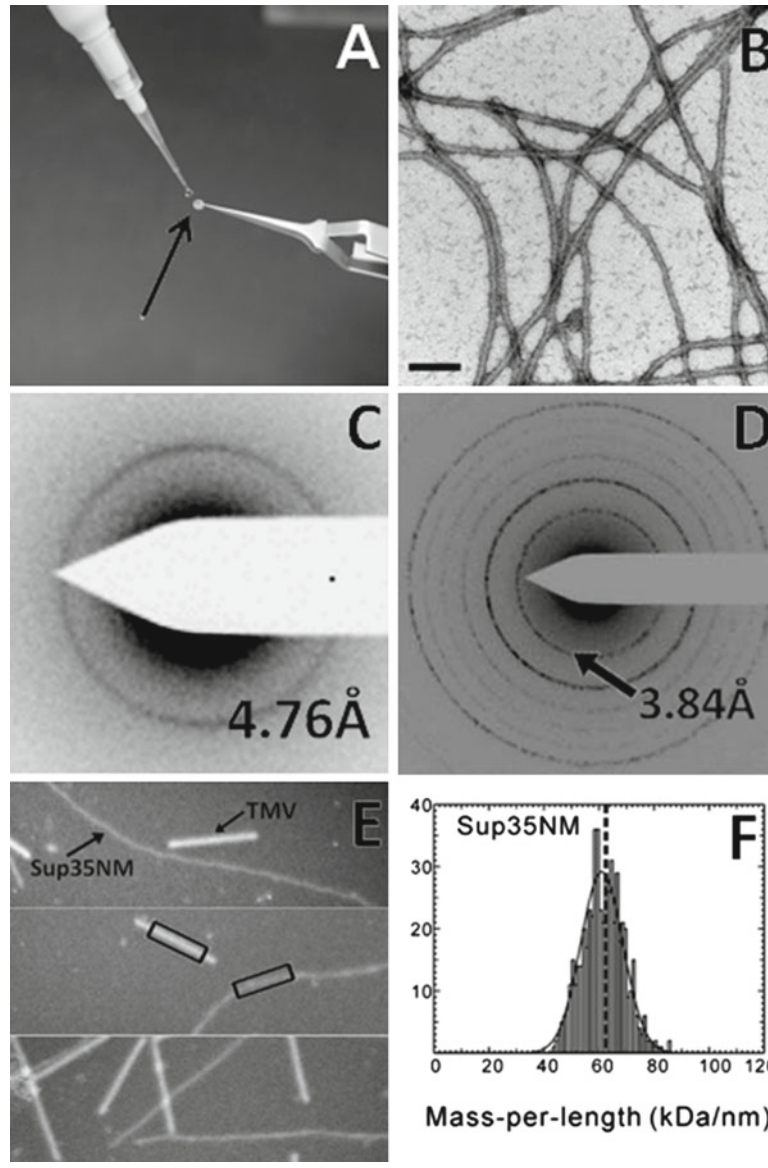

Fig. 2. (**A**) The application of a 10 μl amyloid suspension to a carbon-coated copper grid. (**B**) Sup35 prion domain fibers stained with uranyl acetate. (**C**) Typical amyloid electron diffraction of unaligned fibers (mouse Pmel rpt). (**D**) Electron diffraction of thallous chloride crystals. (**E**) TMV and Sup35NM fibers viewed in the darkfield mode (tilted beam). (**F**) Histogram representation of Sup35NM mass-per-length measurements (from Chen et al. (97)).

chloride crystals, which are not destroyed by the constant electron beam.

11. Electron diffraction images from the thallous chloride control and the amyloid sample can be viewed by image-processing software such as ImageJ (freeware). The atomic spacing of the amyloid diffraction can be determined from the known spacing and diffraction radii of the thallous chloride crystals.

The electron diffraction method described here is for quickly checking if the amyloid sample contains a repeated spacing, such as the 4.7Å spacing seen for all amyloids. To determine cross-β structure, the amyloid fibrils must be laterally aligned to get the additional directional information. Also, the orientation of the aligned fibers with respect to the diffraction pattern must be determined.

This method, developed by Chen et al. (ref. 97), allows determination of mass per length of filaments without access to a scanning transmission electron microscope.

8.2.3. Mass-per-Length Measurements by Tilted-Beam TEM

1. Make serial dilutions each of tobacco mosaic virus (TMV) and the amyloid sample in water or buffer. TMV concentrations around 0.1 mg/ml are in the typical working range.
2. Apply the samples to EM grids and stain with uranyl acetate, as described above.
3. By TEM, determine the proper concentrations and ratios of TMV and amyloid that will yield an even and equal distribution of both amyloid fibrils and virus particles in the microscope field of view. At a magnification of 56,000×, the desired field should have a few individual virus particles along with a few individual amyloid fibrils, without clumping or crowding (Fig. 2e).
4. After the ideal sample concentrations have been determined, prepare the EM grid with amyloid and TMV, but without negative stain. It is best to use a copper grid with an ultra-thin carbon coating (~5 nm) to avoid a high background of electron scatter in the dark field.
5. After application of the sample to the EM grid, wash the grid several times with 10 µl aliquots of water to reduce electron scatter from residual salts.
6. Operate the EM at 80 kV in the dark field, or tilted beam, mode at 56,000× magnification. Use a beam tilt angle of at least 1.2° to prevent the measuring of unscattered electrons.
7. Before viewing the sample, adjust the beam with the condenser stigmators to produce a uniform beam spread over the field of view.
8. Once the initial settings have been adjusted, scan the sample-containing EM grid. Adjust intensity settings and ensure the beam is centered with no visible intensity gradients in the field of view.
9. When pairs of TMV and amyloid fibrils are found in the field of view, quickly adjust focus and acquire an image as a 16-bit TIF file with threshold and tail set to zero. Adjusting the camera to multiple image acquisitions may be necessary to obtain quality pictures. However, it is important to not prolong the exposure of the samples in the electron beam, which can lead to mass loss of the sample.

10. Once sufficient numbers of images have been acquired, image-processing software such as ImageJ can be used to determine the relative intensities of the scattered electrons from TMV particles and amyloid fibrils (see boxes in Fig. 2e). Using the known mass-per-length of TMV (131 kDa/nm), the mass of the amyloid fibril can be determined. Because of the variability of any single measurement, it is typical to make scores of measurements and present the data as a histogram (Fig. 2f).

9. Solid-State NMR

Because amyloid is neither soluble, nor highly mobile, X-ray crystallography and solution NMR are both of little use in studying its structure. Solid-state NMR (ssNMR) has the potential to determine detailed structures of amyloids, as has been done for Aβ peptide (88–90) and the HET-s prion protein (91–93). The application of ssNMR to amyloid structure determination is reviewed by Tycko (94) and by Baldus (95). An excellent introduction to NMR is Levitt's book (96). An excellent explanation of dipolar recoupling by R. Tycko, a pioneer in this method, is available at http://fbml.scripts.mit.edu/Conferences/. We will not attempt to present detailed NMR methods but simply emphasize the importance of this approach in achieving an understanding of amyloid structure.

10. Notes

1. The USA test is sensitive to the presence of various nitrogen sources in the medium. Leucine is particularly able to repress USA uptake even in [URE3] strains. Only required amino acids should be added to the plates with USA. The test cannot be done on -Ura dropout plates.
2. When selecting USA+ clones as a reflection of [URE3] generation, the colony count is generally not linear with cells plated, but is generally sigmoidal, perhaps due to cross-feeding.
3. A cytoduction is denoted, "A→B" where A is the donor strain and B is the recipient. A standard mating with nuclear fusion is denoted "AxB."
4. The BL21(DE3) competent cells are an all-purpose strain for high-level protein expression and easy induction. Other competent cell lines may be used when genes being expressed contain rare codons or proteins are toxic to the cell. BL21(DE3) RIPL cells (Stratagene) overexpress Arg, Ile, Pro, and Leu tRNAs which

are normally poorly expressed in *E. coli* and aid in expression of some eukaryotic proteins.

5. If preparing ^{13}C- or ^{15}N-labeled protein for solid-state NMR experiments, a minimal medium or synthetic complete medium should be used with the appropriate labeled amino acid(s) or $^{15}NH_4Cl$ or U-^{13}C-glucose (76).
6. During centrifugation all viable (unbroken) cells should be removed to avoid false positives. The progress of spheroplasting can be monitored during this incubation by placing 2 μl of cells in 5 μl of 0.5% SDS solution followed by microscopic analysis. Spheroplasts with SDS should appear invisible or as ghost cells. Spheroplasts are sensitive to pressure and must be handled gently. To resuspend spheroplasts, use a 1 ml plastic pipette tip with the narrow tip opening cut off. To increase efficiency of transformation, boil ssDNA at 100°C for 2 min and put immediately on ice just before addition. Also, it is very important to sonicate prion material before addition. Sonication breaks amyloid filaments into smaller pieces, enhancing their infectivity. However, over-sonication may decrease transformation efficiency. Prepare sorbitol agar medium in advance and keep at 50°C (to prevent solidification) to be ready to mix with the spheroplast suspension. Mixing can be done in pre-heated (50°C) sterile 50-ml falcon tubes (Corning). Sorbitol agar medium may contain either 5 mg/l adenine or 0.1 mg/l adenine to select directly for the (PRION+) state of prions, if the yeast strain used for transformation contains an adenine-based genetic system (*ade1-14* or *ade2-1 SUQ5* for [PSI+]; *PDAL5-ADE2* for [URE3]). Such selective pressure during recovery and growth of transformants often improves transformation efficiency likely due to instability of newly arisen prions. Complete absence of adenine may, however, inhibit recovery of transformants (42). Selection stringency may be optimized depending on the particular prion and selection scheme. As a negative control for the transformation, (prion-) cell extract may be used. In our experience, spontaneous prion generation during transformation procedure is hardly detectable. Results from the negative control should be counted when determining the efficiency of transformation.

Acknowledgments

This work was supported by the Intramural Program of the National Institute of Diabetes Digestive and Kidney Diseases. The electron diffraction method was developed by Kent Thurber and Rob Tycko (NIH, Bethesda, MD).

References

1. Gorkovskii, A. A., Bezsonov, E. E., Plotnikova, T. A., Kalebina, T. S., and Kulaev, I. S. (2009) Revealing of *Saccharomyces cerevisiae* yeast cell wall proteins capable of binding thioflavin T, a fluorescent dye specifically interacting with amyloid fibrils, *Biochemistry (Mosc) 74*, 1219–1224.
2. Amberg, D. C., Burke, D. J., and Strathern, J. N. (2005) *Methods in yeast genetics: a Cold Spring Harbor Laboratory Course Manual*, Cold Spring Harbor Laboratory, Cold Spring Harbor, NY.
3. Guthrie, C., and Fink, G. R., (Eds.) (2002) *Methods in Enzymology: Guide to yeast genetics and molecular cell biology, part B*, Vol. **350**, Academic Press.
4. Guthrie, C., and Fink, G. R., (Eds.) (2004) *Guide to yeast genetics and molecular biology, part A*, Vol. 194, Academic Press.
5. Wetzel, R., (Ed.) (1999) *Amyloid, Prions, and other protein aggregates*, Vol. 309, Academic Press.
6. Wetzel, R., and Kheterpal, I., (Eds.) (2006) *Amyloid, Prions, and other protein aggregates, Part B*, Vol. 412, Academic Press.
7. Masison, D. C., (Ed.) (2006) *Identification, analysis and characterization of fungal prions*, Vol. 39(1).
8. Lacroute, F. (1971) Non-Mendelian mutation allowing ureidosuccinic acid uptake in yeast, *J. Bacteriol. **106***, 519–522.
9. Aigle, M., and Lacroute, F. (1975) Genetical aspects of (URE3), a non-Mendelian, cytoplasmically inherited mutation in yeast, *Molec. Gen. Genet. **136***, 327–335.
10. Cox, B. S. (1965) PSI, a cytoplasmic suppressor of super-suppressor in yeast, *Heredity **20***, 505–521.
11. Wickner, R. B. (1994) (URE3) as an altered *URE2* protein: evidence for a prion analog in *S. cerevisiae*, *Science **264***, 566–569.
12. Goldring, E. S., Grossman, L. I., Krupnick, D., Cryer, D. R., and Marmur, J. (1970) The petite mutation in yeast: loss of mitochondrial DNA during induction of petites with ethidium bromide, *J. Mol. Biol. **52***, 323–335.
13. Wickner, R. B. (1974) "Killer character: of Saccharomyces cerevisiae: curing by growth at elevated temperature," *J Bacteriol **117***, 1356–1357.
14. Sommer, S. S., and Wickner, R. B. (1982) Co-curing of plasmids affecting killer double-stranded RNAs of Saccharomyces cerevisiae: (HOK), (NEX), and the abundance of L are related and further evidence that M1 requires L, *J Bacteriol **150***, 545–551.
15. Singh, A. C., Helms, C., and Sherman, F. (1979) Mutation of the non-Mendelian suppressor ψ+ in yeast by hypertonic media, *Proc. Natl. Acad. Sci. USA **76***, 1952–1956.
16. Tuite, M. F., Mundy, C. R., and Cox, B. S. (1981) Agents that cause a high frequency of genetic change from (*psi+*) to (*psi-*) in *Saccharomyces cerevisiae*, *Genetics **98***, 691–711.
17. Chernoff, Y. O., Derkach, I. L., and Inge-Vechtomov, S. G. (1993) Multicopy SUP35 gene induces de-novo appearance of psi-like factors in the yeast *Saccharomyces cerevisiae*, *Curr. Genet. **24***, 268–270.
18. Rizet, G. (1952) Les phenomenes de barrage chez *Podospora anserina*: analyse genetique des barrages entre les souches s et S, *Rev. Cytol. Biol. Veg. **13***, 51–92.
19. Coustou, V., Deleu, C., Saupe, S., and Begueret, J. (1997) The protein product of the *het-s* heterokaryon incompatibility gene of the fungus *Podospora anserina* behaves as a prion analog, *Proc. Natl. Acad. Sci. USA **94***, 9773–9778.
20. Derkatch, I. L., Bradley, M. E., Zhou, P., Chernoff, Y. O., and Liebman, S. W. (1997) Genetic and environmental factors affecting the *de novo* appearance of the (P*SI*+) prion in *Saccharomyces cerevisiae*, *Genetics **147***, 507–519.
21. Sondheimer, N., and Lindquist, S. (2000) Rnq1: an epigenetic modifier of protein function in yeast, *Molec. Cell **5***, 163–172.
22. Derkatch, I. L., Bradley, M. E., Hong, J. Y., and Liebman, S. W. (2001) Prions affect the appearance of other prions: the story of *(PIN)*, *Cell **106***, 171–182.
23. Osherovich, L. Z., and Weissman, J. S. (2001) Multiple Gln/Asn-rich prion domains confer susceptibility to induction of the yeast [*PSI*+] prion, *Cell **106***, 183–194.
24. Masison, D. C., and Wickner, R. B. (1995) Prion-inducing domain of yeast Ure2p and protease resistance of Ure2p in prion-containing cells, *Science **270***, 93–95.
25. TerAvanesyan, A., Dagkesamanskaya, A. R., Kushnirov, V. V., and Smirnov, V. N. (1994) The *SUP35* omnipotent suppressor gene is involved in the maintenance of the non-Mendelian determinant [PSI+] in the yeast *Saccharomyces cerevisiae*, *Genetics **137***, 671–676.
26. Du, Z., Park, K.-W., Yu, H., Fan, Q., and Li, L. (2008) Newly identified prion linked to the chromatin-remodeling factor Swi1 in *Saccharomyces cerevisiae*, *Nat. Genet. **40***, 460–465.
27. Patel, B. K., Gavin-Smyth, J., and Liebman, S. W. (2009) The yeast global transcriptional

co-repressor protein Cyc8 can propagate as a prion, *Nat. Cell Biol.* ***11***, 344–349.

28. Nemecek, J., Nakayashiki, T., and Wickner, R. B. (2009) A prion of yeast metacaspase homolog (Mca1p) detected by a genetic screen, *Proc. Natl. Acad. Sci. USA* ***106***, 1892–1896.
29. Alberti, S., Halfmann, R., King, O., Kapila, A., and Lindquist, S. (2009) A systematic survey identifies prions and illuminates sequence features of prionogenic proteins, *Cell* ***137***, 146–158.
30. Ross, E. D., Baxa, U., and Wickner, R. B. (2004) Scrambled prion domains form prions and amyloid, *Mol Cell Biol* ***24***, 7206–7213.
31. Ross, E. D., Edskes, H. K., Terry, M. J., and Wickner, R. B. (2005) Primary sequence independence for prion formation, *Proc Natl Acad Sci USA* ***102***, 12825–12830.
32. Toombs, J. A., McCarty, B. R., and Ross, E. D. (2010) Compositional determinants of prion formation in yeast, *Mol. Cell. Biol.* ***30***, 319–332.
33. Chiti, F., and Dobson, C. M. (2006) Protein folding, functional amyloid and human disease, *Annu. Rev. Biochem.* ***75***, 333–366.
34. Masison, D. C., Maddelein, M.-L., and Wickner, R. B. (1997) The prion model for (URE3) of yeast: spontaneous generation and requirements for propagation, *Proc. Natl. Acad. Sci. USA* ***94***, 12503-12508.
35. Kochneva-Pervukhova, N. V., Poznyakovski, A. I., Smirnov, V. N., and Ter-Avanesyan, M. D. (1998) C-terminal truncation of the Sup35 protein increases the frequency of de novo generation of a prion-based (*psi+*) determinant in *Saccharmyces cerevisiae*, *Curr. Genet.* ***34***, 146–151.
36. Edskes, H. K., Gray, V. T., and Wickner, R. B. (1999) The (URE3) prion is an aggregated form of Ure2p that can be cured by overexpression of Ure2p fragments, *Proc. Natl. Acad. Sci. USA* ***96***, 1498 – 1503.
37. Sherman, F. (1991) Getting started with yeast, in *Guide to yeast genetics and molecular biology* (Guthrie, C., and Fink, G. R., Eds.), pp 3–21, Academic Press, San Diego.
38. Cooper, T. G. (2002) Transmitting the signal of excess nitrogen in *Saccharomyces cerevisiae* from the Tor proteins to th GATA factors: connecting the dots, *FEMS Microbiol. Revs.* ***26***, 223–238.
39. Magasanik, B., and Kaiser, C. A. (2002) Nitrogen regulation in Saccharomyces cerevisiae, *Gene* ***290***, 1–18.
40. Turoscy, V., and Cooper, T. G. (1987) Ureidosuccinate is transported by the allantoate transport system in *Saccharomyces cerevisiae*, *J. Bacteriol.* ***169***, 2598–2600.
41. Rai, R., Genbauffe, F., Lea, H. Z., and Cooper, T. G. (1987) Transcriptional regulation of the *DAL5* gene in *Saccharomyces cerevisiae*, *J. Bacteriol.* ***169***, 3521–3524.
42. Brachmann, A., Baxa, U., and Wickner, R. B. (2005) Prion generation *in vitro*: amyloid of Ure2p is infectious, *Embo J* ***24***, 3082–3092.
43. Chernoff, Y. O., Lindquist, S. L., Ono, B.-I., Inge-Vechtomov, S. G., and Liebman, S. W. (1995) Role of the chaperone protein Hsp104 in propagation of the yeast prion-like factor (PSI+), *Science* ***268***, 880–884.
44. Conde, J., and Fink, G. R. (1976) A mutant of *Saccharomyces cerevisiae* defective for nuclear fusion, *Proc. Natl. Acad. Sci. USA* ***73***, 3651–3655.
45. Tuite, M. F., Mundy, C. R. and Cox, B. S. (1981) Agents that cause a high frequency of genetic change from (*psi+*) to (*psi-*) in *Saccharomyces cerevisiae. Genetics* ***98***, 691–711.
46. Jung, G., and Masison, D. C. (2001) Guanidine hydrochloride inhibits Hsp104 activity *in vivo*: a possible explanation for its effect in curing yeast prions, *Curr. Microbiol.* ***43***, 7–10.
47. Ferreira, P. C., Ness, F., Edwards, S. R., Cox, B. S., and Tuite, M. F. (2001) The elimination of the yeast (*psi+*) prion by guanidine hydrochloride is the result of Hsp104 inactivation, *Mol Microbiol* ***40***, 1357–1369.
48. Jung, G., Jones, G., and Masison, D. C. (2002) Amino acid residue 184 of yeast Hsp104 chaperone is critical for prion-curing by guanidine, prion propagation, and thermotolerance, *Proc. Natl. Acad. Sci. USA* ***99***, 9936–9941.
49. Derkatch, I. L., Bradley, M. E., Masse, S. V., Zadorsky, S. P., Polozkov, G. V., Inge-Vechtomov, S. G., and Liebman, S. W. (2000) Dependence and independence of (P*SI+*) and [P*IN+*]: a two-prion system in yeast?, *Embo J* ***19***, 1942–1952.
50. Cox, B. S., Ness, F., and Tuite, M. F. (2003) Analysis of the generation and segregation of propagons: entities that propagate the (PSI+) prion in yeast, *Genetics* ***165***, 23–33.
51. Douglas, P. M., Treusch, S., Ren, H. Y., Halfmann, R., Duennwald, M. L., Lindquist, S., and Cyr, D. (2008) Chaperone-dependent amyloid assembly protects cells from prion toxicity, *Proc. Natl. Acad. Sci. USA* ***105***, 7206–7211.
52. Pieri, L., Bucciantini, M., Nosi, D., Formigli, L., Savistchenko, J., Melki, R., and Stefani, M. (2006) The yeast prion Ure2p native-like assemblies are toxic to mammalian cells regardless of their aggregation state, *J. Biol. Chem.* ***281***, 15337–15344.
53. Zhang, C., Jackson, A. P., Zhang, Z. R., Han, Y., Yu, S., Q., H. R., and Perrett, S. (2010)

Amyloid-like aggregates of the yeast prion protein Ure2 enter vertbrate cells by specific endocytic pathways and induce apoptosis, *Plos One* ***5***, e12529.

54. Krammer, C., Suhre, M. H., Kremmer, E., Diemer, C., Hess, S., Schatzl, H. M., Scheibel, T., and Vorberg, I. (2008) Prion protein/protein interactions: fusion with yeast Sup35p-NM modulates cytosolic PrP aggregation in mammalian cells, *FASEB J.* ***22***, 762–773.
55. Krammer, C., Kryndushkin, D., Suhre, M. H., Kremmer, E., Hofmann, A., Pfeifer, A., Scheibel, T., Wickner, R. B., Schatzl, H. M., and Vorberg, I. (2009) The yeast Sup35NM domain propagates as a prion in mammalian cells, *Proc. Natl. Acad. Sci. USA* ***106***, 462–467.
56. Campbell, R. E., Tour, O., Palmer, A. E., Steinbach, P. A., Baird, G. S., D.A., Z., and Tsien, R. Y. (2002) A monomeric red fluorescent protein, *Proc. Natl. Acad. Sci. USA* ***99***, 7877–7882.
57. Cormack, B. P., Bertram, G., Egerton, M., Gow, N. A., Falkow, S., and Brown, A. J. (1997) Yeast-enhanced green flourescent protein (yEGFP) a reporter of gene expression in Candida albicans, *Microbiology* ***143***, 303–311.
58. Sheff, M. A., and Thorn, K. S. (2004) Optimized cassettes for fluorescent protein tagging in *Saccharomyces cerevisiae*, *Yeast* ***21***, 661–670.
59. Song, Y., Wu, Y. X., Jung, G., Tutar, Y., Eisenberg, E., Greene, L. E., and Masison, D. C. (2005) Role for Hsp70 chaperone in *Saccharomyces cerevisiae* prion seed replication, *Eukary. Cell* ***4***, 289–297.
60. Satpute-Krishnan, P., and Serio, T. R. (2005) Prion protein remodelling confers an immediate phenotypic switch, *Nature* ***437***, 262–265.
61. Kawai-Noma, S., Ayano, S., Pack, C. G., Kinjo, M., Yoshida, M., Yasuda, K., and Taguchi, H. (2006) Dynamics of yeast prion aggregates in single living cells, *Genes Cells* ***11***, 1085–1096.
62. Patino, M. M., Liu, J.-J., Glover, J. R., and Lindquist, S. (1996) Support for the prion hypothesis for inheritance of a phenotypic trait in yeast, *Science* ***273***, 622–626.
63. Edskes, H. K., and Wickner, R. B. (2002) Conservation of a portion of the *S. cerevisiae* Ure2p prion domain that interacts with the full - length protein, *Proc. Natl. Acad. Sci. USA* ***99 (Suppl. 4)***, 16384–16391.
64. Zhou, P., Derkatch, I. L., and Liebman, S. W. (2001) The relationship between visible intracellular aggregates that appear after overexpression of Sup35 and the yeast prion-like elements (P*SI*+) and (P*IN*+), *Mol Microbiol* ***39***, 37–46.
65. Mathur, V., Taneja, V., Sun, Y., and Liebman, S. W. (2010) Analyzing the birth and propagation of two distinct prions, (PSI+) and (Het-s) (y), in yeast, *Mol. Biol. Cell.* ***21***, 1449–1461.
66. Speransky, V., Taylor, K. L., Edskes, H. K., Wickner, R. B., and Steven, A. (2001) Prion filament networks in (URE3) cells of *Saccharomyces cerevisiae*, *J. Cell. Biol.* ***153***, 1327–1335.
67. Kawai-Noma, S., Pack, C. G., Kojidani, T., Asakawa, H., Hiraoka, Y., Kinjo, M., Haraguchi, T., Taguchi, H., and Hirata, A. (2010) In vivo evidence for the fibrillar structures of Sup35 prions in yeast cells, *J. Cell. Biol.* ***190***, 223–231.
68. Santoso, A., Chien, P., Osherovich, L. Z., and Weissman, J. S. (2000) Molecular basis of a yeast prion species barrier, *Cell* ***100***, 277–288.
69. Derkatch, I. L., Uptain, S. M., Outeiro, T. F., Krishnan, R., Lindquist, S. L., and Liebman, S. W. (2004) Effects of Q/N-rich, polyQ, and non-polyQ amyloids on the de novo formation of the (PSI+) prion in yeast and aggregation of Sup35 in vitro, *Proc Natl Acad Sci USA* ***101***, 12934–12939.
70. Ganusova, E. E., Ozolins, L. N., Bhagat, S., Newnam, G. P., Wegrzyn, R. D., Sherman, M. Y., and Chernoff, Y. O. (2006) Modulation of prion formation, aggregation, and toxicity by the actin cytoskeleton in yeast, *Mol. Cell. Biol.* ***26***, 617–629.
71. Kryndushkin, D., Shewmaker, F., and Wickner, R. B. (2008) Curing of the (URE3) prion by Btn2p, a Batten disease-related protein, *EMBO J.* ***27***, 2725–2735.
72. Derdowski, A., Sindi, S. S., Klaips, C. L., DiSalvo, S., and Sero, T. R. (2010) A size threshold limits prion transmission and establishes phenotypic diversity, *Science* ***330***, 6 80–683.
73. Wu, Y. X., Greene, L. E., Masison, D. C., and Eisenberg, E. (2005) Curing of yeast (PSI+) prion by guanidine inactivation of Hsp104 does not require cell division, *Proc. Natl. Acad. Sci. USA* ***102***, 12789–12794.
74. Satpute-Krishnan, P., Langseth, S. X., and Sero, T. R. (2007) Hsp104-dependent remodeling of prion complexes mediates protein-only inheritance, *PLoS Biol.* ***5***, e24.
75. Kawai-Noma, S., Pack, C. G., Tsuji, T., Kinjo, M., and Taguchi, H. (2009) Single mother-daughter pair analysis to clarify the diffusion properties of yeast prion Sup35 in guanidine HCl-treated (PSI) cells, *Genes Cells* ***14***, 1045–1054.
76. Blanco, F. J., Hess, S., Pannell, L. K., Rizzo, N. W., and Tycko, R. (2001) Solid-state NMR data support a helix-loop-helix structural model

for the N-terminal half of HIV-1 Rev in fibrillar form, *J. Mol. Biol.* ***313***, 845–859.

77. Maddelein, M. L., Dos Reis, S., Duvezin-Caubet, S., Coulary-Salin, B., and Saupe, S. J. (2002) Amyloid aggregates of the HET-s prion protein are infectious, *Proc Natl Acad Sci USA* ***99***, 7402–7407.
78. King, C. Y., and Diaz-Avalos, R. (2004) Protein-only transmission of three yeast prion strains, *Nature* ***428***, 319–323.
79. Tanaka, M., Chien, P., Naber, N., Cooke, R., and Weissman, J. S. (2004) Conformational variations in an infectious protein determine prion strain differences, *Nature* ***428***, 323–328.
80. Paushkin, S. V., Kushnirov, V. V., Smirnov, V. N., and Ter-Avanesyan, M. D. (1996) Propagation of the yeast prion-like (P*SI*+) determinant is mediated by oligomerization of the *SUP35*-encoded polypeptide chain release factor, *EMBO J.* ***15***, 3127–3134.
81. Bagriantsev, S. N., Gracheva, E. O., Richmond, J. E., and Liebman, S. W. (2008) Variant-specific (PSI+) infection is transmitted by Sup35 polymers within (PSI+) aggregates with heterogeneous protein composition, *Mol. Biol. Cell.* ***19***, 2433–2443.
82. Kryndushkin, D. S., Alexandrov, I. M., Ter-Avanesyan, M. D., and Kushnirov, V. V. (2003) Yeast (P*SI*+) prion aggregates are formed by small Sup35 polymers fragmented by Hsp104, *J. Biol. Chem.* ***278***, 49636–49643.
83. Bagriantsev, S. N., Kushnirov, V. V., and Liebman, S. W. (2006) Analysis of amyloid aggregates using agarose gel electrophoresis, *Methods Enzymol* ***412***, 33–48.
84. Kushnirov, V. V., Alexandrov, I. M., Mitkevich, O. V., Shkundina, I. S., and Ter-Avanesyan, M. D. (2006) Purification and analysis of prion and amyloid aggregates, *Methods* ***39***, 50–55.
85. Tanaka, M., Collins, S. R., Toyama, B. H., and Weissman, J. S. (2006) The physical basis of how prion conformations determine strain phenotypes, *Nature* ***442***, 585–589.
86. Salnikova, A. B., Kryndushkin, D. S., Smirnov, V. N., Kushnirov, V. V., and Ter-Avanesyan, M. D. (2005) Nonsense suppression in yeast cells overproducing Sup35 (eRF3) is caused by its non-heritable amyloids, *J. Biol. Chem.* ***280***, 8808–8812.
87. Aebi, U., and Pollard, T. D. (1987) A glow discharge unit to render electron microscope grids and other surfaces hydrophilic, *J. Electron Microsc. Tech.* ***7***, 29–33.
88. Antzutkin, O. N., Balbach, J. J., Leapman, R. D., Rizzo, N. W., Reed, J., and Tycko, R. (2000) Multiple quantum solid-state NMR indicates a parallel, not antiparallel, organization of beta-sheets in Alzheimer's beta-amyloid fibrils, *Proc. Natl. Acad. Sci. USA* ***97***, 13045–13050.
89. Petkova, A. T., Ishii, Y., Balbach, J. J., Antzutkin, O. N., Leapman, R. D., Delaglio, F., and Tycko, R. (2002) A structural model for Alzheimer's beta-amyloid fibrils based on experimental constraints from solid state NMR, *Proc. Natl. Acad. Sci. USA* ***99***, 16742–16747.
90. Petkova, A. T., Yau, W. M., and Tycko, R. (2006) Experimental constraints on quaternary structure in Alzheimer's beta-amyloid fibrils, *Biochemistry* ***45***, 498–512.
91. Ritter, C., Maddelein, M. L., Siemer, A. B., Luhrs, T., Ernst, M., Meier, B. H., Saupe, S. J., and Riek, R. (2005) Correlation of structural elements and infectivity of the HET-s prion, *Nature* ***435***, 844–848.
92. Siemer, A. B., Ritter, C., Steinmetz, M. O., Ernst, M., Riek, R., and Meier, B. H. (2006) 13C, 15N resonance assignment of parts of the HET-s prion protein in its amyloid form, *J Biomol NMR* ***34***, 75–87.
93. Wasmer, C., Lange, A., Van Melckebeke, H., Siemer, A. B., Riek, R., and Meier, B. H. (2008) Amyloid fibrils of the HET-s(218–79) prion form a beta solenoid with a triangular hydrophobic core, *Science* ***319***, 1523–1526.
94. Tycko, R. (2006) Molecular structure of amyloid fibrils: insights from solid-state NMR, *Quart. Revs. Biophys.* ***1***, 1–55.
95. Baldus, M. (2007) Magnetic resonance in the solid state: applications to protein folding, amyloid fibrils and membrane proteins, *Eur. J. Biophys.* ***36 Suppl. 1***, S37–S48.
96. Levitt, M. H. (2007) *Spin dynamics: basics of nuclear magnetic resonance*, John Wiley & Sons, Ltd., Chichester, England.
97. Chen, B., Thurber, K. R., Shewmaker, F., Wickner, R. B., and Tycko, R. (2009) Measurement of amyloid fibril mass-per-length by tilted-beam transmission electron microscopy, *Proc. Natl. Acad. Sci. USA* ***106***, 14339–14344.
98. Roberts, B. T., and Wickner, R. B. (2003) A class of prions that propagate via covalent autoactivation, *Genes Dev.* ***17***, 2083–2087.
99. Rogoza, T., Goginashvili, A., Rodionova, S., Ivanov, M., Viktorovskaya, O., Rubel, A., Volkov, K., and Mironova, L. (2010) Non-mendelian determinant (ISP+) in yeast is a nuclear-residing prion form of the global transcriptional regulator Sfp1, *Proc. Natl. Acad. Sci. USA* ***107***, 10573–10577.

Chapter 23

Cell-to-Cell Transmission of α-Synuclein Aggregates

Seung-Jae Lee, Paula Desplats, He-Jin Lee, Brian Spencer, and Eliezer Masliah

Abstract

It is now recognized that the cell-to-cell transmission of misfolded proteins such as α-synuclein contributes to the neurodegenerative phenotype in neurological disorders such as idiopathic Parkinson's disease, Dementia with Lewy bodies, and Parkinson's disease dementia. Thus, establishing cell-based models for the transmission of α-synuclein is of importance to understand the mechanisms of neurodegeneration in these disorders and to develop new therapies. Here we describe methods to study the neuron-to-neuron propagation of α-synuclein in an in vitro setting that also has in vivo applications.

Key words: Neurodegeneration, Parkinson's disease, Lewy body disease, α-Synuclein, Propagation, Protein dissemination, Neurons

1. Introduction

Accumulation of protein aggregates across specific brain regions is now recognized as a critical characteristic in major neurodegenerative disorders (1). In Alzheimer's disease (AD), amyloid β (Aβ) protein and tau accumulate in extracellular and intraneuronal compartments (2–4); in Parkinson's disease (PD), the synaptic protein α-synuclein accumulates in axons and neuronal cell bodies (5, 6); in Huntington's disease (HD) and other expansion diseases, polyglutamine (polyQ) proteins accumulate in the nucleus and the cytoplasm (7); and misfolded prions accumulate in the neuropil in Creutzfeldt-Jakob disease (CJD) (10). Neurodegeneration in most of these disorders probably initiates at the synaptic site where discrete protein aggregates denominated oligomers impair neuronal transmission and functioning (8–10). While oligomers are usually diffusible, non-fibrillar, small order aggregates, larger polymers in the form of amyloid fibrils comprise the inclusion bodies characteristic

Einar M. Sigurdsson et al. (eds.), *Amyloid Proteins: Methods and Protocols*, Methods in Molecular Biology, vol. 849,
DOI 10.1007/978-1-61779-551-0_23,

of these disorders and are now believed a pathway for sequestration of more toxic oligomers (11). Alterations in the balance of protein aggregation, clearance, and synthesis play an important role in the formation of toxic oligomers and in the neurodegenerative cascade (12–17). In addition, recent evidence suggests that protein propagation from cell to cell might play an important role in the mechanisms of neurodegeneration (18–24).

α-Synuclein is a cytoplasmic protein, most abundant at the synaptic terminals (25–28), is a 140 kDa molecule with an N-terminus that binds lipids, a central hydrophobic region (NAC) with amyloidogenic capacity and an acidic C-terminus tail (29). Mutations, multiplications, and polymorphisms in α-synuclein have been linked to familial and sporadic forms of Parkinson's disease and Lewy body disease (30). Lewy body disease is an heterogenous group of disorders that includes idiopathic Parkinson's disease, Dementia with Lewy bodies, and Parkinson's disease dementia (31, 32).

In addition to the oligomeric toxic α-synuclein that is retained in the neurons and cell membranes, a small amount of α-synuclein is released from cells, apparently in the absence of serious membrane damage (33). The release of α-synuclein oligomers from neurons is increased under disease conditions and leads to worsening of the synaptic damage and cell death via apoptosis (22, 24). This cell-to-cell transmission of α-synuclein may account for the recent reports showing the spread of α-synuclein with the formation of Lewy bodies from host tissues to long-term fetal cell grafts in Parkinson's patients (21).

For example studies utilizing both oligomeric and fibrillar forms of α-synuclein are taken up by neuronal cells through endocytosis, thereafter targeted to the lysosome for degradation (22, 23). We have demonstrated the dissemination of α-synuclein aggregates through cell-to-cell transmission (20). This study showed that α-synuclein aggregates can be transferred from aggregate-producing cells to aggregate-free cells via endocytosis of the recipient cells. This transmission became more efficient when the lysosomal function was compromised in the recipient cells, suggesting the antagonizing role of lysosomes against the aggregate transmission. When mouse neuronal progenitor cells were transplanted into the brains of transgenic mice overexpressing human α-synuclein, α-synuclein proteins were transferred from host neurons to the grafted cells. Moreover, we have also shown that α-synuclein aggregates can be transferred from neurons to astroglial cells leading to a proinflammatory reaction with toxic consequences (34).

Understanding the mechanisms of cell-to-cell propagation of α-synuclein aggregates is under investigation. While some studies propose a role for exocytosis and endocytosis, others have suggested that α-synuclein might disseminate via a transynaptic pathway,

extrusion after cell death, or nanotube formation (24). Given the important role in disease spreading, neurodegeneration, disease progression, and graft dysfunction understanding the cellular mechanisms of α-synuclein aggregates dissemination in in vitro models is of significant importance. Moreover, dissemination in in vitro models are useful for therapeutical development. In this context, this chapter provides some key protocols to study the process of α-synuclein dissemination in neuronal cultures.

2. Materials

This chapter provides protocols to investigate: (1) the uptake and propagation of tagged recombinant α-synuclein in neuronal stem cells; (2) production and infection of neuronal cells with lentiviral vectors expressing myc-tagged α-synuclein and (3) studies of neuron-to-neuron dissemination of myc-tagged α-synuclein.

2.1. Recombinant α-Synuclein in Neuronal Stem Cells

2.1.1. Cell Culture

1. Cryopreserved mouse cortical neural stem cells (Millipore).
2. DMEM/F12 w/o HEPES, w/L-Glutamine (Mediatech); L-Glutamine (1,000×); PenStrept (1,000×), both from Gibco.
3. B27 supplement (w/o vitamin A, 500×); FGF2; EGF and Heparin (all from Invitrogen).
4. Acid-treated glass coverslips, 12-well cell culture plates, poly-L-ornithine (10 mg/mL), laminin (1 mg/mL) both from Sigma.
5. Paraformaldehyde (4% in PBS).

2.1.2. α-Synuclein Labeling

1. Human recombinant α-synuclein (Calbiochem).
2. Zeba™ Desalt Spin columns (Pierce).
3. Alexa Fluor® 555 Microscale Protein Labeling kit (Invitrogen).

2.2. α-Synuclein myc Lentiviral Vector Production for Infection of Neurons and Propagation Studies

The "packaging" plasmids (Gag-Pol, VSV-G, Rev) should be purified by an endotoxin-free plasmid-prep kit. The DNA concentration should be determined by $A^{260/280}$ and confirmed by gel-electrophoresis. Verify the DNA preparations by restriction digestion analysis, and aliquot the DNA at 1 μg/μl in endotoxin-free TE (10 mM Tris–HCl, 1 mM EDTA, pH 8.0).

2.2.1. Plasmid Preparation

2.2.2. Reagents/Buffers

1. Poly-L-lysine, store 4°C.
   Dilute to 0.01% in 1× DPBS.
2. Reagents for 2× BBS, filter sterilize (0.22 μm), store room temperature.

500 mM BES	10.66 g/100 ml
2.8 M NaCl	16.35 g/100 ml
150 mM Na_2PO_4	2.1 g/100 ml

3. 500 ml 2× BBS, store 4°C.
   50 ml 2.8 M NaCl
   50 ml 500 mM BES
   5 ml 150 mM Na_2HPO_4
   Add water (UltraPure, Invitrogen) to 450 ml
   (a) Adjust pH to 6.95 with 1 M NaOH
   (b) Add water to 500 ml
   (c) Filter sterilize (0.22 μm)
   (d) Store at 4°C for 3–4 days prior to validation.
4. 100 ml 10× $CaCl_2$, store –20°C (will not freeze)
   2.5 M $CaCl_2$, 36.75 g/100 ml
   Dissolve and filter sterilize (0.22 μm) using syringe.
   Store in 1.4 ml aliquots. Do not freeze/thaw.
5. 20% sucrose, store –20°C
   Dissolve 20 g sucrose in 100 ml HBSS.
   Filter sterilize (0.22 μm) using syringe.
   Store in 10 ml aliquots.

2.2.3. Validation of 2× BBS/$CaCl_2$: Combination

Transfect a 10-cm dish of 293T cell (70–80% confluent) with 20 μg GFP reporter plasmid.

Observe transfection efficiency 48 h later (should be at least 90–95% GFP + cells).

Aliquot 2× BBS 14 ml per tube and store at 4°C.

2.3. Studies of Neuron-to-Neuron Dissemination of myc-Tagged α-Synuclein

1. Retinoic acid (100 mM in DMSO).
2. SH-SY5Y cells.
3. Myc-tagged α-synuclein lentiviral vectors.

3. Methods

3.1. Recombinant α-Synuclein in Neuronal Stem Cells

3.1.1. Labeling of α-Synuclein

1. To ensure proper labeling of the protein, replace the buffer from α-synuclein stock solution for PBS using desalting columns (Zeba™ Desalt Spin columns). Following the manufacturer's instructions, wash columns four times with 100 μL PBS. After washing, load 100 μL of α-synuclein stock in the column and

centrifuge at 1,500 × *g* for 1 min. Protein is now in PBS, ready for labeling and should be at a concentration of 1 mg/mL.

2. For labeling of proteins with Alexa 555, follow the instructions of the manufacturer. To calculate the amount of nanomoles of dye that should be added per nanomole of α-synuclein, consider that optimal degree of labeling for α-synuclein is 3 (according with manufacturer's indications, e.g., for labeling of 100 μg of a protein with an MW of 14 kDa, you will need 2.64 μL of stock dye per sample). Transfer up to 100 μL of α-synuclein (1 mg/mL) to a reaction tube. Add 10 μL of 1 M sodium bicarbonate and mix. Add 2.64 μL of reactive dye solution and mix thoroughly by pipetting up and down. Incubate at room temperature for 15 min. Pack the resin in the supplied columns as indicated in the instructions. Load 50 μL of conjugate reaction mix per column and centrifuge at 16,000 × *g* for 1 min. Determine protein concentration and degree of labeling by reading absorbance at 280 and 555 nm and applying the following equations:

$$\text{Protein concentration(mg/mL)} = \frac{[A^{280} - 0.08(A^{555})] \times \text{dilution factor}}{A^{280} \text{ of protein at 1 mg/mL}},$$

where the divisor could be replaced by the molar extinction coefficient of the protein at 280 nm, which for α-synuclein = 0.354.

$$\text{Degree of labeling (moles dye/mole protein)} = \frac{A^{555} \times \text{dilution factor}}{150{,}000 \times \text{protein concentration(M)}}.$$

Labeled α-synuclein should be stored protected from light. For short-term use, store it at 4°C. Alternatively the stock can be aliquoted and stored at −20°C for a few months. Avoid repeated freezing and thawing.

3.1.2. In Vivo Testing of α-Synuclein Uptake

1. Prepare Basal culture media by supplementing DMEM/F12 with L-glutamine, B27 and PenStrept. Filter the media. Freshly prepare aliquots of Expansion media by adding FGF2 (20 ng/mL), EGF (20 ng/mL), and heparin (20 μg/mL) to 50 mL of Basal media. Expansion media can be used for 2 weeks after preparation.
2. Coat culture plates and coverslips with poly-L-ornithine and laminin. Prepare a 1:200 solution of poly-L-ornithine in H_2O and cover the surface of the plates (use 1 mL/well for a 12-well plate containing glass coverslips. Push the covers to the bottom with a pipette tip to ensure that they are well submerged in the solution). Incubate overnight at room temperate in the tissue culture hood. The following day discard the poly-L-ornithine solution and wash the plates two times with PBS before coating with Laminin (1:200 dilution in PBS). Incubate overnight at

room temperate in the tissue culture hood. When coating is done, seal plates and flasks tightly with tape and store at –20°C for up to 6 months. Before use, thaw the laminin, aspirate, and wash once with PBS before plating cells.

3. Grow mouse cortical neural stem cells (MCNSCs) in expansion media, in a 37°C incubator with 5% CO_2. Change media every other day, splitting the cells when they reached 80% confluency. Plate 3×10^4 cell/mL in each cover and incubate overnight.
4. Freshly dilute the necessary amount of Alexa 555-labeled α-synuclein (from Subheading 2.1) in expansion media to obtain a final concentration of 0.3 μM α-synuclein. Incubate the cells in α-synuclein-supplemented media for 24 or 48 h. Finally fix the cells with 4% paraformaldehyde in PBS and keep the fixed covers protected from light at 4°C until processing for microscopy.

3.2. α-Synuclein myc Lentiviral Vector Production for Infection of Neurons and Propagation Studies

3.2.1. Virus Production Planning

Day 1: Coat plates with poly-L-lysine for 15 min at room temperature, aspirate remaining solution.

Plate HEK293T cells so that 24 h later cells will be 70–75% confluent.

Day 2: Transfect cells with packaging plasmid and vector plasmid (according to protocol below).

Day 3: Change medium.

Day 4: 1st collection, refeed cells.

Centrifuge supernatant (according to protocol below).

Day 5: 2nd collection.

Centrifuge supernatant.

Purify virus (according to protocol below).

3.2.2. Transfection/ Collection Procedure

	10 cm plate	15 cm plate	12 × 15 cm plates	24 × 15 cm plates
"Vector"	10.0 μg	22.5 μg	270 μg	540 μg
pGag/Pol	6.5 μg	14.6 μg	176 μg	352 μg
pRev	2.5 μg	5.6 μg	68 μg	136 μg
pVSV-G	3.5 μg	7.9 μg	95 μg	190 μg
H_2O	QS 450 μl	QS 900 μl	QS 12.15 ml	QS 24.3 ml
$CaCl_2$ (10×)	50 μl	100 μl	1.35 ml	2.7 ml
2× BBS	500 μl	1 ml	13.5 ml	27 ml

1. Mix the 4 plasmids according the scheme above.
2. Add H_2O.
3. Add $CaCl_2$, mix thoroughly.
4. Add 2× BBS, mix gently by inverting ~3–5 times, and incubate for 15 min at RT.
5. Add the DNA mix drop wise to dish (2.2 ml per 15-cm plate, 1.0 ml per 10-cm plate), try to spread DNA by carefully rocking the plate.
6. Place the cells in a humidified 37°C incubator at 3% CO_2.
7. Change medium next morning and incubate at 37°C at 10% CO_2.
8. One and 2 days later collect and filter the media through a 0.22-μm cellulose acetate vacuum filter.

3.2.3. Centrifugation

1. Load filtered supernatant into centrifuge tube.
2. Mark tube on one side to indicate location of pellet after centrifugation. This is especially important when using Optimem as the virus pellet is nearly impossible to see.
3. Centrifuge 2 h, 50,000 × *g* at room temperature. If using a fixed angle router, place tubes so mark is facing outward so that the virus pellet can be easily located following centrifugation.
4. Mark location of virus pellet on tube prior to removing supernatant.
5. Discard supernatant and invert tubes on a paper towel. Aspirate excess medium.
6. Resuspend pellets from all tubes in 1,000 μl HBSS. Repeat for collection from day 2 and pool supernatant. Virus from day 1 can be stored at 4°C overnight.
7. Load pooled particles (now in a volume of 2 ml) on 2 ml 20% sucrose in centrifuge tubes. Load very slowly to avoid disrupting sucrose cushion. Wash remaining supernatant from tube with additional 500 μl HBSS and add to centrifuge tube.
8. Centrifuge 2 h, 50,000 × *g* at room temperature.
9. Discard supernatant, resuspend pellet in 250–500 μl HBSS and transfer viral particles into microcentrifuge tube with screw cap and rubber O-ring.
10. Wrap tube with parafilm and shake on vortex at low speed for 1 h at room temperature to resuspend virus.
11. Quick-spin in microcentrifuge (~15 s) and aliquot supernatant in 10–50 μl aliquots into microcentrifuge tubes containing screw cap and rubber O-ring and store at –80°C.

3.2.4. p24-Titer Determination by Perkin-Elmer p24-ELISA

This protocol is basically carried out according to the instructions provided by Perkin-Elmer.

Standards:

Tube	Standard well	p24 (pg/ml)	Preparation
A		4,000	245 µl HBSS + 5 µl control p24 from kit
B	C	100	780 µl HBSS + 20 µl
C	D	50	200 µl HBSS + 200 µl
D	E	25	200 µl HBSS + 200 µl
E	F	12.5	200 µl HBSS + 200 µl
F	G	6.3	200 µl HBSS + 200 µl
G	H	3.1	200 µl HBSS + 200 µl

Sample dilutions

Tube	Dilution	Preparation
1	10^{-3}	1,500 µl HBSS + 1.5 µl virus sample
2	10^{-5}	980 µl HBSS + 10 µl 10^{-3} + 10 µl Triton
3	10^{-6}	900 µl HBSS + 100 µl 10^{-5}
4	10^{-7}	900 µl HBSS + 100 µl 10^{-6}
5	10^{-8}	900 µl HBSS + 100 µl 10^{-7}

ELISA

1. Prewash strips 3× with wash buffer from kit.
2. Load 200 µl samples/standard per well and incubate at 37°C for 2 h (or 4°C overnight).
   (a) Load standards in column 1 as below.
   (b) Load samples in next column in wells A–D or E–H from 10^{-5} to 10^{-8}.
   - A—Empty
   - B—200 µl HBSS
   - C—H as explained above.
3. Dump samples and wash wells 6× with wash buffer.
4. Add 100 µl detector-antibody and incubate at 37°C for 1 h.
5. Dump antibody and wash well 6× with wash buffer.
6. Add 100 µl streptavidin conjugate (10 µl streptavidin per ml diluent) and incubate at 37°C for 30 min.

7. Dump the streptavidin and wash well 6× with wash buffer.
8. Add substrate (1 tablet OPD per 11 ml substrate buffer) and incubate at room temperature for 30 min in the dark.
9. Stop color reaction by adding 100 µl stop solution to each well.
10. Read the plate on a plate reader at 490 nm with a reference filter at 600 nm.
11. Sample concentrations of p24 can be determined by comparing to the standard curve.

3.2.5. Biological Titer Determination by FACS

1. Plate 5×10^4 HEK 293T cells per well of a 24-well plate (0.5 ml each well).
2. 4 h Later, aspirate media from all wells except control samples.
3. Add 200 µl media to each remaining well of cells.
4. Dilute virus as described for the p24 ELISA assay so that you have samples ranging from 10^{-3} to 10^{-8}.
5. To each well, add 100 µl of virus dilution sample from 10^{-3} to 10^{-8} dilution.
6. Incubate for 24 h in a humidified incubator at 37°C with 10% CO_2.
7. Replace media after 24 h and continue incubation for 48 h.
8. Aspirate media, wash with PBS and resuspend cells in 500 µl of PBS for FACS analysis.
9. Calculate the titer a:

$$(\%\ \text{Positive cells}/100) \times (\text{No. of cells}) \times (\text{dilution factor}) \times (1{,}000\ \text{for ml}) = (\text{titer/ml}),$$

i.e., $(0.0223\ \text{transduced cells}) \times (50{,}000\ \text{cells}) \times (1{,}000) \times 1{,}000\ \mu\text{l/ml} = 1.11 \times 10^9$ TU/ml.

This can be used to determine the constant of ng p24/TU of virus typical for your virus preparations. Thus future preparations can be tittered solely by the p24 ELISA using the conversion factor identified from the biological titer determined from the production of LV-GFP.

3.2.6. Lentivirus Infection of Cells

1. To calculate the amount of virus required for infection, determine the optimal multiplicity of infection (MOI) for your specific cell line. In other words, how many virus particles are required per cell for optimal infection?
2. The efficiency of virus infection in each cell line must be determined prior to a full experiment as it can vary dramatically. For example, HEK293T cells can be fully infected with an MOI of 10, while some neuronal cells may require an MOI of 50 or more.

3. Once the optimal MOI has been determined, to calculate the volume of virus required use the following equation:

$$\frac{(\text{No. of cells}) \times (\text{MOI})}{\text{Concentration of virus (titer)}} = \text{volume of virus required},$$

where the concentration of the virus is expressed as transducing units (tdu)/ml (or infectious virus/ml). For example, I have a plate of 1×10^8 cells that I want to infect at an MOI of 50 and my virus has a titer of 5×10^9 tdu/ml.

$$\frac{(2.5 \times 10^6 \text{ cells}) \times 50 \text{ MOI}}{5 \times 10^9 \text{ tdu/ml}} = 0.025 \text{ ml (25 µl of virus)}.$$

Conventionally, cell are counted and plated a few hours before infection just to allow the cells to settle and attach to the dish. Then, the virus is added in a volume of media equal to 1/10 of the total volume of media in the dish. Gene expression usually begins 24–48 h after infection but this depends on the cell type used. It is recommended to avoid freeze/thaw any virus aliquot more than twice since virus infection will be dramatically reduced.

4. Studies of Neuron-to-Neuron Dissemination of myc-Tagged α-Synuclein

1. Setting of SH-SY5Y cells.
   - Acceptor cells: Split SH-SY5Y cells to coverslips in a 12-well plate (1×10^4).
   - Donor cells: Split SH-SY5Y cells (1.5×10^5/dish) to a 35-mm dish.
2. Differentiation (day 0).
   - Change medium with 50 mM all L-*trans* Retinoic acid the next day.
   - Change medium with retinoic acid (50 mM) every 2–3 days.
3. Infection of donor cells with recombinant lentiviral vectors (day 5).
   - Add lentiviral vector (m.o.i. 30) in 1/2 volume of culture medium.
   - 37°C, 1.5 h.
   - Add 1/2 volume of culture medium with retinoic acid.
   - Rinse cells three times with warm DMEM.
4. Labeling of acceptor cells with Qtracker595 (Invitrogen) (day 6).

- Mix component A and B (1:1).
- RT, 5 min.
- Dilute mixture with fresh medium (1:1,000).
- Vortex vigorously for 30 s.
- Replace medium of acceptor cells with the Qtracker mixture.
- 37°C, 2 h.
- Wash five times with warm DMEM.

5. Addition of donor cells to acceptor cells (day 6).
   - Trypsinize donor cells.
   - Resuspend cells in culture medium.
   - Remove medium from acceptor cells and add medium containing donor cells (1:12 diluted from a 35-mm dish).
   - Culture as usual for 1–3 days.
6. Fixation.
   - Wash coverslips twice with cold PBS.
   - Fix cells in 4% paraformaldehyde in PBS for 30 min, RT.
   - Rinse three times with PBS.
7. Immunofluorescence cell staining.
   - Permeabilize cells with ice-cold 0.1% TX-100 in PBS for 5 min RT.
   - Rinse again with PBS for three times
   - Blocking in PBS/5% BSA/3% Goat serum for 30 min RT.
   - Replace with appropriate primary antibodies in blocking solution.
   - RT, 30 min.
   - Wash three times with PBS—20 min each.
   - Add fluorescent dye-conjugated goat anti-mouse antibody in blocking solution.
   - RT, 30 min.
   - Wash three times with PBS—30 min each.
   - TOPRO-3 (Invitrogen) staining of nuclei diluted 1:1,000 in PBS, RT 10 min.
   - Wash three times with PBS—5 min each.
   - Put a drop of anti-fade reagent (Invitrogen) on slide and cover with coverslip. Wait until hardens (in dark). After drying for several hours, seal with clear nail polish.
   - Store at 4°C.
   - Images were obtained with an Olympus FV1000 confocal laser scanning microscope, and the fluorescence intensity was quantified using FV10-ASE 1.7 software (Olympus).

5. Note

The experiments involving the transfer of the myc-tagged α-synuclein from the donor to the acceptor cells can be performed as described here plating the cells together or coculturing using chambers or separate coverslips placed in the same dish. The myc-tagged α-synuclein in the acceptor cells can be detected with antibodies against myc or α-synuclein. The tagging of the acceptor cells can be done with dyes as described in the protocol above or with lentiviral-GFP infection. The protocol described here involves transfer from neuron to neuron; however, the same approach can be used for neurons to glial cells and vice versa.

Acknowledgments

Dr. EM work was supported by NIH grants AG18440, AG022074, NS057096, AG 03097, and AG010435. Dr. SJL work was supported by Mid-career Researcher Program (2010–0015188) and the Diseases Network Research Program (2010–0020610) through NRF grant funded by the Ministry of Education, Science, and Technology.

References

1. Forman, M.S., Trojanowski, J.Q. and Lee, V.M. (2004). Neurodegenerative diseases: a decade of discoveries paves the way for therapeutic breakthroughs. Nat Med **10**, 1055–63.
2. Hanger, D.P. and Wray, S. (2010) Tau cleavage and tau aggregation in neurodegenerative disease. Biochem Soc Trans **38**, 1016–20.
3. Hardy, J. (2006). Alzheimer's disease: the amyloid cascade hypothesis: an update and reappraisal. J Alzheimers Dis **9**, 151–3.
4. Selkoe, D.J. (1994). Normal and abnormal biology of the beta-amyloid precursor protein. Annu Rev Neurosci **17**, 489–517.
5. Goedert, M. (2001). Alpha-synuclein and neurodegenerative diseases. Nat Rev Neurosci **2**, 492–501.
6. Goedert, M. (2001). Parkinson's disease and other alpha-synucleinopathies. Clin Chem Lab Med **39**, 308–12.
7. Ross, C.A. (2004). Huntington's disease: new paths to pathogenesis. Cell **118**, 4–7.
8. Walsh, D.M., Klyubin, I., Fadeeva, J.V., Rowan, M.J. and Selkoe, D.J. (2002). Amyloid-beta oligomers: their production, toxicity and therapeutic inhibition. Biochem Soc Trans **30**, 552–7.
9. Walsh, D.M. and Selkoe, D.J. (2004). Oligomers on the brain: the emerging role of soluble protein aggregates in neurodegeneration. Protein Pept Lett **11**, 213–28.
10. Walsh, D.M. and Selkoe, D.J. (2007). A beta oligomers - a decade of discovery. J Neurochem **101**, 1172–84.
11. El-Agnaf, O.M., Walsh, D.M. and Allsop, D. (2003). Soluble oligomers for the diagnosis of neurodegenerative diseases. Lancet Neurol **2**, 461–2.
12. Alvarez-Erviti, L., Rodriguez-Oroz, M.C., Cooper, J.M., Caballero, C., Ferrer, I., Obeso, J.A. and Schapira, A.H. (2010). Chaperone-mediated autophagy markers in Parkinson disease brains. Arch Neurol **67**, 1464–72.

13. Cherra, S.J., 3 rd, Dagda, R.K. and Chu, C.T. (2010). Review: autophagy and neurodegeneration: survival at a cost? Neuropathol Appl Neurobiol **36**, 125–32.
14. Crews, L. et al. (2010). Selective molecular alterations in the autophagy pathway in patients with Lewy body disease and in models of alpha-synucleinopathy. PLoS One 5, e9313.
15. Cuervo, A.M., Wong, E.S. and Martinez-Vicente, M. (2010). Protein degradation, aggregation, and misfolding. Mov Disord 25 Suppl **1**, S49–54.
16. Luo, G.R. and Le, W.D. (2010). Collective roles of molecular chaperones in protein degradation pathways associated with neurodegenerative diseases. Curr Pharm Biotechnol **11**, 180–7.
17. Matsuda, N. and Tanaka, K. (2010). Does impairment of the ubiquitin-proteasome system or the autophagy-lysosome pathway predispose individuals to neurodegenerative disorders such as Parkinson's disease? J Alzheimers Dis **19**, 1–9.
18. Aguzzi, A., Sigurdson, C. and Heikenwaelder, M. (2008). Molecular mechanisms of prion pathogenesis. Annu Rev Pathol **3**, 11–40.
19. Caughey, B., Baron, G.S., Chesebro, B. and Jeffrey, M. (2009). Getting a grip on prions: oligomers, amyloids, and pathological membrane interactions. Annu Rev Biochem **78**, 177–204.
20. Desplats, P. et al. (2009). Inclusion formation and neuronal cell death through neuron-to-neuron transmission of alpha-synuclein. Proc Natl Acad Sci USA **106**, 13010–5.
21. Kordower, J.H., Chu, Y., Hauser, R.A., Freeman, T.B. and Olanow, C.W. (2008). Lewy body-like pathology in long-term embryonic nigral transplants in Parkinson's disease. Nat Med **14**, 504–6.
22. Lee, H.J., Suk, J.E., Bae, E.J. and Lee, S.J. (2008). Clearance and deposition of extracellular alpha-synuclein aggregates in microglia. Biochem Biophys Res Commun **372**, 423–8.
23. Lee, S.J. (2008). Origins and effects of extracellular alpha-synuclein: implications in Parkinson's disease. J Mol Neurosci **34**, 17–22.
24. Lee, S.J., Desplats, P., Sigurdson, C., Tsigelny, I. and Masliah, E. (2010). Cell-to-cell transmission of non-prion protein aggregates. Nat Rev Neurol **6**, 702–6.
25. Davidson, W.S., Jonas, A., Clayton, D.F. and George, J.M. (1998). Stabilization of alpha-synuclein secondary structure upon binding to synthetic membranes. J Biol Chem **273**, 9443–9.
26. Iwai, A. (2000). Properties of NACP/alpha-synuclein and its role in Alzheimer's disease. Biochim. Biophys. Acta **1502**, 95–109.
27. Iwai, A., Masliah, E., Yoshimoto, M., Ge, N., Flanagan, L., de Silva, H.A., Kittel, A. and Saitoh, T. (1995). The precursor protein of non-A beta component of Alzheimer's disease amyloid is a presynaptic protein of the central nervous system. Neuron **14**, 467–75.
28. Weinreb, P.H., Zhen, W., Poon, A.W., Conway, K.A. and Lansbury, P.T., Jr. (1996). NACP, a protein implicated in Alzheimer's disease and learning, is natively unfolded. Biochemistry **35**, 13709–15.
29. Tsigelny, I.F. et al. (2008). Mechanisms of hybrid oligomer formation in the pathogenesis of combined Alzheimer's and Parkinson's diseases. PLoS One **3**, e3135.
30. Schiesling, C., Kieper, N., Seidel, K. and Kruger, R. (2008). Review: Familial Parkinson's disease-genetics, clinical phenotype and neuropathology in relation to the common sporadic form of the disease. Neuropathol Appl Neurobiol **34**, 255–71.
31. McKeith, I.G. (2006). Consensus guidelines for the clinical and pathologic diagnosis of dementia with Lewy bodies (DLB): report of the Consortium on DLB International Workshop. J Alzheimers Dis **9**, 417–23.
32. McKeith, I.G. et al. (2005). Diagnosis and management of dementia with Lewy bodies: third report of the DLB Consortium. Neurology **65**, 1863–72.
33. Lee, H.J., Patel, S. and Lee, S.J. (2005). Intravesicular localization and exocytosis of alpha-synuclein and its aggregates. J Neurosci **25**, 6016–24.
34. Lee, H.J. et al. (2010). Direct transfer of alpha-synuclein from neuron to astroglia causes inflammatory responses in synucleinopathies. J Biol Chem **285**, 9262–72.

Part III

In Vivo Models and Assays

Chapter 24

Subcutaneous Adipose Tissue Biopsy for Amyloid Protein Studies

Per Westermark

Abstract

Symptoms from a systemic amyloidosis are usually coming from one of the inner organs, e.g., heart or kidney. However, for diagnosis and for material for amyloid protein studies, biopsy from an easier accessible tissue is preferred. This chapter describes biopsy from subcutaneous adipose tissue as a particularly suitable method to obtain amyloid.

Key words: Systemic amyloidosis, Amyloid deposit, Needle biopsy, Subcutaneous fat tissue

1. Introduction

Genetic analyses give important information regarding proteins deposited as amyloid. However, when present as amyloid fibrils, the protein is usually more or less modified. This modification may already take place in the producing cell, in the plasma carrying the precursor to its target tissue, or at the site of deposition. For example, most of the deposited fibril proteins have undergone proteolytic cleavage. This is seen in the three most common systemic amyloid forms derived from serum amyloid A (SAA), monoclonal immunoglobulin light chains, and in most cases, transthyretin (TTR). Typically, in all these three forms, some fragments predominate in the amyloid deposits while others are present at lower concentration or are absent. This has raised the hitherto not fully answered question whether cleavage is pathogenically important as part of the fibrillation process or just a postdeposition event (1). In addition to the modification of the main protein, all amyloid deposits contain additional components, including serum amyloid P component (SAP) and heparan sulfate proteoglycan (HSPG) (2).

Einar M. Sigurdsson et al. (eds.), *Amyloid Proteins: Methods and Protocols*, Methods in Molecular Biology, vol. 849,
DOI 10.1007/978-1-61779-551-0_24,

There are a number of studies which have indicated that variation of cleavage pattern is associated with variations in how amyloid affects different organs and tissues. This has been convincingly shown for AA (3) and ATTR amyloidosis (4). The situation in AL amyloidosis, which is more difficult to study due to the amino acid sequence variations, is more uncertain (5, 6). There may be other posttranslational modifications in the deposited amyloid protein, important for the formation of fibrils at certain places in the body and for other properties of the amyloid. Furthermore, the additional components in the amyloid deposits, such as HSPG, may also vary in composition and amount, and may be of importance for local amyloid fibril formation and deposition. It is therefore of interest to study the composition of the amyloid material itself and not only the precursor gene.

The diagnosis of systemic amyloidosis is most often obtained by a biopsy from a tissue not giving any clinical symptoms, e.g., the rectum or subcutaneous adipose tissue from the abdominal wall. Biopsy from the latter site is particularly easy and can be used for screening of populations (7, 8). The method is also suitable for the obtaining of material for compositional studies of the amyloid. This is at least true for amyloid of AA, AL, and ATTR (nomenclature according to (9)) nature. Biopsy material can be obtained by needle, punch, or a simple surgical procedure. Most individuals in the western world have large amount of subcutaneous fat tissue in the abdominal wall so that biopsy material can be taken without any problem. Biopsy from this region is a convenient method to obtain amyloid material from a living individual by a minimal surgical intervention. The method is very useful for the exact determination of the type of amyloid. This may be obtained by different methods such as enzyme-linked immunosorbent assay (ELISA), Western blot, or mass spectrometry. Subcutaneous adipose tissue has also been used for studies of possible amyloid-associated proteins by proteomics (10).

2. Materials

2.1. Equipment for Biopsy

Locally available material such as sterile needles, syringes, preferably attached to a syringe pistol (Cameco; Precision Dynamics Corporation, Burbank, CA), scalples, forceps, local anesthetic drug, etc.

Dermatological punches (3–8 mm; e.g., from Miltex GMBH (Rietheim-Weilheim, Germany)).

Polarization microscope.

Microscopical slides and cover glasses.

Scissors with curved legs.

Acetone.

Congo red (e.g., from Sigma).
Ethanol.
Sodium chloride.
Ammonium chloride.
Sodium azide.
Xylene.
Mounting medium (e.g., Pertex; Histolab, Gothenburg, Sweden).

3. Methods

Biopsy is preferably performed in the middle of the abdomen, between the umbilicus and the symphysis (see Note 1).

3.1. Biopsy

3.1.1. Needle Biopsy

Use a comparably wide needle of about 1 mm inner diameter (11). After local anesthesia, insert the needle under suction (preferably with equipment used by clinical cytologists) and push the needle back and forth a few times. Equilibrate the pressure and withdraw the needle. Take the needle from the syringe, fill the latter with air, put on the needle again and eject the material in the needle on a microscopical slide or into a tube containing the preferred solution (e.g., fixative, 0.15 M sodium chloride solution, medium for cell culture). The tissue pieces can now be picked up by hand with forceps and then used. An alternative is to withdraw the needle under negative pressure. The material in the needle will then be forced to the syringe from which it can be recovered by washing with a solvent, e.g., buffer or fixative such as 4% formaldehyde solution.

3.1.2. Punch Biopsy

Use the same kind of punch biopsies as used by dermatologists for diagnostic procedures (see Note 2). Preferably, the diameter of the punch should not be less than 5 mm. It is important that the biopsy does not only contain epidermis and dermis but also includes subcutaneous material, the more the better. Lift the biopsy in the dermis with the aid of fine forceps and cut off as deep as possible with a pair of scissors. After being taken out, subcutaneous material can be separated from the dermis and used further. Since also the dermis often contains amyloid, this part should be saved, e.g., by putting it in a freezer immediately.

3.1.3. Surgical Biopsy

This is self-evidently the method that gives the largest amount of tissue. After local anesthesia, a 1–2-cm incision is made between the umbilicus and the symphysis. An approximately 1 cm^3 large subcutaneous piece of tissue can easily be dissected out, usually with little bleeding. The surgical wound has to be closed with a few sutures. Put the biopsy in a jar with 0.15 M NaCl containing 0.02% sodium azide immediately (see Note 3).

3.2. Sampling for Microscopical Analysis of Presence of Amyloid

Subcutaneous adipose tissue is first washed in 0.15 M NaCl, containing 0.02% sodium azide as an anti bacterial agent in order to remove most of the blood (see Note 4). Small pieces (typically 1–2 mm^3) are taken from different parts of the material with scissors, put into a beaker with distilled water to remove salt and then placed on a clean microscopical glass slide (Fig. 1, see Note 5). After that the excess of water has been blotted off with filter paper, the pieces are cut many times (50–100) with a pair of scissors. After that, another clean microscopical slide is placed on top of the material and the two slides are squeezed together between the fingers under a slowly increasing pressure. Fat and water coming out from the sides of this material are absorbed with filter paper or paper towels. When no more material can be pressed out, the slides are separated carefully and both placed on a heating block at +60°C for 10 min. After cooling, the slides are defatted in a jar with

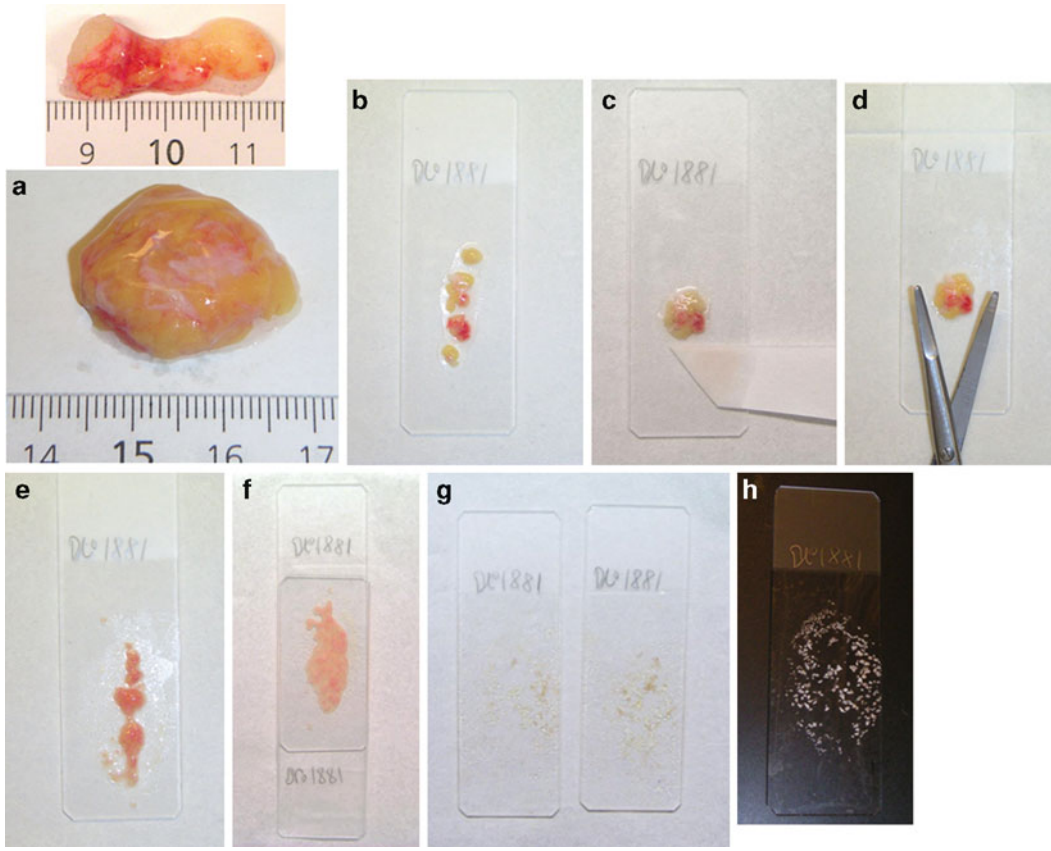

Fig. 1. Summary of the method. Subcutaneous adipose tissue can be obtained by needle biopsy (not shown), punch (**a**, *above*), or by a small surgical procedure (**a**). For demonstration of amyloid, small pieces are taken at different sites of the biopsy, washed in distilled water, and applied to a microscopical slide (**b**). Excess of water is blotted off with filter paper (**c**), cut into small fragments (**d**), and spread on the slide (**e**). Another clean slide is put on the top of the material (**f**) and the two slides are pressed together firmly until no more fat and liquid are coming out from the sides. After separation of the two slides (**g**), they are dried at +60°C for 10 min and then put in acetone for defatting. After the last procedure, the slides can be stained with Congo red or material may be scraped off for other analyses, e.g., SDS-PAGE.

acetone (two changes) for 10 min, air-dried, and stained with Congo red for analysis of the presence of amyloid. The whole procedure is illustrated in Fig. 1. Additional slides may be made simultaneously and after defatting stored dry for further analyses by immunohistochemistry or protein chemistry.

The residual, main part of the subcutaneous adipose tissue is cut into smaller pieces with a pair of scissors and washed in 0.15 M NaCl for several hours at +4°C and then overnight in 0.15 M ammonium chloride, containing 0.02% sodium azide, for the lysis of erythrocytes. After that, salt is removed by washing in distilled water. For further protein analyses, pieces of tissue are defatted in acetone (2–3 changes) and air-dried. After defatting, it may be wise to air-dry the adipose tissue in several small pieces. Otherwise the tissue may shrink to one hard piece of tissue, which may be difficult to use for analytical purposes. This material, which in cases with large amount of amyloid in the subcutaneous tissue may have amyloid as the main constituent, can then be used for purification of amyloid fibril proteins which can be studied in detail.

3.3. Demonstration of Amyloid

3.3.1. Staining of Amyloid with Congo Red

The most universally used method, which when executed properly is very sensitive and specific, is staining with Congo red. According to the literature, the most commonly used protocol is that of Puchtler et al. (12) (see Note 6). There are also commercially available stain mixtures. We have found that these methods often give rise to overstaining with false-positive results, even with green birefringence. The reason is uncertain but it is possible that the dyes used almost 50 years ago were less pure. We have modified the method to the following which results in a specific staining without background (Fig. 2).

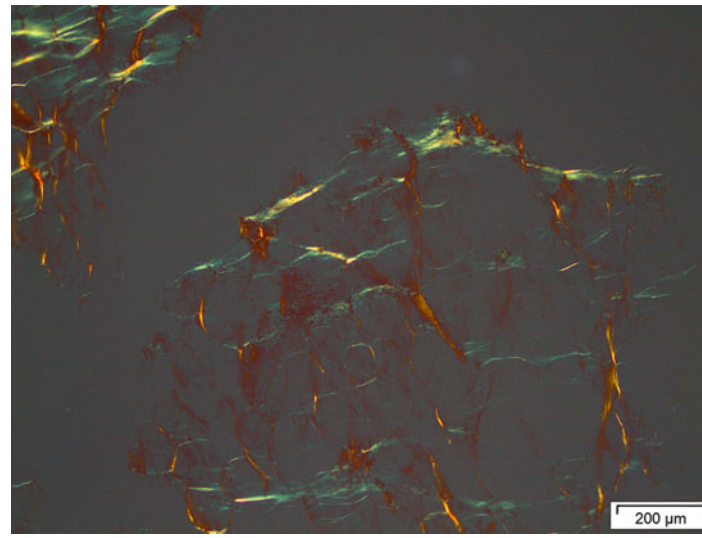

Fig. 2. Typical finding after Congo red staining and polarization microscopy. An amyloid-rich material with *bright green* birefringence.

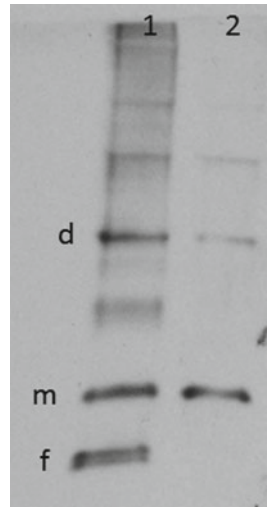

Fig. 3. Example of Western blot analysis of two subcutaneous adipose tissue biopsies from subjects with ATTR V30M amyloidosis. Material in *lane 1* contains dimeric (*d*) and monomeric (*m*) full length TTR as well as C-terminal TTR fragments (*f*) while the amyloid in *lane 2* only contains full length molecules. Visualized with anti-TTR50-127 antibodies.

Make solutions A and B according to the original protocol ((12); see Note 6). To make the modified solution B, add 50 ml of filtered, original B solution to 950 ml of 80% ethanol, saturated with sodium chloride. Before staining, take 1 ml of 1% sodium hydroxide, dissolved in distilled water to 60 ml of the modified solution B. Perform the staining as described in the original protocol (see Note 7). Dehydrate in concentrated ethanol×2, put in xylene×2, and mount for microscopy (see Note 8).

3.3.2. Use of the Material for Western Blot and Mass Spectrometry

The proteins in the dry material can be separated by sodium dodecyl sulfate polyacrylamide gel electrophoresis (SDS-PAGE) immediately. Material can be cut with scissors and then boiled in sample buffer. In order to obtain an efficient solubilization, the tube with material may thereafter be frozen, thawed, and reboiled. After SDS-PAGE, proteins may be visualized by Western blot (Fig. 3) or bands cut out for mass spectrometry (13).

4. Notes

1. The choice of the anterior abdominal skin was based on a systematic study of the occurrence of AA amyloid in the skin of different parts of the body (14). It was found that amyloid most constantly was demonstrated in abdominal skin. This does not necessarily mean that other locations cannot be chosen if there are specific reasons to do so. In most cases of AA, AL,

and ATTR amyloidosis, deposits are present in this tissue. There are no systematic studies about the situation in other, more rare systemic amyloidosis, e.g., derived from fibrinogen alpha chain or apolipoprotein A-I.

2. Disposable dermatological punches can be obtained from different sources. We use punches from Miltex GMBH (Rietheim-Weilheim, Germany). Punch biopsy is a convenient method to obtain material. After cleaning the biopsy site with ethanol and localized anesthesia, small biopsies can be taken without special precautions and a suture is not necessary. When larger (about 5–8 mm), the biopsy is usually regarded as a surgical procedure and a suture may be necessary.
3. Material can be stored in the solution overnight at +4°C without deterioration. It can even be mailed without any particular precaution since the amyloid is comparably resistant to degradation. For clinical diagnostic purposes, we often obtain biopsies sent to us in this way without any problems.
4. Sometimes, local bleeding can create adipose material severely contaminated with blood. In these instances, it is important to carefully rinse in 0.15 M sodium chloride, preferably after that the tissue pieces have been cut up into smaller fragments with the aid of a pair of scissors. A subsequent rinsing with 0.15 M ammonium chloride is important to minimize the amount of hemoglobin since the chains of this protein have a size similar to many amyloid fibril proteins and may disturb further analyses.
5. For diagnostic purposes, it is important to sample from several different parts of the biopsy. Amyloid deposits may occur in a patchy manner. This is, for example, seen with wild-type ATTR amyloid (senile systemic amyloidosis). It may also be important to include some collagen-rich tissue since some types of amyloid has affinity for this type of tissue. However, the problem with nonspecific staining is avoided if our method with diluted Congo red solution is applied.
6. Stock solutions according to the original method: solution A; 80% ethanol saturated with sodium chloride. solution B; solution A saturated with Congo red. Congo red must dissolve for a week, shake the bottle occasionally. Working solution A: Filter and add 1 ml of 1% sodium hydroxide to 100 ml of solution A. Working solution B: Filter and add 1 ml of 1% sodium hydroxide to 100 ml of the diluted solution. Deparaffinize, put in two changes of concentrated ethanol followed by 80% ethanol and transfer the slide to working solution A for 20 min. Then transfer the slide directly to working solution B, stain for 20 min. Dehydrate quickly in two changes of concentrated ethanol, transfer to xylene (or equivalent) and mount. If nuclear staining is needed, this must be performed directly after the deparaffinization step.

7. According to the original protocol, slides should be treated with solution A for 20 min, followed by 20 min in solution B. We often skip solution A without any noticeable negative effects. Also according to the original paper, solutions should be used within 24 h. We have used the solution B for several weeks without any change in specificity or sensitivity. Since the stain is quite diluted, a longer staining time may be necessary. We use 1 h in the solution B but longer staining time can be used, also overnight, without overstaining.
8. Staining with this method is specific but may be weak with some types of amyloid including some AL and ATTR materials. It is important to use a microscope with a strong light source, high-quality polarization filters, and optics that does not change the polarized light. Double microscopes (for more than one examiner) should not be used since the light becomes too weak. Squeeze preparations, as described here have the advantages of being comparably thick, and amyloid is usually appearing with a bright red color and exhibiting clear green birefringence.

Acknowledgments

Supported by the Swedish Research Council, FAMY, FAMY-Norrbotten and AMYL.

References

1. Kisilevsky, R. (2000) Review: Amyloidogenesis - unquestioned answers and unanswered questions. *J. Struct. Biol.* **130**, 99–108.
2. Merlini, G., and Bellotti V.(2003) Molecular mechanisms of amyloidosis. *N. Engl. J. Med.* **349**, 583–596.
3. Westermark, G. T., Sletten, K., and Westermark, P. (1989) Massive vascular AA-amyloidosis: A histologically and biochemically distinctive subtype of reactive systemic amyloidosis. *Scand. J. Immunol.* **30**, 605–613.
4. Ihse, E., Ybo, A., Suhr, O. B., Lindqvist, P., Backman, C., and Westermark, P. (2008) Amyloid fibril composition is related to the phenotype of hereditary transthyretin V30M amyloidosis. *J. Path.* **216**, 253–261,
5. Enqvist, S., Sletten, K., and Westermark, P. (2009) Fibril protein fragmentation pattern in systemic AL-amyloidosis. *J. Path.* **219**, 473–480.
6. Vrana, J. A., Gamez, J. D., Madden, B. J., Theis, J. D., Bergen III, H. R., and Dogan, A. (2009) Classification of amyloidosis by laser microdissection and mass spectrometry-based proteomic analysis in clinical biopsy specimens. *Blood* **114**, 4957–4959.
7. Stenkvist, B., Westermark, P., and Wibell, L. (1974) Simple method of diagnostic screening for amyloidosis. *Ann. Rheum. Dis.* **33**, 75–76.
8. McAdam, K. P. W. J., Westermark, P., Anders, R. F., and Voller, A. (1980) Juvenile amyloidosis in the Anga peoples of Papua New Guinea. In *Amyloid & Amyloidosis*, ed. G.G. Glenner, Costa, P.P., de Freitas, F., pp. 207–210. Amsterdam: Excerpta Medica.
9. Sipe, J. D., Benson, M. D., Buxbaum, J. N., Ikeda, S., Merlini, G., Saraiva, M. J., and Westermark, P. (2010) Amyloid fibril protein nomenclature: 2010 recommendations of the nomenclature committee of the International Society of Amyloidosis. *Amyloid* **17**, 101–104.
10. Lavatelli, F., Perlman, D. H., Spencer, B., Prokaeva, T., McComb, M. E., Théberge, R.,

Connors, L. H., Bellotti, V., Seldin, D. C., Merlini, G., Skinner, M., and Costello, C. E. (2008) Amyloidogenic and associated proteins in systemic amyloidosis proteome of adipose tissue. *Mol. Cell. Proteom.* **7**, 1570–1583.

11. Westermark, P., and Stenkvist, B. (1973) A new method for the diagnosis of systemic amyloidosis. *Arch. Intern. Med.* **132**, 522–523.
12. Puchtler, H., Sweat, F., and Levine, M. (1962) On the binding of Congo red by amyloid. *J. Histochem. Cytochem.* **10**, 355–364.
13. Ihse, E., Stangou, A. J., Heaton, N. D., O'Grady, J., Ybo, A., Hellman, U., Edvinsson, A., and Westermark, P. (2009) Proportion between wild-type and mutant protein in truncated compared to full-length ATTR: an analysis on transplanted transthyretin T60A amyloidosis patients. *Biochem. Biophys. Res. Commun.* **379**, 846–850.
14. Westermark, P. (1972) Occurrence of amyloid deposits in the skin in secondary systemic amyloidosis. *Acta Path. Microbiol. Scand. A* **80**. 718–720.

Chapter 25

Analysis of S100 Oligomers and Amyloids

Hugo M. Botelho, Günter Fritz, and Cláudio M. Gomes

Abstract

The S100 proteins are a large family of 10–12 kDa EF-hand signaling proteins that bind calcium, and in some cases zinc and copper, functioning as central regulators in a diversity of cellular processes. These proteins have tissue, cell, and subcellular-specific expression patterns, and many have an extracellular function. Altogether, these properties underlie their functional diversity and involvement in several pathological conditions including cancer, inflammation, and neurodegeneration. S100 proteins exhibit considerable structural plasticity, being able to exist as monomers or assemble into dimers, higher oligomers, and amyloids, frequently in a metal-dependent manner. Many of these oligomers are functionally relevant, and S100 amyloids have been recently found in prostatic inclusions. Here, we report experimental procedures for the isolation and quantitation of S100 oligomers from tissues, purification of recombinant human S100 protein for assays and use as standards, and an amyloidogenesis assay that allows monitoring the formation of S100 β-oligomers and amyloids in apo- and metal-bound S100 proteins.

Key words: S100 proteins, Brain tissue, Oligomer analysis, Recombinant S100, Thioflavin T, FT-IR, DLS, Amyloid kinetics, Metal ions, Calcium, Zinc

Abbreviations

ATR FT-IR	Attenuated total reflectance Fourier transform infrared spectroscopy
DLS	Dynamic light scattering
KPi	Potassium phosphate
OD	Optical density
ThT	Thioflavin T
SEC	Size exclusion chromatography

1. Introduction

The S100 proteins constitute a protein family involved in Ca^{2+} signal buffering and/or transduction in vertebrates, with an intra- and extracellular action. The relevance of their functions is highlighted by the fact that S100s are the largest subgroup of EF-hand

Einar M. Sigurdsson et al. (eds.), *Amyloid Proteins: Methods and Protocols*, Methods in Molecular Biology, vol. 849,
DOI 10.1007/978-1-61779-551-0_25,

Ca^{2+}-binding proteins, engaged in cell cycle regulation, growth, differentiation, and motility. Ca^{2+} binding (K_d in the micromolar range) typically mediates the exposure of hydrophobic surfaces to which downstream signaling partners bind to (1). Many S100 proteins are also structurally and functionally regulated by binding of other divalent metal ions such as Zn^{2+} and Cu^{2+} at distinct binding sites. These properties and the tissue and cell expression of the S100 proteins results in their involvement in processes related to inflammation, cancer, neurodegenerative disorders, and autoimmune diseases.

Oligomerization is determinant to S100 function. With the exception of monomeric S100G, all S100 proteins are homo- or heterodimers. S100 heterodimers exhibit distinct signaling properties and the functional and structural diversity of S100 proteins is expanded by a number of functional oligomers (2), including tetramers (S100B (3), S100A2 (4), and S100A8/A9 (5)), hexamers (S100B (3), S100A12 (6, 7)), and octamers (S100B (3)). The formation of these species is, in some cases, promoted by metal ion binding, and for S100B, Ca^{2+} promotes tetramerization and tighter interaction with RAGE (3).

Adding to the range of functional oligomers, S100A8/A9 have been recently shown to assemble into amyloid structures *in vivo*, associated with chronic prostate inflammation and cancer (8) in a Ca^{2+}- or Zn^{2+}-dependent manner. This finding has broadened the interest in S100 biology and pathology, as S100 amyloids may have yet unknown roles in human disease, possibly by interfering with physiological S100 functions (2). Indeed, a variety of human S100 proteins have since then been observed to be amyloidogenic (Botelho et al., unpublished observations).

Having in mind the relationship between the functional properties and the S100 oligomeric states, as well as the putative biomedical implications of amyloidogenic processes involving S100 proteins, this chapter details a series of protocols that define the experimental procedures for (a) the isolation and quantitation of S100 oligomers from tissues, (b) the purification of recombinant human S100 protein for assays and use as standards, and (c) an amyloidogenesis assay which allows monitoring the formation of S100 β-oligomers and amyloids in apo- and metal-bound S100 proteins.

2. Materials

Molar protein concentrations refer to the S100 subunit.

2.1. Analysis of S100B Multimers from Brain Tissue

1. 50 mM Tris–Cl, pH 8.0.
2. 20 mM Tris–Cl, 150 mM NaCl, pH 8.0.
3. C0mplete, EDTA free protease inhibitor cocktail (Roche).

4. Potter-Elvehjem homogenizer.
5. Superdex 75 prep grade (GE Healthcare) column (1.6 cm × 60 cm).
6. LIAISON Sangtec 100 assay (AB Sangtec Medical).

2.2. S100 Protein Expression

1. DYT medium supplemented with 0.2% glucose and 100 μg/ml ampicillin.
2. 1.0 M IPTG.

2.3. S100 Protein Purification

1. 50 mM Tris–Cl, pH 7.6.
2. 1.0 M $CaCl_2$.
3. 200 mM EDTA–NaOH, pH 7.6.
4. 20 mM Tris–Cl, 150 mM NaCl, pH 7.6.
5. DNAse I.
6. 1.0 M $MgCl_2$.
7. C0mplete, EDTA-free protease inhibitor cocktail (Roche).
8. Ultracentrifuge.
9. Phenylsepharose High Sub (GE Healthcare) column (1.6 cm × 15 cm).
10. Superdex 75 prep grade (GE Healthcare) column.

2.4. Preparation of Protein Solutions

1. 50 mM Glycine pH 2.5.
2. 100 mM $CaCl_2$.
3. 100 mM $ZnCl_2$.
4. 100 mM $CuSO_4$.
5. 1 M DTT, freshly prepared.
6. 50 mM EDTA (see Note 1).
7. Chelex 100 resin (Sigma).
8. Bradford's reagent.
9. HiTrap Desalting Column (GE Healthcare).
10. Amicon Ultra-4 Centrifugal Filters, cutoff 3 kDa (Millipore).
11. Centrifuge with swinging bucket rotor.
12. Benchtop centrifuge.
13. Water bath or dry bath.
14. UV–visible spectrophotometer.

2.5. Thioflavin T Fluorescence

1. Thioflavin T (ThT) solution: 65 μM ThT (Sigma) in 10 mM potassium phosphate (KPi) pH 7.0, 150 mM NaCl (see Note 2).
2. 10 mg/ml Lysozyme (Fluka) in 50 mM glycine pH 2.5 (see Note 3).

3. 0.22 μm Syringe filters, acetate membrane (e.g., Carl Roth A061.1).
4. 100 μl Multiply PCR tubes (e.g., Sarstedt Safecup, 72.733.200) (see Note 4).
5. Fluorescence cell with stirring (Hellma 119.004F-QS) and magnetic followers (e.g., Carl Roth 0973.1).
6. Spectrofluorimeter with magnetic stirring cell holder.

2.6. Attenuated Total Reflectance Fourier Transform Infrared Spectroscopy

1. FT-IR spectrometer (e.g., Bruker IFS 66).
2. Thermostatized ATR cell suitable for liquid samples (e.g., Harrick BioATR II cell).

2.7. Dynamic Light Scattering

1. Syringe filters (0.22 μm), acetate membrane (Carl Roth).
2. Low volume cuvette (e.g., Hellma 105.215-QS).
3. Mineral oil, for PCR (Sigma).
4. DLS instrument equipped with cell thermostatization (e.g., Malvern Zetasizer Nano ZS).

3. Methods

3.1. Analysis of S100B Multimers from Brain Tissue

S100B forms oligomers in the human brain. To detect such oligomers, a method was designed that does not include any step with non-physiological pH or salt conditions.

1. Thaw brain tissue on ice.
2. Add ice cold 50 mM Tris–Cl, pH 8.0 containing protease inhibitors (C0mplete, Roche) at a 1:2 (v/w) ratio.
3. Homogenize the tissue on ice using a Potter-Elvehjem homogenizer.
4. Ultracentrifuge the brain homogenate at 100,000 × *g* for 60 min.
5. Filter the supernatant through a 0.2 μm membrane.
6. Load filtered supernatant to a size exclusion chromatography column Superdex 75 (GE Healthcare) and elute with 20 mM Tris–Cl, 150 mM NaCl, pH 8.0.
7. Eluted fractions are analyzed for S100B content using a commercial ELISA-based assay kit (LIAISON Sangtec 100 assay, AB Sangtec Medical) that uses a pair of monoclonal S100B antibodies for capture and detection of S100B (Fig. 1).

3.2. S100 Protein Expression

S100 proteins are expressed using *Escherichia coli* as expression host.

1. S100 protein cDNA is cloned into the pGEMEX plasmid by standard cloning techniques.

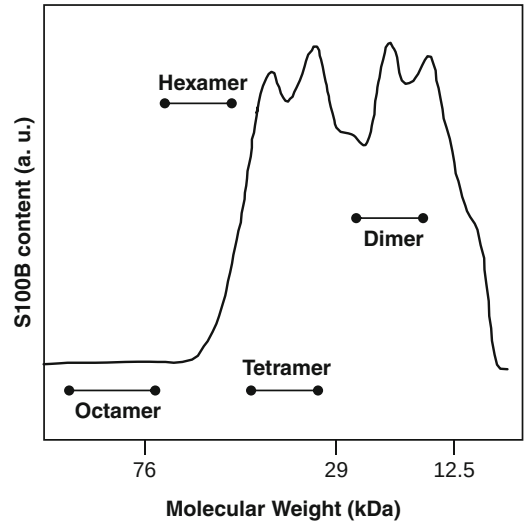

Fig. 1. S100B multimeric species are detected and analyzed by SEC following tissue extraction. The figure shows a typical elution profile of S100B from human brain extract in the presence of EDTA. Redrawn from ref. 3.

2. *E. coli* expression strain BL21(DE3) is transformed with the corresponding plasmid.
3. Select the transformants using solid media plates containing 100 µg/ml ampicillin.
4. Inoculate a single colony of the corresponding expression clone in 10 ml DYT containing 100 µg/ml ampicillin and 0.2% glucose.
5. The culture is grown on a shaker at 37°C overnight.
6. The overnight culture is used to inoculate the expression culture incubated at 37°C. Growth of *E. coli* is followed by OD at 600 nm.
7. As soon as $OD_{600\ nm} = 0.6$ is reached, expression is induced by the addition of 1 mM IPTG. The expression culture is harvested by centrifugation 3–4 h after induction. Cell pellets are frozen at –80°C and stored until further use.

3.3. S100 Proteins Purification

S100 proteins undergo a conformational change upon Ca^{2+} binding which results in exposing a hydrophobic patch for interaction with target proteins. This property is utilized for Ca^{2+}-dependent affinity chromatography on hydrophobic matrices, such as phenyl sepharose. This conformational change is fully reversible and bound protein can be eluted by complexation of the bound Ca^{2+} ions.

1. Frozen cell pellets are thawed on ice.
2. The cells are suspended 50 mM Tris–Cl pH 7.6.
3. A small amount of DNAse I is added to the cell suspension.
4. $MgCl_2$ is added to final concentration of 2 mM.

5. Cells are broken by one passage through a French pressure cell.
6. Crude extracts are subjected to ultracentrifugation at 100,000 × *g* for 1 h.
7. 2 mM $CaCl_2$ is added to the supernatant and subsequently applied to a phenylsepharose column equilibrated in 50 mM Tris–Cl, 2 mM $CaCl_2$, pH 7.6.
8. The column is washed with the same buffer until absorption at 280 nm reaches baseline again.
9. Bound S100 protein is eluted with 50 mM Tris–Cl, 4 mM EDTA, pH 7.6.
10. Fractions containing S100 protein are combined and concentrated by ultrafiltration.
11. Concentrated S100 is applied to a Superdex 75 column equilibrated in 20 mM Tris–Cl, 150 mM NaCl, pH 7.6.
12. Fractions containing S100 protein are combined, concentrated by ultrafiltration, shock-frozen in liquid nitrogen and stored at −80°C until further use.

3.3.1. Obtaining Reduced S100 Proteins

Most S100 proteins have cysteine residues which spontaneously oxidize to the disulfide form (9–11), a process which also occurs *in vivo* for some S100 proteins (12). This step is not required for characterizing S100 amyloidogenesis but must be used to infer the role of disulfides in the process (see Note 5). Since S100 solutions to be used in amyloidogenesis assays are prepared at pH 2.5, they should be manipulated at 4°C at all times to avoid aggregation.

1. Add 300-fold excess of DTT and 0.5 mM EDTA to the as-purified S100 stock.
2. Incubate 2 h at 37°C.
3. Desalt using a HiTrap desalting column equilibrated in oxygen-free 50 mM glycine pH 2.5 at 1 ml/min flow rate (see Note 6). Sample volume should not exceed 1.2 ml. Monitor the elution through the absorption at 280 nm and conductivity. The S100 protein will elute in the void volume of the column; DTT, EDTA and components of the initial buffer will elute at a later volume, as indicated by the perturbation of both the absorbance and conductivity traces.
4. Pool the fractions containing S100 protein, having caution not to include any DTT or EDTA (see Note 7).
5. Reconcentrate the S100 fraction by ultrafiltration using Amicon filters.
6. Centrifuge the concentrate at 12,000 × *g* for 10 min in a benchtop centrifuge at 4°C to pellet any aggregates which formed during concentration.
7. Remove the solution to a new tube, assuring that no pellet is collected.

Table 1
Absorption extinction coefficients (280 nm) for selected human S100 proteins, according to the oxidation state of the cysteine residues

		$\varepsilon^{280\,nm}$ ($M^{-1}.cm^{-1}$)	
Protein	**MW (Da)[a]**	**All cysteines**	**All cysteines**
S100A1	10,546	8,480	8,480
S100A2	10,986	3,230	2,980
S100A3	11,713	15,065	14,440
S100A4	11,729	3,230	2,980
S100A5	10,744	4,595	4,470
S100A6	10,180	4,470	4,470
S100A7	11,457	4,595	4,470
S100A8	10,835	11,460	11,460
S100A9	13,242	6,990	6,990
S100A10	11,187	3,105	2,980
S100A11	11,740	4,595	4,470
S100A12	10,575	2,980[b]	
S100A13	11,340	6,990[b]	
S100A14	11,662	7,115	6,990
S100A15	11,305	4,595	4,470
S100A16	11,801	12,950	12,950
S100B	10,713	1,615	1,490
S100G	9,016	1,490[b]	
S100P	10,400	2,980	2,980
S100Z	11,619	3,105	2,980

Calculated using Expasy (15)
[a] Subunit molecular weight
[b] Proteins containing no cysteines

8. Quantify the S100 solution spectrophotometrically (molar extinction coefficients are supplied in Table 1) or using Bradford's assay.
9. S100 stock solution for amyloidogenesis: amyloidogenesis is favored at higher protein concentrations. The final protein concentration should be at least 3.5 mg/ml (see Note 8). If needed, repeat steps 5 and 6 until the required concentration

is achieved. This is the stock protein solution which is used for preparing all samples in the amyloidogenesis assays.

10. If the S100 proteins are to be studied in the cysteine oxidized state, steps 1 and 2 are omitted (see Note 9).

3.4. Amyloidogenesis Assay of apo- and Metal-Bound S100

Many S100 proteins promptly form amyloids at pH 2.5 (50 mM glycine) at 3 mg/ml or higher concentration. This concentration is adequate for amyloid detection using a variety of biophysical techniques. Tenfold molar excess of metal ions over the S100 subunit (2.3–3.3 mM) is adequate for examining metal binding.

1. All buffers should be passed through a Chelex column to remove trace metal ions. The same applies to the water used in metal ion solutions.
2. Flasks should be previously rinsed in chelex-treated water before storing the trace metal ion-free solutions.

3.4.1. Assessing Amyloid Formation by Extrinsic ThT Fluorescence

The enhancement of ThT fluorescence is one of the hallmarks of amyloid species. Additionally, this assay provides a simple, inexpensive, and quantitative way of detecting amyloids in real-time and deriving kinetic data. Our fluorescence measurements are recorded using a Varian Cary Eclipse spectrofluorimeter.

1. Dilute the S100 protein stock to 100 μl at 3 mg/ml using 50 mM glycine pH 2.5 (see Note 10). Metal ions (Ca^{2+}, Zn^{2+}, Cu^{2+}) may be added as tenfold molar equivalents over the S100 subunit (2.3–3.3 mM, depending on the specific protein). Alternatively, 1 μl 50 mM EDTA is added to obtain apo protein (0.5 mM final concentration).
2. Dilute 5 μl of the S100 solution in 995 μl of ThT solution.
3. Homogenize the solution by inversion.
4. Incubate for at least 2 min at room temperature and in the dark. At pH 7, amyloidogenesis is inhibited and ThT fluorescence is stable for at least 3 h, allowing time for fluorescence measurements.
5. Measure ThT fluorescence at 482 nm: excite the solution at 440 nm using 10 nm excitation and emission slits, 600 V photomultiplier voltage and 0.5 s integration time while maintaining stirring (see Note 11).
6. This is the ThT fluorescence before amyloid formation is promoted. It should be identical to the fluorescence of a blank sample (see Note 12).
7. Incubate the S100 solution at 57°C under quiescent conditions.
8. After 48 h amyloidogenesis is mostly complete. At this time, homogenize the S100 solution by inversion and repeat

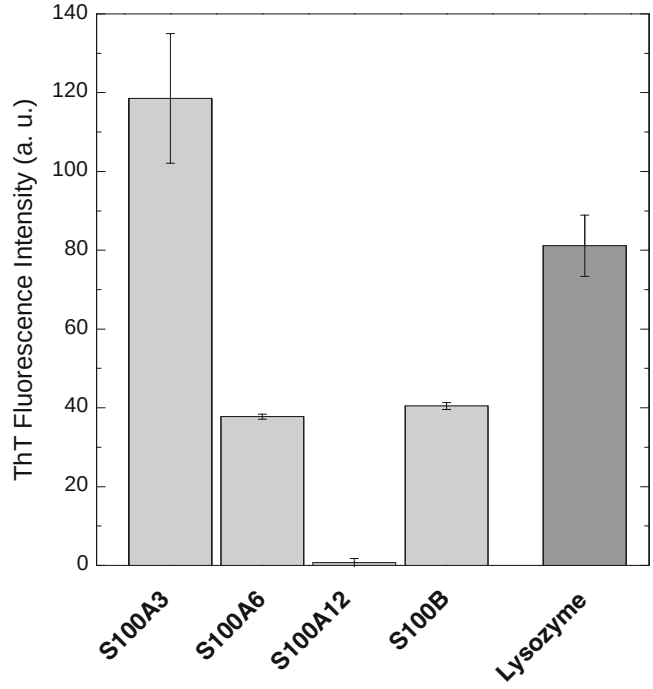

Fig. 2. S100 amyloidogenic species are identifiable by ThT fluorescence after incubation at 3 mg/ml, pH 2.5 and 57°C. For most S100 proteins, the aggregation process is complete after 2 days. AFM analysis further indicates that S100A3 forms amyloid fibrils, S100A6 and S100B assemble into β-oligomers and S100A12 forms non-amyloid oligomers (not binding ThT). Lysozyme (10 mg/ml) serves as a positive control for amyloid formation.

steps 2–5 in triplicate for measuring ThT fluorescence and assessing amyloid/β-oligomer formation.

9. Amyloid species are recognizable by ThT fluorescence emission at 482 nm (Fig. 2 and see Note 13).
10. To calibrate the fluorescence measurement, perform steps 2–9 with a 10 mg/ml lysozyme solution, a positive control for amyloid formation (13). After 10 days, the amyloidogenesis process is complete (Fig. 2).
11. This method can be adapted for obtaining kinetic data by repeating sampling as a function of time and representing ThT fluorescence intensity as a function of time (Fig. 3a, d).

3.4.2. Time Resolved Detection of S100 Oligomers and Amyloids with Attenuated Total Reflectance FT-IR

β-Sheet structures give rise to infrared absorption at specific wavenumbers in the amide I region according to the specific structure, rendering FT-IR an extremely sensitive technique for continuous monitoring of amyloid formation. Our FT-IR measurements are acquired using a Bruker IFS 66/S spectrometer equipped with a nitrogen-cooled MCT detector and a thermostatized Harrick BioATR II cell.

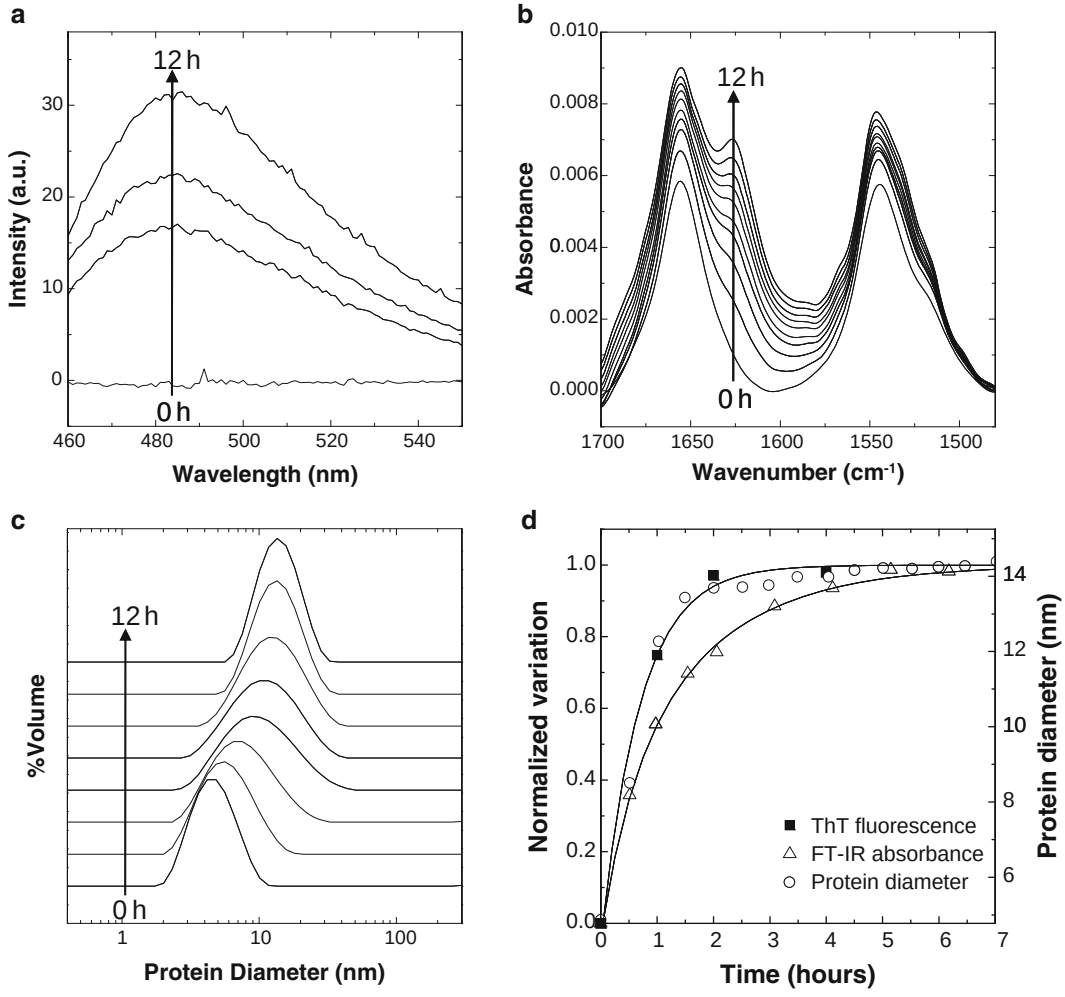

Fig. 3. Kinetic analysis of S100 amyloidogenic pathways. As an example, all data were acquired during incubation of apo S100A6 at pH 2.5, 57°C and 3 mg/ml (0.3 mM) protein concentration. (**a**) ThT fluorescence spectra acquired during the amyloidogenesis assay. The fluorescence band with maximum at 482 nm arises due to intercalation of ThT in β-sheet regions, which are absent in S100A6 in the absence of the thermal challenge. (**b**) Amide I/amide II ATR FT-IR spectra acquired during 12 h of incubation. The buildup of β-oligomers is indicated by the appearance of the band at 1,627 cm^{-1}. (**c**) Time-resolved size distribution as determined from a dynamic light scattering experiment. The distributions indicate the conversion of dimeric S100A6 (4.5 nm diameter) to β-oligomers (14 nm diameter). (**d**) Kinetics of apo S100A6 amyloidogenesis extracted from ThT fluorescence at 482 nm, the ration between infrared absorption at 1,627 cm^{-1} and the spectral maximum (1,655 cm^{-1}) and the DLS-determined protein diameter. Data are fitted with single exponential decay curves.

1. Setup the FT-IR spectrometer: turn it on for enough time to stabilize the light source, cool the MCT detector with liquid nitrogen, align the ATR cell and set the temperature to 57°C according to the manufacturer's instructions.
2. Set acquisition parameters as follows: 1,000–3,000 cm^{-1} spectral range, 4 cm^{-1} resolution, 2 min scan, 20 kHz scanner velocity, 12 mm aperture. Fourier transform may be done using a Blackman–Harris 3 Term apodization function, 5,687 phase

interferogram points, Mertz phase correction mode, and second-order zerofilling factor. Set the acquisition mode to continuous spectra acquisition.

3. Record the baseline spectrum: transfer the buffer solution (containing metal ions or EDTA at the same concentration as the S100 solution) to the ATR cell surface. Close the ATR and sample compartments. Record the spectrum.
4. Remove the blank solution and replace it by the S100 solution at 3 mg/ml (in 50 mM glycine pH 2.5).
5. Immediately start recording spectra.
6. Amyloid formation is assessed by the absorption ratio between the β-sheet band at 1,627 cm^{-1} and the amide I absorption maximum, around 1,655 cm^{-1} (Fig. 3b, d) (14).

3.4.3. Dynamic Light Scattering

Due to the intrinsic sensitivity of DLS to small amounts of aggregated protein material or dust particles, samples should be cleared of such contaminants. We use a Malvern Instruments Zetasizer Nano ZS instrument for DLS measurements. It is equipped with a Peltier-controlled thermostatized cell support. The manufacturer's software automates the autocorrelation analysis of time-resolved light scattering as well as the Mie Theory analysis of the data to extract multimodal particle size distributions.

1. Prepare 200 µl of a 3 mg/ml S100 solution in 50 mM glycine pH 2.5.
2. Filter the S100 solution with a 0.22 µm pore filter (see Note 14).
3. Pipet 50 µl of S100 solution to the DLS cuvette.
4. Carefully place 20 µl mineral oil on top of the solution. This will form an inert seal to prevent evaporation.
5. Setup the DLS instrument to average 15 10 s accumulations in the backscattering mode, using quadratic weighting and 0.01 regularizer. Set the Peltier temperature at 25°C.
6. Make a size measurement. This is the size of the S100 protein in the native-like state at pH 2.5, which should be around 4–5 nm (diameter).
7. Remove the cuvette and keep it at room temperature (see Note 15).
8. Quickly set the Peltier temperature to 57°C and set the instrument for continuous repeated measurements.
9. Replace the cuvette and start the measurement.
10. Retrieve the size distributions (by volume) and plot the distribution maxima as a function of time to obtain kinetic information (Fig. 3c, d). Scattered light intensity can also serve as a kinetic reporter.

4. Notes

1. EDTA is an acid and a 50 mM solution requires pH ~7.0. The pH should be raised by adding NaOH.
2. The 65 μM ThT solution is prepared by diluting a 2.5 mM stock solution which had been filtered though a 0.22 μm filter to remove undisolved particles. ThT should be stored in the dark to avoid photobleaching.
3. Diluting lyophilized lysozyme into 50 mM glycine pH 2.5 will yield a final solution with pH around 4.5. The solution pH should be adjusted to 2.5 with a concentrated HCl solution or lysozyme will not form amyloid under the conditions described. This is better achieved using a micro-pH electrode.
4. These tubes seal the sample, avoiding sample loss through evaporation.
5. S100A3 is an exception. The fully oxidized protein is highly disulfide cross-linked, forms macroscopic insoluble aggregates and requires resolubilization to be amenable to most spectroscopic analyses.
6. After desalting, the column should be washed with 1 M NaCl to remove S100 protein bound to the matrix and equilibrated in 20% ethanol for storage.
7. Both DTT and EDTA chelate metal ions and interfere in the metal binding assays.
8. The working concentration of S100 proteins in amyloidogenesis assays is 3 mg/ml. Preparing a S100 stock solution of at least 3.5 mg/ml allows diluting the solution with additives such as metal ion solutions.
9. For obtaining small amounts (<1 mg) of oxidized S100 proteins, an alternative protocol has been devised: dilute the S100 protein stock 50- to 100-fold in 50 mM glycine pH 2.5, reconcentrate using centrifugal filters and quantify the protein solution.
10. The assay may be upscaled provided that S100 solutions are incubated in tubes appropriate for their volume. Using tubes with capacity much larger than the S100 solution volume will promote sample evaporation at 57°C in amyloidogenesis assays.
11. Report the fluorescence value after subtracting a blank.
12. Most S100 proteins keep a native-like fold at pH 2.5 if kept at 4°C and do not bind ThT, not giving rise to any fluorescence. The α-helical native-like conformation can be assessed by far UV CD spectroscopy.

13. ThT fluorescence identifies both amyloid oligomers and amyloid fibrils. For knowing which type of amyloid structure is formed, the ThT results should be confirmed by Atomic Force or Electron Microscopy imaging.
14. To ensure dust-free conditions, purge the syringe filter with double-distilled water before filtering the S100 solution. Also, all tubes, pipette tips, and other material that comes into contact with the solution after filtration should be rinsed with double-distilled water and dried using a compressed air blower.
15. The cuvette with the S100 sample should be kept at room temperature just for the time required for the Peltier to reach 57°C. It should not be temporarily kept at a cooler temperature (e.g., 4°C) because temperature cycling may produce bubbles in the solution which interfere with DLS measurements.

Acknowledgments

This work was supported by grants POCTI/QUI/45758 and PTDC/QUI/70101 (to CMG) from the Fundação para a Ciência e a Tecnologia (FCT/MCTES, Portugal), by grants FR 1488/3-1 and FR 1488/5-1 from the Deutsche Forschungsgemeinschaft (DFG) (to GF). CMG and GF are recipients of a CRUP/DAAD collaborative grant A-15/08. HMB was a recipient of a Ph. D. fellowship (SFRH/BD/31126/2006) from Fundação para a Ciência e a Tecnologia (FCT/MCTES, Portugal). Ludmilla Morozova-Roche (Umeå University) is gratefully acknowledged for AFM imaging.

References

1. Santamaria-Kisiel, L., Rintala-Dempsey, A. C., and Shaw, G. S. (2006) Calcium-dependent and -independent interactions of the S100 protein family, *Biochem J 396*, 201–214.
2. Fritz, G., Botelho, H. M., Morozova-Roche, L. A., and Gomes, C. M. (2010) Natural and amyloid self-assembly of S100 proteins: structural basis of functional diversity, *FEBS J 277*, 4578–4590.
3. Ostendorp, T., Leclerc, E., Galichet, A., Koch, M., Demling, N., Weigle, B., Heizmann, C. W., Kroneck, P. M., and Fritz, G. (2007) Structural and functional insights into RAGE activation by multimeric S100B, *EMBO J 26*, 3868–3878.
4. Koch, M., Bhattacharya, S., Kehl, T., Gimona, M., Vasak, M., Chazin, W., Heizmann, C. W., Kroneck, P. M., and Fritz, G. (2007) Implications on zinc binding to S100A2, *Biochim Biophys Acta 1773*, 457–470.
5. Korndorfer, I. P., Brueckner, F., and Skerra, A. (2007) The crystal structure of the human (S100A8/S100A9)2 heterotetramer, calprotectin, illustrates how conformational changes of interacting alpha-helices can determine specific association of two EF-hand proteins, *J Mol Biol 370*, 887–898.
6. Moroz, O. V., Blagova, E. V., Wilkinson, A. J., Wilson, K. S., and Bronstein, I. B. (2009) The crystal structures of human S100A12 in apo form and in complex with zinc: new insights into S100A12 oligomerisation, *J Mol Biol 391*, 536–551.
7. Moroz, O. V., Antson, A. A., Dodson, E. J., Burrell, H. J., Grist, S. J., Lloyd, R. M., Maitland, N. J., Dodson, G. G., Wilson, K. S.,

Lukanidin, E., and Bronstein, I. B. (2002) The structure of S100A12 in a hexameric form and its proposed role in receptor signalling, *Acta Crystallogr D Biol Crystallogr* ***58***, 407–413.

8. Yanamandra, K., Alexeyev, O., Zamotin, V., Srivastava, V., Shchukarev, A., Brorsson, A. C., Tartaglia, G. G., Vogl, T., Kayed, R., Wingsle, G., Olsson, J., Dobson, C. M., Bergh, A., Elgh, F., and Morozova-Roche, L. A. (2009) Amyloid formation by the pro-inflammatory S100A8/A9 proteins in the ageing prostate, *PLoS One* ***4***, e5562.
9. Kordowska, J., Stafford, W. F., and Wang, C. L. (1998) Ca2+ and Zn2+ bind to different sites and induce different conformational changes in human calcyclin, *Eur J Biochem* ***253***, 57–66.
10. Raftery, M. J., Collinson, L., and Geczy, C. L. (1999) Overexpression, oxidative refolding, and zinc binding of recombinant forms of the murine S100 protein MRP14 (S100A9), *Protein Expr Purif* ***15***, 228–235.
11. Scotto, C., Mely, Y., Ohshima, H., Garin, J., Cochet, C., Chambaz, E., and Baudier, J. (1998) Cysteine oxidation in the mitogenic S100B protein leads to changes in phosphorylation by catalytic CKII-alpha subunit, *J Biol Chem* ***273***, 3901–3908.
12. Winningham-Major, F., Staecker, J. L., Barger, S. W., Coats, S., and Van Eldik, L. J. (1989) Neurite extension and neuronal survival activities of recombinant S100 beta proteins that differ in the content and position of cysteine residues, *J Cell Biol* ***109***, 3063–3071.
13. Morozova-Roche, L. A., Zurdo, J., Spencer, A., Noppe, W., Receveur, V., Archer, D. B., Joniau, M., and Dobson, C. M. (2000) Amyloid fibril formation and seeding by wild-type human lysozyme and its disease-related mutational variants, *J Struct Biol* ***130***, 339–351.
14. Calero, M., and Gasset, M. (2005) Fourier transform infrared and circular dichroism spectroscopies for amyloid studies. *Methods Mol. Biol.* ***299***, 129–151.
15. Gasteiger, E., Hoogland, C., Gattiker, A., Duvaud, S., Wilkins, M. R., Appel, R. D., Bairoch, A. (2005) Protein identification and analysis tools on the ExPASy server, in *The proteomics protocols handbook* (Walker, J. M., Ed.), pp. 571–607, Humana Press.

Chapter 26

S100A8/A9 Amyloidosis in the Ageing Prostate: Relating Ex Vivo and In Vitro Studies

Anna L. Gharibyan, Dina Raveh, and Ludmilla A. Morozova-Roche

Abstract

The family of S100 proteins encompasses more than 20 members characterized by remarkable conformational and functional diversity. S100 proteins act as central regulators of various cellular processes, including cell survival, proliferation, differentiation, and motility. Many S100 proteins are implicated in various types of cancer as well as neurodegenerative, inflammatory, and autoimmune diseases. Recently, we have found that S100A8/A9 proteins are involved in amyloidogenic process in the ageing prostate, contributing to the formation of calcified corpora amylacea (CA) inclusions, which commonly accompany age-dependent prostate tissue remodelling and cancer. Amyloid formation by S100A8/A9 proteins can also be modelled in vitro. Amyloid assembly of S100A8/A9 proteins into oligomeric and fibrillar complexes is modulated by metal ions such as calcium and zinc. Here, we provide insights into the extraction procedures and review the common structural features of ex vivo and in vitro S100A8/A9 amyloids, showing that they share the same generic origin.

Key words: S100A8, S100A9, Amyloid, Oligomers, Fibrils, Corpora amylacea, Prostate

Abbreviations

CA Corpora amylacea
ThT Thioflavin T

1. Introduction

S100 proteins constitute the largest subfamily within the superfamily of the Ca^{2+}-binding EF-hand proteins. To date, 21 different S100 proteins have been identified in humans and about the same number found in other mammalians by genomic analysis. The name of the family reflects the fact that the first identified S100s were purified from the soluble (S) bovine brain fraction upon fractionation with saturated (100%) ammonium sulphate (1).

Einar M. Sigurdsson et al. (eds.), *Amyloid Proteins: Methods and Protocols*, Methods in Molecular Biology, vol. 849,
DOI 10.1007/978-1-61779-551-0_26,

S100 proteins are characterized by significant conformational plasticity, forming homo- and heterodimers, and tetramers (2). Consequently, their homo- and hetero-oligomeric complexes play distinct roles in cell physiology, including cell adhesion, motility, inflammation, differentiation, and apoptosis (3–6). Although a large number of functions have been found for S100 proteins, their specific role in various biological processes still remains to be defined. In particular, elevated levels of S100 proteins serve as a hallmark of numerous pathological conditions associated with inflammation and recurrent infection (3, 4, 7, 8). Their expression pattern, potential cytokine-like function, up-regulation and regulation via signalling pathways, including the tumour-promoting RAGE receptor, suggest that S100 proteins may play a key role in inflammation-associated cancers (9). Our recent findings showing that calcified amyloid deposits in the ageing prostate known as corpora amylacea (CA) originate from the pro-inflammatory proteins S100A8/A9 and their amyloids (10), indicate that there could be a close link between chronic inflammation, amyloid formation, and cancer.

The age-dependent prostate tissue remodelling associated with reduction of the reproductive role of the prostate gland is often accompanied by serious problems such as benign prostatic hyperplasia observed in 70% of men in their 60s (11) and prostate cancer (12). The latter is the most common non-cutaneous malignant neoplasm in men in the Western world and the incidence of prostate cancer is rising rapidly with increasing lifespan. It is important to note that in Europe the mortality rates from prostate cancer vary significantly amongst different countries (13, 14). There is a marked contrast between Mediterranean regions with below-average mortality and other countries such as Sweden, Denmark, West Germany, Northern France, Ireland, and the Netherlands, which have several high-mortality areas. The factors affecting the increasing incidence of prostate cancer and its obvious geographic pattern are still debated; however, there is growing evidence that inflammation plays a crucial role in prostate pathogenesis. Prostate carcinogenesis is suggested to be associated with exposure to environmental factors such as infectious agents and dietary carcinogens as well as hormonal imbalances that lead to injury of the prostate and to the development of chronic inflammation and regenerative 'risk factor' lesions (11, 15). The inclusion bodies termed CA or calcified deposits often observed adjacent to damaged epithelium and focal inflammatory infiltrates are considered to be risk factors for neoplastic transformation (12). They are highly prevalent in late life and frequently clinically linked with inflammation, infection, and carcinogenesis (12, 16). CA have also been found in the lung, uterus (17), and ovary (18). They may be of a much diversified nature and their incidence is commonly associated with ageing.

Using a combination of approaches, we studied systematically the CAs extracted from the prostate glands of patients diagnosed with prostate cancer and found that their major component is the amyloid form of S100A8 and S100A9 proteins (10). To accumulate in the protease-rich prostate environment, the S100A8/A9 amyloids are stabilized by massive dystrophic calcification. DNA and proteins from *Escherichia coli* are also found in the CA bodies, suggesting that their formation is likely to be associated with bacterial infection. CA inclusions are also accompanied by the activation of macrophages and by an increase in the concentration of S100A8/A9 in the surrounding tissues, indicating on-going inflammatory reactions. These findings suggest a close connection between bacterial infection, inflammation, and amyloid deposition of pro-inflammatory S100A8/A9 proteins in the prostate gland and triggering this self-perpetuating cycle may increase the risk of malignancy in the ageing prostate. The S100A8/A9 amyloid formation can also be studied in vitro solutions. Therefore, here we described some of the procedures used in verifying the amyloid properties of S100A8/A9 deposits.

2. Materials

2.1. CA Inclusion Bodies

CA specimens were dissected from the prostate tissue from patients that underwent radical prostatectomy due to prostate cancer. All patients gave their written informed consent, and the collection of human tissues was approved by the Umeå research ethics board. The dried CA specimens were stored at −80°C. CAs size varied from 0.5 mm to 5–7 mm diameter (Fig. 1).

2.1.1. Materials and Reagents for Protein Extraction from CA

TE buffer: 20 mM Tris–HCl, 10 mM EDTA, pH 7.5.

95% Ethanol (methanol).

1 M Acetic acid.

1.2 M HCl.

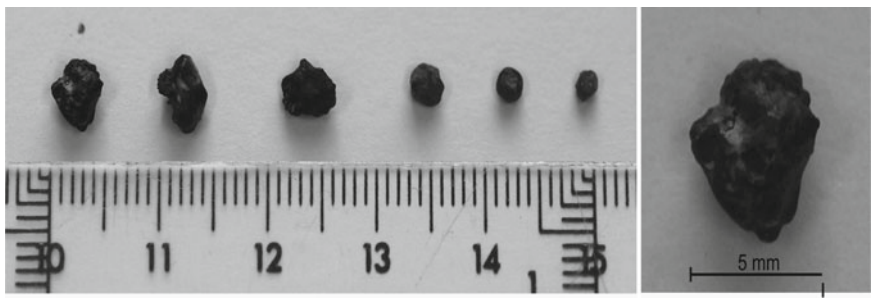

Fig. 1. CA inclusions extracted from human prostate after prostatectomy. The ruler shows their dimension in mm.

0.1 M Tris, 6 M guanidine hydrochloride, pH 7.4.

0.1 M Tris, 6 M guanidine hydrochloride, 0.5 M EDTA, pH 7.4.

Pierce Micro BSA protein assay kit (Pierce).

Grinders.

Microcentrifuge (Eppendorf).

2.2. Identification of Proteins in CA Extracts

0.2 M NH_4HCO_3, 15 mM DTT.

8 M Urea.

80 mM Iodoacetamide.

Trypsin, formic acid 0.5% and 0.1%, TFA 0.1%, acetonitrile 80%.

Poros 50 reverse-phase R2 material (PerSeptive Biosystems).

GELoader tips (Eppendorf).

nanoACQUITY UPLC™ system (Waters).

Q-Tof Ultima™ mass spectrometer (Waters).

2.2.1. Liquid Chromatography Coupled with Electrospray Ionization Mass Spectrometry

2.2.2. Materials and Reagents for Gel Electrophoresis and Western Blotting

PhastGel gradient: 4–25% (GE Healthcare).

Pre-stained molecular weight standards "SeeBlue" (Invitrogen).

Silver nitrate.

Hybond ECL Nitrocellulose Membrane (GE Healthcare).

Non-fat milk.

Tris-buffered saline (TBS) (50 mM Tris–HCl, 150 mM NaCl, pH 7.4) containing 0.05% Tween 20 (TBS-T).

TBS-T containing 5% non-fat milk.

Rabbit polyclonal anti-human S100A8 and anti-human S100A9 antibodies (Santa Cruz).

Horseradish peroxidase-conjugated anti-rabbit IgG (GE Healthcare).

Enhanced chemiluminescence kit (GE Healthcare).

Phast-system equipment (GE Healthcare).

2.3. Immunohistochemical Analysis of CA

Xylene.

Ethanol 99, 70, and 30% solutions.

PBS (phosphate-buffered saline).

Antigen retrieval buffer (10 mM Tris and1 mM EDTA containing 0.05% Tween 20, pH 9.0).

3% Hydrogen peroxide.

Primary antibodies: S100A8 (Calgranulin A) or S100A9 (Calgranulin B) rabbit polyclonal antibodies (Santa Cruz).

Amyloid fibril-specific antibodies (gift of R. Kayed (19)).

Anti-rabbit IgG reagent kit (ImmPRESS, Vector Labs).

Vector VIP and DAB peroxidase substrate kit (Vector Labs).

Vector methyl green counterstain (Vector Labs).

Mounting medium PERTEX (HistoLab).

2.4. Thioflavin T Staining of CA Amyloids

Fresh and filtered (0.22-μm filters) 0.25 mM Thioflavin T (ThT) stock solution.

50 μM ThT working solution (dilute 1:50 the stock solution with 10 mM K_2HPO_4, 150 mM NaCl, pH 7.4 and keep protected from the light).

2.5. Formation of S100A8/A9 Amyloids

Human S100A8/A9 heterodimers isolated from granulocytes and stored in 20 mM Tris, 1 mM DTT, pH 7.2 (20).

Recombinant human S100A8 and S100A9 chains prepared as described (21).

Incubation buffers for amyloid production:

- 50 mM HCl, pH 2.0
- 20 mM Tris, 1 mM DTT, pH 7.2
- 20 mM HEPES, 140 mM NaCl, pH 7.4

  Cation containing buffers: buffers containing 1 mg/ml of either $Ca_3(PO4)_2$ or 10 mM $ZnCl_2$.

  Cation-free buffers: buffers containing 50 mM EDTA.

3. Methods

3.1. Protein Extraction from CA

CA specimens are calcified bodies, comprising 60–70% crystalline phase of hydroxylapatite ($Ca_5(PO_4)_3OH$) and whitlockite ($Ca_2(PO_4)_3$) and remaining 30–40% proteinaceous material (10). To extract proteins from the solid inorganic phase, CA samples need to be subjected to the following procedures:

1. Wash the CA bodies three times with undiluted ethanol (or methanol) to remove the remaining attached tissues and external contaminations.
2. Incubate the washed CA in undiluted ethanol (or methanol) at 4°C overnight.
3. Ground the CA into a fine powder in a homogenizer (22).
4. Extract the protein content by one of the following extraction methods:
   (a) TE extraction:
   - Centrifuge the homogenized material at 15,000 × *g* in a mini-centrifuge (Eppendorf).
   - Resuspend the pellet 3–4 times in sterile TE buffer.

- Homogenize through a 21-gauge needle of a 2-ml syringe and centrifuge again (see Note 1).
- Collect and store all supernatants containing proteins at –20°C (see Note 2).

(b) Extraction with hot acetic acid:

- Add 0.5 ml of hot 1 M acetic acid to 20 mg grounded CA powder and boil for 5 min.
- Cool on ice and ultrasonicate for 1 min.
- Centrifuge at 23,000 × *g* for 15 min, separate the supernatant, and dissolve the pellet in 10% SDS buffer.
- Determine protein content in each fraction using the Pierce Micro BSA protein assay kit following the instruction manual (see Note 3).

(c) Extraction with hydrochloric acid (see Note 4):

- Resuspend the ground CA powder in 1.2 M HCl and incubated overnight at 4°C.
- Centrifuge at 17,500 × *g* for 20 min and collect the supernatant (extract a).
- Resuspend the pellet in 0.1 M Tris, 6 M guanidine hydrochloride, pH 7.4 and incubate for 72 h at 4°C.
- Centrifuge at 17,500 × *g* for 20 min and collect the supernatant (extract b).
- Incubate the pellet for 72 h at 4°C in 0.1 M Tris pH 7.4 containing 6 M guanidine hydrochloride and 0.5 M EDTA for 72 h at 4°C.
- Centrifuge at 17,500 × *g* for 20 min and collect the supernatant (extract c).
- Incubate the remaining pellet in 6 M HCl for 24 h at 4°C.
- Centrifuge at 17,500 × *g* for 20 min and collect the supernatant (extract d).
- Quantify the protein content in extracts (a–d) using the Pierce Micro BSA protein assay kit (Pierce) (see Note 5).

3.2. Identification of Proteins in CA Extracts

The protein composition of CA extract can be analyzed using liquid chromatography coupled with electrospray ionization mass spectrometry, conventional gel electrophoresis, and western blot procedures (10).

3.2.1. Liquid Chromatography Coupled with Electrospray Ionization Mass Spectrometry

1. Dissolve CA extracts in 0.2 M NH_4HCO_3, 15 mM DTT and incubate them at 95°C for 15 min.
2. After cooling to room temperature, mix with 8 M urea and incubate for 1 h.

3. Add iodoacetamide to 80 mM final concentration and incubate at 37°C for 30 min in darkness for alkylation.
4. Reduce urea concentration to 0.8 M by diluting with 0.2 M NH_4HCO_3 and add trypsin at 1:40 enzyme-to-substrate ratio.
5. Perform the tryptic digestion overnight at 37°C and stop the reaction with formic acid (0.5% final concentration).
6. Lyophilize the resulting peptides and resuspend in 1% TFA.
7. Desalt the solution using a Poros 50 reverse-phase R2 material (PerSeptive Biosystems) prepared in a GELoader tip (Eppendorf) using 80% acetonitrile with 0.1% TFA as eluent (23).
8. Lyophilize and resuspended in 0.1% formic acid.
9. Subject the tryptic peptides to a reversed-phase ultra-performance nanoACQUITY UPLC™ system (Waters) (see Note 6).
10. Subject the samples eluted from the trap column to a C18 analytical column (75 μm × 100 mm, 1.7 μm) at 600 nl/min flow speed, using 0.1% formic acid as a solvent A and 0.1% formic acid in acetonitrile as a solvent B in a gradient (see Note 7).
11. Spray the eluted analytes into a Q-Tof Ultima™ mass spectrometer (Waters) with the capillary voltage set to 2.6 kV and cone voltage to 40 V.
12. Perform mass-spectrometry calibration and acquisition of MS/MS spectra (see Note 8).
13. Use ice-cold TE buffer and 0.2 M NH_4HCO_3, 15 mM DTT buffer for dissolving CA material as negative controls and subject them to the same procedures as the CA samples to exclude the general background level of contaminations.
14. Identify proteins by using human sequence library in the International Protein Index (IPI) database (IPI_human_20080409, 72,340 sequences) (see Note 9).

3.2.2. Gel Electrophoresis and Western Blotting

1. Perform gel electrophoresis of CA extracts under reducing conditions by using SDS-PAGE 8–25% gradient gels using 15–20 μg protein per well, including pre-stained molecular weight standards in each run and using silver staining for visualization.
2. For the western blotting, electrotransfer proteins to a nitrocellulose membrane using a Phast-system equipment (GE Healthcare).
3. Block membranes with 5% non-fat milk in TBS-T, at 37°C for 1 h, and then wash three times for 5 min each in TBS-T.
4. Incubated with primary antibodies (rabbit polyclonal anti-human S100A8 and anti-human S100A9 antibodies) overnight at 4°C, prepared in TBS-T containing 5% non-fat milk at the recommended dilution.

5. After three washes of 5 min each with TBS-T, incubate for 1 h at 37°C with anti-rabbit IgG at 1:5,000 dilutions in 5% non-fat milk in TBS-T.
6. Wash three times with TBS-T for 15 min each, and detect immunoreactive proteins by using the enhanced chemiluminescence kit (GE Healthcare, Sweden).

In all CA specimens S100A8, S100A9 and human serum albumin are the major components. Serum albumin can be picked up as a contamination from dried sera stuck to CA bodies and it can remain on CA surface even after washing with ethanol. Several auxiliary and bacterial proteins are also identified, but these proteins vary substantially from patient to patient. Their quantities are also too low to be detected by subsequent gel electrophoresis with silver staining and they are identified only by electrospray ionization mass spectrometry. Strikingly, the gel electrophoresis and western blot analysis indicate that the S100A8 and S100A9 proteins are found not only in monomeric or dimeric forms, which occur naturally in the body, but also as aggregated species of high molecular weight, which remained trapped in the wells of the stacking gels. These species are stained by S100A8, S100A9, and anti-fibrillar antibodies suggesting amyloid features. It must be noted that the high molecular weight species do not interact with anti-serum albumin antibodies excluding its involvement in the CA amyloid.

3.3. Immunohistochemical Analysis of CA and Surrounding Tissues

Archival prostate samples containing intact CA inclusions together with their surrounding tissues can be subjected to immunohistochemical analysis by the following procedures common for paraffin-embedded tissue sections:

1. De-wax the sections in Xylene for 20 min.
2. Rehydrate the tissues gradually by immersing the slides per 2 min in 99, 70, 30% ethanol.
3. Rinse in PBS for 5 min.
4. Retrieve antigens by incubating the sections in 98°C preheated 10 mM Tris and 1 mM EDTA buffer containing 0.05% Tween, pH 9.0 for 20–40 min.
5. Cool the slides to room temperature and rinse with PBS for 5 min.
6. Treat with 3% H_2O_2 for 10 min to quench endogenous peroxidase activities and wash twice with PBS for 3 min.
7. Block non-specific protein immunoreactivity by incubating sections for 20 min in 2.5% normal horse serum (NHS).
8. Incubate the tissues with primary antibodies (S100A8 (Calgranulin A) or S100A9 (Calgranulin B) rabbit polyclonal antibodies at 1:100, and amyloid fibril-specific antibodies at 1:1,000 in NHS during 1 hour at room temperature) (see Note 10).

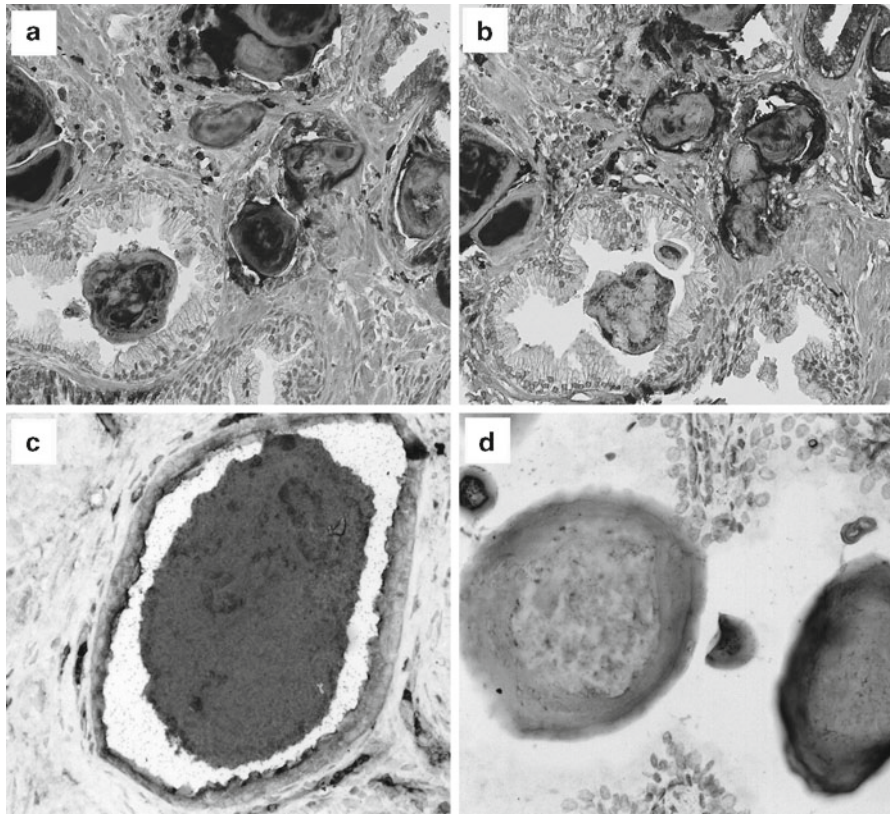

Fig. 2. Immunohistochemistry of CA and surrounding tissues with anti-S100A8 (**a**) and anti-S100A9 (**b**) antibodies, CA co-immunostaining with anti-S100A8 (*darker shade*) and anti-S100A9 (*lighter shade*) antibodies (**c**); CA immunostaining by anti-fibrillar antibodies. Magnification was ×80 in (**a**, **b**), ×100 in (**c**), and ×200 in (**d**).

9. Wash the slides for 5 min in PBS and incubate sections for 30 min with anti-rabbit IgG reagent. (ImmPRESS, Vector Labs).
10. Wash slides for 5 min in PBS and incubate the sections in peroxidase substrate solution (if you use Vector VIP or DAB follow the producers instructions to prepare the working solution) until visible colour is developed usually 2–15 min.
11. Rinse for 5 min in PBS.
12. Counterstain the sections with appropriate dye compatible with your peroxidase substrate (here we stained with Vector methyl green for 5 min).
13. Wash slides in deionized water for 1 min and dehydrate the slides by immersing in 99% ethanol ten times (see Note 11).
14. Immerse five times in xylene and dry at room temperature.
15. Mount the slides (as with permanent-mounting medium PERTEX, HistoLab).
16. Observe under the microscope.

All CAs are stained with S100A8 and S100A9 antibodies as well as amyloid fibril-specific antibodies (Fig. 2).

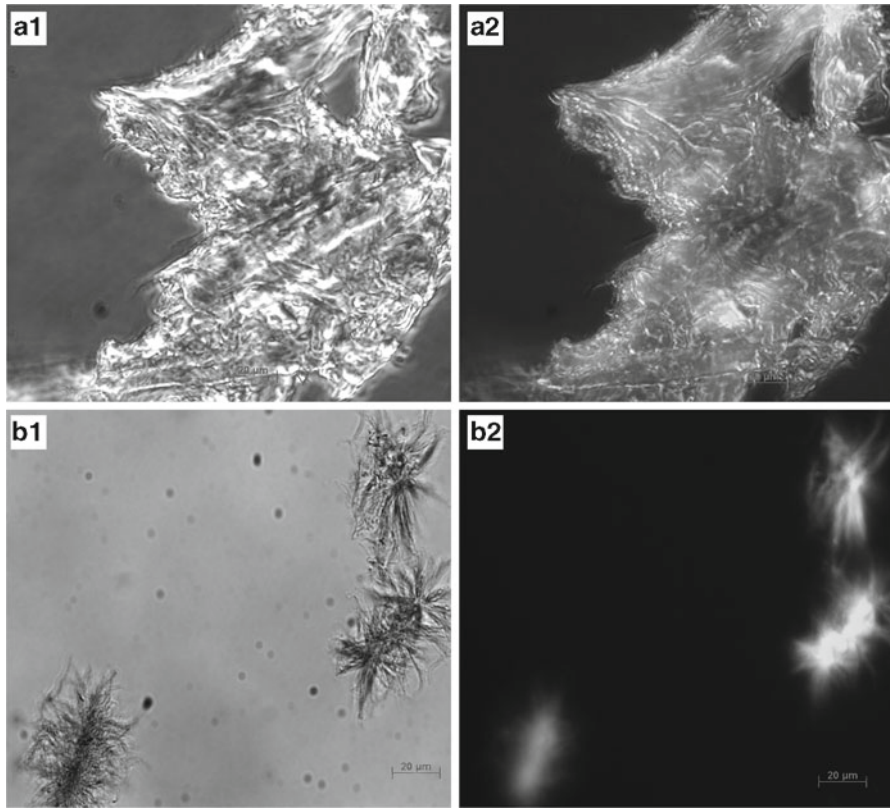

Fig. 3. ThT staining of CA extracts. Optical bright field images (**a1**, **b1**) and related fluorescence images, showing intensive ThT fluorescence (**a2**, **b2**). Scale bar is 20 µm. All extracted CA are characterized by bright ThT fluorescence indicating the presence of amyloids in their bulk mass. Together with unstructured calcified deposits there are also super-molecular filamentous structures of micron scale intensively stained. Similarly, in solutions the S100A8 and S100A9 amyloids extracted from CA and produced in vitro display significant increase of ThT fluorescence compared to free dye, indicative of ThT binding to cross-β-sheet containing structures.

In the normal tissues adjacent to CA inclusions, some areas of glandular epithelial and tissue macrophages infiltrating inflamed glands are also stained with anti-S100A8 and anti-S100A9 antibodies indicating surrounding inflammation (Fig. 2a, b).

3.4. ThT Staining of CA Amyloids

Visualization of amyloids in CA inclusions can also be performed using the following ThT staining:

1. Add 0.5 ml aliquots of 50 µM ThT in 10 mM K_2HPO_4, 150 mM NaCl, pH 7.4 to 60 µg of protein extracts from CA.
2. Place the samples in any suitable optical dish/plate (e.g., 24-well plates).
3. Examine the samples under a fluorescent microscope obtaining both the phase contrast and the fluorescence image (Fig. 3).

3.5. In Vitro Production of S100A8/A9 Amyloids

To validate the capacity of S100A8/A9 proteins to form the amyloid in the ageing prostate and determine the conditions provoking it, development of in vitro model systems is critical. Here we describe two conditions that cause fibrillation of S100A8/A9.

1. Incubate S100A8/A9, either recombinant of isolated from granulocytes, at 2–4 mg/ml concentrations in either:
   (a) 50 mM HCl, pH 2.0, 57°C without agitation (see Note 12).
   (b) 20 mM Tris, 1 mM DTT, pH 7.2, or 20 mM HEPES, 140 mM NaCl, pH 7.4, 37°C with agitation.
2. As CA deposits are calcified and contain an elevated zinc level (10), it is very important to probe their effect on S100A8/A9 fibrillation and then:
   (a) Add 1 mg/ml powdered $Ca_3(PO_4)_2$ or 10 mM $ZnCl_2$ in the incubation buffer to enhance the amyloid formation (compare these structures with those without additives).
   (b) Use as a control a buffer containing 50 mM EDTA (where the amyloid will not be produced).
3. Follow fibrillation by ThT-binding assay and AFM examination in aliquots removed following regular intervals (e.g., every 24 h) within 1–2 weeks (Fig. 4, Note 13).

4. Notes

1. Only sterile needles and syringes are used during the extraction procedures.
2. By this method, we can extract, however, only a portion of the total proteins incorporated in CA and located closer to its surface.
3. This extraction method yields about the same amount of proteins in both fractions, reflecting the extraction of both high and low MW aggregated forms.
4. This method is known as the sequential protein extraction method and was developed by Jiang X. and co-workers (24) for efficient protein extraction from bone tissue. Similar to bones, prostate CAs are also solid, highly mineralized bodies and this method can be most efficient as many protein extraction methods applicable for soft tissues and cells may not extract all the proteins from hard tissues.
5. Proteins are present in all extracts, reflecting the sequential decalcification of the CA and the heterogeneity of the proteinaceous aggregates. The total amount of protein obtained

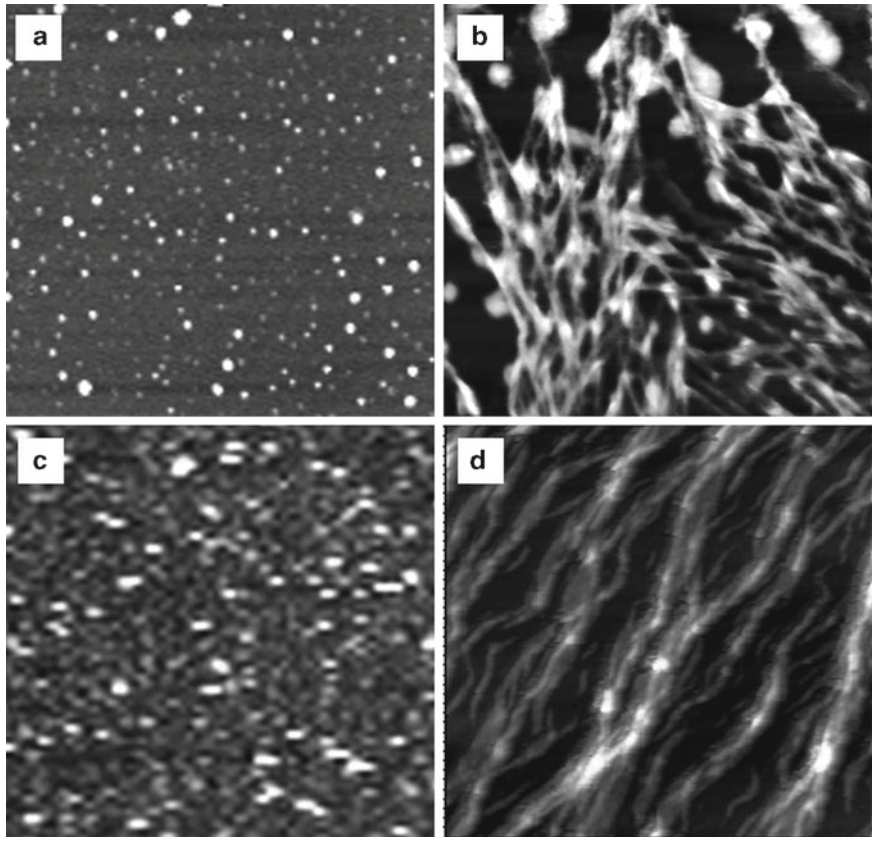

Fig. 4. AFM images of S100A8/A9 amyloid oligomers and fibrils extracted from CA (**a**, **b**) and produced in vitro (**c**, **d**), respectively. Size of images is 4 × 4 μm. Both CA extracts and the S100A8/A9 samples incubated in vitro yield typical oligomeric species of 2–3 nm in height some of which are engaged into chain-like sequences. Extensive networks of fibrillar species of 4–8 nm height and several microns length are observed in CA extracts (**b**) and even thicker bundles of 15–20 nm height are produced at pH 7.4 in vitro (**d**).

using this method is ten-fold higher than by acetic acid extraction. However be aware of the presence of acid or guanidine hydrochloride in the final solutions, which need to be dialyzed further and can potentially affect the initial aggregated state of the proteinaceous material.

6. Each peptide sample is concentrated in a C18 trap column with symmetry of 180 μm × 20 mm, 5 μm and washed with 5% acetonitrile and 0.1% formic acid at 15 μl/min speed for 1 min.
7. The following gradients can be applied: linear from 0 to 40% B in 25 min, linear from 40 to 80% B in 1 min, isocratic at 80% B in 1 min, linear from 80 to 5% B in 1 min and isocratic at 5% B for 7 min.
8. The instrument should be calibrated using MS/MS fragments of GluFib peptide (Sigma Aldrich) and performed the samples

offset calibration as described previously (25). The acquisition of MS/MS spectra is performed with an automated data-directed switching between the MS and MS/MS modes using the instrument software (MassLynx V4.0 SP4). The three most abundant signals of a survey scan (400–1,300 m/z range, 0.87 s scan time and 0.13 s inter-delay) are selected by charge state, and collision energy was applied accordingly for sequential MS/MS fragmentation scanning (50–2,000 m/z range, 0.9 s scan time, 0.1 s inter-delay). ProteinLynx Global Server software (V2.2.5) is used to convert raw data to peak lists for database searching.

9. Proteins were identified by a local version of Mascot search program V2.1.04 and Mascot Daemon application V2.1.6 (Matrix Science Limited, http://www.matrixscience.com). The following settings were used for the database search: trypsin-specific digestion with one missed cleavage allowed, carbamidomethylated cysteine set as fixed modification, oxidized methionine and deamidation in variable mode, peptide tolerance of 60 ppm, and fragment tolerance of 0.1 Da. Peptides with Mascot ion scores exceeding the threshold for statistical significance of $p<0.05$ were selected and also re-processed manually to validate their significance.
10. Negative controls are performed by removing or substituting the primary antibodies with arbitrary antibody to proteins not involved in CA.
11. This and the following steps are suitable for permanent mounting of the slides with alcohol-based mounting mediums (non-aqueous). The whole staining procedure can be modified by choosing another set of compatible peroxidase substrate-counterstain-mounting medium (e.g., in this case of AEC–haematoxylin-aqueous mounting, the slides should not be dehydrated before mounting).
12. The amyloids are self-assembled by the incubation of S100A8/A9 complexes purified from both granulocytes and recombinant protein produced in *E. coli*.
13. Amyloid formation is a concentration-dependent process and by increasing protein concentration you may reduce the incubation period.

Acknowledgments

The research of LMR and ALG were supported by the Swedish Medical Research Council, Insamlingsstiftelsen and Kempe Foundation. The research of DR was supported by EU FP7-PEOPLE-2007-1-1-ITN,PITN-GA-2008-215148.

References

1. Moore, B.W. (1965) A soluble protein characteristics of nervous system. Biochem Biophys Res Commun **19**, 739–744.
2. Fritz, G., Botelho, H.M., Morozova-Roche, L.A., and Gomes, C.M. (2010) Natural and amyloid self-assembly of S100 proteins: structural basis of functional diversity. FEBS *J* **277**, 4578–4590.
3. Foell, D., Frosch, M., Sorg, C., and Roth, J. (2004) Phagocyte-specific calcium-binding S100 proteins as clinical laboratory markers of inflammation. Clin Chim Acta **344**, 37–51.
4. Foell, D., Wittkowski, H., Vogl, T., and Roth, J. (2007) S100 proteins expressed in phagocytes: a novel group of damage-associated molecular pattern molecules. J Leukoc Biol **81**, 28–37.
5. Vogl, T., Tenbrock, K., Ludwig, S., Leukert, N., Ehrhardt, C., van Zoelen, M.A., Nacken, W., Foell, D., van der Poll, T., Sorg, C., and Roth, J. (2007) Mrp8 and Mrp14 are endogenous activators of Toll-like receptor 4, promoting lethal, endotoxin-induced shock. Nat Med **13**, 1042–1049.
6. Ott, H.W., Lindner, H., Sarg, B., Mueller-Holzner, E., Abendstein, B., Bergant, A., Fessler, S., Schwaerzler, P., Zeimet, A., Marth, C., and Illmensee, K. (2003) Calgranulins in cystic fluid and serum from patients with ovarian carcinomas. Cancer Res **63**, 7507–7514.
7. Nacken, W., Roth, J., Sorg, C., and Kerkhoff, C. (2003) S100A9/S100A8: Myeloid representatives of the S100 protein family as prominent players in innate immunity. Microsc Res Tech **60**, 569–580.
8. Sunahori, K., Yamamura, M., Yamana, J., Takasugi, K., Kawashima, M., Yamamoto, H., Chazin, W.J., Nakatani, Y., Yui, S., and Makino, H. (2006) The S100A8/A9 heterodimer amplifies proinflammatory cytokine production by macrophages via activation of nuclear factor kappa B and p38 mitogen-activated protein kinase in rheumatoid arthritis. Arthritis Res Ther **8**:R69.
9. Hermani, A., De Servi, B., Medunjanin, S., Tessier, P.A., and Mayer, D. (2006) S100A8 and S100A9 activate MAP kinase and NF-kappaB signaling pathways and trigger translocation of RAGE in human prostate cancer cells. Exp Cell Res **312**, 184–197.
10. Yanamandra, K., Alexeyev, O., Zamotin, V., Srivastava, V., Shchukarev, A., Brorsson, A.C., Tartaglia, G.G., Vogl, T., Kayed, R., Wingsle, G., Olsson, J., Dobson, C.M., Bergh, A., Elgh, F., and Morozova-Roche, L.A. (2009) Amyloid formation by the pro-inflammatory S100A8/A9 proteins in the ageing prostate. PLoS One **4** (5):e5562.
11. Untergasser, G., Madersbacher, S., and Berger, P. (2005) Benign prostatic hyperplasia: age-related tissue-remodeling. Exp Gerontol **40,** 121–128.
12. De Marzo, A.M., Platz, E.A., Sutcliffe, S., Xu, J., Gronberg, H., Drake, C.G., Nakai, Y., Isaacs, W.B., and Nelson, W.G. (2007) Inflammation in prostate carcinogenesis. Nat Rev Cancer **7**, 256–269.
13. Varenhorst, E., Garmo, H., Holmberg, L., Adolfsson, J., Damber, J.E., Hellstrom, M., Hugosson, J., Lundgren, R., Stattin, P., Tornblom, M., and Johansson, J.E. (2005) The National Prostate Cancer Register in Sweden 1998–2002: trends in incidence, treatment and survival. Scand J Urol Nephrol **39,** 117–123.
14. Adolfsson, J., Garmo, H., Varenhorst, E., Ahlgren, G., Ahlstrand, C., Andren, O., Bill-Axelson, A., Bratt, O., Damber, J.E., Hellstrom, K., Hellstrom, M., Holmberg, E., Holmberg, L., Hugosson, J., Johansson, J.E., Petterson, B., Tornblom, M., Widmark, A., and Stattin, P. (2007) Clinical characteristics and primary treatment of prostate cancer in Sweden between 1996 and 2005. Scand J Urol Nephrol **41**, 456–477.
15. Coussens, L.M., and Werb, Z. (2002) Inflammation and cancer. Nature **420**, 860–867.
16. Christian, J.D., Lamm, T.C., Morrow, J.F., and Bostwick, D.G. (2005) Corpora amylacea in adenocarcinoma of the prostate: incidence and histology within needle core biopsies. Mod Pathol **18**, 36–39.
17. Rocken, C., Linke, R.P., and Saeger, W. (1996) Corpora amylacea in the lung, prostate and uterus. A comparative and immunohistochemical study. Pathol Res Pract **192**, 998–1006.
18. Shintaku, M. (2005) Corpora amylacea in a mature cystic teratoma of the ovary. Neuropathology **25**, 175–176.
19. Kayed, R., Head, E., Sarsoza, F., Saing, T., Cotman, C.W., Necula, M., Margol, L., Wu, J., Breydo, L., Thompson, J.L., Rasool, S., Gurlo, T., Butler, P., and Glabe, C.G. (2007) Fibril specific, conformation dependent antibodies recognize a generic epitope common to amyloid fibrils and fibrillar oligomers that is absent in prefibrillar oligomers. Mol Neurodegener **2**, 18.
20. van den Bos, C., Rammes, A., Vogl, T., Boynton, R., Zaia, J., Sorg, C., and Roth J.

(1998) Copurification of P6, MRP8, and MRP14 from human granulocytes and separation of individual proteins. Protein Expr Purif **13**, 313–318.

21. Vogl, T., Leukert, N., Barczyk, K., Strupat, K., and Roth, J. (2006) Biophysical characterization of S100A8 and S100A9 in the absence and presence of bivalent cations. Biochim Biophys Acta **1763**, 1298–1306.
22. Nelson, S.R., Lyon, M., Gallagher, J.T., Johnson, E.A., and Pepys, M.B. (1991) Isolation and characterization of the integral glycosaminoglycan constituents of human amyloid A and monoclonal light-chain amyloid fibrils. Biochem J **275**, 67–73.
23. Thingholm, T.E., Jorgensen, T.J.D., Jensen, O.N., and Larsen, M.R. (2006) Highly selective enrichment of phosphorylated peptides using titanium dioxide. Nat Protocols **1**, 1929–1935.
24. Jiang, X., Ye, M., Liu, G., Feng S., Cui, L., and Zou, H. (2007) Method development of efficient protein extraction in bone tissue for proteome analysis. J Proteome Res **6**, 2287–2294.
25. Bäckström, S., Elfving, N., Nilsson, R., Wingsle, G., and Björklund, S. (2007) Purification of a Plant Mediator from Arabidopsis thaliana Identifies PFT1 as the Med25 Subunit. Molecular Cell **26**, 717–729.

Chapter 27

Isolation of Amyloid by Solubilization in Water

Dadi Th. Vilhjalmsson, Indiana E. Ingolfsdottir, and Finnbogi R. Thormodsson

Abstract

Amyloid fibrils are highly insoluble in neutral aqueous media of regular ionic strengths making solubilization a difficult task that normally calls for extremely harsh treatment. This is among the reasons for the routine employment of synthetic proteins in amyloid research, where the amylogenic components are needed.

Here we describe a process for solubilizing amyloid in pure water that we adopted from a method developed by Mordechai Pras and associates. We have used it for solubilizing cystatin C amyloid and extracting it out of leptomeningeal tissue and skin from Hereditary Cerebral Hemorrhage with Amyloidosis-Icelandic type (HCHWA-I) patients. HCHWA-I is a rare and very aggressive heritable form of cerebral amyloid angiopathy (CAA)-specific Icelandic type. Similar approach has been employed for solubilization of different forms of amyloid from other organs suggesting broad range of applicability.

Key words: Amyloid, Cell culture, Human, Cystatin C, Human umbilical vascular endothelial cells, Vascular smooth muscle cells, Umbilical cord, Cerebral amyloid angiopathy, HCHWA-I, Immunostaining, Leptomeninges, Cerebral blood vessels

1. Introduction

Although different amyloids consist of dissimilar segments of proteins, all are congophilic and have a characteristic homogeneous and amorphous appearance that stains pink with hematoxylin–eosin, when observed under the microscope. This appearance is, however, vastly misleading since it is a fibrous protein consisting of insoluble fibrils that resist proteolytic digestion (1). Solubilizing amyloid fibrils normally requires harsh treatment since they are highly insoluble in neutral aqueous media of ionic strengths commonly used (2). Consequently, most studies on the mechanisms by which amyloidogenic proteins assemble and may form neurotoxic species have relied on synthetic proteins (3).

Einar M. Sigurdsson et al. (eds.), *Amyloid Proteins: Methods and Protocols*, Methods in Molecular Biology, vol. 849,
DOI 10.1007/978-1-61779-551-0_27,

We have adopted the method developed by Pras and associates to extract amyloid proteins by solubilization in pure water (2). The components of cystatin C amyloid from patients with Hereditary Cerebral Hemorrhage with Amyloidosis-Icelandic type (HCHWA-I) were isolated and used for studying their self-assembly and cytotoxicity (4). This condition, also known as Hereditary Cystatin C Amyloid Angiopathy (HCCAA), is a rare and very aggressive heritable form of cerebral amyloid angiopathy (CAA) specific for Iceland, which displays massive amyloid accumulation into the vasculature of the central nervous system and subsequent intracerebral hemorrhage early in life (5, 6). The amyloid in HCHWA-I is constructed of a truncated L68Q variant of the protease inhibitor cystatin C (7, 8).

Here, we describe the method of solubilizing amyloid in pure water as we use it for extracting leptomeningeal cystatin C amyloid. We have also used this method for extracting cystatin C amyloid from skin; and the solubilizations of different amyloid from other organs have previously been reported by others (9, 10), implying that this method can be applied to most amyloid-laden tissues.

2. Materials

2.1. Special Equipment and Supplies

1. Autoclave.
2. High-speed tissue homogenizer (see Note 1).
3. Stainless steel 8–10-mm probe for the homogenizer.
4. High-speed centrifuge (Sorvall RC5Cplus) with a fixed angle rotor (Sorvall SS-34) or equivalent.
5. 50-mL high-speed polypropylene centrifuge tubes w/screw caps (Nalgene 3119-0050).
6. Ultracentrifuge (Beckman L7-55) with Beckman 50.2 Ti rotor or equivalent.
7. 26.3-mL polycarbonate centrifuge tubes w/cap assembly (Beckman #355618).
8. Freeze drier.
9. Autoclaved fine instruments (forceps and fine scissors).
10. Disposable sterile scalpel.
11. Disposable sterile 50-mL centrifuge tubes.
12. Disposable 90-mm plastic culture dishes.
13. Hypodermic needle 20 G×1.5″.
14. Ice tray and ice bucket.
15. SDS-PAGE equipment.
16. Western blotting equipment.

2.2. Reagents

1. Complete protease inhibitor cocktails (Roch Applied Sciences # 11-697-498-001).
2. Extraction solution (150 mM NaCl): Dissolve 8.8 g NaCl in 1 L of ddH_2O. Sterilize by autoclaving or filtration. Make fresh each time.
3. Ultrapure water.
4. Bradford protein assay kit II (Bio-Rad # 500-0002).
5. Reagents for SDS-PAGE.
6. SilverXpress® Silver Staining Kit (Invitrogen # LC6100).
7. Nitrocellulose membrane (Bio-Rad).
8. Transfer buffer for Western blotting (2 L): 28.8 g glycine; 6.04 g Tris base; 200 mL methanol; 1.6 L ddH2O.
9. Appropriate primary antibody (see Note 2).
10. Horseradish peroxidase-linked secondary antibody.
11. Amersham ECL Plus™ Western Blotting Detection reagents (GE Healthcare # RPN2132).
12. Amersham Hyperfilm ECL (GE Healthcare # 28-9068).

3. Methods

The amyloid proteins were extracted from homogenized leptomeninges by solublilization in ultrapure water. The method is adapted from the procedure developed by Mordechai Pras and others for extracting amyloid from the spleen of patient with primary amyoidosis (2) and from liver and spleen of patients with familial Mediterranean fever (FMF) (9). We have successfully extracted solubilized cystatin C amyloid from HCHWA-I leptomeningens and skin (4).

3.1. Extraction of Cystatin C Amyloid

Our starting material was unfixed HCHWA-I brain section obtained at autopsy and kept frozen at –80°C. After thawing the leptomeninges were stripped off and homogenized at high-speed in salt water and washed a few times to remove all saline-soluble material. The rinsed tissue pellet was subsequently homogenized at high-speed in ultrapure water and spun down by high-speed centrifugation to remove all traces of salt. Subsequent washes by ultrapure water and high-speed centrifugation produced supernatants containing the extracted amyloid proteins (see Fig. 1–3). Finally, the water-extracted amyloid proteins were freeze-dried, making sure that absolutely no moister was left in the material.

3.1.1. Preparing the Tissue

1. In advance, prepare 1 L of the saline washing solution, sterilize and keep it ice-cold.
2. Autoclave instruments (forceps and fine scissors).

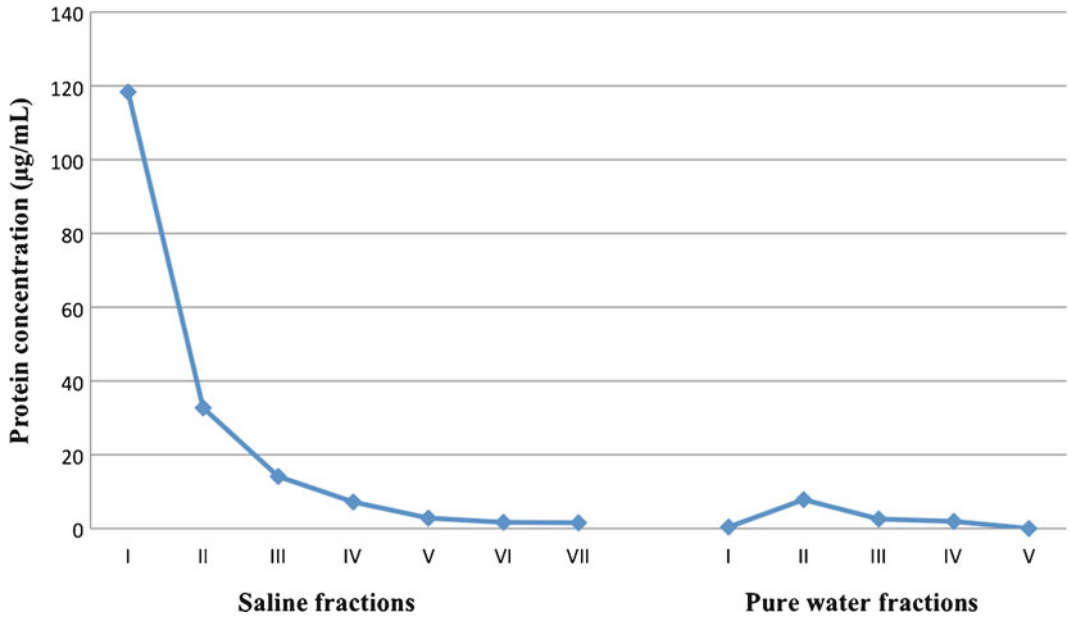

Fig. 1. The figure depicts clearly that most of the saline-soluble proteins were rinsed out in the first few washes. By the fifth wash, the protein concentration was already less than 3 µg/mL. With two more washes, it was safe to conclude that an insignificant amount of saline-soluble proteins remain in the tissue pellet. The first ultrapure water fraction contained no detectable proteins. This is attributed to salt being washed out of the tissue sample. The second fraction showed a protein concentration of 7.8 µg/mL and then a steady declining of protein concentration in the succeeding fractions. By the fourth water fraction protein concentration had fallen below 2 µg/mL and by the fifth fraction the protein concentration was below the level of detection.

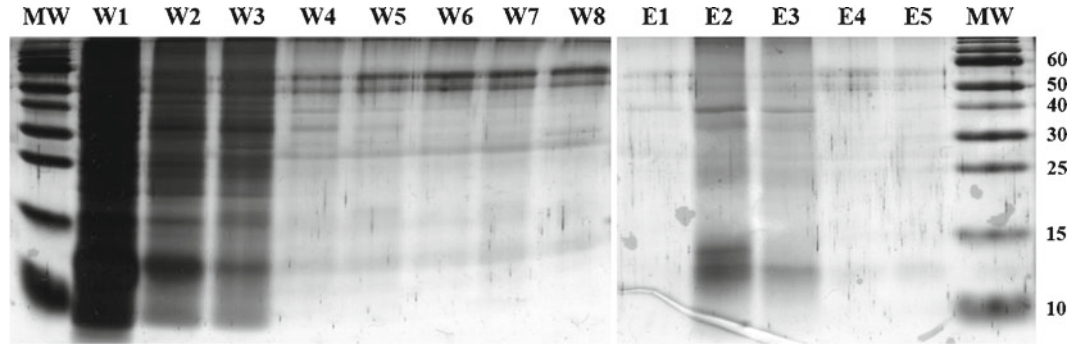

Fig. 2. The silver-stained gel demonstrates decreasing amount of protein in each successive saline wash (*W1–W8*). Silver staining of the first ultrapure water fraction (*E1*) shows no proteins as the salt is washed out of the tissue pellet. In subsequent extractions steps (*E2–E5*), a prominent protein band corresponding to the molecular weight of cystatin C monomer (about 13 kDa) is identified with a ladder of bands above matching cystatin C oligomers.

3. If extracting the amyloid from frozen tissue, it should be taken out of the freezer to thaw well in advance, overnight for large sections.
4. Add one tablet of complete protease inhibitor cocktail to 50 mL of the saline washing solution.

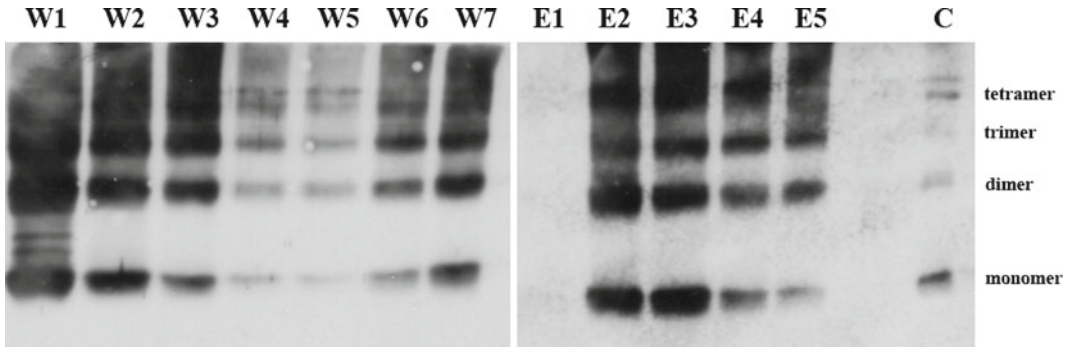

Fig. 3. Western blotting corresponding to silver-stained gels in Fig. 2. There is considerable immunostaining for cystatin C in the saltwater fractions. This is partly due to soluble cystatin C present in the brain; however, the presence of highly abundant oligomeric forms suggests that cystatin C deposits in the cerebral vasculature are the major source. Immunostaining of the pure water fractions confirmed that all the protein bands detected by silver staining are also immunostained for cystatin C.

5. When the tissue has thawed adequately, but not warmed up, place it in a disposable plastic Petri dish arranged on crushed ice.
6. Use the forceps; fine scissors or sterile scalpel to strip away the leptomeninges from the brain slice or dissect away the amyloid rich portion if other tissue is used.
7. Place the tissue in a 50-mL centrifuge tube with 2 mL of ice-cold saline washing solution with protease inhibitors.

3.1.2. Extraction

1. Place the tube in an ice bucket under the high-speed homogenizer.
2. Homogenize the tissue at high-speed on ice for 2 min.
3. Add 18 mL of ice-cold saline washing solution with protease inhibitors.
4. Homogenize the tissue at high-speed on ice for 2.5 min.
5. Centrifuge the homogenate at 10,000 × *g* for half an hour.
6. Decant the supernatant from the tube, keep an aliquot for monitoring the washing progress, and discard the rest.
7. Resuspend the pellet in another 20 mL of the ice-cold saline washing solution.
8. Repeat steps 4–6, until no protein is detectable in the discarded supernatant, or at least eight times.
9. In the final washing step the pellet is resuspended in ice-cold ultrapure water, instead of the saline washing solution.
10. The suspension is transferred to high-speed centrifuge tube.
11. Homogenize the tissue pellet at high-speed for 2.5 min on ice.

12. Centrifuge the homogenate at 100,000 × *g* in an ultra high-speed centrifuge for 1 h.
13. The supernatant containing the salts from the tissue pellet is discarded.
14. Resuspend the pellet in another 20 mL of the ice-cold ultrapure water and homogenize at high-speed for 2 min on ice.
15. Centrifuge the homogenate at 100,000 × *g* in an ultra high-speed centrifuge for 1 h.
16. Take an aliquot from the supernatant for analysis and freeze the rest at −80°C in 50-mL disposable centrifuge tubes.
17. Repeat steps 14–16 for as many times as needed to extract the amyloid from the tissue pellet. In our experience, the bulk of the solubilized amyloid comes out within the first three extractions (see Fig. 1–3).

3.1.3. Freeze-Drying

The tubes containing the frozen supernatant are taken out from the freezer and about ten holes poked on the lid with a sturdy needle. Filter paper cut to fit, is placed inside the lid. Place the tubes in the freeze-dryer flask making sure that the content stays frozen solid. Connect the flask to the instrument and freeze-dry for several days. It is imperative that the drying process is carried out to its conclusion and no moisture left in the sample. The dried amyloid extract is kept frozen at −80°C in a sealed freezer bag with most of the air expelled (see Note 3). Best if used within days of extraction.

3.2. Characterization of the Extracted Aliquots

Protein concentration in each fraction was evaluated by the assay described by Bradford (11). This assay is based on the absorbance change that takes place when the dye Coomassie Brilliant Blue G-250 shift color from red to blue upon binding to proteins under acidic conditions. The assay is linear over the range of 2–120 μg/mL.

We use the Bradford assay kit from Bio-Rad and follow the instructions provided.

SDS-PAGE (polyacrylamide gel electrophoresis) was done according to Laemmli (12) using 12.5% acrylamide gels. The gels were loaded with 15 μL of each fraction and 15 μL of a 2× sample buffer heated to 95°C for 5 min. Gels were silver stained using the SilverXpress® Silver Staining Kit according to manufactures instructions.

Western blotting was performed according to Towbin et al. (13). The proteins were transferred from the gel to a nitrocellulose membrane at 400 mA for 45 min. The blot was immunostained with appropriately diluted antibody of interest and Horseradish peroxidase-labeled secondary antibody. Immunostaining was developed with ECL Plus Western Blotting Detection reagent according to the manufacturer's protocol.

4. Notes

1. For most tissues, high-speed tissue homogenizer is quite adequate. However, when we processed skin from HCHWA-I patients, we resorted to pulverizing samples that were quick frozen in liquid nitrogen. Specific instruments are available for this purpose.
2. The primary antibody used depends on the protein being extracted. In our case, we used rabbit anti-cystatin C (Dako), diluted 1:400.
3. If the material is not completely dry, it will hasten aggregation of the proteins, making them unfit for most applications. This is also the reason why this material does not keep well and should be used freshly prepared.

Acknowledgments

We would like to thank The Icelandic Research Council and The Icelandic HCHWA-I Foundation (Heilavernd) for their support.

References

1. Kyle, R. A. (2001) Amyloidosis: a convoluted story. *Br. J. Haematol.* **114**, 529–538.
2. Pras, M., Schubert, M., Zucker-Franklin, D., Rimon, A., and Franklin, E. C. (1968) The characterization of soluble amyloid prepared in water. *J. Clin. Invest.* **47**, 924–933.
3. Bitan, G., and Teplow, D. B. (2005) Preparation of aggregate-free, low molecular weight amyloid-beta for assembly and toxicity assays. *Methods Mol Biol* **299**, 3–9.
4. Vilhjalmsson, D. T., Blondal, H., and Thormodsson, F. R. (2007) Solubilized cystatin C amyloid is cytotoxic to cultured human cerebrovascular smooth muscle cells., *Experimental and Molecular Pathology* **83**. 357–360.
5. Gudmundsson, G., Hallgrimsson, J., Jonasson, T. A., and Bjarnason, O. (1972) Hereditary cerebral hemorrhage with amyloidosis. *Brain* **95**, 387–404.
6. Bjarnadottir, M., Nilsson, C., Lindstrom, V., Westman, A., Davidsson, P., Thormodsson, F., Blondal, H., Gudmundsson, G., and Grubb, A. (2001) The cerebral hemorrhage-producing cystatin C variant (L68Q) in extracellular fluids. *Amyloid: Int. J. Exp. Clin. Invest.* **8**, 1–10.
7. Cohen, D. H., Feiner, H., Jensson, O., and Frangione, B. (1983) Amyloid fibril in hereditary cerebral hemorrhage with amyloidosis (HCHWA) is related to the gastroenteropancreatic neroendocrine protein, gamma trace. *J. Exp. Med.* **158**, 623–628.
8. Ghiso, J., Jensson, O., and Frangione, B. (1986) Amyloid fibrils in hereditary cerebral hemorrhage with amyloidosis of Icelandic type is a variant of gamma-trace basic protein cystatin C. *Proc. Natl. Acad. Sci. USA* **83**, 2974–2978.
9. Levin, M., Franklin, E. C., Frangione, B., and Pras, M. (1972) The amino acid sequence of a major nonimmunoglobulin component of some amyloid fibrils. *J. Clin. Invest.* **51**, 2773–2776.
10. Nelson, S. R., Lyon, M., Gallagher, J. T., Johnson, E. A., and Pepys, M. B. (1991) Isolation and characterization of the integral glycosaminoglycan constituents of human amyloid A and monoclonal light-chain amyloid fibrils. *Biochem. J.* **275**, 67–73.
11. Bradford, M. M. (1976) A rapid and sensitive method for the quantitation of microgram quantities of protein utilizing the principle of

protein-dye binding. *Anal. Biochem.* **72**, 248–254.

12. Laemmli, U. K. (1970) Cleavage of structural proteins during the assembly of the head of bacteriophage T4. *Nature* **227**, 680–685.
13. Towbin, H., Staehelin, T., and Gordon, J. (1992) Electrophoretic transfer of proteins from polyacrylamide gels to nitrocellulose sheets: procedure and some applications. 1979. *Biotechnology* **24**, 145–149.

Chapter 28

Histological Staining of Amyloid and Pre-amyloid Peptides and Proteins in Mouse Tissue

Hameetha B. Rajamohamedsait and Einar M. Sigurdsson

Abstract

The increased availability of transgenic mouse models for studying human diseases has shifted the focus of many laboratories from in vitro to in vivo assays. Herein, methods are described to allow investigators to obtain well-preserved mouse tissue to be stained with the standard histological dyes for amyloid, Congo Red, and Thioflavin S. These sections can as well be used for immunohistological procedures that allow detection of tissue amyloid and pre-amyloid, such as those composed of the amyloid-β peptide, the tau protein, and the islet amyloid polypeptide.

Key words: Mouse, Perfusion, Brain, Pancreas, Fixation, Histology, Congo red, Thioflavin S, Immunohistochemistry, Amyloid-β, Plaques, Tau, Tangles, Islet amyloid polypeptide

1. Introduction

Over the last couple of decades, numerous transgenic mouse models have been developed for Alzheimer's disease and other amyloid-related disorders. The increased availability of these models continues to shift the focus of many laboratories from in vitro and cell-based assays to animal models. Several tissue preparation methods, histological stains and immunohistochemical procedures can be used for amyloid and pre-amyloid detection, and have been described in varying details by others (1–10). Here, a combined protocol is provided (11–14), that focuses on these methods applied to fixed mouse tissue sections (brain and pancreas). First of all, appropriate tissue preservation is fundamental for any of the following steps; systematic sectioning and storage of tissue sections is as well important for subsequent analysis. Congo Red and Thioflavin S are the two major histological stains used to detect any

Einar M. Sigurdsson et al. (eds.), *Amyloid Proteins: Methods and Protocols*, Methods in Molecular Biology, vol. 849,
DOI 10.1007/978-1-61779-551-0_28,

form of amyloid. These dyes bind to the characteristic β-pleated sheet conformation of amyloid. Additionally, monoclonal mouse antibodies are increasingly employed to detect pre-amyloid and amyloid deposits and their use has led to the development of kits that reduce nonspecific binding of these antibodies to mouse tissue. Although these kits come with detailed protocols, the exact procedure often has to be adjusted depending on the tissue preparation, the antigen and the monoclonal antibodies. Interestingly, less costly reagents can provide similar or better results, at least for certain antibodies.

2. Materials

1. Sodium pentobarbital.
2. Surgical instruments: Scissors, various forceps, feeding needles for newborn mice or birds.
3. Perfusion pump with variable flow (Mini-Pump, Variable flow, Fisher Scientific, Morris Plains, NJ, #138761), with tubing (inner diameter: 0.38 mm).
4. 0.1 M sodium/potassium phosphate buffer, pH 7.4: Dissolve 4.03 g KH_2PO_4 monobasic and 10 g Na_2HPO_4 dibasic, anhydrous in distilled water, pH to 7.4 with dilute NaOH or HCl, fill to 1 L with distilled water.
5. Heparin (1,000 USP units/mL).
6. 4% paraformaldehyde in 0.1 M sodium/potassium phosphate buffer: Prepare 0.2 M sodium/potassium phosphate buffer (8.06 g of KH_2PO_4 monobasic and 20 g of Na_2HPO_4 dibasic, anhydrous dissolved in distilled water, pH to 7.4 and adjust volume to 1 L). A portion of this solution can be diluted to 0.1 M for use in mouse perfusions. The following steps should be performed in a chemical hood. (a) Weigh 40 g of prilled paraformaldehyde. (b) Heat 450 mL of distilled water to 55°C, remove from heat and add paraformaldehyde while stirring. (c) Add 10 N NaOH until the solution clears which occurs when the fixative dissolves (see Note 1). (d) Allow to cool to room temperature and then filter through Whatman #1 (see Note 2). Add water to 500 mL and then add equal volume of 0.2 M phosphate buffer to obtain 1 L of the fixative. Use freshly prepared and/or store refrigerated (see Note 3).
7. Conical tubes, 15 mL.
8. 20% glycerol/2% dimethylsulfoxide in 0.1 M sodium/potassium phosphate buffer, pH 7.4: Prepare buffer as listed above, then add 200 mL of glycerol and 20 mL of dimethylsulfoxide to a total volume of 1 L.

9. Single-edge razor blades No. 9.
10. Paraffin-embedding facility (for pancreatic tissue).
11. Water bath with a temperature controller for mounting paraffin-embedded sections.
12. Tissue Freezing Medium® for frozen tissue specimens.
13. Paint brushes, size 0 and 1.
14. 24-well tissue culture plates.
15. Ethylene glycol-based cryoprotectant: 30% sucrose, 30% ethylene glycol in 0.1 M sodium/potassium phosphate buffer, pH 7.4. Prepare the buffer as listed above, then add 300 g of sucrose and 300 mL of ethylene glycol to a total volume of 1 L.
16. Microscope slides (25 × 75 × 1.0 mm).
17. 95% ethanol: 1.0 M acetic acid (1:1).
18. Gelatin.
19. Chromium potassium sulfate.
20. 1% Congo Red solution in 50% ethanol: Stir 2.5 g of Congo Red into 250 mL of 50% ethanol.
21. 100% ethanol.
22. Xylene or CitriSolv® (Fisher Scientific).
23. Saturated lithium carbonate solution: Stir 2.6 g of lithium carbonate into 200 mL of distilled water.
24. Cell strainers 100 μm nylon, (Falcon, No. 352360, BD Biosciences, Bedford, MA) or equivalent.
25. Six-well culture dishes.
26. MOM® kit (Vector Laboratories, Burlingame, CA) or equivalent.
27. Citrate buffer (10 mM Citric Acid, 0.05 % Tween 20, pH 6.0): Dissolve 1.92 g of anhydrous citric acid and 0.5 mL of Tween 20 in 1,000 mL of distilled water.
28. 80% formic acid.
29. Vectastain ABC Elite kit to detect rabbit IgG primary antibodies (Vector) or equivalent.
30. Primary antibody diluent in phosphate-buffered saline for polyclonal antibodies: 2% Triton X-100, 0.1% sodium azide, 0.01% bacitracin, 2% bovine serum albumin, and 10% normal serum from the same species that the secondary antibody is raised in.
31. Phosphate-buffered saline: 0.01 M phosphate buffer, 0.0027 M potassium chloride, and 0.137 M sodium chloride (PBS tablets (Sigma, St. Louis, MO): dissolve one tablet in 200 mL of water).

32. 0.3% hydrogen peroxide in phosphate-buffered saline (for quenching) or in 0.2 M sodium acetate buffer (for reacting with diaminobenzidine tetrahydrochloride), made fresh from 30% solution.
33. Various antibodies against amyloid-β (Aβ), tau and islet amyloid polypeptide (IAPP).
34. 0.2 M sodium acetate buffer, pH 6.0, adjust pH with 1 M acetic acid.
35. Diaminobenzidine tetrahydrochloride.
36. Nickel ammonium sulfate.
37. Filter disks (0.45 μm).

3. Methods

The methods described below outline (1) a mouse perfusion technique and tissue sectioning (brain and pancreas), (2) preparation of gelatin-coated slides, (3) two amyloid histology procedures, and (4) an immunohistological method for staining of pre-amyloid and amyloid deposits in mouse tissue (Aβ, tau, and IAPP).

3.1. Mouse Perfusion and Tissue Sectioning

1. The mouse has to be deeply anesthetized by intraperitoneal injection of sodium pentobarbital (150 mg/kg).
2. The mouse is subsequently placed over a collection container on a tray or grid that will allow the perfusate to drain into the container (see Note 4).
3. The chest cavity is then exposed and the left ventricle is punctured with pointed forceps.
4. A perfusion cannula is then placed into the ventricle and held in place with hemostats or with forceps that can be secured with a paperclip (see Note 5). The right atrium is then cut and the perfusion pump started. Cutting the atrium allows the perfusate to exit the circulatory system (see Note 6).
5. The initial perfusion should be performed with a physiological solution such as 0.1 M sodium/potassium phosphate buffer or phosphate-buffered saline, pH 7.4.
6. Heparin (1 unit/g bodyweight) may be added to the perfusion solution to eliminate blood clotting (see Note 7). This is especially helpful for investigators that are still learning the perfusion technique.
7. If biochemical analysis is needed on the tissue, the brain can be removed from the skull following perfusion with 25–50 mL of phosphate buffer (5–10 min or until the perfusate runs clear). The whole brain or its portion can then be snap frozen on dry ice

(see Note 8). The remaining portion can then be immersion fixed in 4% paraformaldehyde overnight. If the whole brain is to be used for histology, the perfusion has to be temporarily halted while the tubing is transferred to a 4% paraformaldehyde solution. The same applies to the pancreas (see Note 9).

8. The perfusion is then resumed with about 50–100 mL of fixative. The fixative will shrink the brain which will aid in removing it from the skull, although with experience an unfixed brain can easily be removed intact.
9. The brain/pancreas can then be postfixed overnight at 4°C in the same fixative (see Note 10).
10. The brain is subsequently transferred to 20% glycerol/2% dimethylsulfoxide in 0.1 M phosphate buffer and kept refrigerated overnight. (see Note 11).
11. The pancreas needs to be embedded in paraffin before sectioning. Hence, when fixed it cannot go into a sugar solution (such as glycerol- or sucrose solution) as it interferes with the paraffin embedding and subsequent sectioning. Instead, place the fixed pancreas in PBS and deliver to the in-house paraffin-embedding facility (see Note 12).
12. The brain can then be sectioned at 40 μm on a freezing microtome or in a cryostat (see Note 13). The paraffin-embedded pancreas is ideally sectioned at 5–10 μm and mounted directly onto slides in a heated water bath (37–41°C; see Note 14).
13. It is often necessary to save all the sections and this can be done conveniently by placing them into series in 24-well cell culture tray filled with ethylene glycol cryoprotectant. We usually save sections from each brain into five series at 200-μm intervals. The sections are then stored at –20°C until used (see Note 15).
14. Sections from the pancreas are taken as needed from the paraffin block which is stored at room temperature.

3.2. Preparation of Gelatin-Coated Slides

For immunohistochemical procedures, commercially available coated slides are sufficient but for Congo Red staining of slide-mounted sections, it is preferable to use gelatin-coated slides.

1. Use commercially available precleaned slides (75 × 25 mm).
2. Place in a slide rack (see Note 16).
3. Rinse in distilled water.
4. Dip for 1 min in 1:1 solution of 95% ethanol and 1.0 M acetic acid.
5. Rinse in distilled water until water sheets of slides (15–30 s).
6. Dip for 2 min in freshly prepared filtered gelatin solution. Prepare by heating 300 mL of distilled water to 60°C, then add 3 g of gelatin and stir. When fully dissolved, add 0.3 g of

chromium potassium sulfate to harden the gelatin and stir until dissolved. Filter through Whatman #1 or equivalent filter paper before use.

7. Dry at 30–50°C overnight.
8. Place in slide containers until used.

3.3. Congo Red Staining

1. Prepare a saturated Congo Red solution by adding 2.5 g of Congo Red to a total volume of 250 mL of 50% ethyl alcohol. Undissolved material should be filtered through a Whatman #1 or equivalent filter paper (see Note 17). It is preferable to perform this staining on sections that have been mounted onto slides (see Note 18).
2. After defatting the tissue in xylene or CitriSolv®, it is hydrated by taking it through a series of ethyl alcohol solutions (100, 95, 80, and 70%, 1–2 min in each) before staining in the Congo Red solution for 1 h.
3. The slides are subsequently dipped into a saturated lithium carbonate solution for 10–20 s and then rinsed for a similar period in tap water or distilled water (see Note 19).
4. Dip the slides for 5–60 s in 70% ethanol to get rid of some of the background staining, and then transfer the slides quickly through 80%, 95%, and two sets of 100% ethanol (15 s to 2 min in each) before placing them in xylene or CitriSolv for 5–10 min (see Note 20).
5. The slides can now be coverslipped with mounting media such as DePex (see Note 21).
6. Congo Red staining can then be viewed under plane-polarized light. Amyloid plaques should give apple-green birefringence, usually as a Maltese cross, whereas the neurons that are non-specifically stained will not emit birefringence (see Note 22 and Fig. 1). For an alternative Congo Red staining procedure, please refer to Chapter 24.

3.4. Thioflavin S Staining

1. As with the Congo Red staining method, it is preferable to stain mounted sections with Thioflavin S.
2. Prepare 1% Thioflavin S solution in distilled water, and filter it through Whatman #1 before use (see Note 23).
3. Sections are defatted in xylene or CitriSolv (5–10 min) and then hydrated through a series of ethyl alcohol solutions (100, 95, 80, 70%, 1–2 min in each one), placed for a few seconds in water and then stained with 1% Thioflavin S for 30–60 min (see Note 24).
4. The sections are subsequently dehydrated through a series of ethyl alcohol solutions (70, 80, 95, 100, 100%, 1–2 min in each one) and then placed in xylene or CitriSolv® (5–10 min) before being coverslipped with DePex mounting media.

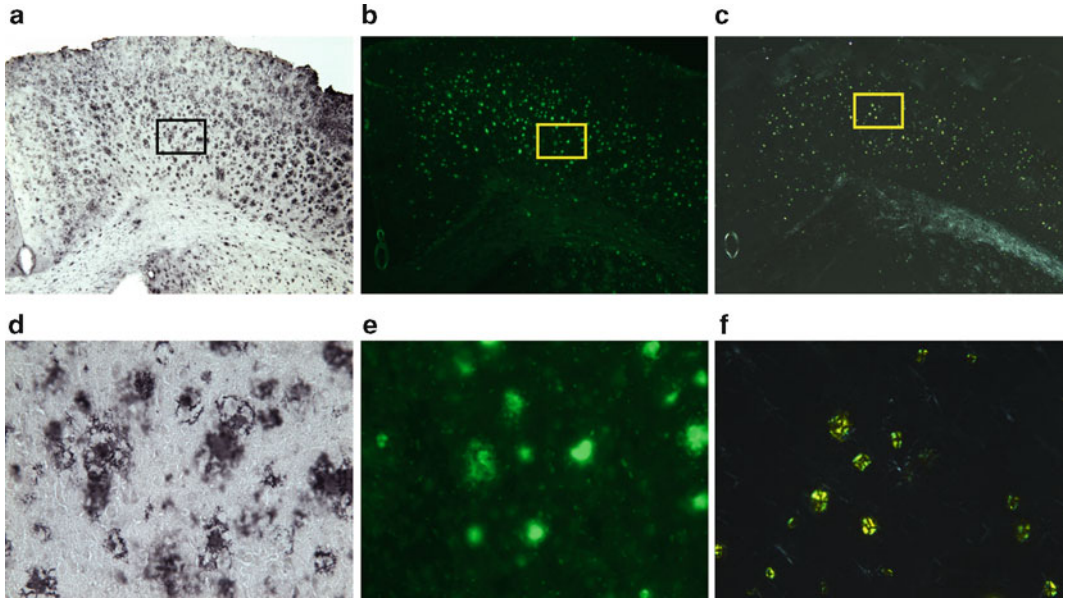

Fig. 1. Coronal brain sections depicting cortical regions (50×) in a 12-month-old 5XFAD mouse stained with 6E10/4G8 (**a**), Thioflavin S (**b**), and Congo Red (**c**). (**d**–**f**) Magnifications (400×) of the boxed areas in (**a**–**c**), respectively. Numerous Aβ plaques are visible, many of which are Thioflavin S and Congo Red positive.

5. The slides are then cleaned as described above for the Congo Red method before being viewed under fluorescence using the filter set recommended for that particular microscope. Thioflavin S bound to amyloid will emit fluorescence (see Note 25 and Fig. 1).
6. The stained sections should be stored in a cool, dark place such as a refrigerator.

3.5. Immunohistochemistry: Staining for Amyloid and Pre-amyloid

The following protocols are for free-floating mouse brain sections (see Note 26). Initially, certain controls should be included such as pre-adsorption of the primary antibody with the antigen and omitting of the primary and secondary antibodies as well as the avidin–peroxidase complex. For mouse-on-mouse detection it is appropriate to include omission of the primary antibody in each run. For optimal immunodetection of Aβ plaques it is not necessary to pretreat the sections with heat or formic acid as is needed for human sections. Likewise, for tau staining, pretreatment is not necessary in mouse sections. However, for IAPP staining of the mouse pancreas, epitope unmasking by boiling in citrate buffer, followed by formic acid treatment, is recommended as detailed below.

3.5.1. Mouse Monoclonal Antibodies

To eliminate background staining it is recommended to use MOM® kit (Vector Laboratories) or equivalent reagents. We have modified the kit instructions to our conditions. It is likely that further adjustments can be performed to save reagents. At least

for certain tau antibodies, less expensive reagents work as well or better (see Note 27).

Aβ Staining

1. Sections are removed from the ethylene glycol cryoprotectant and washed three times for 10 min each in PBS.
2. The sections are treated for 30 min in 0.3% hydrogen peroxide, freshly prepared from a 30% solution, to quench endogenous peroxidase activity.
3. Following two 5-min washes in PBS, the sections are placed in MOM blocking reagent (Vector Laboratories) for 1 h (five drops per 10 mL of PBS; see Note 28), and then washed twice for 5 min in PBS.
4. The sections are then placed for 1 h or longer in mouse primary antibody in MOM diluent (see Note 29). The diluent is prepared by adding 1,200 μL of protein concentrate from the MOM kit into 15 mL of PBS. Control sections are placed in MOM diluent alone.
5. After two 5-min washes in PBS, the sections are incubated for 1 h in biotinylated anti-mouse IgG (secondary antibody) solution that is prepared by adding 20 μL of stock solution into 15 mL of MOM diluent (see Note 30).
6. Following two 5-min washes in PBS, the sections are placed for 30 min in avidin–peroxidase solution that is prepared 30 min in advance by adding two drops of Reagent A and two drops of Reagent B into 40 mL of PBS.
7. Subsequently, the sections are washed for 5–10 min in 0.2 M sodium acetate solution, pH 6.0 (see Note 31), and then reacted with the chromogen of choice. We usually use diaminobenzidine tetrahydrochloride (DAB) as a chromogen and nickel ammonium sulfate to intensify the reaction. This solution can be prepared by dissolving 35 mg of DAB in 100 mL of 0.2 M sodium acetate buffer, pH 6.0. Nickel ammonium sulfate (2.5 g) is subsequently added and once dissolved the solution is filtered through 0.45 μm filter disk by using a 20–60-mL disposable syringe (see Notes 32–34).
8. When in the DAB solution, 20–40 μL of 0.3% hydrogen peroxide (see Note 35) is gradually added to each reaction well (5–10 mL) and the staining reaction allowed to proceed until the sections have reached the desired staining intensity (5–10 min; see Note 36). The sections are then washed in 0.2 M sodium acetate buffer and subsequently transferred to PBS for mounting onto slides (see Note 37).

Tau Staining

For many tau antibodies, the same procedure as described for Aβ can be used except that TBS is recommended in place of PBS for tau phospho-specific antibodies. However, as indicated above, the use of less expensive reagents may give better or equivalent results (see Note 27).

IAPP Staining

1. Deparaffinize sections in two changes of xylene, 5 min each.
2. Hydrate in two changes of 100% ethanol for 3 min each, then in 95 and 80% ethanol for 1 min each. Then rinse in distilled water.
3. Immerse the slides in a slide holder for 10 min in a beaker containing boiling sodium citrate buffer (10 mM citric acid, 0.05% Tween 20, pH 6.0) (see Note 38).
4. Let the sections adjust for 20 min at room temperature.
5. Treat the tissue for 10 min with 80% formic acid (see Note 39).
6. Wash sections twice in PBS with 0.1% Tween 20.
7. Then proceed in the same manner as described in the Aβ staining protocol, starting with treating the sections in 0.3% hydrogen peroxide.

Polyclonal Antibodies

When rabbit polyclonal antibodies are used on mouse brain sections, background staining due to cross-reactivity is less of an issue than with mouse antibodies. Regular secondary antibody kits can be used such as the Vector Elite kit for rabbit IgG antibodies. For Aβ and IAPP, this protocol is the same as the mouse monoclonal protocol except that the primary antibody diluent is different (as detailed in Materials) and the secondary antibody is diluted into PBS (see Note 40).

4. Notes

1. Stop adding NaOH when it does not enhance the clarity of the solution. Powdered paraformaldehyde is more soluble than the prilled version but is not recommended because of enhanced risk of exposure to airborne particles. Although the prilled fixative may not dissolve completely, undissolved material can be filtered away.
2. It is recommended to use double filter paper or to allow the solution to cool down. Warm solution may rupture the filter paper.
3. It is usually recommended to use freshly prepared fixative but we have not noticed any differences in the quality of tissue sections or amyloid staining when the fixative has been refrigerated for up to several weeks prior to use.
4. It is convenient to perform this procedure over a sink but the perfusate should be disposed of according to institutional guidelines.
5. As a perfusion cannula, 22-gauge feeding needle for newborn mice or birds is recommended. Blunted needles as these are less likely to tear the heart during perfusion. The cannula will

fit onto a regular intravenous tubing extension set that also has an injection site for the heparin solution. Alternatively, heparin can be added directly to the perfusion solution.

6. The lungs will expand if there is a buildup of fluids within the circulatory system. The cause is usually that efflux of the perfusate out of the right atrium is blocked and/or the cannula has accidentally been placed in the right ventricle so the perfusion liquid will enter the lungs first instead of the main circulation.
7. Blood clots will give nonspecific staining in immunohistochemistry.
8. If one hemisphere needs to be saved for biochemical analysis it is convenient to place the brain on a cold surface and cut the brain slightly off the midline with a single-edged razor blade. The larger portion should be immersion fixed and it will contain a fraction of the contralateral hemisphere. However, if the brain is cut through the midline between the hemispheres, the hippocampus will often separate from the brain section during staining and/or mounting onto the slides.
9. It can be difficult to distinguish the pancreas from surrounding fat tissue, particularly in older mice that often develop substantial abdominal adipose tissue. Obesity is also induced to promote pancreatic deposition of IAPP aggregates in mouse models which makes this more of an issue. The pancreas is located at the hilus of the spleen and it is best to remove those together. Close examination will reveal that the texture and consistency of the pancreatic tissue is different from associated adipose tissue and these are more easily distinguished after fixation and very clearly with microscopical evaluation of histological sections.
10. If the tissue is fixed by perfusion, postfixation for 6–8 h may be sufficient but overnight fixation does not affect amyloid or preamyloid staining.
11. Without this step, the brain may crack while being frozen for sectioning.
12. Nowadays, only a few laboratories have paraffin-embedding stations but most institutions have central facilities for this procedure, which is much more cost effective and should provide more consistent results.
13. By sectioning the brain at 40 μm, the sections will withstand free-floating staining procedures. Paint brush #1 is convenient to use to move the sections from the blade into the ethylene glycol cryoprotectant solution. Tissue Freezing Medium® or equivalent is used to secure the brain to the specimen holder. It usually takes less time to section the brain on a freezing microtome than in a cryostat.

14. If the paraffin-sectioned tissue does not spread well on the slide when mounted, the temperature of the water bath used for mounting the tissue should be increased gradually from 37°C until ideal conditions are achieved. This typically occurs prior to 41°C.
15. Prolonged storage at –20 to –30°C does not seem to affect staining of amyloid or pre-amyloid.
16. The slide rack should have a handle and an open bottom so that the rack can be moved quickly between solutions (equivalent to Wheaton No. 900200 that includes a staining dish that fits the rack). Nineteen slides will fit in each rack if placed in a zig-zag way. Larger racks can also be used.
17. If the staining will be performed in regular glass slide container, a total volume of 200–250 mL will be sufficient to cover the slides. The solution should be stirred for a few hours or even overnight to ensure that most of the chemical is dissolved. Preferably use freshly made solution. After sitting at room temperature for several days or weeks, the stain will not work properly.
18. Commercially available coated slides, such as Fisherbrand® Superfrost®*/Plus work fine for immunohistochemistry but for histological stains such as Congo Red or Cresyl Violet, it is preferable to use gelatin-coated slides for improved adherence of the sections to the slide.
19. Some protocols suggest washing the sections in running tap water for 15 min. This may be appropriate for human sections but in our experience, mouse and rat sections partially come off the slides when left in water for too long.
20. Protocols for Congo Red staining usually involve counterstains such as Harris hematoxylin but this procedure can be avoided by not washing off the nonspecific Congo Red neuronal staining. Most of this staining comes off in the 70% ethanol so care should be taken to keep the slides only briefly in this solution. The exact time varies a bit but 5–60 s is usually sufficient to reduce the background staining. The remaining intensity should be similar to Cresyl Violet staining. The sections can always be restained in the Congo Red solution if they become too destained in the alcohol solutions. Leave the slides for at least 2 min in the final set of 100% ethanol. Water will turn the xylene or Citrosolv® cloudy and can interfere with microscopic analysis of the tissue sections.
21. Various mounting media can be used. We are particularly fond of DePex mounting media. It does not shrink much while setting which reduces bubble formation and it does not come off in sharp flakes when the slides are cleaned with a razor blade after it has set overnight. It is best to use coverslips (22 × 60 mm)

that are slightly smaller than the slide (25 × 75 mm). The slides will be easier to clean and bubbles are less likely to form.

22. Birefringence is often seen in larger blood vessels and in threads associated with the surface of the brain. This observation does not confirm the presence of amyloid and can be due to Congo Red binding to collagen which is known to result in birefringence.
23. As with Congo Red, a volume of 200–250 mL is sufficient if standard glass staining containers are used. Similar results can be obtained with 0.5% Thioflavin S solution.
24. Less staining time at lower dye concentrations may provide equivalent results, depending on the tissue and the thickness of the sections. For example, for 10-μm thick paraffin-embedded sections of the mouse pancreas, incubation for 2 min in 0.5% Thioflavin S solution is sufficient for staining IAPP deposits.
25. FITC filter which commonly exists in many microscopes works well although the Thioflavin wavelength is slightly different.
26. A similar protocol can be used for slide-mounted sections although incubation periods may have to be increased to allow sufficient penetration of the antibodies. It is most convenient to use cell strainers, with 100-μm nylon mesh, to move the sections between solutions. The strainers can be placed in six-well culture dishes for all the washes. To save material, for all other incubations, the strainers can be placed in small individual Petri dishes of a similar diameter as the wells. Less volume is needed in these dishes to immerse the sections.
27. For example, PHF1 antibody staining of normal mouse tissue can be reduced/eliminated by using the procedure described by Peter Davies (15). For the MC1 antibody, we obtained comparable results with the two methods (Vector MOM kit vs. Davies' protocol), with the latter using less expensive reagents.
28. The MOM blocking solution can be used at least few times.
29. The proper dilution of the monoclonal antibodies will have to be assessed.
30. We have also diluted the secondary antibody into PBS with similar results.
31. It is convenient to prepare 1.0 M sodium acetate, pH 6.0 stock solution. pH can be adjusted with 1.0 M acetic acid. This solution is best kept refrigerated. The 0.2 M solution can be prepared from the stock in 500 mL aliquots and stored refrigerated.
32. The syringes can be used repeatedly and discarded when it becomes difficult to push the plunger through the syringe, which will occur over time.
33. Be sure to use DAB in its salt form (tetrahydrochloride) or it will not dissolve.

34. DAB should not be dissolved in PBS or any other phosphate buffer as phosphates will precipitate it out of solution and these aggregates can then adhere to the sections leading to nonspecific staining. Likewise, when staining is done, the sections should not be moved directly into PBS but rather washed first in 0.2 M sodium acetate to remove any residual DAB.
35. Likewise, hydrogen peroxide used for the reaction should be diluted in the 0.2 M sodium acetate buffer and not in PBS. We usually dilute 10 μL of 30% hydrogen peroxide into 1 mL of the buffer, and then add 20–40 μL of this solution (0.3% hydrogen peroxide) to the reaction (5–10 mL).
36. If the sections reach the desired staining intensity very quickly (seconds to a few minutes), further dilution of the primary and/or secondary antibodies is recommended to preserve these reagents. Typically, 7–8 min staining period is ideal.
37. The sections can be stored overnight or over a weekend in the PBS solution at 4–6°C prior to mounting. Longer storage is not recommended as increased hydration of the sections makes mounting onto slides more difficult.
38. Some unmasking protocols suggest boiling the sections for 20–40 min but this is not necessary to unmask IAPP epitopes in the mouse pancreas. Such a long boiling period causes the mouse tissue to come off the slides and should be avoided.
39. We have noticed that IAPP staining is improved when the boiling period is followed by 10 min formic acid treatment. Longer treatment should be avoided as the tissue can then come of the slides. This improvement may be antibody dependent and the necessity of this additional step should be evaluated for each antibody.
40. For general immunohistochemistry we have often used 0.3% Triton-X in PBS as the wash solution and to dilute the secondary antibody as well as the A+B solution. The detergent may enhance epitope exposure which facilitates detection of certain antigens but is not necessary for staining amyloid plaques in mouse section. The primary antibody diluent can be stored refrigerated prior to use for at least several months.

Acknowledgments

This work was supported by NIHs grant AG20197, AG032611, and DK075494 and the Alzheimer's Association. These protocols were in part adapted from methods obtained from Stanley A. Lorens and Debra Magnuson at Loyola University Chicago. We thank Drs. Fernando Goñi and Ayodeji Asuni for their comments on the original manuscript, which has now been substantially updated and expanded in this second edition of the book.

References

1. Kitamoto, T., Ogomori, K., Tateishi, J., and Prusiner, S. B. (1987) Formic acid pretreatment enhances immunostaining of cerebral and systemic amyloids. *Lab Invest* ***57***, 230–236.
2. Davies, L., Wolska, B., Hilbich, C., Multhaup, G., Martins, R., Simms, G., Beyreuther, K., and Masters, C. L. (1988) A4 amyloid protein deposition and the diagnosis of Alzheimer's disease: prevalence in aged brains determined by immunocytochemistry compared with conventional neuropathologic techniques. *Neurology* ***38***, 1688–1693.
3. Gentleman, S. M., Bruton, C., Allsop, D., Lewis, S. J., Polak, J. M., and Roberts, G. W. (1989) A demonstration of the advantages of immunostaining in the quantification of amyloid plaque deposits. *Histochemistry* ***92***, 355–358.
4. Lamy, C., Duyckaerts, C., Delaere, P., Payan, C., Fermanian, J., Poulain, V., and Hauw, J. J. (1989) Comparison of seven staining methods for senile plaques and neurofibrillary tangles in a prospective series of 15 elderly patients. *Neuropathol. Appl. Neurobiol.* ***15***, 563–578.
5. Wisniewski, H. M., Wen, G. Y., and Kim, K. S. (1989) Comparison of four staining methods on the detection of neuritic plaques. *Acta Neuropathol. (Berl)* ***78***, 22–27.
6. Vallet, P. G., Guntern, R., Hof, P. R., Golaz, J., Delacourte, A., Robakis, N. K., and Bouras, C. (1992) A comparative study of histological and immunohistochemical methods for neurofibrillary tangles and senile plaques in Alzheimer's disease. *Acta Neuropathol. (Berl)* ***83***, 170–178.
7. Raskin, L. S., Applegate, M. D., Price, D. L., Troncoso, J. C., and Hedreen, J. C. (1995) Comparison of new and traditional methods for detection of senile plaques in Alzheimer's disease. *J. Geriatr. Psychiatry Neurol.* ***8***, 125–131.
8. Cullen, K. M., Halliday, G. M., Cartwright, H., and Kril, J. J. (1996) Improved selectivity and sensitivity in the visualization of neurofibrillary tangles, plaques and neuropil threads. *Neurodegeneration*. ***5***, 177–187.
9. Shiurba, R. A., Spooner, E. T., Ishiguro, K., Takahashi, M., Yoshida, R., Wheelock, T. R., Imahori, K., Cataldo, A. M., and Nixon, R. A. (1998) Immunocytochemistry of formalin-fixed human brain tissues: microwave irradiation of free-floating sections. *Brain Res. Brain Res. Protoc.* ***2***, 109–119.
10. Cummings, B. J., Mason, A. J., Kim, R. C., Sheu, P. C., and Anderson, A. J. (2002) Optimization of techniques for the maximal detection and quantification of Alzheimer's-related neuropathology with digital imaging. *Neurobiol. Aging* ***23***, 161–170.
11. Sigurdsson, E. M., Lorens, S. A., Hejna, M. J., Dong, X. W., and Lee, J. M. (1996) Local and distant histopathological effects of unilateral amyloid-β 25-35 injections into the amygdala of young F344 rats. *Neurobiol. Aging* ***17***, 893–901.
12. Sigurdsson, E. M., Lee, J. M., Dong, X. W., Hejna, M. J., and Lorens, S. A. (1997) Bilateral injections of amyloid-β 25-35 into the amygdala of young Fischer rats: Behavioral, neurochemical, and time dependent histopathological effects. *Neurobiol. Aging* ***18***, 591–608.
13. Sigurdsson, E. M., Scholtzova, H., Mehta, P. D., Frangione, B., and Wisniewski, T. (2001) Immunization with a non-toxic/non-fibrillar amyloid-β homologous peptide reduces Alzheimer's disease associated pathology in transgenic mice. *Am. J. Pathol.* ***159***, 439–447.
14. Asuni, A. A., Boutajangout, A., Quartermain, D., and Sigurdsson, E. M. (2007) Immunotherapy targeting pathological tau conformers in a tangle mouse model reduces brain pathology with associated functional improvements. *J. Neurosci.* ***27***, 9115–9129.
15. Davies, P. Tau immunohistochemistry protocol: Mice. http://alzforum.org/res/com/protocol/protocol.aspx?pid=3. Accessed 25 March 2011.

Chapter 29

A Pentameric Luminescent-Conjugated Oligothiophene for Optical Imaging of In Vitro-Formed Amyloid Fibrils and Protein Aggregates in Tissue Sections

K. Peter R. Nilsson, Mikael Lindgren, and Per Hammarström

Abstract

Luminescent-conjugated oligo- and polythiophenes (LCOs and LCPs) are valuable tools for optical imaging of a plethora of protein aggregates associated with amyloidoses. Here, we describe the utilization of an anionic pentameric LCO, p-FTAA, for staining of protein aggregates in a variety of platforms, including in vitro-formed amyloid fibrils and tissue sections.

Key words: Luminescent-conjugated oligothiophenes, Protein aggregates, Optical imaging

1. Introduction

Protein misfolding diseases, also referred to as amyloidoses or proteinopathies, are diseases of disparate etiologies characterized by extracellular or intracellular proteinaceous deposits in tissues and organs (1). These deposits, termed "amyloid" or inclusion bodies, result from misfolding and/or partial unfolding of proteins, followed by the formation of protein aggregates having repetitive cross-β-pleated sheets. The conformational alterations of proteins or peptides when being converted to amyloid, i.e., going from a native fold to β-sheet-rich fibrillar assemblies, makes it hard to specifically identify amyloid with conventional immunochemical reagents such as antibodies. Instead, small hydrophobic molecules have proven useful for visualization and identification of protein deposits. The most common small amyloid ligands are derivatives of Congo red or Thioflavins and in contrast to antibodies these dyes do not bind to specific proteins but are rather selective for protein aggregates having an extensive cross-β-pleated sheet

Einar M. Sigurdsson et al. (eds.), *Amyloid Proteins: Methods and Protocols*, Methods in Molecular Biology, vol. 849,
DOI 10.1007/978-1-61779-551-0_29,

conformation and sufficient structural regularity. Congo red, an aromatic sulfonated azo dye, was introduced more than 80 years ago and its gold-green birefringence under polarized light has been the gold standard for amyloid detection ever since (2, 3).

Lately, a novel class of amyloid imaging agents, luminescent-conjugated oligo- and polythiophenes (LCOs and LCPs), identifying and differentiating a broader subset of protein aggregates than conventional dyes has been described (4–14). LCOs and LCPs contain a swiveling thiophene backbone and upon conformational freedom of this backbone, different emission profiles are observed from the thiophene derivatives. Hence, thiophene-based fluorescent dyes offer the possibility to afford an optical fingerprint corresponding to a distinct conformational state of a specific molecule. The conformational-sensitive optical properties of LCOs and LCPs have proven to be a great asset for studying protein misfolding and aggregation, as binding of the thiophene derivatives to distinct forms of protein aggregates gives rise to specific optical features from the dyes. This is an improvement compared to the other small amyloid imaging, as these probes only change in optical feature whether they are free in solution or upon binding to amyloid fibrils. Here, we present staining protocols for the recently developed anionic pentameric LCO, p-FTAA (11), for a variety of platforms, including in vitro-formed amyloid fibrils and amyloid deposits in tissue sections.

2. Materials

Prepare all solutions using ultrapure water (prepared by purifying deionized water to attain a sensitivity of 18 MΩ cm at 25°C) and analytical grade reagents. Prepare and store all reagents at room temperature (unless indicated otherwise).

2.1. p-FTAA for Kinetic Measurement of Recombinant Aβ Peptide Fibrillation

1. p-FTAA stock solution: 1 mg p-FTAA, synthesized according to (10), in 1 mL deionized water (1.5 mM). Store at 4°C in a test tube wrapped with aluminum foil.
2. Recombinant Aβ1–42 or Aβ1–40 (rPeptide, lyophilized from hexafluoro isopropanol), store at −20°C.
3. Fibrillation buffer: 10 mM Na_2HPO_4/NaH_2PO_4, pH 7.5.
4. 96-well microtiter plates (Costar).

2.2. p-FTAA for Kinetic Measurement of Bovine Insulin Fibrillation

1. p-FTAA stock solution: 1 mg p-FTAA, synthesized according to Åslund et al. (10), in 1 mL deionized water (1.5 mM). Store at 4°C in a test tube wrapped with aluminum foil.
2. Insulin from Bovine pancreas (Sigma, cat. No. I6634), store at −20°C.

3. Fibrillation buffer: 2 M acetic acid (HAc) 500 mM NaCl.
4. Water bath or heating block.
5. 96-well microtiter plates (Costar 3694, Corning Incorporated).

2.3. p-FTAA Staining of Frozen Brain Tissue Sections from Drosophila melanogaster

1. Frozen brain sections from *Drosophila melanogaster* prepared as in (12). Store at –80°C.
2. p-FTAA stock solution: 1 mg p-FTAA, synthesized according to (10), in 1 mL deionized water (1.5 mM). Store at 4°C in a test tube wrapped with aluminum foil.
3. Fixation medium: 95% ethanol.
4. Staining buffer: 100 mM Na_2HPO_4/NaH_2PO_4, pH 7.2 120 mM NaCl.
5. Deionized water.
6. Mounting medium: DakoCytomation (Dako).

2.4. p-FTAA Staining of Frozen Tissue Sections from Human or Mouse

1. p-FTAA stock solution: 1 mg p-FTAA, synthesized according to (10), in 1 mL deionized water (1.5 mM). Store at 4°C in a test tube wrapped with aluminum foil.
2. Fixation medium: ethanol 95%.
3. Staining buffer: phosphate buffer saline (PBS) (100 mM Na_2HPO_4/NaH_2PO_4, pH 7.4 150 mM NaCl).
4. Deionized water.
5. Mounting medium: DakoCytomation (Dako, cat. no. S3023).

2.5. p-FTAA Staining of Formalin-Fixed Paraffin-Embedded Tissue Sections from Human or Mouse

1. p-FTAA stock solution: 1 mg p-FTAA, synthesized according to (10), in 1 mL deionized water (1.5 mM). Store at 4°C in a test tube wrapped with aluminum foil.
2. Fixation medium: ethanol 95%.
3. Staining buffer: PBS (100 mM Na_2HPO_4/NaH_2PO_4, pH 7.4 150 mM NaCl).
4. Deionized water.
5. Mounting medium: DakoCytomation (Dako).

3. Methods

3.1. p-FTAA for Kinetic Measurement of Recombinant Aβ Peptide Fibrillation

1. Solubilize recombinant Aβ1–42 or Aβ1–40 (rPeptide, lyophilized from hexafluoro isopropanol) in 2 mM NaOH at 1 mg/mL followed by dilution in 10 mM Na-phosphate pH 7.5 to a final concentration of 10 μM peptide.
2. Dilute the p-FTAA stock solution (1.5 mM) to a final concentration of 15 μM with deionized water.

3. Mix 100 μL of the Aβ peptide solution with 2 μL p-FTAA solution (15 μM) in a microtiter plate.
4. Incubate the sample at 37°C with repetitive cycles of agitation (8-min agitation, 12-min stagnant sample read) in a Tecan Saphire 2 plate reader and collect spectra between 470 and 700 nm with excitation at 450 nm. The results from typical kinetic measurement of Aβ1–42 or Aβ1–40 fibrillation and the spectra of p-FTAA bound to the respective Aβ amyloid fibrils are shown in Fig. 1a, b.

3.2. p-FTAA for Kinetic Measurement of Bovine Insulin Fibrillation

1. Solubilize bovine insulin (Sigma) in 2 M acetic acid and 500 mM NaCl to a final concentration of 5 mg/mL protein.
2. Dilute the p-FTAA stock solution (1.5 mM) to a final concentration of 15 μM with deionized water.
3. Place the bovine insulin solution in a water bath kept at 50°C to induce formation of amyloid-like insulin fibrils.
4. Withdraw 100 μL aliquots from the fibrillation solution at different time points and mix with 2 μL of the p-FTAA stock solution (see Note 1).
5. Incubate the sample in microtiter plates for 10 min at room temperature and use a Tecan Saphire 2 plate reader to collect spectra between 470 and 700 nm with excitation at 450 nm. The results from typical kinetic measurement of bovine insulin fibrillation are shown in Fig. 1c.

3.3. p-FTAA Staining of Frozen Brain Tissue Sections from Drosophila melanogaster

1. Fix the frozen brain tissue sections in prechilled 95% ethanol at –20°C overnight (see Note 2).
2. Rehydrate the sections to distilled water in 2-min step, using 90, 70, 50, and 0% ethanol.
3. Dilute the p-FTAA stock solution 1:500 in staining buffer (PBS) to achieve the p-FTAA staining solution.
4. Incubate the sections with p-FTAA staining solution for 30 min at room temperature (see Note 3).
5. Wash the sections for 5 min in PBS.
6. Rinse the slides in distilled water.
7. Mount the slides with a cover slip and use DakoCytomation as mounting medium and let the mounting medium solidify for at least 3 h (see Note 4).
8. Seal the slides with nail polish and store at 4°C for at least 2 h (see Note 5).
9. Analyze the sections with a fluorescence microscope. Typical p-FTAA staining of protein aggregates can be observed as green fluorescence with a characteristic spectrum (Fig. 2a) (see Note 6).

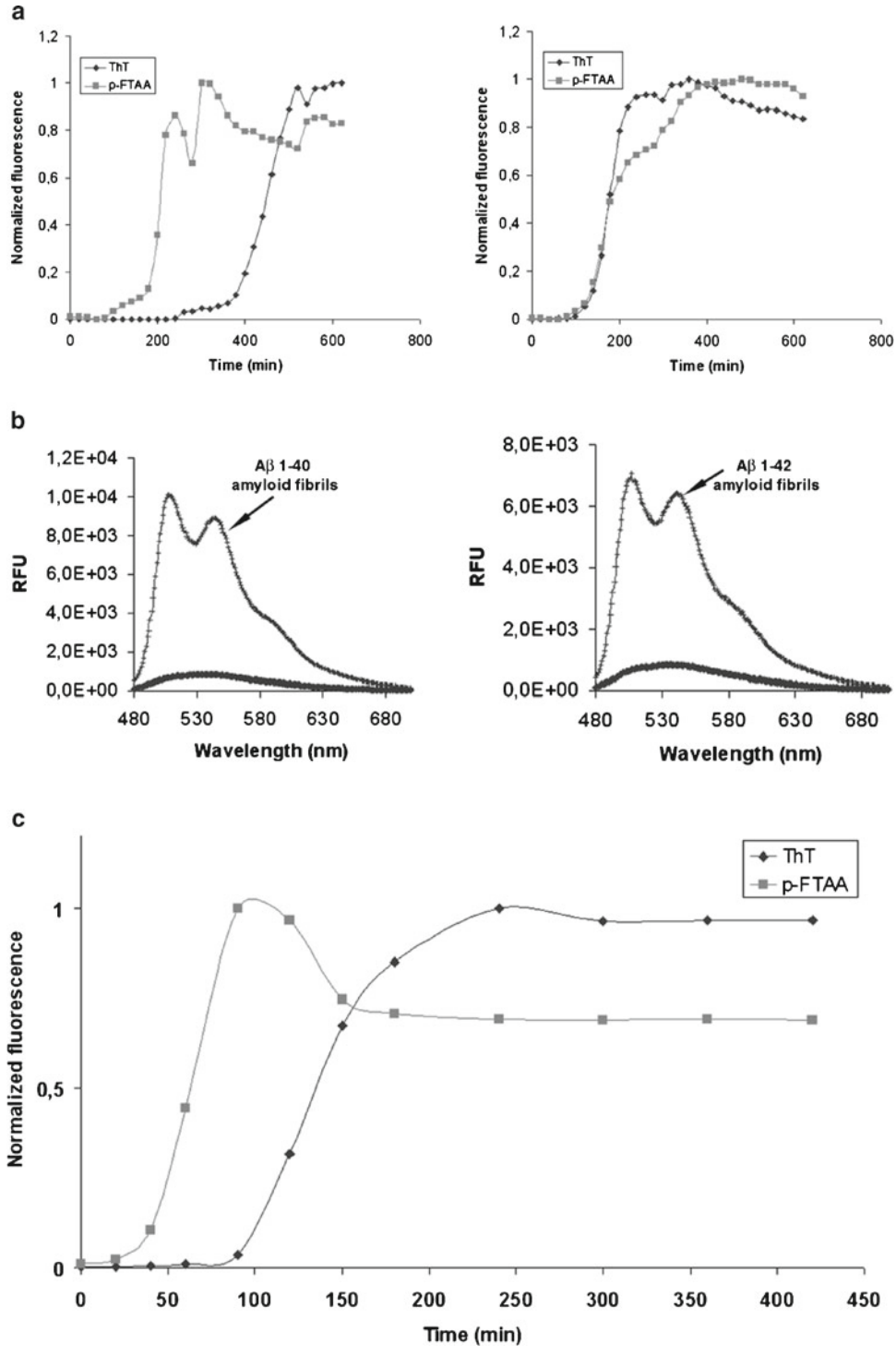

Fig. 1. Kinetics of in vitro fibrillation monitored by p-FTAA. (**a**) Time plots of the kinetics of recombinant Aβ 1–40 (*left*) and Aβ 1–42 (*right*) fibrillation monitored by ThT fluorescence or p-FTAA fluorescence. (**b**) Fluorescence spectra of p-FTAA bound to Aβ 1–40 (*left*) or Aβ 1–42 (*right*) amyloid fibrils. (**c**) Time plots of the kinetics of bovine insulin fibrillation monitored by ThT fluorescence or p-FTAA fluorescence.

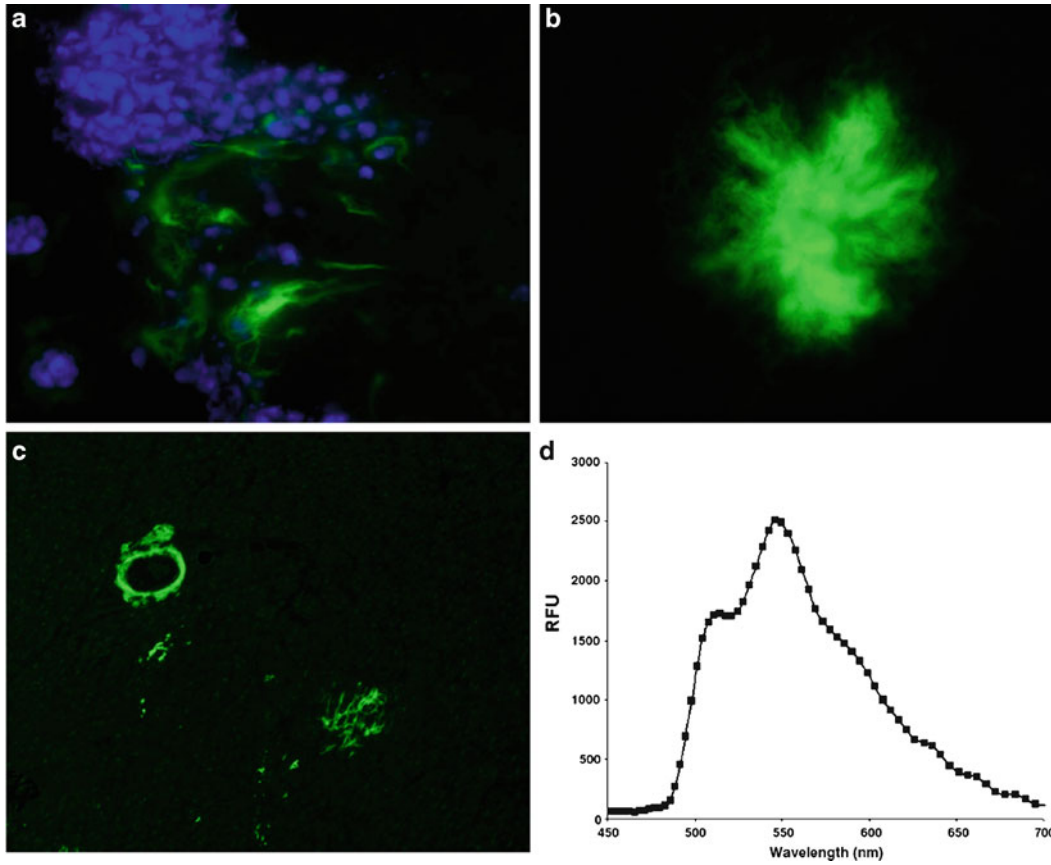

Fig. 2. Fluorescence images of protein aggregates stained by p-FTAA. (**a**) p-FTAA-stained A-β aggregates (*green*) in a brain section from *Drosophila melanogaster*. Nuclei are counterstained by DAPI (*blue*). (**b**) p-FTAA-stained A-β aggregates (*green*) in a brain section from a transgenic mouse. (**c**) Image of p-FTAA-stained amyloid deposits (*green*) in the heart. (**d**) Characteristic emission spectrum from p-FTAA bound to amyloid deposits.

3.4. p-FTAA Staining of Frozen Tissue Sections from Human or Mouse

1. Fix the frozen tissue sections in prechilled 95% ethanol for 10 min (see Note 7).
2. Rehydrate the sections to distilled water in 5-min step, using 90, 70, 50, and 0% ethanol.
3. Incubated the sections in staining buffer for 10 min.
4. Dilute the p-FTAA stock solution 1:500 in staining buffer (PBS) to achieve the p-FTAA staining solution.
5. Incubate the sections with p-FTAA staining solution for 30 min at room temperature (see Note 3).
6. Wash the sections for 10 min in PBS.
7. Mount the slides with a cover slip and use DakoCytomation as mounting medium and let the mounting medium solidify for at least 3 h (see Note 8).
8. Seal the slides with nail polish (see Note 5).

9. Analyze the sections with a fluorescence microscope. Typical p-FTAA staining can be observed as green fluorescence with a characteristic spectral signature (Fig. 2b) (see Notes 6 and 9).

3.5. p-FTAA Staining of Formalin-Fixed Paraffin-Embedded Tissue Sections from Human or Mouse

1. Deparaffinize and rehydrate the sections to distilled water in 20-min step, using xylene, 100% ethanol, 95% ethanol, 70% ethanol, and 0% ethanol (see Note 10).
2. Incubate the sections in staining buffer for 10 min.
3. Dilute the p-FTAA stock solution 1:500 in staining buffer (PBS) to achieve the p-FTAA staining solution.
4. Incubate the sections with p-FTAA staining solution for 30 min at room temperature (see Note 3).
5. Wash the sections for 10 min in PBS.
6. Mount the slides with a cover slip and use DakoCytomation as mounting medium and let the mounting medium solidify for at least 3 h (see Note 8).
7. Seal the slides with nail polish (see Note 5).
8. Analyze the sections with a fluorescence microscope. Typical p-FTAA staining can be observed as green fluorescence with a characteristic spectral signature (Fig. 2c) (see Note 6).

4. Notes

1. The fibrillation of insulin can also be performed having 300 nM of p-FTAA present in situ during fibrillation (13).
2. The fixation solution is critical. Paraformaldehyde (PFA) or formalin fixation is not optimal for p-FTAA staining. To achieve the best p-FTAA staining, with a distinct wavelength shift, a cold ethanol fixation is favorable. To reduce the autofluorescence interference with the p-FTAA spectra, fix the sections overnight. A long fixation time in cold ethanol does not prevent p-FTAA binding. p-FTAA can also be used in combination with antibodies. For a robust staining with both p-FTAA and antibodies, a short, cold acetone fixation is recommended. To not allow the section to swell after acetone treatment, the section protocol must be fully dry. Hence, allow the acetone to evaporate and the section to shrink before the section is rewetted and treated with primary antibody. No blocking is necessary during this protocol. For a detailed protocol regarding combined staining with p-FTAA and antibodies, see ref. 12.
3. Use a covered humidity chamber for processing slides, to minimize the risk of bleached and dried out samples. Always keep processed fluorescent samples and stained specimens in the dark.

4. Allow the mounting medium to solidify for at least 3 h before sealing the slide rims with nail polish. A shorter gelation time can affect spectral shifts of the p-FTAA. Vectashield with DAPI (Vector Laboratories) and Vectashield (Vector Laboratories) can also be used, but these mounting media might influence the spectral signature of p-FTAA to some extent.
5. Mounted slides can be stored for a long time at +4°C in a closed slide folder, but the p-FTAA staining may gradually diffuse. Thus, it is best to proceed to imaging within a few weeks of staining.
6. To image p-FTAA sections it is optimal to use a fluorescence microscope with long band-pass filters equipped with a SpectraView system (Applied Spectral Imaging). For the images in Fig. 2, we used an epifluorescence microscope equipped with a SpectraView 4.0 and a Spectra-Cube (inferometrical optical head SD 300) module with a cooled CCD-camera, through a 405/30 nm (LP450) band-pass filter. The data were processed with the SpectraView 3.0 EXPO software. Spectra were collected in an interval of 450–700 nm with the highest spectral resolution settings ("gas-line settings"). An image of p-FTAA-stained protein aggregates can also be obtained with filters used for fluorescein isothiocyanate (FITC). From our experience spectra can also be recorded with a LSM 510 META (Carl Zeiss, Jena, Germany) confocal laser scanning microscope through Plan-Neofluar 40L/0.75 objectives with an excitation at 458 nm (10) or using multiphoton excitation using Ti:Sapphire laser in the range typically 800–850 nm for p-FTAA (15, 16).
7. Similar as described above for p-FTAA staining of frozen brain tissue sections from *Drosophila melanogaster*, the fixation solution is critical. PFA fixation is not optimal for p-FTAA to achieve optimal staining of, for instance, intracellular protein aggregates such as neurofibrillary tangles (NFTs) and for most favorable spectral resolution (10). Fixation in cold acetone can also be used and this fixation is recommended for combined staining with p-FTAA and antibodies (10, 12).
8. A shorter gelation time can affect spectral shifts of the p-FTAA. Other mounting media such as Vectashield with DAPI (Vector Laboratories) and Vectashield (Vector Laboratories) can also be used. However, these mounting media might influence the spectral signature of p-FTAA. So far we have seen that DakoCytomation (Dako) is the preferable mounting medium for achieving optimal spectral resolution.
9. For increased spectral resolution, spectra can be collected with a mixture of filters. For instance, long band-pass filter 405/30 nm (LP450) and 546/12 (LP590) can be used to get

a complete emission profile between 450 and 700 nm combining two different excitation wavelengths. The spectra can be combined and processed with the SpectraView 3.0 EXPO software.

10. Harsh formalin fixation and extensive cross-linking of the tissue might lead to decreased binding of p-FTAA.

Acknowledgments

This work was supported by the Swedish Research Council (PH), Knut and Alice Wallenberg Foundation (PH, KPRN), Linköping University (PH, KPRN), The Swedish Foundation for Strategic Research (PH, KPRN), The European Union FP7 HEALTH (Project LUPAS) (KPRN, PH, ML), and The European Research Council (ERC, Project MUMID) (KPRN).

References

1. Westermark, P., Benson, M. D., Buxbaum, J. N., Cohen, A. S., Frangione, B., Ikeda, S., Masters, C. L., Merlini, G., Saraiva, M. J., and Sipe, J. D. (2007) A primer of amyloid nomenclature. *Amyloid* **14**, 179–183.
2. Bennhold H. (1922) Eine specifische Amyloidfärbung mit Kongorot. *Münchener Med. Wochenschrift* 44, 1537–1538.
3. Divry P. (1927) Etude histochimique des plaques seniles. *J. Neurol. Psychiatry* **27**, 643–657.
4. Nilsson, K. P. R., Herland, A., Hammarström, P., and Inganäs, O. (2005) Conjugated polyelectrolytes – conformation sensitive optical probes for detection of amyloid fibril formation. *Biochemistry* **44**, 3718–3724.
5. Nilsson, K. P. R., Hammarström, P., Ahlgren, F., Herland, A., Schnell, E. A., Lindgren, M., Westermark, G. T., and Inganäs, O. (2006) Conjugated polyelectrolytes - Conformation-sensitive optical probes for staining and characterization of amyloid deposits. *Chembiochem.* 7, 1096–1104.
6. Nilsson, K. P. R., Åslund, A., Berg, I., Nyström, S., Konradsson, P., Inganäs, O., Stabo-Eeg, F., Lindgren, M., Westermark, G. T., Lannfelt, L., Nilsson, L. N., and Hammarström, P. (2007) Imaging distinct conformational states of amyloid-beta fibrils in Alzheimer's disease using novel luminescent probes. *ACS Chem. Biol.* **2**, 553–560.
7. Sigurdson, C. J., Nilsson, K. P. R., Hornemann, S., Manco, G., Polymenidou, M., Schwarz, P., Leclerc, M., Hammarström, P, Wüthrich, K., and Aguzzi, A. (2007) Prion strain discrimination using luminescent conjugated polymers. *Nature Methods* **12**, 1023–1030.
8. Sigurdson, C. J., Nilsson, K. P. R., Hornemann, S., Heikenwalder, M., Manco, G., Schwarz, P., Ott, D., Rülicke, T., Liberski, P. P., Julius, C., Falsig, J., Stitz, L., Wüthrich, K., and Aguzzi, A. (2009) De novo generation of a transmissible spongiform encephalopathy by mouse transgenesis. *Proc. Natl. Acad. Sci.* USA **106**, 304–309.
9. Nilsson, K. P. R. (2009) Small organic probes as amyloid specific ligands - Past and recent molecular scaffolds. *FEBS Lett.* **583**, 2593–2599.
10. Åslund, A., Sigurdson, C. J., Klingstedt, T., Grathwohl, S., Bolmont, T., Dickstein, D. L., Glimsdal, E., Prokop, S., Lindgren, M., Konradsson, P., Holtzman, D. M., Hof, P. R., Heppner, F. L., Gandy, S., Jucker, M., Aguzzi, A., Hammarström, P., and Nilsson, K. P. R. (2009) Novel pentameric thiophene derivatives for in vitro and in vivo optical imaging of a plethora of protein aggregates in cerebral amyloidoses. *ACS Chem. Biol.* **4**, 673–684.
11. Nilsson, K. P. R., Ikenberg, K., Aslund, Å, Fransson, S., Konradsson, P., Röcken, C., Moch, H., and Aguzzi, A. (2010) Structural typing of systemic amyloidoses by luminescent-conjugated polymer spectroscopy. *Am. J. Pathol.* **176**, 563–574.
12. Berg, I., Nilsson, K. P. R., Thor, S., and Hammarström, P. (2010) Efficient imaging of amyloid deposits in Drosophila models

of human amyloidoses. *Nature Protocols* 5, 935–944.

13. Hammarström, P., Simon, R., Nyström, S., Konradsson, P., Åslund, A., and Nilsson, K. P. R. (2010) A fluorescent pentameric thiophene derivative detects in vitro-formed prefibrillar protein aggregates. *Biochemistry* **49**, 6838–6845.
14. Nilsson, K. P. R., Joshi-Barr, S., Winson, O., and Sigurdson, C. J. (2010) Prion strain interactions are highly selective. *J Neurosci.* **30**, 12094–12102.
15. Stabo-Eeg, F., Lindgren, M., Nilsson, K. P. R., Inganäs, O., and Hammarström, P. (2007) Quantum efficiency and two-photon absorption cross-section of conjugated polyelectrolytes used for protein conformation measurements with applications on amyloid structures. *Chemical Physics* **336**, 121–126.
16. Lindgren, M., Glimsdal, E., Åslund, A., Simon, R., Hammarström, P., Nilsson, K. P. R. (2010) Luminescence and Two-Photon Absorption Cross Section of Novel Oligomeric Luminescent Conjugated Polythiophenes for Diagnostics of Amyloid Fibrils. *Nonlinear Optics, Quantum Optics: concepts in modern optics* **40**, 241–251.

Chapter 30

In Vivo Magnetic Resonance Imaging of Amyloid-β Plaques in Mice

Youssef Zaim Wadghiri, Dung Minh Hoang, Thomas Wisniewski, and Einar M. Sigurdsson

Abstract

Transgenic mice are used increasingly to model brain amyloidosis, mimicking the pathogenic processes involved in Alzheimer's disease (AD). In this chapter, an in vivo strategy is described that has been successfully used to map amyloid-β deposits in transgenic mouse models of AD with magnetic resonance imaging (MRI), utilizing both the endogenous contrast induced by the plaques attributed to their iron content and by selectively enhancing the signal from amyloid-β plaques using molecular-targeting vectors labeled with MRI contrast agents. To obtain sufficient spatial resolution for effective and sensitive mouse brain imaging, magnetic fields of 7-Tesla (T) or more are required. These are higher than the 1.5-T field strength routinely used for human brain imaging. The higher magnetic fields affect contrast agent efficiency and dictate the choice of pulse sequence parameters for in vivo MRI, all addressed in this chapter. Two-dimensional (2D) multi-slice and three-dimensional (3D) MRI acquisitions are described and their advantages and limitations are discussed. The experimental setup required for mouse brain imaging is explained in detail, including anesthesia, immobilization of the mouse's head to reduce motion artifacts, and anatomical landmarks to use for the slice alignment procedure to improve image co-registration during longitudinal studies and for subsequent matching of MRI with histology.

Key words: MRI, Amyloid-β deposits, Susceptibility, Amyloid-β burden, Amyloidosis, Molecular imaging, Contrast agent, Mouse, Transgenic, 2D, 3D

1. Introduction

Based on the hypothesis that amyloidosis plays a major role in the pathogenesis of Alzheimer's disease (AD), a large number of transgenic mouse lines have been developed to model this aspect of AD (1–6). These transgenic mice are currently being used to study the amyloidosis process in vivo, and to test experimental approaches for clearing amyloid-β (Aβ). Noninvasive, in vivo imaging methods to map the distribution of CNS Aβ deposits in these mice would be

Einar M. Sigurdsson et al. (eds.), *Amyloid Proteins: Methods and Protocols*, Methods in Molecular Biology, vol. 849,
DOI 10.1007/978-1-61779-551-0_30,

very valuable for monitoring Aβ plaque formation and progression and to directly assess the efficacy of plaque clearance therapies. Considerable effort has, therefore, gone toward developing imaging approaches using such diverse methods as positron emission tomography (PET), multiphoton optical microscopy, and magnetic resonance imaging (MRI). MRI provides some distinct advantages for whole brain assessment of Aβ burden, including higher spatial resolution than PET and much greater penetration than multiphoton microscopy. MRI is also much more widely available for future clinical-imaging studies in AD patients. As 7-Tesla (T) human scanners have become widely available, the mouse imaging methods described in this chapter at the same field strength are highly relevant to clinical imaging.

MRI methods to image Aβ plaques in human AD patients are not currently available. It has been suggested that iron concentrated in AD plaques may enable their MRI detection using ultra high magnetic field strength (>7-T) and 40-μm×40-μm×40-μm spatial resolution that could only be achieved in postmortem brain tissue from AD patients over several hours of scans (7). This was accomplished using an MR pulse sequence optimized for dark contrast enhancement of lesions that were difficult to reproduce subsequently by Dhenain et al. at 11.7-T (8); an inconsistency likely due to the variable nature in chemical constituents of these plaques. Imaging Aβ lesions in transgenic mouse models of AD, on the other hand, was successfully demonstrated by several groups both ex vivo (9–14) and in vivo (14–24). Results from our laboratories (14) indicate that although some large plaques can be observed in old transgenic mice using susceptibility-induced contrast in T2*-weighted MR images (Fig. 1), the vast majority of plaques in these animals cannot be detected without contrast enhancement with magnetically labeled ligands targeted to Aβ (9, 14, 15, 18, 25, 26).

This chapter describes a method that has been successfully used to map brain Aβ plaques (9, 14, 15, 18, 25, 26) involving high field

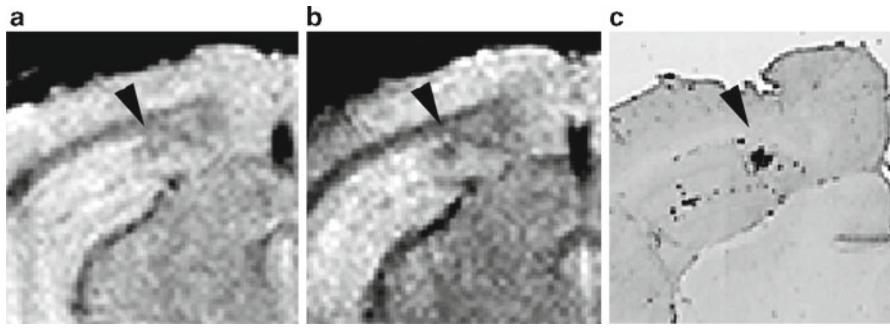

Fig. 1. Large Aβ plaques (*arrowhead*) can be seen in vivo with T2*-weighted 2D multi-slice gradient-echo MRI through subtle signal enhancement (**a**). Injection of PUT-Gd-DTPA-Aβ1-40 in the same mouse significantly enhances the Aβ plaque after 6 h (**b**). The matched immunostained histological section confirms these findings (**c**, *arrowhead*).

(7-T) MRI of transgenic mice, injected with magnetically labeled peptides for susceptibility-induced contrast-enhanced mapping of plaques. Details are provided on the peptides and magnetic labeling methods. Although iron-oxide nanoparticles have also been used for magnetic labeling (15, 26), the protocol provided in this chapter is focused on paramagnetic labeling with a chelated form of gadolinium (GdDTPA) which is the smallest (~1 nm in size) and clinically the most widely used contrast agent (27, 28). Nonetheless, the same approach can easily be extended to larger nanoparticles (29–32), such as iron-oxide particles (15, 26).

The experimental setup and protocols required for optimal in vivo detection of Aβ plaques in the mouse brain are detailed using both 2D and 3D MRI acquisition schemes (33) in less than 2 h.

2. Materials

2.1. Labeling of Amyloid-β Peptide

2.1.1. Equipment

1. ABI 430A peptide synthesizer (AME Bioscience, Chicago, IL).
2. Vydac C18 preparative column, 2.5 × 30 cm (Vydac Separations, Hesperia, CA).

2.1.2. Supplies

All reagents available from Sigma unless otherwise noted.

1. Aβ1-40.
2. K6Aβ1-30-NH_2 (Yale University, Keck Peptide Synthesis Facility).
3. Diethylenetriaminepentaacetic acid (DTPA).
4. Hydrofluoric acid.
5. Acetonitrile.
6. Trifluoroacetic acid.
7. Gd (III) chloride hexahydrate (Aldrich, Milwaukee, WI).
8. 1 N NaOH.
9. 0.4 M Putrescine in water.
10. EDC-coupling agent (Pierce Biotechnology, Rockford, IL).
11. Dialysis membrane (molecular weight cutoff: 2,000 g/mol).
12. Mannitol.
13. Phosphate-buffered saline (PBS).

2.2. MR Microimaging System

2.2.1. Equipment

1. *MR microimaging (μMRI) scanner*: Preferably, mouse brain imaging experiments should be performed at a magnetic field strength of at least 7-T (see Note 1). The experiments described in this chapter were initially performed with a SMIS console (MRRS, Guildford, UK) that was subsequently upgraded to a Bruker Biospec Avance 2 console interfaced to a 7-T 200-mm

horizontal bore magnet (Magnex Scientific, Abingdon, UK) equipped with actively shielded gradient coils (initially Magnex: inner diameter, ID = 120 mm, 250-mT/m gradient strength, 200-μs rise time and then Bruker BGA-9S: ID = 90-mm, 750-mT/m gradient strength, 100-μs rise time). Scanners with very similar performances are also made by other manufacturers such as Agilent Technologies (Varian, Santa Clara, CA, USA).

2. *MRI probe*: A radiofrequency (RF) coil fitting closely around the mouse's head should be used for brain imaging. In these experiments, we used RF coils dedicated for mouse head imaging that were developed in-house or are commercially available (Doty Scientific, Columbia, SC, USA; M2M Imaging Corp., Cleveland, OH, USA; Rapid MR International, Columbus, OH, USA). The results described in this chapter were produced with coils chosen to resonate at a proton frequency of 300 MHz with their inner diameter (ID) designed to fit closely around the mouse's head. The length (L) along the magnet bore axis for each coil was selected to compromise between high coil sensitivity and magnetic field homogeneity over the mouse brain (see Note 2). For the homemade cylindrically shaped Helmholtz coil shown in Fig. 2c, also referred to as a

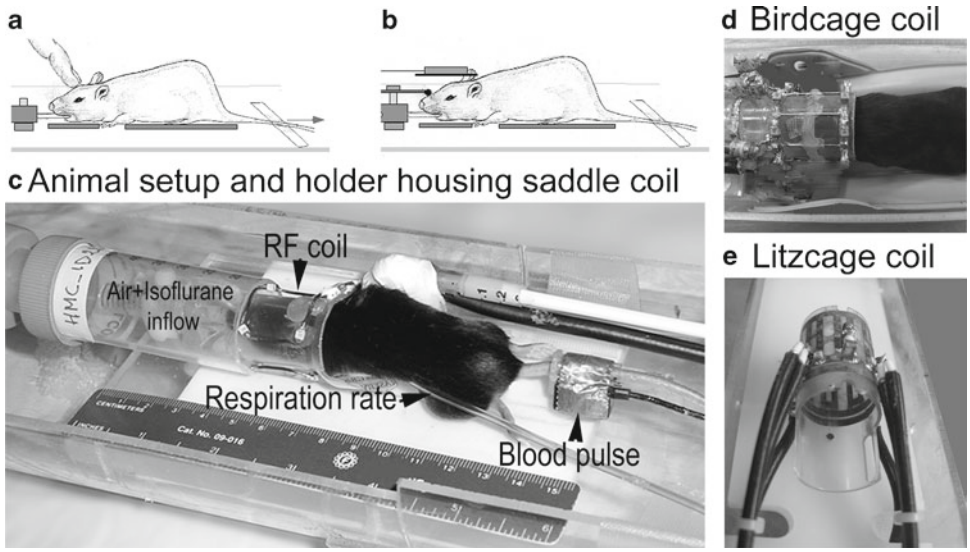

Fig. 2. Overview of mouse positioning/handling in the custom holder. (**a**) Position the mouse head in the bite bar and maintain the head immobilized with hand until taping the tail to stabilize the animal. (**b**) Insert the nosecone to ensure confined anesthetic delivery. (**c**) The mouse holding platform incorporates the RF coil (saddle coil shown) with tooth bar, a nosecone for isoflurane delivery via a vaporizer/scavenger system and a monitoring system measuring rectal temperature, blood pulse, and respiration rate. Multi-rung coils that have in general more homogenous RF field can also be considered such as (**d**) the birdcage coil (here designed in-house) or (**e**) the litzcage coil, in this example purchased from Doty Scientific (Columbia, SC, USA).

saddle coil (34), the dimensions were as follow: ID = 22 mm and L = 20 mm. We also designed in-house a quadrature birdcage coil (35, 36) tailored to cover the mouse head and that one can be seen in Fig. 2d (ID = 21.5 mm and L = 29 mm). A circularly polarized Litz coil available commercially (Doty Scientific, Columbia, SC, USA) (37) was also used (ID = 25 mm and L = 22 mm, Fig. 2e).

3. *Mouse holder*: The rf coil should be incorporated into a holder that stabilizes the mouse's head during MRI and can be fitted with devices for gas anesthesia delivery and physiological monitoring. MR compatible mouse holders are becoming available from commercial vendors of small animal MRI systems as well as rf coils, but most reports to date have used custom-holding devices. We have developed our own holder, incorporating the mouse head coil, a nose cone for isoflurane anesthesia, and several physiological-monitoring devices (Fig. 2; see Note 3). The main design goal of the mouse holder should be to hold the head in a stationary and reproducible position during the 2–3 h that the animal must be maintained inside the magnet. Predictably, the design closely resembles a stereotaxic injection device, but is fabricated from nonmetallic MRI compatible materials (see Note 4). The head holder should be equipped with a calibrated tooth bar allowing enough vertical and horizontal range (5–10 mm) to center any brain region of interest within the RF coil. Ear bars would be helpful to further stabilize the mouse head, but most RF coil designs are not open structures, and it is difficult to incorporate ear bars within the close-fitting head coil.
4. *Gas anesthesia*: Isoflurane vaporizer/anesthesia machine (VMS Matrix Medical, Orchard Park, NY).
5. *Surgical microscope*: (M650, Wild, Heerbrugg, Switzerland or M320F12, Leica Microsystems, Wetzlar, Germany).
6. *Syringe pump*: PHD2000 computer-controlled syringe pump (Harvard Apparatus, Hollison, MA).

2.2.2. Supplies

1. Isoflurane (Aerane, Baxter, Deerfield, IL).
2. Surgical supplies (available from any surgical supplies vendor): small sharp dissection scissors; two pairs of #5 Dumont forceps; 5-0 silk suture; 30-gauge needle; 70% ethanol for cleaning instruments.
3. Cannulae for infusing magnetically labeled peptides: Polyethylene tubing PE-10 (Intramedic, Becton Dickinson, Parsippany, NJ), Inner diameter ID = 0.28 mm (0.011″) and Outer diameter OD = 0.61 mm (0.024″).

3. Methods

3.1. Labeling of Amyloid-β Peptide

The MRI ligands described in this chapter are experimental probes that can be used as control compounds for subsequent animal studies using novel probes. Intact Aβ1-40 is unlikely to be used in humans because of its well-documented intrinsic toxicity that may not be noticeable in acute studies. We are currently developing more soluble nontoxic Aβ derivatives, such as K6Aβ1-30, that are likely to be more suitable as MRI probes for determining brain Aβ load in patients (14).

3.1.1. Peptide Synthesis

1. MR imaging ligand based on Aβ1-40 or K6Aβ1-30 is synthesized on a ABI 430A peptide synthesizer using standard protocols for tBOC (*tert*-butyloxycarbonyl) chemistry, attaching DTPA to the amino terminus of the peptide as the final step of synthesis.
2. The peptides are cleaved from the resins using hydrofluoric acid and purification is performed by high pressure liquid chromatography (HPLC) on a Vydac C18 preparative column, using linear gradients from 0 to 70% of acetonitrile in 0.1% trifluoroacetic acid.

3.1.2. Gadolinium Chelation

1. Gadolinium (Gd) is chelated to DTPA-Aβ1-40 or DTPA-K6Aβ1-30 by incubating the peptide in water or acetonitrile solution at pH 7.0 for 24 h with threefold molar excess of Gd, derived from Gd (III) chloride hexahydrate. For example, if 5 mg of peptide is labeled, the reaction can be performed in 1 ml total volume of 10% acetonitrile (see Note 5). The pH of the solution can be adjusted with a few microliter of 1 N NaOH and monitored with pH test strips. Mass spectroscopy of the lyophilized end-product, Gd-DTPA-Aβ1-40, can be used to verify the expected molecular weight (4,976.6 g/mol).

3.1.3. Putrescine Labeling

For attaching putrescine to Gd-DTPA-Aβ1-40 to increase its blood–brain barrier (BBB) permeability, we have followed the protocol of Poduslo et al. (9) with some minor modifications.

1. Gd-DTPA-Aβ1-40 (10 mg) is dissolved in 1 ml of 0.4 M putrescine, pH 4.7, and added to a solution of 1.4 g EDC in 1 ml of 0.4 M putrescine, pH 4.7.
2. This solution is mixed at room temperature for 4 h and subsequently dialyzed (molecular weight cut off: 2,000 g/mol) at 4°C for 2 days to remove excess putrescine and EDC (see Note 6).
3. Following dialysis, the peptide is relabeled with Gd, as described above for DTPA-Aβ1-40. The resulting Put-Gd-DTPA-Aβ1-40 can be injected intravenously to label amyloid plaques (9).

3.1.4. Mannitol Co-injection

Gd-DTPA-Aβ1-40 does not cross the BBB alone, and must either be modified with compounds such as putrescine (see above) or co-injected into the carotid artery with mannitol. For mannitol co-injection, 400 μg of Gd-DTPA-Aβ1-40 should be suspended in 100 μl of water, and then dissolved in 600 μl of 15% mannitol in PBS immediately before infusion.

3.2. Mouse Preparation

1. *Catheter construction*
   (a) Heat the PE10 polyethylene tubing using either a heat gun or heated oil and stretch to further reduce its diameter from OD = 0.61 mm to an approximate OD of 0.25 mm.
   (b) Cut the tubing to the length required for the syringe pump (see Note 7). The tapered end of the catheter will be inserted into either the artery or the vein during surgery.
2. Anesthetize the mouse with isoflurane: 5% isoflurane in air for 3 min to induce anesthesia, followed by 1–1.5% isoflurane in air to maintain anesthesia.
3. The skin is shaved and cleaned with 70% ethanol.
4. Cut with fine scissors, either on the neck to expose the common carotid artery or on the inside of the thigh to expose the femoral vein.
5. Under a surgical microscope, the vessel of interest is identified and a small section freed from the overlying muscle tissue with two pairs of fine forceps.
6. For injection into the common carotid artery (CCA), a 5-0 silk suture is tied loosely at the cephalic end of the right common artery and an identical suture is ligated at its central portion. Between the ligations, a puncture is made with a 30-gauge needle. A modified PE-10 tubing, attached to a 1-cc syringe filled with labeled peptide, is introduced into the right CCA through the small puncture. The suture at the cephalic CCA is then tightened around the intraluminal catheter to prevent bleeding. During injection, the left CCA is temporarily clamped with a microvascular clip.
7. For injection into the femoral vein, a small hole is made in the vein with a 30-gauge needle, and the modified PE-10 tubing subsequently inserted.
8. The Gd-DTPA-Aβ1-40/mannitol mixture (600–700 μl) is injected into the carotid artery at a rate of 60 μl/min, while a similar volume of Put-Gd-DTPA-Aβ1-40 is injected at the same rate into the femoral vein. In either case, the injection takes approximately 10 min.
9. After injection into the right CCA, the microvascular clip is removed, the catheter is withdrawn from the right CCA and the cephalic CCA is ligated. The puncture is subsequently

sealed with Krazy® glue. The CCA can then be unligated and with the blood flow restored the wound is closed with suture.

10. After injection into the femoral vein, the PE-10 tubing is withdrawn and the puncture is temporarily sealed with a small cotton ball to stop bleeding and the overlying skin then sutured.
11. Mice recover consciousness immediately after removal from anesthesia and should be kept warm until regaining full mobility.

3.3. In Vivo Two-Dimensional Interleaved Multi-slice MR Brain Imaging

2D MRI schemes by their nature are more easily implementable to both gradient echo (GE)- and spin-echo (SE)-based sequences due to the flexibility and ease of adjustment of the parameters. Their use became quickly widespread with the introduction of multiplexing (38, 39) rendering them equally sensitive to their 3D counterpart while offering more possibilities on the tradeoffs between the slice thickness, slice coverage, and the minimum imaging time required (40, 41). In fact, 2D MRI is almost indispensible when a conventional spin-echo sequence is considered due to its slower efficiency (15–17, 42).

1. *Mouse setup*:
   (a) Anesthetize the mouse with isoflurane: 5% isoflurane in air for 3 min to induce anesthesia, followed by 1–1.5% isoflurane in air to maintain anesthesia. Care should be taken to properly secure the mouse in the holder before MRI (Fig. 2; see Note 8).
   (b) After locking the upper inscissors in the tooth bar, press gently with the index finger just above the nose to avoid unhooking the teeth while pulling the tail taut and immobilizing it with tape (Fig. 2; see Note 9). This simple approach has proved to be very efficient for reducing motion artifacts and has provided high-quality MR brain images (Figs. 1 and 4) (15, 18).
2. *Slice alignment*:
   (a) Three single 1-mm thick slices are acquired simultaneously as orthogonal pilot orientations to achieve accurate image alignment after few iterations, ensuring accurate matching to histology and reproducibility between imaging sessions during longitudinal studies (Fig. 3). Pilot scans are low resolution MR images, acquired within several minutes at most, and providing anatomical landmarks adequate to specify the final slice alignment for the high resolution image acquisition. For Aβ plaque imaging in transgenic mice, we acquire multi-slice MR images in the coronal orientation. The mid-sagittal pilot image is used to align the final slices, checking first to ensure that the pilot is well aligned by verifying that the midline blood vessels are obvious throughout the image.

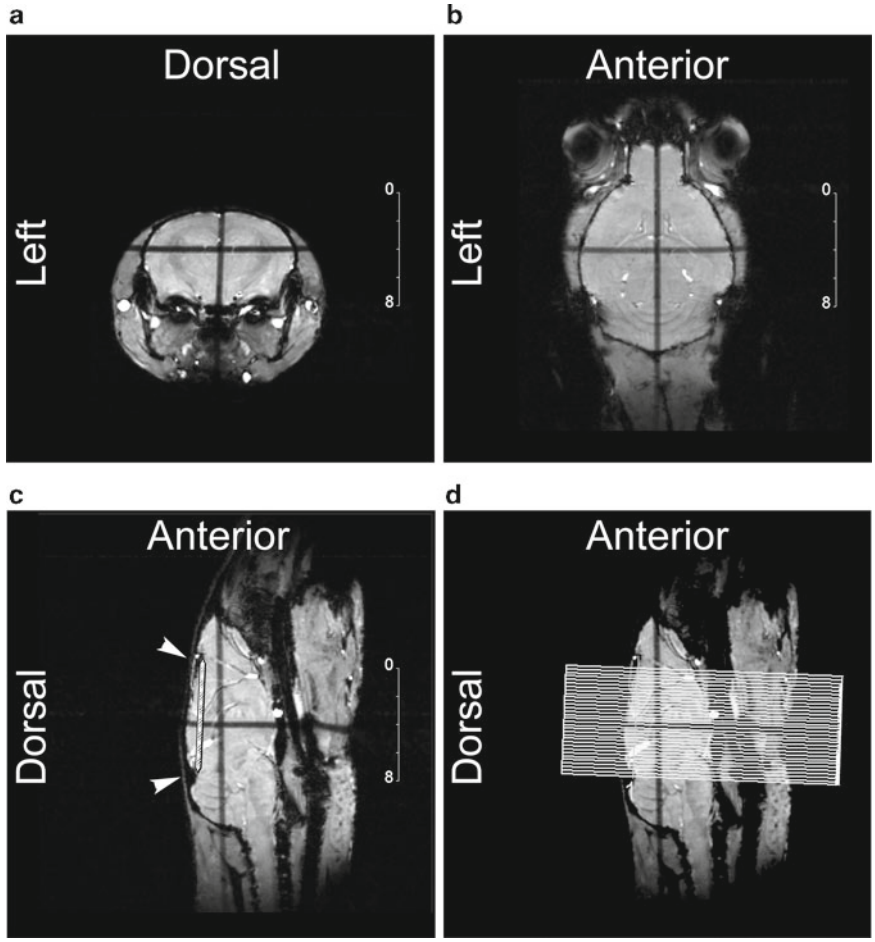

Fig. 3. Orthogonal pilot images (1 mm thick) are acquired corresponding to the coronal (**a**), horizontal (**b**), and sagittal (**c**) orientations (in-plane resolution ranging from 100 to 120 μm), obtained over several minutes using an iterative alignment process. The *crossed dark stripes* seen in all three images are induced by the saturation effect of the slice intercrossing acquired simultaneously, and help in slice positioning. The sagittal pilot orientation (**c**) provides easily identifiable landmarks for the alignment of 2D multi-slice coronal images. A baseline (*white striped segment*) is drawn from the two anatomical notches indicated by the *white arrowheads* in (**c**). Image (**d**) shows the resulting coronal slice grid, placed orthogonally to the baseline and overlaid on the sagittal pilot.

(b) Two "notches" are then identified, anteriorly between the olfactory bulb and the frontal cortex, and posteriorly at the junction of the cerebellum and midbrain (Fig. 3).

(c) The final image slices are placed perpendicular to the line between these two notches, checking for symmetric orientation also on the horizontal pilot image.

3. *High-resolution MRI acquisition*: We determined that Aβ plaques could be better detected with T2*-weighted MRI, 4–6 h after injection of Gd-DTPA-Aβ1-40 and mannitol (15, 18). For each brain, 31 contiguous coronal image slices are acquired from the frontal cortex to the cerebellum, with 78 μm×78 μm in-plane

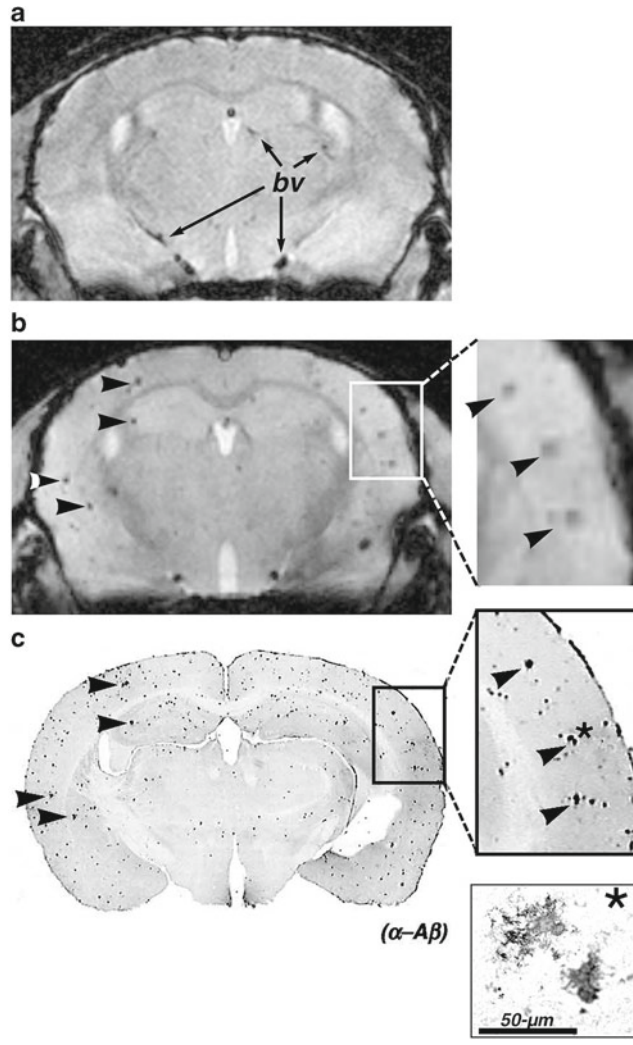

Fig. 4. Aβ plaques were detected with in vivo μMRI, 6 h after injection of Gd-DTPA-Aβ1-40 and 15% mannitol. In vivo T2*-weighted 2D multi-slice gradient-echo coronal μMR images show control (**a**) and transgenic (**b**) mouse brains. Many μMRI lesions could be matched to immunostained Aβ plaques (**c**, *arrowheads*), seen more clearly in the higher-magnification insets. High-power microscopic examination of the immunostained regions revealed that they were indeed parenchymal Aβ plaques, and not blood vessels or vascular amyloid (*inset*, corresponding to the region marked by an *asterisk*). *bv* Blood vessel (reprinted with permission from Wadghiri et al., Magn Reson Med. 2003;50(2):293–302, Wiley InterScience).

resolution using a gradient-echo sequence (TE = 15 ms; TR = 1.5 s; flip angle = 55°; slice thickness = 250 μm; total imaging time = 59 min). This sequence provided good anatomical detail and soft-tissue contrast, with sufficient susceptibility-induced contrast to detect Gd accumulation in plaques in the brains of the transgenic mice (Fig. 4) (15, 18).

3.4. In Vivo Three-Dimensional MR Brain Imaging with 100 μm Isotropic Acquisition

As previously described, 2D sequences provide some distinct advantages in their flexibility between the choice of slice thickness, slice coverage, and the minimum imaging time required (40, 41). However, when narrow slices are needed, they become quickly limited by the gradient strength available.

Additionally, cross-talk due to the multi-slice overlap can be another source of potential artifacts or a loss of signal-to-noise (SNR) likely more noticeable in spin-echo sequence and these issues may require the introduction of a slice gap. In contrast, in 3D sequences each acquisition represents an average of the entire sampled volume acquired through a slab that is less demanding in gradient strength. When combined with fast gradient-echo imaging sequences such as fast low-angle shot (FLASH) (3), whole 3D mouse head datasets can be practically implemented, with a 100 μm isotropic resolution, in less than 2 h as described below. This eases both the co-registration of serial MRI scans and with histologically stained sections for retrospective realignment using either the public domain program ImageJ (NIH Image, NIH, Bethesda, Maryland, USA) or commercially available imaging packages such as Analyze (AnalyzeDirect, Inc., Overland Park, KS, USA) or Amira (Visage Imaging GmbH, Berlin, Germany).

The mouse setup and slice alignment is identical to the 2D protocol in Subheading 3.3. Briefly, anesthetize the mouse with isoflurane and then proceed with identical care as described in the 2D protocol to properly secure the mouse in the holder before MRI to avoid potential motion artifact (Fig. 2; see Note 8). This will ease the co-registration during serial scans and with histology. At the final stage of the high resolution image acquisition for Aβ plaque imaging in transgenic mice, the slab of the 3D sequence is oriented along the dorso-ventral direction to minimize the wrap around by acquiring the horizontal orientation. Although the same two "notches" can be used as landmark to achieve a straightforward co-registration right after the acquisition when alignment is properly done, this stage becomes less critical since it can be replaced by virtual realignment retrospectively (Fig. 5).

1. *High-resolution MRI acquisition*: 4–6 h after injection of Gd-DTPA-Aβ1-40 and mannitol (15, 18) or Gd-DTPA-K6Aβ1-30 and mannitol (14), a 3D Spoiled Gradient Recalled (3D-SPGR) sequence is acquired with 100 μm × 100 μm × 100 μm isotropic resolution using either a single or a four echo train as follow:
   (a) *Single echo*: FOV: 2.56 × 2.56 × 2.56 cm, Matrix: 256 × 256 × 256, TE: 15 ms, TR: 50 ms, FA: 20, NA: 2, BW: 195.312 Hz/pixel (50 KHz total bandwidth) resulting in an effective scan time: 1 h 50 min.
   (b) *Multi-echo*: FOV: 2.56 × 2.56 × 2.56 cm, Matrix: 256 × 256 × 256, TE: 4.07 ms, echo spacing (ES): 6.7 ms,

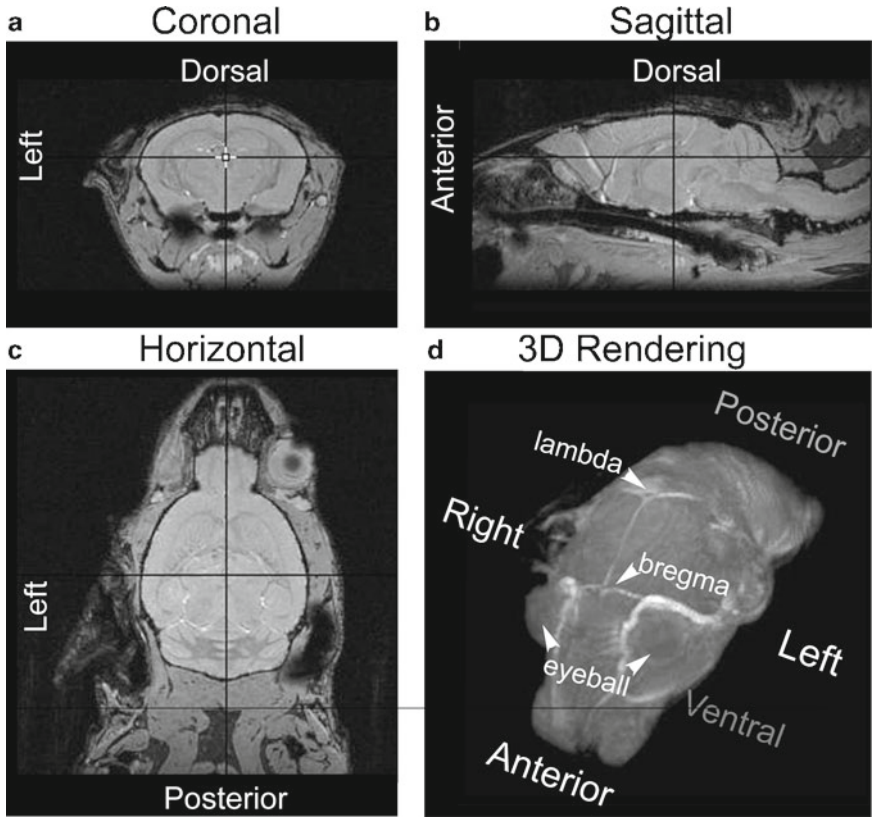

Fig. 5. The three orthogonal brain orientations in the mouse are shown as follow (**a**) coronal, (**b**) sagittal, and (**c**) horizontal. All three orientations were obtained from the same mouse head dataset acquired using a 3D MRI sequence (voxel resolution = 100 μm × 100 μm × 100 μm) shown in (**d**) as a 3D volume rendering in which both eyeballs can be seen. The bregma and lambda are two points that are easily identifiable on the dorsal surface of the mouse skull. Both landmarks are generally used as reference points in mouse brain atlases in which the bregma is the zero coordinate (Paxinos G. and Franklin K.B.J, *the mouse brain in Stereotaxic corordinates*, Elsevier, ISBN). The acquisition of 3D dataset with 100 μm isotropic resolution enables retrospective realignment of the slice sections in any desired orientation without compromising the quality of the resulting images. The co-registration with subsequent histology from the same mouse brain can then be easily achieved.

TR: 65 ms, FA: 20, NA: 2, BW: 195.312 Hz/pixel (50 KHz total bandwidth). Scan time: 2 h 21 min.

Both sequences provide good anatomical detail and soft-tissue contrast, with sufficient susceptibility-induced contrast to detect Gd accumulation in plaques in the brains of the transgenic mice (Fig. 6) (14). The multi-echo sequence can be very advantageous for objectively quantifying the Aβ burden as we previously demonstrated (25, 26).

2. Following in vivo MRI, the mice should be intra-cardially or intra-aortically perfused with PBS followed by 4% paraformaldehyde in PBS.

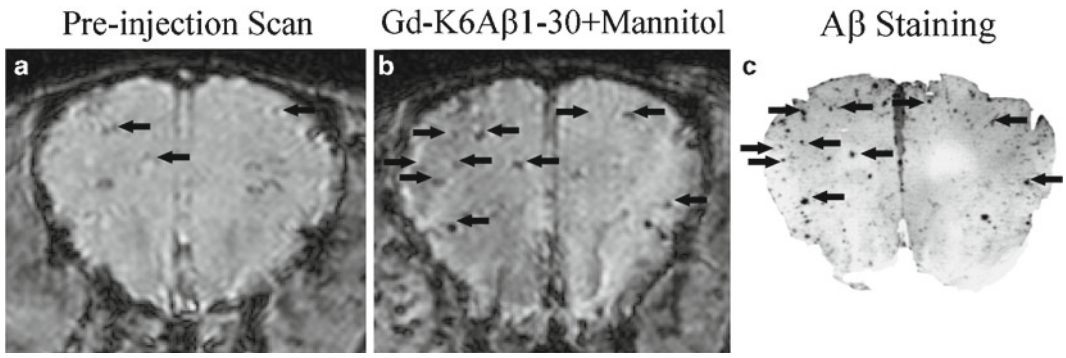

Fig. 6. In vivo Aβ plaque visualization is possible through endogenous detection. (**a**) A few large plaques can be identified in this 20-month-old Tg2576 mouse (see *arrows*) and can most likely be attributed to higher iron content especially in the larger and more mature plaques. The same transgenic mouse was subsequently imaged few weeks later to insure safe recovery and reduce the anesthetic burden. (**b**) Following intracarotid infusion of Gd-DTPA-K6Aβ1-30 co-injected with mannitol, the number of visualized plaques is substantially increased. These plaques by MRI co-register very well with plaques detected with 6E10/4G8 antibody on histological sections as depicted in (**c**) (reprinted with permission from Sigurdsson et al., Neurobiology of Aging 2008;29(6):836–847, Elsevier).

3. Extract brain and submit to fixation by immersion in 4% paraformaldehyde in PBS overnight at 4°C before considering sectioning for subsequent co-registration and validation. See Chapter 28 for details on tissue processing and staining.

3.5. Co-registration of MRI and Histology

1. Using the slice alignment procedure described above, excellent co-registration of MRI and histology can be obtained by blocking the sample, dorsal side down, and cutting coronal sections vertically across the block in the same orientation as the MR image slices. Take care to align the brain in the same manner as for MRI before sectioning.

4. Notes

1. *Static field strength*: The diversity of magnet strengths available for MRI studies raises questions about which field strength is optimal. In most centers, MRI studies will be performed on whatever magnet is available for small animal imaging. However, if there is a choice of field strength, the following factors should be considered. MRI sensitivity, generally measured as the SNR ratio, is linearly proportional to the magnetic field strength. Therefore, increasing the field strength will enable imaging with increased spatial resolution and/or a reduction in the MRI acquisition time. Currently for mouse brain imaging, magnetic field strengths ≥7-T enable in-plane resolution better than 100 μm and slice thickness lower than 500 μm using acquisition times of 1–2 h. MR image contrast,

usually a function of relaxation times T1 and T2, also depends on magnetic field strength. Although a full discussion of MR image contrast is beyond the scope of this chapter, relevant to Aβ plaque MRI is the fact that T1 differences are reduced at higher fields, and as a consequence T1-weighted MRI is less efficient and requires longer acquisition times. On the other hand, T2- and T2*-weighted sequences are more sensitive to small changes in magnetic properties of tissues at high field, and we and others have demonstrated more sensitive detection of magnetically tagged amyloid using T2- and T2*-weighted sequences, compared to T1-weighted MRI (14, 15, 18, 25).

2. *Rf coil*: For the saddle coil, we employed a linear coil design with a relatively simple tuning and impedance matching circuitry to facilitate rapid optimization of the coil sensitivity during the MRI setup. Although this design did not take advantage of the theoretical gain from a quadrature mode (36), it proved very efficient at high fields thanks to its simplified structure. Both the birdcage designed in-house and the commercial Litzcage coil are circularly polarized providing a quadrature detection.
3. *Physiological monitoring*: We have incorporated several devices, available in a computer-controlled system (MP100, Biopac Systems, Inc., Goleta, CA) in our mouse holder, including a rectal temperature probe, an infrared plethysmograph placed around the tail to monitor the blood pulse rate, and an air-filled cushion/pressure transducer placed under the mouse body to measure respiration rate. A respiration monitor is required to implement respiration-gated acquisition, although we have found that motion artifacts can be avoided with the mouse setup described in this chapter, without the need for gated acquisition. A similar MRI compatible setup from Small Animal instruments, Inc. (Stony Brook, NY, USA) can also be considered for effective physiological monitoring in combination with the various sensors described previously.
4. *MR compatible materials*: Plastics are generally used to construct animal holders for MRI: acrylic, polycarbonate, nylon, PVC, or delrin are all good choices. Metallic materials should be avoided except in the coil itself and must be limited to non-ferromagnetic metals, e.g., copper, aluminum, silver, and platinum.
5. Performing this reaction in a buffer should be avoided because ions may interfere with the labeling. Removal of the excess Gd by various means is likely to be accompanied by a loss of chelator bound Gd. Although free Gd can be toxic to mice, the animals seemed to tolerate well Gd-DTPA-Aβ1-40 that was not purified following peptide labeling with threefold molar

excess of Gd. The solubility of DTPA-Aβ1-40 depends on the lot of peptide, and the chelation can be performed in 10–20% acetonitrile in water if needed. Some precipitation can occur when the Gd solution is added, and/or following overnight labeling at 4°C. We have not analyzed the composition of the precipitate, but it can be removed by centrifugation prior to lyophilization or injection. DTPA-K6Aβ1-30 is much more soluble than DTPA-Aβ1-40, and its chelation to Gd can be performed in water.

6. In the original procedure by Poduslo et al. (9), the pH is maintained at pH 4.7 during the incubation period. This should promote putrescine coupling but we have obtained similar mass spectroscopy profile when the pH has not been kept constant during the reaction. The disadvantage of this method is that numerous peaks of similar molecular weight are obtained, indicating a mixture of DTPA-Aβ1-40 peptides with different numbers of attached putrescine molecules. We have also noticed that with one lot of DTPA-Aβ1-40, substantial precipitate formed during the reaction that reduced its yield. To avoid these issues, it may be better to label amino acids prior to peptide synthesis with putrescine or any other ligand that enhances brain uptake.
7. When cutting the polyethylene tubing, use a sharp scalpel blade or razor blade to avoid distorting/crushing the material. Do not use a pair of scissors.
8. Noticeable image artifacts (blurring) can arise from breathing motion in the neck and caudal head, which will make Aβ plaque detection impossible if not corrected. These artifacts can be greatly reduced if the mouse is properly secured in the holder as described in Subheading 3 (Fig. 2).
9. The whole body should remain lightly stretched during MRI, enabling the mouse to breathe freely while greatly reducing head motion from breathing.

Acknowledgments

The research described in this chapter was supported by grants from the NIH (AG020197 and AG032611 to EMS; AG20245, and AG008051 to TW, the Alzheimer's Association (IIRG-08-91618 to YZW, ZEN-08-91006 to EMS), the American Health Assistance Foundation (ADR-A2008-155 to YZW). We thank Yongsheng, Li and Jeffrey A. Blind and Amr Morsi for assistance with the surgical protocols. We also thank Dr Florence Janody for artistic help with Fig. 2.

References

1. Hsiao K, Chapman P, Nilsen S, Eckman C, Harigaya Y, Younkin S, Yang F, *et al.* Correlative memory deficits, Abeta elevation, and amyloid plaques in transgenic mice. Science (New York, NY) 1996, 274: 99–102
2. Holcomb L, Gordon MN, McGowan E, Yu X, Benkovic S, Jantzen P, Wright K, *et al.* Accelerated Alzheimer-type phenotype in transgenic mice carrying both mutant amyloid precursor protein and presenilin 1 transgenes. Nat Med 1998, 4: 97–100
3. McGowan E, Eriksen J, Hutton M. A decade of modeling Alzheimer's disease in transgenic mice. Trends Genet 2006, 22: 281–289
4. Ashe KH, Zahs KR. Probing the biology of Alzheimer's disease in mice. Neuron 2010, 66: 631–645
5. Obulesu M, Rao DM. Animal models of Alzheimer's disease: an understanding of pathology and therapeutic avenues. The International Journal of Neuroscience 2010, 120: 531–537
6. Wisniewski T, Sigurdsson EM. Murine models of Alzheimer's disease and their use in developing immunotherapies. Biochimica et Biophysica Acta 2010, 1802: 847–859
7. Benveniste H, Einstein G, Kim KR, Hulette C, Johnson GA. Detection of neuritic plaques in Alzheimer's disease by magnetic resonance microscopy. Proc. Natl. Acad. Sci. of the United States of America 1999, 96: 14079–14084
8. Dhenain M, Privat N, Duyckaerts C, Jacobs RE. Senile plaques do not induce susceptibility effects in T2*-weighted MR microscopic images. NMR Biomed 2002, 15: 197–203
9. Poduslo JF, Wengenack TM, Curran GL, Wisniewski T, Sigurdsson EM, Macura SI, Borowski BJ, *et al.* Molecular targeting of Alzheimer's amyloid plaques for contrast-enhanced magnetic resonance imaging. Neurobiol Dis 2002, 11: 315–329
10. Helpern JA, Lee SP, Falangola MF, Dyakin VV, Bogart A, Ardekani B, Duff K, *et al.* MRI assessment of neuropathology in a transgenic mouse model of Alzheimer's disease. Magn Reson Med 2004, 51: 794–798
11. Lee SP, Falangola MF, Nixon RA, Duff K, Helpern JA. Visualization of beta-amyloid plaques in a transgenic mouse model of Alzheimer's disease using MR microscopy without contrast reagents. Magn Reson Med 2004, 52: 538–544
12. Zhang J, Yarowsky P, Gordon MN, Di Carlo G, Munireddy S, van Zijl PC, Mori S. Detection of amyloid plaques in mouse models of Alzheimer's disease by magnetic resonance imaging. Magn Reson Med 2004, 51: 452–457
13. Dhenain M, Delatour B, Walczak C, Volk A. Passive staining: a novel ex vivo MRI protocol to detect amyloid deposits in mouse models of Alzheimer's disease. Magn Reson Med 2006, 55: 687–693
14. Sigurdsson EM, Wadghiri YZ, Mosconi L, Blind JA, Knudsen E, Asuni A, Scholtzova H, *et al.* A non-toxic ligand for voxel-based MRI analysis of plaques in AD transgenic mice. Neurobiol Aging 2008, 29: 836–847
15. Wadghiri YZ, Sigurdsson EM, Sadowski M, Elliott JI, Li Y, Scholtzova H, Tang CY, *et al.* Detection of Alzheimer's amyloid in transgenic mice using magnetic resonance microimaging. Magn Reson Med 2003, 50: 293–302
16. Jack CR, Jr., Garwood M, Wengenack TM, Borowski B, Curran GL, Lin J, Adriany G, *et al.* In vivo visualization of Alzheimer's amyloid plaques by magnetic resonance imaging in transgenic mice without a contrast agent. Magn Reson Med 2004, 52: 1263–1271
17. Jack CR, Jr., Wengenack TM, Reyes DA, Garwood M, Curran GL, Borowski BJ, Lin J, *et al.* In vivo magnetic resonance microimaging of individual amyloid plaques in Alzheimer's transgenic mice. J Neurosci 2005, 25: 10041–10048
18. Sigurdsson EM, Wadghiri YZ, Sadowski M, Elliott JI, Li Y, Scholtzova H, Tang CY, *et al.* In vivo magnetic resonance of amyloid plaques in Alzheimer's disease model mice. In: Hyman B, Demonet JF, Christen Y eds., *The living brain and Alzheimer's disease.* Hardcover ed. Berlin: Springer Verlag 2004: 47–59
19. Higuchi M, Iwata N, Matsuba Y, Sato K, Sasamoto K, Saido TC. 19F and 1H MRI detection of amyloid beta plaques in vivo. Nat Neurosci 2005, 8: 527–533
20. Vanhoutte G, Dewachter I, Borghgraef P, Van Leuven F, Van der Linden A. Noninvasive in vivo MRI detection of neuritic plaques associated with iron in APP(V717I) transgenic mice, a model for Alzheimer's disease. Magn Reson Med 2005, 53: 607–613
21. Braakman N, Matysik J, van Duinen SG, Verbeek F, Schliebs R, de Groot HJ, Alia A. Longitudinal assessment of Alzheimer's beta-amyloid plaque development in transgenic mice monitored by in vivo magnetic resonance microimaging. J Magn Reson Imaging 2006, 24: 530–536
22. Borthakur A, Gur T, Wheaton AJ, Corbo M, Trojanowski JQ, Lee VM, Reddy R. In vivo

measurement of plaque burden in a mouse model of Alzheimer's disease. J Magn Reson Imaging 2006, 24: 1011–1017

23. Faber C, Zahneisen B, Tippmann F, Schroeder A, Fahrenholz F. Gradient-echo and CRAZED imaging for minute detection of Alzheimer plaques in an APPV717I x ADAM10-dn mouse model. Magn Reson Med 2007, 57: 696–703
24. Muskulus M, Scheenstra AE, Braakman N, Dijkstra J, Verduyn-Lunel S, Alia A, de Groot HJ, *et al.* Prospects for early detection of Alzheimer's disease from serial MR images in transgenic mice. Current Alzheimer Research 2009, 6: 503–518
25. Scholtzova H, Wadghiri YZ, Douadi M, Sigurdsson EM, Li YS, Quartermain D, Banerjee P, *et al.* Memantine leads to behavioral improvement and amyloid reduction in Alzheimer's-disease-model transgenic mice shown as by micromagnetic resonance imaging. Journal of Neuroscience Research 2008, 86: 2784–2791
26. Yang J, Zaim Wadghiri Y, Minh Hoang D, Tsui W, Sun Y, Chung E, Li Y, *et al.* Detection of amyloid plaques targeted by USPIO-Abeta1–42 in Alzheimer's disease transgenic mice using magnetic resonance microimaging. Neuroimage 2011, 55(4): 1600–1609
27. Weinmann HJ, Brasch RC, Press WR, Wesbey GE. Characteristics of gadolinium-DTPA complex: a potential NMR contrast agent. AJR Am J Roentgenol 1984b, 142: 619–624
28. Weinmann HJ, Laniado M, Mutzel W. Pharmacokinetics of GdDTPA/dimeglumine after intravenous injection into healthy volunteers. Physiological chemistry and physics and medical NMR 1984a, 16: 167–172
29. Bulte JW, Kraitchman DL. Iron oxide MR contrast agents for molecular and cellular imaging. NMR Biomed 2004, 17: 484–499
30. Mulder WJ, Griffioen AW, Strijkers GJ, Cormode DP, Nicolay K, Fayad ZA. Magnetic and fluorescent nanoparticles for multimodality imaging. Nanomedicine (London, England) 2007, 2: 307–324
31. Siddiqui TS, Jani A, Williams F, Muller RN, Vander Elst L, Laurent S, Yao F, *et al.* Lanthanide complexes on Ag nanoparticles: designing contrast agents for magnetic resonance imaging. Journal of Colloid and Interface Science 2009, 337: 88–96
32. Wadghiri YZ, Briley-Saebo K. Nanobiomaterials for Preclinical Studies and Clinical Diagnostic. In: Sitharaman B ed., *Nanobiomaterials Handbook.* Hardback ed. New York: CRC Press. 2011: 1–24
33. Johnson G, Zaim Wadghiri Y, Turnbull DH. Sensitivity in 2D multislice and 3D MR imaging. Magn Reson Med 2003, 49(5): 848–855
34. Hoult DI, Richards RE. The signal-to-noise ratio of the nuclear magnetic resonance experiment. J Magn Reson 1976: 71–85
35. Hayes CE, Edelstein WA, Schenck JF, O.M. M, Eash M. An efficient, highly homogeneous radiofrequency coil for whole-body NMR imaging at 1.5T. J Mag Reson 1985, 63: 622–628
36. Glover GH, Hayes CE, Pelc NJ, Edelstein WA, Mueller OM, Hart HR, O'Donnell M, *et al.* Comparison of linear and circular polarization for magnetic resonance imaging. J Mag Reson 1985, 64: 255–270
37. Doty FD, Entzminger G, Jr., Hauck CD. Error-tolerant RF litz coils for NMR/MRI. J Magn Reson 1999, 140: 17–31
38. Crooks LE, Ortendahl DA, Kaufman L, Hoenninger J, Arakawa M, Watts J, Cannon CR, *et al.* Clinical efficiency of nuclear magnetic resonance imaging. Radiology 1983, 146: 123–128
39. Crooks L, Arakawa M, Hoenninger J, Watts J, McRee R, Kaufman L, Davis PL, *et al.* Nuclear magnetic resonance whole-body imager operating at 3.5 KGauss. Radiology 1982, 143: 169–174
40. Brunner P, Ernst RR. Sensitivity and performance time in NMR imaging. J Magn Reson 1979: 83–106
41. Johnson G, Wadghiri YZ, Turnbull DH. 2D multislice and 3D MRI sequences are often equally sensitive. Magn Reson Med 1999, 41: 824–828
42. Jack CR, Jr., Marjanska M, Wengenack TM, Reyes DA, Curran GL, Lin J, Preboske GM, *et al.* Magnetic resonance imaging of Alzheimer's pathology in the brains of living transgenic mice: a new tool in Alzheimer's disease research. Neuroscientist 2007, 13: 38–48

Chapter 31

The Mouse Model for Scrapie: Inoculation, Clinical Scoring, and Histopathological Techniques

Michele A. Di Bari, Romolo Nonno, and Umberto Agrimi

Abstract

Transmission to mice and other laboratory rodents are central to the study of prion diseases. Bioassays are essential for testing the presence of infectivity, as well as for titration and strain typing studies. Given the peculiar nature of prions, their characterization relies mainly on the measurement of the length of the incubation period in inoculated mice and on the study of a number of parameters, such as the clinical manifestations, the type of pathological changes and the biochemical characteristics of PrP^{Sc}, that call for considerable experience and care in the execution of laboratory procedures and in the reading and interpretation of results. Researchers who are new to the prion field or who would like to expand into studies of rodent models may need information about the practical aspects of prion diseases in mice. This chapter reviews the techniques used in transmission studies, from the preparation of the inocula to pathological investigations, with specific focus on the potential problems that may occur and how to solve them.

Key words: Prion diseases, Bioassays, Infectivity, Histopathology

1. Introduction

Scrapie of sheep and goats is one of the transmissible spongiform encephalopathies, or prion diseases, a group of neurodegenerative diseases caused by unconventional infectious agents known as prions. Other members of the group are bovine spongiform encephalopathy (BSE) in cattle, chronic wasting disease in cervids, and Creutzfeldt–Jakob disease (CJD) in humans. In 1995 a new disease, named variant CJD (vCJD) and caused by the BSE agent, was reported in humans (1, 2).

Prion diseases are invariably fatal. Though transmissible under natural and/or experimental conditions, their pathological picture is typical of neurodegenerative disorders with histological lesions comprising vacuolation, neuronal loss and astrocytosis and the accumulation in the brain of the misfolded isoform (PrP^{Sc}) of a

Einar M. Sigurdsson et al. (eds.), *Amyloid Proteins: Methods and Protocols*, Methods in Molecular Biology, vol. 849,
DOI 10.1007/978-1-61779-551-0_31,

cellular protein named prion protein, or PrP^{C}. According to the protein-only hypothesis, prions are composed mainly or exclusively of PrP^{Sc} (3). Diagnosis of prion diseases is based on histopathology and on the detection of PrP^{Sc} in brain tissue. Since no antibody exists that unequivocally distinguishes between the pathological and cellular isoforms of the prion protein, PrP^{Sc} is routinely identified by its resistance to proteinase K which, in contrast, destroys PrP^{C}.

In spite of recent progress in the development of *in vitro* and cellular models, transmission to laboratory animals remains central to the study of prion diseases. In particular, bioassays are essential for testing the presence of infectivity, as well as for titration and strain typing studies.

Though apparently devoid of nucleic acids, it is well established that prions exhibit strain variation. Different scrapie sources can produce different and well reproducible clinical–pathological characteristics of disease after serial passages in syngeneic mice. Given the absence of nucleic acids and the limited knowledge available on the molecular structure of prions, their characterization relies mainly on the description of disease characteristics. The length of the incubation period is the only "quantitative" parameter used for prion characterization and one of the easiest to measure. All other parameters, such as the clinical manifestations, the type of pathological changes and the biochemical characteristics of PrP^{Sc}, are "qualitative" parameters that call for considerable experience and care in the execution of laboratory procedures and in the reading and interpretation of results.

Although numerous distinct prion strains have been identified in mice by serially passaging scrapie, BSE or CJD, wild-type mice present critical limitations. The transmission of prion diseases from their natural hosts to wild-type mice generally requires very long incubation times and transmission is not always successful. The mouse model has been significantly improved through the development of transgenic mice carrying the PrP gene of sheep, cattle, humans, and deer, in a bid to remove the interspecies transmission barrier (4). These models allow for the study of prion diseases other than mouse-adapted strains, as they have been generally shown to be highly susceptible to prions originating from the species of which they carry the PrP gene. In some cases, overexpression of the heterologous PrP gene has been obtained with the aim of further increasing their susceptibility (4).

Complementary to these specialized models, noteworthy efforts have also been made in recent years to develop the bank vole (*Myodes glareolus*) model, a rodent species that shows a high susceptibility to a wide range of animal and human prion strains (5–7). The Syrian hamster has also been widely used on account of the short incubation time of the scrapie strain adapted to that rodent model (8). As each model presents specific characteristics,

especially with regard to susceptibility, the choice of the most suitable model requires profound knowledge of its characteristics. Several clinical and pathological parameters can be investigated in transmission studies. Their selection depends on the aim of each individual study. Infectivity and titration studies call only for checks on the success of transmission using clinical signs and diagnostic approaches. Strain typing studies, on the other hand, require the measurement and analysis of several parameters; theoretically, the greater the number of parameters studied, the greater the accuracy of strain characterization and the definition of the differences/similarities of a given strain in comparison with others.

Researchers who are new to the prion field or who would like to expand into studies of rodent models may need information about the practical aspects of prion diseases in mice. This chapter reviews the techniques used in transmission studies, from the preparation of the inocula to pathological investigations, with specific focus on the potential problems that may occur and how to solve them.

2. Materials

2.1. Inocula Preparation

1. Sterile phosphate-buffered saline (PBS): weigh and dissolve 1.37 M of sodium chloride (NaCl), 26.8 mM of potassium chloride (KCl), 0.1 M of sodium phosphate (Na_2HPO_4), 17.6 mM of potassium phosphate ($KHPO_4$) in distilled water. Adjust the pH to 7.2 with 1 N NaOH solution.
2. Polypropylene pestle: EPPI-pistill, for exact fitting Eppendorf® test tubes.
3. Eppendorf® test tubes of 1.5–2.0 ml.
4. Analytical balance.
5. Laminar flow hood.

2.2. Anesthesia

1. 1-ml disposable syringes and 26-gauge needles.
2. Injectable anesthetic: 100 mg/kg ketamine and 10 mg/kg xylazine, diluted in sterile physiological solution.
3. Inhalant anesthetic (isoflurane) and the precision vaporizers for its usage.

2.3. Inoculation

1. 0.5-ml disposable syringes with 28-gauge integral needle.
2. 1-ml disposable syringes and 26-gauge needles.
3. Hot plate.
4. Tissue paper.

2.4. Euthanasia and Samples Collection

1. CO_2 chamber.
2. Sodium pentobarbital.
3. Infusion set, 23-gauge needle.
4. 50-ml syringe.
5. Perfusion washing solution: prepare the PBS, as reported above, with 5 mM of EDTA.
6. 10% Neutral-buffered formalin.

2.5. Tissues Preparation

1. Xylene.
2. Graded ethanol at 40, 60, 75, 90, 95, and 100%.
3. Wax paraffin.
4. Embedding cassettes.
5. Automatic tissue processor.
6. Embedding station.

2.6. Hematoxylin and Eosin Staining

1. Microtome.
2. Microscope slides.
3. Xilene.
4. Graded ethanol at 70, 80, 95, and 100%.
5. Mayer's hematoxylin solution.
6. Eosin solution.
7. Eukitt mounting medium.

2.7. Immuno-histochemistry

1. Superfrost Plus slides (cod. J1800AMNZ, Thermo Scientific, UK).
2. Thermostat.
3. Xilene.
4. Graded ethanol at 70, 80, 95, and 100%.
5. Hydrogen peroxidase.
6. Methanol.
7. 98% formic acid.
8. Autoclave.
9. 10 mM citrate buffer pH 6.0.
10. Phosphate buffer saline with Tween 20 (PBST): prepare PBS as reported above and add 0.1% of Tween 20.
11. Normal blocking serum: normal serum from the species the secondary antibody was raised in diluted to 1/20 in PBST.
12. Secondary biotinylated antibody (anti-mouse or anti-rabbit IgG), depending on the species the primary antibody was raised in.

13. Biotin–(Strept)avidin Complex, ABC (Vector Elite ABC, Vector Laboratories).
14. 3,3′-diaminobenzidine (DAB) substrate (Sigma Fast Dab Tablet Sets, Sigma-Aldrich).
15. Mayer's hematoxylin solution.
16. Eukitt mounting medium.
17. Primary antibody: SAF84 (Inalco).

2.8. Paraffin Embedding Blotting

1. 0.45-μm-pore nitrocellulose membrane.
2. Microscope slides.
3. Six-well cell culture cluster.
4. Orbital incubator (MO-OR, Bioscientifica, Roma, Italy).
5. Vacuum pump.
6. Rocking platform.
7. Xilene.
8. Isopropyl alcohol at 50, 70, 80, and 99–100%.
9. Tris–HCl-buffered saline at pH 7.6 for solutions and washing (TBST, pH 7.6): 100 mM of Tris base + 100 mM of NaCl + 0.05% of Tw20. Adjust pH at 7.6 with HCl.
10. Tris–HCl-buffered saline at pH 7.8 for proteinase K solution (TBST, pH 7.8): 10 mM Tris base + 100 mM of NaCl + 0.1% of Tw20. Adjust to pH 7.8 with HCl.
11. Proteinase K solution: 20 μg/ml proteinase K in TBST, pH 7.8.
12. Phenylmethylsulfonyl fluoride solution (PMSF solution): 3 mM of phenylmethylsulfonyl fluoride (PMSF) in TBST, pH 7.6.
13. 3 M guanidine isothiocyanate in TBST, pH 7.6.
14. Blocking solution: 2% dried milk (or 0.2% of casein) in TBST, pH 7.6.
15. Primary antibody solution: antibodies must be diluted in TBST, pH 7.6, at 2% of dried milk (or 0.2% of casein).
16. Secondary antibody solution: alkaline phosphatase-coupled secondary antibody must be diluted in TBST, pH 7.6.
17. Tris–HCl-buffered saline at pH 9.0 for solutions and washing (TBS, pH 9.0): 100 mM of Tris base + 100 mM of NaCl. Mix and adjust at pH 9.0 with HCl.
18. TMN solution: 50 mM of MgCl2 in TBS, pH 9.0.
19. NBC/BCIP: ready to use (PIERCE, Thermo Scientific).
20. 20 mM of EDTA in TBS, pH 9.0.

3. Methods

3.1. Safety Measures

Handling prion-infected material requires extreme caution. Laboratory studies may expose operators to hazardous procedures and to varieties of prion strains with not easily predictable risk. It is therefore imperative to adhere strictly to the safety measures provided in international rules and protocols (9).

3.2. Inoculum Preparation

Prions are extremely resistant to physical and chemical agents (10). Infectivity can persist on contaminated instruments and working surfaces even after severe decontamination procedures have been adopted. The preparation of inocula has therefore to be performed under standard sterile conditions and using procedures able to minimize the risk of prion cross-contamination (see Note 1).

Solutions for injection should be close to neutral pH, as high or low extremes are not tolerated by tissues. For this reason, the use of phosphate-buffered saline (PBS) (see Note 2) is preferable to the physiological solution. Samples are weighed with an analytical balance and homogenized in disposable pestles at 10% (w/v) concentration in sterile PBS. Homogenates are then aliquoted and stored at –25°C.

Because of the time lapse between death and sample collection, brain material from natural sheep scrapie cases, or from any other natural prion diseases, is often inadequately preserved and may be contaminated by bacteria. In these cases, measures should be taken to prevent mortality from contaminated inocula (see Note 3).

3.3. Inoculation

In our laboratory each animal entering experimentation is individually identified by a passive electronic transponder (12-mm glass tag, Wyre Micro Design Ltd., Lancashire, England) injected subcutaneously that allows each animal to be unequivocally identified throughout the experiment.

The route of infection may condition the pathogenesis of prion disease and its choice is dictated by the experimental protocol. Although prions can replicate in several peripheral tissues (especially in the nervous and lymphoid systems), their clinical and pathological manifestations are consequent on neuroinvasion. Hence, the direct inoculation of prions into the brain produces the shortest incubation times. In contrast, after peripheral infection (i.e., oral, intraperitoneal) there is a protracted extraneuronal replication phase before the agent can be detected in the central nervous system.

Before inoculation, animals must be anesthetized (see Note 4). Free-hand inoculation is commonly used for intracerebral infection but a stereotaxic apparatus is needed when the injection has to be performed in a very specific brain area (see Note 5). The injection volumes should not exceed 2% of brain volume (11). For a mouse weighing approximately 20–25 g, 20 µl of homogenate

can be inoculated. Weanling mice aged 4–6 weeks are preferable because of the relative softness of the skull. At this age, 0.5-ml syringes with a 28-gauge integral needle can be used. For the intracerebral inoculation of older mice, 26-gauge needles can be used. A larger size could cause excessive damage to brain tissue and the braincase. Intraperitoneal injection is the route of peripheral infection most frequently used. It is performed as described for the intraperitoneal injection of anesthetic (see Note 4). After inoculation, animals must be closely monitored until they completely recover from anesthesia.

3.4. Clinical Scoring

Prion diseases manifest themselves with behavioral alterations and neurological signs. Clinical scoring should be performed by an experienced technician. It is carried out twice per week until the appearance of neurological signs, after which it is performed daily.

Early clinical signs in mice are often ambiguous and nonspecific; they consist mostly of behavioral abnormalities. Mice display dull, ruffled coat and develop hyperactive behavior.

The most frequent clinical signs are as follows: impaired motor coordination, kyphosis, high stepping gait, straight tail, head tilt, proprioceptive deficits, lethargy, C-shaped tail, blank stare, rolling gait, pruritus. However, depending on prion strain, some of these signs may be absent. In the terminal stage, pronounced ataxia, kyphosis and severe hypo-activity, and hypo-reactivity precede natural death (12).

A standard clinical end point needs to be established in order to define univocally the correct time for sacrifice and proper measurement of the incubation period. This is traditionally defined on the basis of the repeated observation of the same clinical sign over a given period of time. Bearing in mind the variable clinical presentation of these diseases depending on the particular prion strain involved, different clinical end points can be established for different strains. However, standard clinical end points cannot be established *a priori* in primary transmissions where the outcome of inoculation is totally unpredictable. A number of tests have been proposed for the assessment of clinical signs, such as the classical open field and hot plate tests (13), the evaluation of the ability to move on a grid (14) and the tendency of clasping feet when raised by the tail (12). Beside direct clinical observation, computer-assisted methods have been developed for the automated monitoring of the daily activity induced in mice by prion infection. These systems have proved very useful for anticipating a clinical diagnosis and, based on the specific activity profiles recorded, can provide additional criteria for the characterization of prion strains (13).

Clinical signs vary considerably depending on prion strain. Some strains cause severe ataxia, while others produce only insignificant motor dysfunctions. The duration of the clinical stage may also vary among strains. In addition, neurological signs, especially

in the case of primary transmissions, are often subtle and unpredictable, in contrast to what is found in well-established mouse-adapted strains. In these cases, we prefer to measure the survival time, as the interval between infection and sacrifice in the terminal stage of disease, rather than the incubation period. Survival time represents a more reliable measurement than the incubation time and is less affected by the operator's experience. For ethical reasons, mice are culled in the terminal stage but before the neurological impairment and the general conditions are such as to compromise welfare and, especially, adequate drinking and feeding.

3.5. Euthanasia and Collection of Samples

Inhalation and injection of agents can be used for euthanasia (see Note 6). Brain sampling procedures depend on the experimental protocol. To maximize the utilization of brain samples, we usually divide each brain into two parts by a sagittal paramedian cut. The smaller portion is immediately frozen and stored at –20°C for Western blotting analysis and/or inocula preparation. The remaining part is fixed in buffered formalin for at least 24–48 h at room temperature. Fixative volume should be five to ten times tissue volume. For detailed morphological studies, perfusion of the brain may be required (see Note 7). After fixation in formalin, tissues can be decontaminated with formic acid, which makes tissue handling safer by several orders of magnitude (15) (see Note 8).

3.6. Preparation of Tissues

The aim of tissue processing is to embed the tissue in a solid medium that is firm enough to support the tissue and to give it sufficient rigidity to enable thin sections to be cut. The most satisfactory embedding material for routine histology is paraffin wax. To enable impregnation with paraffin, the tissue must be processed through dehydration in ascending concentrations of alcohol, immersion in cleaning agents (generally hydrocarbon solvents) which are miscible with both dehydrating agents and paraffin wax, and finally embedded in paraffin wax.

Given the complex structure of the brain, trimming before processing is critical to guarantee the presence of the expected areas on the section. Lesion profiling, for example, requires four standard levels of the brain (see Fig. 1a) to be available in order to examine nine specific areas of grey matter (see Fig. 1b). This method, though initially developed in mice (16), was subsequently adapted to other rodent species, such as the bank vole (5).

1. Paraffin embedding schedule, to be performed by hand or by automatic tissue processor (total 31.5 h):
   (a) 40% Ethanol, one change, 90 min.
   (b) 60% Ethanol, one change, 90 min.
   (c) 80% Ethanol, one change, 90 min.
   (d) 95% Ethanol, one change, 90 min.

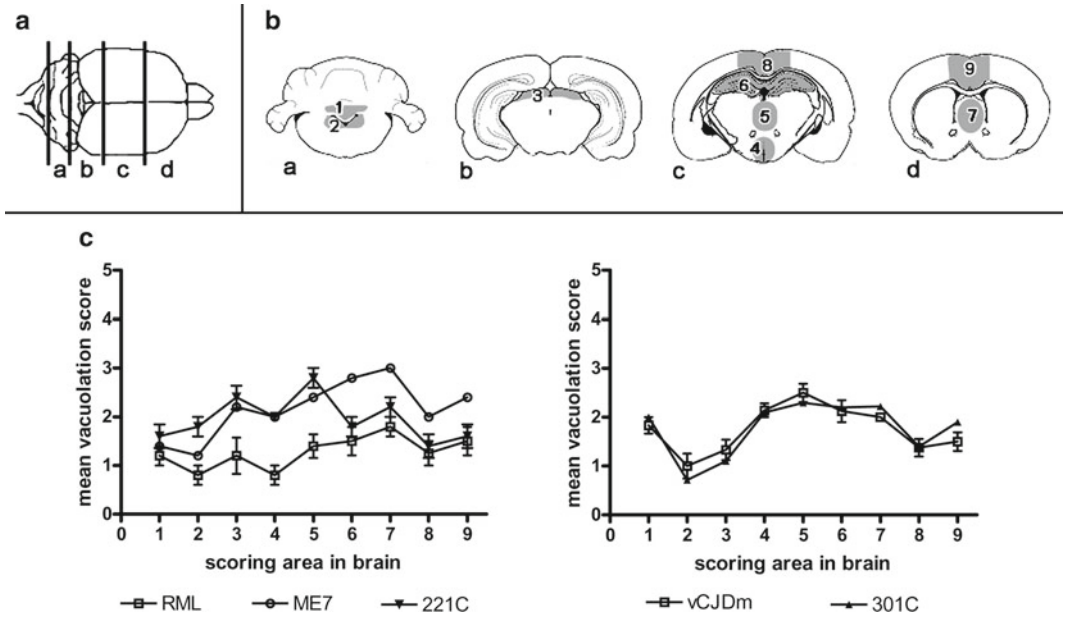

Fig. 1. (**a**) Schematic representation of the brain with the standard cutting levels used for lesion profiles. (**b**) Standard coronal brain sections in which the nine areas scored for lesion profile are shown: (*1*) medulla, (*2*) cerebellum, (*3*) superior colliculus, (*4*) hypothalamus, (*5*) thalamus, (*6*) hippocampus, (*7*) septum, (*8*) retrosplenial and adjacent motor cortex, and (*9*) cingulate and adjacent motor cortex. (**c**) Lesion profiles of three different scrapie strains (RML, ME7, 221C) adapted to C57Bl mice (on the *left*) in comparison with the lesion profiles of 301C (a mouse-adapted BSE strain) and vCJD adapted to C57Bl mice (on the *right*). Note the similar profiles of the two BSE-related sources compared to the different profiles of scrapie strains.

(e) 100% Ethanol, three changes, 90 min each.

(f) Xylene, three changes, 3 h each.

(g) Paraffin wax at 60°C, three changes, 4 h each.

2. Embedding tissues in paraffin blocks.

Embedded blocks are then cut to obtain the sections for hematoxylin and eosin staining (see Fig. 2a), immunohistochemistry (IHC) (see Fig. 2b), PET-blot (paraffin-embedded tissue blot) (see Fig. 2c) and other histological techniques.

3.7. Hematoxylin and Eosin Staining and Lesion Profile

The distribution and severity of spongiform changes in the brain of scrapie-affected mice is variable and depends mainly on the prion strain. This represents the basis of a semiquantitative method of strain discrimination in which the severity of vacuolation is scored from coded sections in specific brain areas to construct a "lesion profile" that is characteristic for each combination of prion strains and mouse lines.

For the purpose of lesion profiling, the brains are trimmed at four standard coronal levels before embedding in paraffin (see Fig. 1a) (16). Vacuolar change is assessed by assigning a score from zero to five, depending on the severity of vacuolation, in nine

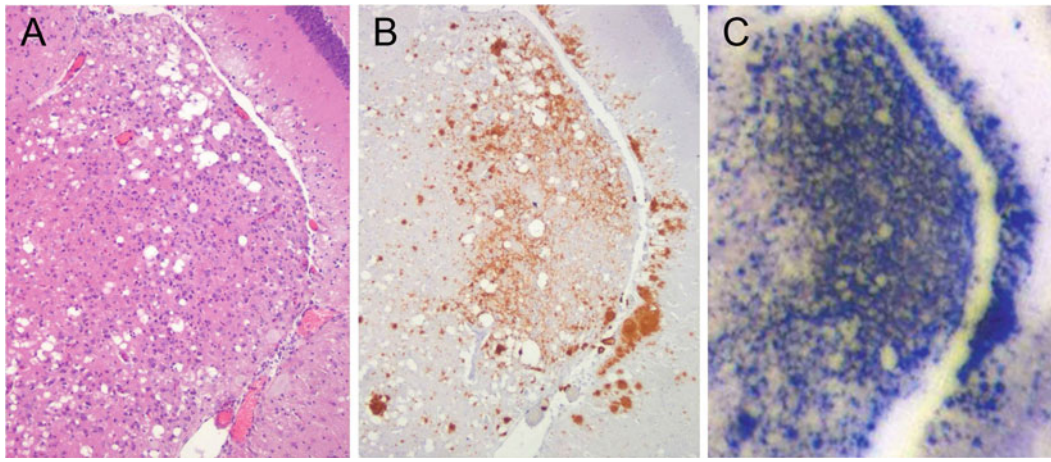

Fig. 2. Serial sections of the geniculate nuclei from voles infected with atypical BSE (BASE) analyzed by (**a**) hematoxylin and eosin, (**b**) immunohistochemistry for PrP^{Sc}, and (**c**) PET-blot.

grey-matter areas of the brain (see Fig. 1b) on hematoxylin and eosin-stained sections. Scoring grid is described as (1) a few vacuoles, widely and unevenly scattered; (2) a few vacuoles evenly scattered; (3) moderate numbers of vacuoles, evenly scattered; (4) many vacuoles with some confluence; and (5) dense vacuolation with most of field confluent (16). At least six individual mice have to be scored to obtain a reliable lesion profile. The results are plotted in a graph as a mean score (see Fig. 1c).

The possible presence of spongiform changes not related to prion infection needs to be taken into consideration during pathological examination (see Note 9).

1. Cut 6-μm-thick sections from embedded blocks at the standard coronal levels (see Fig. 1b). Mount sections on glass slides and dry them at 37°C overnight.
2. Deparaffinize in two changes of xylene, 10 min each.
3. Hydrate in two changes of 100% ethanol for 5 min each. 95, 80, and 70% ethanol for 3 min each. Then rinse in distilled water.
4. Stain in Mayer's hematoxylin solution for 5 min.
5. Wash in running tap water for 10 min.
6. Rinse in distilled water.
7. Counterstain in eosin solution for 1 min.
8. Rinse in distilled water.
9. Rinse in 95% alcohol, ten dips.
10. Dehydrate through two changes of absolute alcohol, 3 min each.
11. Clear in two changes of xylene, 5 min each.
12. Mount with xylene-based mounting medium (Eukitt).

3.8. Immunohistochemistry

IHC exploits the very specific binding exhibited in tissue sections by an antibody for its antigen. The reaction is identified and associated with tissue structures by attaching a microscopically dense probe to the antigen–antibody complex. IHC is commonly used for PrP^{Sc} detection in sections of brain and other tissues.

Treatment of sections with proteinase K, though possible, is not routinely performed by many groups because of its destructive effect on tissue. Instead, pretreatment of the tissue, such as autoclaving or immersion in formic acid, is used to denature PrP^{C} and increase PrP^{Sc} antigenicity (see Note 10). Although PrP^{C} is assumed to be denatured by these pretreatments, when IHC is performed without prior treatment with proteinase K it is possible that PrP^{C} may escape destruction and is detected by IHC in an indefinable mixture with PrP^{Sc}. Given that PrP^{C} and PrP^{Sc} share the same primary structure and that proteinase K is not routinely used in IHC, controls are essential (see Note 11).

1. Cut embedded blocks to 5–6 μm and mount on Superfrost slides. It is always preferable to use freshly cut sections, although sections can be stored for up to 2–3 weeks at +4°C in a sealed container with desiccant.
2. Dry sections at 37°C for at least 30 min or overnight, and then melt at 60°C for 24 h.
3. Deparaffinize in two changes of xylene, 10 min each, and hydrate in two changes of 100% ethanol for 7 min each followed by changes in 95, 80, and 70% ethanol for 5 min each. Then rinse in distilled water for 5 min. Agitate twice in each reagent and drain between reagents.
4. Antigen retrieval (step 1): immerse the sections in undiluted 98% formic acid for 5 min.
5. Immerse sections in container of tap water. Tip out water immediately and replace with slowly running water for 10 min.
6. Rinse in distilled water for 1 min.
7. Antigen retrieval (step 2): autoclaving in citrate buffer. Mount on stainless racks and immerse in abundant citrate buffer contained in an uncovered glass container. The container should be introduced into the autoclave when cold. Autoclave using a liquid cycle at a holding temperature of 121°C for 15 min. The procedure should take at least 90 min. Once the autoclave is safe to open, remove the container and allow to cool to about 50°C before removing slides. Replace the hot buffer slowly with tap or purified water.
8. Rinse the slides carefully with running water for 10 min.
9. Peroxidase blocking: to reduce the risk of unwanted background labeling, endogenous peroxidase activity is inhibited

by immersion of the sections in freshly prepared 3% hydrogen peroxidase in methanol for 20 min.

10. Rinse the slides carefully with running water for 10 min.
11. Rinse in PBST for 2–3 min.
12. Normal serum block: nonspecific binding sites can be blocked by pre-incubation in normal goat serum solution.
13. Rinse in PBST for 2 × 2 min.
14. Primary antibody: incubate sections with primary antibody diluted in PBST overnight at 4°C (see Note 12).
15. Rinse in PBST for 2 × 3 min.
16. Secondary antibody: incubate sections for 30 min with diluted biotinylated secondary antibody solution.
17. Rinse in PBST for 2 × 3 min.
18. Detection: incubate sections in Biotin–(Strept)Avidin (ABC) complex solution for 45 min.
19. Rinse in PBST for 2 × 3 min.
20. Chromogen: add DAB substrate and develop for approximately 7 min. This time may differ depending on the substrate and it is recommended that each user determines the optimal developing time.
21. Rinse in PBST for 3 min.
22. For contrast, stain the nuclei with hematoxylin for approximately 20 s and rinse under tap water in a staining dish for 10 min.
23. Dehydrate by immersing the slides in 80, 95, and 100% ethanol.
24. Clear in xylene for 2 × 5 min.
25. Mount the slides with mounting medium.

3.9. PET-Blot

PET-blot is a very sensitive technique that detects PrP^{Sc} deposits in formalin-fixed and paraffin-embedded tissue after blotting on a nitrocellulose membrane (17). Although conventional IHC has a better microscopic resolution than the PET-blot, one major advantage of the PET-blot technique is that it includes tissue pre-treatment with high concentrations of proteinase K. As a consequence, only PrP^{Sc} is detected by this method. Suitable control sections are needed to verify the efficacy of pretreatments in removing PrP^{C} and the specificity of antibody binding (see Note 12). The satisfactory anatomical resolution of PET-blot makes it possible to map the distribution of PrP^{Sc} in different areas where the protein is deposited. The pattern of PrP^{Sc} distribution in the mouse brain represents an additional useful parameter for typing strains (see Fig. 3).

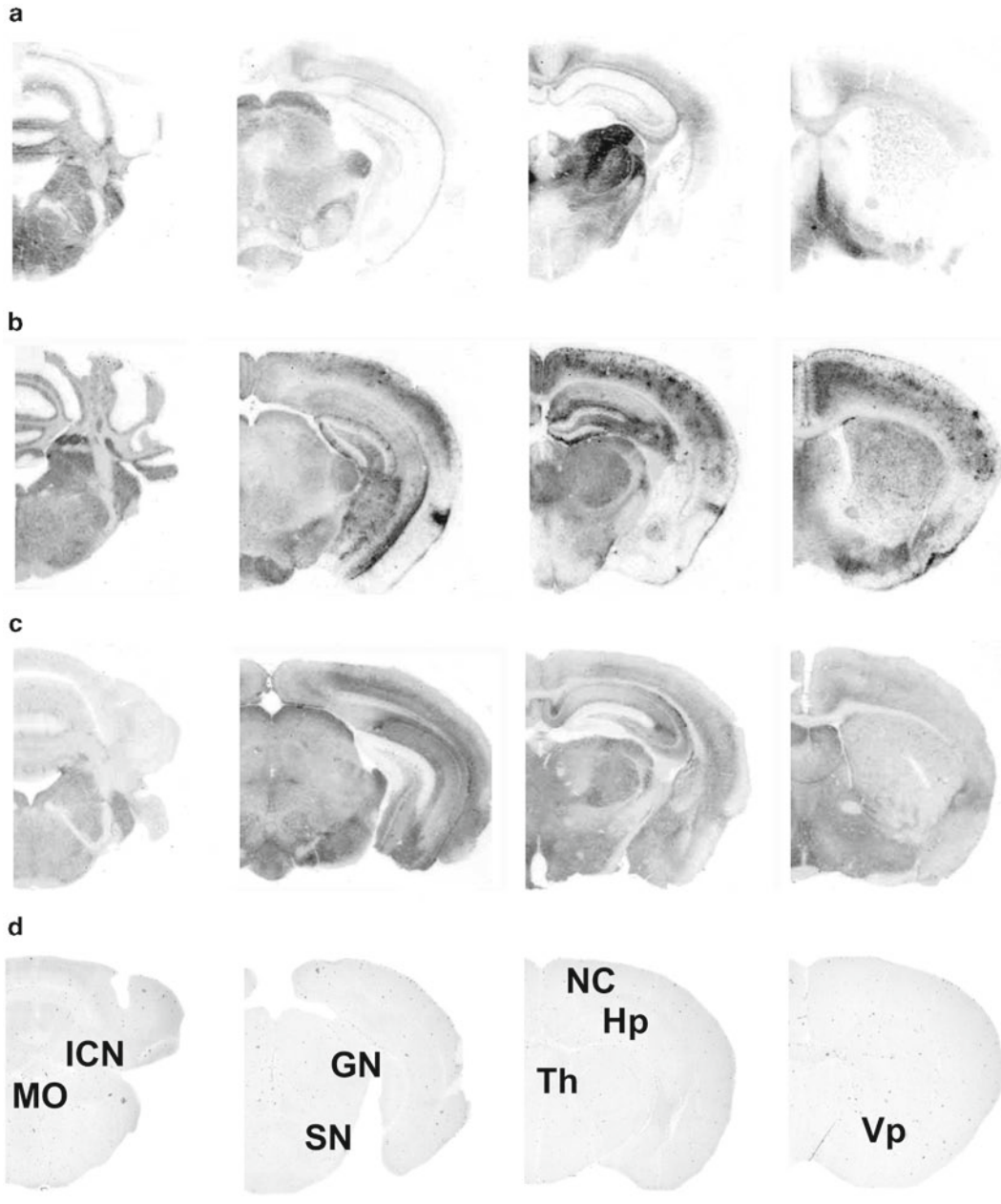

Fig. 3. PET-blot analysis of the pattern of PrP^{Sc} distribution in the brain of voles inoculated with three different vole-adapted scrapie isolates from sheep (lines **a**–**c**). At the lower part of the figure (line **d**), the labeled coronal sections of a negative control brain are shown: *VP* ventral pallidum, *NC* neocortex, *Hp*, hippocampus, *Th* thalamus, *GN* geniculate nuclei, *SN* substantia nigra, *ICN* interposed cerebellar nuclei, *MO* medulla oblongata.

1. Cut nitrocellulose membrane to the shape of microscope slides.
2. Collect the sections at 6 μm on the nitrocellulose membrane, using the microscope glass slides as support for the membrane.
3. Dry the membrane at 37°C overnight and then dry in an incubator set at 60°C for 2–6 h.
4. Deparaffinize the sections in two changes of xylene, 15 min each, then place in isopropyl alcohol 99–100% for 15 min, twice, and then rehydrate through graded isopropyl alcohol: 80% for 10 min, 70% for 5 min, and 50% for 5 min. Rinse in distilled water for 5 min and finally in TBST, pH 7.6, solution for 5 min.
5. Fill each well of a six-well cell culture cluster with TBST, pH 7.6.
6. Cut the membrane so that only the part covered by tissue is left (do this quickly, taking care not to dry the section) and gently put sections in the prefilled wells.
7. Incubate for 5 min.
8. Empty wells by inverting the plate or by vacuum pump. Add the proteinase K solution and incubate overnight at 55°C with gentle shaking.
9. Empty wells by inverting the plate or by vacuum pump and wash with two changes of TBST, pH 7.6 on the rocking platform, 5 min each time.
10. Carry out all the following steps on a rocking platform.
11. Add PMSF solution for 15 min.
12. Wash as in step 9.
13. Add guanidine isothiocyanate solution for 15 min.
14. Wash three times with abundant TBST, pH 7.6, 5 min each time.
15. Add blocking solution for 60 min.
16. Empty the wells and incubate with primary antibody solution for 90 min.
17. Wash three times with abundant TBST, pH 7.6, 5 min each time.
18. Add second antibody alkaline phosphatase-coupled solution for 90 min.
19. Wash two times with abundant TMN solution, 5 min each time.
20. Add NBC/BCIP 1–5 min.
21. Wash two times with EDTA solution, 10 min each time.
22. Dry in the air for at least 12 h on the tissue paper. Keep the membrane between two microscope slides.

4. Notes

1. Disposable instruments—and especially disposable polypropylene pestles for homogenization—are crucial. When the same prion strain is repeatedly used, a teflon-glass potter (Omini International, Kennesaw, USA) dedicated only to that strain can be used. In these cases, our decontamination procedure includes immersion in 1 N NaOH for at least 48 h and two cycles of autoclaving at 136°C for 1 h.
2. PBS must be autoclaved for 20 min at 121°C. All procedures for the preparation of PBS must be performed in a prion-free laboratory.
3. Different methods can be used to overcome the problem of contamination by bacteria or toxic substances. Heat treatment of the inoculum at 70°C for 10 min in a thermomixer (Thermomixer Comfort, Eppendorf, Milano, Italy) is the most frequently used approach. The supplementary dilution in PBS (from 10% w/v to 1% or even less) or the addition of antibiotics (10% of Penicillin/Streptomycin solution—10,000 units of penicillin base and 10,000 µg streptomycin, Omega Scientific, Inc., USA) are possible alternatives. When these treatments are used, the possible sensitivity of prions, and of some strains in particular, to heat (18) and some antibiotics (amphotericin, tetracyclines) (19, 20) needs to be taken into consideration, and their use should be avoided or appropriate measures adopted.
4. Injectable anesthetics are typically administered by the intraperitoneal route. Intraperitoneal injections in rodents are given in the lower left or right quadrant of the abdomen as there are no vital organs in the area. The quadrants are defined by the midline and a line perpendicular to it passing through the umbilicus. The animal should be held either by an assistant or in one hand on its back, and the needle angled at 45° to the skin. Ketamine and xylazine may be administered together in a single injection using insulin syringes of 1 cc. A dose of 0.3 ml of ketamine/xylazine solution (0.5 ml of Ketavet 100 and 0.15 ml of Rompun in 9.35 ml of sterile physiological solution) is usually sufficient for mice weighing 25–30 g.

   The most frequently used inhalational anesthetic for laboratory mice is isoflurane, delivered in concentrations of 1–3% in oxygen, using a precision vaporizer. This allows a rapid induction and recovery. Anesthesia is administered to the mouse until rear foot reflexes are abolished, following which continual observation of the respiratory pattern and responsiveness to manipulation and reflexes must be carried out throughout the procedure. It is possible that prolonged anesthesia may

cause unwanted death due to hypothermia. To prevent this, after an intracerebral injection, the mouse should be held in a cage placed on a hot plate at 37–38°C until recovery.

5. The free-hand method is both simple and rapid to perform. After deep anesthesia, the mouse should be placed on absorbent tissue paper. Before the injection, the inoculum should be resuspended and vortexed in its vials for 30–40 s. The intracerebral injection should be performed in the frontal region, in proximity to the basal ganglia. The animal should be kept under the palm of the hand with its head held in place with thumb and forefinger at ear level. The needle should enter perpendicularly to the braincase and must be blocked at 3–4 mm of depth. The injection must be administered very slowly.
6. For euthanasia, carbon dioxide is the inhalational agent of choice; it produces rapid anesthesia followed by death. This agent causes rapid loss of consciousness without hypoxia, limiting the damage to brain tissue. It is generally recommended that animals be placed immediately in >70% CO_2 so that they lose consciousness very quickly, while 100% CO_2 may cause severe dyspnoea and distress. CO_2, in common with other inhalational agents, must be used with appropriate chambers to ensure even distribution of the gas.

   Barbiturates are the most widely used and accepted injectable agents for euthanasia. Sodium pentobarbitone is administered both intravenously and intraperitoneally at a dosage of 200 mg/kg for euthanasia. Cessation of respiration and heartbeat together with an absence of reflexes are good standard indicators of death in rodents.
7. The objective of perfusion is to remove the blood from the brain and to replace it with tissue fixative. Perfusion allows the homogeneous and rapid fixation of the brain. After CO_2 euthanasia, the heart continues to palpitate for about 2–4 min. During this period the mouse is perfused by inserting the needle into the left ventricle and making a small incision in the right atrium. The needle should be introduced perpendicularly to the tip of the heart. It is useful to block the needle, tightening it with a microplier. A 50-ml syringe, connected to the needle with a silicone tube, should be used to introduce PBS, QS wash solution, into the ventricle. After perfusion with the buffer, perfuse with 50 ml of buffered formalin. Remove the brain and immerse immediately in the fixative.
8. Samples are decontaminated by immersion in undiluted 98% formic acid for 1 h. This treatment helps to enhance the detection of PrP^{Sc}, but it has a serious drawback as it reduces the adhesion of the sections to the slides.
9. Lesion profiling is a well-established method; however, several aspects may affect the efficient assessment of spongiform changes

and need to be taken into consideration: the status of conservation of brain tissue, the clinical stage of animals, the areas of the brain available for examination and the age of animals.

After death, brain tissue undergoes rapid degradative processes that may interfere with the proper assessment of spongiform changes. Lesion profiling should be carried out only on well-preserved brains, in other words avoiding those collected from animals that have died before being sacrificed.

The degree of brain damage is directly related to the clinical stage of the disease. For this reason, lesion profiling should be performed on animals culled at a standard clinical end point or, in the case of primary transmissions, in the terminal stage.

As the reliability of lesion profiling also depends on the exact level of brain regions available for analysis, great care should be taken when trimming brains before embedding them in paraffin.

Sometimes vacuoles are found occurring naturally in the brain of older animals. In our experience, senile vacuolization is most frequently found in the white matter of the cerebellum, and in the medulla oblongata and midbrain. Healthy, age-matched controls should be included in the analyses in order to distinguish vacuoles due to senility from spongiform changes related to prion disease.

Assessment of the degree of spongiform changes in lesion profiling is a subjective measurement. Consequently, lesion profiling is a very consistent method when it is performed by the same operator but requires caution when lesion profiles obtained by different operators are compared.

10. In IHC, antigen demonstration is improved by the use of antigen retrieval procedures that break down the protein cross-links formed by fixatives, thereby exposing hidden antigen sites. The precise mechanisms by which pretreatments enhance the immunoreactivity of PrP^{Sc} are unknown. However, the effect of these chemical procedures is intended to break down the structure of amyloid fibrils in order to expose the buried epitopes. These procedures may also help to denature PrP^{C}. Because pretreatment of sections by autoclaving or immersion in formic acid can cause the sections to detach from the slides and may generate alterations in tissue morphology, it is imperative to use glass slides specific for IHC or coated with appropriate adhesives.
11. Positive controls are necessary to test the reactivity of the antigen and the antibody. Negative controls asses nonspecific immunolabeling and verify the effectiveness of pretreatments. Ideally, sections from a negative (noninfected mice) and a positive (known infected mice) control should always be included. Control sections in which the primary antibody was either

omitted or replaced with normal rabbit or mouse serum are also important to assess nonspecific binding of secondary antibody. In the case of transgenic mice overexpressing PrP, the use of more extensive controls, including age-matched noninfected animals, should be taken into consideration in order to assess the potentially increased nonspecific immunolabeling due to PrP^{C} overexpression.

12. Numerous monoclonal and polyclonal antibodies are currently available for the IHC detection of PrP^{Sc} in tissue sections. Given the numerous rodent models currently available, including a continuously increasing number of transgenic mice expressing PrP of various species, the antibodies need to be carefully selected on the basis of their specificity for a given PrP sequence. The antibody most used in our laboratory for IHC and PET-blot is SAF84 for both mice and voles.

Acknowledgments

The authors wish to thank Dr Claudia D'Agostino, Mr Paolo Frassanito, Mr Shimon Simson, Ms Geraldina Riccardi, and Ms Nadia Palazzini for their technical assistance.

References

1. Will, R.G., Ironside, J.W., Zeidler, M., Cousens, S.N., Estibeiro, K., Alperovitch, A., Poser, S., Pocchiari, M., Hofman, A. and Smith, P.G. (1996) A new variant of Creutzfeldt-Jakob disease in the UK. *Lancet* **347**, 921–925.
2. Bruce, M., Will, R.G., Ironside, J.W., McConnell, I., Drummond, D., Suttie, A., McCardle, L., Chree, A., Hope, J., Birkett, C., Cousens, S., Fraser, H. and Bostock, C.J. (1997) Transmissions to mice indicate that "new variant" CJD is caused by the BSE agent. *Nature* **389**, 498–501.
3. Prusiner, S.B. (1982) Novel proteinaceous infectious particles cause scrapie. *Science* **216**, 136–144.
4. Groschup, M.H. and Buschmann, A. (2008) Rodent models for prion diseases. *Vet Res* **39**:32.
5. Nonno, R., Di Bari, M.A., Cardone, F., Vaccari, G., Fazzi, P., Dell'Omo, G., Cartoni, C., Ingrosso, L., Boyle, A., Galeno, R., Sbriccoli, M., Lipp, H.-P., Bruce, M., Pocchiari, M. and Agrimi, U. (2006) Efficient transmission and characterization of Creutzfeldt–Jakob disease strains in bank voles. *PLOS Pathogens* **2**, 112–120.
6. Agrimi, U., Nonno, R., Dell'Omo, G., Di Bari, M.A., Conte, M., Chiappini, B., Esposito, E., Di Guardo, G., Windl, O., Vaccari, G. and Lipp, H.P. (2008) Prion protein amino acid determinants of differential susceptibility and molecular feature of prion strains in mice and voles. *PLoS Pathogens* **4**, 1–9.
7. Di Bari, M.A., Chianini, F., Vaccari, G., Esposito, E., Conte, M., Eaton, S.L., Hamilton, S., Finlayson, J., Steele, P.J., Dagleish, M.P, Reid, H.W, Bruce, M., Jeffrey, M., Agrimi, U. and Nonno, R. (2008) The bank vole (Myodes glareolus) as a sensitive bioassay for sheep scrapie. *J. Gen. Virol.* **89**, 2975–2985.
8. Kimberlin, R.H. and Walker, C. (1977) Characteristics of a short incubation model of scrapie in the golden hamster. *J Gen Virol* **34**, 295–304.
9. Baron, H. and Prusiner, S.B. (2000) Biosafety of Prion Diseases. In: Fleming DO and Hunt DL (ed) Biological Safety, Principles and practices, 3rd edn. Wiley, New York.
10. Taylor, D.M. (1999) Inactivation of prions by physical and chemical means. *J Hosp. Infect.* **43**, S69–S76.

11. Morton, D.B., Jennings, M., Bukwell, A., Ewbank, R., Godfrey, C., Holgate, B., Inglis, I., James, R., Page, C., Sharman, I., Verschoyle, R., Westall, L. and Wilson, A.B. (2001) Refining procedures for the administration of substances. *Laboratory animals* **35**, 1–41.
12. Thackray, A.M., Klein, M.A., Aguzzi, A. and Bujdoso, R. (2002) Chronic subclinical prion disease induced by low-dose inoculum. *J Virol* **76**, 2510–2517.
13. Dell'Omo, G., Vannoni, E., Vyssotski, A.L., Di Bari, M.A., Nonno, R., Agrimi, U. and Lipp H-P (2002) Early behavioural changes in mice infected with BSE and scrapie: automated home cage monitoring reveals prion strains differences. *Eur. J. Neurosci.* 735–742.
14. Carp, R.I., Callahan, S.M., Sersen, E.A. and Moretz, R.C. (1984) Preclinical changes in weight of scrapie-infected mice as a function of scrapie agent-mouse strain combination. *Intervirol.* **21**, 61–69.
15. Brown, P., Wolff, A. and Gajdusek, D.C. (1990) A simple and effective method for inactivating virus infectivity in formalin-fixed tissue samples from patients with Creutzfeldt-Jakob disease. *Neurology* **40**, 887–890.
16. Fraser, H. and Dickinson, A.G. (1968) The sequential development of the brain lesions of scrapie in three strains of mice. *J Comp Pathol* **78**, 301–311.
17. Schulz-Schaeffer, W.J., Tschöke, S., Kranefuss, N., Dröse, W., Hause-Reitner, D., Giese, A., Groschup, M.H. and Kretzschmar, H.A. (2000) The Paraffin-Embedded Tissue Blot Detects PrP^{Sc} early in the incubation time in prion diseases. *Am. J. Pathol.* **156**, 51–56.
18. Somerville, R.A., Oberthür, R.C., Havekost, U., MacDonald, F., Taylor, D.M., and Dickinson, A.G. (2002) Characterisation of thermodynamic diversity between transmissible spongiform encephalopathy agent strains and its theoretical implications. *J. Biol. Chem.* **277**, 11084–11089.
19. Xi, Y.G., Ingrosso, L., Ladogana, A., Masullo, C. and Pocchiari, M. (1992) Amphotericin B treatment dissociates in vivo replication of the scrapie agent from PrP accumulation. *Nature* **356**, 598–601.
20. Forloni, G., Iussich, S., Awan, T., Colombo, L., Angeretti, N., Girola, L., Bertani, I., Poli, G., Caramelli, M.G., Bruzzone, M., Farina, L., Limido, L., Rossi, G., Giaccone, G., Ironside, J.W., Bugiani, O., Salmona, M. and Tagliavini, F. (2002) Tetracyclines affect prion infectivity. *Proc. Natl. Acad. Sci.* USA **99**, 10849–10854.

Chapter 32

Biochemical Isolation of Insoluble Tau in Transgenic Mouse Models of Tauopathies

Carl Julien, Alexis Bretteville, and Emmanuel Planel

Abstract

Tau is a highly soluble microtubule-associated protein (MAP) that is abundant in the central nervous system and expressed mainly in neuronal axons. Intracellular aggregates of insoluble tau protein are present in a group of neurodegenerative diseases called tauopathies, which include Alzheimer's disease. Numerous transgenic mouse models of tauopathies have been produced in the last decade, and analysis of insoluble tau in these animals has provided a powerful tool to understand the development of tau pathology. In this short chapter, we aim at reviewing the two main isolation methods, sarkosyl and formic acid extraction (and their variations), used for the biochemical isolation of insoluble tau in transgenic mouse models of tauopathy, and discuss their advantages and drawbacks.

Key words: Tauopathies, Insoluble tau, Sarkosyl, Formic acid, Mouse models

1. Introduction

Tau is a highly soluble microtubule-associated protein (MAP) that is abundant in the central nervous system and expressed mainly in axons. The microtubule-binding domain of tau mediates its most characterized biological function: to stabilize microtubules (MT) and promote their polymerization (1, 2). Tau binding to MT and its ability to promote MT assembly is negatively regulated by phosphorylation at multiple sites in, and around, the MT binding domain (3, 4).

Neurofibrillary tangles (NFTs) are intracellular aggregates of abnormally hyperphosphorylated tau present in a group of neurodegenerative diseases called tauopathies (4). Tau hyperphosphorylation can induce aggregation in vitro (5, 6), and it is thought to induce NFT formation in the brain (7). In Alzheimer's disease, the

Einar M. Sigurdsson et al. (eds.), *Amyloid Proteins: Methods and Protocols*, Methods in Molecular Biology, vol. 849,
DOI 10.1007/978-1-61779-551-0_32,

accumulation of NFT in neurons is preceded by appearance of hyperphosphorylated tau. The distribution pattern of NFT in the brain of patients is highly hierarchical and has been divided into six stages (8, 9). The gradual invasion of the brain by NFT changes has also been confirmed biochemically and has been classified into ten stages according to the affected region (10). Tau pathology is correlated to dementia in AD, and to memory loss in normal aging and mild cognitive impairment (11–14).

In the past decade, numerous transgenic mouse models of tauopathy have been produced in an effort to better understand the development of tau pathology and its relationship with many genetic, biological, and environmental factors. Analysis of insoluble tau has provided a powerful tool for the quantitative evaluation of the evolution of the pathology in these models. We define here "insoluble tau" as tau insoluble in 1% sarkosyl, or tau insoluble in Radio-immunoprecipitation buffer (RIPA) and extracted with 70% formic acid, at the exclusion of all other forms of differential solubility assays. In this short chapter, we aim at reviewing the sarkosyl and formic acid methods (and their variations), used for the biochemical isolation of insoluble tau in transgenic mouse models of tauopathy, and discuss their advantages and drawbacks.

1.1. Sarkosyl-Based Extraction Methods

In 1990, Sharon Greenberg and Peter Davies published their seminal article on the isolation of insoluble tau from Alzheimer's disease patients' brains (15). The originality of their method is that they did not attempt to extract highly insoluble population of tau-paired helical filaments (PHFs) from isolated NFTs—an approach that led to inconsistent results between groups and controversies about the possibility to completely solubilize NFTs (16, 17)—but rather selected less-aggregated populations of PHFs directly from AD brain homogenates. The PHFs isolated with this method were similar in structure and many antigenic properties to PHFs from isolated NFTs and allowed immediate consistent PAGE results between groups (18). The method is summarized in Fig. 1. The first step is the homogenization of brain tissues in a buffer containing 0.8 M NaCl and 10% sucrose (see Note 1). The most important step is the isolation of insoluble tau with 1% sarkosyl and 1% 2-mercaptoethanol for 2–2.5 h at 37°C (see Note 2). The following filtration step aims to remove aggregates and trapped soluble proteins, while the discontinuous sucrose gradient further enriches the preparation (15).

In 2000, the first transgenic mouse model of FTDP-17 (JNPL3) was published and Greenberg and Davies' method was used for the biochemical characterization of insoluble tau (19). The method has proven to be popular since it has been used in many modified versions by many groups, in the majority of models reporting biochemical characterization of insoluble tau. However, it has generally been poorly referenced, with many groups failing

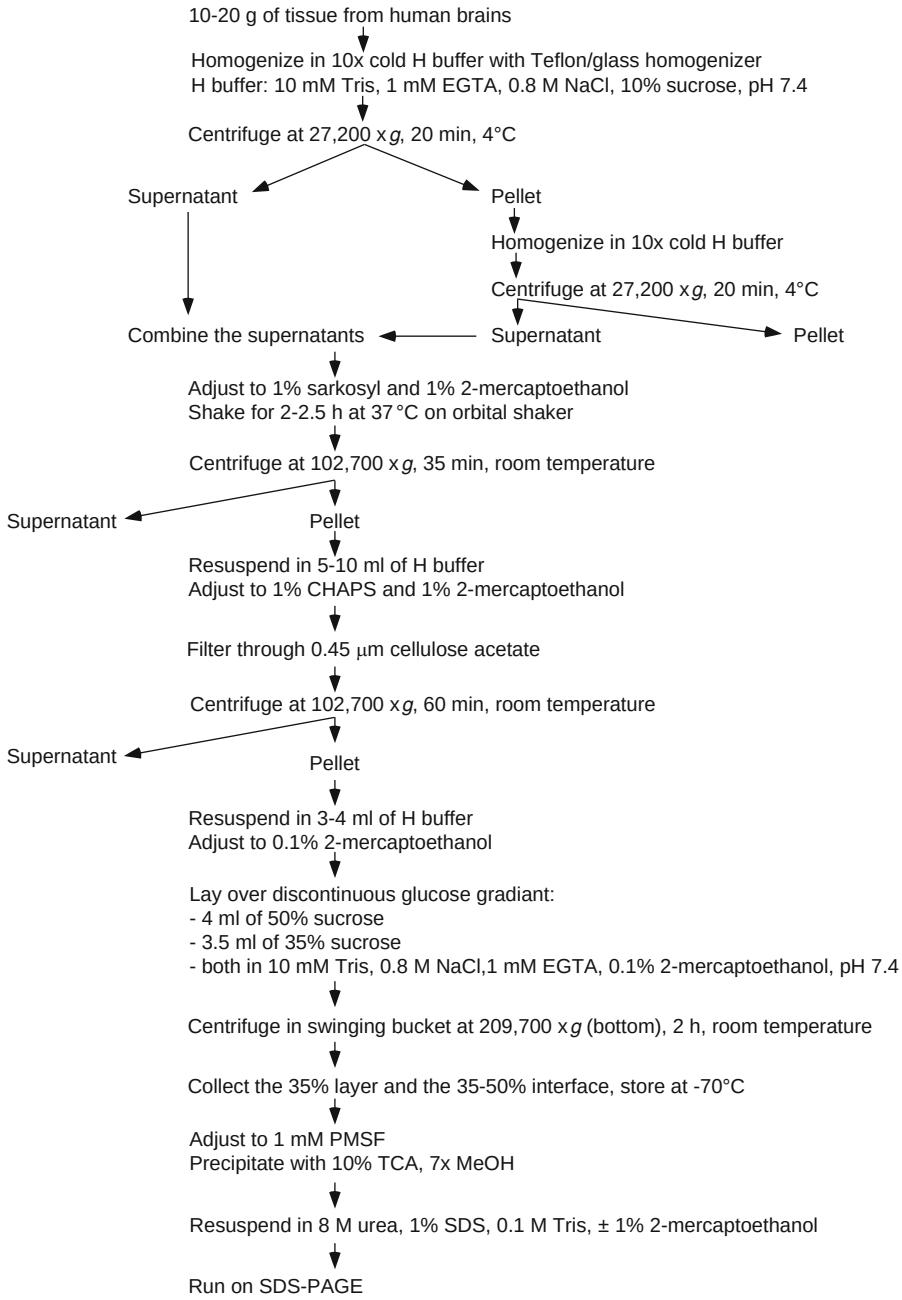

Fig. 1. Insoluble tau isolation with 1% sarkosyl by Greenberg and Davies (15). The original method proposed by Sharon Greenberg and Peter Davies to isolate insoluble tau from AD brains for consistent SDS-PAGE results.

to acknowledge the original article of Greenberg and Davies in the materials and methods, while other referenced modified versions of it without citing the original paper. The mouse models of tau pathology using 1% sarkosyl isolation of insoluble tau for their initial

characterization are summarized in Table 1 (see Note 3). For animal models of tauopathies, it is generally not necessary to follow the exact method of Greenberg and Davies because the NFTs in these mice are not as compact and numerous as in AD brains, so the filtration and sucrose gradient steps can be omitted. Moreover, the method is complex and requires a lot of tissue, which is not practical when working on mouse brain. This has led to the development of many variations of the original protocol, with different cell dissociation buffers (from H buffer, to TBS, to RIPA), different centrifugation speeds and temperatures, and different sarkosyl extraction methods (with or without 2-mercaptoethanol, from 2 h incubation at 37°C to 30 min on ice), but with 1% sarkosyl as a constant factor (see Table 1) (see Note 4). One of the most detailed protocol published early on came from the group that published the JNPL3 model (19): in the original publication in 2000, the article of Greenberg and Davies was cited, but the protocol was not described; however, in 2002, Sahara et al. (20) proposed a very detailed method to analyze the sarkosyl-insoluble tau from JNPL3 mice (see Fig. 2). The most faithful adaptation of the protocol of Greenberg and Davies to a mouse model of tauopathy was published in 2007 by the group of Dr Mandelkow (21): all the buffers composition and initial steps are the same as in the original PNAS article (see Fig. 3). We have ourselves used a modified version of the protocol of Greenberg and Davies (see Fig. 4) in which we replaced the initial H buffer by a RIPA buffer without sodium dodecyl sulfate (SDS) (22, 23). This modification allows for the study of both cytosolic and membrane-associated proteins involved in AD pathogenesis, such as p35 or APP, in the same extracts.

1.2. Formic Acid-Based Extraction Methods

The formic acid extraction is derived from a method used to analyze Aβ solubility (24), and was first used in a transgenic tau mouse model in 1999 by the groups of Drs. Trojanowski and Lee (25). It consists in evaluating the differential solubility of tau in reassembly buffer (RAB) containing 0.75 M NaCl, followed by homogenization of the pellet in RAB with 1 M sucrose to remove myelin and associated lipids, then extraction of the next pellet with RIPA containing the anionic detergents deoxycholate and SDS combined with non-ionic Nonidet P-40 (NP-40), and reextracting the final pellet in formic acid (see Fig. 5) (see Notes 5 and 6).

2. Materials

Prepare all solutions using ultrapure water (prepared by purifying deionized water to attain a resistivity of 18 MΩ/cm at 25°C) and analytical-grade reagents. Diligently follow all waste disposal regulations when disposing waste materials.

Table 1
Tau transgenic mouse models of tauopathy displaying insoluble tau

Name	Mutation	Human tau isoform	Promoter	Reference	Protocol reference	Tissue extraction for insoluble tau procedure	Insoluble tau isolation
Line 7	No mutation	3R0N (352aa)	Mouse PrP	(25)	No reference	RAB: 0.1 M MES pH 7.0, 1 mM EGTA, 0.5 mM $MgSO_4$, 0.75 M NaCl, 100 mM EDTA, inhibitors	RIPA followed by 70% formic acid
JNPL3	P301L	4R0N (383aa)	Mouse PrP	(19)	(15)	No detailed protocol	No detailed protocol
ALZ17	No mutation	4R2N (441aa)	Thy1.2	(46)	No reference	RAB: 0.1 M MES, 1 mM EGTA, 0.5 mM $MgSO_4$, 0.75 M NaCl, 100 mM EDTA inhibitors	RIPA followed by 70% formic acid
VLW	G272V/ P301L/ R406W	4R2N (441aa)	Thy1.2	(27)	(49)	No detailed protocol	No detailed protocol
pR5-183	P301L	4R2N (441aa)	Thy1.2	(28)	(50)	10 mM Tris pH7.4, 1 mM EGTA, 0.8 M NaCl, 10% sucrose	1% sarkosyl, 1 h at room temperature
G272V Tg	G272V	4R2N (441aa)	Mouse PrP tet off	(47)	(46)	RAB: 0.1 M MES pH 8.0, 1 mM EGTA, 0.5 mM $MgSO_4$, 0.75 M NaCl, inhibitors	RIPA followed by 70% formic acid
Tg214	V337M	4R2N (441aa)	PDGF	(48)	No reference	RAB: 0.1 M MES pH 7.0, 1 mM EGTA, 0.5 mM $MgSO_4$, 0.75 M NaCl, inhibitors	RIPA followed by 70% formic acid
R406W Tg	R406W	4R2N (441aa)	aCaMKII	(29)	(15)	TBS: 10 mM Tris pH 7.4, 150 mM NaCl, inhibitors	No detailed protocol
Line 14	No mutation	3RT	Tubulin a1	(41)	No reference	RAB: 0.1 M MES pH 7.0, 1 mM EGTA, 0.5 mM $MgSO_4$, 0.75 M NaCl, 100 mM EDTA, inhibitors	RIPA followed by 70% formic acid
Line 2541	P301S	4R0N (383aa)	Thy1.2	(30)	No reference	No detailed protocol	No detailed protocol

(continued)

Table 1 (continued)

Name	Mutation	Human tau isoform	Promoter	Reference	Protocol reference	Tissue extraction for insoluble tau procedure	Insoluble tau isolation
hTau	No mutation	All isoforms	Human MAPT	(31)	(15)	TBS pH 7.4, inhibitors	1% sarkosyl, 30 min
RW Tau Tg	R406W	4R2N (441aa)	Mouse PrP	(42)	(25)	RAB: 0.1 M MES pH 7.0, 1 mM EGTA, 0.5 mM $MgSO_4$, 0.75 M NaCl, 100 mM EDTA, inhibitors	RIPA followed by 70% formic acid
TgTau R406W	R406W	4R2N (441aa)	Hamster PrP	(32)	No reference	TS buffer: 50 mM Tris–HCl, 150 mM NaCl pH 7.6, 1 mM EGTA, inhibitors	1% sarkosyl in TS, 30 min on ice
rTg4510	P301L	4R0N (383aa)	Inducible CaMKII	(33)	No reference	TBS, inhibitors	1% sarkosyl, 1 h at 37°C
GFAP-Tau	No mutation	4R1N (412aa)	GFAP	(43)	No reference	HS-TBS: 50 mM Tris pH 7.6, 750 mM NaCl, 1 mM EGTA, 0.5 mM $MgSO_4$, inhibitors	RIPA followed by 70% formic acid
PL L12	P301L	4R1N (412aa)	Mouse CNP	(44)	(41)	RAB: 0.1 M MES pH 7.0, 1 mM EGTA, 0.5 mM $MgSO_4$, 0.75 M NaCl, 100 mM EDTA, inhibitors	RIPA followed by 70% formic acid
Tau 4R/2N-P301L	P301L	4R2N (441aa)	Thy1	(34)	No reference	25 mM Tris–HCl pH 7.6, 150 mM NaCl, 1 mM EDTA, 1 mM EGTA	1% sarkosyl, 1 h at room temperature
3xTG-AD	P301L	4R0N (383aa)	Thy1.2	(51)	No reference	Tissue protein extraction reagent (Pierce)	70% formic acid, ELISA
GFAP/Tau P301L Tg	P301L	4R1N (412aa)	GFAP	(52)	No reference	Not documented	Not documented
TgTau P301L	P301L	4R2N (441aa)	Hamster PrP	(35)	No reference	TS buffer: 50 mM Tris–HCl, 150 mM NaCl pH 7.6, 1 mM EGTA, inhibitors	1% sarkosyl in TS, 30 min on ice

Tg30Tau	G272V/P301S	4R1N (412aa)	Thy1	(36)	(53)	10 mM Tris–HCl pH 7.4, 0.8 M NaCl, 1 mM EDTA, sucrose 10%	1% sarkosyl
Lines PS5, PS19	P301S	4R1N (412aa)	Mouse PrP	(45)	(25)	RAB: 0.1 M MES, 1 mM EGTA, 0.5 mM $MgSO_4$, 0.75 M NaCl, inhibitors	RIPA followed by 70% formic acid
ht40delta K280	deltaK280	4R2N (441aa)	Inducible CaMKII	(21)	No reference	Buffer H: 10 mM Tris pH 7.4, 0.8 M NaCl, 1 mM EGTA, 10% sucrose, inhibitors RAB: 0.1 M MES pH 7, 1 mM EGTA, 0.5 mM $MgSO_4$, 0.75 M NaCl, inhibitors	1% sarkosyl, 1% 2-mercapto ethanol, 1 h at 37°C RIPA followed by 70% formic acid
DM	K257T/P301S	4R0N (383aa)	Rat MAPT	(37)	No reference	10 mM Tris–HCl pH 7.4, 0.15 M NaCl, 2 mM EGTA	1% sarkosyl, 1 h at room temperature
TauRD/ deltaK280	deltaK280	4RT domain (244–372)	Inducible CaMKII	(38)	(15)	Buffer H: 10 mM Tris–HCl pH 7.4, 1 mM EGTA, 0.8 M NaCl, 10% sucrose	1% sarkosyl, 60–90 min at 37°C
K3	K369I	4R1N (412aa)	Thy1.2	(39)	(50)	10 mM Tris pH7.4, 1mM EGTA, 0.8 M NaCl, 10% sucrose	1% sarkosyl, 1 h at room temperature
mTau	No mutation	All mouse isoforms	Mouse MAPT	(40)	(15)	50 mM Tris pH 8.0, 274 mM NaCl, 5 mM KCl, 2 mM EGTA, 2 mM EDTA	1% sarkosyl, 1 h at 37°C

We list here the mouse models expressing human or mouse tau transgenes, in which insoluble tau was demonstrated to be present in the original publication. Because of space constraints, we do not reference subsequent analysis of these models

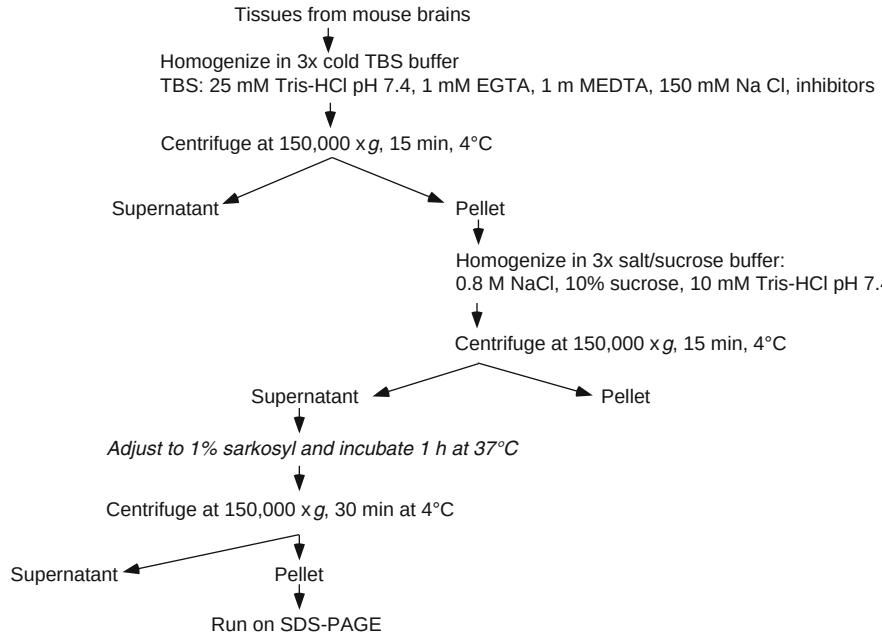

Fig. 2. Insoluble tau isolation with 1% sarkosyl by Sahara et al. (20). A method described in details to analyze insoluble tau from JNPL3 mice.

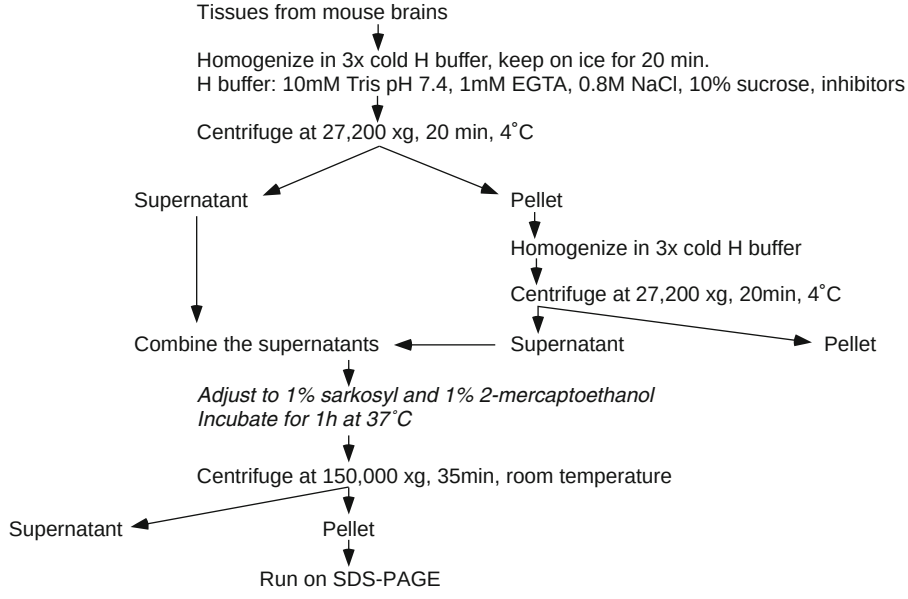

Fig. 3. Insoluble tau isolation with 1% sarkosyl by Eckermann et al. (21). A method following most closely the protocol of Greenberg and Davies.

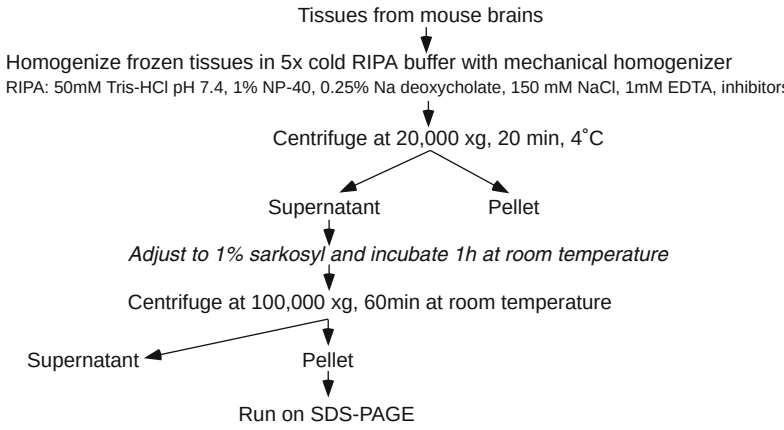

Fig. 4. Insoluble tau isolation with 1% sarkosyl by Planel et al. (23). A method replacing the original H buffer with RIPA buffer without SDS.

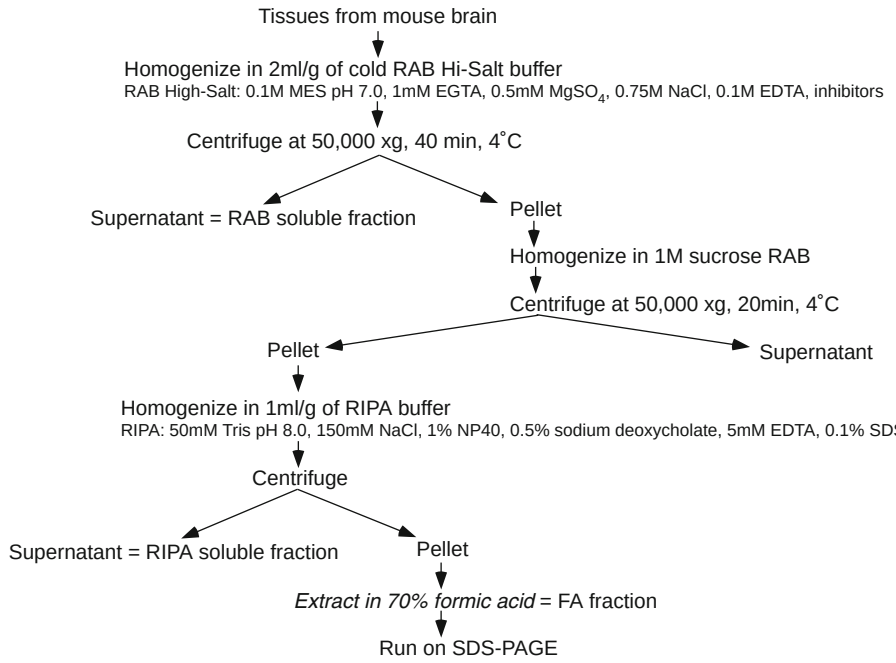

Fig. 5. Insoluble tau isolation with formic acid by Ishihara et al. (25). A method used for the characterization of numerous tau transgenic mice.

2.1. Insoluble Tau Isolation with 1% Sarkosyl by Greenberg and Davies (15)

1. Sarkosyl or *N*-Lauroylsarcosine sodium salt (Sigma, St Louis, MO, USA, #L9150).
2. H buffer: 10 mM Tris (Sigma, #T1503), 1 mM Ethylene glycol-bis(2-aminoethylether)-*N*,*N*,*N*′,*N*′-tetraacetic acid (EGTA) (Sigma, #E0396), 0.8 M NaCl (Sigma, #S3014), 10% sucrose (Sigma, #84097), pH 7.4.
3. H buffer including 0.1% (v/v) 2-mercaptoethanol (Sigma, #M7154).

4. H buffer including 1% (w/v) 3-[(3-cholamidopropyl) dimethylammonio]-1-propanesulfonate (CHAPS) (Sigma, #C9426) and 1% (v/v) 2-mercaptoethanol (Sigma, #M7154).
5. 50% (w/v) sucrose (Sigma, #84097) in 10 mM Tris (Sigma, #T1503), 0.8 M NaCl (Sigma, #S3014), 1 mM EGTA (Sigma, #E0396), 0.1% (v/v) 2-mercaptoethanol (Sigma, #M7154), pH 7.4.
6. 35% (w/v) of sucrose (Sigma, #84097) in 10 mM Tris (Sigma, #T1503), 0.8 M NaCl (Sigma, #S3014), 1 mM EGTA (Sigma, #E0396), 0.1% (v/v) 2-mercaptoethanol (Sigma, #M7154), pH 7.4.

2.2. Insoluble Tau Isolation with 1% Sarkosyl by Sahara et al. (20)

1. Sarkosyl or *N*-Lauroylsarcosine sodium salt (Sigma, St Louis, MO, USA).
2. Tris-buffered saline (TBS): 25 mM Tris–HCl (Sigma, #T5941), pH 7.4, 150 mM NaCl (Sigma, #S3014), 1 mM Ethylenediaminetetraacetic acid (EDTA) (Sigma, #EDS), 1 mM EGTA (Sigma, #E0396), containing phosphatase and protease inhibitors 5 mM sodium pyrophosphate (Sigma, #71501), 30 mM β-glycerophosphate (Sigma, #G9422), 30 mM sodium fluoride (Sigma, #S7920), 1 mM phenylmethylsulfonyl fluoride (PMSF) (Sigma, #P7626).
3. Salt/sucrose buffer: 0.8 M NaCl (Sigma, #S3014), 10% sucrose (Sigma, #84097), 10 mM Tris–HCl (Sigma, #T5941), pH 7.4.

2.3. Insoluble Tau Isolation with 1% Sarkosyl by Eckermann et al. (21)

1. Sarkosyl or *N*-Lauroylsarcosine sodium salt (Sigma, St Louis, MO, USA, #L9150).
2. H buffer: 10 mM Tris (Sigma, #T1503), 1 mM EGTA (Sigma, #E0396), 0.8 M NaCl (Sigma, #S3014), 10% sucrose (Sigma, #84097), pH 7.4, containing 1 mM PMSF (Sigma, #P7626).
3. Tris-buffered saline (TBS): 10 mM Tris (Sigma, #T1503), 154 mM NaCl (Sigma, #S3014).

2.4. Insoluble Tau Isolation with 1% Sarkosyl by Planel et al. (23)

1. RIPA: 50 mM Tris–HCl (Sigma, #T5941), pH 7.4, 1% Nonidet P-40 (Sigma, #74385), 0.25% Na-deoxycholate (Sigma, #D6750), 150 mM NaCl (Sigma, #S3014), 1 mM EDTA (Sigma, #EDS) containing phosphatase and protease inhibitors [1 mM PMSF (Sigma, #P7626), 1 mM Na_3VO_4 (Sigma, #S6508), 1 mM NaF (Sigma, #S7920), and 10 µl/ml of protease inhibitor cocktail Sigma #P8340].
2. O+ buffer: 62.5 mM Tris–HCl (Sigma, #T5941), pH 6.8, 10% glycerol (Sigma, #G8773), 5% 2-mercaptoethanol (Sigma, #M7154), 0.1% SDS (Sigma, #L3771), 1 mM EGTA (Sigma, #E0396), 1 mM EDTA (Sigma, #EDS), containing phosphatase and protease inhibitors [1 mM PMSF (Sigma, #P7626), 1 mM Na_3VO_4 (Sigma, #S6508), 1 mM NaF (Sigma, #S7920), and 10 µl/ml of protease inhibitor cocktail Sigma #P8340].

2.5. Insoluble Tau Isolation with Formic Acid by Ishihara et al. (25)

1. RAB High-Salt buffer: 0.1 M morpholineethanesulfonic acid (MES) (Sigma, #M3671), pH 7.0, 1 mM EGTA (Sigma, #E0396), 0.5 mM $MgSO_4$ (Sigma, #M2643), 0.75 M NaCl (Sigma, #S3014), 0.1 M EDTA (Sigma, #EDS), containing phosphatase and protease inhibitors: 1 mM PMSF (Sigma, #P7626), 1 mM Na_3VO_4 (Sigma, #S6508), 1 mM NaF (Sigma, #S7920) and 10 µl/ml of protease inhibitor cocktail (Sigma #P8340).
2. 1 M sucrose RAB buffer: RAB High-Salt buffer containing 1 M sucrose.
3. RIPA buffer: 50 mM Tris (Sigma, #T1503), pH 8.0, 150 mM NaCl (Sigma, #S3014), 1% Nonidet P-40 (Sigma, #74385), 0.5% Na-deoxycholate (Sigma, #D6750), 5 mM EDTA (Sigma, #EDS), 0.1% SDS (Sigma, #L3771), containing phosphatase and protease inhibitors: 1 mM PMSF (Sigma, #P7626), 1 mM Na_3VO_4 (Sigma, #S6508), 1 mM NaF (Sigma, #S7920) and 10 µl/ml of protease inhibitor cocktail (Sigma #P8340).
4. Neutralization buffer: 1 M Tris (Sigma, #T1503), 0.5 M NaH_2PO_4 (Sigma, #S3139).

3. Methods

Here, we describe five reported protocols used for the biochemical isolation of insoluble tau in transgenic mouse models of tauopathy by sarkosyl (see Subheadings 3.1–3.4) and formic acid extraction (see Subheading 3.5) (see Notes 7–9).

3.1. Insoluble Tau Isolation with 1% Sarkosyl by Greenberg and Davies (15) (see Fig. 1)

1. Collect 10–20 g of tissue from human brains.
2. Homogenize with 10 vol. (v/w) of cold H buffer with Teflon/glass homogenizer. For example, use 100 ml of cold H buffer for 10 g of tissue.
3. Centrifuge at 27,200 × *g* during 20 min at 4°C.
4. Recover and save the supernatant.
5. From the pellet, homogenize again with 10 vol. of cold H buffer (same volume determined in step 2), centrifuge at 27,200 × *g* during 20 min at 4°C, and combine the two supernatants. Discard the pellet.
6. From 27,200 × *g* supernatants, adjust to 1% sarkosyl and 1% 2-mercaptoethanol. For example, add 11.11 µl of 10% sarkosyl in water and add 1.11 µl of 2-mercaptoethanol for 100 µl of supernatants.
7. Incubate for 2–2.5 h at 37°C on orbital shaker.
8. Centrifuge at 102,700 × *g* for 35 min at room temperature.
9. Discard the supernatant.

10. Resuspend the pellet in 5–10 ml of H buffer including 1% (w/v) CHAPS and 1% (v/v) 2-mercaptoethanol.
11. Filter through 0.45 µm cellulose acetate.
12. Centrifuge at 102,700 × *g* for 60 min at room temperature.
13. Discard the supernatant.
14. Resuspend the pellet in 3–4 ml of H buffer including 0.1% (v/v) 2-mercaptoethanol.
15. Lay over a discontinuous sucrose gradient consisting of 4 ml of 50% (w/v) sucrose and 3.5 ml of 35% (w/v) of sucrose both in 10 mM Tris, 0.8 M NaCl, 1 mM EGTA, 0.1% (v/v) 2-mercaptoethanol, pH 7.4.
16. Centrifuge at 210,000 × *g* (35,000 rpm in a Beckman SW 41Ti Swinging Bucket rotor (Beckman Coulter, Brea, CA, USA, #331362) with Beckman centrifuge tubes (Beckman Coulter, #358120)) during 2 h at room temperature.
17. Collect the 35% layer and the 35–50% interface with a 5-ml syringe attached to an 18-gauge, 1.5-inch needle inserted through the side of the centrifuge tube. Store at –70°C.
18. Adjust to 1 mM PMSF.
19. Precipitate with 10% (w/v) Trichloroacetic acid (TCA) (Sigma, #T9159), 7 vol. (v/v) of MeOH or with 7 vol. (v/v) of MeOH/0.1% (w/v) TCA. Either method can be used with no difference in results.
20. Resuspend in 8 M urea, 1% (w/v) SDS, 0.1 M Tris pH 6.8, and with or without 1% (v/v) 2-mercaptoethanol.
21. Run on 10% acrylamide (Sigma, #A3553)/Bis-acrylamide (Sigma, #146072) (29:1) SDS-PAGE. Use Precision Plus Protein All Blue Standards (BIO-RAD; #161-0373) as molecular weight markers or other suitable protein standard to identify 60–80 kDa proteins.

3.2. Insoluble Tau Isolation with 1% Sarkosyl by Sahara et al. (20) (see Fig. 2)

1. Collect tissue from mouse brains.
2. Homogenize with 3 vol. (v/w) of cold TBS buffer containing the protease and phosphatase inhibitors. For example, use 3 ml of cold TBS buffer for 1 g of tissue.
3. Centrifuge at 150,000 × *g* during 15 min at 4°C.
4. Discard the supernatant.
5. From the pellet, homogenize with 3 vol. (v/w) of salt/sucrose buffer.
6. Centrifuge at 150,000 × *g* during 15 min at 4°C.
7. Discard the pellet.
8. From the supernatant, adjust to 1% sarkosyl. For example, add 1 g of sarkosyl (or 5.26 ml of 20% (v/v) sarkosyl diluted in cold TBS buffer) for 100 ml of supernatant.

9. Incubate for 1 h at 37°C on orbital shaker.
10. Centrifuge at 150,000 × *g* for 30 min at 4°C.
11. Discard the supernatant.
12. Resuspend the pellet in 50 µl of TBS buffer and store at −80°C.
13. Run on 10% acrylamide (Sigma, #A3553)/Bis-acrylamide (Sigma, #146072) (29:1) SDS-PAGE. Use Precision Plus Protein All Blue Standards (BIO-RAD; #161-0373) as molecular weight markers or other suitable protein standard to identify 60–80 kDa proteins.

3.3. Insoluble Tau Isolation with 1% Sarkosyl by Eckermann et al. (21) (see Fig. 3)

1. Collect cortices from mouse brains.
2. Homogenize with 3 vol. (v/w) of cold H buffer with protease inhibitor. Keep on ice for 20 min.
3. Centrifuge at 27,200 × *g* during 20 min at 4°C.
4. Recover and save the supernatant.
5. From the pellet, homogenize again with 3 vol. of cold H buffer (same volume determined in step 2), centrifuge at 27,200 × *g* during 20 min at 4°C, and combine the two supernatants. Discard the pellet.
6. From 27,200 × *g* supernatants, adjust to 1% sarkosyl and 1% 2-mercaptoethanol.
7. Incubate for 1 h at 37°C on orbital shaker.
8. Centrifuge at 150,000 × *g* for 35 min at room temperature.
9. Discard the supernatant.
10. Resuspend the pellet with 0.5 vol. of TBS.
11. Run on 10% acrylamide (Sigma, #A3553)/Bis-acrylamide (Sigma, #146072) (29:1) SDS-PAGE. Use Precision Plus Protein All Blue Standards (BIO-RAD; #161-0373) as molecular weight markers or other suitable protein standard to identify 60–80 kDa proteins.

3.4. Insoluble Tau Isolation with 1% Sarkosyl by Planel et al. (23) (see Fig. 4)

1. Collect tissue from mouse brains.
2. Homogenize in 5 vol. (v/w) of cold RIPA buffer without SDS containing protease and phosphatase inhibitors with a mechanical homogenizer.
3. Centrifuge at 20,000 × *g* during 20 min at 4°C.
4. Discard the pellet.
5. From the supernatant, adjust to 1% sarkosyl.
6. Incubate for 1 h at room temperature on orbital shaker.
7. Centrifuge at 100,000 × *g* for 60 min at room temperature.
8. Discard the supernatant, rinse with 1% sarkosyl.

9. Resuspend the pellet in O+ buffer.
10. Boil for 3 min, and keep at –20°C.
11. Run on 10% acrylamide (Sigma, #A3553)/Bis-acrylamide (Sigma, #146072) (29:1) SDS-PAGE. Use Precision Plus Protein All Blue Standards (BIO-RAD; #161-0373) as molecular weight markers or other suitable protein standard to identify 60–80 kDa proteins.

3.5. Insoluble Tau Isolation with Formic Acid by Ishihara et al. (25) (see Fig. 5)

1. Collect tissue from mouse brains.
2. Homogenize in 2 vol. (v/w) of cold RAB Hi-Salt buffer containing protease and phosphatase inhibitors with mechanical homogenizer. For example, use 20 ml of cold RAB Hi-Salt buffer for 10 g of tissue.
3. Centrifuge at 50,000 × *g* during 40 min at 4°C.
4. Recover and save the supernatant for the RAB soluble fraction.
5. From the pellet, homogenize with the volume determined on step 2 of cold 1 M sucrose RAB containing protease and phosphatase inhibitors.
6. Centrifuge at 50,000 × *g* during 20 min at 4°C.
7. Discard the supernatant.
8. From the pellet, homogenize with 1 vol. (v/w) of cold RIPA buffer containing phosphatase and protease inhibitors.
9. Centrifuge at 50,000 × *g* during 20 min at 4°C.
10. Recover and save the supernatant for the RIPA soluble fraction.
11. Extract the RIPA-insoluble pellet with 1 vol. (v/w) of cold 70% (v/v) formic acid.
12. Dilute the formic acid fraction with 1:20 (v/v) neutralization buffer.
13. Run on 10% acrylamide (Sigma, #A3553)/Bis-acrylamide (Sigma, #146072) (29:1) SDS-PAGE. Use Precision Plus Protein All Blue Standards (BIO-RAD; #161-0373) as molecular weight markers or other suitable protein standard to identify 60–80 kDa proteins.

4. Notes

1. The high salt allows for dissociation of soluble tau from microtubules and better recovery of AD-specific antigens, such as Alz-50, than with lower concentration of NaCl (15), while the sucrose allows the elimination of myelin and associated lipids.

2. Sarkosyl was used instead of SDS because it allows for the preservation of antigenic epitopes that are lost during the isolation of insoluble tau by SDS, probably because of conformational changes (26).
3. Initial characterization of mouse models is described in detail elsewhere: JNPL3 (19), VLW (27), pR5-183 (28), R406W Tg (29), Line 2541 (30), hTau (31), TgTauR406W (32), rTG4510 (33), Tau 4R/2N-P301L (34), TgTauP301L (35), Tg30Tau (36), ht40deltaK280 (21), DM (37), TauRD/deltaK280 (38), K3 (39), and mTau (40).
4. It should be noted that the protocols are often not described in details, and that there is usually no justification as to why the buffers and procedures are different from Greenberg and Davies one (if it is referenced at all; see Table 1).
5. It is unclear what tau species are present in the pellet since it has not been characterized by immuno-electron microscopy.
6. This technique has been used mainly by the Trojanowski and Lee groups through the years for the characterization of multiple mice models of tauopathy such as Line 14 (41), RW Tau Tg (42), GFAP-Tau (43), PL L12 (44), Lines PS5 and PS19 (45), but also by the groups of Drs Goedert (46), Gotz (47), Mandelkow (21), or Takashima (48). The procedure has been remarkably consistent through the years and in different groups.
7. The decision to use either the sarkosyl or the formic acid method to analyze insoluble tau in a transgenic mouse model of tauopathy depends on several factors. For example, the formic acid method is convenient for models with both Aβ and tau pathologies because both can be quantified with this protocol. On the other hand, if electron microscopy of the aggregates is necessary, then sarkosyl extraction is the method of choice. Overall, the choice of one or the other method is not crucial when working with an already well-characterized transgenic mouse model of tauopathy and looking at one condition vs. another in the same mouse model. It becomes a concern when looking for insoluble tau in a new transgenic tau mouse model, and especially when analyzing animals that are not transgenic for tau; we found that many proteins other than tau can be present in the final insoluble fractions, and may include neurofilaments or MAP2 proteins, which can have cross-reactivity with some anti total- and phospho-tau antibodies. For such animal we would recommend the sarkosyl extraction closest to the original method of Greenberg and Davies, as it will allow for the crucial characterization of the aggregates by electron microscopy.

8. Whatever the chosen method, it is very important to include positive controls (AD brains and/or brains from well-characterized tauopathy models), as well as negative controls (brains from tau knock-out mice). Finally, the use of pan-tau polyclonal antibodies should be discouraged for the biochemical characterization of insoluble tau in new mouse models.
9. In any case, we think that the field is in need of a consensus and standardized protocol to be used for the biochemical characterization of insoluble tau in animal models, especially considering the proliferation of variations on the sarkosyl method. All these methods should be compared to see which one reflects more accurately the presence of tau pathological aggregates.

Acknowledgments

We are grateful to Dr. Peter Davies (Albert Einstein College of Medicine, Bronx, NY, USA) for helpful comments. This work was made possible by grants from the CIHR, FRSQ, NSERC, RQRV/AFIRMAQ and FCI (to EP), and by a postdoctoral award from Alzheimer Society of Saskatchewan and from Alzheimer Society of Canada (to CJ). We apologize in advance if we missed an essential reference in this review.

References

1. Weingarten, M. D., Lockwood, A. H., Hwo, S. Y., and Kirschner, M. W. (1975) A protein factor essential for microtubule assembly, *Proc Natl Acad Sci USA 72*, 1858–1862.
2. Cleveland, D. W., Hwo, S. Y., and Kirschner, M. W. (1977) Purification of tau, a microtubule-associated protein that induces assembly of microtubules from purified tubulin, *J Mol Biol 116*, 207–225.
3. Avila, J., Lucas, J. J., Perez, M., and Hernandez, F. (2004) Role of tau protein in both physiological and pathological conditions, *Physiol Rev 84*, 361–384.
4. Buee, L., Bussiere, T., Buee-Scherrer, V., Delacourte, A., and Hof, P. R. (2000) Tau protein isoforms, phosphorylation and role in neurodegenerative disorders, *Brain Res. Brain. Res. Rev. 33*, 95–130.
5. Alonso, A. C., Zaidi, T., Novak, M., Grundke-Iqbal, I., and Iqbal, K. (2001) Hyperphosphorylation induces self-assembly of tau into tangles of paired helical filaments / straight filaments, *Proc. Natl. Acad. Sci. USA. 98*, 6923–6928.
6. Sato, S., Tatebayashi, Y., Akagi, T., Chui, D. H., Murayama, M., Miyasaka, T., Planel, E., Tanemura, K., Sun, X., Hashikawa, T., Yoshioka, K., Ishiguro, K., and Takashima, A. (2002) Aberrant tau phosphorylation by glycogen synthase kinase-3beta and JNK3 induces oligomeric tau fibrils in COS-7 cells, *J Biol Chem 277*, 42060–42065.
7. Trojanowski, J. Q., and Lee, V. M. (1994) Paired helical filament tau in Alzheimer's disease. The kinase connection, *Am. J. Pathol. 144*, 449–453.
8. Braak, H., and Braak, E. (1991) Neuropathological stageing of Alzheimer-related changes, *Acta Neuropathol*, *82*, 239–259.
9. Braak, H., and Braak, E. (1997) Frequency of stages of Alzheimer-related lesions in different age categories, *Neurobiol. Aging 18*, 351–357.
10. Delacourte, A., David, J. P., Sergeant, N., Buee, L., Wattez, A., Vermersch, P., Ghozali, F., Fallet-Bianco, C., Pasquier, F., Lebert, F., Petit, H., and Di Menza, C. (1999) The biochemical pathway of neurofibrillary degeneration in aging and Alzheimer's disease, *Neurology 52*, 1158–1165.

11. Arriagada, P. V., Growdon, J. H., Hedley-Whyte, E. T., and Hyman, B. T. (1992) Neurofibrillary tangles but not senile plaques parallel duration and severity of Alzheimer's disease, *Neurology 42*, 631–639.
12. Guillozet, A. L., Weintraub, S., Mash, D. C., and Mesulam, M. M. (2003) Neurofibrillary tangles, amyloid, and memory in aging and mild cognitive impairment, *Arch Neurol 60*, 729–736.
13. Wilcock, G. K., and Esiri, M. M. (1982) Plaques, tangles and dementia. A quantitative study, *J Neurol Sci 56*, 343–356.
14. Bretteville, A., and Planel, E. (2008) Tau aggregates: toxic, inert, or protective species?, *J Alzheimers Dis 14*, 431–436.
15. Greenberg, S. G., and Davies, P. (1990) A preparation of Alzheimer paired helical filaments that displays distinct tau proteins by polyacrylamide gel electrophoresis, *Proc Natl Acad Sci USA 87*, 5827–5831.
16. Selkoe, D. J. (1986) Altered structural proteins in plaques and tangles: what do they tell us about the biology of Alzheimer's disease?, *Neurobiol Aging 7*, 425–432.
17. Wisniewski, H. M., Iqbal, K., Grundke-Iqbal, I., and Rubenstein, R. (1987) The solubility controversy of paired helical filaments: a commentary, *Neurochem Res 12*, 93–95.
18. Ksiezak-Reding, H., Binder, L. I., and Yen, S. H. (1990) Alzheimer disease proteins (A68) share epitopes with tau but show distinct biochemical properties, *J Neurosci Res 25*, 420–430.
19. Lewis, J., McGowan, E., Rockwood, J., Melrose, H., Nacharaju, P., Van Slegtenhorst, M., Gwinn-Hardy, K., Paul Murphy, M., Baker, M., Yu, X., Duff, K., Hardy, J., Corral, A., Lin, W. L., Yen, S. H., Dickson, D. W., Davies, P., and Hutton, M. (2000) Neurofibrillary tangles, amyotrophy and progressive motor disturbance in mice expressing mutant (P301L) tau protein, *Nat Genet 25*, 402–405.
20. Sahara, N., Lewis, J., DeTure, M., McGowan, E., Dickson, D. W., Hutton, M., and Yen, S. H. (2002) Assembly of tau in transgenic animals expressing P301L tau: alteration of phosphorylation and solubility, *J Neurochem 83*, 1498–1508.
21. Eckermann, K., Mocanu, M. M., Khlistunova, I., Biernat, J., Nissen, A., Hofmann, A., Schonig, K., Bujard, H., Haemisch, A., Mandelkow, E., Zhou, L., Rune, G., and Mandelkow, E. M. (2007) The beta-propensity of Tau determines aggregation and synaptic loss in inducible mouse models of tauopathy, *J Biol Chem 282*, 31755–31765.
22. Noble, W., Planel, E., Zehr, C., Olm, V., Meyerson, J., Suleman, F., Gaynor, K., Wang, L., LaFrancois, J., Feinstein, B., Burns, M., Krishnamurthy, P., Wen, Y., Bhat, R., Lewis, J., Dickson, D., and Duff, K. (2005) Inhibition of glycogen synthase kinase-3 by lithium correlates with reduced tauopathy and degeneration in vivo, *Proc Natl Acad Sci USA 102*, 6990–6995.
23. Planel, E., Bretteville, A., Liu, L., Virag, L., Du, A. L., Yu, W. H., Dickson, D. W., Whittington, R. A., and Duff, K. E. (2009) Acceleration and persistence of neurofibrillary pathology in a mouse model of tauopathy following anesthesia, *FASEB J 23*, 2595–2604.
24. Skovronsky, D. M., Doms, R. W., and Lee, V. M. (1998) Detection of a novel intraneuronal pool of insoluble amyloid beta protein that accumulates with time in culture, *J Cell Biol 141*, 1031–1039.
25. Ishihara, T., Hong, M., Zhang, B., Nakagawa, Y., Lee, M. K., Trojanowski, J. Q., and Lee, V. M. (1999) Age-dependent emergence and progression of a tauopathy in transgenic mice overexpressing the shortest human tau isoform, *Neuron 24*, 751–762.
26. Kondo, J., Honda, T., Mori, H., Hamada, Y., Miura, R., Ogawara, M., and Ihara, Y. (1988) The carboxyl third of tau is tightly bound to paired helical filaments, *Neuron 1*, 827–834.
27. Lim, F., Hernandez, F., Lucas, J. J., Gomez-Ramos, P., Moran, M. A., and Avila, J. (2001) FTDP-17 mutations in tau transgenic mice provoke lysosomal abnormalities and Tau filaments in forebrain, *Mol Cell Neurosci 18*, 702–714.
28. Gotz, J., Chen, F., Barmettler, R., and Nitsch, R. M. (2001) Tau filament formation in transgenic mice expressing P301L tau, *J Biol Chem 276*, 529–534.
29. Tatebayashi, Y., Miyasaka, T., Chui, D. H., Akagi, T., Mishima, K., Iwasaki, K., Fujiwara, M., Tanemura, K., Murayama, M., Ishiguro, K., Planel, E., Sato, S., Hashikawa, T., and Takashima, A. (2002) Tau filament formation and associative memory deficit in aged mice expressing mutant (R406W) human tau, *Proc Natl Acad Sci USA 99*, 13896–13901.
30. Allen, B., Ingram, E., Takao, M., Smith, M. J., Jakes, R., Virdee, K., Yoshida, H., Holzer, M., Craxton, M., Emson, P. C., Atzori, C., Migheli, A., Crowther, R. A., Ghetti, B., Spillantini, M. G., and Goedert, M. (2002) Abundant tau filaments and nonapoptotic neurodegeneration in transgenic mice expressing human P301S tau protein, *J Neurosci 22*, 9340–9351.

31. Andorfer, C., Kress, Y., Espinoza, M., de Silva, R., Tucker, K. L., Barde, Y. A., Duff, K., and Davies, P. (2003) Hyperphosphorylation and aggregation of tau in mice expressing normal human tau isoforms, *J Neurochem 86*, 582–590.
32. Ikeda, M., Shoji, M., Kawarai, T., Kawarabayashi, T., Matsubara, E., Murakami, T., Sasaki, A., Tomidokoro, Y., Ikarashi, Y., Kuribara, H., Ishiguro, K., Hasegawa, M., Yen, S. H., Chishti, M. A., Harigaya, Y., Abe, K., Okamoto, K., St George-Hyslop, P., and Westaway, D. (2005) Accumulation of filamentous tau in the cerebral cortex of human tau R406W transgenic mice, *Am J Pathol 166*, 521–531.
33. Santacruz, K., Lewis, J., Spires, T., Paulson, J., Kotilinek, L., Ingelsson, M., Guimaraes, A., DeTure, M., Ramsden, M., McGowan, E., Forster, C., Yue, M., Orne, J., Janus, C., Mariash, A., Kuskowski, M., Hyman, B., Hutton, M., and Ashe, K. H. (2005) Tau suppression in a neurodegenerative mouse model improves memory function, *Science 309*, 476–481.
34. Terwel, D., Lasrado, R., Snauwaert, J., Vandeweert, E., Van Haesendonck, C., Borghgraef, P., and Van Leuven, F. (2005) Changed conformation of mutant Tau-P301L underlies the moribund tauopathy, absent in progressive, nonlethal axonopathy of Tau-4R/2N transgenic mice, *J Biol Chem 280*, 3963–3973.
35. Murakami, T., Paitel, E., Kawarabayashi, T., Ikeda, M., Chishti, M. A., Janus, C., Matsubara, E., Sasaki, A., Kawarai, T., Phinney, A. L., Harigaya, Y., Horne, P., Egashira, N., Mishima, K., Hanna, A., Yang, J., Iwasaki, K., Takahashi, M., Fujiwara, M., Ishiguro, K., Bergeron, C., Carlson, G. A., Abe, K., Westaway, D., St George-Hyslop, P., and Shoji, M. (2006) Cortical neuronal and glial pathology in TgTauP301L transgenic mice: neuronal degeneration, memory disturbance, and phenotypic variation, *Am J Pathol 169*, 1365–1375.
36. Leroy, K., Bretteville, A., Schindowski, K., Gilissen, E., Authelet, M., De Decker, R., Yilmaz, Z., Buee, L., and Brion, J. P. (2007) Early axonopathy preceding neurofibrillary tangles in mutant tau transgenic mice, *Am J Pathol 171*, 976–992.
37. Rosenmann, H., Grigoriadis, N., Eldar-Levy, H., Avital, A., Rozenstein, L., Touloumi, O., Behar, L., Ben-Hur, T., Avraham, Y., Berry, E., Segal, M., Ginzburg, I., and Abramsky, O. (2008) A novel transgenic mouse expressing double mutant tau driven by its natural promoter exhibits tauopathy characteristics, *Exp Neurol 212*, 71–84.
38. Mocanu, M. M., Nissen, A., Eckermann, K., Khlistunova, I., Biernat, J., Drexler, D., Petrova, O., Schonig, K., Bujard, H., Mandelkow, E., Zhou, L., Rune, G., and Mandelkow, E. M. (2008) The potential for beta-structure in the repeat domain of tau protein determines aggregation, synaptic decay, neuronal loss, and coassembly with endogenous Tau in inducible mouse models of tauopathy, *J Neurosci 28*, 737–748.
39. Ittner, L. M., Fath, T., Ke, Y. D., Bi, M., van Eersel, J., Li, K. M., Gunning, P., and Gotz, J. (2008) Parkinsonism and impaired axonal transport in a mouse model of frontotemporal dementia, *Proc Natl Acad Sci U S A 105*, 15997–16002.
40. Adams, S. J., Crook, R. J., Deture, M., Randle, S. J., Innes, A. E., Yu, X. Z., Lin, W. L., Dugger, B. N., McBride, M., Hutton, M., Dickson, D. W., and McGowan, E. (2009) Overexpression of wild-type murine tau results in progressive tauopathy and neurodegeneration, *Am J Pathol 175*, 1598–1609.
41. Higuchi, M., Ishihara, T., Zhang, B., Hong, M., Andreadis, A., Trojanowski, J., and Lee, V. (2002) Transgenic mouse model of tauopathies with glial pathology and nervous system degeneration, *Neuron 35*, 433.
42. Zhang, B., Higuchi, M., Yoshiyama, Y., Ishihara, T., Forman, M. S., Martinez, D., Joyce, S., Trojanowski, J. Q., and Lee, V. M. (2004) Retarded axonal transport of R406W mutant tau in transgenic mice with a neurodegenerative tauopathy, *J Neurosci 24*, 4657–4667.
43. Forman, M. S., Lal, D., Zhang, B., Dabir, D. V., Swanson, E., Lee, V. M., and Trojanowski, J. Q. (2005) Transgenic mouse model of tau pathology in astrocytes leading to nervous system degeneration, *J Neurosci 25*, 3539–3550.
44. Higuchi, M., Zhang, B., Forman, M. S., Yoshiyama, Y., Trojanowski, J. Q., and Lee, V. M. (2005) Axonal degeneration induced by targeted expression of mutant human tau in oligodendrocytes of transgenic mice that model glial tauopathies, *J Neurosci 25*, 9434–9443.
45. Yoshiyama, Y., Higuchi, M., Zhang, B., Huang, S. M., Iwata, N., Saido, T. C., Maeda, J., Suhara, T., Trojanowski, J. Q., and Lee, V. M. (2007) Synapse loss and microglial activation precede tangles in a P301S tauopathy mouse model, *Neuron 53*, 337–351.
46. Probst, A., Gotz, J., Wiederhold, K. H., Tolnay, M., Mistl, C., Jaton, A. L., Hong, M., Ishihara, T., Lee, V. M., Trojanowski, J. Q., Jakes, R., Crowther, R. A., Spillantini, M. G., Burki, K., and Goedert, M. (2000) Axonopathy and amyotrophy in mice transgenic for human four-

repeat tau protein, *Acta Neuropathol 99*, 469–481.

47. Gotz, J., Tolnay, M., Barmettler, R., Chen, F., Probst, A., and Nitsch, R. M. (2001) Oligodendroglial tau filament formation in transgenic mice expressing G272V tau, *Eur J Neurosci 13*, 2131–2140.
48. Tanemura, K., Murayama, M., Akagi, T., Hashikawa, T., Tominaga, T., Ichikawa, M., Yamaguchi, H., and Takashima, A. (2002) Neurodegeneration with tau accumulation in a transgenic mouse expressing V337M human tau, *J. Neurosci. 22*, 133–141.
49. Perez, M., Valpuesta, J. M., de Garcini, E. M., Quintana, C., Arrasate, M., Lopez Carrascosa, J. L., Rabano, A., Garcia de Yebenes, J., and Avila, J. (1998) Ferritin is associated with the aberrant tau filaments present in progressive supranuclear palsy, *Am J Pathol 152*, 1531–1539.
50. Goedert, M., Spillantini, M. G., Cairns, N. J., and Crowther, R. A. (1992) Tau proteins of Alzheimer paired helical filaments: abnormal phosphorylation of all six brain isoforms, *Neuron 8*, 159–168.
51. Oddo, S., Vasilevko, V., Caccamo, A., Kitazawa, M., Cribbs, D. H., and LaFerla, F. M. (2006) Reduction of soluble abeta and tau, but not soluble abeta alone, ameliorates cognitive decline in transgenic mice with plaques and tangles, *J Biol Chem 281*, 39413–39423.
52. Dabir, D. V., Robinson, M. B., Swanson, E., Zhang, B., Trojanowski, J. Q., Lee, V. M., and Forman, M. S. (2006) Impaired glutamate transport in a mouse model of tau pathology in astrocytes, *J Neurosci 26*, 644–654.
53. Brion, J. P., Hanger, D. P., Bruce, M. T., Couck, A. M., Flament-Durand, J., and Anderton, B. H. (1991) Tau in Alzheimer neurofibrillary tangles. N- and C-terminal regions are differentially associated with paired helical filaments and the location of a putative abnormal phosphorylation site, *Biochem. J. 273*, 127–133.

Chapter 33

Tissue Processing Prior to Analysis of Alzheimer's Disease Associated Proteins and Metabolites, Including Aβ

Stephen D. Schmidt, Ralph A. Nixon, and Paul M. Mathews

Abstract

Amyloid-containing tissue, whether from human patients or an animal model of a disease, is typically characterized by various biochemical and immunohistochemical techniques, many of which are described in detail in this volume. In this chapter, we describe a straightforward technique for the homogenization of tissue prior to these analyses. The technique is particularly well suited for performing a large number of different biochemical analyses on a single mouse brain hemisphere. Starting with this homogenate multiple characterizations can be done, including western blot analysis and isolation of membrane-associated proteins, both of which are described here. Additional analyses can readily be performed on the tissue homogenate, including the ELISA quantitation of Aβ in the brain of a transgenic mouse model of β-amyloid deposition. The ELISA technique is described in detail in Chapter 34.

Key words: Aβ, Alzheimer's disease, Amyloid, Amyloid precursor protein, APP, Brain, Dissection, Fractionation, Homogenization, Membrane protein, SDS-PAGE, Western blot analysis

1. Introduction

It is often valuable to characterize and quantitate multiple proteins from a tissue sample in addition to the amyloid species of interest. Unfortunately, the tissue extraction techniques used to solubilize amyloid, such as formic acid extraction of β-amyloid to fully recover Aβ in human Alzheimer's disease brain or in β-amyloid depositing transgenic mice (1), are frequently incompatible with other methods of protein analysis because of the extensive denaturation to which the tissue is subjected. The extraction protocol described here, however, is compatible with numerous biochemical analyses while allowing for quantitation of Aβ levels both prior to and following β-amyloid deposition (2–18). In this chapter, we describe the preparation of a sucrose homogenate from a mouse brain hemisphere and from human brain tissue, and the

Einar M. Sigurdsson et al. (eds.), *Amyloid Proteins: Methods and Protocols*, Methods in Molecular Biology, vol. 849,
DOI 10.1007/978-1-61779-551-0_33,

subsequent western blot analysis of various proteins. Additionally, fractionation of membrane-associated proteins from soluble proteins, which may be used to separate amyloid precursor protein (APP) from the soluble, secreted N-terminal fragment of APP (sAPP) (19–22), is described.

As illustrated in Chapter 34, a portion of this tissue homogenate can also be subjected to standard amyloid extraction techniques, which allows for the quantitation of Aβ in β-amyloid plaques. This reduces the amount of tissue required to obtain multiple readouts and allows for a direct comparison of the levels of an amyloid precursor to the aggregated amyloid within a single sample. This approach is particularly valuable in the analysis of β-amyloid depositing transgenic mice, where a single hemibrain can be used as the starting material for multiple biochemical analyses, preserving the other hemibrain for additional purposes, such as fixation and immunohistochemistry. This greatly increases the numbers and types of analyses one can obtain from a single mouse, and thus represents significant savings in the number of animals necessary for an informative data set.

2. Materials

1. Tissue of interest or, as described here, a relevant β-amyloid mouse model for dissection of the brain. A generally useful quantity of tissue is approximately 200 mg.
2. Homogenization equipment, such as a 5-mL Wheaton Potter-Elvehjem tissue grinder with a piston-type polytetrafluoroethylene (e.g., Teflon) pestle and glass vessel (available from Fisher Scientific; Pittsburgh, PA, cat. no. 08-414-16C), driven by an electric stirrer. Other homogenization techniques can also be employed (see Note 1).
3. Neutral pH, phosphate-buffered 10% formalin (Fisher Diagnostics, Middletown, VA, cat. no. 245-685).
4. Ultracentrifuge and rotor (e.g., Beckman Coulter Optima TLX or MAX-E centrifuge and TLA-100.1 rotor).
5. 0.5-mL thick-walled polycarbonate ultracentrifuge tubes (Beckman Instruments, Palo Alto, CA, cat. no. 343776).
6. Tissue homogenization buffer (THB): 250 mM sucrose, 20 mM Tris (pH 7.4), 1 mM EDTA, 1 mM EGTA at 4°C. Stable for months when sterile-filtered, handled aseptically, and stored at 4°C.
7. 100 mM phenylmethylsulfonyl fluoride (PMSF; Sigma, St. Louis, MO) in 100% ethanol. Stable for months when stored at –20°C.
8. 1,000× LAP: 5 mg each of leupeptin hemisulfate salt, antipain HCl, and pepstatin A, all dissolved in 1 mL of

N,N-dimethylformamide (all available from Sigma, St. Louis, MO). Stable for months when stored at –20°C.

9. DC Protein Assay Reagents Package (Bio-Rad, Hercules, CA, cat. no. 500-0116).
10. 96-well EIA/RIA plates, medium binding (Corning, Corning, NY, cat. no. 9017).
11. 10 mg/mL bovine serum albumin (BSA). Store at –20°C in aliquots.
12. Microplate spectrophotometer capable of reading the optical density at 750 nm of samples in a 96-well plate.
13. 2× Sample diluent containing urea (2× SD): 9.6% sodium dodecyl sulfate (SDS), 4 M urea, 16% sucrose, 0.5 mg/mL bromophenol blue. Add 46 μL of 2-mercaptoethanol per 1 mL of sample diluent to the amount of 2× SD to be used daily (2-mercaptoethanol final concentration: 700 mM).
14. Precast Criterion Tris–HCl polyacrylamide gels (e.g., 4–20% polyacrylamide, 18-well, 30-μL wells; available from Bio-Rad, Hercules, CA, cat. no. 345-0033).
15. Sodium dodecyl sulfate-polyacrylamide gel electrophoresis (SDS-PAGE) and western blot transfer equipment (e.g., Criterion brand cell and Criterion blotter with plate electrodes, available from Bio-Rad, Hercules, CA, cat. nos. 165-6001 and 170-4070, respectively).
16. Polyvinylidene fluoride (PVDF) membrane (e.g., Immobilon-P transfer membrane, Millipore Corporation, Bedford, MA, cat. no. IPVH 00010).
17. 10× Ponceau S solution: prepared by mixing 2% Ponceau S (w/v; Sigma, St. Louis, MO, cat. no. P-3504) into 30% trichloroacetic acid until the Ponceus S fully dissolves. Dilute this 1:10 in H_2O prior to use. Both the stock solution and diluted solution are stable at room temperature.
18. Phosphate-buffered saline (PBS).
19. 5% Nonfat milk powder (Bio-Rad, Hercules, CA, cat. no. 170-6404) in PBS, prepared fresh.
20. 1% Bovine serum albumin (BSA), 0.02% NaN_3 in PBS.
21. Appropriate primary and secondary antibodies (for western blot analysis).

3. Methods

The value of the extraction protocol presented here is its flexibility: a homogenate that is compatible with many biochemical analyses is prepared from a tissue sample. The methods below describe the preparation of a sucrose homogenate from a mouse hemibrain or human

brain tissue. Also illustrated are some of the biochemical analyses, such as western blot analysis of total proteins and the separation and analysis of secreted and membrane-associated forms of APP, that can be used to characterize protein expression and processing in the sample.

3.1. Tissue Homogenization

After sacrifice, the two hemispheres of a mouse brain are separated and processed differently: one hemisphere is homogenized in sucrose for biochemical analyses, while the other is immersion-fixed for histological examinations (see Fig. 1). Other tissue types or tissue from patients can also be used as the starting material.

3.1.1. Brain Dissection

Rapidly sacrifice the mouse in accordance with current institute animal care and use committee procedures. With scissors, decapitate the mouse and cut along the midline through the skin over the skull (see Fig. 2). Expose the skull and using clean, small scissors carefully cut through the skull along the midline working rostral from the base of the skull. Avoid cutting into the brain with the scissors; chipping away at the skull with small cuts of the scissors is a useful technique to avoid damaging the underlying brain. At the level of the eye orbits, cut laterally though the skull in both directions. With forceps, carefully lift and pull laterally the two pieces of skull to expose the brain. Additional cuts may be required to fully expose the skull and some practice may be required—on a wild-type animal—to develop a rapid technique that does not damage the brain.

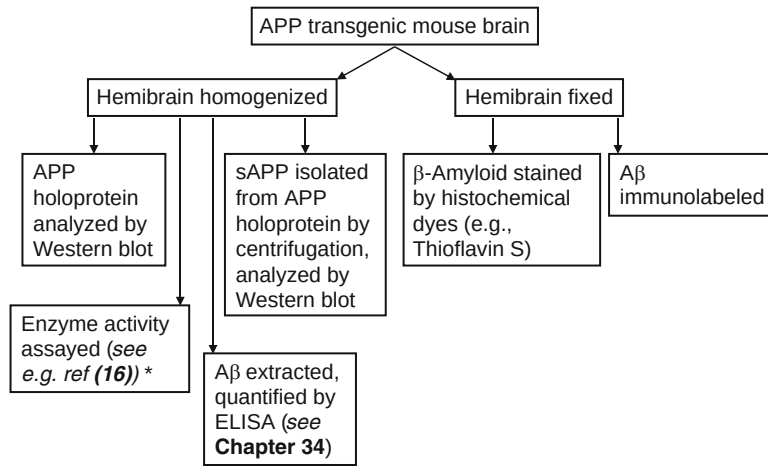

Fig. 1. Flowchart of procedures possible when tissue is processed as described in this chapter. *Note: certain enzymes are inhibited by the protease inhibitor cocktail that is added to THB prior to homogenization. An inhibitor of an enzyme of interest can be omitted from the protease inhibitor mixture and, immediately after homogenization, an aliquot can be frozen separately for the enzyme assay. The inhibitor that was left out can then be mixed into the remaining homogenate before dividing it into aliquots and freezing.

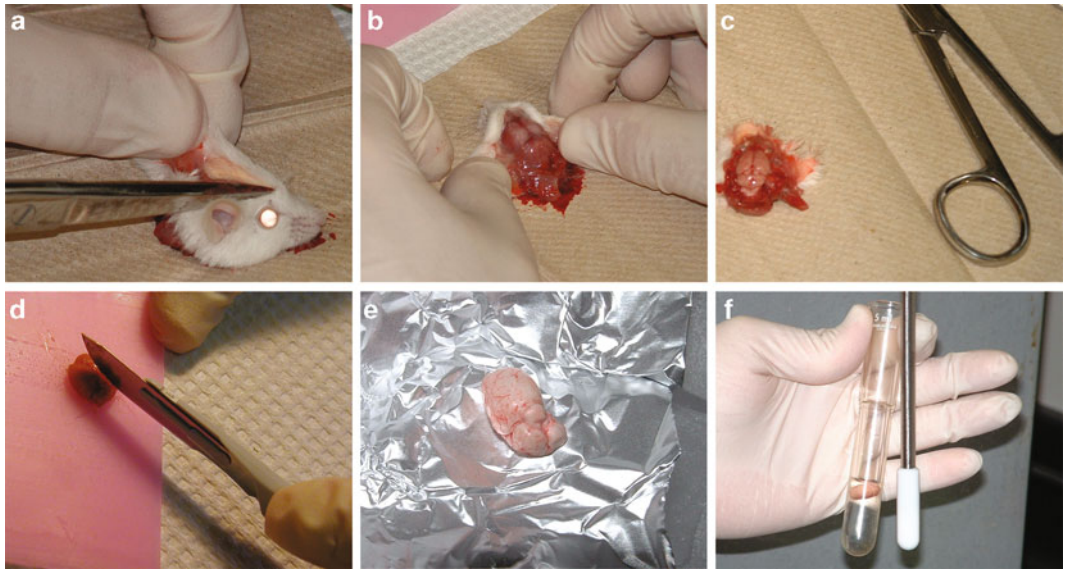

Fig. 2. Removal of a mouse brain in preparation for homogenization. The skin covering the skull is cut with scissors (**a**) and spread apart to expose the skull (**b**). The top of the skull is removed, exposing the brain (**c**). The brain is cut through the midline at the corpus callosum (**d**) and frozen as individual hemispheres on aluminum foil on dry ice (**e**). A Teflon-coated pestle and glass vessel used for homogenization (**f**).

Once the brain is fully exposed, cut through the spinal cord at the base of the brain, carefully insert forceps under the brain, and gently lift it from the brain case. The olfactory bulbs at the anterior end of the brain often remain within the skull unless special care is taken to free them from the bone. Place the brain on a clean, non-stick surface and use a razor blade or scalpel to cut through the midline at the corpus callosum such that the brain is separated into two equal hemispheres (Fig. 2). Specific brain regions may be further isolated. (We routinely remove and discard the olfactory bulbs but retain the cerebellum.) Rapidly freeze one hemisphere on a piece of aluminum foil placed on dry ice. The other hemisphere can be used for other purposes, such as histological analysis following immersion fixation (see Subheading 3.1.2) or stored frozen as reserve tissue. Transfer the frozen hemisphere to a labeled microcentrifuge tube that has been prechilled on dry ice and store at −80°C. Tissue can be stored frozen at −80°C for an extended period if necessary. Only a single mouse should be sacrificed at a time and the tissue properly frozen before a second animal is dissected (see Note 2).

Human brain tissue samples are typically dissected to isolate gray matter from white matter, vessels, and meninges prior to homogenization. The gray matter may be used for western blot and other analyses, while the lipid-rich white matter and other tissue are commonly discarded. Cutting the tissue into ~0.5 cm^3 pieces facilitates obtaining a sample of nearly pure gray matter. To preserve labile proteins during the dissection, the procedure can be

performed on a chilled platform created by inverting an aluminum weighing dish on dry ice pellets. The tips of blunt-tipped forceps should be placed in dry ice pellets prior to using them to hold tissue, while scalpel blades can be warmed to facilitate passage through the frozen tissue.

3.1.2. Fixation of the Second Brain Hemisphere for Neuropathology and/or Immunohistochemistry

Immediately drop the remaining brain hemisphere into 15 mL of neutral pH, phosphate-buffered 10% formalin chilled to 4°C. Allow the tissue to immersion fix at 4°C for a minimum of 24 h prior to sectioning and subsequent analysis (see Chapter 28).

3.1.3. Preparation of the Sucrose Homogenate

This section of the protocol describes the preparation of a 10% sucrose homogenate (weight of tissue/volume) from the frozen mouse brain hemisphere. Such a homogenate can similarly be prepared from human brain or other tissues obtained from patients or animals by dissecting the tissue of interest, weighing it, and adjusting volumes as needed. It is important to work quickly and to keep samples cold throughout.

1. Determine the weight of the tissue (see Note 3): use an empty microcentrifuge tube to tare the balance and weigh the frozen hemibrains to the nearest 10 mg. This should be done quickly to prevent thawing and samples should be stored on dry ice until homogenized.
2. Cool on ice the glass vessel to be used for homogenization.
3. Calculate the amount of THB that will be needed for a given group of samples: 1 mL of buffer is needed per 100 mg of tissue. Immediately prior to beginning homogenization, mix protease inhibitors into the THB (1/100th volume of 100 mM PMSF and 1/1,000th volume 1,000× LAP; see Note 4). If a precipitate is seen in the 100 mM PMSF solution, dissolve it by warming to 37°C. Prepare slightly more (~10% additional) of the THB + inhibitors than the minimum needed. Keep on ice.
4. Pipet the necessary amount of cold THB + inhibitors (e.g., 1.9 mL for a 190 mg tissue sample, the approximate wet weight of a mouse brain hemisphere) into the glass vessel to be used for homogenization. Drop the frozen brain hemisphere into the cold THB + inhibitors using a small spatula to pry the tissue from the microcentrifuge tube if necessary.
5. Fully homogenize the tissue using 20 complete up-and-down strokes of the glass vessel while the pestle is rapidly spinning (see Note 1). Care should be taken not to cause excess foaming by removing the pestle completely from the homogenate, as this denatures proteins.
6. Generate multiple aliquots of the homogenate in pre-labeled microcentrifuge tubes to minimize subsequent refreezing of aliquots following a particular analysis. A useful scheme for

subsequent formic acid extraction of Aβ is to dispense the homogenate into several aliquots of 350–500 µL, including a single 5 µL aliquot to be used for protein quantitation (see Subheading 3.1.4; see also Note 5). For the diethylamine extraction procedure described in Chapter 34, make a single 1.3 mL aliquot, with the remaining homogenate distributed into smaller volumes.

7. Freeze aliquots on dry ice immediately.
8. Rinse the pestle with water and dry it with a lint-free tissue. Rinse the vessel three times, invert for several seconds, and shake out excess water before homogenizing the next sample. Store aliquoted homogenates at −80°C. Discard any remaining THB to which protease inhibitors have been added.

3.1.4. Determining Protein Concentration in the Homogenate

The protein concentration in each homogenate is determined so that equal amounts of total protein from each sample can be analyzed by SDS-PAGE. This may be done using the DC Protein Assay Reagents Package or a similar kit. Diluted aliquots of homogenates and standards are dispensed into duplicate wells of a 96-well plate, followed by the reagents from the kit as described below:

1. Add 20 µL of H_2O to the 5 µL aliquot of homogenate set aside for protein quantitation.
2. Dilute the 10 mg/mL BSA stock solution to 0.2, 0.4, 1.0, 2.0, and 4.0 mg/mL and load 5 µL of the diluted standards and samples and a 5 µL H_2O blank into duplicate wells.
3. Proceed with the manufacturer's protocol. The 15-min incubation specified in the protocol may be eliminated and the optical density may be read immediately after the addition of reagent B. Typically, the mouse hemibrain homogenization described here yields ~10 mg/mL total protein.

3.2. Western Blot Analysis of Total Proteins

SDS-PAGE and western blot have become routine laboratory procedures and the specifics of each electrophoresis and transfer apparatus are typically well described by the manufacturer's protocol. Choices of polyacrylamide percentage and whether isocratic or gradient gels are more appropriate depend on the molecular weight of the protein being characterized. Sources for useful information and precast SDS-polyacrylamide gels include Bio-Rad (Hercules, CA) and Invitrogen (Carlsbad, CA).

Figure 3a, b shows representative analyses of mouse and human brain homogenates by western blot, and the specific method used for these western blots is described here.

1. Pipet 50 µL of 2× SD into microcentrifuge tubes.
2. Pipet the volume of each homogenate that equals 200 µg of protein into the tubes containing 2× SD (e.g. 20 µL of a homogenate containing 10 mg/mL of protein).

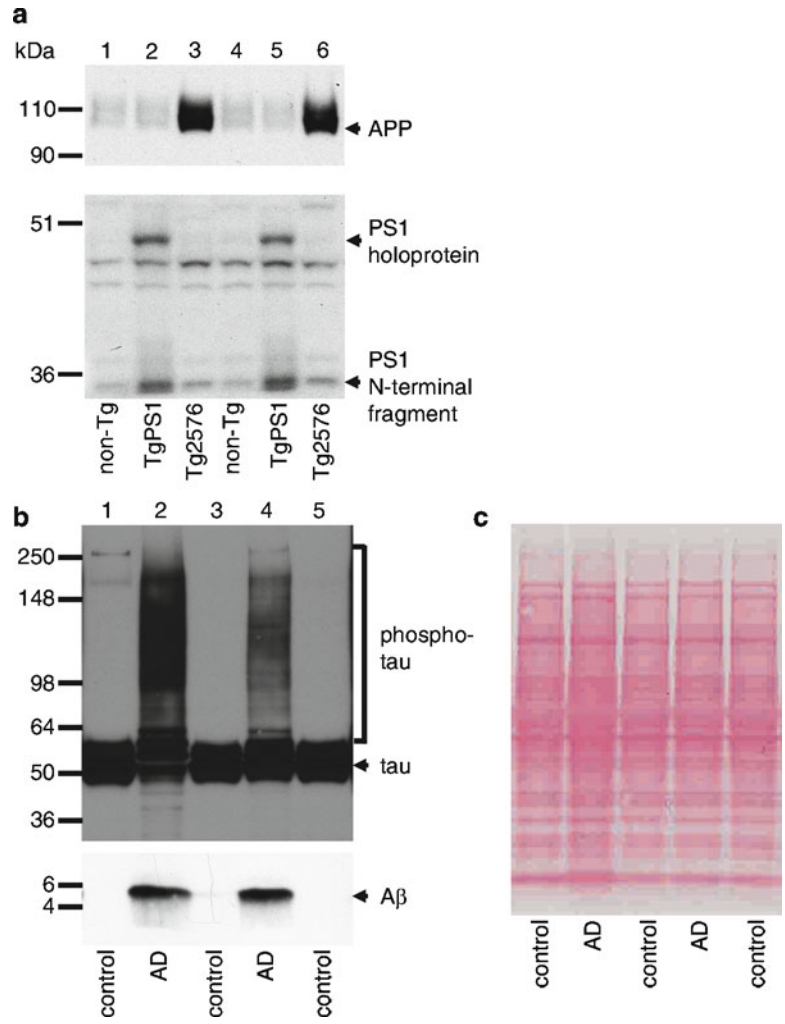

Fig. 3. Western blot analysis of APP and presenilin 1 from transgenic mouse brain homogenates and tau and Aβ from human AD brain homogenates. Homogenates were prepared from hemibrains isolated from non-transgenic mice (non-Tg), and mice overexpressing a mutant form of human presenilin 1 (TgPS1; (26)) or Swedish mutant APP (Tg2576; (27)) and subjected to SDS-PAGE as described. Following transfer, one membrane (**a**, *upper panel*) was probed with an antibody that binds to the C-terminal of APP and recognizes both the murine and human proteins (C1/6.1, generated by our laboratory and available from Covance, Princeton, NJ; (23)) and a second (**a**, *lower panel*) was probed with an anti-PS1 antibody (NT1, generated by our laboratory and available from Covance, Princeton, NJ; (25)). The increased expression of APP is seen in the APP transgenic mice (*lanes 3* and *6*) when compared to the endogenous APP expression in the other animals. Similarly, an increase in PS1 expression is seen in the PS1 transgenic mice (*lanes 2* and *5*). Homogenates correspondingly prepared from human control and AD brain (Brodmann area 10) were likewise resolved and transferred. The membranes were probed with either T46 (Tau 46.1) antibody for detection of tau protein (**b**, *upper panel*) (28) or JRF/Aβtot/17 antibody for Aβ (**b**, *lower panel*) (23). The AD samples show characteristic phosphorylated tau (phospho-tau) and accumulated Aβ (*lanes 2* and *4*) in contrast to the controls (*lanes 1, 3*, and *5*). The AD samples were from Braak stage 5 brains. In (**c**), temporary Ponceau S staining of a membrane with the samples in (**b**) demonstrates that protein was uniformly loaded and transferred for each sample.

3. Add H_2O to bring each volume to 100 µL (e.g., 30 µL).
4. Heat tubes to 95°C for 5 min. Vortex each tube vigorously for ~15 s to shear DNA (see Note 6).
5. Load 20 µL of the prepared sample into the wells of a 4–20% Tris–HCL polyacrylamide gel. Electrophorese according to the manufacturer's protocol.
6. Transfer sized proteins onto a PVDF membrane (e.g. Immobilon-P) according to the manufacturer's protocol.
7. Confirm the uniformity of protein loading and transfer by Ponceau S staining. Transfer the wet membrane to a small volume (~25 mL) of Ponceau S solution and incubate at room temperature with gentle agitation for 30 s. Wash with multiple changes of PBS until the red-stained protein bands in each lane are visible (Fig. 3c). The membrane can be dried at this point and stored prior to antibody labeling. The water soluble Ponceau S can be completely removed by washing with PBS for ~15 min.
8. Rewet the membrane according to the manufacturer's protocol if it has been allowed to dry.
9. Block excess protein-binding sites by incubating the membrane in 5% nonfat milk powder in PBS for 1 h at room temperature with gentle rocking. Wash the membrane 3× 15 min with PBS.
10. Bind primary antibody in 1% BSA, 0.02% NaN_3, PBS, followed by 3× 15 min washes with PBS and secondary antibody diluted in 5% nonfat milk powder in PBS. (Note: commercially obtained primary antibodies may be expensive, but when diluted in 1% BSA, 0.02% NaN_3, PBS and stored at 4°C are stable for more than a year and can be reused several times). Choice of antibody-binding conditions, type of secondary antibody and detection technique will need to be guided by the specifics of the primary antibody used.

3.3. Fractionation of Soluble and Membrane-Associated Proteins

A number of the precursor proteins from which amyloids are derived are membrane-associated proteins (e.g., APP, prion protein, and the familial British dementia precursor protein BRI). One advantage of preparing, as the first step in protein characterization and isolation, a sucrose homogenate lacking detergents is that membranes are preserved and fractionation techniques can be used to differentiate membrane-associated proteins from soluble cytosolic or extracellular proteins. We have applied this technique to differentiate the membrane-associated APP holoprotein from the soluble, N-terminal proteolytic fragments of APP that are released from the cell into the extracellular space, the so-called sAPP fragments (19–22). Western blot analysis of APP holoprotein and sAPP isolated from mouse brain by this technique is shown in Fig. 4 (see also (23, 24) for further examples). Samples should be

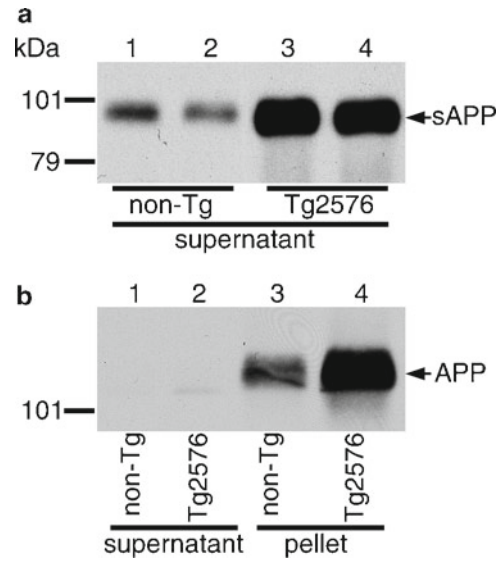

Fig. 4. Detection of sAPP in mouse brain. Sucrose homogenates were prepared from non-transgenic (non-Tg) and Swedish APP transgenic mice (Tg2576) mice and a portion of this homogenate centrifuged at 100,000 × *g* for 1 h. In *panel* ***a***, a portion of the supernatant was examined by western blot using an antibody that recognizes the N-terminal region of APP (22C11; (29); available from Chemicon, Temecula, CA). The 22C11 epitope is common to both APP holoprotein and the extracellular, secreted fragment of APP (sAPP) generated following α- or β-cleavage of the parental molecule (see ref. 23). The soluble sAPP fragment remains in the supernatant fraction while the membrane-associated APP holoprotein pellets during the 100,000 × *g* centrifugation. Much more sAPP was detected in the APP transgenic (*lanes 3* and *4*) than in the non-transgenic (*lanes 1* and *2*) mice. In *panel* ***b***, both supernatant (*lanes 1* and *2*) and membrane-pellet-associated (*lanes 3* and *4*) proteins were electrophoresed and subjected to western blot analysis with an antibody (C1/6.1; (23)) that recognizes APP holoprotein but does not bind to sAPP. No APP holoprotein was detected in the supernatant. APP holoprotein, however, was readily detected in both the membrane pellet prepared from the non-transgenic mouse (*lane 3*) and, at a higher level, in the membrane pellet from the APP transgenic animal (*lane 4*) (17, 18).

kept from warming above 4°C throughout the procedure, and rotors and tubes should be prechilled (see Note 7).

1. Thaw on ice one of the smaller volume aliquots of the 10% sucrose homogenate.
2. Pipet 0.2 mL into a 0.5 mL thick-walled ultracentrifuge tube.
3. Centrifuge for 1 h at 100,000 × *g* (48,000 rpm using a TLA-100.1 rotor) at 4°C.
4. Transfer the supernatant to a new tube and place on ice if SDS-PAGE is to be done immediately, otherwise freeze the supernatant on dry ice and store at –80°C. Multiple aliquots can be prepared prior to freezing to avoid unnecessary freeze-thaw cycles. Soluble, non-membrane-associated proteins are contained within this supernatant.

5. Directly resuspend the pellet in 0.4 mL of 1× SD containing urea (prepared by diluting 2× SD with H_2O) (see Note 8). Vortex to fully resuspend the pellet and spin briefly to collect droplets within the tube. The membrane-associated, non-soluble proteins within this resuspended pellet can be immediately analyzed by SDS-PAGE and western blot (see Subheading 3.2) or the samples can be stored at −80°C for future analysis.
6. Prior to running the gel add an equal volume of 2× SD to the supernatant samples and heat these and the resuspended pellets to 95°C for 5 min.
7. Load equal volumes of the supernatant and pellet samples into the wells of the gel and electrophorese (see Note 8). Following migration, transfer to PVDF membrane and probe the membrane with an antibody of interest.

4. Notes

1. While many tools for tissue homogenization can be used to prepare a homogenate from a mouse brain, a Teflon pestle against a glass vessel produces a uniform and consistent homogenate with intact membrane vesicles. In general, the more gentle the technique the better, although the production of a homogenate of uniform consistency is critical. If a motorized stirrer is not available to spin the pestle while moving the vessel up and down, the entire procedure can be done by hand, although more up-and-down strokes will be required.
2. The quality of the tissue rapidly deteriorates after the animal is sacrificed, so it is critical to dissect rapidly and progress to the point at which tissue is frozen or in fixative before pausing. For this reason we always freeze the hemibrains one mouse at a time, even if only a small number of hemibrain homogenates will be prepared the same day.
3. In order to obtain equal protein amounts for various assays (such as ELISA, see Chapter 34), it is critical that the hemibrain is accurately weighed and that the volume of THB used is adjusted to reflect the weight of each sample. This greatly improves the uniformity across samples in all subsequent analyses.
4. The protease inhibitors have a limited half-life in an aqueous solution and should be diluted immediately prior to use. Other inhibitors and inhibitor cocktails can be substituted. Maintaining samples on ice is as critical to preventing proteolysis in the homogenate as are the inhibitors. It is normal for the PMSF to form a cloudy colloid when diluted into THB.

5. The volume of aliquots prepared from the homogenate should reflect the anticipated downstream uses of each sample and should be done to minimize the need to refreeze and reuse an aliquot. The volumes suggested here are ideal for the downstream Aβ ELISA analyses described in Chapter 34.
6. DNA in the tissue sample interferes with protein migration on an SDS polyacrylamide gel. However, the urea in the sample diluent denatures the DNA more fully and allows for better protein resolution (25). The protein-DNA solution can still be viscous and therefore should be vortexed sufficiently to shear DNA and to allow for accurate pipetting of small volumes.
7. Whenever working with the homogenates, they must be kept cold to prevent unwanted proteolysis. Because of the long centrifugation time it is essential that the rotor and centrifuge be prechilled to 4°C. Samples should be refrozen immediately if necessary. Once SD has been added to samples, they are considerably more stable.
8. The amount of protein in the supernatant may differ from that in the pellet, which contains membrane-associated proteins. However, the volume of sample diluent used to resuspend the pellet is twice the volume of homogenate used for centrifugation. This is done so that when equal volumes of the supernatant plus sample diluent and the pellet resuspended in sample diluent are analyzed by western blot, the relative distribution of proteins in these two fractions can be directly compared. In order to determine the volume of these fractions to be used for SDS-PAGE, first calculate the volume of homogenate for a given sample that will contain the amount of protein necessary to give a signal by western blot. For example, in a homogenate containing 10 mg/mL of protein and where 40 μg of protein is typically loaded on the gel, this amount of homogenate would be 4 μL. Remembering that the supernatant has been diluted with an equal volume of SD and pellet resuspended in the same total volume, one would load 8 μL of the supernatant in SD and 8 μL of the resuspended pellet.

Acknowledgments

This work has been supported by the Alzheimer's Association (IIRG-07-60047 to P.M.M.) and the National Institute on Aging (AG017617 to P.M.M., R.A.N.). We thank Dr. Karen Duff (Columbia University) for the transgenic mouse brains used in the sample data.

References

1. Gravina, S. A., Ho, L., Eckman, C. B., Long, K. E., Otvos, L., Jr., Younkin, L. H., Suzuki, N., and Younkin, S. G. (1995) Amyloid beta protein (A beta) in Alzheimer's disease brain. Biochemical and immunocytochemical analysis with antibodies specific for forms ending at A beta 40 or A beta 42(43), *J Biol Chem* ***270***, 7013–7016.
2. Janus, C., Pearson, J., McLaurin, J., Mathews, P. M., Jiang, Y., Schmidt, S. D., Chishti, M. A., Horne, P., Heslin, D., French, J., Mount, H. T., Nixon, R. A., Mercken, M., Bergeron, C., Fraser, P. E., St George-Hyslop, P., and Westaway, D. (2000) A beta peptide immunization reduces behavioural impairment and plaques in a model of Alzheimer's disease, *Nature* ***408***, 979–982.
3. Refolo, L. M., Pappolla, M. A., LaFrancois, J., Malester, B., Schmidt, S. D., Thomas-Bryant, T., Tint, G. S., Wang, R., Mercken, M., Petanceska, S. S., and Duff, K. E. (2001) A cholesterol-lowering drug reduces beta-amyloid pathology in a transgenic mouse model of Alzheimer's disease, *Neurobiol Dis* ***8***, 890–899.
4. Rozmahel, R., Huang, J., Chen, F., Liang, Y., Nguyen, V., Ikeda, M., Levesque, G., Yu, G., Nishimura, M., Mathews, P., Schmidt, S. D., Mercken, M., Bergeron, C., Westaway, D., and St George-Hyslop, P. (2002) Normal brain development in PS1 hypomorphic mice with markedly reduced gamma-secretase cleavage of betaAPP, *Neurobiol Aging* ***23***, 187–194.
5. Rozmahel, R., Mount, H. T., Chen, F., Nguyen, V., Huang, J., Erdebil, S., Liauw, J., Yu, G., Hasegawa, H., Gu, Y., Song, Y. Q., Schmidt, S. D., Nixon, R. A., Mathews, P. M., Bergeron, C., Fraser, P., Westaway, D., and George-Hyslop, P. S. (2002) Alleles at the Nicastrin locus modify presenilin 1-deficiency phenotype, *Proc Natl Acad Sci USA* ***99***, 14452–14457.
6. Pfeifer, M., Boncristiano, S., Bondolfi, L., Stalder, A., Deller, T., Staufenbiel, M., Mathews, P. M., and Jucker, M. (2002) Cerebral hemorrhage after passive anti-Abeta immunotherapy, *Science* ***298***, 1379.
7. Phinney, A. L., Drisaldi, B., Schmidt, S. D., Lugowski, S., Coronado, V., Liang, Y., Horne, P., Yang, J., Sekoulidis, J., Coomaraswamy, J., Chishti, M. A., Cox, D. W., Mathews, P. M., Nixon, R. A., Carlson, G. A., St George-Hyslop, P., and Westaway, D. (2003) In vivo reduction of amyloid-beta by a mutant copper transporter, *Proc Natl Acad Sci USA* ***100***, 14193–14198.
8. Herzig, M. C., Winkler, D. T., Burgermeister, P., Pfeifer, M., Kohler, E., Schmidt, S. D., Danner, S., Abramowski, D., Sturchler-Pierrat, C., Burki, K., van Duinen, S. G., Maat-Schieman, M. L., Staufenbiel, M., Mathews, P. M., and Jucker, M. (2004) Abeta is targeted to the vasculature in a mouse model of hereditary cerebral hemorrhage with amyloidosis, *Nat Neurosci 7*, 954–960.
9. Lacombe, P., Mathews, P. M., Schmidt, S. D., Breidert, T., Heneka, M. T., Landreth, G. E., Feinstein, D. L., and Galea, E. (2004) Effect of anti-inflammatory agents on transforming growth factor beta over-expressing mouse brains: a model revised, *J Neuroinflammation* ***1***, 11.
10. Pawlik, M., Sastre, M., Calero, M., Mathews, P. M., Schmidt, S. D., Nixon, R. A., and Levy, E. (2004) Overexpression of human cystatin C in transgenic mice does not affect levels of endogenous brain amyloid Beta Peptide, *J Mol Neurosci* ***22***, 13–18.
11. Yao, J., Petanceska, S. S., Montine, T. J., Holtzman, D. M., Schmidt, S. D., Parker, C. A., Callahan, M. J., Lipinski, W. J., Bisgaier, C. L., Turner, B. A., Nixon, R. A., Martins, R. N., Ouimet, C., Smith, J. D., Davies, P., Laska, E., Ehrlich, M. E., Walker, L. C., Mathews, P. M., and Gandy, S. (2004) Aging, gender and APOE isotype modulate metabolism of Alzheimer's Abeta peptides and F-isoprostanes in the absence of detectable amyloid deposits, *J Neurochem* ***90***, 1011–1018.
12. Mastrangelo, P., Mathews, P. M., Chishti, M. A., Schmidt, S. D., Gu, Y., Yang, J., Mazzella, M. J., Coomaraswamy, J., Horne, P., Strome, B., Pelly, H., Levesque, G., Ebeling, C., Jiang, Y., Nixon, R. A., Rozmahel, R., Fraser, P. E., St George-Hyslop, P., Carlson, G. A., and Westaway, D. (2005) Dissociated phenotypes in presenilin transgenic mice define functionally distinct gamma-secretases, *Proc Natl Acad Sci USA* ***102***, 8972–8977.
13. Gandy, S., Zhang, Y. W., Ikin, A., Schmidt, S. D., Bogush, A., Levy, E., Sheffield, R., Nixon, R. A., Liao, F. F., Mathews, P. M., Xu, H., and Ehrlich, M. E. (2007) Alzheimer's presenilin 1 modulates sorting of APP and its carboxyl-terminal fragments in cerebral neurons in vivo, *J Neurochem* ***102***, 619–626.
14. Mi, W., Pawlik, M., Sastre, M., Jung, S. S., Radvinsky, D. S., Klein, A. M., Sommer, J., Schmidt, S. D., Nixon, R. A., Mathews, P. M., and Levy, E. (2007) Cystatin C inhibits amyloid-beta deposition in Alzheimer's disease mouse models, *Nat Genet* ***39***, 1440–1442.

15. Trinchese, F., Fa, M., Liu, S., Zhang, H., Hidalgo, A., Schmidt, S. D., Yamaguchi, H., Yoshii, N., Mathews, P. M., Nixon, R. A., and Arancio, O. (2008) Inhibition of calpains improves memory and synaptic transmission in a mouse model of Alzheimer disease, *J Clin Invest* ***118***, 2796–2807.
16. Yang, D. S., Stavrides, P., Mohan, P. S., Kaushik, S., Kumar, A., Ohno, M., Schmidt, S. D., Wesson, D., Bandyopadhyay, U., Jiang, Y., Pawlik, M., Peterhoff, C. M., Yang, A. J., Wilson, D. A., St George-Hyslop, P., Westaway, D., Mathews, P. M., Levy, E., Cuervo, A. M., and Nixon, R. A. (2011) Reversal of autophagy dysfunction in the TgCRND8 mouse model of Alzheimer's disease ameliorates amyloid pathologies and memory deficits, *Brain* ***134***, 258–277.
17. Choi, J. H., Berger, J. D., Mazzella, M. J., Morales-Corraliza, J., Cataldo, A. M., Nixon, R. A., Ginsberg, S. D., Levy, E., and Mathews, P. M. (2009) Age-dependent dysregulation of brain amyloid precursor protein in the Ts65Dn Down syndrome mouse model, *J Neurochem* ***110***, 1818–1827.
18. Morales-Corraliza, J., Mazzella, M. J., Berger, J. D., Diaz, N. S., Choi, J. H., Levy, E., Matsuoka, Y., Planel, E., and Mathews, P. M. (2009) In vivo turnover of tau and APP metabolites in the brains of wild-type and Tg2576 mice: greater stability of sAPP in the beta-amyloid depositing mice, *PLoS One* ***4***, e7134.
19. Weidemann, A., Konig, G., Bunke, D., Fischer, P., Salbaum, J. M., Masters, C. L., and Beyreuther, K. (1989) Identification, biogenesis, and localization of precursors of Alzheimer's disease A4 amyloid protein, *Cell* ***57***, 115–126.
20. Golde, T. E., Estus, S., Younkin, L. H., Selkoe, D. J., and Younkin, S. G. (1992) Processing of the amyloid protein precursor to potentially amyloidogenic derivatives, *Science* ***255***, 728–730.
21. Seubert, P., Oltersdorf, T., Lee, M. G., Barbour, R., Blomquist, C., Davis, D. L., Bryant, K., Fritz, L. C., Galasko, D., Thal, L. J., and et al. (1993) Secretion of beta-amyloid precursor protein cleaved at the amino terminus of the beta-amyloid peptide, *Nature* ***361***, 260–263.
22. Caporaso, G. L., Gandy, S. E., Buxbaum, J. D., Ramabhadran, T. V., and Greengard, P. (1992) Protein phosphorylation regulates secretion of Alzheimer beta/A4 amyloid precursor protein, *Proc Natl Acad Sci USA* ***89***, 3055–3059.
23. Mathews, P. M., Jiang, Y., Schmidt, S. D., Grbovic, O. M., Mercken, M., and Nixon, R. A. (2002) Calpain activity regulates the cell surface distribution of amyloid precursor protein: inhibition of calpains enhances endosomal generation of beta-cleaved C-terminal APP fragments, *J Biol Chem* ***277***, 36415–36424.
24. Mathews, P. M., Guerra, C. B., Jiang, Y., Grbovic, O. M., Kao, B. H., Schmidt, S. D., Dinakar, R., Mercken, M., Hille-Rehfeld, A., Rohrer, J., Mehta, P., Cataldo, A. M., and Nixon, R. A. (2002) Alzheimer's disease-related overexpression of the cation-dependent mannose 6-phosphate receptor increases Abeta secretion: role for altered lysosomal hydrolase distribution in beta-amyloidogenesis, *J Biol Chem* ***277***, 5299–5307.
25. Mathews, P. M., Cataldo, A. M., Kao, B. H., Rudnicki, A. G., Qin, X., Yang, J. L., Jiang, Y., Picciano, M., Hulette, C., Lippa, C. F., Bird, T. D., Nochlin, D., Walter, J., Haass, C., Levesque, L., Fraser, P. E., Andreadis, A., and Nixon, R. A. (2000) Brain expression of presenilins in sporadic and early-onset, familial Alzheimer's disease, *Mol Med* ***6***, 878–891.
26. Duff, K., Eckman, C., Zehr, C., Yu, X., Prada, C. M., Perez-tur, J., Hutton, M., Buee, L., Harigaya, Y., Yager, D., Morgan, D., Gordon, M. N., Holcomb, L., Refolo, L., Zenk, B., Hardy, J., and Younkin, S. (1996) Increased amyloid-beta42(43) in brains of mice expressing mutant presenilin 1, *Nature* ***383***, 710–713.
27. Hsiao, K., Chapman, P., Nilsen, S., Eckman, C., Harigaya, Y., Younkin, S., Yang, F., and Cole, G. (1996) Correlative memory deficits, Abeta elevation, and amyloid plaques in transgenic mice, *Science* ***274***, 99–102.
28. Kosik, K. S., Orecchio, L. D., Binder, L., Trojanowski, J. Q., Lee, V. M., and Lee, G. (1988) Epitopes that span the tau molecule are shared with paired helical filaments, *Neuron* ***1***, 817–825.
29. Hilbich, C., Monning, U., Grund, C., Masters, C. L., and Beyreuther, K. (1993) Amyloid-like properties of peptides flanking the epitope of amyloid precursor protein-specific monoclonal antibody 22C11, *J Biol Chem* ***268***, 26571–26577.

Chapter 34

Aβ Measurement by Enzyme-Linked Immunosorbent Assay

Stephen D. Schmidt, Matthew J. Mazzella, Ralph A. Nixon, and Paul M. Mathews

Abstract

The neuritic plaque in the brain of Alzheimer's disease patients consists of an amyloid composed primarily of Aβ, an approximately 4-kDa peptide derived from the amyloid precursor protein. Multiple lines of evidence suggest that Aβ plays a key role in the pathogenesis of the disease, and potential treatments that target Aβ production and/or Aβ accumulation in the brain as β-amyloid are being aggressively pursued. Methods to quantitate the Aβ peptide are, therefore, invaluable to most studies aimed at a better understanding of the molecular etiology of the disease and in assessing potential therapeutics. Although other techniques have been used to measure Aβ in the brains of AD patients and β-amyloid-depositing transgenic mice, the enzyme-linked immunosorbent assay (ELISA) is one of the most commonly used, reliable, and sensitive methods for quantitating the Aβ peptide. Here we describe methods for the recovery of both soluble and deposited Aβ from brain tissue and the subsequent quantitation of the peptide by sandwich ELISA.

Key words: Aβ, Amyloid, Enzyme-linked immunosorbent assay, ELISA, Extraction, Quantification, Quantitation, Alzheimer's disease, Amyloid precursor protein, APP, Formic acid, Brain

1. Introduction

In 1984–1985, Glenner, Masters and colleagues determined that neuritic plaques, one of the defining features of Alzheimer's disease (AD), consist primarily of the small Aβ peptide (1, 2). This peptide, most commonly consisting of 40 or 42 amino acid residues, varies in length at its C-terminus and is derived from the amyloid precursor protein (APP) by specific proteolytic steps (3). The accumulation of Aβ and its deposition as insoluble β-amyloid plaque in the brain parenchyma is generally thought to be central to the pathogenesis of the disease. Much support for this amyloid-cascade model of AD pathobiology has come from the identification of mutations within the amyloid precursor protein (APP) (4–6) and the presenilin

Einar M. Sigurdsson et al. (eds.), *Amyloid Proteins: Methods and Protocols*, Methods in Molecular Biology, vol. 849,
DOI 10.1007/978-1-61779-551-0_34,

proteins (PS1 and PS2) (7–10) that cause early-onset familial AD (FAD) in humans. These mutations result in either more Aβ generation (11, 12) or increased levels of particularly pathogenic forms of Aβ (e.g., Aβ42 (13–15)). Expression in mice of FAD-mutant human APP transgenes either alone (16–18) or in combination with mutant presenilin transgenes (13, 19, 20) has resulted in animals that deposit substantial β-amyloid. These amyloid-depositing transgenic mice are now perhaps the most important experimental system in which to evaluate potential AD therapies, such as inhibitors of Aβ generation and Aβ immunotherapy (see, e.g., (21)).

Enzyme-linked immunosorbent assay (ELISA) is one of the most commonly employed biochemical techniques for the quantification of the Aβ peptide in the brain of humans and transgenic mice. Following the homogenization of the appropriate tissue (see Chapter 33) and a subsequent extraction to dissociate Aβ from the β-amyloid plaque, ELISA is used to precisely and rapidly measure levels of the peptide. Additionally, C-terminal epitope-specific antibodies are frequently used to differentiate Aβ40 from Aβ42, allowing the investigator to separately quantitate these two Aβ species. In this chapter, we describe the methodology used in our laboratory (21–37) for extracting Aβ from brain tissue and the subsequent quantitation of Aβ40 and Aβ42 by sandwich ELISA.

2. Materials

1. Ultracentrifuge and rotors (e.g., Beckman Coulter Optima TLX or MAX-E ultracentrifuge, TLA-100.1 and TLA 100.3 rotors).
2. Microplate spectrophotometer capable of reading the optical density (OD) at 450 nm of samples in a 96-well plate.
3. Platform rocker.
4. Sonic dismembrator with a probe capable of processing samples of approximately 600 µL.
5. 7-mL dounce glass tissue grinder (Kontes brand; available from Fisher Scientific, Pittsburgh, PA, cat. no. K885300-0007).
6. 8- or 12-channel pipette, with a minimum range of 50–200 µL.
7. 0.5-mL thick-walled polycarbonate ultracentrifuge tubes (8 × 34 mm, Beckman Instruments, Palo Alto, CA, cat. no. 343776).
8. 3.5-mL thick-walled polycarbonate ultracentrifuge tubes (13 × 51 mm, Beckman Instruments, Palo Alto, CA, cat. no. 349622).
9. 96-well high-binding microtiter plates (Nunc-Immuno 96 MicroWell Maxisorp plates recommended, Nalge Nunc

International, Rochester, NY, cat. no. 439454; available from Fisher Scientific, Pittsburgh, PA, cat. no. 12-565-135).

10. Adhesive sealing film for microplates (non-sterile, SealPlate brand recommended, cat. no. 100-SEAL-PLT, Excel Scientific, Wrightwood, CA; available from Sigma-Aldrich, St. Louis, MO, cat. no. Z36,965-9).
11. Multichannel pipetter basins (V-shaped bottom, non-sterile; available from Fisher Scientific, Pittsburgh, PA, cat. no. 13-681-100).
12. Centricon Centrifugal Filter, 10-kDa cutoff (Centricon YM-10, Millipore, Bedford, MA, cat. no. 4241).
13. Peroxidase Labeling Kit (Roche Diagnostics Corp., Indianapolis, IN, cat. no. 1 829 696).
14. 0.5 mg human $A\beta_{1-40}$ (lyophilized peptide, American Peptide Co., Sunnyvale, CA, cat. no. 62-0-78A).
15. 0.5 mg human $A\beta_{1-42}$ (lyophilized peptide, American Peptide Co., Sunnyvale, CA, cat. no. 62-0-80A).
16. 0.5 mg mouse/rat $A\beta_{1-40}$ (lyophilized peptide, American Peptide Co., Sunnyvale, CA, cat. no. 62-0-86A).
17. 0.5 mg mouse/rat $A\beta_{1-42}$ (lyophilized peptide, American Peptide Co., Sunnyvale, CA, cat. no. 62-0-84A).
18. Formic acid (minimum 95% purity).
19. FA neutralization solution (1 M Tris base, 0.5 M Na_2HPO_4, 0.05% NaN_3). Store at room temperature; stable for months.
20. 0.4% diethylamine, 100 mM NaCl. Store at 4°C; stable for months.
21. 0.5 M Tris base, pH 6.8. Store at 4°C; stable for months.
22. 10 mM EDTA in PBS.
23. Dimethyl sulfoxide (DMSO).
24. Purified Aβ40- and Aβ42-specific capture antibodies (see Note 1).
25. Purified anti-Aβ antibody with an epitope not overlapping with the epitopes of the capture antibodies (see Note 2).
26. 10% NaN_3. Store at room temperature. Very toxic, so be careful when preparing stock solution from powder.
27. Coating buffer: 30 mM $NaHCO_3$, 70 mM Na_2CO_3, 0.05% NaN_3, pH 9.6. (2.52 g $NaHCO_3$, 7.42 g Na_2CO_3, 5 mL 10% NaN_3, ddH_2O to 1 L; adjust pH to 9.6). Store at 4°C; stable for months.
28. 10× PBS: 1,369 mM NaCl, 27 mM KCl, 43 mM Na_2HPO_4, 15 mM KH_2PO_4. (80 g NaCl, 2 g KCl, 11.5 g $Na_2HPO_4{\cdot}7H_2O$, 2 g KH_2PO_4, ddH_2O to 1 L; adjust pH to 7.4). Store at room temperature. Make fresh monthly in a sterile container.

29. Blocking buffer: 1% Block Ace, 0.05% NaN_3, in PBS, pH 7.4. (4 g Block Ace powder, 2 mL 10% NaN_3, 1× PBS to 400 mL; adjust pH to 7.4). Store at 4°C; stable for months (see Notes 3 and 4).
30. ELISA capture (EC) buffer: 5 mM NaH_2PO_4, 15 mM Na_2HPO_4, 2 mM EDTA, 400 mM NaCl, 0.2% bovine albumin, 0.05% CHAPS, 0.4% Block Ace, 0.05% NaN_3, pH 7.0. (0.69 g $NaH_2PO_4 \cdot H_2O$, 2.13 g Na_2HPO_4, 0.74 g EDTA disodium salt, 23.3 g NaCl, 2.0 g bovine albumin, 0.5 g CHAPS, 4 g Block Ace powder, 5 mL 10% NaN_3, ddH_2O to 1 L; adjust pH to 7.0). Store at 4°C; stable for months (see Note 4).
31. PBST: 0.05% Tween 20 in PBS. Store at room temperature. Make fresh monthly in a sterile container.
32. Detection antibody buffer: 3 mM NaH_2PO_4, 17 mM Na_2HPO_4, 2 mM EDTA, 400 mM NaCl, 1% BSA, pH 7.0. (0.41 g $NaH_2PO_4 \cdot H_2O$, 2.41 g Na_2HPO_4, 0.74 g EDTA disodium salt, 23.3 g NaCl, 10.0 g bovine albumin, ddH_2O to 1 L; adjust pH to 7.0). Sterile filter and make ~11 mL aliquots under sterile conditions in a tissue culture hood. Store at 4°C; stable for months (see Notes 4 and 5).
33. TMB Microwell Peroxidase Substrate System (Kirkegaard & Perry Laboratories, Gaithersburg, MD, cat. no. 507600).
34. Stop solution: 5.7% *o*-phosphoric acid. Store at room temperature; stable for months (see Note 6).

3. Methods

3.1. Designing an ELISA and Preparing Solutions and Standards

3.1.1. Designing an ELISA

A sandwich ELISA consists of a "capture" antibody and a "detection" antibody, both of which bind to the peptide one wants to quantitate, but at distinct and nonoverlapping epitopes. Initially, the capture antibody is coated onto the plastic of the microtiter plate. When a complex mixture of proteins (such as those in a brain homogenate) is then incubated in this microtiter plate well, those peptides that are recognized by the capture antibody are bound and "captured" onto the ELISA plate. This reaction is driven by the high concentration and high affinity of the capture antibody, which allows for very small amounts of a peptide, such as Aβ, to be efficiently tethered to the plate via the antibody. Extraneous proteins are then washed away and a second antibody, conjugated to a reporter molecule or enzyme such as horseradish peroxidase, is used to detect the Aβ now bound to the initial capture antibody. Using such a "detection" antibody confers a number of advantages. First, this sandwich method greatly increases the sensitivity of the ELISA. Second, the ELISA gains specificity for a particular protein

or peptide by combining the specificities of the two antibodies. For example, we commonly employ antibodies with specificity for the C-terminus of Aβ (e.g., an anti-Aβ40 antibody) to specifically capture Aβ40 from the complex mixture of proteins found in a brain extract (21–37). Importantly, this step eliminates Aβ42, APP, and other APP metabolites that may also be recognized by the detection antibody (see Note 7). The captured Aβ40 is then detected using an antibody that binds to the N-terminal region of Aβ (as well as other APP metabolites, which, if present, would potentially confound the specific quantitation of Aβ40). The following methodology will focus on the use of sandwich ELISAs to quantitate human Aβ40 and Aβ42 from β-amyloid-depositing human APP transgenic mouse brain (see Fig. 1). These protocols are also applicable to human brain from Alzheimer's disease patients. In these cases, insoluble Aβ that has been deposited into β-amyloid plaques is first solubilized in formic acid (see Subheading 3.2). Additionally, sensitive sandwich ELISAs can also quantitate Aβ from non-β-amyloid-containing tissue, such as APP transgenic mouse brain prior to β-amyloid deposition and nontransgenic mouse brain (see Subheading 3.3.1) or from human or mouse plasma (see Subheading 3.3.2).

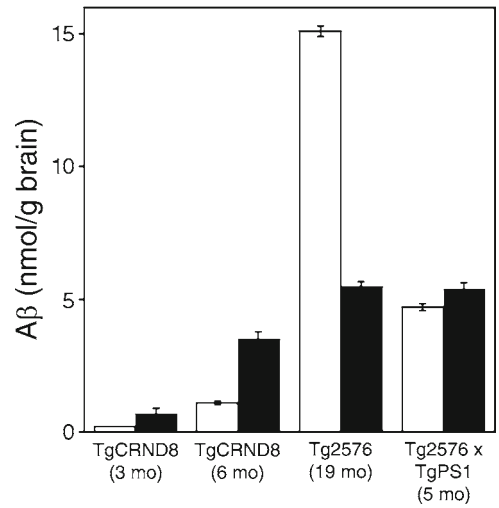

Fig. 1. Brain Aβ levels in transgenic mice determined by sandwich ELISA. Aβ was quantitated from formic acid-extracted 10% brain homogenates as described in this chapter. Data from three different β-amyloid-depositing transgenic mouse lines analyzed at the indicated ages (mo) are presented: TgCRND8 mice ((42); see also ref. 21) and Tg2576 mice (16) overexpress mutant forms of human APP while the Tg2576 × TgPS1 is a cross with a mutant presenilin 1 expressing line (19, 20). *Open bars* represent Aβ40, *solid bars* represent Aβ42. The increase in the amount of deposited Aβ40 and Aβ42 that occurs as the TgCRND8 mice age from 3 to 6 months is apparent. Additionally, both the TgCRND8 and Tg2576 × TgPS1 lines deposit more Aβ42 relative to Aβ40 than does the Tg2576 line, which is evident from this ELISA analysis. The sandwich ELISAs have high specificity for Aβ40 and Aβ42 due to the use of C-terminal specific anti-Aβ40 and Aβ42 antibodies (see Fig. 2).

The specificity and sensitivity of an ELISA is dependent upon the purity, affinity, and epitope specificity of the antibodies used. In general, good monoclonal antibodies make for successful ELISAs; polyclonal antibodies tend to be more variable, and much effort needs to be put into the affinity-purification of the antiserum prior to its use in an ELISA. Thus, for success in any ELISA, the first step must be the identification of appropriate antibodies, preferably in quantities that will permit the investigator to expend the necessary amounts of antibody in the critical task of ELISA development and quality control. To date, we have primarily used monoclonal antibodies to detect Aβ by sandwich ELISA, antibodies which were the kind gift of Dr. Marc Mercken (Johnson and Johnson Pharmaceutical Research and Development/Janssen Pharmaceutica; see, e.g., refs. 21–39). These, and any particular set of antibodies used by others, however, may not be available to a given investigator and much preliminary effort may need to be made to obtain an antibody repertoire that will be suitable. In Notes 1 and 2, we describe commercially available antibodies that have been successfully used in our laboratory and would therefore allow most laboratories to develop a sandwich ELISA to detect human Aβ. The selection of antibodies is best guided by extensive conversations with laboratories and/or commercial suppliers that have had success detecting the protein of interest, prior to initiating any study. The user should be prepared to try a number of antibodies and antibody combinations during the development of an in-house ELISA. The less abundant the protein or peptide of interest, the more will rest on the pairing of the best antibodies in the sandwich ELISA. Commercial ELISA kits are also available from a number of sources for the quantitation of Aβ, and much of the preparation of samples and standards described in this chapter applies to the use of these kits. Covance (Princeton, NJ) currently markets ELISA kits, some of which use antibodies developed or characterized by our group as described in this chapter.

3.1.2. Preparing Solutions

In our laboratory, quantitating a peptide at low fmol/mL levels seems to be remarkably dependent upon the quality of the distilled, reverse osmosis-filtered H_2O used to make solutions; contamination of solutions or the H_2O source with fungus or other microorganisms can be problematic. We therefore recommend periodically disinfecting water storage containers by autoclaving or other means. For the same reason, PBS, including the 10× stock solution, and PBST should also frequently be made fresh, in sterile containers. Several of the solutions contain 0.05% NaN_3 (sodium azide) as a preservative (1/200th volume of a 10% NaN_3 stock solution).

3.1.3. Preparing Aβ Standards

Aβ standards for the ELISA are prepared from high quality synthetic peptides. The peptides are dissolved in dimethyl sulfoxide (DMSO), diluted in ELISA capture (EC) buffer, divided into

aliquots, and stored at –80°C. To minimize the possibility of aggregation of the Aβ standard, carry out the following steps quickly and keep the EC buffer on ice. Allow vials of lyophilized peptide to equilibrate to room temperature before opening.

1. Preparation of 1 mg/mL master stock solutions: dissolve 0.5 mg of peptide in 500 µL of room temperature DMSO. Make 25 µL aliquots, freeze on dry ice, and store at –80°C. This stock solution is 231 nmol/mL for human $A\beta_{1-40}$, 222 nmol/mL for human $A\beta_{1-42}$, 236 nmol/mL for murine $A\beta_{1-40}$, and 226 nmol/mL for murine $A\beta_{1-42}$.
2. Preparation of 1 nmol/mL stock solutions: thaw an aliquot of the 1 mg/mL master stock solution from above and dilute 8 µL into the following volumes of EC buffer:
   - 1,840 µL for human $A\beta_{1-40}$
   - 1,764 µL for human $A\beta_{1-42}$
   - 1,888 µL for murine $A\beta_{1-40}$
   - 1,808 µL for murine $A\beta_{1-42}$

   Divide each into 250-µL aliquots, freeze on dry ice, and store at –80°C.
3. Preparation of 5 pmol/mL working stock solutions: thaw an aliquot of 1 nmol/mL solution and dilute 200 µL into 40 mL of EC buffer. Divide into 100-µL aliquots, freeze on dry ice, and store at –80°C. You will need about 400 small tubes to make these aliquots, so label and arrange the tubes before thawing the 1 nmol/mL stock solution.

3.1.4. Preparation of an HRP-Coupled Detection Antibody

Our experience is that the linear range of the sandwich ELISA is best if the detection antibody is directly coupled to horseradish peroxidase (HRP), rather than when coupled to biotin and then detected using streptavidin–HRP. Although suitable biotinylated anti-Aβ detection antibodies can be purchased (see Note 2) and may suffice for some applications, a group that is investing in the development of highly sensitive ELISAs is better off using HRP-coupled antibodies, which they may need to produce themselves. This section describes the preparation of the antibody, the HRP coupling, quality control, and storage of an HRP-coupled detection antibody.

1. Start with the appropriate purified antibody (see Note 2). The antibody cannot contain azide in subsequent steps. Dialyze against PBS if an azide-free antibody source cannot be found.
2. The coupling reaction requires that the antibody concentration be ~4 mg/mL in a volume of 300 µL. Most antibody solutions are more dilute than this, and if so the antibody first needs to be concentrated using a 10-kDa cutoff Centricon Centrifugal

Filter according to the manufacturer's protocol. Apply a sufficient amount of antibody to the column to obtain the needed amount of concentrated antibody. Ensure that the column never completely dries during centrifugation.

3. Follow the Roche Peroxidase Labeling Kit's protocol for the coupling of HRP to an antibody. Per the protocol, remember that the PBS-antibody solution must be initially alkalinized before coupling.
4. The HRP-coupled antibody should not be frozen, but stored at 4°C as freezing can inactivate the peroxidase. Do not add azide as this also inactivates the peroxidase. For long-term storage, thimerosal can be added to 0.002% to the coupled antibody. A 2% (1,000×) thimerosal stock solution may be prepared, and should be stored at 4°C. We find that with proper storage HRP-coupled antibodies can remain active for more than 1 year at 4°C.

The efficiency of the coupling reaction must be determined empirically for each batch of HRP-coupled detection antibody. This is done by testing the ability of different dilutions of the newly coupled antibody to detect Aβ standards. When prepared according to the Roche kit protocol, which gives a final antibody volume of approximately 1 mL, an HRP-coupled anti-Aβ antibody can typically be diluted 1:1,000 or more for the ELISA (see Note 8).

3.2. Solubilization of Aβ from β-Amyloid Plaques Prior to ELISA

This procedure dissociates the aggregated Aβ in β-amyloid plaques so that it is possible to quantitate the peptide by ELISA. A small volume of homogenized β-amyloid-containing tissue (prepared as described in Chapter 33) is first sonicated in the presence of formic acid, which solubilizes Aβ from the densely aggregated β-amyloid plaque, and then subjected to high-speed centrifugation. Three layers result: a thin upper lipid layer that is not collected, the predominant intermediate phase that contains the Aβ peptides, and a barely discernable pellet (40). The intermediate phase is recovered and neutralized for the ELISA; the upper lipid layer and the pellet are discarded.

1. Mix 200 µL of a 10% (w/v) brain homogenate (see Chapter 33) into 440 µL of cold formic acid (minimum 95% purity) in a 1.7-mL microcentrifuge tube.
2. Sonicate each sample individually for 1 min on ice: immerse the tip of the probe in the sample and move the tube up and down over the probe while sonicating. Keep the tube on ice during this process by holding it in a small (e.g., 50 mL) beaker filled with ice. Rinse the probe and wipe it dry before processing the next sample.

3. Centrifuge 400 µL of the sonicated mixture at 100,000 × *g* for 1 h at 4°C (48,000 rpm using a Beckman Coulter TLA-100.1 rotor), in a 0.5-mL thick-walled polycarbonate ultracentrifuge tube.
4. Dilute 210 µL of the intermediate phase into 4 mL of room temperature FA neutralization solution. Vortex briefly.
5. Divide the neutralized solution into six 0.5-mL aliquots. Freeze the aliquots on dry ice. Each aliquot is more than sufficient for 4 ELISA well readings (typically Aβ40 and Aβ42 measurements, each in duplicate). These samples can be loaded onto the ELISA plate neat or, more typically, diluted in EC buffer as necessary (see Subheading 3.4).

3.3. Preparation of Non-β-Amyloid-Containing Tissue and Blood Plasma Prior to ELISA

3.3.1. Extraction of Aβ from Tissue Without Plaque Pathology

This section describes the extraction of Aβ from homogenates of tissue without β-amyloid plaque pathology. Although the Aβ present in a tissue that lacks β-amyloid is generally soluble, Aβ is a "sticky" peptide and the uniformity of its recovery and subsequent ELISA quantitation is improved if the Aβ is first extracted in diethylamine (23, 26, 41). Other agents, such as Triton X-100, can be used, but we find that the presence of nonionic detergents in the sample frequently increases the nonspecific background of the ELISA. Additionally, diethylamine extraction has the advantage of eliminating lipids (which are particularly abundant in brain and can nonspecifically increase background) and membrane-associated proteins such as APP, which remain in the pellet fraction following extraction (41). Diethylamine does, however, disrupt membrane vesicles so that intracellular as well as extracellular Aβ is recovered. In contrast to the formic acid extraction technique described in Subheading 3.2, the diethylamine-extracted sample is much less dilute prior to applying to the ELISA (see Subheading 3.5.4). This allows for the quantitation of the typically low levels of Aβ found in tissue without plaques [e.g., young APP transgenic mice prior to β-amyloid deposition and non-transgenic mice (see Note 9)] (22–24, 26–32, 35, 36). Tissue homogenates prepared as described in Chapter 33 are first mixed with diethylamine using a dounce. Following a high-speed centrifugation, Aβ is recovered in the supernatant, which is pH-neutralized and applied to the ELISA plate. Plaque-associated Aβ, however, is not completely extracted with this method and therefore formic acid extraction should be used in tissues containing β-amyloid.

1. Mix 1 mL of a 10% (w/v) brain homogenate (see Chapter 33) with 1 mL of cold 0.4% diethylamine (DEA), 100 mM NaCl with six up and down strokes of a glass pestle in the dounce glass tissue grinder. Keep the thawed homogenates, 0.4% DEA, 100 mM NaCl, and the dounce on ice. Transfer 1.9 mL of the homogenate–DEA mixture to a 3.5-mL thick-walled polycarbonate ultracentrifuge tube.

2. Between samples, rinse the pestle and dounce with H_2O and dry.
3. Centrifuge the tube containing the homogenate–DEA mixture at 100,000×*g* for 1 h at 4°C (43,000 rpm in a TLA 100.3 rotor).
4. Add 1.7 mL of the supernatant to a tube containing 170 µL of 0.5 M Tris base, pH 6.8 and vortex briefly. Divide into four 440-µL aliquots, freeze on dry ice, and store at −80°C. (440 µL is sufficient to run ELISAs for both Aβ40 and Aβ42 when loading 100 µL neat into duplicate wells for each assay.) These samples can be loaded onto the ELISA plate neat or diluted in EC buffer as necessary (see Subheading 3.4).
5. Discard the pellet.

3.3.2. Preparation of Blood Plasma Prior to ELISA

Aβ levels in blood plasma can also be determined by ELISA. The best method to prevent clotting is to mix the blood immediately with EDTA to chelate Ca^{++} as heparin may bind Aβ and interfere with the ELISA measurement. Plasma prepared this way can be directly applied to an ELISA plate following a freeze–thaw cycle to inactivate endogenous peroxidase. Without this freeze–thaw cycle, the endogenous peroxidase in blood can give a high background when the ELISA is developed using an HRP-coupled detection antibody.

1. Immediately mix the blood sample as it is being collected with an equal volume of 10 mM EDTA in PBS.
2. Gently mix the sample and centrifuge at 10,000×*g* for 5 min at room temperature.
3. Collect the supernatant and divide the plasma into aliquots prior to freezing at −80°C. These samples can be loaded onto the ELISA plate neat or diluted in EC buffer as necessary (see Subheading 3.4).

3.4. Quantification of Aβ by Sandwich ELISA

Solutions should be kept on ice during the following steps with the exception of the PBS, PBST, and 5.7% *o*-phosphoric acid, which are stored and used at room temperature. Plates should be tightly sealed with sealing film during all incubations to prevent drying. The sandwich ELISA takes 3 days to complete.

Day 1

1. The capture antibody is coated onto the necessary number of wells of a 96-well high-binding microtiter plate by adding 100 µL/well of antibody diluted in coating buffer. Incubate overnight at 4°C with rocking. Typically, the capture antibodies are diluted to 2–10 µg/mL for coating. The antibody diluted in coating buffer must be free of any other proteins (see Note 1).

Day 2

2. Wash wells twice with PBS. This step can be done by various methods, including a wash bottle containing PBS which is used to spray PBS into the wells. Invert the plate quickly over a sink to discard the solution between washes. Residual wash solution can be removed by inverting the plate and patting on a paper towel.
3. Block nonspecific binding sites on the plastic by adding 200 μL/well of blocking buffer and incubating for 4 h at room temperature with gentle rocking. This blocking step can be extended for significantly longer than 4 h, and plates may even be left at this step for up to 1 week if stored at 4°C.
4. Prepare by thawing and diluting as necessary all samples and standards. Immediately before loading or diluting formic acid extracts, they should be incubated at 37°C for 5 min to solubilize any precipitate and not placed on ice before being diluted or a precipitate will quickly reform. Samples may need to be diluted with EC buffer to generate readings within the linear range of the standards. The approximate dilution needs to be determined empirically, and may require that multiple dilutions be tested in a trial ELISA and/or that assays are repeated with additional dilutions. Typically, formic acid-extracted samples from human tissue or transgenic mouse models with significant β-amyloid deposition will need to be diluted from 1:10 to 1:100 for an ELISA with a linear range of approximately 25–400 fmol/mL. DEA extracts prepared from non-β-amyloid-containing tissue and blood plasma is typically loaded onto the ELISA plate neat or up to a 1:10 dilution. Aβ standards are similarly diluted in EC buffer immediately prior to the ELISA. As previously noted, the concentration of the standards used will depend on the inherent sensitivity of the ELISA and must match the range of the Aβ concentrations found within the samples. As described in Subheading 3.5, care needs to be taken that the values for all samples fall between values obtained for the standards and within the linear range of the standard curve. As an example, standards at 400, 200, 100, 50, 25, 12.5, and 6.25 fmol/mL would be used for samples optimally diluted to give readings of ~25–200 fmol/mL.
5. Immediately prior to proceeding with the ELISA and after samples are fully prepared for loading, dump the blocking buffer. Quickly add 50 μL/well of EC buffer to prevent the wells from drying while the individual samples are being added.
6. Add 100 μL of standards and samples to wells containing 50 μL of EC buffer (final volume in each well is now 150 μL; see Note 10). For a measurement of background signal, blank wells should contain 150 μL of EC buffer.
7. Incubate overnight at 4°C with rocking.

Day 3

8. Wash wells twice with PBST, then once with PBS.
9. Add 100 µL of HRP-conjugated detection antibody, diluted in detection antibody buffer (see Note 8), to each well. Incubate for 4 h at room temperature with rocking.
10. Wash wells twice with PBST, then once with PBS.
11. Add to the wells 100 µL of a 1:1 mixture of the two solutions (TMB peroxidase substrate and peroxidase substrate solution B) of the TMB microwell peroxidase substrate system (see Note 11). Allow plates to develop until the second to the least concentrated standard has a slight blue color change, and then stop the reaction by adding 100 µL of stop solution to each well (see Note 6). If the samples change color rapidly, the reaction may be stopped more quickly. If the samples have a low signal, however, a longer reaction time may produce more useful results. Regardless, samples and standards need to be stopped as simultaneously as possible. If the plates are allowed to overdevelop, the linear range of the ELISA will be compromised.
12. Read the OD_{450} with a microplate spectrophotometer. Aβ concentrations in the sample are interpolated from the OD_{450} using a standard curve generated from the known Aβ amounts in the standards (see Fig. 2).

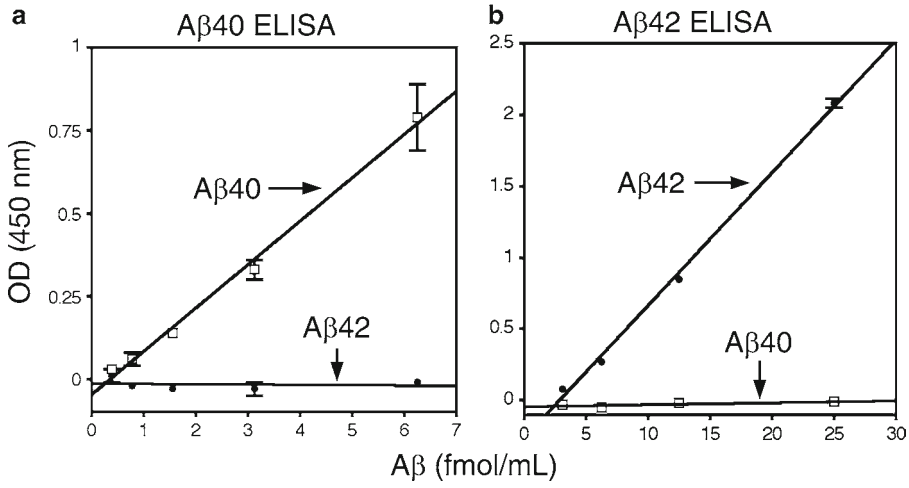

Fig. 2. Assessing antibody specificity. Affinity-purified polyclonal antibodies from a commercial source (Covance, Princeton, NJ; see Note 1) were coated on microtiter plates at 5 µg/mL and allowed to capture human Aβ standards. One of the antibodies, made against an Aβ40 epitope, showed sensitivity to sub-fmol/mL levels to Aβ40 (**a**, *open boxes*) while exhibiting no cross-reactivity to Aβ42 standards included on the same plate (**a**, *closed circles*). The second antibody, made against an Aβ42 epitope, showed similar specificity to Aβ42 but with a higher linear range and lower sensitivity (**b**). Both Aβ40 and Aβ42 were detected with the human Aβ-specific monoclonal antibody JRF/Aβtot/17, which binds to the N-terminus of Aβ, as previously described (43).

3.5. Assessing Antibody Specificity, Discarding Below Sensitivity and Saturated Points from Standard Curves, Accounting for Dilutions

3.5.1. Assessing Antibody Specificity

Once a combination of capture and detection antibodies has been obtained, pilot assays should be performed to determine the specificity of the antibody combinations for Aβ40 or Aβ42. This is accomplished by coating a microtiter plate with the putative Aβ40- or Aβ42-specific antibody. If an antibody has good specificity for Aβ40 vs. Aβ42, it should not recognize Aβ42 standards (Fig. 2a). Similarly, an Aβ42 antibody should not recognize Aβ40 standards (Fig. 2b). Such specificity assays are very useful in pointing out unexpected cross-reactivity in an ELISA.

3.5.2. Determining Sensitivity and Discarding Measurements Below a Meaningful Sensitivity Limit

The majority of the serially diluted standards in an Aβ ELISA should show a linear relationship, but at some point a "bottoming-out" effect will be observed in which there is no longer a linear change in OD with successively lower concentration standards (Fig. 3). The lowest concentration at which a point is still linear with the other points on the curve, and for which duplicate readings are in close agreement, thus becomes a given assay's "sensitivity limit."

Several different concentrations of capture and detection antibodies should be tested in initial pilot assays to determine which antibody concentrations produce the optimal sensitivity for

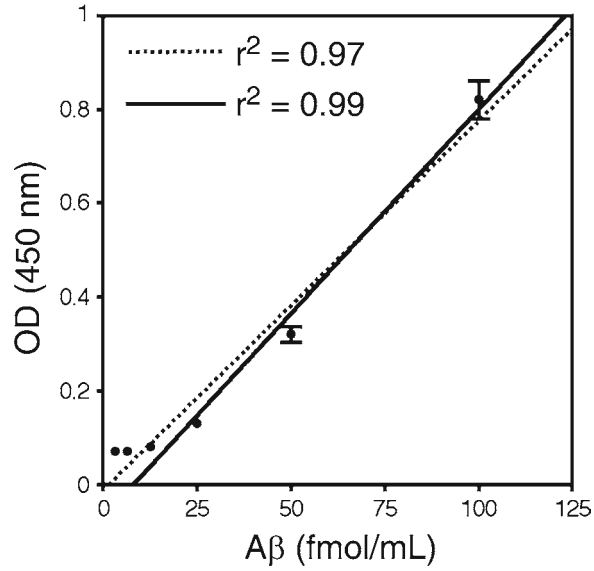

Fig. 3. Determining sensitivity and discarding standards that are below sensitivity. The OD representing various concentrations of human Aβ40 standard was determined by sandwich ELISA. The bottom two points, representing the lowest concentrations of Aβ40, were below sensitivity and skew a linear curve fit away from the other points (*dotted line*, $r^2 = 0.97$). Discarding these two points from the analysis improves the curve fit (*solid line*, $r^2 = 0.99$) and would be more appropriate for calculating the amount of Aβ40 in samples containing ~25–100 fmol/mL Aβ40.

the concentration of Aβ expected in the samples. Since sensitivity will vary somewhat from assay to assay it should be determined for each ELISA, even after pilot assays have demonstrated a general sensitivity limit for a given combination and concentration of antibodies. OD values obtained for standards below this sensitivity limit are meaningless and may skew the standard curve, particularly in the region relevant to the OD measurements obtained from the samples (Fig. 3, dotted line). These "below sensitivity" values should be excluded in a consistent fashion before a curve fit is applied (Fig. 3, solid line).

3.5.3. Determining Linear Range and Discarding Saturated Standards

Frequently, the highest concentration standards develop rapidly, become saturated, and are nonlinear relative to lower concentration standards. Interpolating from a saturated region of the standard curve may cause significant differences between samples to be underestimated. Standard points that show signs of saturation should therefore be discarded and interpolation should only be from within the linear range of the standards (Fig. 4, solid line). This will often require additional dilution of the samples in a subsequent assay to ensure that all sample measurements are within the linear range of the ELISA.

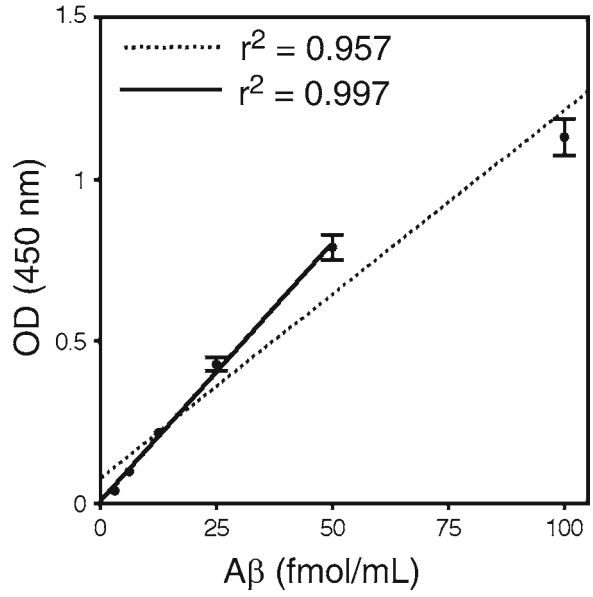

Fig. 4. Discarding a saturated point to improve the linear curve fit. Human Aβ42 standards of various concentrations were analyzed by sandwich ELISA to produce a standard curve. The 100 fmol/mL Aβ42 standard was beginning to saturate when this ELISA was developed, and the linear relationship between peptide concentration and OD is not optimal. This produces a relatively poor linear curve fit (*dotted line*, $r^2 = 0.957$); removing the 100 fmol/mL Aβ42 standard data point generates a better linear curve (*solid line*, $r^2 = 0.997$), which would be more appropriate for calculating Aβ42 concentrations in samples from approximately 5 to 50 fmol/mL.

Indeed, an ELISA with a broad linear range is desirable in that this will increase the likelihood that a given sample will be within range on a first ELISA run and that the assay will not have to be repeated. As with optimizing antibody concentrations to produce good sensitivities, pilot assays may be used to determine which antibody concentrations produce the broadest linear range. Interassay variability dictates that the linear range be determined for every assay, however, and that saturated standards be discarded wherever necessary.

3.5.4. Accounting for Dilutions Made During the Assay

Multiple steps throughout this protocol introduce dilution factors that must be taken into account. Aβ amounts are often reported as femto-, pico-, or nano-mole per gram of tissue. If the neutralized formic acid extract of a 10% tissue homogenate is loaded directly into the ELISA well as described in this chapter, the Aβ value determined in fmol/mL by the ELISA needs to be multiplied by 704 to convert to fmol/g of brain tissue (see Note 12). If the neutralized DEA extract of a 10% tissue homogenate is loaded directly onto the ELISA plate, the Aβ value determined in fmol/mL by the ELISA needs to be multiplied by 24.2 to convert to fmol/g of brain tissue (see Note 12).

4. Notes

1. Capture antibodies must be purified IgG and in PBS or a similar protein-free buffer. Any other proteins will compete with the antibody for binding to the microtiter plate. Thus, ascites fluid, antiserum, etc.—which contain many other proteins—are not suitable and only purified IgG or affinity-purified antibody from these sources can be used. Typically, capture antibodies are coated at 2–10 μg/mL. Increasing the coating antibody concentration more than this is often a waste of expensive antibody and will not improve the ELISA's sensitivity. Using the minimal amount of antibody for coating is cost effective, but this amount must be determined empirically and a useful linear range of standards must be maintained. Covance (Princeton, NJ) sells high-affinity Aβ40 and Aβ42 affinity-purified polyclonal antibodies under their Signet product line; these antibodies were used for the assays shown in Fig. 2. Additional sources of Aβ antibodies are available and others will undoubtedly become available, so the investigator is advised to search for the most cost-effective source of high-affinity antibodies during the development phase of an ELISA.
2. As with the capture antibodies, the detection antibody must be purified IgG and in PBS or a similar protein-free buffer.

A commonly used monoclonal antibody that binds to an epitope within the N-terminus of human Aβ is 6E10 (available from Covance, Princeton, NJ). A very serviceable sandwich ELISA for Aβ40 and Aβ42 can be constructed from the C-terminal-specific capture antibodies available from Covance and 6E10. Biotinylated 6E10 can also be purchased, and HRP–streptavidin used to detect the 6E10 bound during the ELISA, but this often results in a narrower linear range and therefore a less useful ELISA than one using directly HRP-coupled antibody. Regardless, if biotinylated antibody followed by HRP–streptavidin is used, much attention needs to be given to ensuring that the ELISA remains linear in the range of all samples (see Subheading 3.5).

An alternative detection strategy is to use a coating antibody of one species (e.g., mouse) and a detection antibody from another (e.g., rabbit). In this case, one could use an HRP-coupled anti-rabbit secondary antibody prior to developing the ELISA. However, we have found that this rarely works in practice, particularly if a high-sensitivity ELISA is required, as very minimal cross-reactivity of the anti-rabbit secondary antibody with murine IgG leads to overwhelming background.

3. Block Ace powder is a product of Dainippon Pharmaceutical Co., Osaka, Japan and is available from Serotec, Raleigh, NC, cat. no. BUF029. Other protein-blocking reagents are often used for ELISAs (BSA, casein). Our laboratory's experience has been that while these reagents work, Block Ace gives the lowest nonspecific background and the most consistent assays over time, and we therefore recommend it. However, 3% BSA in PBS with azide can be substituted in many applications.
4. Preparing the solutions containing protein (e.g., blocking buffer, EC buffer, and detection antibody buffer) is easiest if all of the dry components are added to half of the final volume of the solution and stirred very vigorously—denaturation of these blocking proteins by foaming is not a problem and may even be advantageous. After the protein is dissolved, the solution is brought up to the appropriate final volume.
5. Do not add sodium azide to detection antibody buffer as the azide will inactivate the horseradish peroxidase conjugated to the detection antibodies in later steps.
6. In addition to 5.7% *o*-phosphoric acid, other acids such as H_2SO_4 and HCl are sometimes used to stop the TMB reaction. *O*-phosphoric acid, however, is more efficient in stopping color development and is recommended by the manufacturer.
7. Aβ sandwich ELISAs are typically done using C-terminal Aβ40- or Aβ42-specific antibodies as the capture antibody. This offers some advantages as N-terminal-directed anti-Aβ

antibodies bind all Aβ species and usually recognize APP and other APP metabolites. If sufficiently abundant, these may compete with the Aβ of interest during the initial binding to the capture antibody. In practical application, however, this is not of significant concern when detecting the abundant Aβ extracted from a β-amyloid-depositing mouse, for example. Therefore, in some applications, the capture antibody can be N-terminal directed with other antibodies, recognizing other epitopes within either the Aβ sequence or at the C-terminus, used for detection.

8. The Roche Peroxidase Labeling Kit generally gives quite tractable HRP coupling reactions if the starting antibody concentration is carefully adjusted to 4 mg/mL. Nevertheless, the efficiency of the coupling must always be determined by trying each new batch of detection antibody in a trial ELISA. A straightforward way to do this is to test the newly coupled antibody at various dilutions in detection antibody buffer on a series of Aβ standards. A typical scheme would include the detection antibody diluted 1:1,000, 1:2,000, 1:5,000 and perhaps 1:10,000 against Aβ standards ranging from ~3 to 200 fmol/mL. Frequently, using the detection antibody at higher concentrations will increase the sensitivity of the ELISA, although eventually higher concentrations will nonspecifically increase the background.
9. Murine and human Aβ differ in their N-terminal region at three residues. Thus, most antibodies that recognize the N-terminus of Aβ are species specific, with the vast majority of the available antibodies recognizing the human and not the murine peptide (e.g., 6E10). However, two well-characterized monoclonal antibodies have been used to quantitate endogenous murine Aβ by ELISA: JRF/rAβ1-15/2 and m3.2 (22–24, 26–32, 35, 36). The m3.2 antibody, unlike JRF/rAβ1-15/2, also recognizes other murine APP metabolites by Western blot (36). Antibody m3.2, which was generated by our group, is available from Covance (Princeton, NJ).
10. As both the samples and standards are diluted equally 2:3 in EC buffer at this point, no arithmetic adjustment for this dilution is necessary when calculating Aβ concentrations from the standard curve.
11. Warm the two bottles of TMB Microwell Peroxidase Substrate System to 37°C, then prepare the developing solution immediately before use by mixing an equal volume from each bottle. Change pipettes between bottles to prevent cross-contamination. For every set of two plates his mixture should be made fresh and used immediately.

12. This correction factor of 704 for the formic acid-extracted homogenate takes into account the 1:11 dilution when the tissue is initially homogenized (see Chapter 33), the further 1:3.2 dilution in formic acid, and the 1:20 dilution when the formic acid extract is neutralized. The correction factor of 24.2 for the DEA-extracted homogenate takes into account the 1:11 dilution when the tissue is initially homogenized (see Chapter 33), the further 1:2 dilution in DEA, and the 1:1.1 dilution when the DEA is neutralized.

Acknowledgments

This work has been supported by the Alzheimer's Association (IIRG-07-60047 to P.M.M.) and the National Institute on Aging (AG017617 to P.M.M., R.A.N.). We thank Drs. Karen Duff (Columbia University) and David Westaway (University of Alberta) for the transgenic mouse brains used in the sample data. We are very indebted to Dr. Marc Mercken (Johnson and Johnson Pharmaceutical Research and Development/Janssen Pharmaceutica) for the use of his anti-Aβ antibodies.

References

1. Glenner, G. G., and Wong, C. W. (1984) Alzheimer's disease: initial report of the purification and characterization of a novel cerebrovascular amyloid protein, *Biochem Biophys Res Commun **120***, 885–890.
2. Masters, C. L., Simms, G., Weinman, N. A., Multhaup, G., McDonald, B. L., and Beyreuther, K. (1985) Amyloid plaque core protein in Alzheimer disease and Down syndrome, *Proc Natl Acad Sci USA **82***, 4245–4249.
3. De Strooper, B., and Annaert, W. (2000) Proteolytic processing and cell biological functions of the amyloid precursor protein, *J Cell Sci **113***, 1857–1870.
4. Chartier-Harlin, M. C., Crawford, F., Houlden, H., Warren, A., Hughes, D., Fidani, L., Goate, A., Rossor, M., Roques, P., Hardy, J., and et al. (1991) Early-onset Alzheimer's disease caused by mutations at codon 717 of the beta-amyloid precursor protein gene, *Nature **353***, 844–846.
5. Levy, E., Carman, M. D., Fernandez-Madrid, I. J., Power, M. D., Lieberburg, I., van Duinen, S. G., Bots, G. T., Luyendijk, W., and Frangione, B. (1990) Mutation of the Alzheimer's disease amyloid gene in hereditary cerebral hemorrhage, Dutch type, *Science **248***, 1124–1126.
6. Tanzi, R. E., and Bertram, L. (2001) New frontiers in Alzheimer's disease genetics, *Neuron **32***, 181–184.
7. Mullan, M., Houlden, H., Windelspecht, M., Fidani, L., Lombardi, C., Diaz, P., Rossor, M., Crook, R., Hardy, J., Duff, K., and et al. (1992) A locus for familial early-onset Alzheimer's disease on the long arm of chromosome 14, proximal to the alpha 1-antichymotrypsin gene, *Nat Genet **2***, 340–342.
8. Levy-Lahad, E., Wasco, W., Poorkaj, P., Romano, D. M., Oshima, J., Pettingell, W. H., Yu, C. E., Jondro, P. D., Schmidt, S. D., Wang, K., and et al. (1995) Candidate gene for the chromosome 1 familial Alzheimer's disease locus, *Science **269***, 973–977.
9. Rogaev, E. I., Sherrington, R., Rogaeva, E. A., Levesque, G., Ikeda, M., Liang, Y., Chi, H., Lin, C., Holman, K., Tsuda, T., and et al. (1995) Familial Alzheimer's disease in kindreds with missense mutations in a gene on chromosome 1 related to the Alzheimer's disease type 3 gene, *Nature **376***, 775–778.
10. Wasco, W., Pettingell, W. P., Jondro, P. D., Schmidt, S. D., Gurubhagavatula, S., Rodes, L., DiBlasi, T., Romano, D. M., Guenette, S. Y., Kovacs, D. M., and et al. (1995) Familial

Alzheimer's chromosome 14 mutations, *Nat Med* ***1***, 848.

11. Cai, X. D., Golde, T. E., and Younkin, S. G. (1993) Release of excess amyloid beta protein from a mutant amyloid beta protein precursor, *Science* ***259***, 514–516.
12. Citron, M., Oltersdorf, T., Haass, C., McConlogue, L., Hung, A. Y., Seubert, P., Vigo-Pelfrey, C., Lieberburg, I., and Selkoe, D. J. (1992) Mutation of the beta-amyloid precursor protein in familial Alzheimer's disease increases beta-protein production, *Nature* ***360***, 672–674.
13. Borchelt, D. R., Thinakaran, G., Eckman, C. B., Lee, M. K., Davenport, F., Ratovitsky, T., Prada, C. M., Kim, G., Seekins, S., Yager, D., Slunt, H. H., Wang, R., Seeger, M., Levey, A. I., Gandy, S. E., Copeland, N. G., Jenkins, N. A., Price, D. L., Younkin, S. G., and Sisodia, S. S. (1996) Familial Alzheimer's disease-linked presenilin 1 variants elevate Abeta1-42/1-40 ratio in vitro and in vivo, *Neuron* ***17***, 1005–1013.
14. Citron, M., Westaway, D., Xia, W., Carlson, G., Diehl, T., Levesque, G., Johnson-Wood, K., Lee, M., Seubert, P., Davis, A., Kholodenko, D., Motter, R., Sherrington, R., Perry, B., Yao, H., Strome, R., Lieberburg, I., Rommens, J., Kim, S., Schenk, D., Fraser, P., St George Hyslop, P., and Selkoe, D. J. (1997) Mutant presenilins of Alzheimer's disease increase production of 42- residue amyloid beta-protein in both transfected cells and transgenic mice, *Nat Med* ***3***, 67–72.
15. Lemere, C. A., Lopera, F., Kosik, K. S., Lendon, C. L., Ossa, J., Saido, T. C., Yamaguchi, H., Ruiz, A., Martinez, A., Madrigal, L., Hincapie, L., Arango, J. C., Anthony, D. C., Koo, E. H., Goate, A. M., and Selkoe, D. J. (1996) The E280A presenilin 1 Alzheimer mutation produces increased A beta 42 deposition and severe cerebellar pathology, *Nat Med* ***2***, 1146–1150.
16. Hsiao, K., Chapman, P., Nilsen, S., Eckman, C., Harigaya, Y., Younkin, S., Yang, F., and Cole, G. (1996) Correlative memory deficits, Abeta elevation, and amyloid plaques in transgenic mice, *Science* ***274***, 99–102.
17. Games, D., Adams, D., Alessandrini, R., Barbour, R., Berthelette, P., Blackwell, C., Carr, T., Clemens, J., Donaldson, T., Gillespie, F., and et al. (1995) Alzheimer-type neuropathology in transgenic mice overexpressing V717F beta-amyloid precursor protein, *Nature* ***373***, 523–527.
18. Sturchler-Pierrat, C., Abramowski, D., Duke, M., Wiederhold, K. H., Mistl, C., Rothacher, S., Ledermann, B., Burki, K., Frey, P., Paganetti, P. A., Waridel, C., Calhoun, M. E., Jucker, M., Probst, A., Staufenbiel, M., and Sommer, B. (1997) Two amyloid precursor protein transgenic mouse models with Alzheimer disease-like pathology, *Proc Natl Acad Sci USA* ***94***, 13287–13292.
19. Duff, K., Eckman, C., Zehr, C., Yu, X., Prada, C. M., Perez-tur, J., Hutton, M., Buee, L., Harigaya, Y., Yager, D., Morgan, D., Gordon, M. N., Holcomb, L., Refolo, L., Zenk, B., Hardy, J., and Younkin, S. (1996) Increased amyloid-beta42(43) in brains of mice expressing mutant presenilin 1, *Nature* ***383***, 710–713.
20. Holcomb, L., Gordon, M. N., McGowan, E., Yu, X., Benkovic, S., Jantzen, P., Wright, K., Saad, I., Mueller, R., Morgan, D., Sanders, S., Zehr, C., O'Campo, K., Hardy, J., Prada, C. M., Eckman, C., Younkin, S., Hsiao, K., and Duff, K. (1998) Accelerated Alzheimer-type phenotype in transgenic mice carrying both mutant amyloid precursor protein and presenilin 1 transgenes, *Nat Med* ***4***, 97–100.
21. Janus, C., Pearson, J., McLaurin, J., Mathews, P. M., Jiang, Y., Schmidt, S. D., Chishti, M. A., Horne, P., Heslin, D., French, J., Mount, H. T., Nixon, R. A., Mercken, M., Bergeron, C., Fraser, P. E., St George-Hyslop, P., and Westaway, D. (2000) A beta peptide immunization reduces behavioural impairment and plaques in a model of Alzheimer's disease, *Nature* ***408***, 979–982.
22. Refolo, L. M., Pappolla, M. A., LaFrancois, J., Malester, B., Schmidt, S. D., Thomas-Bryant, T., Tint, G. S., Wang, R., Mercken, M., Petanceska, S. S., and Duff, K. E. (2001) A cholesterol-lowering drug reduces beta-amyloid pathology in a transgenic mouse model of Alzheimer's disease, *Neurobiol Dis* ***8***, 890–899.
23. Rozmahel, R., Huang, J., Chen, F., Liang, Y., Nguyen, V., Ikeda, M., Levesque, G., Yu, G., Nishimura, M., Mathews, P., Schmidt, S. D., Mercken, M., Bergeron, C., Westaway, D., and St George-Hyslop, P. (2002) Normal brain development in PS1 hypomorphic mice with markedly reduced gamma-secretase cleavage of betaAPP, *Neurobiol Aging* ***23***, 187–194.
24. Rozmahel, R., Mount, H. T., Chen, F., Nguyen, V., Huang, J., Erdebil, S., Liauw, J., Yu, G., Hasegawa, H., Gu, Y., Song, Y. Q., Schmidt, S. D., Nixon, R. A., Mathews, P. M., Bergeron, C., Fraser, P., Westaway, D., and George-Hyslop, P. S. (2002) Alleles at the Nicastrin locus modify presenilin 1-deficiency phenotype, *Proc Natl Acad Sci USA* ***99***, 14452–14457.
25. Pfeifer, M., Boncristiano, S., Bondolfi, L., Stalder, A., Deller, T., Staufenbiel, M.,

Mathews, P. M., and Jucker, M. (2002) Cerebral hemorrhage after passive anti-Abeta immunotherapy, *Science* ***298***, 1379.

26. Phinney, A. L., Drisaldi, B., Schmidt, S. D., Lugowski, S., Coronado, V., Liang, Y., Horne, P., Yang, J., Sekoulidis, J., Coomaraswamy, J., Chishti, M. A., Cox, D. W., Mathews, P. M., Nixon, R. A., Carlson, G. A., St George-Hyslop, P., and Westaway, D. (2003) In vivo reduction of amyloid-beta by a mutant copper transporter, *Proc Natl Acad Sci USA* ***100***, 14193–14198.
27. Herzig, M. C., Winkler, D. T., Burgermeister, P., Pfeifer, M., Kohler, E., Schmidt, S. D., Danner, S., Abramowski, D., Sturchler-Pierrat, C., Burki, K., van Duinen, S. G., Maat-Schieman, M. L., Staufenbiel, M., Mathews, P. M., and Jucker, M. (2004) Abeta is targeted to the vasculature in a mouse model of hereditary cerebral hemorrhage with amyloidosis, *Nat Neurosci 7*, 954–960.
28. Lacombe, P., Mathews, P. M., Schmidt, S. D., Breidert, T., Heneka, M. T., Landreth, G. E., Feinstein, D. L., and Galea, E. (2004) Effect of anti-inflammatory agents on transforming growth factor beta over-expressing mouse brains: a model revised, *J Neuroinflammation* ***1***, 11.
29. Pawlik, M., Sastre, M., Calero, M., Mathews, P. M., Schmidt, S. D., Nixon, R. A., and Levy, E. (2004) Overexpression of human cystatin C in transgenic mice does not affect levels of endogenous brain amyloid Beta Peptide, *J Mol Neurosci* ***22***, 13–18.
30. Yao, J., Petanceska, S. S., Montine, T. J., Holtzman, D. M., Schmidt, S. D., Parker, C. A., Callahan, M. J., Lipinski, W. J., Bisgaier, C. L., Turner, B. A., Nixon, R. A., Martins, R. N., Ouimet, C., Smith, J. D., Davies, P., Laska, E., Ehrlich, M. E., Walker, L. C., Mathews, P. M., and Gandy, S. (2004) Aging, gender and APOE isotype modulate metabolism of Alzheimer's Abeta peptides and F-isoprostanes in the absence of detectable amyloid deposits, *J Neurochem* ***90***, 1011–1018.
31. Mastrangelo, P., Mathews, P. M., Chishti, M. A., Schmidt, S. D., Gu, Y., Yang, J., Mazzella, M. J., Coomaraswamy, J., Horne, P., Strome, B., Pelly, H., Levesque, G., Ebeling, C., Jiang, Y., Nixon, R. A., Rozmahel, R., Fraser, P. E., St George-Hyslop, P., Carlson, G. A., and Westaway, D. (2005) Dissociated phenotypes in presenilin transgenic mice define functionally distinct gamma-secretases, *Proc Natl Acad Sci USA* ***102***, 8972–8977.
32. Gandy, S., Zhang, Y. W., Ikin, A., Schmidt, S. D., Bogush, A., Levy, E., Sheffield, R., Nixon, R. A., Liao, F. F., Mathews, P. M., Xu, H., and Ehrlich, M. E. (2007) Alzheimer's presenilin 1 modulates sorting of APP and its carboxyl-terminal fragments in cerebral neurons in vivo, *J Neurochem* ***102***, 619–626.
33. Mi, W., Pawlik, M., Sastre, M., Jung, S. S., Radvinsky, D. S., Klein, A. M., Sommer, J., Schmidt, S. D., Nixon, R. A., Mathews, P. M., and Levy, E. (2007) Cystatin C inhibits amyloid-beta deposition in Alzheimer's disease mouse models, *Nat Genet* ***39***, 1440–1442.
34. Trinchese, F., Fa, M., Liu, S., Zhang, H., Hidalgo, A., Schmidt, S. D., Yamaguchi, H., Yoshii, N., Mathews, P. M., Nixon, R. A., and Arancio, O. (2008) Inhibition of calpains improves memory and synaptic transmission in a mouse model of Alzheimer disease, *J Clin Invest* ***118***, 2796–2807.
35. Choi, J. H., Berger, J. D., Mazzella, M. J., Morales-Corraliza, J., Cataldo, A. M., Nixon, R. A., Ginsberg, S. D., Levy, E., and Mathews, P. M. (2009) Age-dependent dysregulation of brain amyloid precursor protein in the Ts65Dn Down syndrome mouse model, *J Neurochem* ***110***, 1818–1827.
36. Morales-Corraliza, J., Mazzella, M. J., Berger, J. D., Diaz, N. S., Choi, J. H., Levy, E., Matsuoka, Y., Planel, E., and Mathews, P. M. (2009) In vivo turnover of tau and APP metabolites in the brains of wild-type and Tg2576 mice: greater stability of sAPP in the beta-amyloid depositing mice, *PLoS One* ***4***, e7134.
37. Yang, D. S., Stavrides, P., Mohan, P. S., Kaushik, S., Kumar, A., Ohno, M., Schmidt, S. D., Wesson, D., Bandyopadhyay, U., Jiang, Y., Pawlik, M., Peterhoff, C. M., Yang, A. J., Wilson, D. A., St George-Hyslop, P., Westaway, D., Mathews, P. M., Levy, E., Cuervo, A. M., and Nixon, R. A. (2011) Reversal of autophagy dysfunction in the TgCRND8 mouse model of Alzheimer's disease ameliorates amyloid pathologies and memory deficits, *Brain* ***134***, 258–277.
38. Mathews, P. M., Guerra, C. B., Jiang, Y., Grbovic, O. M., Kao, B. H., Schmidt, S. D., Dinakar, R., Mercken, M., Hille-Rehfeld, A., Rohrer, J., Mehta, P., Cataldo, A. M., and Nixon, R. A. (2002) Alzheimer's disease-related overexpression of the cation-dependent mannose 6-phosphate receptor increases Abeta secretion: role for altered lysosomal hydrolase distribution in beta-amyloidogenesis, *J Biol Chem 277*, 5299–5307.
39. Grbovic, O. M., Mathews, P. M., Jiang, Y., Schmidt, S. D., Dinakar, R., Summers-Terio, N. B., Ceresa, B. P., Nixon, R. A., and Cataldo, A. M. (2003) Rab5-stimulated up-regulation of the endocytic pathway increases intracellular beta-cleaved amyloid precursor protein carboxyl-terminal fragment levels and Abeta production, *J Biol Chem* ***278***, 31261–31268.

40. Gravina, S. A., Ho, L., Eckman, C. B., Long, K. E., Otvos, L., Jr., Younkin, L. H., Suzuki, N., and Younkin, S. G. (1995) Amyloid beta protein (A beta) in Alzheimer's disease brain. Biochemical and immunocytochemical analysis with antibodies specific for forms ending at A beta 40 or A beta 42(43), *J Biol Chem 270*, 7013–7016.
41. Savage, M. J., Trusko, S. P., Howland, D. S., Pinsker, L. R., Mistretta, S., Reaume, A. G., Greenberg, B. D., Siman, R., and Scott, R. W. (1998) Turnover of amyloid beta-protein in mouse brain and acute reduction of its level by phorbol ester, *J Neurosci 18*, 1743–1752.
42. Chishti, M. A., Yang, D. S., Janus, C., Phinney, A. L., Horne, P., Pearson, J., Strome, R., Zuker, N., Loukides, J., French, J., Turner, S., Lozza, G., Grilli, M., Kunicki, S., Morissette, C., Paquette, J., Gervais, F., Bergeron, C., Fraser, P. E., Carlson, G. A., George-Hyslop, P. S., and Westaway, D. (2001) Early-onset amyloid deposition and cognitive deficits in transgenic mice expressing a double mutant form of amyloid precursor protein 695, *J Biol Chem 276*, 21562–21570.
43. Mathews, P. M., Jiang, Y., Schmidt, S. D., Grbovic, O. M., Mercken, M., and Nixon, R. A. (2002) Calpain activity regulates the cell surface distribution of amyloid precursor protein: inhibition of calpains enhances endosomal generation of beta-cleaved C-terminal APP fragments, *J Biol Chem 277*, 36415–36424.

Chapter 35

Cognitive and Sensorimotor Tasks for Assessing Functional Impairments in Mouse Models of Alzheimer's Disease and Related Disorders

Allal Boutajangout, Yong Sheng Li, David Quartermain, and Einar M. Sigurdsson

Abstract

In the last couple of decades, substantial progress has been made in the development of transgenic mouse models developing amyloid-β deposits and/or neurofibrillary tangles. These mouse models of Alzheimer's disease and related disorders provide an excellent tool for investigating etiology, pathogenic mechanisms, and potential treatments. An essential component of their characterization is a detailed behavioral assessment, which clarifies the functional consequences of these pathologies. We have selected and refined a series of cognitive and sensorimotor tasks that are ideal for studying these models and the efficacy of various treatments.

Key words: Mouse, Behavior, Cognition, Memory, Motor function, Alzheimer's disease, Amyloid-β, Tau, Plaques, Neurofibrillary tangles

1. Introduction

Several transgenic mouse models have been developed that show age-related deposition of amyloid-β (Aβ) and/or tau aggregates as observed in Alzheimer's disease (AD) and related disorders. These models are very useful for clarifying the etiology and pathogenesis of these diseases and to evaluate potential therapeutic interventions.

Numerous mouse models have been developed with familial AD mutations in the amyloid precursor protein and/or the presenilins, with most if not all developing cognitive impairments with age (1, 2). Tangle mouse models appeared later after the first tau mutations were discovered, with at least some of these developing

Einar M. Sigurdsson et al. (eds.), *Amyloid Proteins: Methods and Protocols*, Methods in Molecular Biology, vol. 849,
DOI 10.1007/978-1-61779-551-0_35,

motor impairments because of tau pathology in the spinal cord and brain stem (3). This feature precludes thorough cognitive characterization, which requires extensive maze navigation but allows rapid evaluation of the progression of the pathology and therapy efficacy by using tests for motor coordination (4). Several other tangle models have now been generated and shown to develop cognitive impairments (e.g., see refs. 5, 6).

In our laboratory, we have primarily characterized the functional impairments of the following models, Tg2576 (7), JNPL3 (8), and htau/PS1 (6), with or without a therapeutic intervention. Toward this end, we have used two types of behavioral tests: (1) Sensorimotor tasks to (a) verify that any treatment-related effects observed in the cognitive tasks cannot be explained by differences in sensorimotor abilities or (b) as the primary functional measure of models that develop motor impairments (such as JNPL3). These include traverse beam, locomotor activity, and rotarod. (2) Cognitive tests, including (a) one designed to test short-term memory (object recognition) and (b) two that test spatial/working memory (closed-field symmetrical maze and radial arm maze).

2. Materials

2.1. Traverse Beam

1. Wooden beam (1.1 cm wide and 50.8 cm long).
2. Goal box is a shaded rectangular box made of plastic material and open at one end (length: 16 cm; height and width: 7 cm).
3. Light socket and a bulb (30 W).
4. Two support rods and clamps, such as standard laboratory equipment support rods with tripod base and corresponding clamps to hold the beam.
5. Soft cushion to be placed underneath the entire beam.
6. Mirror allows the observation of footslips on the side that is not facing the observer.

2.2. Rotarod

1. Rotarod 7650 accelerating model. UgoBasile, Varese, Italy. Various other models can be used, some of which allow several animals to be tested simultaneously.
2. Soft cushion to be placed under the rotating rod.

2.3. Locomotor Activity

1. Circular open field (75 cm in diameter).
2. Tracking system (such as Hamilton-Kinder Smart-frame Photobeam System or ANY-MAZE, San Diego Instruments, San Diego, CA, or Noldus Ethovision XT, Noldus, The Netherlands).

2.4. Object Recognition

1. Square-shaped open-field box (48 cm square with 18-cm-high walls made from Plexiglas).
2. Tracking system (such as Hamilton-Kinder Smart-frame Photobeam System or ANY-MAZE, San Diego Instruments, or Noldus Ethovision XT, Noldus, The Netherlands).
3. Objects (such as 250-ml Erlenmeyer flasks, colored soda/beer bottles, glassware, and cans).

2.5. Closed-Field Symmetrical Maze

1. This apparatus is a square open-field box (61 cm square, divided into 36, 9.5 cm squares colored in white).
2. Walls constructed from wood painted in gray.
3. Different lengths of barriers (length: 20 cm, 30.5 cm, 40.5 cm; thickness: 1 cm; height: 8 cm).
4. Saccharine solution (0.1%) colored with green food color (McCormick & Co. Inc., MD, USA).
5. Froot Loops cereal or similar type of a sweet cereal.

2.6. Radial Arm Maze

1. An eight-arm elevated radial maze, constructed from Plexiglas or similar material.
2. Each arm is 35 cm long, 7 cm wide with a water/food cup 1 cm in diameter positioned at the end of each arm.
3. Sidewalls (15 cm high that extend 12 cm into each arm). Remaining sidewalls are 1.5 cm high.
4. The central area is an octagonal-shaped hub (14 cm in diameter).
5. Eight clear guillotine doors constructed from Plexiglas.
6. The maze is elevated 75 cm above floor level.
7. Saccharine solution (0.1%) colored with green food color (McCormick & Co. Inc., MD, USA).
8. Froot Loops cereal or similar type of a sweet cereal.

3. Methods

Before enrolling an animal in a study, all protocols must be approved by Institutional Animal Care and Use Committee (IACUC).

It is necessary to habituate/train animals in the apparatus, prior to behavioral testing, and the mice should always be adapted to the room and its light intensity. In all tests, the level of light is kept relatively low with the use of a dimmer or screens. It is important as well to minimize distracting odors by cleaning each equipment and related objects with water and a 50–70% alcohol solution after each animal's run of the test. Subsequent drying of the surface with tissue shortens the interval between animals. Finally, close

attention should be given to possible visual deficits which are relatively common in mice. Those animals should obviously not be included in tests that require intact sight. Certain strains are prone to having a mutation that causes retinal degeneration, and its presence can be detected by PCR (9).

3.1. Sensorimotor Tests

One major objective of performing sensorimotor tasks is to verify that the outcome in cognitive tasks, which require maze running, cannot be explained by differences in sensorimotor abilities. These tasks are also ideal as a primary measure in mice that develop motor impairments such as the JNPL3 model.

3.1.1. Traverse Beam

This task tests balance and general motor coordination (Fig. 1). Mice are assessed by measuring their ability to traverse a narrow wooden beam to reach a goal box (modification of ref. 12) which specifically examines hindlimb function. The mice are placed on a 1.1-cm-wide beam 50.8 cm long, suspended 30 cm above a padded surface by two identical columns. Attached at one end of the beam is a darkened goal box. The animals are habituated to the apparatus 1 day before test. Mice are placed on the beam and are then monitored for a maximum of 60 s. The number of foot slips each mouse commits before falling or reaching the goal box is recorded for each of the four successive trials (see Note 1). A mirror allows the observation of foot slips on the side that is not facing the observer. The average number of foot slips for all the four trials is calculated and recorded. These foot slips are errors in the test

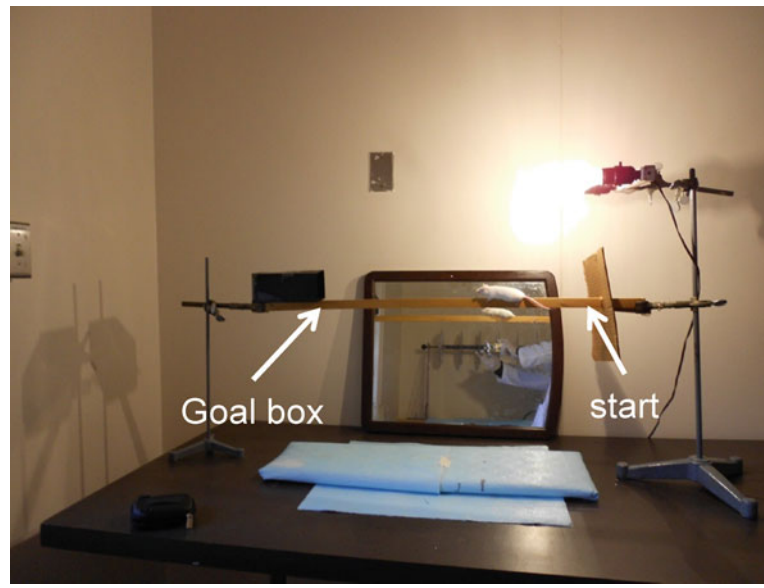

Fig. 1. Traverse beam. Mice are placed on a wooden beam and the number of foot slips each mouse makes before reaching the goal box is recorded in four trials (4, 10, 11).

and are recorded numerically (see Note 2). To prevent injury from falling, a soft foam cushion is always kept underneath the beam.

3.1.2. Rotarod

The animal is placed onto the rod (diameter 3.6 cm) apparatus to measure forelimb and hindlimb motor coordination and balance (Rotarod 7650 accelerating model; Ugo Basile, Biological Research Apparatus, Varese, Italy (13, 14); Fig. 2). The animals are habituated to the apparatus by receiving training sessions of two trials, a sufficient number to reach a baseline level of performance. The mice are then tested an additional three times, increasing the speed of the rotating rod throughout the trial. During habituation and testing, the rotating rod is set at 1.0 rpm. The speed of the rotation is gradually increased at 30-s intervals. A soft foam cushion is placed beneath the apparatus to prevent potential injury from falling. Each animal is tested for a total of three sessions, with each session separated by 15 min, and measures are taken for latency to fall or invert (by clinging) from the top of the rotating barrel (see Note 2).

3.1.3. Locomotor Activity

A tracking system such as the Hamilton-Kinder Smart-Frame Photobeam System (San Diego Instruments) is used to make a video recording of animal's activity over a designated period of time (see Note 3; Fig. 3). Exploratory locomotor activity is recorded in a

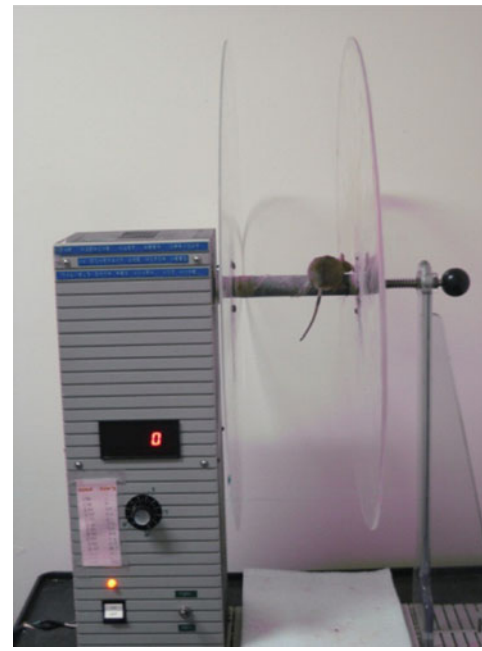

Fig. 2. Rotarod. Mice are placed on the rotating rod (1.0 rpm) when habituated and its rotating speed raised every 30 s by 0.5 rpm. Each mouse is tested three times with 15 min between trials. Measures are taken for latency to fall off the rod (4, 10).

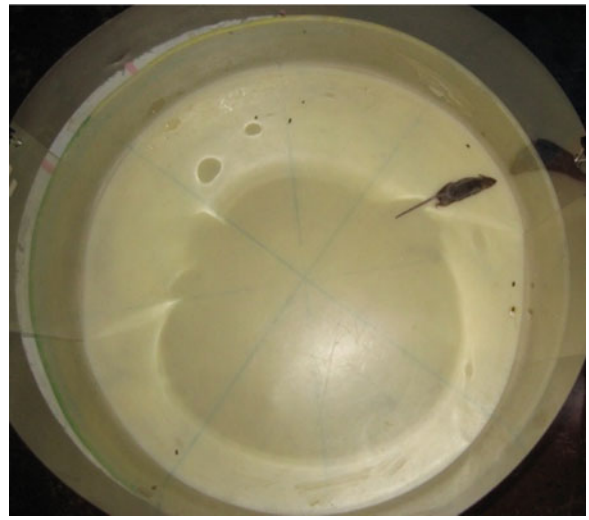

Fig. 3. Locomotor activity. Recorded in a circular open field measuring 75 cm in diameter using a video tracking system. Distance (cm), mean resting time (s), and velocity (average and maximum (cm/s)) are calculated (4, 6, 10).

circular open field measuring 75 cm in diameter (see Note 4). Mice are habituated in a session in which they are allowed to explore the open field for 15 min. A video camera mounted in the ceiling above the chamber automatically records movements in the open field in each dimension (i.e., *x*, *y*, and *z* planes). The total distance is measured in centimeters (cm) traveled. The duration of the test is 15 min. Results are reported based on distance traveled (cm), mean resting time (s), and velocity (average and maximum, cm/s) of the mouse.

3.2. Cognitive Tests

3.2.1. Object Recognition

The spontaneous object recognition test measures short-term memory and is conducted in a square-shaped open-field box (48 cm square, with 18-cm-high walls constructed from black Plexiglas), raised 50 cm above the floor.

Mice are individually habituated in a session in which they are allowed to explore in the open field two identical objects for 15 min (Fig. 4a). These objects are placed diagonally in the center of two zones. Twenty-four hours later this procedure is repeated with two novel identical objects (see Note 5; Fig. 4b). For any given trial, the objects in a pair are about 15–16 cm high, and composed of the same material so that they cannot readily be distinguished by olfactory cues. The amount of time spent exploring each object within a defined zone of the arena is automatically monitored by a tracking system (San Diego Instruments, San Diego, CA) (Fig. 4c). At the end of the training phase, the mouse is removed from the box for the duration of the retention delay (3 h).

Fig. 4. Object recognition. Measures short memory in an open-field box (48 cm square). Mice are habituated to explore different objects within the box, such as those depicted in (**a**, **b**). (**c**) The amount of time spent exploring each object within a defined zone of the arena is measured by a tracking system (4, 6). (**d**) During retention test, one of the familiar objects is replaced by a novel object (*arrow*).

Normal mice remember a specific object after a delay of at least 3 h and spend the majority of their time (about 70%) investigating the novel object during the retention trial. During retention tests, one of the previous familiar objects used during training is replaced by a second novel object, after which the animal is placed in the center of the box and allowed to explore freely for 6 min (see Note 6; Fig. 4d). The time spent exploring the novel and familiar objects is recorded for 6 min. The percentage short-term memory score is the time spent exploring any one of the two objects (training session) compared with the novel one (retention session).

3.2.2. Closed-Field Symmetrical Maze

This apparatus is a rectangular field of 61 cm square with 9-cm-high walls divided into 36, 9.5 cm squares and covered by a clear Plexiglas top (Fig. 5). Endboxes, each 11 × 16 × 9 cm (width × depth × height), are situated at diagonal corners of the field. The symmetrical maze

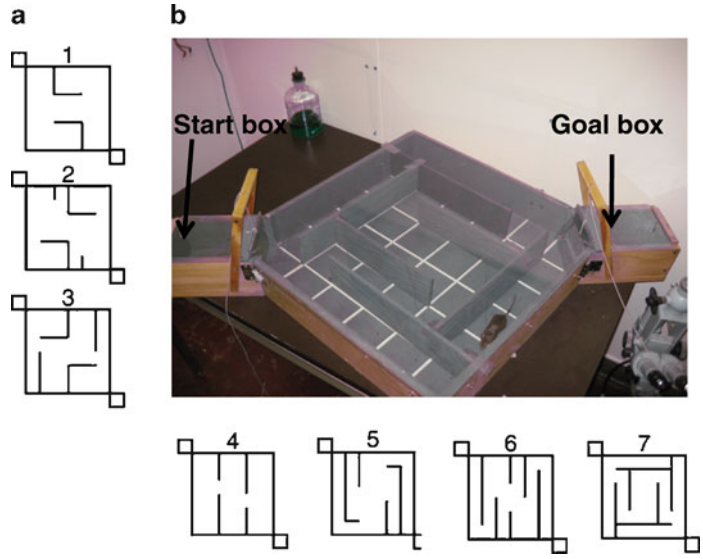

Fig. 5. Closed-field symmetrical maze. (**a**, **b**) Measures spatial/working memory. Schematic *panels 1–7* represent seven problems graded in difficulty to test the spatial and working memory of mice. The barriers are placed in the field in symmetrical patterns, so that mice face the same turns going in either direction within a given problem, which eliminates intertrial handling.

(15) is a modification of the Hebb–Williams (16) and Rabinovitch–Rosvold (17) type of tests, and we have further modified this test (10). The main difference is that each end-compartment now functions as both a startbox and a goalbox, and the mice run in opposite direction on alternate trials, thereby eliminating intertrial handling. The barriers are placed in the field in symmetrical patterns, so that mice face the same turns going in either direction within a given problem. Twenty-four hours prior to testing, the mice are adapted to a water restriction schedule (2 h daily access to water; see Note 7). The mice are given at least two adaptation sessions prior to the beginning of testing. In the first session, each animal is given 0.1% saccharine flavored water in the goal box for 10 min. In the second habituation session 24 h later, the mouse is placed in the start chamber and permitted to explore the field and enter the goal box in which the saccharine solution reward (0.05 ml) is available (see Note 8). When the mice are running reliably from the start chamber to the goal box, they are given three practice sessions on simple problems (24 h apart); in which one or two barriers are placed in different positions in the field so as to obstruct direct access to the goal box (see Note 9). Formal testing consists of the presentation of three to seven problems graded in difficulty (Fig. 5). One problem is presented per day and the mice are given five trials on each problem with a wait period of 2 min between trials. Performance is

scored manually by the same observer in terms of errors (i.e., entries and reentries into designated error zones) and the time needed to complete each trial.

3.2.3. Radial Arm Maze

Spatial learning can also be evaluated in an eight-arm radial maze (Fig. 6). Apparatus is an eight-arm elevated radial maze constructed from Plexiglas or similar material. Each arm is 35 cm long and 7 cm wide with a water/food cup 1 cm in diameter positioned at the end of each arm. Sidewalls, 15 cm high, extend 12 cm into each arm to prevent animals from crossing between arms. The height of the remaining sidewalls is 1.5 cm. The central area is an octagonal shaped hub 14 cm in diameter. Clear Plexiglas guillotine doors, operated remotely by a pulley system control access to the arms. The maze is elevated 75 cm above floor level and situated in a room in which several distinctive objects of a constant location serve as extra maze cues. Prior to testing, mice are adapted to a water or food restriction schedule. If a water restriction is used, water is restricted for 24 h before adapting the mice, and during the adaptation/testing period (2 h daily access to water, see Note 7).

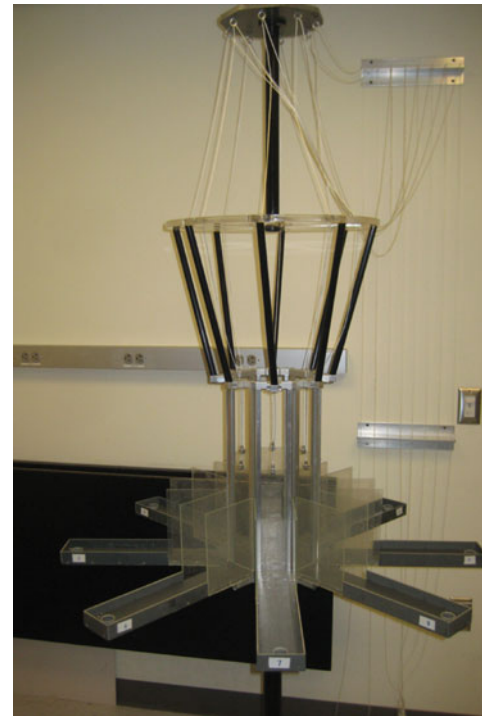

Fig. 6. Radial arm maze. Measures spatial/working memory. Apparatus is an eight-arm elevated radial maze with access to the arms controlled by guillotine doors operated by a pulley system (6, 10).

If a food restriction is used, body weight should be maintained at 90–92% of ad libitum levels (see Note 10). The mice are first adapted in a Y maze for 2 days, and thereafter, in the eight-arm maze for 2–3 days. Mice are initially adapted to the test procedure by allowing them free exploration of the maze for 10 min. During adaptation, drops of 0.1% saccharine solution (water restriction schedule) or pieces of Froot Loops cereal (food restriction schedule) are sprinkled over the floor of the maze and the doors of the Radial Arm Maze are raised and lowered periodically to accustom the animals to the sound associated with their operation. Adaptation is continued until animals are consuming the sugar solution or eating the cereal and freely entering all arms. This typically requires two sessions (1 day apart). On the training trials, a few drops of the saccharine solution or one piece of cereal is placed in the well of each of the eight arms and the trial is begun by placing the mouse in the central area and raising all doors. When an arm is entered all doors are lowered. After the sugar solution is consumed or the food is eaten, the door to that arm is raised allowing the mouse to return to the central arena. After a 5-s interval, the next trial is initiated by again raising all of the doors simultaneously. This procedure is continued until the animal has entered all arms or until 15 min has elapsed (see Note 9). Daily acquisition sessions are continued for 9–10 days. An error is defined as a reentry to a previously visited arm.

4. Notes

1. If an animal falls while performing the traverse beam test, it should be placed back on the beam to continue the test.
2. It is often difficult for obese animals (>35 g) to complete certain tests (traverse beam, rotarod). It is advised to emphasize alternative tests if many of the animals fall into this category or exclude these animals from the study.
3. Locomotor activity can be analyzed by several tracking programs. We originally used the SMART program from San Diego Instruments which has now been replaced by ANY-MAZE. More recently, we have been using Noldus Ethovision XT (Noldus, The Netherlands).
4. Gray-colored open field gives good flexibility in tracking mice with different fur colors. Marking the fur with a contrasting nontoxic marker may facilitate tracking.
5. For example, each bottle has blue water in the bottom third portion, the middle of the bottle is clear, and the upper third is painted in gray (see Fig. 4b). When a black/brown mouse is being tested, the surface of the apparatus is white and a white

cap/can (height approx. 3.5 cm) is placed on the top of the objects to allow tracking of the animal (Fig. 4d). Conversely, darker surface and cap are used when white mice are being tracked.

6. We have used as novel object colored glassware (shown by arrow in Fig. 4d) that is different in shape and color from objects used for training sessions (see Fig. 4b).
7. In our experience, it is better for reinforcement to restrict water rather than food. The mice do better under these conditions. This approach also eliminates confounding variables associated with trail of food morsels in the maze that can distract the mice and/or aid them in finding their way to the reinforcer.
8. If the mice do not drink the water, this session is repeated the following day, and again the next day if needed which is rare.
9. If the animal is not navigating the maze during habituation, it is encouraged with a gentle touch. If this does not help, after repeated attempts and continued habituation, the mouse is excluded from the study.
10. This can be achieved by depriving the mice of food for 24 h on the first day of the habituation and then maintain the animals on 2.0–2.5 g of chow per day for the duration of the study, making adjustments based on body weights recorded 2–3 times per week. Mice maintain good health on this schedule and do not lose additional body weight over the testing period.

Acknowledgments

This work was supported by National Institutes of Health Grants AG032611 and AG020197 and the Alzheimer's Association.

References

1. Ashe, K. H. and Zahs, K. R. (2010) Probing the biology of Alzheimer's disease in mice. *Neuron* ***66***, 631–645.
2. Morrissette, D. A., Parachikova, A., Green, K. N., and LaFerla, F. M. (2009) Relevance of transgenic mouse models to human Alzheimer disease. *J. Biol. Chem.* ***284***, 6033–6037.
3. Gotz, J. and Ittner, L. M. (2008) Animal models of Alzheimer's disease and frontotemporal dementia. *Nat. Rev. Neurosci.* ***9***, 532–544.
4. Asuni, A. A., Boutajangout, A., Quartermain, D., and Sigurdsson, E. M. (2007) Immunotherapy targeting pathological tau conformers in a tangle mouse model reduces brain pathology with associated functional improvements. *J. Neurosci.* ***27***, 9115–9129.
5. Polydoro, M., Acker, C. M., Duff, K., Castillo, P. E., and Davies, P. (2009) Age-dependent impairment of cognitive and synaptic function in the htau mouse model of tau pathology. *J. Neurosci.* ***29***, 10741–10749.
6. Boutajangout, A., Quartermain, D., and Sigurdsson, E. M. (2010) Immunotherapy targeting pathological tau prevents cognitive decline in a new tangle mouse model. *J. Neurosci.* ***30***, 16559–16566.
7. Hsiao, K., Chapman, P., Nilsen, S., Eckman, C., Harigaya, Y., Younkin, S., Yang, F., and

Cole, G. (1996) Correlative memory deficits, Aβ elevation, and amyloid plaques in transgenic mice. *Science* ***274***, 99–102.

8. Lewis, J., McGowan, E., Rockwood, J., Melrose, H., Nacharaju, P., Van Slegtenhorst, M., Gwinn-Hardy, K., Paul, M. M., Baker, M., Yu, X., Duff, K., Hardy, J., Corral, A., Lin, W. L., Yen, S. H., Dickson, D. W., Davies, P., and Hutton, M. (2000) Neurofibrillary tangles, amyotrophy and progressive motor disturbance in mice expressing mutant (P301L) tau protein. *Nat. Genet.* ***25***, 402–405.
9. Gimenez, E. and Montoliu, L. (2001) A simple polymerase chain reaction assay for genotyping the retinal degeneration mutation (Pdeb(rd1)) in FVB/N-derived transgenic mice. *Lab Anim* *35*, 153–156.
10. Asuni, A. A., Boutajangout, A., Scholtzova, H., Knudsen, E., Li, Y. S., Quartermain, D., Frangione, B., Wisniewski, T., and Sigurdsson, E. M. (2006) Vaccination of Alzheimer's model mice with Aβ derivative in alum adjuvant reduces Aβ burden without microhemorrhages. *Eur. J Neurosci.* ***24***, 2530–2542.
11. Boutajangout, A., Ingadottir, J., Davies, P., and Sigurdsson, E. M. (2011) Passive immunization targeting pathological phospho-tau protein in a mouse model reduces functional decline and clears tau aggregates from the brain. *J. Neurochem.* ***118***, 658–67.
12. Torres, E. M., Perry, T. A., Blockland, A., Wilkinson, L. S., Wiley, R. G., Lappi, D. A., and Dunnet, S. B. (1994) Behavioural, histochemical and biochemical consequences of selective immunolesions in discrete regions of the basal forebrain cholinergic system. *Neuroscience* ***63***, 95–122.
13. Carter, R. J., Lione, L. A., Humby, T., Mangiarini, L., Mahal, A., Bates, G. P., Dunnett, S. B., and Morton, A. J. (1999) Characterization of progressive motor deficits in mice transgenic for the human Huntington's disease mutation. *J Neurosci.* ***19***, 3248–3257.
14. Hyde, L. A., Crnic, L. S., Pollock, A., and Bickford, P. C. (2001) Motor learning in Ts65Dn mice, a model for Down syndrome. *Dev. Psychobiol.* ***38***, 33–45.
15. Davenport, J. W. (1970) Cretinism in rats: enduring behavioral deficit induced by tricyanoaminopropene. *Science* ***167***, 1007–1008.
16. Hebb, D. O. and Williams, K. A. (1946) A method of rating animal intelligence. *J. Gen. Psychol.* ***34***, 59–65.
17. Rabinovitch, M. S. and Rosvold, H. E. (1951) A closed-field intelligence test for rats. *Can. J Psychol.* ***5***, 122–128.

INDEX

A

B

Einar M. Sigurdsson et al. (eds.), *Amyloid Proteins: Methods and Protocols*, Methods in Molecular Biology, vol. 849,
DOI 10.1007/978-1-61779-551-0, © Springer Science+Business Media, LLC 2012

C

D

E

F

G

H

I

J

K

L

M

N

O

P

Q

R

S

T

U

V

X

Y

Z